Atlas of Clinical PET-CT in Treatment Response Evaluation in Oncology

Stefano Fanti
Gopinath Gnanasegaran
Ignasi Carrió
Editors

Springer

Atlas of Clinical PET-CT in Treatment Response Evaluation in Oncology

Stefano Fanti • Gopinath Gnanasegaran
Ignasi Carrió
Editors

Atlas of Clinical PET-CT in Treatment Response Evaluation in Oncology

Springer

Editors
Stefano Fanti
Department of Metropolitan Nuclear Medicine
Policlinico S.Orsola-Malpighi
Bologna
Italy

Ignasi Carrió
Hospital Sant Pau, Nuclear Medicine De
Autonomous University of Barcelona
Barcelona
Spain

Gopinath Gnanasegaran
Department of Nuclear Medicine
Royal Free London NHS Foundation Trust
London, UK

ISBN 978-3-030-68857-8 ISBN 978-3-030-68858-5 (eBook)
https://doi.org/10.1007/978-3-030-68858-5

This Springer imprint is published by the registered company Springer Nature Switzerland AG
The registered company address is: Gewerbestrasse 11, 6330 Cham, Switzerland

Contents

Part II Therapy Response Evaluation: Clinical Atlas

List of Contributors

Archi Agrawal Department of Nuclear Medicine and Molecular Imaging, Tata Memorial Hospital, Homi Bhabha National University (HBNI), Mumbai, India

Kanhaiyalal Agrawal Department of Nuclear Medicine, All India Institute of Medical Sciences (AIIMS), Bhubaneswar, India

Haseeb Ahmed Department of Nuclear Medicine, Guy's & St. Thomas' NHS Foundation, London, England

Valentina Ambrosini Nuclear Medicine, DIMES, S.Orsola-Malpighi Hospital, University of Bologna, Bologna, Italy

A. I. J. Arens Department of Radiology and Nuclear Medicine, Radboud University Medical Center, Nijmegen, The Netherlands

Salma Audi Department of Nuclear Medicine, Royal Free London NHS Foundation Trust, London, UK

Agustí Barnadas Department of Medical Oncology, Hospital Sant Pau, Universitat Autònoma Barcelona, Barcelona, Spain

T. Barwick Department of Radiology, Imperial College Healthcare NHS Trust, London, UK

S. Bisdas Lysholm Department of Neuroradiology, National Hospital for Neurology and Neurosurgery, London, UK

Mateos Bogoni PET/CT Center, Quanta – Diagnóstico e Terapia, Curitiba, PR, Brazil

Jamshed Bomanji Institute of Nuclear Medicine, University College London Hospital, University College London Hospitals NHS Trust, London, UK

Gabriel Buschner Technical University Munich, Munich, Germany

Ignasi Carrió Department of Nuclear Medicine, Hospital Sant Pau, Universitat Autònoma Barcelona, Barcelona, Spain

Angelo Castello Nuclear Medicine Unit, IRCCS-Humanitas Research Hospital, Rozzano, Italy

Francesco Ceci Nuclear Medicine, Department of Medical Sciences, University of Turin, Turin, Italy

Juliano Julio Cerci PET/CT Center, Quanta – Diagnóstico e Terapia, Curitiba, PR, Brazil

Sayak Choudhury Department of Nuclear Medicine and Molecular Imaging, Tata Memorial Hospital, Mumbai, India

Gary J. R. Cook Cancer Imaging Department, School of Biomedical Engineering and Imaging Sciences, King's College London, London, UK

King's College London and Guy's & St Thomas' PET Centre, St Thomas' Hospital, London, UK

D. J. Coope Department of Neurosurgery, Salford Royal NHS Foundation Trust, Manchester, UK

Lea Cuppari Nuclear Medicine Unit, Veneto Institute of Oncology IOV—IRCCS, Padua, Italy

Laura Evangelista Nuclear Medicine Unit, Veneto Institute of Oncology IOV—IRCCS, Padua, Italy

Stefano Fanti Nuclear Medicine, Sant'Orsola Hospital, Bologna, Italy

Nuclear Medicine, DIMES, S.Orsola-Malpighi Hospital, University of Bologna, Bologna, Italy

Rashika Fernando Department of Nuclear Medicine and Radiology, Royal Liverpool University Hospitals NHS Foundation Trust, Liverpool, UK

Francesco Fraioli University College London Hospitals (UCLH), London, UK

L. F. de Geus-Oei Department of Radiology, Leiden University Medical Center, Leiden, The Netherlands

Gopinath Gnanasegaran Department of Nuclear Medicine, Royal Free London NHS Foundation Trust, London, UK

Fahim Ul Hassan Department of Nuclear Medicine, Guy's & St. Thomas' NHS Foundation, London, England

L. Heijmen Department of Radiology, Leiden University Medical Center, Leiden, The Netherlands

D. E. Hilling Department of Surgery, Leiden University Medical Center, Leiden, The Netherlands

Roland Hustinx Division of Nuclear Medicine and Oncological Imaging, University Hospital of Liege, Liege, Belgium

Alessio Imperiale Biophysics and Nuclear Medicine, University Hospitals of Strasbourg, Strasbourg, France

Molecular Imaging – DRHIM, IPHC, UMR 7178, CNRS/Unistra, Strasbourg, France

S. Islam Department of Surgery and Cancer, Imperial College London, London, UK

Department of Radiology, Imperial College Healthcare NHS Trust, London, UK

Yash Jain Department of Nuclear Medicine and Molecular Imaging, Tata Memorial Hospital, Homi Bhabha National Institute, Mumbai, India

Radhakrishnan Jayan Department of Nuclear Medicine and Radiology, Royal Liverpool University Hospitals NHS Foundation Trust, Liverpool, UK

Kalevi Kairemo Department of Nuclear Medicine, University of Texas MD Anderson Cancer Center, Houston, TX, USA

Department of Theragnostics, Docrates Cancer Center, Helsinki, Finland

Irfan Kayani Institute of Nuclear Medicine, University College London Hospital, University College London Hospitals NHS Trust, London, UK

Alessandro Lambertini Nuclear Medicine, Department of Medical Sciences, University of Turin, Turin, Italy

Egesta Lopci Nuclear Medicine Unit, IRCCS-Humanitas Research Hospital, Rozzano, Italy

Pierre Lovinfosse Division of Nuclear Medicine and Oncological Imaging, University Hospital of Liege, Liege, Belgium

Homer A. Macapinlac Department of Nuclear Medicine, University of Texas MD Anderson Cancer Center, Houston, TX, USA

M. V. Manikandan Department of Nuclear Medicine and Molecular Imaging, Tata Memorial Hospital, Homi Bhabha National Institute, Mumbai, India

Margaret Masukawa PET/CT Center, Quanta – Diagnóstico e Terapia, Curitiba, PR, Brazil

Boon Mathew Department of Nuclear Medicine and Molecular Imaging, Tata Memorial Hospital, Homi Bhabha National University (HBNI), Mumbai, India

A. S. Mehdi Department of Radiology, Imperial College Healthcare NHS Trust, London, UK

Bhagwant Rai Mittal Department of Nuclear Medicine, PGIMER, Chandigarh, India

Cristina Nanni Nuclear Medicine Department, AOU S.Orsola-Malpighi, Bologna, Italy

Malavika Nathan Department of Nuclear Medicine, Royal Free London NHS Foundation Trust, London, UK

Andrea Paccagnella Nuclear Medicine, Sant'Orsola Hospital, Bologna, Italy

Emanuela Palmerini IRCCS Istituto Ortopedico Rizzoli, Bologna, Italy

E. L. van Persijn van Meerten Department of Radiology, Leiden University Medical Center, Leiden, The Netherlands

Giulia Polverari Nuclear Medicine, Department of Medical Sciences, University of Turin, Turin, Italy

Dimitrios Priftakis University College London Hospitals (UCLH), London, UK

Nilendu C. Purandare Department of Nuclear Medicine and Molecular Imaging, Tata Memorial Hospital, Homi Bhabha National University (HBNI), Mumbai, India

Ameya D. Puranik Department of Nuclear Medicine and Molecular Imaging, Tata Memorial Hospital, Homi Bhabha National Institute, Mumbai, India

Venkatesh Rangarajan Department of Nuclear Medicine and Molecular Imaging, Tata Memorial Hospital, Homi Bhabha National University (HBNI), Mumbai, India

Joan Duch Renom Department of Nuclear Medicine, Hospital de la Santa Creu i Sant Pau, Barcelona, Spain

Saima Riaz University College London Hospitals (UCLH), London, UK

M. J. Roef Department of Nuclear Medicine, Catharina Hospital, Eindhoven, The Netherlands

Nagabhushan Seshadri Department of Nuclear Medicine and Radiology, Royal Liverpool University Hospitals NHS Foundation Trust, Liverpool, UK

Sneha Shah Department of Nuclear Medicine and Molecular Imaging, Tata Memorial Hospital, Homi Bhabha National University (HBNI), Mumbai, India

Sweni Shah Department of Nuclear Medicine, Royal Free London NHS Foundation Trust, London, UK

Arvind Suresh Department of Nuclear Medicine and Molecular Imaging, Tata Memorial Hospital, Mumbai, India

David Taïeb Department of Nuclear Medicine, La Timone University Hospital, European Center for Research in Medical Imaging, Aix-Marseille University, Marseille, France

G. Thompson Centre for Clinical Brain Sciences, University of Edinburgh, Edinburgh, UK

Sharjeel Usmani Department of Nuclear Medicine, Kuwait Cancer Control Center (KCCC), Shuwaikh, Kuwait

Shelvin Kumar Vadi Department of Nuclear Medicine, PGIMER, Chandigarh, India

A. L. Vahrmeijer Department of Surgery, Leiden University Medical Center, Leiden, The Netherlands

Stefan Vöö Institute of Nuclear Medicine, University College London Hospital, University College London Hospitals NHS Trust, London, UK

Biomedical Research Centre, Inflammation, Immunity and Immunotherapeutics, University College London Hospital, London, UK

F. A. Vuijk Department of Surgery, Leiden University Medical Center, Leiden, The Netherlands

Thomas Wagner Department of Nuclear Medicine, Royal Free London NHS Foundation Trust, London, UK

A. D. Waldman Centre for Clinical Brain Sciences, University of Edinburgh, Edinburgh, UK

Simon Wan PETMRI unit, Institute of Nuclear Medicine, University College London Hospital, London, UK

Wolfgang Weber Technical University Munich, Munich, Germany

Part I

Therapy Response Evaluation: Science and Practice

Treatment Response Evaluation: Science and Practice

1

Agustí Barnadas and Ignasi Carrió

1.1 Introduction

Imaging of cancer has long played an important role in defining the local and regional extent of the disease and to exclude the presence of metastatic spread that would generally preclude cure in most cases. In patients with systemic disease, the primary role of imaging has been to provide a baseline evaluation to assess treatment response. There is an increasing recognition that imaging will have an important role in characterizing disease, for testing activity of novel therapies, and in the proper evaluation of therapeutic efficacy. Traditionally, treatment response evaluation in oncology has been based on comparing the size and/or volume of the tumor before and after treatment. However, the introduction of molecular imaging techniques such as FDG PET/CT has improved the characterization of disease and the evaluation of therapies. Advanced molecular imaging approaches appear now in most recent guidelines as part of the recommendations on appropriate use of optimal imaging in solid tumors and lymphoma [1, 2].

A. Barnadas
Department of Medical Oncology, Hospital Sant Pau, Universitat Autònoma Barcelona, Barcelona, Spain

I. Carrió (✉)
Department of Nuclear Medicine, Hospital Sant Pau, Universitat Autònoma Barcelona, Barcelona, Spain
e-mail: icarrio@santpau.cat

In clinical practice, the oncologist needs imaging for assessment of cancer patients in four main scenarios: staging, follow-up of the patient without relapse, assessment of patients with advanced disease including evaluation of response to therapy, and the assessment of the patient with suspected progression because of worsening symptoms. On the other hand, in the current era of precision oncology, there has been an exponential growth in the armamentarium of genomically targeted therapies and immunotherapy. In day-to-day practice, evaluating responses to such precision therapy modalities becomes essential for routine "go" versus "no go" decisions. While this book is focused on the role and value of molecular imaging in the assessment of therapies in most common cancer types, this chapter intends to offer a clinical perspective of the current challenges in this particular area.

Our understanding of tumor biology is rapidly evolving; such knowledge developments are soon translated into new targeted therapeutic approaches for cancer therapy, bringing new challenges to traditional ways of assessing tumor response. Early response prediction after the onset of treatment can lead to alteration of the initial treatment plan, or to the intensification of treatment in those patients who are likely going to respond, aiming to improve outcome, and finally to eventual discontinuation or alteration of treatment in those patients with clear disease progression. Therefore, the evaluation of early

S. Fanti et al. (eds.), *Atlas of Clinical PET-CT in Treatment Response Evaluation in Oncology*,
https://doi.org/10.1007/978-3-030-68858-5_1

response to precision therapies is essential for appropriate clinical management of patients under these molecular targeted drugs. Another role for pretreatment imaging lies in the integrated approach for the determination of the individual tumor risk profile. In this perspective, predictive biomarkers of response, such as imaging biomarkers offered by functional imaging modalities, must be integrated with other clinical and laboratory biomarkers for personalized treatment stratification according to individual prognostic profiles.

1.2 Criteria for Evaluating Response

Treatment response evaluation in oncology has been traditionally based on comparing the size and/or volume of the tumor before and after treatment. However, with the continuing development of new classes of anticancer drugs, the wider availability of new anatomic and functional imaging modalities, and the better understanding of tumor biology, it has become clear that one response assessment criteria may not suffice for appropriate evaluation in all types of tumors. In particular, for those criteria that do not take into account changes in various biologic tumor characteristics apart from size, such as tumor viability, metabolic activity, and cellular density that may be associated with tumor response.

This has led the efforts by various specialized groups and professional organizations to define improved tumor-specific response criteria. During first decade of 2000, various site-specific and defined criteria were proposed. Meanwhile, the European Organization for Research and Treatment of Cancer (EORTC) developed Response Evaluation Criteria in Solid Tumors (RECIST 1.1) to address updates on various measurement rules, such as the number of lesions need to be assessed. The use of RECIST in various clinical trial scenarios, the utilization of newer imaging technologies like 18-Fluorodeoxyglucose positron emission tomography (FDG-PET) and MRI, the proper assessment of lymph nodes, when confirmation is truly needed, and the applicability in trials of targeted noncytotoxic drugs represent new challenges for this methodology.

1.3 Traditional Response Criteria

Various criteria to assess tumor response to therapy by measuring changes of tumor size on imaging studies were developed in the 1960s and 1970s. The World Health Organization (WHO) recognized the need for standardized criteria across clinical trials and published the "WHO handbook for reporting results of cancer treatment" in 1979 [3]. These "WHO criteria" for assessing tumor response were refined and simplified by the "RECIST," which were developed jointly by the EORTC, the National Cancer Institute (NCI) of the USA, and the National Cancer Institute of Canada Clinical Trials group, and have been widely adopted [4]. RECIST 1.0 criteria were initially published in 2000 and updated (RECIST 1.1) in 2009 [5].

The fundamental principles of assessing tumor response, however, have not substantially changed since the initial publication of the WHO criteria in 1979. Overall, "tumor burden" is quantified by summing the size of tumor lesions in a baseline scan before the start of a new therapy. Bidimensional measurements are used for the WHO criteria and unidimensional measurements for RECIST. Tumor response is then quantified by measuring the relative change of this sum of lesion sizes. Importantly, for clinical decision-making and for reporting the results of clinical trials, this continuous parameter is then dichotomized in responders and nonresponders. For bidimensional measurements (WHO criteria), response is defined as a decrease of the sum of tumor sizes by at least 50%. For spherical tumors, this is equivalent to a decrease of the diameter by 30% (RECIST). It must be recognized that large retrospective analyzes have shown that response assessment by WHO criteria and RECIST 1.0 and RECIST 1.1 lead to very similar response classifications [6, 7].

In general, RECIST may not be necessarily representative for changes in tumor volumes in

irregular shaped tumors, given the unidimensional measurement employed. Moreover, RECIST does not address any other measurements of antitumor changes other than tumor shrinkage. With the progressive introduction of novel anticancer therapeutic agents that do not immediately result in decrease of size, the RECIST guideline seems to be of limited value, good examples of which are provided by the effects of immunotherapy in different tumors or bevacizumab in the treatment of colorectal cancer metastases or sorafenib for hepatocellular cancer [8, 9].

To address the issue of tumor necrosis, modified RECIST (mRECIST) criteria were developed [5, 6]. These criteria include enhancement of the target lesions during the arterial phase of either contrast-enhanced CT or MRI. Necrotic areas (nonenhanced during arterial phase) are excluded from the measurement, resulting in a more reliable assessment of the viable tumor remnant. The updated criteria further clarify which lesions should be measured to monitor tumor response and how these lesions are measured. Certainly, additional updates and modifications of RECIST may come in the future.

1.4 Incorporation of Molecular Imaging into Response Criteria

The arrival of molecular imaging approaches brought new insights on the natural history of cancers and offered improved means to assess therapeutic response in oncology. With FDG-PET, the metabolic status of tumors can be imaged, typically showing a decrease in metabolic activity after therapy. Quantitative 18F-FDG PET was introduced for the early sequential monitoring of tumor response of breast cancer in 1993 [10]. Since then, there has been growing interest in using 18F-FDG PET to quickly assess tumor response to therapy. With increasing availability of PET-imaging techniques and adequate evidence of usefulness of PET imaging in the assessment of response to cancer therapy, new response criteria using PET/CT were proposed. The EORTC PET response criteria were proposed in 1999, and subsequently, PERCIST 1.0 was proposed in 2009 [11, 12]. As FDG uptake can be readily quantified, the semiquantitative SUV measurement was adopted and has been observed to decrease after therapy in good responding patients with lymphoma, breast cancer, non-small cell lung cancer, esophageal cancer, and colorectal cancer. Many groups have described early SUV effects observed during serial PET scanning that can already be detected, starting several days after initiation of treatment. Although the optimal timing of image acquisition during treatment is not yet clear and probably differs depending on the tumor type, this early response assessment appears to be one of the most promising applications of PET.

Progressive metabolic disease is then classified as an increase in FDG tumor SUV of greater than 25% within the tumor region defined on the baseline scan, visible increase in the extent of FDG tumor uptake (20% in the longest dimension), or the appearance of new FDG uptake in metastatic lesions. Stable metabolic disease would be classified as an increase in tumor FDG SUV of less than 25% or a decrease of less than 15% and no visible increase in extent of FDG tumor uptake (20% in the longest dimension). Partial metabolic response would be classified as a reduction of a minimum of 15% ± 25% in tumor FDG SUV after one cycle of chemotherapy and greater than 25% after more than one treatment cycle. Complete metabolic response would be complete resolution of FDG uptake within the tumor volume so that it was indistinguishable from surrounding normal tissue. The 25% threshold of SUV change to define a response was mainly based on the limited data on the repeatability of tumor SUV measurements in patients undergoing no therapy. The standard deviation of relative changes of SUVs was approximately 10% and showed no major deviation from a normal distribution. Therefore, 2.5 times the standard deviation should include about 99% of the fluctuations of the measurements that are not caused by a therapeutic effect. A comparison with the limited literature data on changes in FDG uptake during treatment also supported that

a decrease in tumor FDG uptake by 25% or more was correlated with a more favorable outcome.

Overall, EORTC PET response criteria and PET response criteria in solid tumors (PERCIST) follow the model of RECIST and define four response categories with similar names as RECIST: complete metabolic response, partial metabolic response, stable metabolic disease, and progressive metabolic disease. However, there are some differences in the exact definitions of the response categories, and PERCIST provides much more details on which lesions are considered "measurable" and how scans with multiple FDG-avid lesions should be analyzed. In EORTC criteria, standardization and rules were proposed on the following headings: patient preparation, timing of FDG PET scans, attenuation correction and dose of FDG, methods to measure FDG uptake, tumor sampling, reproducibility and definition of FDG tumor response.

According to the PERCIST criteria, response to therapy is assessed as a continuous variable and expressed as percentage change in SUL (SUV normalized by lean body mass) peak or in the sum of lesion (SULs) between the pre and posttreatment scans [13, 14]. A complete metabolic response is defined as visual disappearance of all metabolically active tumors. A partial response is considered more than a 30% and a 0.8 unit decline in SUL peak between the most intense lesion before treatment and the most intense lesion after treatment, although not necessarily the same lesion. More than a 30% and 0.8 unit increase in SUL peak or new lesions, if confirmed, is classified as progressive disease. A greater than 75% increase in total lesion glycolysis is proposed as another metric of progression.

Overall, criteria for assessing tumor response to therapy with FDG PET/CT, initially published in 1999, have now come of age. The original EORTC PET criteria have formalized the concept of assessing tumor response in clinical trials by quantifying changes in FDG uptake. Clinical research during the last 20 years has demonstrated that this concept is valid and that metabolic changes during therapy are correlated with patient outcome. PERCIST has refined response assessment by FDG PET/CT and provides a much more detailed framework for lesion selection, region of interest definition, and response classification. A series of studies have shown that EORTC criteria and PERCIST provide very similar assessment of tumor response, but the use of PERCIST is preferable for clinical trials because PERCIST is a much more specific standard. Therefore, it is likely that PERCIST will replace EORTC criteria in the same way that RECIST replaced the WHO criteria. There is some evidence that PERCIST is a better approach to assess tumor response than RECIST, but this still needs to be proven by systematic clinical studies. These studies should include randomized trials to determine if the response rate by PERCIST predicts the clinical benefit of new anticancer drugs better than the response rate by RECIST [13].

1.5 Response Criteria and Immunotherapy

Since the approval of ipilimumab by the Food and Drug Administration (FDA) and European Medicines Agency (EMA) in 2011, immune checkpoint inhibitors have substantially changed the field of oncology. At the same time, this new approach has unveiled new patterns of tumor response as compared to conventional cytotoxic cancer therapies. Clearly, immune checkpoint inhibitors offer an alternative treatment strategy by exploiting the patients' immune system, resulting in a T cell-mediated antitumor response. These therapies have proven to be effective in multiple different tumor types.

Monoclonal antibody-based therapies targeting cytotoxic T-lymphocyte antigen 4 (CTLA-4), programmed cell death 1 (PD-1), or programmed cell death ligand 1 (PD-L1) have improved patient survival across various tumor types. Immune checkpoint inhibitor therapies target the ability of cancer cells to evade the patient's immune system through disruption of inhibitory ligand-receptor interactions. This allows effector T cells to recognize and eradicate tumor cells. Currently, seven immune checkpoint inhibitors have been approved for clinical use by the FDA and EMA. These are the anti-CTLA-4 antibody

ipilimumab, the anti-PD1 antibodies nivolumab, pembrolizumab and cemiplimab, and the anti-PD-L1 antibodies atezolizumab, avelumab, and durvalumab. These antibodies are currently used to treat multiple tumor types including: melanoma, hepatocellular carcinoma, small cell lung cancer, non-small cell lung carcinoma, renal cell carcinoma, urothelial carcinoma, Hodgkin lymphoma, head and neck squamous cell carcinoma, Merkel cell carcinoma, gastric cancer, breast cancer, primary mediastinal large B-cell lymphoma, and cervical cancer. Moreover, the FDA approved pembrolizumab and nivolumab as tumor agnostic therapy for patients with microsatellite instability-high or deficient DNA mismatch repair tumors. This list of indications is steadily growing as research progresses. In this rapidly growing area, molecular imaging using PET/CT has the potential to provide noninvasive whole-body visualization of tumor and immune cell characteristics and might support patient selection or response evaluations for immune checkpoint inhibitor therapies in solid tumors as well as in lymphoma.

The European Association of Nuclear Medicine has provided recommendations on the proper use of FDG PET/CT to assess response to immune checkpoint inhibitors (Aide). Relevant issues with implications for patient management appear to be pseudoprogression, including frequency and timeline, hyperprogression, and immune-related side effects.

Patterns of response to immunotherapeutic agents also differ from those to chemotherapeutic and molecularly targeted agents. First, although responses usually occur early, they can also be delayed. Second, responses may be preceded by apparent disease progression, retrospectively termed pseudoprogression. These patterns of response have mainly been reported in melanoma patients receiving anti-CLTA-4 agents, with approximately 15% of patients experiencing pseudoprogression. Pseudoprogression appears to be much rarer in all other tumor types (less than 3%), especially with the use of anti-PD1/PD-L1 agents, indicating that in the vast majority of patients, progression seen on morphological imaging is authentic progression. Pseudoprogression should only be considered when the clinical condition of the patient is concomitantly improving. Patients whose clinical condition is not improving and who have disease progression on imaging should discontinue immunotherapy. The risk of continuing treatment beyond progression is that it may prevent commencement of a new line of treatment once the progression is confirmed because of clinical deterioration.

Despite the EORTC criteria were the first to be applied for the assessment of response of solid tumors to immunotherapy, the observation of pseudoprogression in a subgroup of patients treated primarily with ipilumumab and similar reports in other groups of patients led to the modification of the existing definitions of therapeutic response based on morphological imaging techniques using the RECIST. Two slightly different modifications have been recently proposed, known as irRECIST and iRECIST [15]. The latter was developed by the RECIST Working Group and, therefore, is the version more likely to be adopted widely [16]. Essentially, iRECIST has a new category of unconfirmed progression that requires progression to be confirmed by a further follow-up scan. This can also include identification of new lesions, which need to be categorized as measurable or not using RECIST 1.1 principles but that are not included in the sum of target lesions measured at baseline assessment. It is suggested that if the patient is clinically stable, treatment should be continued.

In an attempt to properly harmonize morphological and metabolic responses, additional criteria have been formulated. PET/CT Criteria for Early Prediction of Response to Immune Checkpoint Inhibitor Therapy (PECRIT) included either a change in the sum of RECIST 1.1-based target lesion diameters (method 1) or a change in SULpeak of >15.5% of the hottest lesion [17]. Combining morphological and metabolic criteria can lead to an accuracy of 95% (sensitivity 100%, specificity 93%). The PET Response Evaluation Criteria for Immunotherapy (PERCIMT) [18] classification takes into consideration the observed relevance of the absolute number of new lesions on FDG PET scan and its more robust predictive role compared to pure

SUV changes during the course of treatment with ipilimumab. In particular, such criteria dichotomize patients according to clinical benefit from the treatment (complete or partial response and stable disease) or no clinical benefit from the treatment, that is, progressive disease determined as the appearance of: (a) four or more new lesions <1 cm in functional diameter, (b) three or more new lesions >1.0 cm in functional diameter, or (c) two or more new lesions >1.5 cm in functional diameter. In all cases, the functional diameter is considered the lesion diameter measured in centimeters based on the fused PET/CT images.

Generally speaking, it seems that FDG-PET imaging has to be performed before the start of immunotherapy, together with conventional contrast-enhanced CT. The metabolic information obtained at this time allows adequate restaging and proper evaluation of disease extent at baseline [19]. The scan should be repeated at the first treatment response evaluation, which in most cancer types is 8 or 9 weeks after the start of immunotherapy, which is generally after two or three cycles of treatment, depending on the regimen used. The added value of FDG-PET imaging during treatment is generally found in patients with no morphological response on contrast-enhanced CT or presenting with symptoms, or with signs of immune-related adverse effects. Along with clinical benefit, the presence of a metabolic response despite morphological progression should support clinicians in decision-making. Subsequent imaging with FDG-PET is recommended at the end of immunotherapy [15].

1.6 Practical Considerations

For therapy assessment, use of state of the art equipment is mandatory. Accurate quantification and repeatability/reproducibility of measurements is necessary, with adequate harmonization and quality assurance and control.

Response assessment can be done visually or by using quantitative approaches, depending on the clinical or research question. However, reports must be clinically meaningful, facilitating clinical categorization of response.

EORTC PET criteria and PERCIST lead to very similar response classifications. There may be significant differences between response assessment by PERCIST and RECIST. PERCIST may correlate better with patient outcomes.

Accurate response assessment has to facilitate response-adapted therapies with the goal to de-escalate chemotherapy and reduce long-term side effects.

Inflammatory reactions can occur during immunotherapy and may be associated with pseudoprogression and immune-related adverse effects. It is always recommended to correlate image evolution with the clinical status of the patient.

References

1. Trabulsi E, Rumble B, Jadvar H, Hope T, Pomper M, et al. Optimum imaging strategies for advanced prostate cancer: ASCO Guideline. J Clin Oncol. 2020;38:1–34.
2. Cheson BD, Ansell S, Schwartz L, et al. Refinement of the Lugano classification lymphoma response criteria in the era of immunomodulatory therapy. Blood. 2016;128:2489–96.
3. World Health Organization. WHO handbook for reporting results of cancer treatment: World Health Organization; 1979. https://apps.who.int/iris/handle/10665/37200.
4. Therasse P, et al. New guidelines to evaluate the response to treatment in solid tumors. European Organization for Research and Treatment of Cancer, National Cancer Institute of the United States, National Cancer Institute of Canada. J Natl Cancer Inst. 2000;92:205–16.
5. Eisenhauer EA, Therasse P, Bogaerts J, Schwartz LH, Sargent D, et al. New response evaluation criteria in solid tumours: revised RECIST guideline (version 1.1). Eur J Cancer. 2009;45:228–47.
6. Forner A, et al. Evaluation of tumor response after locoregional therapies in hepatocellular carcinoma: are response evaluation criteria in solid tumors reliable? Cancer. 2009;115:616–23.
7. Subbiah V, Chuang HH, Gambhire D, Kairemo K. Defining clinical response criteria and early response criteria for precision oncology: current state-of-the-art and future perspectives. Diagnostics. 2017;7:10.
8. Martens MH, Lambregts D, Kluza E, Beets-Tan RGH. Tumor response to treatment: prediction and assessment. Curr Radiol Rep. 2014;2:64–7.
9. James PB, O'Connor EO, Aboagye JE, Aerts JWL, Barrington SF, Beer AJ, Boellaard R, et al. Imaging

biomarker roadmap for cancer studies. Nat Rev Clin Oncol. 2017;14:169–86.
10. Wahl RL, Zasadny K, Helvie M, Hutchins GD, Weber B, et al. Metabolic monitoring of breast cancer chemohormonotherapy using positron emission tomography: initial evaluation. J Clin Oncol. 1993;11:2101–11.
11. Wahl RL, Jacene H, Kasamon Y, Lodge MA. From RECIST to PERCIST. Evolving considerations for PET response criteria in solid tumors. J Nucl Med. 2009;50(Suppl 1):122S–50S.
12. O JH, Lodge MA, Wahl RL. Practical PERCIST: a simplified guide to PET response criteria in solid tumors. Radiology. 2016;280:576–84.
13. Pinker K, Riedl C, Weber WA. Evaluating tumor response with FDG PET: updates on PERCIST, comparison with EORTC criteria and clues to future developments. Eur J Nucl Med Mol Imaging. 2017;44(Suppl 1):55–66.
14. Aide N, Charline L, Veit-Haiback P, Sera T, Sattler B, Boellard R. EANM/EARL harmonization strategies in PET quantification: from daily practice to multicentre oncological studies. Eur J Nucl Med Mol Imaging. 2017;44(Suppl I):S17–31.
15. Aide N, Hicks RJ, Le Tourneau C, Lheureux S, Fanti S, et al. FDG PET/CT for assessing tumour response to immunotherapy. Report on the EANM symposium on immune modulation and recent review of the literature. Eur J Nucl Med Mol Imaging. 2019;46:238–50.
16. Seymour L, Bogaerts J, Perrone A, Ford R, Schwartz LH, et al. iRECIST: guidelines for response criteria for use in trials testing immunotherapeutics. Lancet Oncol. 2017;18:e143–52.
17. Cho SY, Lipson EJ, Im HJ, Rowe SP, Gonzalez EM, Blackford A, et al. Prediction of response to immune checkpoint inhibitor therapy using early-time-point (18)F-FDG PET/CT imaging in patients with advanced melanoma. J Nucl Med. 2017;58:1421–8.
18. Sachpekidis C, Anwar H, Winkler J, Kopp-Schneider A, Larribere L, Haberkorn U, et al. The role of interim (18)F-FDG PET/CT in prediction of response to ipilimumab treatment in metastatic melanoma. Eur J Nucl Med Mol Imaging. 2018;45:1289–96.
19. van de Donk PP, Kist de Ruijter L, Lub-de Hooge MN, Adrienne H, Brouwers AH, Anthonie J, van der Wekken AJ, et al. Molecular imaging biomarkers for immune checkpoint inhibitor therapy. Theranostics. 2020;10:1708–18.

2 CT in Treatment Response Assessment in Oncology

Malavika Nathan

2.1 Introduction

In oncological clinical trials, the objective assessment of treatment response to novel pharmaceuticals is a crucial part of the drug development process. Surrogate imaging end points combined with traditional clinical end points of morbidity and mortality are assessed to determine the effectiveness of a drug, eventually determining whether it will have a role in routine oncological management [1].

It follows that having a standardized method of assessing treatment response of tumours with imaging is vital to objectively assess the efficacy of novel chemotherapeutic regimens. Cross-sectional imaging, primarily with computed tomography (CT) is the mainstay. The World Health Organization (WHO) was the first to publish its criteria in 1981, and since then, there have been several iterations, namely Response Evaluation Criteria in Solid tumours (RECIST) versions 1.0 in 2000 and 1.1 in 2009. Modifications and adaptations of the RECIST criteria have evolved to assess treatment response in specific tumours such as hepatocellular carcinoma (HCC), gastrointestinal stromal tumours (GISTs) and lymphoma.

M. Nathan (✉)
Department of Nuclear Medicine, Royal Free London NHS Foundation Trust, London, UK
e-mail: malavika.nathan@nhs.net

More recently, the advent of immunotherapy has demonstrated a variety of novel tumour responses, some of which are distinct from those of traditional chemotherapy and molecular targeted therapies. These novel responses have not always been accurately categorized by RECIST criteria, necessitating the development of new response criteria, prefixed with 'i' to reflect immunotherapy, such as immune-related response criteria (irRC), from the WHO in 2009 and most recently iRECIST from the original RECIST working group in 2017.

This chapter will provide an overview of these criteria, highlighting the similarities and differences as well as the pitfalls.

2.2 Current Response Assessment Criteria for Chemotherapy and Targeted Therapies

Table 2.1 highlights the main response criteria for solid tumours and lymphoma [1–9]. mRECIST and Choi criteria are adaptations of the conventional RECIST criteria, specifically for HCC and GIST, respectively, to assess response to targeted therapies. Targeted therapies refer to the use of protein-kinase inhibitors to inhibit tumour cell proliferation. The Lugano classification is used for response assessment in lymphoma. ^{18}F-fluorodeoxyglucose (^{18}F-FDG) PET/CT is the

S. Fanti et al. (eds.), *Atlas of Clinical PET-CT in Treatment Response Evaluation in Oncology*,
https://doi.org/10.1007/978-3-030-68858-5_2

Table 2.1 Comparison of different response criteria for solid organ tumours and lymphoma

Response	WHO	RECIST 1.1	mRECIST	Choi criteria	Lugano classification
Complete response (CR)	Disappearance of all lesions for at least 4 weeks.	Disappearance of all target lesions.	Disappearance of all arterial phase enhancement in all target lesions.	Disappearance of all target lesions.	Complete resolution of disease. Decrease in size of target lymph nodes to <1.5 cm longest diameter. Resolution of all extranodal sites of disease if identified as target lesions. Return to normal size of all involved organomegaly. No new lesions. Absent non-measured lesions.
Partial Response (PR)	≥50% decrease in SBP from baseline, confirmed at 4 weeks.	>30% decrease in SLDs of target lesions.	>30% decrease in SLDs of arterially enhancing target lesions.	≥10% decrease in tumour size of ≥15% decrease in attenuation of target lesions on CT; no new lesions.	>50% decrease in size of SBP of target lesions. >50% reduction in spleen length from normal length. No increase in non-measured lesions.
Progressive disease (PD)	≥25% increase in SBD in one or more lesions. Development of new lesions.	>20% increase in SLDs of target lesions with an absolute increase of ≥5 mm in any target lesions. Development of new lesions.	>20% increase in SLDs of arterially enhancing target lesions.	≥10% increase in SLD of lesions; does not meet the criteria for PR for tumour attenuation, new intra-tumoural nodules, or an increase in the size of the existing intra-tumoural nodules.	One of the following criteria should be met: Longest diameter >1.5 cm. >50% increase in size of SBP of target lesions from nadir. Increase in size of longest diameter of perpendicular short axis from nadir (5 mm increase for lesions <20 mm or 10 mm increase for lesions >20 mm. Splenomegaly: >50% increase in size from previous measurement. Increase in length by 20 mm if previously not enlarged. New/recurrent splenomegaly. New/recurrent nodal or extranodal disease.
Stable disease (SD)	Neither CR, PR or PD.	Neither CR, PR or PD.	Neither CR, PR or PD.	Neither CR, PR or PD.	Decrease in <50% SBP of target lesions (six target nodal or target extranodal sites) from baseline, provided no criteria for progressive disease are met. No new lesions suggesting lymphoma. No increase in organ enlargement or non-measured lesions in a manner consistent with lymphoma.

Adapted from [1, 9]
mRECIST modified RECIST, *SBP* sum of bidimensional product, *SLD* sum of longest diameter

mainstay imaging modality for FDG avid lymphomas. However, CT is recommended for non-FDG avid lymphomas or where PET/CT is unavailable.

WHO criteria recommended evaluating changes in the sum of the bidimensional product (SBP) of tumour lesions from baseline on each post-treatment scan [6]. The bidimensional product refers to the longest diameter multiplied by the longest perpendicular diameter for each lesion measured.

Whilst the WHO criteria attempted to standardize response evaluation, there were a number of issues, namely, which lesions to measure, the minimum size of the lesion, number of lesions and how progression should be defined. Furthermore, a significant pitfall was the intra- and inter-observer variability in lesion measurement, even by a few millimetres, potentially inaccurately categorizing the response as progressive disease [1].

RECIST 1.0, an international collaboration between the WHO, European Organisation for Research and Treatment of Cancer (EORTC) and the National Cancer Institute of North America (NCI) produced a revised set of response evaluation guidelines, addressing the pitfalls of the original WHO criteria [5]. The significant changes were:

- The use of a single longest dimension (SLD) of the lesion instead of bidimensional measurements. Therefore, the sum of the longest dimension was to be used for pre- and post-treatment comparison.
- Defined 'measurable' lesions based on minimum size of 10 mm on spiral CT and 20 mm on conventional CT. Solid lesions were preferred to cystic lesions as measurable disease. Non-measurable disease included all those lesions that did not comply with the size cut-offs as well as truly non-measurable disease such as pleural/pericardial effusions, ascites, leptomeningeal disease, etc. Sclerotic bone lesions were also considered non-measurable.
- Defined ten lesions (up to five in any one organ) as maximum number of target lesions to be measured on baseline and follow-up scans.
- Refined PD definition by stating that 20% increase in sum of longest diameters (SLD) constituted disease progression and also unequivocal new lesions [5].

The four response categories of the original WHO version remained, but criteria defining PR and PD differed from WHO. PR was redefined as greater than 30% decrease in SLD of target lesions compared with baseline. PD was redefined as greater than 20% increase in SLD compared to the nadir. CR and SD definitions were unaltered.

In 2009, RECIST was further refined in response to issues raised from the original 1.0 version [7, 10]. Major changes included:

- A reduction in the number of target lesions required to determine response assessment from 10 to 5 (with a maximum of 2 per organ).
- Inclusion of pathological lymph nodes with short axis measurement greater than 15 mm as target/measurable lesions. Lytic or mixed lytic bone lesions with a significant soft tissue component were included as measurable disease and could be considered as target lesions.
- Further refinement of PD to include an absolute increase in size of 5 mm of the sum of SLDs (to guard against overcalling PD when the total sum is very small). For example, a minimal increase in size due to measurement variability could meet the 20% increase criteria by RECIST 1.0 without a true increase in tumour burden [10].
- Inclusion of ^{18}F-FDG PET/CT findings in response assessment.

Table 2.2 highlights the overall response category based on the responses of target lesions, non-target lesions and development of new lesions according to RECIST 1.1.

Table 2.2 Overall response categories in RECIST 1.1

Response of target lesions	Response of non-target lesions	New lesions	Overall response
CR	CR	No	CR
CR	Neither CR nor PD	No	PR
CR	Not assessed	No	PR
PR	No PD or not assessed	No	PR
SD	No PD or not assessed	No	SD
PD	Any	Possible	PD
Any	Any	Possible	PD
Any	Any	Yes	PD

Adapted from [1]

2.3 Pitfalls of RECIST 1.1

- Increases in tumour size due to intra-tumoural haemorrhage or necrosis.
  - Certain targeted therapeutic agents, namely tyrosine kinase inhibitors and anti-angiogenesis agents, induce intra-tumoural haemorrhage or necrosis, which can result in a paradoxical increase in size of lesions. This is often seen in primary liver tumours, such as HCC, as well as liver metastases from GIST and melanoma [11, 12]. This is a pitfall of response assessment by RECIST, potentially miscategorizing the patient as progressive disease and should be recognized in order to avoid this error. Confirmation of response can be performed with MRI or ^{18}F-FDG PET/CT.
- CT attenuation changes due to intra-tumoural haemorrhage or necrosis.
  - This phenomenon particularly pertains to GIST (primary lesion and liver metastases) treated with tyrosine kinase inhibitors, where significant reduction in CT attenuation due to myxoid degeneration, haemorrhage or necrosis is an important response parameter and may precede any changes in size [3, 4]. It is also of particular relevance in the context of 'new' liver lesions—pre-existing liver lesions that are isodense to liver (and not seen)—becoming more conspicuous on post-treatment imaging due to tumour degeneration. Choi et al. modified RECIST criteria to incorporate these CT attenuation changes, as well as including the assessment of intra-tumoural nodules in response [3, 4, 12]. Aside from GIST, CT attenuation changes have also been shown to be of relevance in other soft tissue sarcomas [13].
- Lung nodule cavitation.
  - Cavitation as a manifestation of tumour response can also result in an increase in size of the nodule. Proposals have been suggested to exclude the cavity when measuring lung nodules, to provide a more accurate assessment of tumour burden [14], however, this is yet to be validated.

2.4 mRECIST in HCC

RECIST criteria have been modified for HCC treated with tyrosine kinase inhibitors, namely sorafenib, to account for tumour hypervascularity on arterial phase imaging as a measure of viable tumour [8, 15]. Complete loss of arterial phase enhancement of the tumour is considered as complete response. Any residual or new hypervascularity of the tumour post-treatment indicates the presence of viable tumour.

2.5 Lugano Classification in Lymphoma

CT is only used for response assessment in non ^{18}F-FDG avid lymphomas such a chronic lymphocytic leukaemia, lymphoplasmacytic lymphoma, marginal zone lymphoma and mycosis fungoides to name a few, or where PET/CT is unavailable.

There are several differences between the Lugano classification (LC) and RECIST criteria:

- LC measures the longest diameter on the lymph node rather than short axis as in RECIST. Measurable nodal disease is considered longer than 1.5 cm as opposed to 1.0 cm

short axis with RECIST. However, extranodal disease is deemed measurable if it is >1.0 cm.
- LC uses the sum of bidimensional product compared with sum of unidimensional measurements in RECIST.
- Criteria for CR, PR and PD are different in LC compared with RECIST as indicated in Table 2.1.

2.6 Response Assessment Criteria in Immunotherapy

The advent of immunotherapy has had a significant impact in the treatment of several cancers, such as cutaneous malignant melanoma, non-small cell lung cancer, renal cell cancer and head and neck squamous cell carcinomas, through activation of patients' immune systems to eliminate tumour cells. T cell activation and response are regulated by immune checkpoints—a balance of stimulatory and inhibitory signals—which control the magnitude of the immune response. The most commonly used form of immunotherapy targets several checkpoint inhibitors.

In contrast to chemotherapy, where response can be immediate, the effect of immunotherapy usually takes significantly longer. Different patterns of tumour response have been identified, most, distinct from traditional chemotherapeutic responses [16]:

- Immediate tumour response with no new lesions.
- Durable stable disease.
- Response after initial progression in tumour burden—termed 'pseudoprogression' or 'flare effect'.
- Tumour response but with development of new lesions.

These patterns do not conform well to RECIST 1.1 criteria, where the development of new lesions automatically categorizes the response as PD, potentially resulting in the premature termination of therapy or removal of patients from clinical trials.

Novel response criteria have been developed for immunotherapy, namely irRC in 2009, which uses WHO criteria, but is rarely used currently [16], immune-related RECIST (irRECIST) in 2013, which combines aspects of irRC and RECIST 1.1 [17] and finally immune RECIST (iRECIST) in 2017 by the RECIST working group, which standardizes the immune response criteria [18].

Table 2.3 highlights the similarities and differences between irRECIST, iRECIST and RECIST 1.1.

Table 2.3 Comparison of immune response criteria [16–18]

	RECIST 1.1	irRECIST	iRECIST
Lesion measurement	Unidimensional	Bidimensional	Unidimensional
Target lesion size	≥10 mm	≥10 mm	≥10 mm
Target lesion number	five lesions total, two per organ.	five lesions total, two per organ.	five lesions total, two per organ.
New lesions	Always represents PD.	Incorporated into total tumour burden.	iUPD
Response	CR: disappearance of all lesions. PR: ≥30% decrease from baseline SLD. PD: ≥20% increase SLD from nadir. SD: neither CR, PR, PD.	CR: disappearance of all lesions. PR: ≥30% decrease from baseline SLD. PD: ≥20% increase SLD from nadir. SD: neither CR, PR, PD.	CR: disappearance of all lesions. PR: ≥30% decrease from baseline SLD. PD: ≥20% increase SLD from nadir. SD: neither CR, PR, PD.
Confirmation of PD	No unless response is primary end point.	Yes, imaging up to 12 weeks later to confirm PD and account for pseudoprogression.	Yes, imaging 4–8 weeks after first assessment.

SLD sum of longest diameter, *iUPD* immune unconfirmed progressive disease

Much of the criteria is concordant between RECIST 1.1 and iRECIST. The main change is in the definition of PD—to consider 'pseudoprogression' and the development of new lesions. First iRECIST PD is termed 'immune unconfirmed PD' (iUPD). True PD is then confirmed with imaging 4–8 weeks later.

2.7 Conclusion

CT is the main imaging modality used to assess treatment response. This chapter has summarized the standard response criteria employed to assess treatment response to chemotherapy, targeted therapy and immunotherapy, highlighting the similarities and differences as well as the pitfalls of the current criteria.

References

1. Tirkes T, Hollar MA, Tann M, Kohli MD, Akisik F, Sandrasegaran K. Response criteria in oncologic imaging: review of traditional and new criteria. Radiographics. 2013;33(5):1323–41.
2. Cheson BD, Fisher RI, Barrington SF, Cavalli F, Schwartz LH, Zucca E, et al. Recommendations for initial evaluation, staging, and response assessment of Hodgkin and non-Hodgkin lymphoma: the Lugano classification. J Clin Oncol. 2014;32(27):3059–68.
3. Choi H, Charnsangavej C, de Castro Faria S, Tamm EP, Benjamin RS, Johnson MM, et al. CT evaluation of the response of gastrointestinal stromal tumors after imatinib mesylate treatment: a quantitative analysis correlated with FDG PET findings. AJR Am J Roentgenol. 2004;183(6):1619–28.
4. Choi H, Charnsangavej C, Faria SC, Macapinlac HA, Burgess MA, Patel SR, et al. Correlation of computed tomography and positron emission tomography in patients with metastatic gastrointestinal stromal tumor treated at a single institution with imatinib mesylate: proposal of new computed tomography response criteria. J Clin Oncol. 2007;25(13):1753–9.
5. Therasse P, Arbuck SG, Eisenhauer EA, Wanders J, Kaplan RS, Rubinstein L, et al. New guidelines to evaluate the response to treatment in solid tumors. European Organization for Research and Treatment of Cancer, National Cancer Institute of the United States, National Cancer Institute of Canada. J Natl Cancer Inst. 2000;92(3):205–16.
6. World Health Organization. WHO handbook for reporting results of cancer treatment. Geneva Albany, NY: World Health Organization; sold by WHO Publications Centre USA; 1979. 45 p.
7. Eisenhauer EA, Therasse P, Bogaerts J, Schwartz LH, Sargent D, Ford R, et al. New response evaluation criteria in solid tumours: revised RECIST guideline (version 1.1). Eur J Cancer. 2009;45(2):228–47.
8. Bruix J, Sherman M, Llovet JM, Beaugrand M, Lencioni R, Burroughs AK, et al. Clinical management of hepatocellular carcinoma. Conclusions of the Barcelona-2000 EASL conference European Association for the Study of the Liver. J Hepatol. 2001;35(3):421–30.
9. Naveen MK, Daniella FP, Srikala N, Avinash RK, Jeremy SA, Dushyant VS. Imaging for oncologic response assessment in lymphoma. Am J Roentgenol. 2017;208(1):18–31.
10. Nishino M, Jackman DM, Hatabu H, Yeap BY, Cioffredi LA, Yap JT, et al. New Response Evaluation Criteria in Solid Tumors (RECIST) guidelines for advanced non-small cell lung cancer: comparison with original RECIST and impact on assessment of tumor response to targeted therapy. AJR Am J Roentgenol. 2010;195(3):W221–8.
11. Horger M, Lauer UM, Schraml C, Berg CP, Koppenhofer U, Claussen CD, et al. Early MRI response monitoring of patients with advanced hepatocellular carcinoma under treatment with the multikinase inhibitor sorafenib. BMC Cancer. 2009;9:208.
12. Shankar S, vanSonnenberg E, Desai J, Dipiro PJ, Van Den Abbeele A, Demetri GD. Gastrointestinal stromal tumor: new nodule-within-a-mass pattern of recurrence after partial response to imatinib mesylate. Radiology. 2005;235(3):892–8.
13. Stacchiotti S, Collini P, Messina A, Morosi C, Barisella M, Bertulli R, et al. High-grade soft-tissue sarcomas: tumor response assessment--pilot study to assess the correlation between radiologic and pathologic response by using RECIST and Choi criteria. Radiology. 2009;251(2):447–56.
14. Crabb SJ, Patsios D, Sauerbrei E, Ellis PM, Arnold A, Goss G, et al. Tumor cavitation: impact on objective response evaluation in trials of angiogenesis inhibitors in non-small-cell lung cancer. J Clin Oncol. 2009;27(3):404–10.
15. Bruix J, Reig M, Rimola J, Forner A, Burrel M, Vilana R, et al. Clinical decision making and research in hepatocellular carcinoma: pivotal role of imaging techniques. Hepatology. 2011;54(6):2238–44.
16. Wolchok JD, Hoos A, O'Day S, Weber JS, Hamid O, Lebbe C, et al. Guidelines for the evaluation of immune therapy activity in solid tumors: immune-related response criteria. Clin Cancer Res. 2009;15(23):7412–20.
17. Nishino M, Giobbie-Hurder A, Gargano M, Suda M, Ramaiya NH, Hodi FS. Developing a common language for tumor response to immunotherapy: immune-related response criteria using unidimensional measurements. Clin Cancer Res. 2013;19(14):3936–43.
18. Seymour L, Bogaerts J, Perrone A, Ford R, Schwartz LH, Mandrekar S, et al. iRECIST: guidelines for response criteria for use in trials testing immunotherapeutics. Lancet Oncol. 2017;18(3):e143–e52.

3 MRI and Diffusion-Weighted MRI in Treatment Response Evaluation Overview

Simon Wan

3.1 Introduction

Magnetic resonance imaging (MRI) is an established imaging modality integral to many modern cancer management pathways. Amongst the many strengths of MRI are its superior soft tissue contrast resolution, multi-planar capability and the lack of ionising radiation. MRI is also widely available in many hospitals.

With MRI, the anatomical arrangement of normal and pathological structures, and their tissue properties, are probed by echoes returned from radiofrequency pulse sequences targeted at regions of interest in the body, within magnetic fields in the scanner [1]. Exogenous contrast agents are often used in conjunction [2]. Current clinical MRI examinations utilise multiple pulse sequences to generate images with different weighting to tissue contrast. These images can provide important details of oncological disease status, such as nature and structure of tumours, tumour size, tissue planes, adjacent neuromuscular bundle or organ invasion.

Anatomical coverage of clinical MRI examinations is traditionally limited to individual body parts (such as brain, liver, pelvis). This is as a trade-off for meticulous spatial and contrast resolution and for scan times to be reasonably tolerable for patients. Clinical MRI examinations are, therefore, adept to loco-regional disease assessment and response evaluation.

Functional MRI parameters have recently been enabled by advances in MRI hardware and sequence developments. Diffusion-weighted imaging (DWI) sequences are now widely adopted. Tumour vascularity and perfusion can be assessed with different methods, such as with dynamic contrast enhanced sequences using exogenous contrast agents [3], or arterial spin labelling [4], with MR tagging of blood as endogenous tracer. Tissue hypoxia can be probed with sequences such as blood oxygen level-dependent (BOLD) MRI [5]. Chemical composition within tumours and its microenvironment may be glimpsed by techniques such as MRI spectroscopy or chemical exchange saturation transfer [6, 7]. Functional MRI sequence development continues to be an expanding field of research.

Another area of development has been the expansion to whole body coverage. While this may not be a novel concept, improvement in hardware, such as improved gradient systems, interconnected phase array coils and protocol and sequence designs, such as parallel imaging strategies, have enabled adequate quality images with full body coverage to be attainable within an acceptable scan duration. These have paved ways for the technique to be entering routine clinical use in malignancy with tendency for disseminated

S. Wan (✉)
PETMRI unit, Institute of Nuclear Medicine, University College London Hospital, London, UK
e-mail: mwan@nhs.net

S. Fanti et al. (eds.), *Atlas of Clinical PET-CT in Treatment Response Evaluation in Oncology*,
https://doi.org/10.1007/978-3-030-68858-5_3

lesions, such as in metastatic prostate, breast cancer and in multiple myeloma [8–10].

MRI has been shown to be of high accuracy in primary disease assessment in a multitude of cancer type and location, for example, in the brain, head and neck, hepatobiliary, rectum, gynaecological tract and in the prostate, bones and soft tissues [11–17]. It is intuitive then that MRI would be the natural candidate of choice for response evaluation for these tumours. Depending on the treatment options for the particular clinical context, this may be after the use of ablation, chemotherapy or radiation for loco-regional disease (in neoadjuvant, primary treatment or adjuvant setting), or after systemic treatment in more widespread disease.

It is important to note that while many MRI techniques are now feasible and available for response evaluation, there is much variation in the extent to which these have been validated or adopted into clinical practice. For many indications (e.g. in post-neoadjuvant rectal tumour), use of MRI has been well studied [12, 18, 19]. In other areas (e.g. whole body MRI in multiple myeloma [8]), robust validation of MRI evaluation of treatment response remains work in progress. Some advanced techniques may show potential, but clinical translation may be further away on the horizon.

The rest of the chapter would focus on some of the general concepts underpinning response evaluation with MRI, with particular emphasis on established criteria and DWI.

3.2 Response Evaluation by Tumour Burden or Anatomical Parameters

Change in tumour burden, as visualised on radiological images, is widely thought of as useful for response evaluation in cancer management. Its acceptance is built on the premise that changes in tumour burden (such as size and number of lesions) can act as surrogate predictors for patients' survival and quality of life, the ultimate end points of cancer therapeutics.

3.2.1 WHO and RECIST Criteria

In 1981, the World Health Organization (WHO) first published tumour response criteria [20]. Over the next decades, Response Evaluation Criteria in Solid Tumours (RECIST) was published in 2000 [21], attempting to further standardise measurement of tumour burden on anatomical imaging. This was further validated in cohorts of patients with metastatic cancer undergoing cytotoxic therapy treatment, resulting in the refined criteria published as RECIST 1.1 in 2009 [22].

By providing internationally agreed principles and common languages, they provide standardised frameworks for reporting tumour response, thereby increasing robustness and comparability of clinical trial results from different research centres. This is important for when an 'objective response' may be an important end point in determining the success of a phase II clinical trial, or for when a clear definition of disease progression is needed for trials using progression-free survival as an end point, such as in a phase III trial [21].

While the main use of these criteria may be for clinical trials reporting, especially in the metastatic disease context, it is undoubted that many key features have influence on day-to-day clinical oncological imaging practice. Common to the evolving WHO, RECIST 1.0 and 1.1 criteria are:

1. Definitions of measurable lesions
2. Specification of how dimensions should be measured and
3. How changes of these measurements over time should be computed to generate response categories

In RECIST 1.1, multiple strategies are adopted to increase practicality, precision, reproducibility and robustness of response evaluation. For example, defining a minimum size for individual measurable lesion (at least 10 mm for longest dimension of a tumour, 15 mm for short axis measurement of nodes) and summing together of the diameters of target lesions as a single parameter (SPD) to define response category may help

to limit impact of individual measurement errors. Limiting the number of lesions, which needs to be longitudinally measured to up to five 'target lesions' (selected based on size, perceived reproducibility on repeated measurements and representativeness of all involved organs), reduces the burden to reporters. Clarity of the different response categories with appropriate thresholds increases robustness and reproducibility at the response category level (e.g. Partial response is defined when there has been at least 30% in the SPD of target lesions. Progressive disease can be defined when there is new lesion, or at least 20% increase (and at least 5 mm absolute increase) in the SPD of target lesions compared to baseline, or the smallest SPD, achieved on the study).

MRI may be used under RECIST1.1. It is acknowledged that there are many acquisition variables in MRI, which may impact greatly on image quality, lesion conspicuity and measurement. Rather than specifying exact sequences to be used in any particular MRI study, RECIST1.1 stipulated that scanning sequences should be optimised, and the same scanner and protocol should be matched as closely as possible across imaging time points. Unless for isotropic acquisition, maximal diameter of each target lesion should always be measured on the planes in which a particular MRI sequence is acquired in (not re-formatted).

3.2.2 iRECIST

With increasing use of immune modulators as anticancer therapy, it has become recognised that some patients may demonstrate unusual pattern of response as per anatomical parameters. These may include a delayed response or even apparent initial increases in tumour burden, which is followed by late, deep and durable responses (pseudoprogression). In light of this, investigators began to apply different modifications to the conventional RECIST, culminating in the RIECIST steering group to propose an additional response evaluation algorithm for use in studies evaluating efficacy of immunotherapies in 2017 (iRECIST) [23, 24].

Many key features, particularly surrounding lesion measurements and summations remain similar to RECIST1.1. A main new change is the requirement of a confirmatory imaging study in 4–8 weeks if there are features of progressive disease on initial response evaluation studies. Termed iUPD (unconfirmed PD) at this initial time point, if there are features reaching threshold of further growth on the following confirmatory study, then disease progression is confirmed (confirmed PD, iCPD). Assuming the patient remains clinically stable, it has been recommended that treatment be continued after iUPD. It is acknowledged that it is challenging to differentiate between pseudo and true progression. The proposed strategy hoped to strike the balance between the undesirable early discontinuation of an effective treatment and equally undesirable continuation of a non-effective therapy. Robust validation of this approach is an on-going effort.

3.2.3 Other Response Evaluation by Anatomical MRI in Specific Disease Contexts

Comprehensive coverage and detail critique of all the individual scenarios, where MRI can be used for response evaluation, are beyond the scope of this chapter, but some of the more established areas in use in clinical practice are described.

3.2.3.1 Brain Tumour

Specific challenges in measuring brain tumour burden for response evaluation had led to the community adopting specific response criteria (e.g. that proposed by the Response Assessment in Neuro-Oncology (RANO) working group) [25], such as for high-grade and low-grade gliomas, leptomeningeal metastases and brain metastasis. MRI is an indispensable tool in these.

With irregular shapes of gliomas, bidimensional measures are used for measurements of gliomas in RANO criteria, unlike single-dimension measures used in RECIST. Furthermore, how response evaluation of gliomas may be described on differ-

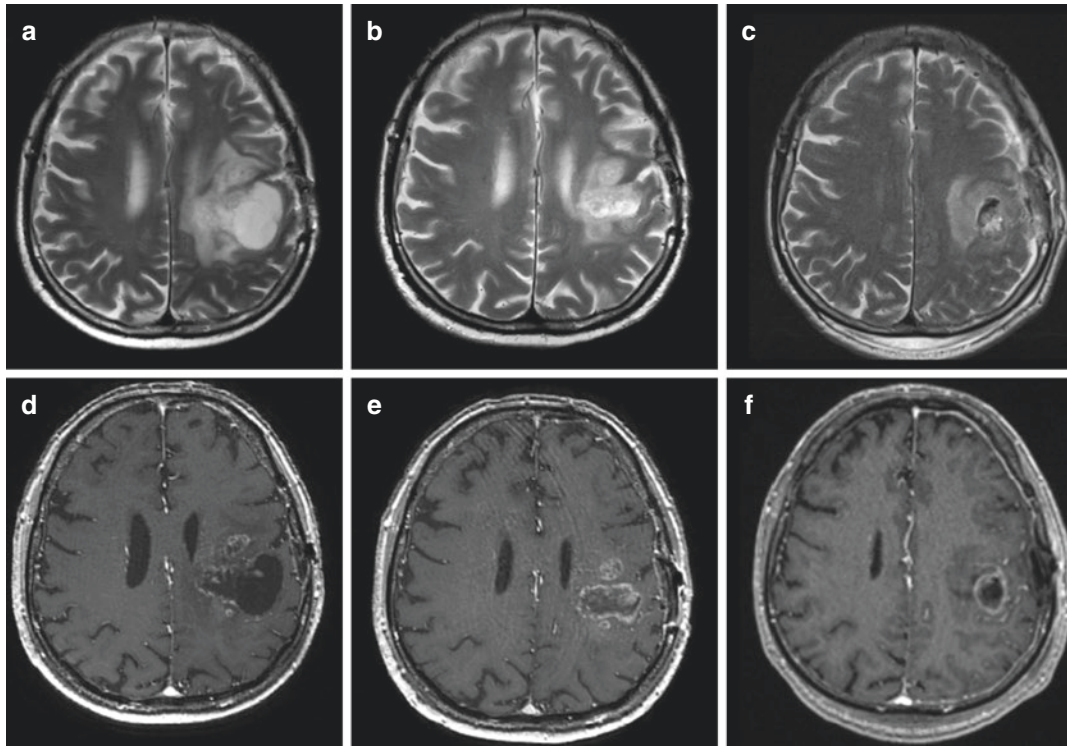

Fig. 3.1 Glioblastoma multiforme response evaluation. Top row T2 weighted axial images of the brain; bottom row corresponding T1 post-contrast axial images; from right, (**c**, **f**)—baseline post debulking surgery; (**b**, **e**) 2 months post-radiotherapy and commencement of steroid and temozolomide; (**a**, **d**) 5 months post-radiotherapy and commencement of steroid and temozolomide. (**c**, **f**) show residual tumour manifesting as enhancing cavitating tumour with intermediate to high surrounding T2 tumour signal. (**b**, **e**) show increase in size of enhancing cavitating lesion with new adjacent nodules, and some increase in T2 signal change, in keeping with radiological progression; however, the patient remained stable and well at this stage. (**a**, **d**) similar further progressive radiological change, and by this time point, there was parallel clinical deterioration, further supporting progressive disease despite treatment

ent specific MRI sequences has been specified. This is because tumoural changes in different MR sequences may carry different biological significance.

For example, anti-angiogenic agent, such as bevacizumab, is believed to reduce vascular permeability, even if a glioma is biologically progressing. Definition of PD has, therefore, been expanded to include changes such as significant increase of T2/FLAIR signal areas and emergence of new lesion (beyond the more intuitive increased of enhancing tumour area). These are in order to capture patients with non-enhancing but progressing disease. In addition, post-contrast images are not used in response criteria for low-grade glioma, as these tumours do not often show contrast enhancement.

Other key features of the RANO criteria are the incorporation of clinical status and the patient's reliance on corticosteroid use as part of overall response evaluation criteria (Fig. 3.1). Pseudoprogression can also confound response evaluation of brain tumours, leading to some authors to propose additional immune-related response criteria (irRC) for immunotherapy trials. These adopt similar concepts of iRECIST by specifying need for a confirmatory scan at a later time point to confirm PD.

3.2.3.2 Hepatocellular Carcinoma (HCC)

HCC is the third most common cause of cancer related death. Liver-directed, loco-regional therapies are commonly used as a stand-alone palliative modality or as a bridge to selected patients for whom liver transplant may be a curative option. These may include thermal ablations, or transarterial embolization with varying agents to include chemotherapy, drug-eluting beads or radioactive spheres. These treatments induce local disease control through tumour necrosis, and it is recognised that there can be poor correlation between the clinical benefit and conventional size-based methods of response assessment. For instance, following adequate radiofrequency ablation, it would be anticipated that the focal area of the ablation zone would be greater than the pre-treatment tumour size.

Modified RECIST (mRECIST) was proposed as an improved tool, which has also been adopted by the European Association for the Study of the Liver (EASL) [26, 27]. Hepatic carcinogenesis is associated with a peculiar vascular derangement, manifesting as arterial enhancement, followed by washout on portal venous and/or delayed phases on imaging including MRI. For a lesion >1 cm and in a high pre-test population cohort (cirrhotic patient), this typical imaging appearance is considered diagnostic of HCC, which in turn also provides a handle for MRI evaluation of response evaluation. One of the key modifications in mRECIST is of taking measurements of only the viable (arterial enhancing) component of tumour for assessment of tumour volume and for summation to compute overall response at a patient level. Necrotic areas are ignored. mRECIST has been validated by studies showing that responders had better survival compared to non-responders to these loco-regional treatments.

Furthermore, the Liver Imaging Reporting and Data System (LI-RADS) lexicon [28], originally proposed by the American College of Radiology, has recently expanded with addition of a treatment response algorithm. This has some similarities and overlaps with mRECIST, including placing emphasis on the arterially enhancing tumour residuum. On the other hand, LI-RADS provides a more detail lexicon of MRI features and is a lesion-by-lesion response assessment tool.

3.2.3.3 Rectal Cancer

Neoadjuvant chemoradiation (CRT) has become standard treatment for patients with locally advanced rectal cancer. Neoadjuvant treatment aims to downsize and downstage tumours, with an aim to increasing resectability and long-term local disease control. In a minority of patients showing complete response, it is becoming apparent that they may be spared the morbid surgical resection without significantly comprising long-term outcome. Standardised and accurate MRI response evaluation is thus of paramount importance [29].

Change in tumour length is advocated as a useful measure for response evaluation, as a compromise between the measurements on any one imaging plane, which may not be reproducible, given the often complex non-orthogonal planes on which tumour grows, and ultimate 3D volumetry [29] (Fig. 3.2). Treatment effect can also be inferred by reduction of often intermediate T2 signal representing viable tumour and emergence of low-signal fibrotic tissues. This had been used in a semi-quantitative scoring system (MRI tumour regression grade), with a five-point scale of relative proportion of tumour signal and fibrotic signal, which has shown moderate success when validated with pathological tumour regression [30]. In addition, some primary non-mucinous tumour undergo mucinous change with CRT, manifesting as increasing high T2 signal, which is also a form of treatment response [31].

Furthermore, specific to the neoadjuvant, pre-surgical setting is the need to precisely describe residual tumour extent for assessment of resectability and planning surgical approach. MRI has been shown to be able to predict feasibility of successful sphincter preserving low-rectal cancer surgery, and with lesser success also at predicting outcome of clearance of the mesorectal fascia, an important surgical landmark [30].

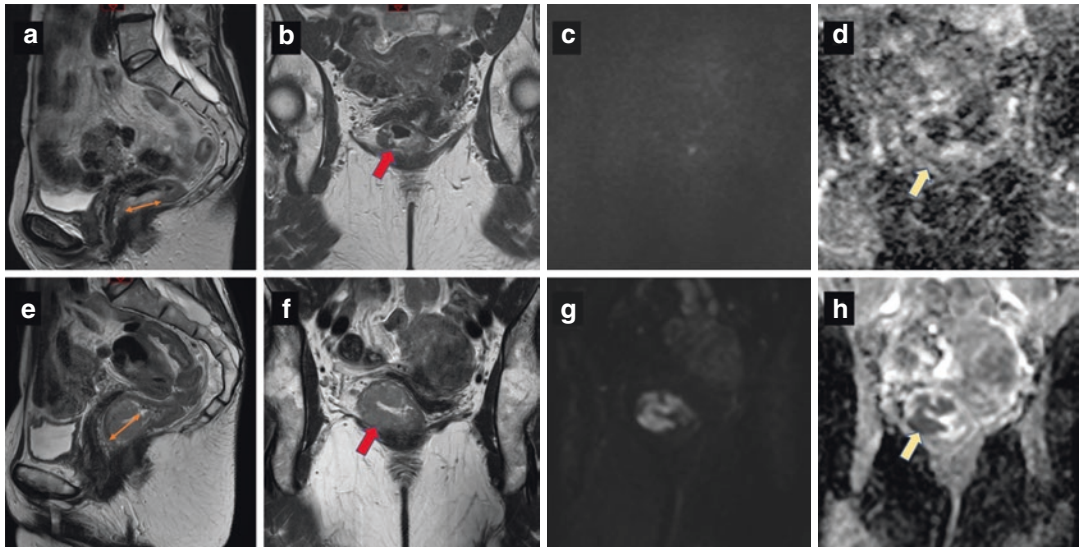

Fig. 3.2 Rectal tumour response evaluation post-neoadjuvant treatment. Top row: post-neoadjuvant treatment MRI; bottom row: pre-treatment scan for comparison; from left to right: sagittal T2 TSE, coronal oblique T2 TSE, b-1000 DWI images, ADC maps. (**a**, **b**, **e**, **f**) show the primary rectal tumour in different planes pre- and post-treatment, highlighting complex orientation of the tumour. These also show the potential limitation of using single measurement of tumour length as a parameter for response evaluation (significant reduction in tumour bulk on both imaging planes: red arrows in (**b**, **f**) and orange arrow in (**a**, **e**), but only comparatively modest change in tumour length demonstrated by the orange arrows in (**a**, **e**)). Images (**g**, **h**) show high DWI signal on b-1000 images and corresponding low ADC value (yellow arrow in **h**), inferring restricted water diffusion due to increased cellularity pre-treatment. These has improved post treatment (**c**, **d**). A persistent low ADC band in (**d**) may represent a residual fibrotic band when correlated to the same region in image (**b**)

3.3 Response Evaluation with Diffusion-Weighted Imaging (DWI)

Diffusion of water could be probed in vivo by DWI MRI. A basic DWI sequence involves a pair of de-phasing and refocusing pulses. Water molecules, which had moved away of its voxel between these pulses, would lead to incomplete rephasing, and hence signal loss. The degree of signal loss is related to the degree of water motion [32].

The sensitivity of the diffusion sequence to water motion can be varied by changing the parameter known as the b-value (a higher b value may be more sensitive, but at the expense of signal to noise ratio and/or acquisition time) [32]. In clinical practice, DWI MRI is usually performed with at least two *b*-values (e.g. $b = 50$ or 0 s/mm^2 and other *b*-values from 0 to 1000 s/mm^2), which enable calculation of an apparent diffusion coefficient (ADC), latter often presented in the form of a parametric map.

In biological tissues, diffusion of water molecules is thought to be 'restricted' by increased cell membranes and macromolecules [33]. DWI-derived parameter of 'diffusivity' can, therefore, act as a surrogate imaging marker of cellularity. This may be exploited for assessment of tumour response to treatment.

Some authors had proposed that DWI may act as a predictor for response to treatment, postulating that hypoxic tumours, which may have areas of necrosis (manifesting as tumours with higher ADC on pre-treatment MRI) would have a poorer response. This has been observed in some studies showing an inverse relationship between pre-treatment ADC values and eventual treatment outcome, for example, in primary colorectal tumour and liver metastases. However, such relationship is not observed consistently across tumour types and contexts [32, 34].

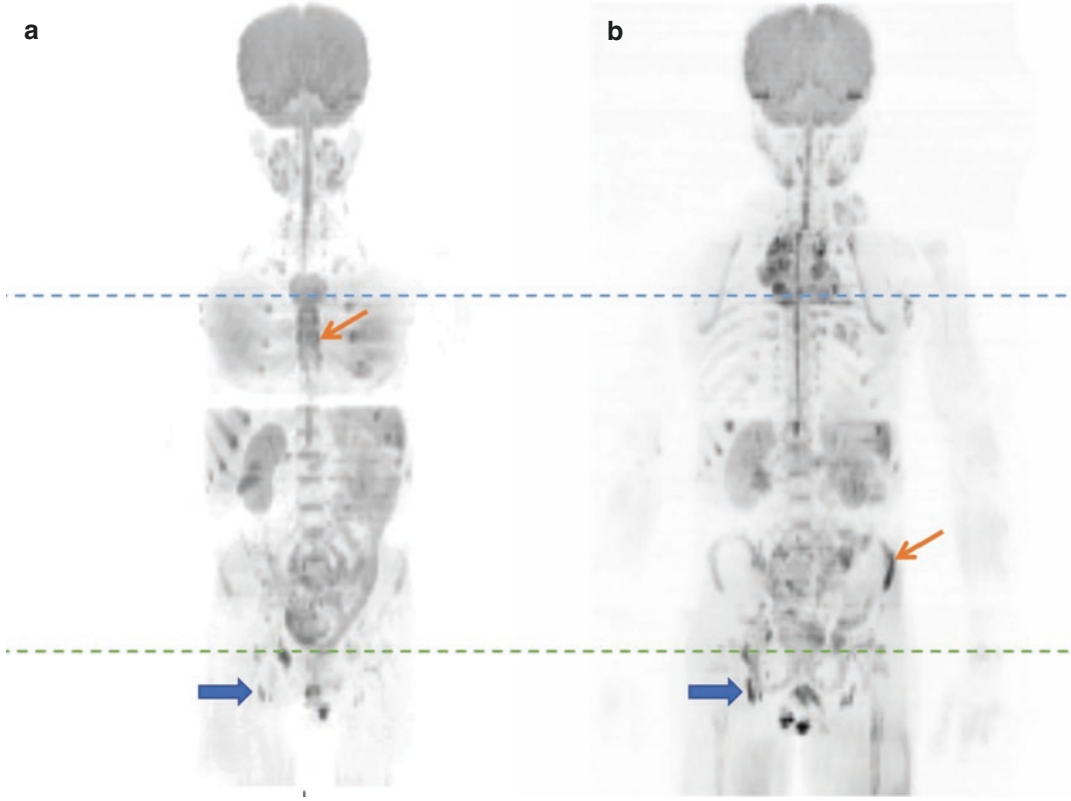

Fig. 3.3 Paediatric lymphoma response evaluation. Whole body MRI with DWI. 3D maximal intensity projection (MIP) of b-800 images. (**a**) Interim study post two cycles of treatment, (**b**) baseline image. See also Figs. 3.4 and 3.5. At baseline, there are extensive thoracic lymphadenopathy showing enlargement and increased DWI signal, in keeping with known diagnosis of classical Hodgkin lymphoma (stage 2). Blue arrows on both images show prominent right inguinal lymph nodes, which have high DWI signal but with normal morphology (see Fig. 3.5). These are confirmed benign on FDG PET and ultrasound (not shown). Orange arrows show 'false-positive' areas of high DWI signal at the sternum and anterior ends of ribs on the interim study and left anterior ilium of the baseline study; these are thought to be as a result of combination of field inhomogeneity and imperfect fat suppression, as well as respiratory motion on the interim study. This is confirmed by absence of signal abnormalities on other structural sequences (not shown). Dotted green and blue lines correspond to approximate levels of axial images in Figs. 3.4 and 3.5

Use of DWI MRI in early and interim response evaluation had shown success in some studies (e.g. in breast cancer, melanoma, head and neck), although more widespread validation remains lacking.

In conventional post-treatment response evaluation settings, many studies have confirmed that responded tumours have an increased ADC, supporting the general notion that cellularity decreases with treatment response [35–38]. There are, however, important caveats. Some tumour response may be accompanied by reduced ADC, reflecting treatment response with fibrosis and scarring (Fig. 3.2). Response evaluation in lymph nodes is difficult with inherent 'physiological' low ADC (high cellularity) (Figs. 3.3, 3.4, and 3.5). Increases in T2 signal of tumour as a result of treatment may result in apparent increase in DWI signal (T2 shine through) though this should be readily appreciable by reviewing the ADC parametric map. Interpretation of bone marrow lesion DWI response may sometimes be difficult because of potential for development of reactive marrow hyperplasia, fatty replacement or fibrosis as a result of post-treatment change, which also influence DWI signal return [39]. Standardisation of techniques remains a challenge, from varia-

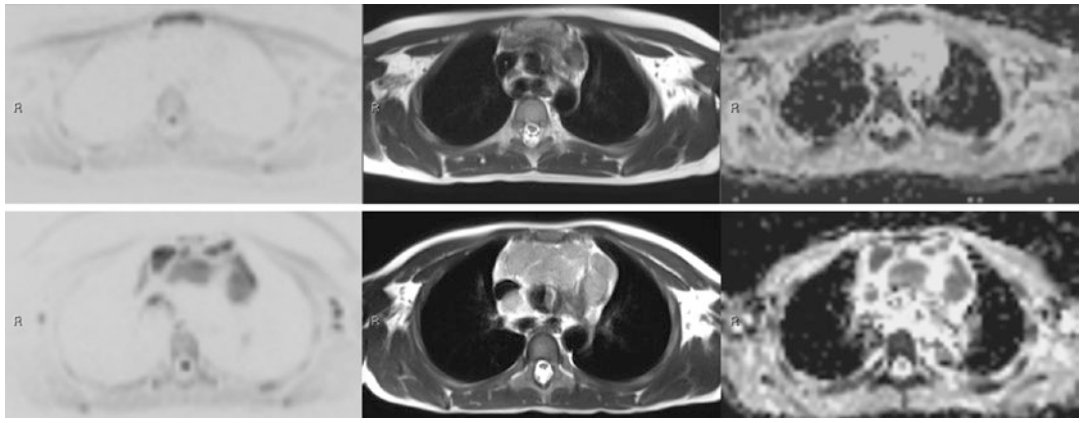

Fig. 3.4 Paediatric lymphoma response evaluation. Bottom row showing baseline appearances with intermediate T2 signal (middle column) enlarged anterior mediastinal nodes; these demonstrate high DWI signal on b-800 images (left hand column) and corresponding low ADC value (right hand column). There is reduction in size and DWI signal on the interim study (top row)

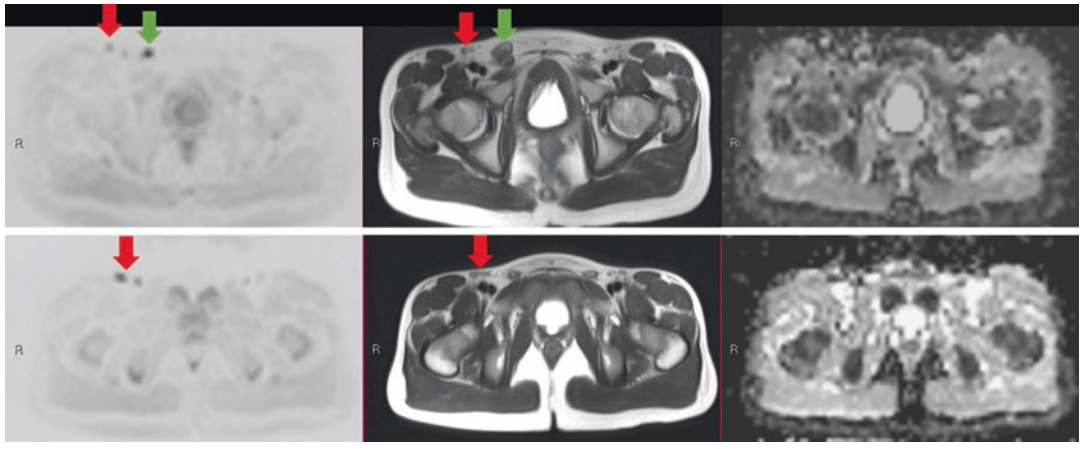

Fig. 3.5 Paediatric lymphoma response evaluation. Bottom row showing baseline appearances of the inguinal level. Small right inguinal lymph nodes (red arrows) have normal morphology including retained fatty hilum, corroborated to be benign on FDG PET and ultrasound (not shown). These show inherent 'physiological' high DWI signal. These remain unchanged on the interim response scan (top row). Green arrows show retracted right testis in the right inguinal canal as an incidental finding

tions of acquisition techniques to models for ADC calculations. Quantitative measures of DWI (changes in absolute ADC values, volumetry) had been studied with success, but qualitative assessment of change remains the routine mainstay assessment method. Despite advances, it remains the case that DWI is an adjunctive MRI response evaluation tool, and it should be assessed in conjunction with other MRI, clinical and laboratory findings (Fig. 3.3).

More sophisticated methods of DWI modelling may allow extraction of additional biologically relevant imaging markers. For instance, diffusion tensor imaging (DTI) exploits the directionality of water molecular diffusion and could be used to study tumour microstructural changes with treatment [40]. Intravoxel incoherent motion (IVIM) explores the bulk motion of water flow within tumour microvasculature (as supposed to water diffu-

sion), which may be dominant in low b-values images and may be modelled through bi-exponential decay of DWI signal loss [41, 42]. These are more resource-intensive with need for longer acquisition and post-processing time. Tumour response evaluation with these parameters had been shown to be feasible, but these remain exploratory.

3.4 Conclusion

With superior soft tissue contrast resolution and widespread availability, MRI has established roles in a multitude of tumour response evaluation setting. Evaluation of anatomical tumour burden change remains the main parameter for response evaluation. Tumour and MRI sequence specific parameters and criteria may be necessary in different clinical scenarios for optimal assessment.

In addition, with its versatility, advances in hardware and sequence design, a vast number of functional MRI parameters are available, which are at different stages of validation. DWI had been described briefly in this chapter, but many exciting developments are beyond the scope of this chapter. Standardisation and validation remain a challenge to implementation.

References

1. Pooley RA. Fundamental physics of MR imaging. Radiographics. 2005;25(4):1087–99.
2. American College of Radiology, Committee on Drugs and Contrast Media. ACR manual on contrast media [Internet]. 2015 [cited 2020 July 16]. Available from: http://www.acr.org/~/link.aspx?_id=29C40D1FE0EC4E5EAB6861BD213793E5&_z=z.
3. Jackson A, O'Connor JPB, Parker GJM, Jayson GC. Imaging tumor vascular heterogeneity and angiogenesis using dynamic contrast-enhanced magnetic resonance imaging. Clin Cancer Res. 2007;13(12):3449–59.
4. Grade M, Hernandez Tamames JA, Pizzini FB, Achten E, Golay X, Smits M. A neuroradiologist's guide to arterial spin labeling MRI in clinical practice. Neuroradiology. 2015;57(12):1181–202.
5. O'Connor JPB, Robinson SP, Waterton JC. Imaging tumour hypoxia with oxygen-enhanced MRI and BOLD MRI. Br J Radiol. 2019;92(1096):20180642.
6. Horská A, Barker PB. Imaging of brain tumors: MR spectroscopy and metabolic imaging. Neuroimaging Clin N Am. 2010;20(3):293–310.
7. Wu B, Warnock G, Zaiss M, Lin C, Chen M, Zhou Z, et al. An overview of CEST MRI for non-MR physicists. EJNMMI Phys. 2016;3(1):19.
8. Messiou C, Hillengass J, Delorme S, Lecouvet FE, Moulopoulos LA, Collins DJ, et al. Guidelines for acquisition, interpretation, and reporting of whole-body MRI in myeloma: myeloma response assessment and diagnosis system (MY-RADS). Radiology. 2019;291(1):5–13.
9. Padhani AR, Lecouvet FE, Tunariu N, Koh D-M, De Keyzer F, Collins DJ, et al. METastasis reporting and data system for prostate cancer: practical guidelines for acquisition, interpretation, and reporting of whole-body magnetic resonance imaging-based evaluations of multiorgan involvement in advanced prostate cancer. Eur Urol. 2017;71(1):81–92.
10. Kosmin M, Makris A, Joshi PV, Ah-See M-L, Woolf D, Padhani AR. The addition of whole-body magnetic resonance imaging to body computerised tomography alters treatment decisions in patients with metastatic breast cancer. Eur J Cancer. 2017;77:109–16.
11. Villanueva-Meyer JE, Mabray MC, Cha S. Current clinical brain tumor imaging. Neurosurgery. 2017;81(3):397–415.
12. Taylor FGM, Swift RI, Blomqvist L, Brown G. A systematic approach to the interpretation of preoperative staging MRI for rectal cancer. Am J Roentgenol. 2008;191(6):1827–35.
13. Weinreb JC, Barentsz JO, Choyke PL, Cornud F, Haider MA, Macura KJ, et al. PI-RADS prostate imaging—reporting and data system: 2015, version 2. Eur Urol. 2016;69(1):16–40.
14. Kaur H, Hindman NM, Al-Refaie WB, Arif-Tiwari H, Cash BD, Chernyak V, et al. ACR appropriateness criteria® suspected liver metastases. J Am Coll Radiol. 2017;14(5):S314–25.
15. Becker M, Burkhardt K, Dulguerov P, Allal A. Imaging of the larynx and hypopharynx. Eur J Radiol. 2008;66(3):460–79.
16. Crombé A, Marcellin P-J, Buy X, Stoeckle E, Brouste V, Italiano A, et al. Soft-tissue sarcomas: assessment of mri features correlating with histologic grade and patient outcome. Radiology. 2019;291(3):710–21.
17. Balcacer P, Shergill A, Litkouhi B. MRI of cervical cancer with a surgical perspective: staging, prognostic implications and pitfalls. Abdom Radiol N Y. 2019;44(7):2557–71.
18. Brown G, Kirkham A, Williams GT, Bourne M, Radcliffe AG, Sayman J, et al. High-resolution MRI of the anatomy important in total mesorectal excision of the rectum. Am J Roentgenol. 2004;182(2):431–9.
19. Lambregts DMJ, Maas M, Stokkel MPM, Beets-Tan RGH. Magnetic resonance imaging and other imaging modalities in diagnostic and tumor response evaluation. Semin Radiat Oncol. 2016;26(3):193–8.
20. Hoogstraten B, Staquet M, Winkler A. Reporting results of cancer treatment. Cancer. 1981;47(1):207–14.

21. Therasse P, Arbuck SG, Eisenhauer EA, Wanders J, Kaplan RS, Rubinstein L, et al. New guidelines to evaluate the response to treatment in solid tumors. J Natl Cancer Inst. 2000;92(3):12.
22. Eisenhauer EA, Therasse P, Bogaerts J, Schwartz LH, Sargent D, Ford R, et al. New response evaluation criteria in solid tumours: revised RECIST guideline (version 1.1). Eur J Cancer. 2009;45(2):228–47.
23. Seymour L, Bogaerts J, Perrone A, Ford R, Schwartz LH, Mandrekar S, et al. iRECIST: guidelines for response criteria for use in trials testing immunotherapeutics. Lancet Oncol. 2017;18(3):e143–52.
24. Persigehl T, Lennartz S, Schwartz LH. iRECIST: how to do it. Cancer Imaging. 2020;20(1):2.
25. Chukwueke UN, Wen PY. Use of the response assessment in neuro-oncology (RANO) criteria in clinical trials and clinical practice. CNS Oncol. 2019;8(1):CNS28.
26. Lencioni R, Llovet J. Modified RECIST (mRECIST) assessment for hepatocellular carcinoma. Semin Liver Dis. 2010;30(01):052–60.
27. Galle PR, Forner A, Llovet JM, Mazzaferro V, Piscaglia F, Raoul J-L, et al. EASL clinical practice guidelines: management of hepatocellular carcinoma. J Hepatol. 2018;69(1):182–236.
28. Chernyak V, Fowler KJ, Kamaya A, Kielar AZ, Elsayes KM, Bashir MR, et al. Liver imaging reporting and data system (LI-RADS) version 2018: imaging of hepatocellular carcinoma in at-risk patients. Radiology. 2018;289(3):816–30.
29. Beets-Tan RGH, Lambregts DMJ, Maas M, Bipat S, Barbaro B, Curvo-Semedo L, et al. Magnetic resonance imaging for clinical management of rectal cancer: updated recommendations from the 2016 European Society of Gastrointestinal and Abdominal Radiology (ESGAR) consensus meeting. Eur Radiol. 2018;28(4):1465–75.
30. Lambregts DMJ, Boellaard TN, Beets-Tan RGH. Response evaluation after neoadjuvant treatment for rectal cancer using modern MR imaging: a pictorial review. Insights Imaging. 2019;10(1):15.
31. Kalisz KR, Enzerra MD, Paspulati RM. MRI evaluation of the response of rectal cancer to neoadjuvant chemoradiation therapy. Radiographics. 2019;39(2):538–56.
32. Heijmen L, Verstappen MCHM, ter Voert EEGW, Punt CJA, Oyen WJG, de Geus-Oei L-F, et al. Tumour response prediction by diffusion-weighted MR imaging: ready for clinical use? Crit Rev Oncol Hematol. 2012;83(2):194–207.
33. Koh D-M, Collins DJ. Diffusion-weighted MRI in the body: applications and challenges in oncology. Am J Roentgenol. 2007;188(6):1622–35.
34. Bains LJ, Zweifel M, Thoeny HC. Therapy response with diffusion MRI: an update. Cancer Imaging. 2012;12(2):395–402.
35. Afaq A. Diffusion-weighted magnetic resonance imaging for tumour response assessment: why, when and how? Cancer Imaging. 2010;10(1A):S179–88.
36. Li SP, Padhani AR. Tumor response assessments with diffusion and perfusion MRI. J Magn Reson Imaging. 2012;35(4):745–63.
37. Bonekamp S, Corona-Villalobos CP, Kamel IR. Oncologic applications of diffusion-weighted MRI in the body. J Magn Reson Imaging. 2012;35(2):257–79.
38. Chavhan GB, Caro-Dominguez P. Diffusion-weighted imaging in pediatric body magnetic resonance imaging. Pediatr Radiol. 2016;46(6):847–57.
39. Koh D-M, Blackledge M, Padhani AR, Takahara T, Kwee TC, Leach MO, et al. Whole-body diffusion-weighted MRI: tips, tricks, and pitfalls. Am J Roentgenol. 2012;199(2):252–62.
40. Furman-Haran E, Nissan N, Ricart-Selma V, Martinez-Rubio C, Degani H, Camps-Herrero J. Quantitative evaluation of breast cancer response to neoadjuvant chemotherapy by diffusion tensor imaging: initial results. J Magn Reson Imag JMRI. 2018;47(4):1080–90.
41. Kato H, Esaki K, Yamaguchi T, Tanaka H, Kajita K, Furui T, et al. Predicting early response to chemoradiotherapy for uterine cervical cancer using intravoxel incoherent motion MR imaging. Magn Reson Med Sci. 2019;18(4):293–8.
42. Marzi S, Piludu F, Forina C, Sanguineti G, Covello R, Spriano G, et al. Correlation study between intravoxel incoherent motion MRI and dynamic contrast-enhanced MRI in head and neck squamous cell carcinoma: evaluation in primary tumors and metastatic nodes. Magn Reson Imaging. 2017;37:1–8.

4 PET and PET-CT in Treatment Response Evaluation: Overview

Gabriel Buschner and Wolfgang Weber

4.1 Introduction: Why Is Tumor Response Assessed by Imaging?

Assessing tumor response to therapy is one of the most common applications of imaging in oncology. The fundamental reason for the frequent use of imaging to assess response is tumor heterogeneity. Tumors with the same clinical, histologic, and molecular features often respond very differently to the same treatment: while tumors shrink significantly in some patients, there is continued tumor growth in others.

An alternative approach to assess response is the measurement of tumor markers in the serum. For example, prostate-specific antigen (PSA) is commonly used to monitor response to therapy in prostate cancer. More recently, changes in the number of circulating tumor cells have been introduced to assess tumor response. However, these approaches cannot capture intermetastatic heterogeneity of tumor response. It is quite common that in the same patient, some metastases decrease in size during therapy while others increase, and new metastases develop. Thus, the overall tumor burden may fall, but treatment needs to be changed (Fig. 4.1). Only imaging can provide such critical information.

In addition to its crucial clinical role for managing treatments in individual patients, response assessment by imaging is critical for oncologic drug development. Regulatory authorities have accepted evidence of tumor shrinkage or delay of tumor progression on imaging studies as a surrogate end point for clinical trials and as a basis for drug approvals [1]. Using imaging-based end points instead of survival end points can shorten the duration of clinical trials and make new therapeutics for diseases with limited therapeutic options available significantly earlier.

4.2 Assessment of Tumor Response: When and How?

In clinical trials, tumor response to new therapeutic agents is classified as "complete response," "partial response," "stable disease," and "progressive disease." This terminology goes back to the 1970s and was internationally standardized in 1979 by the so-called "WHO criteria." These criteria were later refined as "response evaluation criteria in solid tumors" (RECIST) in 2000 [2]. The current version is RECIST 1.1 [3]. RECIST has been developed by an international collaboration of the European Organization for Research and Treatment of Cancer (EORTC), the National Cancer Institute (NCI) of the United States, and

G. Buschner · W. Weber (✉)
Technical University Munich, Munich, Germany
e-mail: gabriel.buschner@mri.tum.de; w.weber@tum.de

S. Fanti et al. (eds.), *Atlas of Clinical PET-CT in Treatment Response Evaluation in Oncology*,
https://doi.org/10.1007/978-3-030-68858-5_4

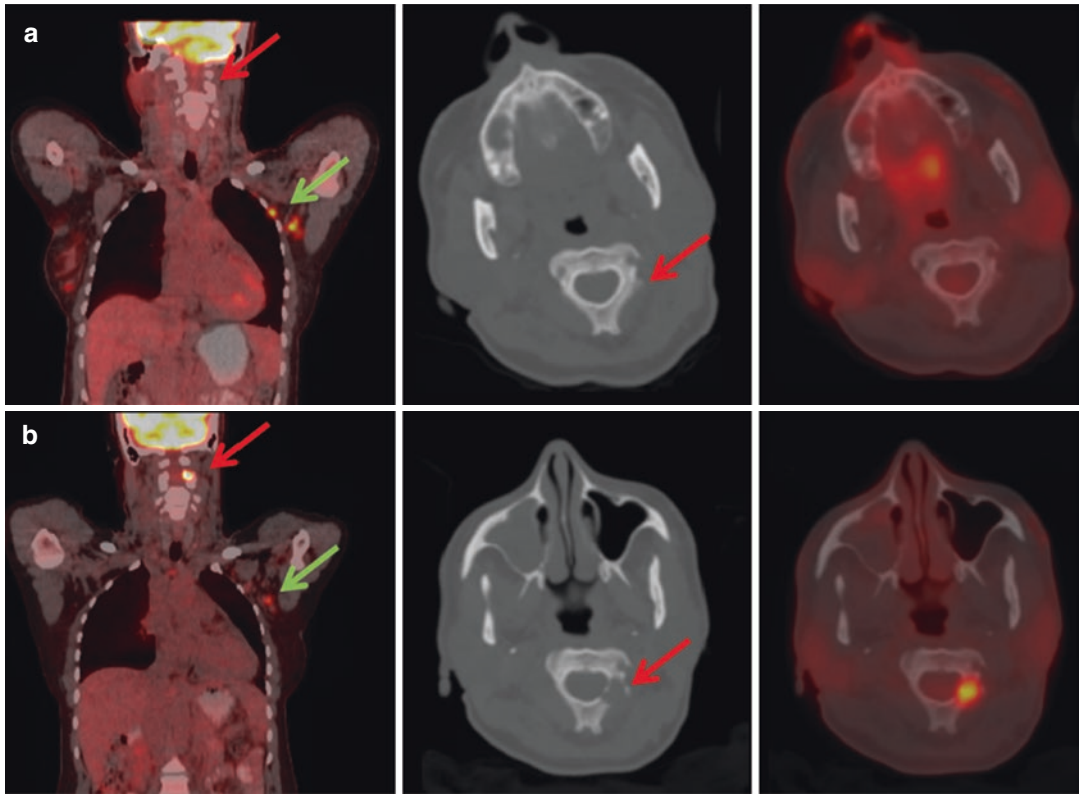

Fig. 4.1 Patient with axillary recurrence of breast cancer. FDG PET/CT at baseline shows hypermetabolic left axillary lymph nodes (green arrow) but no evidence of osseous metastases (**a**). Follow-up imaging after initiation of hormonotherapy demonstrates clearly reduced metabolic activity of the lymph nodes but also shows a new osteolytic metastasis in the cerebral spine (red arrows **b**)

the Canadian Cancer Trials Group (CCTG), as well as several pharmaceutical companies. The goal of RECIST is to provide a pragmatic methodology to evaluate the efficacy of new cancer therapeutics in clinical trials by assessing changes in tumor burden during therapy [3]. Table 4.1 provides an abbreviated summary of RECIST. The basic concept of RECIST is to use the sum of the maximum diameters of up to five well-measurable target lesions as an index for tumor burden. The relative changes of this index after therapy determine how tumor response is classified. A decrease by at least 30% defines a partial response and an increase by at least 20% progressive disease. Changes in the sum of tumor diameters between minus 30% and plus 20% are classified as stable disease. Complete response and partial response are frequently grouped together as "response" and "stable disease" and "progressive disease" as nonresponse. The response rate is the percentage of patients classified as responders ("complete response" and "partial response" combined). The term disease stabilization rate is used for the percentage of patients that are classified as "complete response," "partial response," and "stable disease."

4.2.1 Response Assessment by FDG PET

In 1999, the EORTC published the first criteria for assessing tumor response by FDG-PET (EORTC criteria) [4]. Similar to RECIST, the goal of the EORTC criteria was to define a standard for monitoring tumor response to therapy in clinical trials. A summary of the EORTC criteria is given in Table 4.2.

At the time of the publication of the EORTC criteria, PET/CT scanners were not yet available clinically, and treatment monitoring with FDG PET was at its infancy. EORTC criteria

Table 4.1 Response assessment in solid tumors by anatomic imaging

Response category		Target lesions	Nontarget lesions
Complete response	CR	Disappearance of all target lesions. Any pathological lymph nodes must have reduction in short axis to <10 mm	Disappearance of all nontarget lesions and normalization of tumor marker level. All lymph nodes must be <10 mm short axis
Partial response	PR	At least a 30% decrease in the sum of diameters of target lesions, taking as reference the baseline sum diameters	*Non-CR/non-PD* Persistence of one or more nontarget lesion(s) and/or maintenance of tumor marker level above the normal limits
Stable disease	SD	Neither sufficient shrinkage to qualify for PR nor sufficient increase to qualify for PD, taking as reference the smallest sum diameters while on study	
Progressive disease	PD	At least a 20% increase in the sum of diameters of target lesions, taking as reference the smallest sum on study or one or more new lesions The sum of diameters must also increase by at least 5 mm	Unequivocal progression of existing nontarget lesions or one or more new lesions

Table 4.2 Response assessment in solid tumors by FDG PET and PET/CT

	EORTC (1999)	PERCIST 1.0 (2009)
Quantitative parameter	SUVmean, normalized body surface area	SUVpeak, normalized to lean body mass (SUL)
Objective response	*CMR* Complete resolution of 18F-FDG uptake within tumor volume (indistinguishable from surrounding normal tissue) *PMR* After one cycle of chemotherapy reduction of 15–25% of 18F-FDG SUV is required or >25% after more than one treatment cycle *SMD* SUV increase in tumor by <25% or decrease of <15% and No increase in extent (at least <20% in longest diameter) *PMD* Increase of tumor SUV >25% or Increase in extent (20% in longest dimension) or New lesions with FDG-uptake	*CMR* Measurable target lesion with no FDG uptake and uptake < mean liver activity and indistinguishable from surrounding background blood pool levels disappearance of all other lesions No new FDG-avid lesions in pattern typical of cancer *PMR* In target measurable tumor decrease of SUL by ≥30% and drop in units difference in SUL ≥0.8 SUL And no size increase of the target lesion >30%; no increase of nontarget lesions or in SUL and no new lesions *SMD* <30% increase/decrease in metabolic target lesion *PMD* Increasing of SUL by ≥30% in target lesion (at least 0.8 SUL units difference) or Visible increase in extent of 18F-FDG tumor uptake (75% in TLG volume with no decline in SUL or Detection of at least one new lesion, which is typical for cancer and not treatment or infection related Progression of non-target lesions

CMR complete metabolic response, *PMR* partial metabolic response, *SMD* stable metabolic disease, *PMD* progressive metabolic disease, *CR* complete remission, *SUV* standardized uptake value, *TLG* total lesion glycolysis, *CMR* complete metabolic response, *PMR* partial metabolic response, *SMD* stable metabolic disease, *PMD* progressive metabolic disease, *CR* complete remission, *SUV* standardized uptake value, *TLG* total lesion glycolysis

are, therefore, based on expert opinion and limited data on the test-retest reproducibility of FDG uptake in untreated tumors.

In 2009, Wahl et al. [5] introduced the PET response criteria in solid tumors (PERCIST) to assess metabolic tumor response (Table 4.3). PERCIST incorporates 10 more years of clinical experience with FDG PET and PET/CT and includes many more details regarding the definitions of measurable lesions, quality control pro-

Table 4.3 Response assessment in malignant lymphomas by RECIL [6]

	Anatomic imaging	Metabolism FDG PET	New lesions	Bone marrow involvement
CR	Complete disappearance of all target lesions and all nodes with long axis <10 mm ≥30% decrease in the sum of longest diameters of target lesions (PR) with normalization of FDG-PET	Negative (Deauville score 1–3)	No	No
PR	≥30% decrease in the sum of longest diameters of target lesions but not a CR	Positive (Deauville score 4–5)	No	Any
MR	≥10% decrease in the sum of longest diameters of target lesions but not a PR (<30%)	Any	No	Any
SD	<10% decrease or ≤20% increase in the sum of longest diameters of target lesions	Any	No	Any
PD	>20% increase in the sum of longest diameters of target lesions For small lymph nodes measuring <15 mm post therapy, a minimum absolute increase of 5 mm and the long diameter should exceed 15 mm Appearance of a new lesion	Any	Yes/no	Any

CR complete response, *PR* partial response, *MR* minor response, *SD* stable disease, *PD* progressive disease

cedures as well as recommendations on how scans with multiple FDG-avid lesions should be analyzed [5]. EORTC criteria and PERCIST follow the model of RECIST and define four response categories with similar names as RECIST: complete metabolic response (CMR), partial metabolic response (PMR), stable metabolic disease (SMD), and progressive metabolic disease (PMD).

Briefly, RECIST defines tumor response by a decrease in the FDG uptake of index lesions. Index lesions are the malignant lesions with the highest FDG uptake on the baseline and follow-up scans, respectively. In most cases, the same lesions are analyzed on the baseline and follow-up scan, but in principle, the lesions can be different. For example, the index lesions could be three liver and two bone metastases on the baseline scan and one liver, one bone, and three lung metastases on the follow-up scan [5].

FDG uptake is measured by standardized uptake values normalized to the lean body mass of the patient (SUL). Lean body mass is estimated from patient height and actual mass by an empiric formula. The reason for recommending SULs is that SUVs are systematically overestimated in obese patients than in nonobese patients. As a measure for FDG uptake of tumor lesions, PERCIST recommends the "peak SUL" (SULpeak). SULpeak is the average SUL in a small sphere placed in the lesion at the site of maximum FDG uptake. SULpeak is less affected by statistical noise than maximum standardized uptake values and more quickly to define and less operator-dependent than delineating the whole lesion and measuring the mean SUL.

The criterion for a response is a decrease in SUL by at least 30%, which is based on a series of studies that have determined the variability of test-retest measurements of SUVs or SULs [7, 8]. A relative increase or decrease of tumor FDG uptake by more than 30% was exceedingly rare in these studies and, therefore, used as a criterion for a treatment-induced effect. An increase in FDG uptake of index lesions by at least 30% is a criterion for progression by PERCIST. This is again justified by the variability of the FDG signal in untreated tumors.

PERCIST provides no strict definition for the number of index lesions to be analyzed. The primary approach is to only use one index lesion on the baseline and one index lesion on the follow-up scan. An alternative is to average the SUL of up to five lesions and use this sum of SUL as an

index of tumor burden. Relatively few and rather small studies have compared these different approaches. These studies showed a comparable prognostic value for the analysis of one or five index lesions [9, 10].

4.2.1.1 Response Assessment in Lymphoma

The biology of lymphomas and their response to therapy differ significantly from solid tumors. Generally, lymphomas show significantly more rapid tumor shrinkage in response to chemotherapy than solid tumors. Furthermore, several lymphomas are curable by chemotherapy, even if multiple lymph node areas are involved. Incurable lymphomas generally respond well to chemotherapy but recur later. In contrast, only palliative therapy is available for most of the metastatic solid tumors, and generally, tumor shrinkage is moderate.

Response assessment in Hodgkin and non-Hodgkin lymphomas has been harmonized by the international working group criteria, first published in 2007 and revised in 2014 (Lugano criteria) [11]. The Lugano criteria use a combination of FDG PET and CT to assess response. In FDG avid lymphomas, such as Hodgkin's lymphoma and diffuse large B cell lymphoma. In contrast to RECIST, international working group criteria initially recommend bidimensional measurements of tumor size for response assessment. However, a recent analysis has demonstrated that unidimensional measurements provide similar results. The new response classification response evaluation criteria in lymphoma (RECIL) uses unidimensional measurements of three lesions to define tumor burden and similar criteria for response and progression as RECIST.

A five-point scoring system is used to classify the degree of FDG uptake ("Deauville score," Table 4.3). A Deauville score of 1–3 after therapy is considered a complete response and a Deauville score of 4 or 5 as a partial response if there is a decrease of the sum of lesion diameters by at least 30%. Progression is defined by an increase of the sum lesion diameters by 20% or the appearance of new lesions on FDG PET or CT [6].

4.2.2 Response Assessment with Other PET Imaging Agents

In several countries, somatostatin receptor (SSTR) and prostate specific membrane antigen (PSMA) PET are now routinely used for staging of neuroendocrine tumors and prostate cancer. There is also preliminary evidence that treatment monitoring with these two types of ligands is feasible [12]. It is, therefore, tempting to apply PERCIST (or a slightly modified version of PERCIT) for response monitoring with other tracers, but it is currently unclear if this is appropriate. The uptake mechanism of SSTR and PSMA ligands (receptor binding) is quite different from FDG (tracer of metabolic flux). Furthermore, there is no obvious reason why downregulation of SSTR or PSMA expression is an indicator of a favorable response. Therefore, future research on the utility of SSTR and PSMA PET for treatment monitoring is necessary.

4.2.3 Timing of Response Assessment

There is no general answer to the question when response assessment should be performed. With chemotherapy, FDG uptake decreases rather rapidly in well-responding tumors. It is, therefore, feasible to monitor response already after 2–3 treatment cycles. However, this varies between different tumor types. If there is no significant decrease of FDG uptake at such an early time point, this generally indicates a low likelihood for later tumor shrinkage.

The sensitivity of FDG PET to detect residual disease after completion of therapy increases with the time between the PET scan and the end of treatment, likely due to tumor growth. Therefore, FDG PET should be performed "as late as clinically meaningful" [13] if detection of residual disease is the primary aim of the study.

4.3 Responders vs. Nonresponders

Many studies have shown that response by RECIST, in general, correlates with patient outcome, that is, patients classified as responders by RECIST live on average longer than patients classified as nonresponders. In randomized clinical trials of new cancer therapeutics, a response by RECIST often predicts drug efficacy, that is, treatment with the drug that shows the higher response rate results in longer survival.

On a smaller scale, clinical studies have also shown that tumor response on FDG PET also correlates with patient outcome. There is also evidence that FDG PET can assess tumor response earlier than anatomic imaging [14]. When FDG PET and CT are performed at the same time, tumor response on FDG PET is frequently more closely correlated with outcome than tumor response on CT. This has been most extensively shown in lymphomas but also some solid tumors [15].

For clinical practice, however, disease stabilization is generally a more meaningful than tumor response. Systemic therapies of solid tumors are usually continued until there is disease progression (or severe toxicity). Furthermore, clinical response evaluation is rather multidimensional and includes not only imaging results, but also symptom control/reduction, improved quality of life, as well as changes in laboratory parameters such as tumor markers. By this combination of parameters, clinicians implement individualized treatment strategies that aim to optimize treatment outcomes. Thus, clinical response assessment is inherently different from the standardized testing of drugs in a clinical trial. Nevertheless, RECIST and PERCIST provide an important framework for response assessment and patient management because they define parameters that can be reliably measured by clinical imaging studies. In addition, the established prognostic value of a response by RECIST or PERCIST can be reassuring for the management of individual patients.

4.4 Management and Type of Treatment

Clinically, the most frequent impact of response assessment in solid tumors is to change treatment in case of tumor progression. In the neoadjuvant setting, response-adapted therapies have also been investigated [16]. The underlying idea is to stop neoadjuvant therapy in case of insufficient response and to perform surgery. Such an approach can reduce the side effects and costs of ineffective therapy [17]. FDG PET has shown significant promise in multiple tumor types for identifying nonresponding tumors early in the course of neoadjuvant therapy [18–22]. These studies provide a strong rationale for FDG PET response-adapted neoadjuvant therapies. Unfortunately, however, solid tumors are frequently cross-resistant to several chemotherapy drugs. Thus, resistance to one chemotherapy regimen often makes response to a different chemotherapy regimen unlikely. Progress in response-adapted therapies of solid tumors has, therefore, been rather slow. However, a recent randomized study in gastroesophageal-junction cancer has demonstrated improvement of outcome by intensifying chemotherapy or adding radiotherapy in FDG PET nonresponders [23].

Response-adapted therapies have, however, become a standard for treatment in certain lymphomas. Here the goal is both escalation and de-escalation of therapy. A “negative” (Deauville score 1–3) FDG PET scan after chemotherapy is a strong predictor for a favorable prognosis and allows to avoid additional radiotherapy in patients with early stage Hodgkin’s disease [24–26]. While omitting radiotherapy is associated with a small increase in the risk for recurrence, this is considered to be outweighed by the reduced risk for long-term complications of radiotherapy in this group of patients with an overall very favorable prognosis [27]. Conversely, a positive interim PET scan may lead to treatment intensification by a more intense chemotherapy regimen [28].

4.5 Common Patterns, Pitfalls, Variants, Advantages, and Limitations

4.5.1 Standardized Imaging Protocol

For assessing response to therapy, it is critical that FDG uptake on the baseline and follow-up scans is comparable. Therefore, it is necessary to follow a standardized protocol, which ensures that patient preparation, image acquisition, and image reconstruction are performed in a similar way. The European Association of Nuclear Medicine (EANM) FDG PET/CT imaging guidelines provided detailed instructions for standardized imaging protocols [29].

Importantly, attention to standardized protocol is not only necessary to accurately quantify FDG uptake by SUVs, but also for visual image analysis. For example, imaging later after FDG injection will not only increase tumor SUVs, but also contrast between tumor and liver. Therefore, the Deauville score of lymphomas will also be affected by significant variations in uptake time.

It is increasingly common that patients are scanned on different generations of PET/CT systems, for example, when the baseline scan and follow-up scans are performed at different institutions. Newer scanners generally provide higher image contrast for small lesions due to time of flight information and improved reconstruction algorithms. This may affect both quantitative assessment of FDG uptake as well as visual interpretation. For example, if a small "new" lesion is seen on the follow-up scan with a newer system, it may be impossible to rule out that this lesion was already present before but was undetectable by the older system.

4.5.2 Impact of Therapy on FDG Metabolism

A "metabolic flare phenomenon" and "metabolic stunning" are sometimes discussed as pitfalls for response assessment by FDG PET/CT. However, clinical evidence for both phenomena is rather scant. There is plenty of data from in vitro studies that surviving cancer cells show increased FDG uptake after exposure to chemotherapeutic agents. This increased metabolism is believed to be due to ongoing repair processes in the surviving cells. In vivo, however, the loss of viable cells due to effective therapy usually outweighs a temporary increase in FDG uptake by the surviving cells [14, 30].

"Metabolic stunning" describes a potential opposite treatment effect. In response to therapy, cancer cells stop proliferation and, therefore, accumulate less FDG but remain viable. There is some evidence for this because the sensitivity of FDG PET to detect metastases is lower when FDG PET is performed during or early after completion of chemotherapy. However, it is mostly unclear if the reason for this is "metabolic stunning" or simply because the density of viable tumor cells has decreased during therapy [13, 14].

4.5.3 Radiation Therapy

Assessment of tumor response to radiotherapy is complicated by the common inflammatory changes of surrounding normal tissues, such as the lungs. A further challenge is that local tumor control rates of modern radiotherapy regimens are excellent. The risk for false-positive findings after radiotherapy is, therefore, high. Radiation-induced inflammation can remain FDG-avid for several months. Therefore, FDG PET is more commonly used for surveillance after radiotherapy than for treatment monitoring in the strict sense [31].

4.5.4 Immunotherapy

Cancer immunotherapy has made incredible progress during the last 10 years and is now a standard form of therapy in many malignancies, including malignant melanoma, lung cancer, head-and-neck cancer, and urothelial carcinomas. During the clinical development of immunotherapy, it has been noted that tumor shrinkage can occur later than typically observed for che-

motherapy. In some cases, tumor size may even increase temporarily. A modified version of RECIST, iRECIST, therefore, introduces the term unconfirmed progression [32]. Thus, progression by iRECIST needs to be confirmed by follow-up imaging studies. Specific criteria to assess response to immunotherapy by FDG PET/CT have been proposed but still need validation. However, current experience suggests that standard PERCIST and EORTC criteria can in principle also be applied to assess response to immunotherapy [10, 33].

4.5.5 Clinical Image Interpretation

Well-defined and preferably quantitative criteria are important to assess tumor response to therapy in a standardized way. Still, the basis for response assessment is clinical image interpretation. Differentiation of tumor- and treatment-induced changes can be challenging and requires careful image interpretation. Furthermore, the presence of new metastases is generally the strongest negative prognostic factor on imaging studies. Sensitive and specific detection of new metastases requires knowledge about the typical spread of a given malignancy and should include on a joint interpretation of PET and CT findings. New metastases need to be differentiated from inflammatory lesions, such as sarcoid-like reactions, inflammatory pulmonary nodules, inflammation due to trauma, etc. Like for tumor staging, knowledge of tumor biology and clinical experience are, therefore, critical for correct assessment of tumor response to therapy.

References

1. FDA. Clinical trial endpoints for the approval of cancer drugs and biologics guidance for industry. 2018. Available from: https://www.fda.gov/media/71195/download.
2. Therasse P, Arbuck SG, Eisenhauer EA, Wanders J, Kaplan RS, Rubinstein L, et al. New guidelines to evaluate the response to treatment in solid tumors. European Organization for Research and Treatment of Cancer, National Cancer Institute of the United States, National Cancer Institute of Canada. J Natl Cancer Inst. 2000;92(3):205–16.
3. Eisenhauer EA, Therasse P, Bogaerts J, Schwartz LH, Sargent D, Ford R, et al. New response evaluation criteria in solid tumours: revised RECIST guideline (version 1.1). Eur J Cancer. 2009;45(2):228–47.
4. Young H, Baum R, Cremerius U, Herholz K, Hoekstra O, Lammertsma AA, et al. Measurement of clinical and subclinical tumour response using [18F]-fluorodeoxyglucose and positron emission tomography: review and 1999 EORTC recommendations. European Organization for Research and Treatment of Cancer (EORTC) PET Study Group. Eur J Cancer. 1999;35(13):1773–82.
5. Wahl RL, Jacene H, Kasamon Y, Lodge MA. From RECIST to PERCIST: evolving considerations for PET response criteria in solid tumors. J Nucl Med. 2009;50(Suppl 1):122s–50s.
6. Younes A, Hilden P, Coiffier B, Hagenbeek A, Salles G, Wilson W, et al. International Working Group consensus response evaluation criteria in lymphoma (RECIL 2017). Ann Oncol. 2017;28(7):1436–47.
7. de Langen AJ, Vincent A, Velasquez LM, van Tinteren H, Boellaard R, Shankar LK, et al. Repeatability of 18F-FDG uptake measurements in tumors: a meta-analysis. J Nucl Med. 2012;53(5):701–8.
8. Weber WA, Gatsonis CA, Mozley PD, Hanna LG, Shields AF, Aberle DR, et al. Repeatability of 18F-FDG PET/CT in advanced non-small cell lung cancer: prospective assessment in 2 multicenter trials. J Nucl Med. 2015;56(8):1137–43.
9. Pinker K, Riedl CC, Ong L, Jochelson M, Ulaner GA, McArthur H, et al. The impact that number of analyzed metastatic breast cancer lesions has on response assessment by 18F-FDG PET/CT using PERCIST. J Nucl Med. 2016;57(7):1102–4.
10. Ito K, Teng R, Schöder H, Humm JL, Ni A, Michaud L, et al. (18)F-FDG PET/CT for monitoring of ipilimumab therapy in patients with metastatic melanoma. J Nucl Med. 2019;60(3):335–41.
11. Cheson BD, Fisher RI, Barrington SF, Cavalli F, Schwartz LH, Zucca E, et al. Recommendations for initial evaluation, staging, and response assessment of Hodgkin and non-Hodgkin lymphoma: the Lugano classification. J Clin Oncol Off J Am Soc Clin Oncol. 2014;32(27):3059–68.
12. Seitz AK, Rauscher I, Haller B, Krönke M, Luther S, Heck MM, et al. Preliminary results on response assessment using (68)Ga-HBED-CC-PSMA PET/CT in patients with metastatic prostate cancer undergoing docetaxel chemotherapy. Eur J Nucl Med Mol Imaging. 2018;45(4):602–12.
13. Akhurst T, Kates TJ, Mazumdar M, Yeung H, Riedel ER, Burt BM, et al. Recent chemotherapy reduces the sensitivity of [18F]fluorodeoxyglucose positron emission tomography in the detection of colorectal metastases. J Clin Oncol Off J Am Soc Clin Oncol. 2005;23(34):8713–6.
14. Weber WA. Assessing tumor response to therapy. J Nucl Med. 2009;50(Suppl 1):1s–10s.

15. Riedl CC, Pinker K, Ulaner GA, Ong LT, Baltzer P, Jochelson MS, et al. Comparison of FDG-PET/CT and contrast-enhanced CT for monitoring therapy response in patients with metastatic breast cancer. Eur J Nucl Med Mol Imaging. 2017;44(9):1428–37.
16. Weber WA, Ott K, Becker K, Dittler HJ, Helmberger H, Avril NE, et al. Prediction of response to preoperative chemotherapy in adenocarcinomas of the esophagogastric junction by metabolic imaging. J Clin Oncol Off J Am Soc Clin Oncol. 2001;19(12):3058–65.
17. Lordick F, Ott K, Krause BJ, Weber WA, Becker K, Stein HJ, et al. PET to assess early metabolic response and to guide treatment of adenocarcinoma of the oesophagogastric junction: the MUNICON phase II trial. Lancet Oncol. 2007;8(9):797–805.
18. Brenner W, Bohuslavizki KH, Eary JF. PET imaging of osteosarcoma. J Nucl Med. 2003;44(6):930–42.
19. de Geus-Oei LF, van Laarhoven HW, Visser EP, Hermsen R, van Hoorn BA, Kamm YJ, et al. Chemotherapy response evaluation with FDG-PET in patients with colorectal cancer. Ann Oncol. 2008;19(2):348–52.
20. Herrmann K, Benz MR, Czernin J, Allen-Auerbach MS, Tap WD, Dry SM, et al. 18F-FDG-PET/CT imaging as an early survival predictor in patients with primary high-grade soft tissue sarcomas undergoing neoadjuvant therapy. Clin Cancer Res. 2012;18(7):2024–31.
21. Lau LF, Williams DS, Lee ST, Scott AM, Christophi C, Muralidharan V. Metabolic response to preoperative chemotherapy predicts prognosis for patients undergoing surgical resection of colorectal cancer metastatic to the liver. Ann Surg Oncol. 2014;21(7):2420–8.
22. Wang C, Guo W, Zhou M, Zhu X, Ji D, Li W, et al. The predictive and prognostic value of early metabolic response assessed by positron emission tomography in advanced gastric cancer treated with chemotherapy. Clin Cancer Res. 2016;22(7):1603–10.
23. Barbour AP, Walpole ET, Mai GT, Barnes EH, Watson DI, Ackland SP, et al. Preoperative cisplatin, fluorouracil, and docetaxel with or without radiotherapy after poor early response to cisplatin and fluorouracil for resectable oesophageal adenocarcinoma (AGITG DOCTOR): results from a multicentre, randomised controlled phase II trial. Ann Oncol. 2020;31(2):236–45.
24. Radford J, Illidge T, Counsell N, Hancock B, Pettengell R, Johnson P, et al. Results of a trial of PET-directed therapy for early-stage Hodgkin's lymphoma. N Engl J Med. 2015;372(17):1598–607.
25. Barrington SF, Phillips EH, Counsell N, Hancock B, Pettengell R, Johnson P, et al. Positron emission tomography score has greater prognostic significance than pretreatment risk stratification in early-stage hodgkin lymphoma in the UK RAPID study. J Clin Oncol Off J Am Soc Clin Oncol. 2019;37(20):1732–41.
26. Straus DJ, Jung SH, Pitcher B, Kostakoglu L, Grecula JC, Hsi ED, et al. CALGB 50604: risk-adapted treatment of nonbulky early-stage Hodgkin lymphoma based on interim PET. Blood. 2018;132(10):1013–21.
27. Ansell SM. Hodgkin lymphoma: 2020 update on diagnosis, risk-stratification, and management. Am J Hematol. 2020;95(8):978–89.
28. André MPE, Girinsky T, Federico M, Reman O, Fortpied C, Gotti M, et al. Early positron emission tomography response-adapted treatment in stage i and ii hodgkin lymphoma: final results of the randomized EORTC/LYSA/FIL H10 trial. J Clin Oncol Off J Am Soc Clin Oncol. 2017;35(16):1786–94.
29. Boellaard R, Delgado-Bolton R, Oyen WJ, Giammarile F, Tatsch K, Eschner W, et al. FDG PET/CT: EANM procedure guidelines for tumour imaging: version 2.0. Eur J Nucl Med Mol Imaging. 2015;42(2):328–54.
30. Plathow C, Weber WA. Tumor cell metabolism imaging. J Nucl Med. 2008;49(Suppl 2):43s–63s.
31. Van den Wyngaert T, Helsen N, Carp L, Hakim S, Martens MJ, Hutsebaut I, et al. Fluorodeoxyglucose-positron emission tomography/computed tomography after concurrent chemoradiotherapy in locally advanced head-and-neck squamous cell cancer: the ECLYPS study. J Clin Oncol Off J Am Soc Clin Oncol. 2017;35(30):3458–64.
32. Seymour L, Bogaerts J, Perrone A, Ford R, Schwartz LH, Mandrekar S, et al. iRECIST: guidelines for response criteria for use in trials testing immunotherapeutics. Lancet Oncol. 2017;18(3):e143-e52.
33. Tan AC, Emmett L, Lo S, Liu V, Kapoor R, Carlino MS, et al. FDG-PET response and outcome from anti-PD-1 therapy in metastatic melanoma. Ann Oncol. 2018;29(10):2115–20.

5 Conventional Radiological Techniques and PET-CT in Treatment Response Evaluation in Postsurgical Setting

Dimitrios Priftakis, Saima Riaz, and Francesco Fraioli

5.1 Introduction

Surgery is the curative treatment of choice in many types of cancer, which are diagnosed at an early stage when the disease is still localized, and there is no evidence of distant metastatic spread. The success of curative surgery depends on the removal of the tumor with a margin of healthy tissue around it in order to ensure that no malignant cells are left behind. In many cases, dissection of regional lymph nodes is also necessary in order to remove known metastatic lymph nodes or to prevent spread of the disease from potentially undetected micrometastases. Although these strategies have improved the survival of the patients, the recurrence rates after complete surgical resection with curative intent remain high in many types of cancer (e.g., 30–75% in non-small cell lung cancer depending on final pathologic staging [1]). Therefore, there is need for postsurgical surveillance, usually with biomarkers and imaging, to detect potential evidence of recurrence as early as possible.

In some cases, although curative surgery is not feasible, patients may benefit from primary debulking surgery, followed by radiotherapy or chemotherapy. Follow-up with imaging is necessary after debulking surgery to assess residual disease or for surveillance since these patients have a higher chance of early recurrence.

Moreover, imaging plays an important role in the assessment of postoperative complications, which may have an impact not only on the patients' quality of life, but also on their survival [2].

Having established the crucial role of imaging in postoperative surveillance, the optimal choice of modality for each indication needs to be addressed. In this chapter, we will compare the advantages and limitations of conventional imaging (X-ray, CT, and MRI) and PET/CT in the postsurgical setting of various types of cancer and review the respective guidelines and recommendations. Potential pitfalls in the interpretation of imaging findings will also be discussed, as these are common due to distortion of the anatomy and postoperative inflammation.

5.2 Computed Tomography (CT)

Computed Tomography is usually the first imaging modality considered for postoperative surveillance in cancer patients because of the anatomical details that it provides and its wide availability. The performance of CT differs among the various types of cancer, and there are certain advantages and limitations depending on the anatomical area, which guide the selection of patients who should be monitored with this method.

D. Priftakis (✉) · S. Riaz · F. Fraioli
University College London Hospitals (UCLH), London, UK
e-mail: dimitris.priftakis@nhs.net

S. Fanti et al. (eds.), *Atlas of Clinical PET-CT in Treatment Response Evaluation in Oncology*,
https://doi.org/10.1007/978-3-030-68858-5_5

In non-small cell lung cancer, recurrence after surgery can appear at the bronchial stump, adjacent to a surgical staple, in the parietal pleura or in mediastinal lymph nodes [3]. Such local or locoregional recurrence occurs in up to 25% of patients with resected early-stage NSCLC, usually in the first 2 years [4]. Therefore, it is recommended that patients after surgery with curative intent for NSCLC should be monitored with chest CT every 6 months for the first 2–3 years and with low-dose CT annually thereafter [5]. The radiographic features of recurrence vary, and the differentiation from postoperative fibrosis is often hard. A growing mass at the level of resection on serial CT scans is a strong indication of recurrence. In some cases, the recurrent tumor may not be visible due to its small size, or there may be indirect findings of recurrence such as a change of position in mediastinal structures [4]. The use of CT in the postsurgical surveillance of NSCLC has been reported to have high negative predictive value (NPV) but not satisfactory positive predictive value (PPV) (53%) [6].

In colorectal cancer, CT can be used for surveillance after surgery with curative intent along with CEA marker monitoring. The data on the usefulness of CT in following patients with non-metastatic colorectal cancer are controversial and show that the impact on patient management (earlier salvage surgery with curative intent) is not associated with improved survival [7]. Nevertheless, imaging with contrast-enhanced chest/abdominal/pelvic CT is recommended in this group of patients every 6–12 months for up to 5 years [8].

In patients with head and neck cancer, a new postsurgery baseline CT is recommended within 6 months of the surgery and annual monitoring for recurrence thereafter [9]. Because of the postsurgical distortions in areas with already complex anatomy, it is important to establish the postsurgical baseline in order to guide the future assessment for recurrence. The radiologist must be aware of the exact surgical technique as the myocutaneous flaps that are used for reconstruction may initially look like masses with soft-tissue attenuation, but also because their margins are the most common sites of local recurrence [10]. Postoperative complications such as infection, abscess, fistula, or flap necrosis can be evaluated as they have characteristic morphology on CT. Additionally, monitoring of the lungs with chest CT is necessary in head and neck cancer patients, especially smokers, because they run a high risk not only for lung metastases, but also for a second primary lung cancer [11].

In summary, CT is very successful in the establishment of postoperative anatomy, in the assessment of complications, as well as in the detection of locoregional recurrence in a wide range of tumors. Additionally, CT has the advantage of being one of the most accessible and cost-effective imaging modalities. Nevertheless, there are certain categories of patients where CT is not accurate enough for evaluation in the postsurgical setting or where it provides equivocal findings that need further imaging for clarification. These limitations will be addressed in the following sections on MRI and PET.

5.3 Magnetic Resonance Imaging (MRI)

Magnetic resonance imaging (MRI) shows a trend of increased use in oncology [12, 13] due to the high sensitivity of the method for soft-tissue abnormalities, which makes it ideal for detecting primary or metastatic tumors in dedicated body parts, such as brain, breast, liver, colon, pelvis, head, and neck. Moreover, the development of new sequences and techniques, such as diffusion-weighted imaging (DWI), apparent diffusion coefficient (ADC), or dynamic contrast enhanced (DCE), opens new ways in detecting and monitoring cancer with higher accuracy [13, 14].

In colorectal cancer, MRI has shown higher per-lesion sensitivity than the CT in detecting pelvic recurrence and liver metastases in patients after resection of primary tumor. However, considering its higher cost and a relatively high proportion of false-positive tests (14%), it is not recommended for routine follow-up but is reserved for planning the surgical resection of such lesions [15]. MRI can also be used as an alternative surveillance imaging method in

patients with renal failure who cannot have contrast-enhanced CT [8]. Another role for MRI can be in the surveillance of the liver in patients with resected liver metastases [16].

MRI has emerged as an important imaging tool in head and neck cancer and particularly in tumors of the nasopharynx, the nasal sinuses, and the skull base. In the postsurgical setting, MRI is better in the assessment of late complications such as chylous fistulas and posttraumatic neuromas. The greatest added value of MRI, however, is in assessment of recurrence and differentiation from posttherapy changes [10, 17]. Particularly, with the addition of the more advanced sequences, the sensitivity and specificity of MRI for the detection of recurrent or residual tumors increase (94% and 100%, respectively) [18]. MRI spectroscopy is another MRI modality that may have up to 100% PPV in the confirmation of malignancy in a posttherapy mass [17].

In women with ovarian cancer, despite the high accuracy of MRI in staging, the superiority of MRI in recurrence assessment is controversial. The overall accuracy of MRI in ovarian cancer recurrence is approximately 89%. Nevertheless, some studies show high specificity of MRI but lower sensitivity, while other studies conclude that MRI is more sensitive for detecting local pelvic recurrence and peritoneal lesions of recurrent ovarian tumors [19, 20].

Postoperative surveillance of breast cancer relies almost exclusively on annual mammography [21, 22]. MRI surveillance may be considered as a supplemental imaging tool, according to some guidelines, for clarification of equivocal findings or in subgroups of patients such as women with dense breasts or women diagnosed before the age of 50 [23]. Studies have shown that despite the low diagnostic yield of MRI in the postoperative surveillance of breast cancer, the PPV of the method is acceptable, possibly higher than the PPV of surveillance ultrasound and potentially more effective after more than 3 years after surgery [24].

In summary, MRI is not routinely used in the follow-up of cancer patients after surgery but may be considered as a complementary imaging method in certain subgroups of patients. The high cost and relatively low availability are some of the main disadvantages of the method, as its cost-effectiveness remains largely unproven. However, the development of novel sequences, such as DWI, ADC, DCE, and the emerging use of magnetic spectroscopy bear the promise of more accurate postsurgical monitoring of cancer.

5.4 Positron Emission Tomography (PET)

Positron emission tomography (PET) is a type of nuclear imaging based on the use of radiotracers labeled with positron-emitting isotopes, such as ^{18}F, ^{68}Ga, etc. The positrons emitted from the decay of these isotopes are antimatter counterparts of electrons, and as such, they quickly interact with surrounding electrons through a process called annihilation, producing two 511 keV photons, which travel in opposite directions. The detectors in the PET scanner are configured in a circular array and record pairs of photons that arrive simultaneously in opposite ends, creating a map of radiotracer accumulation in the body [25]. PET imaging is routinely coupled with CT for attenuation correction of the images and for anatomical localization of the PET findings. The modern scanners are hybrid PET/CT scanners, and fusion of PET and CT images is part of the reconstruction [26]. Hybrid imaging with PET/MRI is a more recent development for better soft-tissue characterization and with the advantage of lower exposure to radiation, however, with inferior attenuation correction when compared with PET/CT and higher costs which limit its availability [27].

The most commonly used radiotracer for PET imaging in oncology is ^{18}F-FDG, a radiolabeled glucose analogue, which is accumulated by cancer cells due to their high metabolic needs. FDG-PET imaging has been proven beneficial not only in primary staging, but also in the assessment of response to treatment, the accurate characterization of residual disease, and the early detection of recurrence with impact on survival and quality of life [28]. Among these, surveillance and restaging disease after surgery are commonly recom-

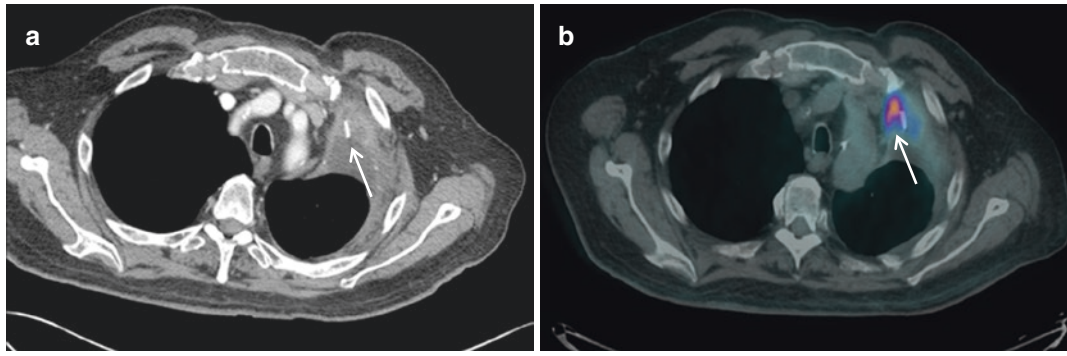

Fig. 5.1 78-year-old male patient who had left upper lobectomy for T3N2M0 non-small cell lung cancer. The patient was followed up with chest CT every 6 months. On the second follow-up, 1 year after the surgery, the contrast-enhanced CT (**a**) showed suspicious localized pleural thickening at the level of the surgical clips. On PET/CT (**b**), there was FDG uptake in this area, confirming local recurrence

mended indications for FDG-PET for many types of malignancy, provided that it is performed in an appropriate and timely manner.

The timing of FDG-PET imaging is crucial in the postsurgical setting. Tissue injury in the operative bed triggers an inflammatory response with the formation of granulation tissue, where there can also be increased FDG uptake. Gradually, the granulation tissue undergoes apoptosis and is replaced by scar tissue, within 2 months, and as this happens, FDG uptake tends to decrease and eventually resolve [29]. Therefore, it is generally recommended to delay FDG PET/CT for 4–8 weeks after surgery to reduce the chance of a diagnostic error due to interference of FDG-avid postsurgical changes [29–31].

Apart from the expected inflammatory postsurgical changes, other complications including infections, abscesses, fistulae, fat necrosis, and reactive lymph nodes can demonstrate increased FDG activity, which may be persistent for a long time after surgery, even years in some cases [32]. Postsurgical fat necrosis, in particular, may be difficult to differentiate from malignancy because it usually has a mass-like appearance with focal FDG uptake. Fat necrosis is more commonly met after surgery in the abdominal region as a result of omental infarction. CT can help in the characterization of such lesions, as they demonstrate a central fat-attenuation area surrounded by a rim of fibrous tissue. Follow up of fat necrosis with PET/CT shows gradual decrease and resolution of FDG avidity over time [33, 34].

In patients with non-small cell lung cancer after complete resection, FDG PET/CT has shown high accuracy in the detection of recurrence with high impact on management and survival [35]. High sensitivity and specificity of FDG PET/CT are accompanied by good PPV (89.5%) and NPV (98.8%), leading to a change in management in approximately 30% of patients with positive PET, whereas, a negative PET is very reliable for absence of disease [36, 37] (Fig. 5.1). A positive scan must always be differentiated by potentially FDG-avid mimickers of malignancy such as inflammatory changes at the bronchial stump, persistent postpleurodesis inflammation, postbiopsy infections (e.g., empyema), and reactive regional lymph nodes [29]. FDG PET/CT can also be useful in the detection or exclusion of recurrence in patients with serum CEA elevation after curative resection [38]. Despite the efficiency of FDG PET/CT, its potential impact on survival and encouraging reports on cost-effectiveness, the method is not recommended for routine surveillance imaging after primary lung cancer resection [35].

In colorectal cancer, PET/CT may complement conventional imaging in the surveillance after surgery with curative intent. FDG PET/CT is a very accurate and specific method for early

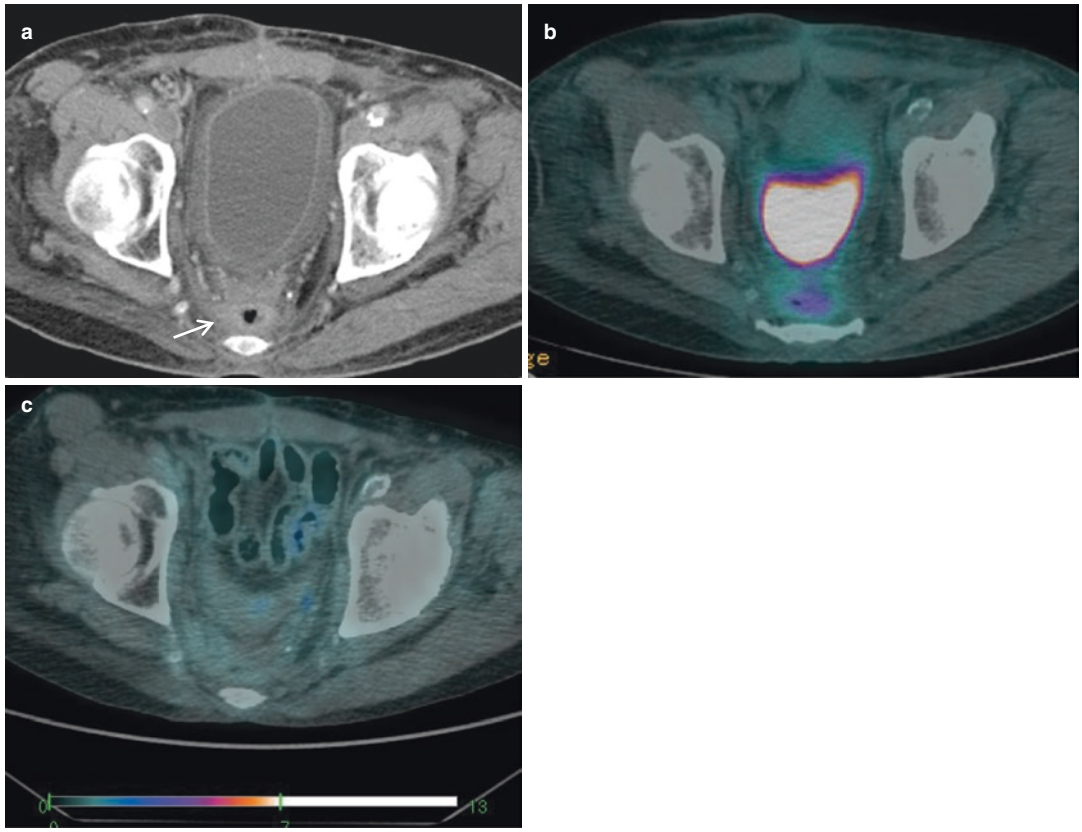

Fig. 5.2 Previous rectal adenocarcinoma treated with radiotherapy and end ileostomy. Recent history of enterocutaneous fistula repair. Most recent CT (**a**) shows enhancing soft tissue around a small air cavity in the precoccygeal region. PET/CT (**b**) done at the same time of CT shows low-grade activity in that region, which is most compatible with inflammatory changes. PET/CT (**c**) at 1 month shows complete resolution of the uptake with small residual tissue in keeping with granulation tissue and postsurgical change in the pelvis and no evidence of recurrence

detection of recurrence and has the best performance in patients with high suspicion [39, 40]. In patients with rising CEA, FDG PET/CT has superior per-lesion sensitivity than CT and can detect recurrence even in cases with negative conventional imaging. This leads to a change in management in 30–56% of patients with suspected colorectal cancer recurrence, providing chances for surgical resection or other local treatments earlier in the course of disease, but also helping to avoid unnecessary operations in patients with more advanced disease [41] (Fig. 5.2).

Although postoperative surveillance of head and neck cancers relies primarily on CT, as mentioned earlier, several studies have shown superiority of FDG PET/CT in the detection of locoregional recurrence [29, 42]. Particularly, FDG PET/CT has the advantage of a very high NPV (>94%) in this setting [43] and the ability to detect distant metastases and second primaries, which are relatively frequent in these patients, especially smokers. On the other hand, FDG PET/CT has suboptimal PPV (<60%) for recurrence in the primary site or cervical nodes [43] due to various postsurgical inflammatory complications, which can result in increased FDG uptake (Fig. 5.3). An example of a pitfall is the asymmetrical FDG uptake in the vocal cords after injury of the recurrent laryngeal nerve during surgery, where the compensatory overactivity of the normal vocal cord can be interpreted as

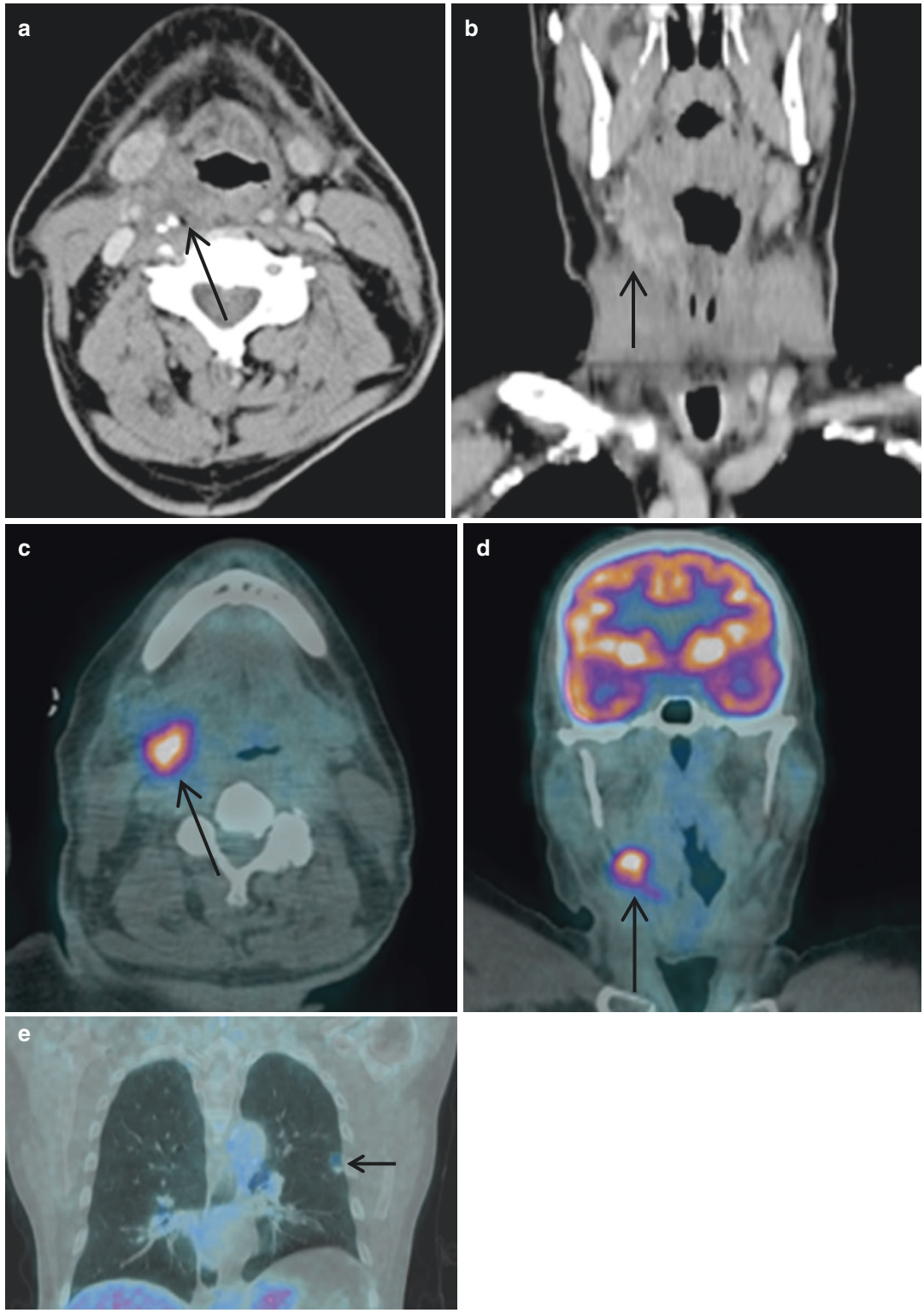

Fig. 5.3 66-year-old male patient 8 months after laryngectomy for pT4N1M0 squamous cell carcinoma. Follow-up contrast-enhanced CT of the neck (**a**, **b**) showed an area of heterogeneous enhancement in the deep aspect of the right oropharynx suspicious for recurrence, which was not easily accessible for biopsy. PET/CT 3 weeks later showed high-focal FDG uptake compatible with local recurrence (**c**, **d**), but also an FDG-avid left lung lesion (**e**), which could represent either a metastasis or a second primary

suspicious for malignancy [29]. Due to the relatively high false-positive rate, biopsy is recommended in the majority of patients with positive postoperative PET findings.

In the postoperative surveillance of ovarian cancer, the value of PET/CT has been found similar or higher than conventional imaging in many studies, being particularly sensitive in the detection of peritoneal deposits and of recurrence in normal-sized lymph nodes [44, 45]. In this context, FDG PET/CT can be considered as an equivalent alternative to contrast-enhanced CT despite occasional false-negative results due to postoperative peritoneal inflammation and bowel adhesions, which may obscure metastatic peritoneal deposits. False-negative results are also frequent in certain ovarian cancer subtypes such as mucinous adenocarcinomas or in the presence of cystic and necrotic deposits [45]. A significant advantage of FDG PET/CT is the ability to detect recurrence earlier and with higher sensitivity than CA-125, the biomarker routinely used for ovarian cancer surveillance [46]. It has been reported that the high sensitivity of FDG-PET imaging in patients with suspected recurrence of ovarian cancer (i.e., increased CA-125 and negative or equivocal conventional imaging) leads to a change in the intended management in a substantial proportion of patients, higher than 50% [46, 47] (Fig. 5.4).

Local postoperative assessment with FDG-PET in patients with breast cancer has been demonstrated to be more sensitive but not significantly more specific than with CT. Also, FDG-PET imaging did not show significant difference in accuracy when compared with MRI in this setting [48]. The lack in specificity can be explained by common postsurgical inflammatory complications such as fat necrosis, cellulitis, or fistulae [29]. Nevertheless, the use of FDG PET/CT is sometimes consid-

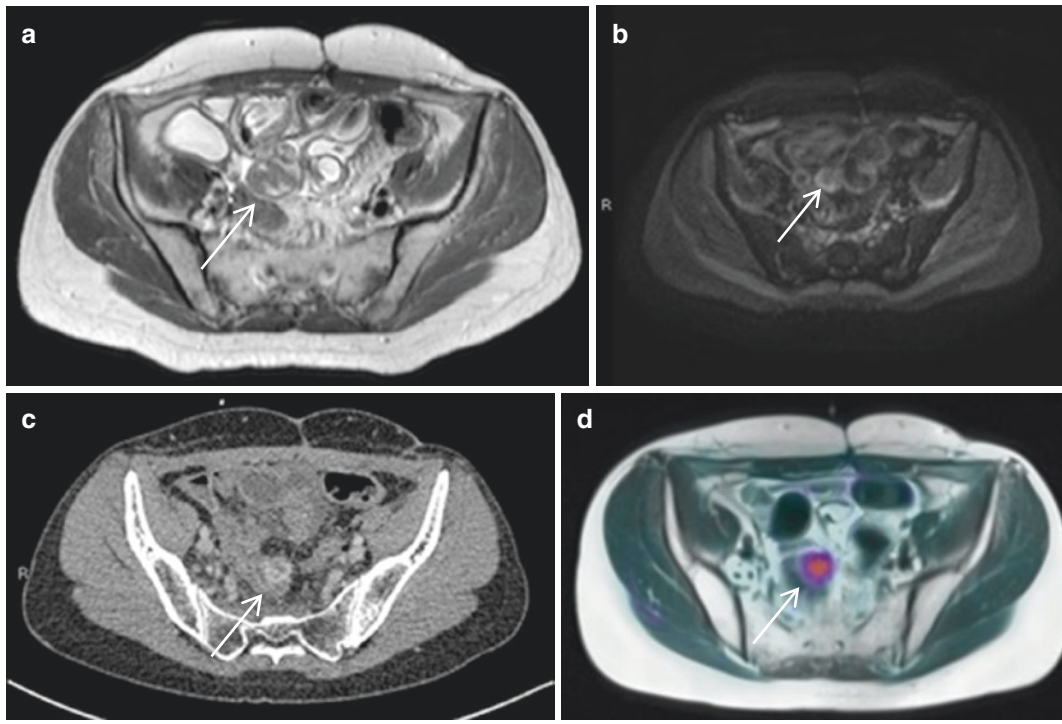

Fig. 5.4 34-year-old woman, 2 years after resection of nonmetastatic uterine leiomyosarcoma FIGO IIA. MRI (**a**. T2 sequence, **b**. DWI sequence) and contrast-enhanced CT (**c**) show a serosal sigmoid lesion suspicious for recurrence. Follow-up FDG PET/MRI (**d**) shows increased metabolic activity of this lesion, confirming recurrence in the sigmoid mesentery

ered appropriate for restaging for detection of local recurrence [49], and it is particularly efficient in asymptomatic patients with elevated biomarkers (e.g., CA15-3), thus offering the chance for earlier initiation of treatment with increased odds for cure or long-term palliation [50].

In summary, FDG-PET imaging has a proven value in the postsurgical assessment in a wide range of cancer types and disease scenarios. A common indication for the use of FDG-PET imaging is the localization of early recurrence suspected by the elevation of a tumor marker with negative or equivocal findings in conventional imaging. Caution should be taken in imaging patients after recent surgery as a variety of inflammatory postoperative complications can produce false-positive results.

5.5 Other Radiotracers (Neuroendocrine Tumors, Prostate Cancer)

Despite the success of PET imaging with FDG in Oncology, there are types of cancer which have indolent course and do not exhibit sufficient increase in metabolic activity to benefit from this radiotracer (Fig. 5.5). Examples of such neoplasms include well-differentiated neuroendocrine tumors and prostate cancer, for which alternative radiotracers have been developed. In this section, we will examine the postoperative value of PET imaging with these specific radiotracers.

Well-differentiated neuroendocrine tumors (NET) are known to overexpress somatostatin receptors, and for the purpose of PET imaging, radiolabeled somatostatin agonists have been developed to target these receptors. The most commonly used NET-targeting PET radiotracers are ^{68}Ga-DOTA-TATE, ^{68}Ga-DOTA-TOC, and ^{68}Ga-DOTA-NOC.

Somatostatin-receptor PET imaging has brought forth important support in clinical diagnosis and treatment of various types of NETs. However, there is no consensus in the appropriateness of its use for follow-up after surgery with curative intent [51]. There is no evidence that somatostatin-receptor PET imaging has an impact on patient management in the postoperative setting even if small-volume residual disease is visualized. In patients with biochemical or clinical evidence of recurrence, conventional imaging is routinely the first choice, followed by somatostatin-receptor PET in cases with equivocal findings [51].

Prostate cancer is one of the most prevalent cancers in men, and radical prostatectomy with curative intent is one of the most common choices for fit patients with no evidence of metastatic disease. After prostatectomy, follow-up is done with PSA levels, which should be undetectable, and any rise in PSA is suspicious for recurrence (biochemical recurrence). Conventional imaging methods are often unable to localize the site of recurrence. On

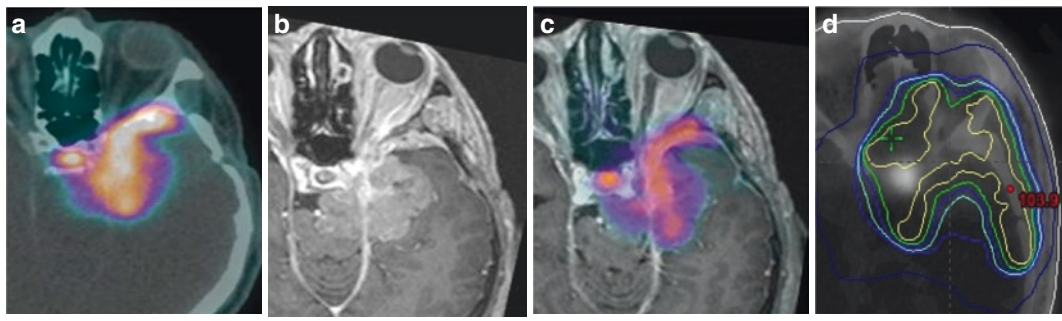

Fig. 5.5 47-year-old with meningioma already underwent surgery. Candidate to radiotherapy. PET/CT (**a**) demonstrates a ^{68}Ga-DOTA-TATE avid lesion in the left middle fossa. MR (**b**) shows high anatomical details. However, neither modality can assess the infiltration of the pituitary fossa. Approach to radiotherapy without this information is difficult as may cause hypopituitarism following irradiation. PET MR (**c**) allows to visualize the exact extension of this disease and, consequently, modulates the radiation beam, sparing as much normal tissue as possible (**d**)

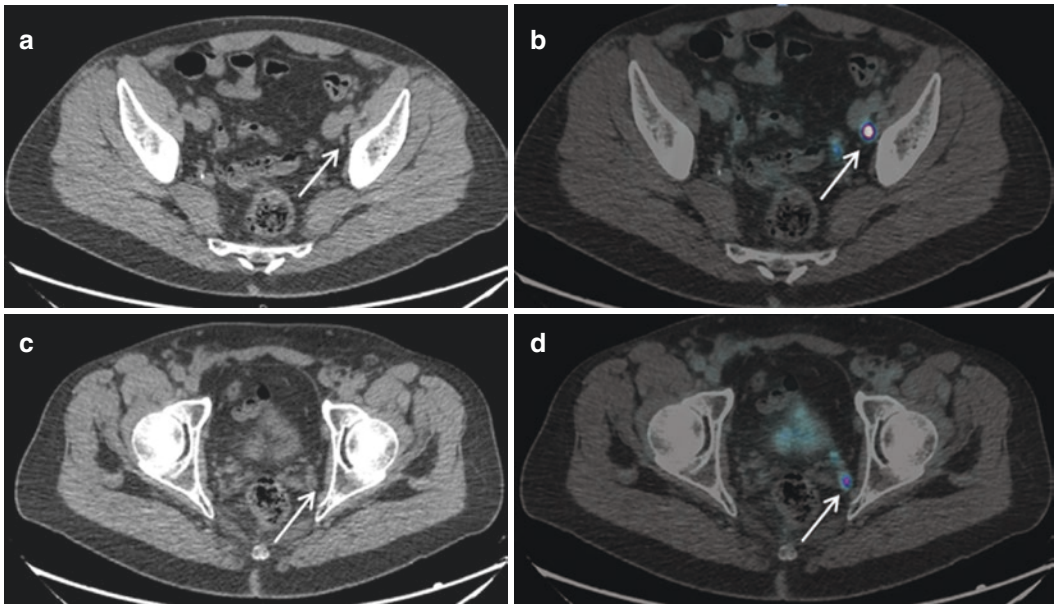

Fig. 5.6 68-year-old man with rising PSA (0.48 ng/ml, doubling time 3 months) 2.5 years after radical prostatectomy for high-volume Gleason 6 prostate cancer confined to the prostate with negative margins. ^{68}Ga-PSMA PET/CT (**a**–**d**) shows intense uptake in two small left-sided pelvic lymph nodes measuring up to 6 mm (below the 8 mm threshold for a lymph node to be considered positive in conventional imaging)

the contrary, imaging with sensitive and specific PET radiotracers such as ^{18}F-choline, ^{68}Ga- or ^{18}F-PSMA, and ^{18}F-fluciclovine can detect even small volume of disease, leading to targeted therapeutic approaches.

Radiolabeled choline is targeting the high membrane turnover in prostate cancer cells. ^{18}F-choline PET/CT has shown good results in the biochemical recurrence setting, with high sensitivity and specificity, particularly in the detection of metastatic lymph nodes [52]. Emphasis should be given to the fact that the detection rate of ^{18}F-choline PET/CT is higher when PSA levels are higher than 1 ng/ml and when PSA doubling time is 6 months or less. Therefore, guidelines advocate for the use of ^{18}F-choline PET/CT in patients with biochemical recurrence after radical prostatectomy when PSA is higher than 1 ng/ml [53].

More recently, the development of ^{68}Ga-PSMA PET imaging, based on the overexpression of a transmembrane glycoprotein by prostate cancer cells, has shown promise to further improve recurrence detection in patients with rising PSA levels after radical prostatectomy. Like ^{18}F-choline, the detection rate of ^{68}Ga-PSMA is influenced by PSA levels and kinetics, but it is very sensitive even in PSA levels as low as 0.2 ng/ml, thus leading to earlier disease localization. As a result, ^{68}Ga-PSMA PET imaging has a high impact on management, leading to a change of treatment in 54% of the patients [54, 55] (Fig. 5.6). Despite its excellent performance, ^{68}Ga-PSMA PET imaging is not yet widely available and, therefore, not routinely recommended. More studies regarding the impact on disease outcomes, patients' quality of life, and cost-effectiveness are needed.

5.6 Conclusion

In this chapter, the utility of conventional imaging (CT, MRI) and PET/CT imaging with FDG and other radiotracers in the postsurgical setting of various types of cancer has been reviewed. The most common indications have been summarized, and the accuracy of the methods for a variety of clinical scenarios has been presented according to published medical literature. Guideline recom-

mendations have been discussed in each section. Emphasis has been given to the description of postoperative complications and the problem of differentiation from disease recurrence.

Selecting the appropriate method and time of imaging is crucial for the response assessment in the postsurgical setting. CT and MRI are widely available methods with the advantage of providing rich anatomical information for the evaluation of postoperative complications and for the detection of recurrence. On the other hand, PET can add functional information, which in some cases may lead to earlier identification of recurrence, particularly when there is suspicion based on biochemical evidence (tumor markers) with negative or equivocal conventional imaging findings. The evidence-based knowledge of what each method can offer will allow the clinicians to order the imaging test, which will have the best positive impact on their patients' disease outcome.

References

1. Sugimura H, Nichols FC, Yang P, et al. Survival after recurrent nonsmall-cell lung cancer after complete pulmonary resection. Ann Thorac Surg. 2007;83:409–18. https://doi.org/10.1016/j.athoracsur.2006.08.046.
2. Tevis SE, Kohlnhofer BM, Stringfield S, et al. Postoperative complications in patients with rectal cancer are associated with delays in chemotherapy that Lead to worse disease-free and overall survival. Dis Colon Rectum. 2013;56:1339–48. https://doi.org/10.1097/DCR.0b013e3182a857eb.
3. Shepard J-AO, McLoud TC. Thoracic imaging. 3rd ed. Philadelphia, PA: Elsevier; 2019.
4. Kelsey CR, Marks LB, Hollis D, et al. Local recurrence after surgery for early stage lung cancer: an 11-year experience with 975 patients. Cancer. 2009;115:5218–27. https://doi.org/10.1002/cncr.24625.
5. National Comprehensive Cancer Network Imaging Appropriate Use Criteria. Non-small cell lung cancer (Version 5.2019). 2019. Retrieved from https://www.nccn.org/professionals/imaging/content/.
6. Korst RJ, Kansler AL, Port JL, et al. Accuracy of surveillance computed tomography in detecting recurrent or new primary lung cancer in patients with completely resected lung cancer. Ann Thorac Surg. 2006;82:1009–15. https://doi.org/10.1016/j.athoracsur.2006.03.062.
7. Jeffery M, Hickey BE, Hider PN, See AM. Follow-up strategies for patients treated for non-metastatic colorectal cancer. Cochrane Database Syst Rev. https://doi.org/10.1002/14651858.CD002200.pub3.
8. National Comprehensive Cancer Network Imaging Appropriate Use Criteria. Colon cancer (Version 1.2019). 2019. Retrieved from https://www.nccn.org/professionals/imaging/content/.
9. National Comprehensive Cancer Network Imaging Appropriate Use Criteria. Head and neck cancers (Version 5.2019). 2019. Retrieved from https://www.nccn.org/professionals/imaging/content/.
10. Saito N, Nadgir RN, Nakahira M, et al. Posttreatment CT and MR imaging in head and neck Cancer: what the radiologist needs to know. Radiographics. 2012;32:1261–82. https://doi.org/10.1148/rg.325115160.
11. Pagedar NA, Jayawardena A, Charlton ME, Hoffman HT. Second primary lung cancer after head and neck cancer: implications for screening computed tomography. Ann Otol Rhinol Laryngol. 2015;124:765–9. https://doi.org/10.1177/0003489415582259.
12. Wise J. MRI scanning increases eightfold in Canadian women with breast cancer. BMJ. 2015;351:h5088. https://doi.org/10.1136/bmj.h5088.
13. Oberlin DT, Casalino DD, Miller FH, Meeks JJ. Dramatic increase in the utilization of multiparametric magnetic resonance imaging for detection and management of prostate cancer. Abdom Radiol. 2017;42:1255–8. https://doi.org/10.1007/s00261-016-0975-5.
14. Méndez CA, Pizzorni Ferrarese F, Summers P, et al. DCE-MRI and DWI integration for breast lesions assessment and heterogeneity quantification. Int J Biomed Imag. 2012;2012:1–8. https://doi.org/10.1155/2012/676808.
15. Miles K. Colorectal cancer: imaging surveillance following resection of primary tumour. Cancer Imaging. 2007;7:S143–9. https://doi.org/10.1102/1470-7330.2007.9011.
16. Hyder O, Dodson RM, Mayo SC, et al. Posttreatment surveillance of patients with colorectal cancer with surgically treated liver metastases. Surgery. 2013;154:256–65. https://doi.org/10.1016/j.surg.2013.04.021.
17. Moore AG, Srinivasan A. Postoperative and postradiation head and neck: role of magnetic resonance imaging. Top Magn Reson Imaging. 2015;24:3–13. https://doi.org/10.1097/RMR.0000000000000042.
18. Tshering Vogel DW, Zbaeren P, Geretschlaeger A, et al. Diffusion-weighted MR imaging including bi-exponential fitting for the detection of recurrent or residual tumour after (chemo)radiotherapy for laryngeal and hypopharyngeal cancers. Eur Radiol. 2013;23:562–9. https://doi.org/10.1007/s00330-012-2596-x.
19. Kubik-Huch RA, Dörffler W, von Schulthess GK, et al. Value of (18F)-FDG positron emission tomography, computed tomography, and magnetic resonance imaging in diagnosing primary and recurrent ovarian carcinoma. Eur Radiol. 2000;10:761–7. https://doi.org/10.1007/s003300051000.

20. Kim CK, Park BK, Choi JY, et al. Detection of recurrent ovarian cancer at MRI: comparison with integrated PET/CT. J Comput Assist Tomogr. 2007;31:868–75. https://doi.org/10.1097/rct.0b013e31803e8c45.
21. Runowicz CD, Leach CR, Henry NL, et al. American Cancer Society/American Society of Clinical Oncology breast cancer survivorship care guideline. JCO. 2016;34:611–35. https://doi.org/10.1200/JCO.2015.64.3809.
22. National Comprehensive Cancer Network Imaging Appropriate Use Criteria. Breast cancer (Version 1.2019). 2019. Retrieved from https://www.nccn.org/professionals/imaging/content/.
23. Swinnen J, Keupers M, Soens J, et al. Breast imaging surveillance after curative treatment for primary non-metastasised breast cancer in non-high-risk women: a systematic review. Insights Imaging. 2018;9:961–70. https://doi.org/10.1007/s13244-018-0667-5.
24. Park VY, Kim E-K, Kim MJ, et al. Breast magnetic resonance imaging for surveillance of women with a personal history of breast cancer: outcomes stratified by interval between definitive surgery and surveillance MR imaging. BMC Cancer. 2018;18:91. https://doi.org/10.1186/s12885-018-3998-1.
25. Kapoor V, McCook BM, Torok FS. An introduction to PET-CT imaging. Radiographics. 2004;24:523–43. https://doi.org/10.1148/rg.242025724.
26. Delbeke D, Schöder H, Martin WH, Wahl RL. Hybrid imaging (SPECT/CT and PET/CT): improving therapeutic decisions. Semin Nucl Med. 2009;39:308–40. https://doi.org/10.1053/j.semnuclmed.2009.03.002.
27. Fraioli F, Punwani S. Clinical and research applications of simultaneous positron emission tomography and MRI. BJR. 2014;87:20130464. https://doi.org/10.1259/bjr.20130464.
28. Israel O, Kuten A. Early detection of cancer recurrence: 18F-FDG PET/CT can make a difference in diagnosis and patient care. J Nucl Med. 2007;48(Suppl 1):28S–35S.
29. Garg G, Benchekroun MT, Abraham T. FDG-PET/CT in the postoperative period: utility, expected findings, complications, and pitfalls. Semin Nucl Med. 2017;47:579–94. https://doi.org/10.1053/j.semnuclmed.2017.07.005.
30. Ulaner GA, Lyall A. Identifying and distinguishing treatment effects and complications from malignancy at FDG PET/CT. Radiographics. 2013;33:1817–34. https://doi.org/10.1148/rg.336125105.
31. Boellaard R, Delgado-Bolton R, Oyen WJG, et al. FDG PET/CT: EANM procedure guidelines for tumour imaging: version 2.0. Eur J Nucl Med Mol Imaging. 2015;42:328–54. https://doi.org/10.1007/s00259-014-2961-x.
32. Makis W, Ciarallo A, Rush C, Hickeson M. Infectious and inflammatory complications of surgical management of cancer patients imaged with 18F-FDG PET/CT: a pictorial essay. Clin Imaging. 2013;37:669–79. https://doi.org/10.1016/j.clinimag.2013.02.003.
33. Rydzak C, Chauhan A, Gupta N, et al. Fat-containing hypermetabolic masses on FDG PET/CT: a spectrum of benign and malignant conditions. Am J Roentgenol. 2016;207:1095–104. https://doi.org/10.2214/AJR.16.16066.
34. Davidson T, Lotan E, Klang E, et al. Fat necrosis after abdominal surgery: a pitfall in interpretation of FDG-PET/CT. Eur Radiol. 2018;28:2264–72. https://doi.org/10.1007/s00330-017-5201-5.
35. Sudarski S, Henzler T, Schoenberg SO. Post-therapeutic positron emission tomography/computed tomography for early detection of non-small cell lung cancer recurrence. Transl Lung Cancer Res. 2013;2:295–303. https://doi.org/10.3978/j.issn.2218-6751.2013.05.02.
36. Toba H, Sakiyama S, Otsuka H, et al. 18F-fluorodeoxyglucose positron emission tomography/computed tomography is useful in postoperative follow-up of asymptomatic non-small-cell lung cancer patients. Interact Cardio Vascul Thorac Surg. 2012;15:859–64. https://doi.org/10.1093/icvts/ivs368.
37. Keidar Z, Haim N, Guralnik L, et al. PET/CT using 18F-FDG in suspected lung cancer recurrence: diagnostic value and impact on patient management. J Nucl Med. 2004;45:1640–6.
38. Isobe K, Hata Y, Takai Y, et al. Usefulness of fluoro-2-deoxyglucose positron emission tomography for investigating unexplained rising carcinoembryonic antigen levels that occur during the postoperative surveillance of lung cancer patients. Int J Clin Oncol. 2009;14:497–501. https://doi.org/10.1007/s10147-009-0905-4.
39. Sobhani I, Tiret E, Lebtahi R, et al. Early detection of recurrence by 18FDG-PET in the follow-up of patients with colorectal cancer. Br J Cancer. 2008;98:875–80. https://doi.org/10.1038/sj.bjc.6604263.
40. Maas M, Rutten IJG, Nelemans PJ, et al. What is the most accurate whole-body imaging modality for assessment of local and distant recurrent disease in colorectal cancer? A meta-analysis: imaging for recurrent colorectal cancer. Eur J Nucl Med Mol Imaging. 2011;38:1560–71. https://doi.org/10.1007/s00259-011-1785-1.
41. Zhang Y. Value of 18 F-FDG PET-CT in surveillance of postoperative colorectal cancer patients with various carcinoembryonic antigen concentrations. WJG. 2014;20:6608. https://doi.org/10.3748/wjg.v20.i21.6608.
42. Kostakoglu L, Fardanesh R, Posner M, et al. Early detection of recurrent disease by FDG-PET/CT leads to management changes in patients with squamous cell cancer of the head and neck. Oncologist. 2013;18:1108–17. https://doi.org/10.1634/theoncologist.2013-0068.
43. Gupta T, Master Z, Kannan S, et al. Diagnostic performance of post-treatment FDG PET or FDG PET/CT imaging in head and neck cancer: a systematic review and meta-analysis. Eur J Nucl Med Mol Imaging. 2011;38:2083–95. https://doi.org/10.1007/s00259-011-1893-y.
44. Rangarajan V, Agrawal A. Appropriateness criteria of FDG PET/CT in oncology. Indian

J Radiol Imaging. 2015;25:88. https://doi.org/10.4103/0971-3026.155823.
45. Kang SK, Reinhold C, Atri M, et al. ACR appropriateness criteria ® staging and follow-up of ovarian cancer. J Am Coll Radiol. 2018;15:S198–207. https://doi.org/10.1016/j.jacr.2018.03.015.
46. Suppiah S, Chang W, Hassan H, et al. Systematic review on the accuracy of positron emission tomography/computed tomography and positron emission tomography/magnetic resonance imaging in the management of ovarian cancer: is functional information really needed? World J Nucl Med. 2017;16:176. https://doi.org/10.4103/wjnm.WJNM_31_17.
47. Simcock B, Neesham D, Quinn M, et al. The impact of PET/CT in the management of recurrent ovarian cancer. Gynecol Oncol. 2006;103:271–6. https://doi.org/10.1016/j.ygyno.2006.03.004.
48. Pennant M, Takwoingi Y, Pennant L, et al. A systematic review of positron emission tomography (PET) and positron emission tomography/computed tomography (PET/CT) for the diagnosis of breast cancer recurrence. Health Technol Assess. 2010;14 https://doi.org/10.3310/hta14500.
49. Jadvar H, Colletti PM, Delgado-Bolton R, et al. Appropriate use criteria for 18 F-FDG PET/CT in restaging and treatment response assessment of malignant disease. J Nucl Med. 2017;58:2026–37. https://doi.org/10.2967/jnumed.117.197988.
50. Champion L, Brain E, Giraudet A-L, et al. Breast cancer recurrence diagnosis suspected on tumor marker rising: value of whole-body 18FDG-PET/CT imaging and impact on patient management. Cancer. 2011;117:1621–9. https://doi.org/10.1002/cncr.25727.
51. Hope TA, Bergsland EK, Bozkurt MF, et al. Appropriate use criteria for somatostatin receptor PET imaging in neuroendocrine tumors. J Nucl Med. 2018;59:66–74. https://doi.org/10.2967/jnumed.117.202275.
52. Evangelista L, Zattoni F, Guttilla A, et al. Choline PET or PET/CT and biochemical relapse of prostate cancer: a systematic review and meta-analysis. Clin Nucl Med. 2013;38:305–14. https://doi.org/10.1097/RLU.0b013e3182867f3c.
53. Mottet N, Bellmunt J, Bolla M, et al. EAU-ESTRO-SIOG guidelines on prostate cancer. Part 1: screening, diagnosis, and local treatment with curative intent. Eur Urol. 2017;71:618–29. https://doi.org/10.1016/j.eururo.2016.08.003.
54. Afaq A, Alahmed S, Chen S-H, et al. Impact of 68Ga-prostate-specific membrane antigen PET/CT on prostate cancer management. J Nucl Med. 2018;59:89–92. https://doi.org/10.2967/jnumed.117.192625.
55. Han S, Woo S, Kim YJ, Suh CH. Impact of ^{68}Ga-PSMA PET on the management of patients with prostate cancer: a systematic review and meta-analysis. Eur Urol. 2018;74:179–90. https://doi.org/10.1016/j.eururo.2018.03.030.

6 Conventional Radiological and PET-CT Assessment of Treatment Response Evaluation in Chemotherapy Setting

Nagabhushan Seshadri, Rashika Fernando, and Radhakrishnan Jayan

6.1 Introduction

Imaging modalities, both conventional and functional techniques, have contributed significantly to the evaluation of disease and the decision to identify the most efficient form of treatment. The ability to combine imaging information with key clinical end points has become important in cancer therapeutics, which provides valuable information in assessing response to chemotherapy agents. Imaging characteristics and interpretation criteria have been developed to act as surrogate markers to assess presence and severity of disease state to strategically plan therapeutic management. This in turn has not only helped improve treatment efficacy, but also reduce unwanted side effects and address other dimensions such as patient's quality of life and prognosis.

6.2 Conventional Radiological Techniques

Conventional imaging methods measuring morphological parameters still forms the cornerstone of response assessment in oncology. Treatment response evaluation using these techniques in oncology is traditionally based on comparing the size and/or volume of the tumour before and after treatment. In 1979, the World Health Organization (WHO) proposed uniform criteria, known as the WHO criteria, to report the results of cancer treatment [1]. It was based on bi-dimensional measurements of the tumour and defined response as a decrease of at least 50% in the sum of the product of the longest perpendicular diameters of measured lesions. The rationale for using a 50% threshold for the definition of response was based on data evaluating the reproducibility of measurements of tumour size by palpation and on planar chest radiographs [2]. A widely adopted measure of response is the 'Response Evaluation Criteria in Solid Tumours (RECIST) system, which was introduced in 2000 [3]. Using this system, the uni-dimensional measurement of target lesions, the number of lesions to be followed and the minimum size of these lesions were defined to provide a simple and standardized way of response assessment. The criteria were revised in 2009 (RECIST 1.1), reducing the number of lesions to be assessed, introducing the assessment of lymph nodes to simplify and optimize assessment of response [4] (Table 6.1).

RECIST provides a standardized and practical method to assess response in solid tumours in general, but pitfalls and limitations of RECIST have been noted in various clinical scenarios. Some of the pitfalls are cancer and treatment-specific.

N. Seshadri (✉) · R. Fernando · R. Jayan
Department of Nuclear Medicine and Radiology, Royal Liverpool University Hospitals NHS Foundation Trust, Liverpool, UK
e-mail: nagabhushan.seshadri@Liverpoolft.nhs.uk

S. Fanti et al. (eds.), *Atlas of Clinical PET-CT in Treatment Response Evaluation in Oncology*,
https://doi.org/10.1007/978-3-030-68858-5_6

Table 6.1 WHO, RECIST 1.0 and RECIST 1.1

Criteria	WHO	RECIST	RECIST 1.1
Complete response (CR)	Disappearance of all lesions	Disappearance of all lesions	Disappearance of all lesions
Partial response (PR)	>50% decrease in area	>30% decrease in the sum of longest diameter	>30% decrease in the sum of longest diameter
Stable disease (SD)	Neither PR nor PD	Neither PR nor PD	Neither PR nor PD
Progressive disease (PD)	>25% increase in the sum of area	>20% increase in the sum of smallest sum of diameters of lesions	>20% increase in the sum of smallest sum of diameters of lesions or 5 mm absolute increase or new lesions

Table 6.2 (mRECIST)

Criteria	Definition
Complete response (CR)	Disappearance of all enhancing lesions
Partial response (PR)	>30% decrease in the sum of longest diameter of lesion-enhancing component vs baseline sum of diameters
Stable disease (SD)	Neither PR nor PD
Progressive disease (PD)	>20% increase in the sum of diameters of viable lesions

Table 6.3 (MASS criteria)

Criteria	Definition
Favourable response	No new lesion and decrease in tumour size of ≥20% or one or more predominantly solid enhancing lesions with marked central necrosis or marked decreased attenuation (≥40 HU)
Indeterminate response	Neither favourable nor unfavourable
Unfavourable response	Increase in tumour size of ≥20% in the absence of marked central necrosis or marked decreased attenuation or new metastases, marked central fill-in or new enhancement of a previously homogeneously hypo-attenuating non-enhancing mass

For example, difficulties are often encountered in measuring target lesions (e.g. breast and prostate cancers). RECIST does not take into account changes in shape, size and irregular shape of tumours, given the uni-dimensional measurement undertaken [5]. Moreover, RECIST does not address any other measurement of anti-tumour changes other than tumour shrinkage. It has been noted that with some of the novel anti-cancer therapeutic agents, there is no immediate result in decrease of size. A good example is Sorafenib for hepatocellular cancer [6].

To address the issue of tumour necrosis, modified RECIST (mRECIST) criteria were developed to include enhancement of the target lesions during the arterial phase of either contrast-enhanced CT or MRI as a criteria [7] (Table 6.2).

The Choi response criteria, which incorporates tumour density and uses small changes in tumour size on CT, was proposed in the assessment of response of GIST treated with imatinib as one of the first cancer and therapy-specific criteria in solid tumours to overcome the limitations of RECIST [8]. With this, response is defined as a 10% decrease in uni-dimensional tumour size or a 15% decrease in CT attenuation, as opposed to a 30% decrease in uni-dimensional tumour size defined by RECIST. Tumour progression using these criteria is defined as the appearance of new intra-tumour nodules or an increase in the size of existing intra-tumour nodules, or an increase in overall tumour size by more than 20%, in the absence of post-treatment hypodense change.

MASS criteria was proposed to include Morphology, Attenuation, Size and Structure to overcome limitations of size and attenuation on CT and include specific morphologic or structural changes in treated metastatic RCC (Renal Cell Carcinoma) treated with anti-angiogenic agents [9]. MASS criteria also use morphologic or structural changes and classify objective response into three categories: favourable response, indeterminate response and unfavourable response (Table 6.3).

6.3 PET/CT in Response Assessment to Chemotherapy

Unlike conventional imaging methods, functional imaging methods define response to treatment as changes in molecular or functional characteristics that precede structural or anatomic changes. Integrated PET/CT provides information on early metabolic and volumetric changes and thus acts as a functional biomarker, which correlates with disease status.

Various quantitative parameters derived from Positron Emission Tomography (PET) studies based on concentration of fluorine-18-fluorodeoxyglucose (FDG) in tumours, which include standardized uptake values (SUVs), total lesion glycolysis (TLG) and metabolic tumour volume (MTV), have been proposed. SUV is a widely used quantitative parameter. It is defined as the ratio between the activity concentration in the tumour and the activity concentration in the whole body if the radioactivity were homogeneously distributed throughout the patient [10].

6.3.1 EORTC

The EORTC (European Organisation for Research and Treatment of Cancer) published published preliminary criteria for the assessment of tumour response in 1999 [11]. Recommendations of EORTC for determining tumour response with FDG-PET was based on SUV change as compared to the baseline study. These were classified into progressive metabolic disease, stable metabolic disease, partial metabolic response and complete metabolic response (Table 6.4).

Table 6.4 (EORTC)

Criteria	Definition
Complete metabolic response (CR)	No FDG uptake
Partial metabolic response (PR)	Decrease of a minimum of 15–25% SUV after one cycle of chemotherapy or greater than 25% after more than one cycle
Stable disease (SD)	Increase of SUV <25% or decrease <15% and no visible change in extent
Progressive disease (PD)	Increase of SUV >25% Increase of extend of FDG uptake

Table 6.5 (IHP)

Organ	Criteria for presence of disease
Liver or spleen	• Any size with uptake > liver/spleen: Positive • >1.5 cm with uptake < liver/spleen: Negative • Spleen diffuse uptake > liver: Positive if no cytokine administration for past 10 days
Lung	• New nodule >1.5 cm with FDG uptake > blood pool is considered positive if lung involvement present at baseline • New nodule <1.5 cm and FDG negative: Indeterminate • New nodule FDG positive with otherwise complete response: Infection/inflammation
Bone marrow	• Multifocal FDG uptake: Positive • Diffuse FDG uptake > liver: Hyperplasia
Lymph node	• For residual mass >2 cm: Positive if FDG uptake > mediastinal blood pool • For lesions <2 cm: Positive if any uptake > background

6.3.2 IHP Criteria for Lymphoma

In 2007, revised response criteria incorporating FDG PET were developed by the Response Assessment Subcommittee of the International Harmonization Project (IHP) to ensure consistency across clinical trials [12]. The definition proposed for a positive PET is focal or diffuse FDG uptake above the mediastinal blood pool (MBP) for residual nodal masses ≥2 cm, and any visible uptake above background for masses <2 cm, using visual assessment. Other specific criteria were provided for extra-nodal disease (Table 6.5).

6.3.3 Deauville Criteria for Lymphoma

There was need for binary criteria (positive or negative) that are simple to interpret, reproducible and have a high positive and negative predictive value. More recently, the Deauville criteria, which is a visual interpretation criteria based on a

Table 6.6 (Deauville score)

Score	Definition
1	No uptake
2	Uptake ≤ mediastinum
3	Uptake > mediastinum but ≤ liver
4	Moderately increased uptake compared to the liver
5	Markedly increased uptake compared to the liver and/or new lesions
6	New areas of uptake unlikely to be related to lymphoma

five-point scale of uptake on FDG PET/CT, has been proposed for response assessment in Lymphoma [13]. This is a five-point grading system based on the most intense uptake in a site of initial disease, if present (Table 6.6).

An international validation study using this grading system showed the inter-observer agreement was very high between six independent PET/CT reviewers using the Deauville criteria for HL (Hodgkins Lymphoma), FL (Follicular Lymphoma) and DLBCL (Diffuse Large B Cell Lymphoma) [14].

6.3.4 PERCIST

PET Response Criteria in Solid Tumours (PERCIST 1.0) were introduced in 2009 as guidelines for systematic and structured assessment of response to therapy with FDG-PET in patients with cancer, with suggested application in clinical trials and, potentially, in the clinical practice of PET reporting [15]. PERCIST has been used to measure clinical outcomes after treatment in a variety of tumours such as small-cell lung cancer, colorectal cancer, non-Hodgkin lymphoma, oesophageal cancer and Ewing sarcoma (Table 6.7).

Table 6.7 PERCIST

Criteria	Definition
Complete metabolic response (CR)	Complete resolution of FDG uptake in the target lesion with FDG uptake less than the mean SUL (SUV corrected for lean body mass) of the liver and indistinguishable from that of the surrounding background
Partial metabolic response (PR)	Partial metabolic response is defined as a decrease of greater than or equal to 30%, and of at least 0.8 SUL units must be shown between the target lesion at baseline and the most intense evaluable lesion at follow-up
Stable disease (SD)	Stable disease is defined as an increase or decrease in SUL of less than 30%
Progressive disease (PD)	Progressive disease is defined as progressive metabolic disease, lesions must show an increase of greater than or equal to 30% and an increase of at least 0.8 SUL units in a target lesion or development of a new lesion

6.4 MRI and CT in Response Assessment to Chemotherapy

Diffusion-weighted imaging (DWI) is probably the most useful MRI sequence for assessing response to chemotherapy. The assessment of tumour cellular density by DWI is one of the most intensively studied therapy evaluation strategies in recent years. This is due to the fact that the majority of current anti-cancer therapies result in loss of tumour cellularity, and DWI is sensitive to this effect [16]. Moreover, DWI is a completely non-invasive method, exploiting the tissue water diffusion at a cellular level and, therefore, acting as a useful biomarker for reduction of cellular density post-treatment. Typically, ADC (Apparent Diffusion Coefficient) values tend to increase following successful treatment, as a result of post-treatment necrosis, although ADC values can later decrease with establishment of fibrosis. Quantitative use of ADC, however, has shown conflicting results and is not yet suitable for clinical application. MRI with DWI imaging is useful in assessment of therapeutic response in rectal and gynaecological malignancies, liver and brain. Assessing tissue perfusion changes with CT perfusion imaging and dynamic contrast-enhanced MRI imaging is also a promising tool, especially in drugs that cause changes in angiogenesis of the tumour.

6.5 Evaluation of Response to Chemotherapy in Individual Tumours

6.5.1 Oesophageal and Gastric Cancer

Preoperative chemotherapy is particularly useful in oesophageal and oesophago gastric junctional tumours to downstage the tumour and facilitate surgical resection, improving local control and eradicating micro-metastases. The adjuvant use of chemotherapy aims to eradicate any remaining micro-metastatic disease after a potentially curative resection [17]. NICE recommends assessment with CT and FDG PET/CT for all patients with oesophageal and junctional tumours fit for surgery [18]. FDG-PET is more useful than CT in identifying the subset of patients who are chemosensitive, and these patients are likely to have a better prognosis following surgery [19]. CT is used more than FDG-PET in response assessment to gastric cancer as FDG-PET is less useful than in oesophageal and junctional tumours. In contrast, FDG PET is useful for monitoring response to therapy in gastrointestinal stromal tumours (GIST).

6.5.2 Colorectal Cancer

Response assessment after preoperative treatment in anal and colorectal cancers is to confirm resectability and determine the surgical approach. In patients with complete tumour regression after preoperative treatment, controversial treatment such as deferral from surgery and wait-and-watch approach is now being discussed. Follow-up imaging with MRI for local re-staging and CT for whole body staging is useful. The role of FDG PET is limited for patients with advanced stage disease with hepatic or peritoneal metastases to improve accuracy of re-staging after chemotherapy. FDG-PET is also useful before surgery for liver metastases to exclude extra-hepatic disease.

6.5.3 Hepatocellular Carcinoma

In HCC (Hepatocelluclar Carcinoma) treatment assessment, criteria such as mRECIST and European association of Study of Liver (EASL), which assess changes in tumour vascularization, are more useful than conventional criteria such as WHO or RECIST. Several studies have highlighted the difficulty in using CT to reassess locoregional tumour extension after completion of preoperative neoadjuvant chemo-radiotherapy. CT criteria based on the extent of tumour contact with vessels such as portal vein, hepatic artery and superior mesenteric vein are useful. FDG-PET has a very limited role in this setting.

6.5.4 Pancreatic Cancer

Compared to normal pancreas, most malignant tumours are hypermetabolic. In the context of treatment response, post-chemotherapy-reduced FDG uptake may occur prior to morphological changes and, therefore, PET/CT is more sensitive in assessing response and recurrence and also predicts survival [20]. Studies have also shown that the sensitivity of PET/CT is higher than contrast-enhanced CT for assessing response post-chemoradiation and surgery [20–23].

6.5.5 Lung Cancer

Tumour progression occurs in approximately one third of patients during first-line chemotherapy, therefore, there is a clear need for better techniques to monitor treatment response in order to allow for treatment alternatives and predict outcome [24].

Given the limitations of size-based response criteria, particularly its inability to differentiate benign changes such as consolidation and cavitation from tumour, several studies have reported the valuable role of FDG PET in response assessment to chemotherapy and, therefore, in the prognosis [25]. In a study of patients with advanced NSLCL (Non Small Cell Lung Cancer), FDG PET/CT after one treatment cycle is predictive of

outcome to first-line chemotherapy identifying patients at risk of treatment failure, permitting early switch to a different therapy [26]. A similar study to assess response was undertaken by Weber et al. that included 57 patients after one cycle of treatment and showed a reduction in metabolic activity correlated with end of treatment response [27]. Multiple studies have also found a significant difference in SUVmax pre- and post-treatment in patients who respond to chemo-radiotherapy [28, 29]. Studies have also shown the utility of FDG PET/CT for determining survival outcomes post-treatment [30–32].

In locally advanced lung cancer when considering surgical resection after neoadjuvant chemotherapy, it is vital to confirm nodal status, but the use of FDG PET/CT in re-staging is a controversial issue. While some studies have shown the usefulness of FDG PET/CT post-induction therapy [33, 34], the technique is not accurate enough to influence management with regards to mediastinal nodal involvement [35]. One study showed the false-negative rate of PET/CT was 25% vs 9% on histopathological confirmation with primary mediastinoscopy [36].

Therefore, although FDG PET/CT has an important role in treatment response to chemotherapy in lung cancer, there are still limitations compared to more invasive techniques.

6.5.6 Lymphoma

Residual masses at the end of treatment are frequently seen in lymphoma patients. Response has hitherto been based using morphological criteria with CT as the most commonly used modality in patients at treatment completion. It is difficult on CT alone to assess whether the residual mass represents viable tumour, scar or necrosis. The inclusion of FDG PET/CT has addressed some of the limiting factors of CT with its improved ability to distinguish between viable tumour and necrosis/fibrosis in residual masses after treatment.

Meta-analysis and systematic studies involving large number of patients have showed the pooled sensitivity and specificity for detection of residual disease in HL to be 84% and 90%, respectively. Likewise for NHL (Non Hodgkin's Lymphoma), the pooled sensitivity and specificity were 72% and 100%, respectively [37]. Further studies with FDG PET/CT for response at the end of treatment in early and advanced HL have demonstrated a very high negative and positive predictive value [38, 39].

The usefulness of interim imaging in lymphoma (during active chemotherapy treatment) is being studied both for prognosis and for developing risk-adapted strategies. FDG PET/CT is superior to CT alone in the evaluation of therapeutic response as early as after 1–2 cycles of chemotherapy. There is emerging data reporting the predictive value of interim FDG PET/CT, mostly after two cycles in HL and DLBCL. In HL, interim PET has shown a 2-year PFS (progression free survival) of approximately 95% in PET-negative patients, whereas, it was only about 13% in PET-positive patients for advanced disease treated with initial chemotherapy. Interim PET in DLBCL has a lower predictive value than in HL with 2-year PFS rates of 73%–86% in PET-negative patients and a variable PFS for PET-positive patients, ranging from 18% to 74% [40, 41].

PET/CT is by far the best modality for response assessment in lymphoma with a potential to influence risk-adapted therapy in these patients.

6.5.7 Head and Neck Cancer

In patients with locally advanced head and neck tumours, monitoring of response to neoadjuvant therapy by FDG-PET may lead to significant changes in patient management by accurately differentiating responders from non-responders, and thereby lead to timely alteration in therapeutic strategy [42]. In a large meta-analysis of 51 studies involving 2335 patients, the sensitivity, specificity, positive predictive value (PPV) and NPV of FDG PET/CT for the detection of

residual primary HNSCC were reported to be 94%, 82%, 75% and 95%, respectively [43]. It has also been suggested that early prediction of therapy response using PET/CT in such patients may lead to timely alterations in therapeutic strategy [44, 45].

6.5.8 Breast Cancer

Several early studies have reported that FDG PET/CT may have a role in the evaluation of response to treatment and help differentiate responders from non-responders following first-line chemotherapy, therefore, in the prognosis of breast cancer patients [46, 47]. A meta-analysis to evaluate the accuracy of ^{18}F-FDG PET/CT in predicting the pathological response to neoadjuvant chemotherapy in breast cancer patients showed a pooled sensitivity, specificity and diagnostic odds ratio with 95% confidence intervals of 81.9% (76.0–86.6%), 79.3% (72.1–85.1%) and 17.35 (10.98–27.42), respectively, indicating moderate accuracy in predicting the pathological response [48]. It has been showed that the results for PET/CT depend on breast cancer subtype, indicating good performance in ER-positive and triple-negative tumours, but relatively poor performance in HER2-positive tumours, and hence the variability in results [49].

6.5.9 Other Tumours

PET/CT has also been used in the evaluation of response to chemotherapy in some of the other less commonly occurring tumours such as cholangiosarcoma, testicular, ovarian, cervical cancers, sarcoma and multiple myeloma. But the evidence for its use in these tumours has not been studied systematically and requires further evaluation. In tumours such as these and a few others, a single imaging test may not accurately predict response to treatment, and multimodality imaging tests need to be employed in such situations.

6.6 Conclusion

Conventional imaging modalities rely on changes in size or morphologic characteristics to evaluate tumour response and frequently present a limited diagnostic efficacy in the evaluation of response to oncologic treatments. Further, in the evolution of disease morphological changes appear later and are preceded by functional and molecular alterations. Functional imaging techniques such as PET/CT evaluate specific biomarkers such as vascular, metabolic, biochemical and molecular changes in cancer cells, allowing earlier assessment of response to chemotherapy, and thereby help tailor treatment.

References

1. World Health Organization. WHO handbook for reporting results of cancer treatment: offset publication no. 48. Geneva: World Health Organization; 1979.
2. Miller AB, Hoogstraten B, Staquet M, Winkler A. Reporting results of cancer treatment. Cancer. 1981;47:207–14.
3. Therasse P, et al. New guidelines to evaluate the response to treatment in solid tumors. European Organization for Research and Treatment of Cancer, National Cancer Institute of the United States, National Cancer Institute of Canada. J Natl Cancer Inst. 2000;92(3):205–16.
4. Eisenhauer EA, et al. New response evaluation criteria in solid tumours: revised RECIST guideline (version 1.1). Eur J Cancer. 2009;45(2):228–47.
5. Coche E. Recist and beyond. JBR-BTR. 2013;96(3):167–71.
6. Arizumi T, et al. Comparison of systems for assessment of post-therapeutic response to sorafenib for hepatocellular carcinoma. J Gastroenterol. 2014;49(12):1578–87. https://doi.org/10.1007/s00535-014-0936-0.
7. Llovet JM, et al. Design and endpoints of clinical trials in hepatocellular carcinoma. J Natl Cancer Inst. 2008;100(10):698–711.
8. Choi H, et al. Correlation of computed tomography and positron emission tomography in patients with metastatic gastrointestinal stromal tumor treated at a single institution with imatinib mesylate: proposal of new computed tomography response criteria. J Clin Oncol. 2007;25(13):1753–9.
9. Smith AD, Shah SN, Rini BI, Lieber ML, Remer EM. Morphology, attenuation, size, and structure (MASS) criteria: assessing response and pre-

dicting clinical outcome in metastatic renal cell carcinoma on antiangiogenic targeted therapy. AJR. 2010;194:1470–8.
10. Thie JA. Understanding the standardized uptake value, its methods, and implications for usage. J Nucl Med. 2004;45:1431–4.
11. Young H, Baum R, Cremerius U, et al. Measurement of clinical and subclinical tumour response using F-18-fluorodeoxyglucose and positron emission tomography:review and 1999 EORTC recommendations. Eur J Cancer. 1999;35:1773–82.
12. Juweid ME, Stroobants S, Hoekstra OS, Mottaghy FM, Dietlein M, Guermazi A, et al. Use of positron emission tomography for response assessment of lymphoma: consensus of the imaging Subcommittee of International Harmonization Project in Lymphoma. J Clin Oncol. 2007;25:571–8.
13. Barrington SF, Mikhaeel NG, Kostakoglu L, Meignan M, Hutchings M, Mueller SP, et al. Role of imaging in the staging and response assessment of lymphoma: consensus of the International Conference on Malignant Lymphomas Imaging Working Group. J Clin Oncol. 2014;32:3048–58.
14. Barrington SF, Qian W, Somer EJ, Franceschetto A, Bagni B, Brun E, Almquist H, Loft A, Højgaard L, Federico M, Gallamini A, Smith P, Johnson P, Radford J, O'Doherty MJ. Concordance between four European centres of PET reporting criteria designed for use in multicentre trials in Hodgkin lymphoma. Eur J Nucl Med Mol Imaging. 2010;37(10):1824–33.
15. Wahl RL, Jacene H, Kasamon Y, Lodge MA. From RECIST to PERCIST: evolving considerations for PET response criteria in solid tumors. J Nucl Med. 2009;50(Suppl 1):122S–50S.
16. Martens MH, Lambregts DMJ, Kluza E, et al. Tumor response to treatment: prediction and assessment. Curr Radiol Rep. 2014;2:62.
17. Thomas AL, O'Byrne K, Steward WP. Chemotherapy for upper gastrointestinal tumours. Postgrad Med J. 2000;76:321.
18. National Guideline Alliance (UK). Oesophagogastric cancer assessment and management in adults. London: National Institute for Health and Care Excellence (UK); 2018.
19. Alcindor T, et al. Perioperative chemotherapy for upper gastrointestinal cancer: correlation between response to treatment and outcome. J Clin Oncol. 2012;30(4_Suppl):95. https://doi.org/10.1200/jco.2012.30.4_suppl.95.
20. Cameron K, Golan S, Simpson W, et al. Recurrent pancreatic carcinoma and cholangiocarcinoma: 18F-fluorodeoxyglucose positron emission tomography/computed tomography (PET/CT). Abdom Imaging. 2011;36:463–71.
21. Sperti C, Pasquali C, Chierichetti F, et al. 18-Fluorodeoxyglucose positron emission tomography in predicting survival of patients with pancreatic carcinoma. J Gastrointest Surg. 2003;7:953–9. discussion 959–960.
22. Ruf J, Lopez Hänninen E, Oettle H, et al. Detection of recurrent pancreatic cancer: comparison of FDG-PET with CT/MRI. Pancreatology. 2005;5:266–72.
23. Pery C, Meurette G, Ansquer C, et al. Role and limitations of 18F-FDG positron emission tomography (PET) in the management of patients with pancreatic lesions. Gastroenterol Clin Biol. 2010;34:465–74.
24. Nishino M, Hatabu H, Johnson BE, McLoud TC. State of the art: response assessment in lung cancer in the era of genomic medicine. Radiology. 2014;271:6–27.
25. Delgado Bolton RC, Izarduy LP, Carreras Delgado JL. Positron emission tomography and positron emission tomography/computed tomography in the evaluation of response to chemotherapy. Cancer Chemother Rev. 2008;3(2):77–86.
26. Usmanij EA, Natroshvili T, Timmer-Bonte JNH, Oyen WJG, van der Drift MA, Bussink J, de Geus-Oei L-F. The predictive value of early in-treatment 18F-FDG PET/CT response to chemotherapy in combination with bevacizumab in advanced non-squamous non–small cell lung cancer. J Nucl Med. 2017;58(8):1243–8.
27. Weber WA, Petersen V, Schmidt B, et al. Positron emission tomography in NSCLC: prediction of response to chemotherapy by quantitative assessment of glucose use. J Clin Oncol. 2003;21:2651–7.
28. Bahce I, Vos CG, Dickhoff C, et al. Metabolic activity measured by FDG PET predicts pathological response in locally advanced superior sulcus NSCLC. Lung Cancer. 2014;85:205–12.
29. Yamamoto Y, Nishiyama Y, Monden T, et al. Correlation of FDG-PET findings with histopathology in the assessment of response to induction chemoradiotherapy in non-small cell lung cancer. Eur J Nucl Med Mol Imaging. 2006;33:140–7.
30. Dingemans AM, de Langen AJ, van den Boogaart V, et al. First-line erlotinib and bevacizumab in patients with locally advanced and/or metastatic non-small-cell lung cancer: a phase II study including molecular imaging. Ann Oncol. 2011;22:559–66.
31. Mileshkin L, Hicks RJ, Hughes BG, et al. Changes in 18F-fluorodeoxyglucose and 18F-fluorodeoxythymidine positron emission tomography imaging in patients with non-small cell lung cancer treated with erlotinib. Clin Cancer Res. 2011;17:3304–15.
32. de Langen AJ, van den Boogaart V, Lubberink M, et al. Monitoring response to antiangiogenic therapy in non-small cell lung cancer using imaging markers derived from PET and dynamic contrast-enhanced MRI. J Nucl Med. 2011;52:48–55.
33. Kremer R, Peysakhovich Y, Dan LF, et al. FDG PET/CT for assessing the resectability of NSCLC patients with N2 disease after neoadjuvant therapy. Ann Nucl Med. 2016;30:114–21.
34. De Leyn P, Stroobants S, De Wever W, et al. Prospective comparative study of integrated positron emission tomography-computed tomography scan compared with remediastinoscopy in the assessment of residual mediastinal lymph node disease

after induction chemotherapy for mediastinoscopy-proven stage IIIA-N2 non-small-cell lung cancer: a Leuven Lung Cancer Group Study. J Clin Oncol. 2006;24:3333–9.
35. Stamatis G. Staging of lung cancer: the role of non-invasive, minimally invasive and invasive techniques. Eur Respir J. 2015;46:521–31.
36. Rami-Porta R, Call S. Invasive staging of mediastinal lymph nodes: mediastinoscopy and remediastinoscopy. Thorac Surg Clin. 2012;22:177–89.
37. Zijlstra JM, Lindauer-van der Werf G, Hoekstra OS, Hooft L, Riphagen II. Huijgens PC. 18F-fluorodeoxyglucose positron emission tomography for post-treatment evaluation of malignant lymphoma: a systematic review. Haematologica. 2006;91(4):522–9.
38. AU Barrington SF, Mikhaeel NG, Kostakoglu L, Meignan M, Hutchings M, Müeller SP, Schwartz LH, Zucca E, Fisher RI, Trotman J, Hoekstra OS, Hicks RJ, O'Doherty MJ, Hustinx R, Biggi A, Cheson BDSO. Role of imaging in the staging and response assessment of lymphoma: consensus of the International Conference on Malignant Lymphomas Imaging Working Group. J Clin Oncol. 2014;32(27):3048–58.
39. Zanoni L, Cerci JJ, Fanti S. Use of PET-CT to assess response to therapy in lymphoma. Q J Nucl Med Mol Imaging. 2011;55:533–47.
40. Mikhaeel NG, Hutchings M, Fields PA, O'Doherty MJ, Timothy AR. FDG-PET after two to three cycles of chemotherapy predicts progression-free and overall survival in high-grade non-Hodgkin lymphoma. Ann Oncol. 2005 Sep;16(9):1514–23.
41. Terasawa T, Dahabreh IJ, Nihashi T, et al. Fluorine-18-fluorodeoxyglucose positron emission tomography in response assessment before high-dose chemotherapy for lymphoma: a systematic review and meta-analysis. Oncologist. 2010;15:750–9.
42. Kostakoglu L. Goldsmith SJ. PET in the assessment of therapy response in patients with carcinoma of the head and neck and of the esophagus. J Nucl Med. 2004;45:56–68.
43. Gupta T, Master Z, Kannan S, et al. Diagnostic performance of post-treatment FDG PET or FDG PET/CT imaging in head and neck cancer: a systematic review and meta-analysis. Eur J Nucl Med Mol Imaging. 2011;38:2083–95.
44. Abgral R, Le Roux P-Y, Keromnes N, Rousset J, Valette G, Gouders D, et al. Early prediction of survival following induction chemotherapy with DCF (docetaxel, cisplatin, 5-fluorouracil) using FDG PET/CT imaging in patients with locally advanced head and neck squamous cell carcinoma. Eur J Nucl Med Mol Imaging. 2012;39(12):1839–47.
45. Yoon DH, Cho Y, Kim SY, Nam SY, Choi SH, Roh JL, et al. Usefulness of interim FDG-PET after induction chemotherapy in patients with locally advanced squamous cell carcinoma of the head and neck receiving sequential induction chemotherapy followed by concurrent chemoradiotherapy. Int J Radiat Oncol Biol Phys. 2011;81(1):118–25.
46. Jansson T, Westlin JE, Ahlstrom H, et al. Positron emission tomography studies in patients with locally advanced and/or metastatic breast cancer: a method for early therapy evaluation? J Clin Oncol. 1995;13:1470–7.
47. Schelling M, Avril N, Nahrig J, et al. Positron emission tomography using 18F-fluorodeoxyglucose for monitoring primary chemotherapy in breast cancer. J Clin Oncol. 2000;18:1689–95.
48. Tian F, Shen G, Deng Y, Diao W, Jia Z. The accuracy of ^{18}F-FDG PET/CT in predicting the pathological response to neoadjuvant chemotherapy in patients with breast cancer: a meta-analysis and systematic review. Eur Radiol. 2017 Nov;27(11):4786–96.
49. Koolen BB, Pengel KE, Wesseling J, Vogel WV, Vrancken Peeters MJ, Vincent AD, et al. FDG PET/CT during neoadjuvant chemotherapy may predict response in ER-positive/HER2-negative and triple negative, but not in HER2-positive breast cancer. Breast. 2013 Oct;22(5):691–7.

7 Conventional Radiological Techniques and PET-CT in Treatment Response Evaluation in Post-Radiotherapy Setting

Stefan Vöö, Irfan Kayani, and Jamshed Bomanji

7.1 Introduction

In most Western countries, radiotherapy forms part of 40% of oncology treatment pathways and is the mainstay of 19% of curative treatment [1]. Intensity-modulated radiotherapy has become the standard of care for multiple malignancies by virtue of the ability to deliver highly conformal doses while minimizing damage to adjacent tissues [2].

Accurate response assessment informs future treatment decisions and in some situations guides the need for potentially curative surgical salvage. Early recognition of treatment success or failure can, therefore, impact on patient survival. Traditionally, this assessment relied upon anatomical measurement of disease, such as CT evaluation using Response Evaluation Criteria in Solid Tumors (RECIST). However, such measurements are of inherently limited value following radiotherapy, as residual masses/tissue abnormalities are common posttreatment and do not necessarily infer the presence of viable clonogenic tumor cells. For example, in head and neck cancer, residual lymph node masses are well recognized following radiotherapy and, particularly with human papillomavirus-related disease, can continue to regress many months following completion of treatment [3]. Anatomic imaging assessments performed with CT or MR imaging are usually less capable of depicting small residual disease deposits. In addition, because surgery, chemotherapy, and radiotherapy produce edema, hyperemia, scarring, and loss of facial planes, differentiation of residual or recurrent disease from posttherapy changes using conventional imaging techniques including CT and MRI is particularly challenging. Moreover, novel therapeutic agents may be cytostatic instead of cytoreductive in which case treatment response may not be reflected in a decrease in tumor size [4].

The challenge of determining the presence or absence of viable tumor within residual masses following radiotherapy provides a powerful rationale for the incorporation of functional imaging into response assessment protocols.

PET/CT employs radioactive tracers to assess molecular characteristics of tissues. Malignancies have distinctive molecular profiles, which differ compared with surrounding normal tissue and may, therefore, be exploited by PET/CT imaging with appropriate tracers [4].

S. Vöö (✉)
Institute of Nuclear Medicine, University College London Hospital, University College London Hospitals NHS Trust, London, UK

Biomedical Research Centre, Inflammation, Immunity and Immunotherapeutics, University College London Hospital, London, UK
e-mail: stefan.voo@nhs.net

I. Kayani · J. Bomanji
Institute of Nuclear Medicine, University College London Hospital, University College London Hospitals NHS Trust, London, UK

S. Fanti et al. (eds.), *Atlas of Clinical PET-CT in Treatment Response Evaluation in Oncology*,
https://doi.org/10.1007/978-3-030-68858-5_7

PET/CT in radiotherapy response assessment is useful for several reasons. Firstly, molecular response to radiotherapy may precede anatomical response, and PET/CT may allow a more accurate assessment at an earlier stage than standard cross-sectional imaging. Secondly, use of specific tracers allows a more reliable discrimination of tumor from treatment-related inflammation or fibrosis. Thirdly, tumors respond heterogeneously during radiotherapy [5]. Although this may not be apparent on anatomical imaging, by using an appropriate molecular biomarker, which changes at an early stage and correlates with response, this variability may be demonstrated with PET/CT and the treatment adapted accordingly [4].

PET/CT has potential utility at different stages of radiotherapy response. Firstly, a growing area of research focuses on employing PET/CT during radiotherapy; this can facilitate an adaptive individualized approach to treatment with potential for escalation or de-escalation strategies depending on the quality/speed of on-treatment response or switching of treatment approach, for example, to surgery in the event of an absent early response to radiotherapy. Secondly, imaging can be used after radiotherapy to stratify patients who are responding and conversely identify nonresponders and discriminate this from treatment effects, allowing for early aggressive treatment of persistent or progressive disease [4].

7.2 Functional Imaging for Disease Response Assessment to Radiotherapy

The use of functional MR imaging techniques to assess biomarkers of early response has also been proposed. The use of apparent diffusion coefficient (ADC) values from diffusion-weighted MR imaging has been reported to result in a lower false-positive rate for both primary and nodal disease response than the use of uptake at ^{18}F-labeled Fluorodeoxyglucose (FDG) PET [6].

Overall, functional imaging appears to be a promising addition to clinical examination and anatomic imaging for assessing the response of head and neck squamous cell carcinoma (SCC) tumors to radiation therapy. This is particularly true in the clinical scenario of residual masses, where anatomic imaging techniques are inaccurate. The use of FDG PET/CT is now supported by considerable data [7]. A role also may be established for other PET- and MR imaging-based techniques.

7.2.1 Functional, Metabolic PET Imaging

Various PET tracers are available for imaging cellular processes such as metabolism, proliferation, hypoxia, and cell membrane synthesis. PET tracers, along with advances in understanding of molecular cancer biology, can help individualize therapeutic approaches.

7.2.1.1 Glucose Metabolism

The use of FDG PET/CT to demonstrate altered cellular glucose metabolism is the most widely used application of molecular imaging. Complementary anatomical and functional information facilitates an accurate noninvasive assessment of surrogate biomarkers of disease activity. FDG PET has an emerging role as a response assessment tool in treatment response to radiotherapy. FDG PET/CT is a useful modality for assessing treatment response because it is able to evaluate the metabolic activity as a marker of tumor cell viability, overcoming the known limitations of morphologic imaging modalities.

FDG PET/CT is recommended by the NCCN guidelines for therapy assessment after chemoradiotherapy (CRT) or radiotherapy (RT). For example, in patients with head and neck SCCs, the pooled sensitivity, specificity, positive predictive value, and negative predictive value of PET/CT for assessing disease response were 87.7%, 87.8%, 75.7%, and 94.3%, according to the results of two meta-analyses [7, 8]. PET had a higher diagnostic accuracy if performed more than 12 weeks after the completion of treatment. The high negative predictive value of a finding of complete metabolic response can be used to guide management decisions. In a study of FDG PET-based response assessment performed by Porceddu et al. [9], 41 patients with PET-negative residual nodal masses were observed

without subsequent nodal failure. Therefore, a complete metabolic response at PET can be used to avoid unnecessary surgery to residual masses.

7.2.1.2 Tumor Hypoxia

Hypoxia is an established indicator of poor prognosis for patients with different cancers [10]. It leads to radiation resistance in tumor cells by preventing irreversible damage to cell deoxyribonucleic acid (DNA) by free radicals induced by ionizing radiation; oxygen is needed for the production of free radicals. Cell DNA, thus, undergoes repair and tumor cells survive [11]. The critical partial pressure of oxygen (pO_2) threshold, below which solid tumors show resistance to radiation therapy, is approximately 10–15 mmHg [10]. The amount of radiation needed to achieve cell kill in hypoxic conditions is three times that needed in normoxic conditions [6]. There is limited evidence of improved treatment outcomes with a reduction in hypoxia [12], which can be achieved by adding oxygen-mimicking agents to radiation therapy or by giving radiation therapy along with an oxygen-enhanced gas mixture such as carbogen (a mixture consisting of 95% oxygen and 5% carbon dioxide) [10].

Tumor hypoxia can be assessed by a number of invasive techniques, including polarographic oxygen electrodes and immunohistochemical staining of pathologic specimens to allow detection of hypoxia-specific markers. In addition, there are a number of PET tracers available that allow noninvasive visualization of hypoxia. At present, there is no consensus on which hypoxia-specific agent is most effective for PET; each of these agents has its advantages and disadvantages and may be better suited for evaluating some tumor types than others.

FMISO is the most extensively investigated PET imaging agent and has been used for the assessment of head and neck SCCs [13–16]. Studies have shown that uptake of FMISO is not necessarily correlated with uptake of FDG [15, 16] and, thus, that the two agents represent different tumor properties. However, high uptake of FMISO before radiation therapy can be predictive of local-regional treatment failure, and thus indicative of a poor prognosis. However, further work is needed to investigate the normal variation in FMISO uptake and tumor oxygenation kinetics before therapy, as well as changes in the hypoxic subvolume during therapy, before FMISO imaging can be clinically used to guide hypoxia-mediated intensity modulated radiation therapy (IMRT) [17, 18].

^{18}F-fluoroazomycin arabinoside (FAZA) is a hypoxia-specific PET agent that clears the blood more rapidly than FMISO and, as a result, produces a higher target-to-background signal ratio [19]. Fluorine ^{18}F-erythronitroimidazole (FETNIM) is theoretically a more potent indicator of hypoxia than FMISO, owing to its greater hydrophilia and better pharmacokinetics [20]. FAZA and FETNIM both appear to be promising hypoxia-specific radiotracers, but further studies of these agents are needed, especially in direct comparison with FMISO.

Radioactive copper-labeled diacetyl-bis-(N4-methylthiosemicarbazone) (ATSM) is a different type of hypoxia-specific PET tracer. ATSM is a neutral lipophilic compound that can permeate cell membranes. In hypoxic conditions, ATSM molecules are reduced and negatively charged, causing the agent to accumulate selectively in hypoxic cells while it washes out rapidly from normoxic cells. ATSM clearance through the blood leads to a high tumor-to-background signal ratio on PET images [21]. Pilot studies of the effectiveness of ATSM for evaluating different tumors showed a significant difference in the uptake of this tracer between patients with residual or recurrent tumor and those without residual or recurrent tumor; by contrast, there was no significant difference in FDG uptake between the two patient groups [22]. The disparity in uptake between the two tracers suggests that ATSM may be more useful for predicting early tumor response to chemoradiation therapy.

7.2.1.3 Tumor Cell Proliferation

Radiation therapy and chemotherapy can lead to a rapid decrease in the rate of cellular proliferation in responding tumors, a change that usually precedes a decrease in tumor size [23]. By contrast, accelerated tumor cell repopulation is an important indicator of underlying radiation resistance and, hence, treatment failure [11]. Imaging

strategies for identifying tumor cell repopulation as part of the early response assessment and for delineating areas of high cell turnover as targets for dose escalation are, therefore, desirable.

^{18}F-labeled FLT PET is the functional imaging technique most widely used to assess cellular proliferation [24]. FLT, unlike FDG, is taken up only by actively dividing cells, not by surrounding inflammatory cells, and thus allows specific detection of cellular division. Changes in the intensity of FLT uptake can be used to monitor cellular response to treatment even before there are visible changes in tumor volume [11, 25].

Promising results have been reported from studies in which FLT was used to assess early disease response to therapy in patients with head and neck SCCs, with good reproducibility of SUV measurements and changes in uptake preceding changes in tumor volume [25–27]. The ability to delineate areas of high cellular proliferation means that dose escalation to these areas is technically feasible [25].

However, definitive histologic validation for this use of FLT is lacking. Linecker et al. found no correlation between FLT uptake and the Ki-67 index, an endogenous marker of cellular proliferation in a study of 19 patients with head and neck SCCs [28]. FLT does not allow reliable differentiation between benignity and malignancy of abnormal cervical lymph nodes because its uptake by the germinal centers of reactive lymph nodes leads to a low positive predictive value [29]. Further research will be needed before a role may be established for FLT in early treatment response assessment and adaptive radiation therapy planning.

7.2.1.4 Apoptosis

Apoptosis, also known as programmed cell death, is an important mechanism by which chemotherapy and radiation therapy regimens induce tumor cell death. Radiation resistance and subsequent treatment failure may result from mutations that lead to deregulated cellular proliferation and suppression of apoptotic mechanisms [30]. Noninvasive imaging of apoptosis, therefore, has the potential to allow early monitoring of response to therapy. The use of technetium 99m (^{99m}Tc)–labeled annexin V, a protein that binds to a major phospholipid constituent of cell membranes, has been investigated for imaging apoptosis in various malignancies, including head and neck SCCs [31].

The difficulty of radiolabeling annexin V with fluorine 18 has led to the development of other apoptosis-specific PET tracers. ^{18}F-labeled compound 2-[5-fluoro-pentyl]-2-methyl-malonic acid (ML-10) is one of a set of novel small-molecule probes designed to allow visualization of the unique complex of apoptosis-related cellular alterations [32]. This compound, the first apoptosis-specific PET tracer to undergo clinical testing, produced promising results in several small clinical trials in patients with acute ischemic stroke or metastases to the brain after whole-brain radiation therapy, in whom it allowed early detection of response to treatment [32]. ML-10 is also useful for differentiating between apoptotic and necrotic cells.

7.2.1.5 Amino Acid Transport and Protein Synthesis

Carbon 11 (^{11}C)-labeled methionine (MET) is a PET tracer used to image amino acid transport and accelerated protein synthesis in malignant tissue [33]. MET allows effective visualization of different cancers but not differentiation of the histologic grade [34]. Lindholm et al. showed a good correlation between FDG and MET, with similar sensitivities and specificities for tumor detection [35].

A study evaluating early treatment response in patients with head and neck SCCs showed a greater decline in uptake at tumor sites with histology-confirmed complete response in comparison with sites of residual tumor tissue after radiation therapy [36]. In another study performed in patients with head and neck SCCs, an early decrease in MET uptake was reported to correlate with an end-of-treatment tumor volume reduction seen at MR imaging, a finding that suggested that MET could be used for early treatment adaptation [37]. By contrast, Nuutinen et al. observed a substantial early decline in MET uptake after radiation therapy in 15 patients with head and neck SCCs but found that the rate of

decrease in tracer uptake was comparable between patients with disease recurrence and those with preserved local control [38]. At present, there is no clear role for the use of MET in the imaging of head and neck cancers.

^{18}F-labeled fluoroethyltyrosine (FET) is another amino acid analog that is taken up by tumor cells through amino acid transport systems [39]. High diagnostic accuracies have been achieved with the use of FET in patients with brain tumors, but the tracer has lower sensitivities (64%–75%) in comparison with FDG (89%–95%) in the evaluation of head and neck SCCs [40–42]. Although its specificity (90%–100%) is higher than that of FDG (50%–79%), the consensus is that FET is not a suitable replacement for FDG in the initial assessment of different malignancies, owing to its poorer sensitivity. It may, however, have a role in helping differentiate between residual tumor tissue and inflammatory tissue after therapy.

7.2.1.6 Cell Membrane Synthesis

Choline is a ubiquitous substance that is incorporated into phospholipids, which are the major constituent of cell membrane synthesis [43]. Up until now, there is a paucity of data on the use of radiolabeled-choline in malignancies and response to treatment. In an initial feasibility study on 45 patients, C-labeled choline was found to be as effective as FDG for detecting malignant head and neck tumors at PET [44]. However, the usefulness of this tracer for assessing posttreatment response requires further evaluation; in one study, choline PET/CT was not found to be superior to FDG PET/CT for the detection of recurrent disease [45].

7.2.1.7 Epidermal Growth Factor Receptor Status

The status of epidermal growth factor receptor (EGFR) is an important tumor microenvironment factor, and blockade of EGFR by cetuximab increases the effectiveness of radiation therapy [46]. EGFR activation causes tumor cell proliferation, apoptosis, and production of hypoxia-related proteins, all of which can cause resistance to chemotherapy and radiation therapy [47]. Because PET can be used to assess both EGFR status and cetuximab uptake, this imaging modality may be useful for treatment selection and treatment response assessment [48].

7.2.2 Functional MR Imaging Techniques

Advanced MR imaging techniques such as dynamic contrast-enhanced imaging, diffusion-weighted imaging, blood oxygenation level–dependent (BOLD) imaging, and spectroscopy hold the promise of providing functional information about disease [49]. These techniques can be used for planning, monitoring, and assessing the results of radiation therapy in patients with head and neck SCCs [50].

7.2.2.1 Dynamic Contrast-Enhanced MR Imaging

Dynamic contrast-enhanced MR imaging is a noninvasive technique that helps characterize the microvasculature, thereby providing markers specific to perfusion, permeability of blood vessels, and the volume of extracellular space. Abnormal microvessels seen at dynamic contrast-enhanced MR imaging themselves may be a marker of hypoxia: Tumor angiogenesis is associated with chaotic vessel formation and incompetent arteriovenous shunts, which lead to less effective perfusion and a more hypoxic environment than exists in normal tissues [51].

The identification of hypoxic tumors allows hypoxia-modifying therapy, treatment escalation, or even primary surgery [52]. Newbold et al. demonstrated a statistically significant correlation between various dynamic contrast-enhanced MR imaging parameters, particularly K_{trans} (which represents the permeability of blood vessels) and pimonidazole staining (an exogenous marker for hypoxia) [53]. The appearance of head and neck SCCs at dynamic contrast-enhanced MR imaging, for example, has been used to successfully predict treatment response to chemoradiation therapy in the tumors [54].

7.2.2.2 Diffusion-Weighted MR Imaging

Diffusion-weighted MR imaging is a noninvasive imaging technique that facilitates tissue characterization on the basis of the molecular motion of water molecules. Diffusion is quantified by using the ADC, which is inversely correlated with cellularity and is a potential biomarker for apoptosis [55]. The increased density of cells within malignant lymph nodes reduces their ADC at diffusion-weighted MR imaging. Studies have shown that diffusion-weighted MR imaging can be useful for differentiating small malignant lymph nodes from nonmalignant ones [56, 57].

In a study on 33 patients with head and neck SCCs, change in ADC was used as a marker of tumor response 1 week after the commencement of chemoradiation therapy [58]. Change in tumor ADC after 1 week of treatment had a high sensitivity and specificity for identifying patients who would have a partial or complete response to treatment. Dirix et al. evaluated the usefulness of diffusion-weighted MR imaging for radiation therapy planning and found that patients with local-regional recurrence had lower ADC values within the tumor after 4 weeks of radiation therapy [59]. This finding suggests that diffusion-weighted imaging would be useful for identifying patients who might benefit from adaptive escalation of the radiation dose.

7.2.2.3 BOLD Imaging

BOLD imaging, also known as intrinsic susceptibility-weighted MR imaging, is a functional imaging technique that is primarily used to evaluate brain activity triggered by exercise or other external stimuli. In recent years, it also has been used as a hypoxia-specific imaging technique.

Contrast at BOLD imaging depends on the quantity of paramagnetic deoxyhemoglobin within red blood cells, which generates an MR signal based on the transverse relaxation rate (i.e., R2*) [60]. This imaging technique was used to assess reoxygenation of tumors while patients breathed oxygen-enriched gas (i.e., carbogen) [61]. In another study, a heterogeneous response in different tumors during carbogen breathing at BOLD MR imaging permitted the identification of patients who would be likely to benefit from carbogen-induced sensitization to radiation [62]. Hypoxic tumors with high blood flow have a high R2* and are more likely to respond to carbogen for radiation sensitization. Conversely, in small animal studies, hypoxic tumors with low blood volumes were found to have low R2* values and to be less likely to respond to carbogen [63].

7.2.2.4 MR Spectroscopy

MR spectroscopy allows noninvasive molecular imaging of cellular metabolism. Both phosphorus 31 MR spectroscopy and proton (hydrogen 1) MR spectroscopy have been studied extensively. An early study of proton MR spectroscopy performed by Mukherji et al. demonstrated a qualitatively consistent pattern between in vitro and in vivo metabolic profiles of different carcinomas [64]. Increased choline-to-creatine ratios and consistently narrow lipid resonances were noted in spectral waveforms from in vitro and in vivo MR spectroscopy. The technique is potentially useful for differentiating tumors from benign abnormalities, and the choline-to-creatine ratio may be useful in monitoring for response to treatment. In addition, MR spectroscopy can be used to identify certain amino acids in tumors that are not detected in normal tissues, findings that may have prognostic implications, and may lead to changes in therapy [65]. However, Le et al. investigated the usefulness of in vivo lactate resonances at MR spectroscopy for assessing cervical lymph nodes in patients with stage IV head and neck SCCs and reported that these measurements do not correlate with either tumor pO_2 or treatment outcome [66].

7.2.3 Functional Imaging with Perfusion CT

Perfusion CT, or dynamic contrast-enhanced CT, relies on the passage of iodinated contrast material through a region of interest to produce changes in attenuation, which may be used as markers of microvascular blood flow [67]. A kinetic model analysis of these changes in attenu-

ation allows the derivation of several physiologic parameters, including blood flow (BF) or perfusion, blood volume (BV), mean transit time (MTT), and permeability.

CT perfusion has been studied in cancer patients for the diagnosis and characterization of disease and the prognostication and evaluation of its response to treatment. The development of new blood vessels (i.e., neoangiogenesis), an adaptive response to hypoxia within the tumor, is an indirect marker that is depicted on perfusion CT images as an increase in tumor perfusion, BV, MTT, permeability, or a combination thereof. Gandhi et al. showed that BF, BV, and permeability were all increased, whereas MTT was reduced, in tumors compared with surrounding normal structures [68]. In another study, tumors that did not respond to CRT were found to have had significantly lower baseline BF and BV values [69]. In a larger study, in which tumor response to chemoradiation therapy was assessed over 4 years of follow-up, findings were similar, with significantly lower baseline BF and permeability in patients with local-regional treatment failure [70]. The results of these studies support the hypothesis that tumors with low perfusion have greater levels of hypoxia and, therefore, exhibit more resistance to treatment.

7.2.4 Emerging Integrated Hybrid Imaging Techniques

7.2.4.1 Integrated PET/CT Perfusion Imaging

The combined use of PET and CT to determine the relationship between the metabolic status of tumors and their perfusion shows promise [71–73]. Further understanding of the multitude of hypoxia-driven adaptive responses and their relations to tumor perfusion and aerobic and anaerobic glycolysis is required before more extensive clinical application of this technique can be considered.

7.2.4.2 Integrated PET-MR Imaging

Responding to the global success of PET/CT, commercial scanner manufacturers brought the first integrated PET-MR imaging systems to market in 2011. This newly developed technology offers potential advantages over PET/CT, including reduced radiation exposure, superior soft-tissue contrast resolution, and the ability to acquire functional PET and MR imaging data simultaneously, and thus facilitates a spatially and temporally correlated multiparametric analysis of PET and MR functional biomarkers. Although this technology remains in its infancy, early clinical experience has shown that it may have great promise [74].

7.3 Assessment of Treatment Response After Radiotherapy

There is great interest in surrogate metrics for survival after investigational cancer treatments, such as response rate, time to tumor progression, or progression-free survival [75]. Changes in tumor size after treatment are often, but not invariably, related to duration of survival. A variety of approaches to measuring response rate have been developed, beginning with the original reports by Moertel on physical examination in 1976 and continuing to the subsequent World Health Organization (WHO) criteria (1979) and RECIST 1.1 (2009) [76–78]. Response rate typically refers to how often a tumor shrinks anatomically and has been defined in several ways. Not uncommonly, complete response, partial response, stable disease, and progressive disease are defined as in the WHO and RECIST criteria (Tables 7.1 and 7.2) [78].

Response rates must be viewed with some caution when one is trying to predict outcomes in newer cancer therapies that may be more cytostatic than cytocidal. With such newer treatments, lack of progression may be associated with a good improvement in outcome, even in the absence of major shrinkage of tumors as evidenced by partial response or complete response [80]. To determine lack of progression by changes in tumor size requires regular and systematic assessments of tumor burden. The newer PET metrics may be more informative [81].

Table 7.1 Comparison of WHO response criteria and RECIST

Characteristic	WHO	RECIST	RECIST v1.1
Measurability of lesion at baseline	1. Measurable, bidimensional[a] (product of LD and greatest perpendicular diameter)	1. Measurable, unidimensional (LD only: Size with conventional techniques ≥20 mm, with spiral CT ≥10 mm)	1. Measurable, unidimensional (LD only: Size with conventional techniques ≥20 mm, with spiral CT ≥10 mm; nodes: Target short axis ± 15 mm, nontarget 10–15 mm nodes, normal <10 mm)
	2. Nonmeasurable/evaluable (e.g., lymphangitic pulmonary metastases, abdominal masses)	2. Nonmeasurable: All other lesions, including small lesions; evaluable is not recommended	2. Nonmeasurable: All other lesions, including small lesions; evaluable is not recommended
Objective response	1. Measurable disease (change in sum of products of the LD and greatest perpendicular diameters, no maximal number of lesions specified): CR, disappearance of all known disease, confirmed at ≥4 weeks; PR, ≥50% decrease from baseline, confirmed at ≥4 weeks; PD, ≥25% increase of one or more lesions or appearance of new lesions; NC, neither PR nor PD criteria met	1. Target lesions (change in sum of LD, maximum of five per organ up to ten total [more than one organ]): CR, disappearance of all target lesions, confirmed at ≥4 weeks; PR, ≥30% decrease from baseline, confirmed at 4 weeks; PD, ≥20% increase over smallest sum observed or appearance of new lesions; SD, neither PR nor PD criteria met	1. Target lesions (change in sum of LDs, maximum of two per organ up to five total [more than one organ]): CR, disappearance of all target lesions, confirmed at ≥4 weeks; PR, ≥30% decrease from baseline, confirmed at 4 weeks; PD, ≥20% increase over smallest sum observed and overall 5 mm net increase or appearance of new lesions; SD, neither PR nor PD criteria met
	2. Nonmeasurable disease: CR, disappearance of all known disease, confirmed at ≥4 weeks; PR, estimated decrease of ≥50%, confirmed at 4 weeks; PD, estimated increase of ≥25% in existent lesions or new lesions; NC, neither PR nor PD criteria met	2. Nontarget lesions: CR, disappearance of all nontarget lesions and normalization of tumor markers, confirmed at ≥4 weeks; PD, unequivocal progression of nontarget lesions or appearance of new lesions; non-PD, persistence of one or more nontarget lesions or tumor markers above normal limits	2. Nontarget lesions: CR, disappearance of all nontarget lesions and normalization of tumor markers, confirmed at ≥4 weeks; PD, unequivocal progression of nontarget lesions or appearance of new lesions; non-PD: Persistence of one or more nontarget lesions or tumor markers above normal limits; PD must be "unequivocal" in nontarget lesions (e.g., 75% increase in volume); PD can also be new "positive PET" scan with confirmed anatomic progression. Stably positive PET is not PD if it corresponds to anatomic non-PD
Overall response	1. Best response is recorded in measurable disease	1. Best response is recorded in measurable disease from treatment start to disease progression or recurrence	1. Best response is recorded in measurable disease from treatment start to disease progression or recurrence

Table 7.1 (continued)

Characteristic	WHO	RECIST	RECIST v1.1
	2. NC in nonmeasurable lesions will reduce CR in measurable lesions to overall PR	2. Non-PD in nontarget lesions will reduce CR in target lesions to overall PR	2. Non-PD in nontarget lesions will reduce CR in target lesions to overall PR
	3. NC in nonmeasurable lesions will not reduce PR in measurable lesions	3. Non-PD in nontarget lesions will not reduce PR in target lesions	3. Non-PD in nontarget lesions will not reduce PR in target lesions
		4. Unequivocal new lesions are PD, regardless of response in target and nontarget lesions	4. Unequivocal new lesions are PD, regardless of response in target and nontarget lesions
Duration of response	1. CR: From date CR criteria are first met to date PD is first noted	1. Overall CR: From date CR criteria are first met to date recurrent disease is first noted	1. Overall CR: From date CR criteria are first met to date recurrent disease is first noted
	2. Overall response: From date of treatment start to date PD is first noted	2. Overall response: From date CR or PR criteria are first met (whichever status came first) to date recurrent disease is first noted	2. Overall response: From date CR or PR criteria are first met (whichever status came first) to date recurrent disease is first noted
	3. In patients who achieve only PR, only period of overall response should be recorded	3. SD: From date of treatment start to date PD is first noted	3. SD: From date of treatment start to date PD is first noted

LD longest diameter, *CR* complete response, *PR* partial response, *PD* progressive disease, *SD* stable disease, *NC* no change

[a]Lesions that can be measured only unidimensionally are considered measurable (e.g., mediastinal adenopathy or malignant hepatomegaly)

Table 7.2 Time point response: patients with target (±nontarget) disease (RECIST 1.1) [79]

Target lesions	Nontarget lesions	New lesions	Overall response
CR	CR	No	CR
CR	Non-CR/non-PD	No	PR
CR	Not evaluated	No	PR
PR	Non-PD or not all evaluated	No	PR
SD	Non-PD or not all evaluated	No	SD
Not all evaluated	Non-PD	No	NE
PD	Any	Yes or no	PD
Any	PD	Yes or no	PD
Any	Any	Yes	PD

CR complete response, *PR* partial response, *SD* stable disease, *NE* not evaluable, *PD* progressive disease

Surrogate end points for survival should provide earlier, hopefully correct, answers about the efficacy of treatment and should allow better decisions on whether a drug should be advanced from early phase I to phase II or III trials. Until now, for drug development and regulatory approval purposes, indices of efficacy of treatment of solid tumors have been based solely on systematic assessments of tumor size, including the WHO, RECIST, and International Workshop Criteria (IWC) for lymphoma. However, for many years, there has been evidence that nuclear medicine imaging techniques could provide unique, biologically relevant, and prognostically important information unavailable through anatomic imaging [82].

Quantitative FDG PET/CT was introduced for the early sequential monitoring of tumor response of breast cancer in 1993 [83]. Since then, there

has been growing interest in using FDG PET/CT to quickly assess whether a tumor is—or is not—responding to therapy [83]. In the initial report, women with newly diagnosed breast cancer had a rapid and significant decline in standardized uptake value (SUV), influx rate for FDG determined by Patlak analysis and estimated phosphorylation rate of FDG to FDG-6 phosphate within 8 days of the start of effective treatment. These parameters continued to decline with each progressive treatment in the responding patients, antedating changes in tumor size. By contrast, the nonresponding patients did not have a significant decline in their SUV. Since that report, there have been many others in a wide range of tumors [84, 85]. Abundant data now exist that PET is a useful tool for response assessment in a variety of diseases, at the end of treatment, at mid treatment, and when performed soon after treatment is initiated. Quantitative nonanatomic imaging approaches can be used as a biomarker of cancer response to predict or assess the efficacy of treatments [86–88]. PET with FDG appears, thus, to be one of the most powerful biomarkers introduced to date for clinical trials and for individual patients.

7.3.1 Anatomic Response Criteria (WHO, RECIST)

7.3.1.1 WHO Criteria

The proposed WHO methods included determining the product of the bidimensional measurement of tumors (i.e., greatest perpendicular dimensions), summing these dimensions over all tumors, and then categorizing changes in these summed products as follows: complete response—tumor has disappeared for at least 4 weeks; partial response—50% or greater reduction in sum of tumor size products from baseline confirmed at 4 weeks; no change—neither partial response nor complete response nor progressive disease; and progressive disease—at least a 25% increase in tumor size in one or more lesions, with no complete response, partial response, or stable disease documented before increase in size, or development of new tumor sites [82].

The WHO criteria is not explicit on such factors as how many tumor foci should be measured, how small a lesion could be measured, and how progression should be defined. Thus, despite efforts at standardization, the WHO criteria do not fully standardize response assessment. The WHO criteria are still in use in some trials and are the criteria used to define clinical response rates in many trials from the past two decades—which are important reference studies. Although not as commonly used at present, familiarity with the WHO response criteria is essential for comparison with more recent studies using RECIST, especially as relates to the issue of when tumors progress (Table 7.1) [82].

7.3.1.2 RECIST v1.1

The RECIST group, which included representatives from, among others, the EORTC, the National Cancer Institute (NCI), the National Cancer Research Network, and industry reported response criteria for solid tumors, RECIST v1.1 [79].

RECIST v1.1 requires that:

- A maximum of five target lesions, with a maximum of two per organ with a longest diameter of at least 10 mm.
- In lymph nodes, the short axis rather than the long axis should be measured, with normal nodes measuring <10 mm, nontarget nodes ≥10 mm but <15 mm and target nodes ≥15 mm.
- Osteolytic lesions with a soft tissue component and cystic tumors may serve as target lesions (Table 7.1).

Additionally, within RECIST v1.1, there are guidelines for reporting findings of lesions that are too small to measure and for measuring lesions that appear to have fragmented or coalesced at follow-up imaging [78].

The RECIST categories for response include (Table 7.2):

- Complete response (CR)—disappearance of all tumor foci for at least 4 weeks.
- Partial response (PR)—a decline of at least 30% in tumor diameters for at least 4 weeks.
- Stable disease (SD)—neither partial response nor progressive disease.
- Progressive disease (PD)—at least a 20% increase in the sum of all tumor diameters from the lowest tumor size. Additionally, an augmentation of the criteria defining progressive disease or target lesions was introduced in RECIST v1.1 to not only include a ≥20% increase in the sum of the longest diameter (SLD) from the nadir, but also a ≥5 mm absolute increase in the SLD.

PD of nontarget lesions can only be applied if the increase in nontarget lesions is representative of change in overall tumor burden. RECIST v1.1 has the inclusion of PET findings among the indicators of disease response [78].

Thus, essential elements within structured reports in oncologic imaging could include: (1) the identification with appropriate terminology of target lesion (their localization, size [two dimensions for primary lesions and for nodal disease if for lymphoma, long axis for metastases, and short axis for nodal disease for solid tumors]), (2) nonmeasurable and (3) new disease.

Although these anatomic criteria may appear to be arcane, the RECIST 1.1 criteria are used in virtually every clinical trial of new solid tumor therapeutics, as response is essentially always measured. Further, regulatory agencies have accepted RECIST as the de facto standard in response assessment for clinical trials in many countries. Familiarity with the implications of trials in which response is measured using the WHO, RECIST, and RECIST v1.1 criteria is essential, as they are not identical and do not produce identical results. Inclusion of the RECIST information in the reports will minimize errors in response allocation and, thus potential patient harm, while at the same time can be helpful for minimizing secondary reviews of examinations should patients subsequently enter into clinical trials [78].

7.3.1.3 Limitations of Anatomic Response Criteria

There is increasing awareness that anatomical approaches based on measurements of tumor size such as RECIST have significant limitations including the presence of tumors that cannot be measured, poor measurement reproducibility and mass lesions of unknown activity that persist following therapy, reducing intrinsically continuous data on tumor size, and tumor response to a series of four bins in response. Faced with these limitations, more sophisticated measurements (including tumor volume and lesion regression rates) have been applied to the evaluation of tumor response to therapy. Other more recent approaches make use of CT density (Hounsfield units) measurements for the evaluation of gastrointestinal stromal tumors or contrast enhancement patterns after vascular interventional therapies in hepatic lesions (European Association for the Study of the Liver) [76–79].

7.3.2 Metabolic Response Criteria

7.3.2.1 Qualitative Assessment

PET scans for diagnosis and primary staging, response assessment, and restaging in clinical practice are typically interpreted using qualitative methods in which the distribution and intensity of tracer uptake in potential tumor foci are compared with tracer uptake in normal structures such as blood pool, muscle, brain, and liver.

The IWC + PET criteria developed through the efforts of Juweid and Cheson dichotomizes PET results into positive and negative relative to the intensity of tracer uptake, as compared with the blood pool or nearby normal structures (Tables 7.3 and 7.4).

Such a dichotomous reporting has been introduced in clinical reporting in lymphoma, including response to radiotherapy, and proposed in evaluation of gastrointestinal and lung tumors after chemoradiation therapy.

Table 7.3 Response definitions for clinical trials: lymphoma response [89]

Response	Definition	Nodal masses	Spleen, liver	Bone marrow
CR	Disappearance of all evidence of disease	(a) FDG–avid or PET-positive before therapy must be PET-negative after therapy; mass of any size is permitted if PET is negative; (b) variably FDG–avid or PET-negative; regression to normal size on CT	Not palpable, nodules disappeared	Infiltrate has cleared on repeated biopsy; if indeterminate by morphology, immunohistochemistry should be negative for CR
PR	Regression of measurable disease and no new sites	≥50% decrease in SPD of up to six largest dominant masses; no increase in size of other nodes;(a) FDG–avid or PET-positive before therapy; one or more PET-positive at previously involved site; (b) variably FDG–avid or PET-negative; regression on CT	≥50% decrease in SPD of nodules (for single nodule in greatest transverse diameter); no increase in size of liver or spleen	Irrelevant if positive before therapy; cell type should be specified
SD	Failure to attain CR/PR or PD	(a) FDG–avid or PET-positive before therapy; PET-positive at prior sites of disease and no new sites on CT or PET; (b) variably FDG–avid or PET-negative; no change in size of previous lesions on CT		
Relapsed disease or PD	Any new lesion or increase of previously involved sites by ≥50% from nadir	Appearance of new lesions >1.5 cm in any axis, ≥50% increase in SPD of more than one node, or ≥50% increase in longest diameter of previously identified node >1 cm in short axis; lesions PET-positive if FDG–avid lymphoma or PET-positive before therapy	>50% increase from nadir in SPD of any previous lesions	New or recurrent involvement

CR complete remission, *PR* partial remission, *SPD* sum of product of diameters, *SD* stable disease, *PD* progressive disease

7.3.2.2 Quantitative Assessment (PERCIST v1.0)

PET Response Criteria in Solid Tumors (PERCIST 1.0) were introduced in 2009 as guidelines for systematic and structured assessment of response to therapy with PET in patients with cancer, with suggested application in clinical trials, and, potentially, in the clinical practice of PET reporting. PERCIST v1.0 describes in detail methods for controlling the quality of PET imaging conditions to ensure the comparability of PET images from different time points and to allow quantitative expression of the changes in PET measurements and assessment of the overall response according to PET results. PERCIST has been referenced widely, and authors of several articles have reported that the metrics described in PERCIST 1.0 are associated with clinical outcomes after therapy in patients with several different types of cancer, including small-cell lung cancer, colorectal cancer, non-Hodgkin lymphoma, esophageal cancer, and the Ewing sarcoma family of tumors [82].

Table 7.4 Comparison of qualitative PET response criteria and IWC + PET [89–91]

Characteristic	Hicks criteria	IWC + PET (lymphoma)
Measurability of lesion at baseline	1. FDG–avid	1. DG–avid tumor; baseline PET scan is desirable
	2. Standardized display with normalization to liver	2. Variably FDG–avid tumor; FDG baseline PET scan is required
		3. Follow-up PET at least 3 weeks after last chemotherapy session or at least 8–12 weeks after last radiation therapy session
Objective response	Complete metabolic response: FDG–avid lesions revert to background of normal tissues in which they are located	Complete response in FDG–avid tumors: No focal or diffuse increased FDG uptake over background in location consistent with tumor, regardless of CT abnormality; new lung nodules in lymphoma patient, without history of lung involvement (regardless of FDG avidity), are not considered lymphoma; increased focal or multifocal marrow uptake is not considered tumor unless biopsy is done
	Partial metabolic response: "Significant reduction in SUV in tumors"	Noncomplete response: Diffuse or focal uptake exceeding mediastinal blood pool if >2 cm in size; in nodes <2 cm diameter, uptake of FDG greater than background is positive; lesions >1.5 cm in size in liver or spleen, with uptake equal to or greater than spleen, are considered tumor
	SMD: "No visible change in metabolic activity of tumors"	Partial remission: See Table 7.2
	Progressive metabolic disease: "Increase in intensity or extent of tumor metabolic activity or new sites"	Progressive disease: See Table 7.2

7.4 Current Uses of FDG PET/CT in Treatment Response Following Radiation Therapy

7.4.1 Head and Neck Cancer

Head and neck cancer has an annual incidence of 550,000 worldwide [92]. Chemoradiotherapy (CRT) is the standard of care for locally advanced HNSCC for both unresectable disease and to achieve organ preservation [93]. The avoidance of unnecessary post-CRT neck dissection in complete responders depends on accurate posttreatment response assessment. Conventional imaging is hampered by treatment-related anatomical distortion and residual masses as well as the possibility of small occult deposits.

FDG PET/CT has an established role in post-CRT assessment in locally advanced HNSCC. Posttreatment FDG PET/CT has an NPV up to 99% for nodal disease (when performed at 4 months) [94], benefit over conventional assessment (anatomical imaging and clinical examination) [95], and a high probability of long-term regional control (2.3% regional failure rate at 36 months) [96]. A recent randomized controlled trial, the UK PET-NECK study, demonstrated that PET/CT surveillance had equivalent survival outcome at lower overall cost, when compared with routine neck dissection for N2/3 nodal disease post-CRT for advanced nodal disease [97]. In this study, PET/CT took place 12 weeks following CRT. In line with this, a prior meta-analysis had shown that diagnostic accuracy was improved when response assessment was performed more than 12 weeks posttreatment [7]. Some groups have adopted a policy of response assessment at least 4 months posttreatment [94, 98]. The clinical management of equivocal results remains problematic [94, 97, 99]. The majority of published data relate to the use of response assessment PET/CT following CRT for

oropharyngeal carcinoma; the test characteristics of PET/CT for other head and neck tumor sites and following the use of radiotherapy alone remain less clear. Future work includes the incorporation of standardized qualitative interpretative response assessment criteria, for example, Hopkins criteria [100], which may help stratify management and the use of FDG PET/CT during radiotherapy to optimize the therapeutic ratio [101].

7.4.2 Esophageal Carcinoma

Neoadjuvant CRT is a standard of care for locally advanced disease, but responders and nonresponders have a significantly differing prognosis [102]. Use of interim post-CRT FDG PET/CT prior to surgery can help guide appropriate further management, specifically by identifying interim metastatic disease (which may occur in up to 17%) preventing futile surgery [103, 104].

The added benefit of surgery for those with complete metabolic response (CMR) is less well defined. A substantial minority (20–30%) of patients with resectable disease have a complete pathologic response (CPR) to CRT [105]. Multiple groups have described the correlation between CMR on post-CRT FDG PET/CT, CPR and survival benefit [106]. Monjazeb et al. [107] suggested patients with CMR may be spared surgery. Cervino et al. [108] described a 91% 18-month disease-free survival for patients with a negative FDG PET/CT, who did not undergo surgery post-neoadjuvant treatment. However, the reported data are heterogeneous, for example, Elliot et al. [109] found that CMR on post-CRT FDG PET/CT and CPR did not correlate. This may partly relate to study timing, as radiation-induced esophagitis can mimic residual active disease and limit the utility of interim and posttreatment PET/CT. Many advocate surgery for even complete responders post-CRT and consider the role of FDG PET/CT to be guiding biopsy and highlighting patients requiring escalation of treatment [110].

7.4.3 Rectal Carcinoma

Neoadjuvant CRT prior to resection is the standard of care for locally advanced rectal cancer (LARC). Early evidence of treatment response can alter surgical management, and accurate restaging is critical.

MRI is the mainstay of radiological staging of rectal cancer but has limited value in response assessment following CRT [111]. International guidelines do not yet reflect a role for FDG PET/CT in the post-CRT restaging of LARC. However, several small studies have indicated a correlation between metabolic and pathologic response and demonstrated a superior NPV (up to 95.5%) of FDG PET/CT for CPR compared with MRI in LARC restaging [112–114]. Furthermore, a recent systematic review combining results of over 1500 patients found a high-pooled accuracy for early PET restaging post-CRT for LARC [115].

The role of PET/CT should not be overstated. Two systematic reviews of post-CRT FDG PET/CT suggest the main role for functional imaging was in identification of nonresponders rather than selection for organ-sparing strategies [115, 116]. However, post-CRT FDG PET/CT has a role in early outcome prediction with markers for metabolic response correlating with overall survival and disease-free survival [117].

7.4.4 Brain Tumors

Following radiotherapy for brain tumors, radiation necrosis can occur and mimic tumor progression or recurrence on conventional imaging.

FDG PET/CT has an established role in differentiating radiation necrosis from tumor progression. Stereotactic radiotherapy can result in apparent expansion and increased enhancement of treated lesions. FDG PET has a reported sensitivity of 75% and specificity of 81% for distinguishing radiation necrosis from recurrent tumor at sites of radiosurgery [118].

Distinction of radiation necrosis from residual tumor after fractionated radiotherapy can be problematic. The two often coexist, radiation

necrosis may be hypermetabolic, and local seizure activity may falsely increase uptake [119]. Increased uptake relative to contralateral grey matter has been demonstrated to have 68% accuracy in the diagnosis of recurrent tumor [120].

The role of FDG PET/CT postradiotherapy is largely problem-solving and biopsy guidance in combination with MRI and other advanced imaging techniques. However, owing to the suboptimal sensitivity and specificity of FDG-PET, other PET tracers may have superior accuracy [121]. Fluorine-18 fluoro-ethyl-tyrosine is an amino acid analog with improved tumor-to-background contrast compared with FDG and higher sensitivity for detection of recurrent glioma [122]. Fluoro-ethyl-tyrosine does not require an on-site cyclotron, and cost-effectiveness has been reported in diagnostic and recurrent indications [123], although not yet specifically for postradiosurgery indications.

7.4.5 Cervical Carcinoma

Cervical cancer is the third most common malignancy worldwide [124]. Locally advanced disease is treated with CRT (typically external beam radiotherapy plus cisplatin with subsequent intrauterine brachytherapy), but 20–40% of patients suffer disease persistence or recurrence [125]. Preexisting methods of assessment such as International Federation of Gynaecology and Obstetrics stage do not reliably predict early treatment response or outcome [126]. Hence, the development of noninvasive surrogate biomarkers to predict poor treatment response and facilitate treatment escalation is of clinical pertinence. Opportunities to use PET/CT for this purpose may exist both during and after completion of treatment.

Evidence suggests that early treatment (prebrachytherapy) FDG PET/CT may be used to delineate metabolically active disease, allowing treatment field adaptation [127]. Furthermore, CMR predicts end of treatment response; Kidd et al. [128] found that maximum standardized uptake values (SUV_{max}) and FDG heterogeneity at 4 weeks during treatment correlated with 3-month posttreatment PET response. Yoon et al. [129] reported that in patients with FDG-avid pelvic nodal disease, failure to achieve nodal CMR correlated with a markedly reduced disease-free survival (71% with CMR vs. 18%; $p < 0.001$). While such use remains experimental, this may represent a method to flag those in need of treatment escalation.

A number of trials have demonstrated that FDG PET/CT at 3 months post-CRT predicts prognosis. Persistent abnormal or new FDG activity post-CRT represented the most important predictor of disease-related death by 5 years in one study [130]. However, posttherapy PET biomarkers remain of uncertain value in assessing long-term treatment success; one study suggested that delta $SUV_{max} > 60\%$ predicted disease-free survival, and [127] another study reported a limited NPV with 21% of patients with CMR on posttreatment FDG PET/CT, developing disease recurrence during the median 28-month follow-up [131], with tumor size and stage acting as predictors for recurrent disease. Furthermore, a systematic review suggests that although more accurate than MRI, PET/CT is less cost-effective in posttreatment surveillance [132] than standard follow-up. Therefore, while PET/CT offers promise in posttreatment assessment of cervical cancer, its potential to add value to the treatment pathway remains to be fully realized.

7.4.6 Lung Carcinoma

Non-small-cell lung cancer (NSCLC) is the leading cause of cancer-related mortality [133]. FDG PET/CT is well established as a cost-effective staging tool prior to radical treatment. CRT is the standard treatment in locally advanced disease, but locoregional treatment failure rates are 15–40%, and treatment escalation can cause morbidity [134]. Anatomical imaging response assessment post-CRT does not correlate well with histopathological response, and distinction of posttreatment fibrosis from residual tumor is problematic. Therefore, the use of noninvasive surrogate biomarkers to flag nonresponders early in treatment is crucial.

Studies suggest that surrogate PET biomarkers such as total lesion glycolysis [135] and SUV_{max} [136] may predict treatment response during CRT. However, the applicability of metabolic markers in predicting long-term outcomes post-CRT in NSCLC remains unclear. One study suggested that FDG PET poststereotactic radiotherapy did not reliably predict long-term outcome [137]. More recently, Ding et al. [138] found that metabolic tumor volume (MTV) at FDG PET/CT post-CRT was predictive of recurrence-free survival post-CRT at 2 years.

Surgical resection post-CRT is a potential curative treatment option for selected patients with Stage IIIA NSCLC, and the high NPV of FDG PET/CT may aid interim treatment decisions post-CRT. Kim et al. [139] demonstrated improved disease-free survival and overall survival in patients who demonstrated CMR.

FDG PET/CT may also have a role in adaptive radiotherapy planning in NSCLC, with changes in MTV [140] and gross tumor volume [138] being used to adapt treatment. The use of FDG PET/CT to distinguish tumor recurrence from fibrosis has been reported to guide posttreatment problem-solving [141] but can be challenging.

7.4.7 Hepato-Pancreatico-Biliary Tumors, Particularly Pancreatic Carcinoma and Liver Metastases (Postselective Internal Radiotherapy Treatment)

CRT is a standard of care for locally advanced pancreatic cancer. However, local relapse rates are high (42–68%) and distant recurrence is common [142].

FDG PET/CT performed 12 weeks post-CRT demonstrated that increased delta SUV_{max} predicts overall survival and progression-free survival. The use of FDG PET/CT during CRT is limited by the inflammation caused by bile duct occlusion. Allowing for this, in the future, integration of PET/CT as a response assessment tool may help define futility owing to interim distant metastatic disease and allow adaptation of the therapy field and selection for aggressive treatment [143].

Selective internal radiotherapy treatment is an important palliative treatment for unresectable metastatic liver disease. Early assessment of treatment response can help guide further treatment [144]. FDG PET/CT can provide an earlier and more accurate assessment of response to ^{90}Y-microsphere therapy than CT imaging alone [145]. MTV and total lesion glycolysis are reported to be the best predictors of survival in colorectal metastatic disease [146]. However, recent evidence suggests that diffusion-weighted MRI may be the superior modality with an NPV of 92% vs. 56% for FDG PET/CT [147], and further investigation is required for clarification.

References

1. Crellin AM, Burnet NG. Proton beam therapy: the context, future direction and challenges become clearer. Clin Oncol. 2014;26:736–8.
2. McGarry CK, Butterworth KT, Trainor C, McMahon SJ, O'Sullivan JM, Prise KM, Hounsell AR. In-vitro investigation of out-of-field cell survival following the delivery of conformal, intensity-modulated radiation therapy (imrt) and volumetric modulated arc therapy (vmat) plans. Phys Med Biol. 2012;57:6635–45.
3. Huang SH, O'Sullivan B, Xu W, Zhao H, Chen DD, Ringash J, Hope A, Razak A, Gilbert R, Irish J, Kim J, Dawson LA, Bayley A, Cho BC, Goldstein D, Gullane P, Yu E, Perez-Ordonez B, Weinreb I, Waldron J. Temporal nodal regression and regional control after primary radiation therapy for n2-n3 head-and-neck cancer stratified by hpv status. Int J Radiat Oncol Biol Phys. 2013;87:1078–85.
4. Cliffe H, Patel C, Prestwich R, Scarsbrook A. Radiotherapy response evaluation using fdg pet-ct-established and emerging applications. Br J Radiol. 2017;90:20160764.
5. Castadot P, Geets X, Lee JA, Gregoire V. Adaptive functional image-guided imrt in pharyngo-laryngeal squamous cell carcinoma: is the gain in dose distribution worth the effort? Radiother Oncol. 2011;101:343–50.
6. Vandecaveye V, De Keyzer F, Nuyts S, Deraedt K, Dirix P, Hamaekers P, Vander Poorten V, Delaere P, Hermans R. Detection of head and neck squamous cell carcinoma with diffusion weighted mri after (chemo)radiotherapy: correlation between radiologic and histopathologic findings. Int J Radiat Oncol Biol Phys. 2007;67:960–71.

7. Gupta T, Master Z, Kannan S, Agarwal JP, Ghsoh-Laskar S, Rangarajan V, Murthy V, Budrukkar A. Diagnostic performance of post-treatment fdg pet or fdg pet/ct imaging in head and neck cancer: a systematic review and meta-analysis. Eur J Nucl Med Mol Imaging. 2011;38:2083–95.
8. Isles MG, McConkey C, Mehanna HM. A systematic review and meta-analysis of the role of positron emission tomography in the follow up of head and neck squamous cell carcinoma following radiotherapy or chemoradiotherapy. Clin Otolaryngol. 2008;33:210–22.
9. Porceddu SV, Pryor DI, Burmeister E, Burmeister BH, Poulsen MG, Foote MC, Panizza B, Coman S, McFarlane D, Coman W. Results of a prospective study of positron emission tomography-directed management of residual nodal abnormalities in node-positive head and neck cancer after definitive radiotherapy with or without systemic therapy. Head Neck. 2011;33:1675–82.
10. Nordsmark M, Bentzen SM, Rudat V, Brizel D, Lartigau E, Stadler P, Becker A, Adam M, Molls M, Dunst J, Terris DJ, Overgaard J. Prognostic value of tumor oxygenation in 397 head and neck tumors after primary radiation therapy. An international multicenter study. Radiother Oncol. 2005;77:18–24.
11. Bussink J, van Herpen CM, Kaanders JH, Oyen WJ. Pet-ct for response assessment and treatment adaptation in head and neck cancer. Lancet Oncol. 2010;11:661–9.
12. Overgaard J. Hypoxic radiosensitization: adored and ignored. J Clin Oncol Off J Am Soc Clin Oncol. 2007;25:4066–74.
13. Eschmann SM, Paulsen F, Reimold M, Dittmann H, Welz S, Reischl G, Machulla HJ, Bares R. Prognostic impact of hypoxia imaging with 18f-misonidazole pet in non-small cell lung cancer and head and neck cancer before radiotherapy. J Nucl Med. 2005;46:253–60.
14. Rischin D, Hicks RJ, Fisher R, Binns D, Corry J, Porceddu S, Peters LJ. Trans-Tasman Radiation Oncology Group S. prognostic significance of [18f]-misonidazole positron emission tomography-detected tumor hypoxia in patients with advanced head and neck cancer randomly assigned to chemoradiation with or without tirapazamine: a substudy of trans-Tasman radiation oncology group study 98.02. J Clin Oncol Off J Am Soc Clin Oncol. 2006;24:2098–104.
15. Zimny M, Gagel B, DiMartino E, Hamacher K, Coenen HH, Westhofen M, Eble M, Buell U, Reinartz P. Fdg--a marker of tumour hypoxia? A comparison with [18f]fluoromisonidazole and po2-polarography in metastatic head and neck cancer. Eur J Nucl Med Mol Imaging. 2006;33:1426–31.
16. Thorwarth D, Eschmann SM, Holzner F, Paulsen F, Alber M. Combined uptake of [18f]fdg and [18f] fmiso correlates with radiation therapy outcome in head-and-neck cancer patients. Radiother Oncol. 2006;80:151–6.
17. Rajendran JG, Hendrickson KR, Spence AM, Muzi M, Krohn KA, Mankoff DA. Hypoxia imaging-directed radiation treatment planning. Eur J Nucl Med Mol Imaging. 2006;33(Suppl 1):44–53.
18. Wang W, Lee NY, Georgi JC, Narayanan M, Guillem J, Schoder H, Humm JL. Pharmacokinetic analysis of hypoxia (18)f-fluoromisonidazole dynamic pet in head and neck cancer. J Nucl Med. 2010;51:37–45.
19. Piert M, Machulla HJ, Picchio M, Reischl G, Ziegler S, Kumar P, Wester HJ, Beck R, McEwan AJ, Wiebe LI, Schwaiger M. Hypoxia-specific tumor imaging with 18f-fluoroazomycin arabinoside. J Nucl Med. 2005;46:106–13.
20. Gronroos T, Eskola O, Lehtio K, Minn H, Marjamaki P, Bergman J, Haaparanta M, Forsback S, Solin O. Pharmacokinetics of [18f]fetnim: a potential marker for pet. J Nucl Med. 2001;42:1397–404.
21. Vavere AL, Lewis JS. Cu-atsm: a radiopharmaceutical for the pet imaging of hypoxia. Dalton Trans. 2007;(43):4893–902.
22. Minagawa Y, Shizukuishi K, Koike I, Horiuchi C, Watanuki K, Hata M, Omura M, Odagiri K, Tohnai I, Inoue T, Tateishi U. Assessment of tumor hypoxia by 62cu-atsm pet/ct as a predictor of response in head and neck cancer: a pilot study. Ann Nucl Med. 2011;25:339–45.
23. Weber WA. Monitoring tumor response to therapy with 18f-flt pet. J Nucl Med. 2010;51:841–4.
24. Rasey JS, Grierson JR, Wiens LW, Kolb PD, Schwartz JL. Validation of flt uptake as a measure of thymidine kinase-1 activity in a549 carcinoma cells. J Nucl Med. 2002;43:1210–7.
25. Troost EG, Bussink J, Hoffmann AL, Boerman OC, Oyen WJ, Kaanders JH. 18f-flt pet/ct for early response monitoring and dose escalation in oropharyngeal tumors. J Nucl Med. 2010;51:866–74.
26. Menda Y, Boles Ponto LL, Dornfeld KJ, Tewson TJ, Watkins GL, Schultz MK, Sunderland JJ, Graham MM, Buatti JM. Kinetic analysis of 3′-deoxy-3′-(18) f-fluorothymidine ((18)f-flt) in head and neck cancer patients before and early after initiation of chemoradiation therapy. J Nucl Med. 2009;50:1028–35.
27. de Langen AJ, Klabbers B, Lubberink M, Boellaard R, Spreeuwenberg MD, Slotman BJ, de Bree R, Smit EF, Hoekstra OS, Lammertsma AA. Reproducibility of quantitative 18f-3′-deoxy-3′-fluorothymidine measurements using positron emission tomography. Eur J Nucl Med Mol Imaging. 2009;36:389–95.
28. Linecker A, Kermer C, Sulzbacher I, Angelberger P, Kletter K, Dudczak R, Ewers R, Becherer A. Uptake of (18)f-flt and (18)f-fdg in primary head and neck cancer correlates with survival. Nuklearmedizin. J Nucl Med. 2008;47:80–5. quiz N12.
29. Troost EG, Vogel WV, Merkx MA, Slootweg PJ, Marres HA, Peeters WJ, Bussink J, van der Kogel AJ, Oyen WJ, Kaanders JH. 18f-flt pet does not discriminate between reactive and metastatic lymph nodes in primary head and neck cancer patients. J Nucl Med. 2007;48:726–35.

30. Cotter TG. Apoptosis and cancer: the genesis of a research field. Nat Rev Cancer. 2009;9:501–7.
31. Hoebers FJ, Kartachova M, de Bois J, van den Brekel MW, van Tinteren H, van Herk M, Rasch CR, Valdes Olmos RA, Verheij M. 99mtc hynic-rh-annexin v scintigraphy for in vivo imaging of apoptosis in patients with head and neck cancer treated with chemoradiotherapy. Eur J Nucl Med Mol Imaging. 2008;35:509–18.
32. Hoglund J, Shirvan A, Antoni G, Gustavsson SA, Langstrom B, Ringheim A, Sorensen J, Ben-Ami M, Ziv I. 18f-ml-10, a pet tracer for apoptosis: first human study. J Nucl Med. 2011;52:720–5.
33. Hoffman RM. Altered methionine metabolism, DNA methylation and oncogene expression in carcinogenesis. A review and synthesis. Biochim Biophys Acta. 1984;738:49–87.
34. Leskinen-Kallio S, Nagren K, Lehikoinen P, Ruotsalainen U, Teras M, Joensuu H. Carbon-11-methionine and pet is an effective method to image head and neck cancer. J Nucl Med. 1992;33:691–5.
35. Lindholm P, Leskinen-Kallio S, Minn H, Bergman J, Haaparanta M, Lehikoinen P, Nagren K, Ruotsalainen U, Teras M, Joensuu H. Comparison of fluorine-18-fluorodeoxyglucose and carbon-11-methionine in head and neck cancer. J Nucl Med. 1993;34:1711–6.
36. Lindholm P, Leskinen-Kallio S, Grenman R, Lehikoinen P, Nagren K, Teras M, Ruotsalainen U, Joensuu H. Evaluation of response to radiotherapy in head and neck cancer by positron emission tomography and [11c]methionine. Int J Radiat Oncol Biol Phys. 1995;32:787–94.
37. Chesnay E, Babin E, Constans JM, Agostini D, Bequignon A, Regeasse A, Sobrio F, Moreau S. Early response to chemotherapy in hypopharyngeal cancer: assessment with (11)c-methionine pet, correlation with morphologic response, and clinical outcome. J Nucl Med. 2003;44:526–32.
38. Nuutinen J, Jyrkkio S, Lehikoinen P, Lindholm P, Minn H. Evaluation of early response to radiotherapy in head and neck cancer measured with [11c]methionine-positron emission tomography. Radiother Oncol. 1999;52:225–32.
39. Wester HJ, Herz M, Weber W, Heiss P, Senekowitsch-Schmidtke R, Schwaiger M, Stocklin G. Synthesis and radiopharmacology of o-(2-[18f] fluoroethyl)-l-tyrosine for tumor imaging. J Nucl Med. 1999;40:205–12.
40. Pauleit D, Zimmermann A, Stoffels G, Bauer D, Risse J, Fluss MO, Hamacher K, Coenen HH, Langen KJ. 18f-fet pet compared with 18f-fdg pet and ct in patients with head and neck cancer. J Nucl Med. 2006;47:256–61.
41. Balogova S, Perie S, Kerrou K, Grahek D, Montravers F, Angelard B, Susini B, El Chater P, St Guily JL, Talbot JN. Prospective comparison of fdg and fet pet/ct in patients with head and neck squamous cell carcinoma. Mol Imaging Biol. 2008;10:364–73.
42. Haerle SK, Fischer DR, Schmid DT, Ahmad N, Huber GF, Buck A. 18f-fet pet/ct in advanced head and neck squamous cell carcinoma: an intra-individual comparison with 18f-fdg pet/ct. Mol Imaging Biol. 2011;13:1036–42.
43. Roivainen A, Forsback S, Gronroos T, Lehikoinen P, Kahkonen M, Sutinen E, Minn H. Blood metabolism of [methyl-11c]choline; implications for in vivo imaging with positron emission tomography. Eur J Nucl Med. 2000;27:25–32.
44. Khan N, Oriuchi N, Ninomiya H, Higuchi T, Kamada H, Endo K. Positron emission tomographic imaging with 11c-choline in differential diagnosis of head and neck tumors: comparison with 18f-fdg pet. Ann Nucl Med. 2004;18:409–17.
45. Ito K, Yokoyama J, Kubota K, Morooka M, Shiibashi M, Matsuda H. 18f-fdg versus 11c-choline pet/ct for the imaging of advanced head and neck cancer after combined intra-arterial chemotherapy and radiotherapy: the time period during which pet/ct can reliably detect non-recurrence. Eur J Nucl Med Mol Imaging. 2010;37:1318–27.
46. Manning HC, Merchant NB, Foutch AC, Virostko JM, Wyatt SK, Shah C, McKinley ET, Xie J, Mutic NJ, Washington MK, LaFleur B, Tantawy MN, Peterson TE, Ansari MS, Baldwin RM, Rothenberg ML, Bornhop DJ, Gore JC, Coffey RJ. Molecular imaging of therapeutic response to epidermal growth factor receptor blockade in colorectal cancer. Clin Cancer Res. 2008;14:7413–22.
47. Bussink J, van der Kogel AJ, Kaanders JH. Activation of the pi3-k/akt pathway and implications for radioresistance mechanisms in head and neck cancer. Lancet Oncol. 2008;9:288–96.
48. Niu G, Cai W, Chen K, Chen X. Non-invasive pet imaging of egfr degradation induced by a heat shock protein 90 inhibitor. Mol Imaging Biol. 2008;10:99–106.
49. Gallagher FA. An introduction to functional and molecular imaging with mri. Clin Radiol. 2010;65:557–66.
50. Brunt JN. Computed tomography-magnetic resonance image registration in radiotherapy treatment planning. Clin Oncol. 2010;22:688–97.
51. Dewhirst MW, Ong ET, Braun RD, Smith B, Klitzman B, Evans SM, Wilson D. Quantification of longitudinal tissue po2 gradients in window chamber tumours: impact on tumour hypoxia. Br J Cancer. 1999;79:1717–22.
52. Overgaard J, Hansen HS, Overgaard M, Bastholt L, Berthelsen A, Specht L, Lindelov B, Jorgensen K. A randomized double-blind phase iii study of nimorazole as a hypoxic radiosensitizer of primary radiotherapy in supraglottic larynx and pharynx carcinoma. Results of the danish head and neck cancer study (dahanca) protocol 5-85. Radiother Oncol. 1998;46:135–46.
53. Newbold K, Castellano I, Charles-Edwards E, Mears D, Sohaib A, Leach M, Rhys-Evans P, Clarke P, Fisher C, Harrington K, Nutting C. An exploratory

study into the role of dynamic contrast-enhanced magnetic resonance imaging or perfusion computed tomography for detection of intratumoral hypoxia in head-and-neck cancer. Int J Radiat Oncol Biol Phys. 2009;74:29–37.
54. Agrawal S, Awasthi R, Singh A, Haris M, Gupta RK, Rathore RK. An exploratory study into the role of dynamic contrast-enhanced (dce) mri metrics as predictors of response in head and neck cancers. Clin Radiol. 2012;67:e1–5.
55. Vandecaveye V, De Keyzer F, Dirix P, Lambrecht M, Nuyts S, Hermans R. Applications of diffusion-weighted magnetic resonance imaging in head and neck squamous cell carcinoma. Neuroradiology. 2010;52:773–84.
56. Vandecaveye V, De Keyzer F, Vander Poorten V, Dirix P, Verbeken E, Nuyts S, Hermans R. Head and neck squamous cell carcinoma: value of diffusion-weighted mr imaging for nodal staging. Radiology. 2009;251:134–46.
57. King AD, Ahuja AT, Yeung DK, Fong DK, Lee YY, Lei KI, Tse GM. Malignant cervical lymphadenopathy: diagnostic accuracy of diffusion-weighted mr imaging. Radiology. 2007;245:806–13.
58. Kim S, Loevner L, Quon H, Sherman E, Weinstein G, Kilger A, Poptani H. Diffusion-weighted magnetic resonance imaging for predicting and detecting early response to chemoradiation therapy of squamous cell carcinomas of the head and neck. Clin Cancer Res. 2009;15:986–94.
59. Dirix P, Vandecaveye V, De Keyzer F, Stroobants S, Hermans R, Nuyts S. Dose painting in radiotherapy for head and neck squamous cell carcinoma: value of repeated functional imaging with (18)f-fdg pet, (18) f-fluoromisonidazole pet, diffusion-weighted mri, and dynamic contrast-enhanced mri. J Nucl Med. 2009;50:1020–7.
60. Padhani AR, Krohn KA, Lewis JS, Alber M. Imaging oxygenation of human tumours. Eur Radiol. 2007;17:861–72.
61. Robinson SP, Rodrigues LM, Ojugo AS, McSheehy PM, Howe FA, Griffiths JR. The response to carbogen breathing in experimental tumour models monitored by gradient-recalled echo magnetic resonance imaging. Br J Cancer. 1997;75:1000–6.
62. Taylor NJ, Baddeley H, Goodchild KA, Powell ME, Thoumine M, Culver LA, Stirling JJ, Saunders MI, Hoskin PJ, Phillips H, Padhani AR, Griffiths JR. Bold mri of human tumor oxygenation during carbogen breathing. J Magn Reson Imaging. 2001;14:156–63.
63. Rodrigues LM, Howe FA, Griffiths JR, Robinson SP. Tumor r2* is a prognostic indicator of acute radiotherapeutic response in rodent tumors. J Magn Reson Imaging. 2004;19:482–8.
64. Mukherji SK, Schiro S, Castillo M, Kwock L, Muller KE, Blackstock W. Proton mr spectroscopy of squamous cell carcinoma of the extracranial head and neck: in vitro and in vivo studies. AJNR. Am J Neuroradiol. 1997;18:1057–72.
65. Maheshwari SR, Mukherji SK, Neelon B, Schiro S, Fatterpekar GM, Stone JA, Castillo M. The choline/creatine ratio in five benign neoplasms: comparison with squamous cell carcinoma by use of in vitro mr spectroscopy. Am J Neuroradiol. 2000;21:1930–5.
66. Le QT, Koong A, Lieskovsky YY, Narasimhan B, Graves E, Pinto H, Brown JM, Spielman D. In vivo 1h magnetic resonance spectroscopy of lactate in patients with stage iv head and neck squamous cell carcinoma. Int J Radiat Oncol Biol Phys. 2008;71:1151–7.
67. Miles KA. Molecular imaging with dynamic contrast-enhanced computed tomography. Clin Radiol. 2010;65:549–56.
68. Gandhi D, Hoeffner EG, Carlos RC, Case I, Mukherji SK. Computed tomography perfusion of squamous cell carcinoma of the upper aerodigestive tract. Initial results. J Comput Assist Tomogr. 2003;27:687–93.
69. Zima A, Carlos R, Gandhi D, Case I, Teknos T, Mukherji SK. Can pretreatment ct perfusion predict response of advanced squamous cell carcinoma of the upper aerodigestive tract treated with induction chemotherapy? AJNR. Am J Neuroradiol. 2007;28:328–34.
70. Bisdas S, Rumboldt Z, Surlan-Popovic K, Baghi M, Koh TS, Vogl TJ, Mack MG. Perfusion ct in squamous cell carcinoma of the upper aerodigestive tract: long-term predictive value of baseline perfusion ct measurements. AJNR. Am J Neuroradiol. 2010;31:576–81.
71. Bisdas S, Spicer K, Rumboldt Z. Whole-tumor perfusion ct parameters and glucose metabolism measurements in head and neck squamous cell carcinomas: a pilot study using combined positron-emission tomography/ct imaging. AJNR Am J Neuroradiol. 2008;29:1376–81.
72. Hirasawa S, Tsushima Y, Takei H, Hirasawa H, Taketomi-Takahashi A, Takano A, Oriuchi N, Endo K. Inverse correlation between tumor perfusion and glucose uptake in human head and neck tumors. Acad Radiol. 2007;14:312–8.
73. Abramyuk A, Wolf G, Shakirin G, Haberland U, Tokalov S, Koch A, Appold S, Zophel K, Abolmaali N. Preliminary assessment of dynamic contrast-enhanced ct implementation in pretreatment fdg-pet/ct for outcome prediction in head and neck tumors. Acta Radiol. 2010;51:793–9.
74. Drzezga A, Souvatzoglou M, Eiber M, Beer AJ, Furst S, Martinez-Moller A, Nekolla SG, Ziegler S, Ganter C, Rummeny EJ, Schwaiger M. First clinical experience with integrated whole-body pet/mr: comparison to pet/ct in patients with oncologic diagnoses. J Nucl Med. 2012;53:845–55.
75. Schuetze SM, Baker LH, Benjamin RS, Canetta R. Selection of response criteria for clinical trials of sarcoma treatment. Oncologist. 2008;13(Suppl 2):32–40.

76. Moertel CG, Hanley JA. The effect of measuring error on the results of therapeutic trials in advanced cancer. Cancer. 1976;38:388–94.
77. Miller AB, Hoogstraten B, Staquet M, Winkler A. Reporting results of cancer treatment. Cancer. 1981;47:207–14.
78. Therasse P, Arbuck SG, Eisenhauer EA, Wanders J, Kaplan RS, Rubinstein L, Verweij J, Van Glabbeke M, van Oosterom AT, Christian MC, Gwyther SG. New guidelines to evaluate the response to treatment in solid tumors. European organization for research and treatment of cancer, national cancer institute of the United States, national cancer institute of Canada. J Natl Cancer Inst. 2000;92:205–16.
79. Eisenhauer EA, Therasse P, Bogaerts J, Schwartz LH, Sargent D, Ford R, Dancey J, Arbuck S, Gwyther S, Mooney M, Rubinstein L, Shankar L, Dodd L, Kaplan R, Lacombe D, Verweij J. New response evaluation criteria in solid tumours: revised recist guideline (version 1.1). Eur J Cancer. 2009;45:228–47.
80. Ratain MJ, Eckhardt SG. Phase ii studies of modern drugs directed against new targets: if you are fazed, too, then resist recist. J Clin Oncol Off J Am Soc Clin Oncol. 2004;22:4442–5.
81. Michaelis LC, Ratain MJ. Measuring response in a post-recist world: from black and white to shades of grey. Nat Rev Cancer. 2006;6:409–14.
82. Wahl RL, Jacene H, Kasamon Y, Lodge MA. From recist to percist: evolving considerations for pet response criteria in solid tumors. J Nucl Med. 2009;50(Suppl 1):122S–50S.
83. Wahl RL, Zasadny K, Helvie M, Hutchins GD, Weber B, Cody R. Metabolic monitoring of breast cancer chemohormonotherapy using positron emission tomography: initial evaluation. J Clin Oncol Off J Am Soc Clin Oncol. 1993;11:2101–11.
84. Juweid ME, Cheson BD. Positron-emission tomography and assessment of cancer therapy. N Engl J Med. 2006;354:496–507.
85. Weber WA, Wieder H. Monitoring chemotherapy and radiotherapy of solid tumors. Eur J Nucl Med Mol Imaging. 2006;33(Suppl 1):27–37.
86. Kidd EA, Siegel BA, Dehdashti F, Grigsby PW. The standardized uptake value for f-18 fluorodeoxyglucose is a sensitive predictive biomarker for cervical cancer treatment response and survival. Cancer. 2007;110:1738–44.
87. Weber WA. Positron emission tomography as an imaging biomarker. J Clin Oncol Off J Am Soc Clin Oncol. 2006;24:3282–92.
88. Larson SM, Schwartz LH. 18f-fdg pet as a candidate for “qualified biomarker”: functional assessment of treatment response in oncology. J Nucl Med. 2006;47:901–3.
89. Cheson BD, Pfistner B, Juweid ME, Gascoyne RD, Specht L, Horning SJ, Coiffier B, Fisher RI, Hagenbeek A, Zucca E, Rosen ST, Stroobants S, Lister TA, Hoppe RT, Dreyling M, Tobinai K, Vose JM, Connors JM, Federico M, Diehl V. International harmonization project on L. revised response criteria for malignant lymphoma. J Clin Oncol Off J Am Soc Clin Oncol. 2007;25:579–86.
90. Kalff V, Duong C, Drummond EG, Matthews JP, Hicks RJ. Findings on 18f-fdg pet scans after neoadjuvant chemoradiation provides prognostic stratification in patients with locally advanced rectal carcinoma subsequently treated by radical surgery. J Nucl Med. 2006;47:14–22.
91. Hicks RJ, Kalff V, MacManus MP, Ware RE, McKenzie AF, Matthews JP, Ball DL. The utility of (18)f-fdg pet for suspected recurrent non-small cell lung cancer after potentially curative therapy: impact on management and prognostic stratification. J Nucl Med. 2001;42:1605–13.
92. Jemal A, Bray F, Center MM, Ferlay J, Ward E, Forman D. Global cancer statistics. CA Cancer J Clin. 2011;61:69–90.
93. Adelstein DJ, Li Y, Adams GL, Wagner H Jr, Kish JA, Ensley JF, Schuller DE, Forastiere AA. An intergroup phase iii comparison of standard radiation therapy and two schedules of concurrent chemoradiotherapy in patients with unresectable squamous cell head and neck cancer. J Clin Oncol Off J Am Soc Clin Oncol. 2003;21:92–8.
94. Slevin F, Subesinghe M, Ramasamy S, Sen M, Scarsbrook AF, Prestwich RJ. Assessment of outcomes with delayed (18)f-fdg pet-ct response assessment in head and neck squamous cell carcinoma. Br J Radiol. 2015;88:20140592.
95. Mak D, Hicks RJ, Rischin D, Solomon B, Peters L, Bressel M, Young RJ, Corry J. Treatment response in the neck: P16+ versus p16- oropharyngeal cancer. J Med Imaging Radiat Oncol. 2013;57:364–72.
96. Ul-Hassan F, Simo R, Guerrero-Urbano T, Oakley R, Jeannon JP, Cook GJ. Can (18)f-fdg pet/ct reliably assess response to primary treatment of head and neck cancer? Clin Nucl Med. 2013;38:263–5.
97. Mehanna H, Wong WL, McConkey CC, Rahman JK, Robinson M, Hartley AG, Nutting C, Powell N, Al-Booz H, Robinson M, Junor E, Rizwanullah M, von Zeidler SV, Wieshmann H, Hulme C, Smith AF, Hall P, Dunn J, Group P-NTM. Pet-ct surveillance versus neck dissection in advanced head and neck cancer. N Engl J Med. 2016;374:1444–54.
98. Zundel MT, Michel MA, Schultz CJ, Maheshwari M, Wong SJ, Campbell BH, Massey BL, Blumin J, Wilson JF, Wang D. Comparison of physical examination and fluorodeoxyglucose positron emission tomography/computed tomography 4-6 months after radiotherapy to assess residual head-and-neck cancer. Int J Radiat Oncol Biol Phys. 2011;81:e825–32.
99. Prestwich R, Sen M, Scarsbrook A. Qualitative 18f-fdg pet/ct response evaluation after chemotherapy or radiotherapy for head and neck squamous cell carcinoma: is there an equivocal group? Journal of nuclear medicine: official publication. Soc Nucl Med. 2014;55:2081.
100. Marcus C, Ciarallo A, Tahari AK, Mena E, Koch W, Wahl RL, Kiess AP, Kang H, Subramaniam

RM. Head and neck pet/ct: therapy response interpretation criteria (Hopkins criteria)-interreader reliability, accuracy, and survival outcomes. J Nucl Med. 2014;55:1411–6.
101. Bhatnagar P, Subesinghe M, Patel C, Prestwich R, Scarsbrook AF. Functional imaging for radiation treatment planning, response assessment, and adaptive therapy in head and neck cancer. Radiographics. 2013;33:1909–29.
102. Schmidt T, Lordick F, Herrmann K, Ott K. Value of functional imaging by pet in esophageal cancer. J Natl Compr Cancer Netw. 2015;13:239–47.
103. Kim TJ, Kim HY, Lee KW, Kim MS. Multimodality assessment of esophageal cancer: preoperative staging and monitoring of response to therapy. Radiographics. 2009;29:403–21.
104. Stiekema J, Vermeulen D, Vegt E, Voncken FE, Aleman BM, Sanders J, Boot H, van Sandick JW. Detecting interval metastases and response assessment using 18f-fdg pet/ct after neoadjuvant chemoradiotherapy for esophageal cancer. Clin Nucl Med. 2014;39:862–7.
105. Wu AJ, Goodman KA. Clinical tools to predict outcomes in patients with esophageal cancer treated with definitive chemoradiation: are we there yet? J Gastrointest Oncol. 2015;6:53–9.
106. Flamen P, Van Cutsem E, Lerut A, Cambier JP, Haustermans K, Bormans G, De Leyn P, Van Raemdonck D, De Wever W, Ectors N, Maes A, Mortelmans L. Positron emission tomography for assessment of the response to induction radiochemotherapy in locally advanced oesophageal cancer. Ann Oncol. 2002;13:361–8.
107. Monjazeb AM, Riedlinger G, Aklilu M, Geisinger KR, Mishra G, Isom S, Clark P, Levine EA, Blackstock AW. Outcomes of patients with esophageal cancer staged with [(1)(8)f]fluorodeoxyglucose positron emission tomography (fdg-pet): can postchemoradiotherapy fdg-pet predict the utility of resection? J Clin Oncol Off J Am Soc Clin Oncol. 2010;28:4714–21.
108. Cervino AR, Pomerri F, Alfieri R, Sileni VC, Castoro C, Galuppo S, Evangelista L. 18f-fluorodeoxyglucose pet/computed tomography and risk stratification after neoadjuvant treatment in esophageal cancer patients. Nucl Med Commun. 2014;35:160–8.
109. Elliott JA, O'Farrell NJ, King S, Halpenny D, Malik V, Muldoon C, Johnston C, Reynolds JV. Value of ct-pet after neoadjuvant chemoradiation in the prediction of histological tumour regression, nodal status and survival in oesophageal adenocarcinoma. Br J Surg. 2014;101:1702–11.
110. Kukar M, Alnaji RM, Jabi F, Platz TA, Attwood K, Nava H, Ben-David K, Mattson D, Salerno K, Malhotra U, Kanehira K, Gannon J, Hochwald SN. Role of repeat 18f-fluorodeoxyglucose positron emission tomography examination in predicting pathologic response following neoadjuvant chemoradiotherapy for esophageal adenocarcinoma. JAMA Surg. 2015;150:555–62.
111. van der Paardt MP, Zagers MB, Beets-Tan RG, Stoker J, Bipat S. Patients who undergo preoperative chemoradiotherapy for locally advanced rectal cancer restaged by using diagnostic mr imaging: a systematic review and meta-analysis. Radiology. 2013;269:101–12.
112. Bampo C, Alessi A, Fantini S, Bertarelli G, de Braud F, Bombardieri E, Valvo F, Crippa F, Di Bartolomeo M, Mariani L, Milione M, Biondani P, Avuzzi B, Chiruzzi C, Pietrantonio F. Is the standardized uptake value of fdg-pet/ct predictive of pathological complete response in locally advanced rectal cancer treated with capecitabine-based neoadjuvant chemoradiation? Oncology. 2013;84:191–9.
113. Calvo FA, Sole CV, de la Mata D, Cabezon L, Gomez-Espi M, Alvarez E, Madariaga P, Carreras JL. (1)(8)f-fdg pet/ct-based treatment response evaluation in locally advanced rectal cancer: a prospective validation of long-term outcomes. Eur J Nucl Med Mol Imaging. 2013;40:657–67.
114. Huh JW, Kwon SY, Lee JH, Kim HR. Comparison of restaging accuracy of repeat fdg-pet/ct with pelvic mri after preoperative chemoradiation in patients with rectal cancer. J Cancer Res Clin Oncol. 2015;141:353–9.
115. Maffione AM, Chondrogiannis S, Capirci C, Galeotti F, Fornasiero A, Crepaldi G, Grassetto G, Rampin L, Marzola MC, Rubello D. Early prediction of response by (1)(8)f-fdg pet/ct during preoperative therapy in locally advanced rectal cancer: a systematic review. Eur J Surg Oncol. 2014;40:1186–94.
116. Joye I, Deroose CM, Vandecaveye V, Haustermans K. The role of diffusion-weighted mri and (18) f-fdg pet/ct in the prediction of pathologic complete response after radiochemotherapy for rectal cancer: a systematic review. Radiother Oncol. 2014;113:158–65.
117. Memon S, Lynch AC, Akhurst T, Ngan SY, Warrier SK, Michael M, Heriot AG. Systematic review of fdg-pet prediction of complete pathological response and survival in rectal cancer. Ann Surg Oncol. 2014;21:3598–607.
118. Chao ST, Suh JH, Raja S, Lee SY, Barnett G. The sensitivity and specificity of fdg pet in distinguishing recurrent brain tumor from radionecrosis in patients treated with stereotactic radiosurgery. Int J Cancer. 2001;96:191–7.
119. Shah R, Vattoth S, Jacob R, Manzil FF, O'Malley JP, Borghei P, Patel BN, Cure JK. Radiation necrosis in the brain: imaging features and differentiation from tumor recurrence. Radiographics. 2012;32:1343–59.
120. Ricci PE, Karis JP, Heiserman JE, Fram EK, Bice AN, Drayer BP. Differentiating recurrent tumor from radiation necrosis: time for re-evaluation of positron emission tomography? AJNR. Am J Neuroradiol. 1998;19:407–13.
121. Nihashi T, Dahabreh IJ, Terasawa T. Diagnostic accuracy of pet for recurrent glioma diagnosis: a meta-analysis. AJNR. Am J Neuroradiol. 2013;34:944–50. S941-911

122. Gotz I, Grosu AL. [(18)f]fet-pet imaging for treatment and response monitoring of radiation therapy in malignant glioma patients - a review. Front Oncol. 2013;3:104.
123. Heinzel A, Muller D, Langen KJ, Blaum M, Verburg FA, Mottaghy FM, Galldiks N. The use of o-(2-18f-fluoroethyl)-l-tyrosine pet for treatment management of bevacizumab and irinotecan in patients with recurrent high-grade glioma: a cost-effectiveness analysis. J Nucl Med. 2013;54:1217–22.
124. Jemal A, Siegel R, Ward E, Hao Y, Xu J, Thun MJ. Cancer statistics, 2009. CA Cancer J Clin. 2009;59:225–49.
125. Schwarz JK, Siegel BA, Dehdashti F, Grigsby PW. Metabolic response on post-therapy fdg-pet predicts patterns of failure after radiotherapy for cervical cancer. Int J Radiat Oncol Biol Phys. 2012;83:185–90.
126. Barwick TD, Taylor A, Rockall A. Functional imaging to predict tumor response in locally advanced cervical cancer. Curr Oncol Rep. 2013;15:549–58.
127. Oh D, Lee JE, Huh SJ, Park W, Nam H, Choi JY, Kim BT. Prognostic significance of tumor response as assessed by sequential 18f-fluorodeoxyglucose-positron emission tomography/computed tomography during concurrent chemoradiation therapy for cervical cancer. Int J Radiat Oncol Biol Phys. 2013;87:549–54.
128. Kidd EA, Thomas M, Siegel BA, Dehdashti F, Grigsby PW. Changes in cervical cancer fdg uptake during chemoradiation and association with response. Int J Radiat Oncol Biol Phys. 2013;85:116–22.
129. Yoon MS, Ahn SJ, Nah BS, Chung WK, Song HC, Yoo SW, Song JY, Jeong JU, Nam TK. Metabolic response of lymph nodes immediately after rt is related with survival outcome of patients with pelvic node-positive cervical cancer using consecutive [18f]fluorodeoxyglucose-positron emission tomography/computed tomography. Int J Radiat Oncol Biol Phys. 2012;84:e491–7.
130. Grigsby PW, Siegel BA, Dehdashti F, Rader J, Zoberi I. Posttherapy [18f] fluorodeoxyglucose positron emission tomography in carcinoma of the cervix: response and outcome. J Clin Oncol Off J Am Soc Clin Oncol. 2004;22:2167–71.
131. Onal C, Reyhan M, Guler OC, Yapar AF. Treatment outcomes of patients with cervical cancer with complete metabolic responses after definitive chemoradiotherapy. Eur J Nucl Med Mol Imaging. 2014;41:1336–42.
132. Auguste P, Barton P, Meads C, Davenport C, Malysiak S, Kowalska M, Zapalska A, Guest P, Martin-Hirsch P, Borowiack E, Khan K, Sundar S, Roberts T. Evaluating pet-ct in routine surveillance and follow-up after treatment for cervical cancer: a cost-effectiveness analysis. BJOG. 2014;121:464–76.
133. Saintigny P, Burger JA. Recent advances in non-small cell lung cancer biology and clinical management. Discov Med. 2012;13:287–97.
134. Furuse K, Fukuoka M, Kawahara M, Nishikawa H, Takada Y, Kudoh S, Katagami N, Ariyoshi Y. Phase iii study of concurrent versus sequential thoracic radiotherapy in combination with mitomycin, vindesine, and cisplatin in unresectable stage iii non-small-cell lung cancer. J Clin Oncol Off J Am Soc Clin Oncol. 1999;17:2692–9.
135. Usmanij EA, de Geus-Oei LF, Troost EG, Peters-Bax L, van der Heijden EH, Kaanders JH, Oyen WJ, Schuurbiers OC, Bussink J. 18f-fdg pet early response evaluation of locally advanced non-small cell lung cancer treated with concomitant chemoradiotherapy. J Nucl Med. 2013;54:1528–34.
136. Vera P, Mezzani-Saillard S, Edet-Sanson A, Menard JF, Modzelewski R, Thureau S, Meyer ME, Jalali K, Bardet S, Lerouge D, Houzard C, Mornex F, Olivier P, Faure G, Rousseau C, Mahe MA, Gomez P, Brenot-Rossi I, Salem N, Dubray B. Fdg pet during radiochemotherapy is predictive of outcome at 1 year in non-small-cell lung cancer patients: a prospective multicentre study (rtep2). Eur J Nucl Med Mol Imaging. 2014;41:1057–65.
137. Henderson MA, Hoopes DJ, Fletcher JW, Lin PF, Tann M, Yiannoutsos CT, Williams MD, Fakiris AJ, McGarry RC, Timmerman RD. A pilot trial of serial 18f-fluorodeoxyglucose positron emission tomography in patients with medically inoperable stage i non-small-cell lung cancer treated with hypofractionated stereotactic body radiotherapy. Int J Radiat Oncol Biol Phys. 2010;76:789–95.
138. Ding X, Li H, Wang Z, Huang W, Li B, Zang R, Sun H, Yi Y. A clinical study of shrinking field radiation therapy based on (18)f-fdg pet/ct for stage iii non-small cell lung cancer. Technol Cancer Res Treat. 2013;12:251–7.
139. Kim SH, Lee JH, Lee GJ, Jeong S, Kwak YK, Kim HK, Cho DG, Park YH, Yu M, Yoon SC. Interpretation and prognostic value of positron emission tomography-computed tomography after induction chemotherapy with or without radiation in iiia-n2 non-small cell lung cancer patients who receive curative surgery. Medicine. 2015;94:e955.
140. Mahasittiwat P, Yuan S, Xie C, Ritter T, Cao Y, Ten Haken RK, Kong FM. Metabolic tumor volume on pet reduced more than gross tumor volume on ct during radiotherapy in patients with non-small cell lung cancer treated with 3dcrt or sbrt. J Radiat Oncol. 2013;2:191–202.
141. Nakajima N, Sugawara Y, Kataoka M, Hamamoto Y, Ochi T, Sakai S, Takahashi T, Kajihara M, Teramoto N, Yamashita M, Mochizuki T. Differentiation of tumor recurrence from radiation-induced pulmonary fibrosis after stereotactic ablative radiotherapy for lung cancer: characterization of 18f-fdg pet/ct findings. Ann Nucl Med. 2013;27:261–70.
142. Topkan E, Parlak C, Kotek A, Yapar AF, Pehlivan B. Predictive value of metabolic 18fdg-pet response on outcomes in patients with locally advanced pancreatic carcinoma treated with definitive con-

current chemoradiotherapy. BMC Gastroenterol. 2011;11:123.
143. Topkan E, Parlak C, Yapar AF. Fdg-pet/ct-based restaging may alter initial management decisions and clinical outcomes in patients with locally advanced pancreatic carcinoma planned to undergo chemoradiotherapy. Cancer Imaging. 2013;13:423–8.
144. Sabet A, Meyer C, Aouf A, Sabet A, Ghamari S, Pieper CC, Mayer K, Biersack HJ, Ezziddin S. Early post-treatment fdg pet predicts survival after 90y microsphere radioembolization in liver-dominant metastatic colorectal cancer. Eur J Nucl Med Mol Imaging. 2015;42:370–6.
145. Bienert M, McCook B, Carr BI, Geller DA, Sheetz M, Tutor C, Amesur N, Avril N. 90y microsphere treatment of unresectable liver metastases: changes in 18f-fdg uptake and tumour size on pet/ct. Eur J Nucl Med Mol Imaging. 2005;32:778–87.
146. Fendler WP, Philippe Tiega DB, Ilhan H, Paprottka PM, Heinemann V, Jakobs TF, Bartenstein P, Hacker M, Haug AR. Validation of several suv-based parameters derived from 18f-fdg pet for prediction of survival after sirt of hepatic metastases from colorectal cancer. J Nucl Med. 2013;54:1202–8.
147. Barabasch A, Kraemer NA, Ciritsis A, Hansen NL, Lierfeld M, Heinzel A, Trautwein C, Neumann U, Kuhl CK. Diagnostic accuracy of diffusion-weighted magnetic resonance imaging versus positron emission tomography/computed tomography for early response assessment of liver metastases to y90-radioembolization. Investig Radiol. 2015;50:409–15.

8 Conventional Radiological Techniques and PET-CT in Treatment Response Evaluation in Immunotherapy Settings

Angelo Castello and Egesta Lopci

8.1 Introduction

The introduction of targeted therapies and, mostly, immune checkpoint inhibitors (ICI) has positively revolutionized the scenario of cancer treatment. Starting from the encouraged results obtained in melanoma patients [1–3], ICI have been tested and approved in several other solid tumors in the metastatic stage, including renal cell carcinoma [4], urothelial carcinoma [5], Hodgkin Lymphoma [6], head and neck squamous cell carcinoma [7], and non-small cell lung carcinoma [8–10].

In 2011, ipilimumab, a fully human antibody against cytotoxic T lymphocyte antigen 4 (CTLA-4), was the first ICI approved in the USA and Europe by Food and Drug Administration and European Medicines Agency, respectively. Afterwards, another class of ICI, such as nivolumab and pembrolizumab which inhibit the programmed death-1 (PD-1), were approved. Finally, atezolizumab, durvalumab, and avelumab, anti-PD-ligand (L)-1 antibodies, were the molecules most recently approved for cancer treatment.

In this chapter, we provide an overview of the current landscape of ICI as well as the continue challenge of response assessment towards these new agents facing in the clinical practice.

A. Castello · E. Lopci (✉)
Nuclear Medicine Unit, IRCCS-Humanitas Research Hospital, Rozzano, Italy

8.2 Management: Type of Treatments/Regimes

8.2.1 Melanoma

As abovementioned ipilimumab was the first ICI approved for treatment of metastatic melanoma, based on the results of randomized trial demonstrating improved overall survival (OS) and durable response in 676 patients [1]. The authors showed 3-year survival rates ranging from 20% to 26%, although objective response rate (ORR) was comprised between 12% and 19%, thus suggesting that a larger part of patients had clinical benefit with stable disease [11]. Approved dosage of ipilimumab is 3 mg/kg every 3 weeks for a total of 4 cycles, since the evidence that a dosage of 10 mg/kg was associated with higher rate of severe (grade 3) or life-threatening (grade 4) adverse events respect to 3 mg/kg (34% vs. 18–28%), even though a higher dose demonstrated a longer median OS (11.5 vs. 15.7 months) [12].

In 2014, a new class of antibodies has appeared in the scenario of metastatic melanoma therapy, i.e., nivolumab and pembrolizumab, both directed against PD-1 [2, 3]. Response rates were higher for these new antibodies compared to

S. Fanti et al. (eds.), *Atlas of Clinical PET-CT in Treatment Response Evaluation in Oncology*,
https://doi.org/10.1007/978-3-030-68858-5_8

chemotherapy (27% vs. 10%), as well as compared to ipilimumab (36% vs. 13% for nivolumab; 44% vs. 19% for pembrolizumab) [13–17]. Likewise, OS and progression-free survival (PFS) were significantly higher in patients treated with either nivolumab or pembrolizumab compared with ipilimumab [18, 19]. Following the success in metastatic melanoma setting, in 2016 ipilimumab was also approved as adjuvant therapy in patients at high risk of relapse after surgery (stage III). Based on EORTC 18071 clinical trial, high dose (10 mg/kg) of ipilimumab every 3 weeks, then every 3 months for 3 years was associated with clinical benefit in terms of recurrence-free survival (RFS) (HR 0.77, 95% CI 0.64–0.90), distant metastasis-free survival (HR 0.76, 95% CI 0.64–0.92), and OS (HR 0.72, 95% CI 0.58–0.88). Nevertheless, there were higher rates of immune-related adverse events (approximately 40%) in the arm of ipilimumab [20, 21]. In addition, also nivolumab and pembrolizumab have been approved by FDA for use in the adjuvant setting in patients with stage III or IV. Indeed, CheckMate-238 and KEYNOTE-054 trials demonstrated longer RFS (relapse-free survival) than ipilimumab or placebo. Furthermore, a better toxicity profile was associated to nivolumab arm compared to ipilimumab [22, 23].

ICI in neoadjuvant context is another setting where these new drugs are under investigations. The hypothesis behind this application is that neoadjuvant therapy would be less toxic and potentially more effective if administered before surgery. In fact, a larger tumor volume may favorite the exposition of more antigens than after surgery. Conversely, if patients progress or show severe toxicities during ICI as neoadjuvant therapy, surgery time will not be possible or will be at high risk [24].

8.2.2 NSCLC

Beside approval in patients affected by melanoma, ICI were also applied in patients with metastatic NSCLC. The first clinical trial, CheckMate-017, demonstrated significant longer OS and ORR in patients with squamous NSCLC treated with nivolumab than those treated with docetaxel [8]. Likewise, nivolumab was associated with longer OS and median duration of response in 582 patients with non-squamous NSCLC [9].

In the same time, results from KEYNOTE-001 trial determined approval of pembrolizumab in patients with metastatic NSCLC. In addition, ORR was significantly improved among patients with PD-L1 tumor expression ≥50%, therefore pembrolizumab was also approved either as first-line treatment in tumors with high PD-L1 expression or in patients with low PD-L1 expression (i.e., 1%) with progression disease in course of or after platinum-based chemotherapy according to KEYNOTE-010 trial [10, 25].

Furthermore, atezolizumab (anti-PD-L1) was approved for metastatic NSCLC patients with progression on/after platinum and in patients bearing EGFR or ALK mutations after progression disease during specific drugs for these genetic alterations [26].

Similar to melanoma, a recent paper by Forde et al. [27] reported encouraging data on the use of nivolumab as neoadjuvant therapy in NSCLC. The authors demonstrated a safety profile, no delayed surgery time, and a major pathologic response (i.e., <10% viable tumor cells) in approximately half of patients.

8.2.3 Other Solid Tumors

Beyond their application in melanoma and NSCLC, ICI have showed promising results also in other solid tumors. For instance, atezolizumab was the first approved for metastatic urothelial cancer after progression with platinum chemotherapy [28]. In the same setting, subsequently, durvalumab and avelumab (two anti-PD-L1 antibodies) were approved [29, 30]. Moreover, nivolumab and pembrolizumab were approved as second line for metastatic urothelial carcinoma based on the results of CheckMate-032, CheckMate-275, KEYNOTE-012, and KEYNOTE-045 trials [31–34]. Afterwards, pembrolizumab has been approved in the first line [35].

Several clinical trials are evaluating the efficacy of ICI, either alone or in combination with

other therapies, in the first-line and second-line settings in head and neck squamous cell carcinoma, advanced gastric, gastroesophageal adenocarcinoma, and in the third-line setting for advanced/metastatic squamous cell carcinoma of the esophagus [36, 37].

There is great interest in developing new regimes of treatment based on the combination of ICI with other agents, such as chemotherapy, radiotherapy, kinase inhibitors, or epigenetic drugs in order to improve clinical efficacy or to decrease adverse events. Preliminary data show encouraging results, although several limitations need to be addressed in the current trials (e.g., small size, lack of comparison, short follow-up) [38].

An overview of ongoing clinical trials with ICI is summarized in Table 8.1.

Table 8.1 Summary of the ongoing clinical trials with ICI (source: https://clinicaltrials.gov/)

Cancer type	Trial identifier number	Phase/status	ICI
Melanoma	NCT03963518	III, no recruiting	Not specified
	NCT03293784	I, recruiting	Nivolumab, ipilimumab
	NCT03711188	II, recruiting	Nivolumab, ipilimumab
	NCT02073123	I/II, no recruiting	Nivolumab, ipilimumab, pembrolizumab
	NCT03161756	I/II, recruiting	Nivolumab, ipilimumab
	NCT03425461	I, recruiting	Nivolumab, ipilimumab
	NCT03384836	I/II, recruiting	Pembrolizumab
	NCT03597282	I, recruiting	Nivolumab, ipilimumab
	NCT02565992	I, recruiting	Pembrolizumab
	NCT02307149	I, recruiting	Ipilimumab
	NCT03563729	II, recruiting	Nivolumab, pembrolizumab, ipilimumab
	NCT02535078	I/II, recruiting	Durvalumab, tremelimumab
Lung cancer	NCT03233724	I/II, recruiting	Pembrolizumab
	NCT03469960	III, recruiting	Nivolumab, ipilimumab
	NCT03906071	III, recruiting	Nivolumab
	NCT03996473	I/II, no recruiting	Pembrolizumab
	NCT03035890	NA, recruiting	Nivolumab, atezolizumab, pembrolizumab
	NCT03325816	I/II no recruiting	Nivolumab
	NCT03257722	I/II, recruiting	Pembrolizumab
	NCT02599454	I, recruiting	Atezolizumab
	NCT03468426	I, recruiting	BI 754091 (anti-PD-1)
	NCT03041311	II, no recruiting	Atezolizumab
	NCT03994744	II, no recruiting	Sintilimab
	NCT03380871	I, no recruiting	Pembrolizumab
	NCT02439450	I,II recruiting	Nivolumab, pembrolizumab
	NCT02973789	III, recruiting	Not specified
	NCT02403193	I,II recruiting	PDR001 (anti-PD-1)
	NCT03554473	I/II, recruiting	M7824 (anti-PD-L1/TGFβ trap)
Mesothelioma	NCT03644550	II, recruiting	Pembrolizumab
Head & Neck	NCT03532737	II, recruiting	Pembrolizumab
	NCT03878979	II, no recruiting	Nivolumab
	NCT03673735	III, no recruiting	Durvalumab
	NCT03522584	I/II, recruiting	Durvalumab, tremelimumab
	NCT02819752	I, no recruiting	Pembrolizumab
	NCT03906526	I, no recruiting	Tislelizumab
	NCT03162224	I,II recruiting	Durvalumab

(continued)

Table 8.1 (continued)

Cancer type	Trial identifier number	Phase/status	ICI
Oropharyngeal squamous cell carcinoma	NCT03144778	I, no recruiting	Durvalumab, tremelimumab
Nasopharyngeal carcinoma	NCT03427827	III, recruiting	Not specified
	NCT03984357	II, no recruiting	Nivolumab
GI tract	NCT03453164	I/II, recruiting	Nivolumab
HCC, biliary tract cancer	NCT03695952	Recruiting	Nivolumab, pembrolizumab
HCC, liver transplant	NCT03966209	I, recruiting	JS001(PD-1 inhibitor)
Pancreatic cancer	NCT02734160	I, no recruiting	Durvalumab
HCC, GI adenocarcinoma	NCT03511222	I, recruiting	Nivolumab, pembrolizumab
HCC	NCT03867084	III, recruiting	Pembrolizumab
Colorectal cancer	NCT03658772	I, no recruiting	Pembrolizumab
HCC	NCT02795429	I/II, recruiting	PDR001 (anti-PD-1)
HCC	NCT03337841	II, no recruiting	Pembrolizumab
Pancreatic cancer	NCT03331562	II, recruiting	Pembrolizumab
Pancreatic cancer	NCT03767582	I/II, no recruiting	Nivolumab
Esophageal squamous cell carcinoma	NCT03792347	I, recruiting	Pembrolizumab
Biliary tract carcinoma	NCT04003636	III, no recruiting	Pembrolizumab
Brain	NCT03173950	II, recruiting	Nivolumab
	NCT03277638	I/II, recruiting	Pembrolizumab
	NCT02852655	I, no recruiting	MK-3475
	NCT03576612	I, recruiting	Nivolumab
	NCT03893903	I, recruiting	Avelumab
	NCT03491683	I/II, no recruiting	Cemiplimab(anti-PD-1)
	NCT03925246	II, no recruiting	Nivolumab
	NCT02798406	II, recruiting	Pembrolizumab
Genitourinary tract RCC	NCT03200717	II, recruiting	Pazopanib
Metastatic ovarian cancer	NCT03287674	I/II, no recruiting	Nivolumab, ipilimumab
Metastatic RCC	NCT02989714	I/II, no recruiting	Nivolumab
Urothelial carcinoma	NCT03179943	II, recruiting	Atezolizumab
Prostate cancer	NCT03506997	II, recruiting	Pembrolizumab
Prostate cancer	NCT03406858	II, recruiting	Pembrolizumab
Urothelial carcinoma	NCT03486197	II, recruiting	Pembrolizumab
Bladder cancer	NCT02901548	II, recruiting	Durvalumab
Ovarian cancer	NCT03558139	I, recruiting	Avelumab
Urothelial carcinoma, bladder cancer	NCT03601455	II, recruiting	Durvalumab, tremelimumab
RCC	NCT03977571	III, recruiting	Nivolumab, ipilimumab
Ovarian cancer	NCT02608684	II, no recruiting	Pembrolizumab
Prostate cancer	NCT03315871	II, recruiting	M7824 (anti-PD-L1/TGFβ trap)
Uterine cancer	NCT03951415	II, recruiting	Durvalumab
Cervical cancer	NCT03612791	II, recruiting	Atezolizumab
Urothelial carcinoma Bladder cancer	NCT03288545	I, recruiting	Pembrolizumab

Table 8.1 (continued)

Cancer type	Trial identifier number	Phase/status	ICI
Urothelial carcinoma Bladder cancer	NCT03123055	I/II, recruiting	Pembrolizumab
Others Advanced solid tumors	NCT03388632	I, recruiting	Nivolumab, ipilimumab
	NCT03841110	I, recruiting	Nivolumab, pembrolizumab, atezolizumab
	NCT03945253	I, no recruiting	ASP8374, pembrolizumab
	NCT02467361	I/II, no recruiting	Nivolumab, ipilimumab, pembrolizumab
	NCT03260322	I, recruiting	ASP8374, pembrolizumab
	NCT03228667	II, recruiting	Nivolumab Pembrolizumab atezolizumab Avelumab
	NCT04009681	I/II recruiting	Not specified
	NCT02671435	I/II, no recruiting	Durvalumab, monalizumab
	NCT03986606	I, no recruiting	PSB205 (anti-PD-1/CTLA-4)
	NCT03810339	II, recruiting	Toripalimab
	NCT03990233	I, recruiting	BI 754091 (anti-PD-1)
	NCT02836834	I, no recruiting	JS001(PD-1 inhibitor)
	NCT03474640	I, recruiting	Toripalimab
	NCT03013491	I/II, recruiting	CX-072 (anti-PD-L1), ipilimumab
	NCT03667716	I, recruiting	Nivolumab
	NCT03993379	II, no recruiting	CX-072 (anti-PD-L1)
	NCT02805660	I/II, no recruiting	Durvalumab
	NCT03172936	I, recruiting	PDR001 (anti-PD-1)
	NCT03884556	I, recruiting	Pembrolizumab
	NCT03301896	I, recruiting	PDR001 (anti-PD-1)
	NCT03289962	I, recruiting	Atezolizumab
	NCT02608268	I,II recruiting	PDR001 (anti-PD-1)
	NCT03549000	I, recruiting	PDR001 (anti-PD-1)
Melanoma, NSCLC, HNSCC, RCC, urothelial carcinoma	NCT03311334	I, recruiting	Nivolumab, atezolizumab
HNSCC, NSCLC, GI adenocarcinoma	NCT03735290	I/II, recruiting	Pembrolizumab
Colorectal cancer, breast cancer, NSCLC, bladder cancer, GI adenocarcinoma RCC MSI-H	NCT03775850	I/II, recruiting	Pembrolizumab
Melanoma, NSCLC, breast cancer, anaplastic thyroid cancer	NCT02404441	I/II, no recruiting	PDR001 (anti-PD-1)
NSCLC, HNSCC, esophageal SCC, GIST, colorectal cancer	NCT04000529	I, no recruiting	Spartalizumab
Urothelial carcinoma, melanoma, RCC, NSCLC, HNSCC	NCT03511391	II, recruiting	Nivolumab, pembrolizumab

(continued)

Table 8.1 (continued)

Cancer type	Trial identifier number	Phase/status	ICI
Breast cancer	NCT03366844	I, recruiting	Pembrolizumab
	NCT03237572	I, recruiting	Pembrolizumab
	NCT03591276	I/II, recruiting	Pembrolizumab
	NCT03988036	II, no recruiting	Pembrolizumab
Melanoma, breast cancer	NCT02981303	II, no recruiting	Pembrolizumab
Colorectal cancer, breast cancer	NCT02484404	I/II, recruiting	Durvalumab
Breast cancer, sarcoma	NCT02936102	I, no recruiting	FAZ053 (anti-PD-L1), PDR001 (anti-PD-1)
Sarcoma	NCT03116529	I/II, recruiting	Durvalumab, tremelimumab
Merkel cell carcinoma	NCT03853317	II, no recruiting	Avelumab
HCC, colorectal cancer, gastric cancer, NSCLC	NCT03259867	II, recruiting	Nivolumab, pembrolizumab
Melanoma, NSCLC, bladder cancer	NCT02897765	I, no recruiting	Nivolumab
Pediatric solid tumors	NCT02793466	I, recruiting	Durvalumab
Ovarian cancer, colorectal cancer, breast cancer, SCLC	NCT03761914	I/II, recruiting	Pembrolizumab

8.3 Pathophysiology

Evaluation of response assessment should be rationally based on the knowledge of the mechanism of action of the administered drugs. The physiologic function of checkpoints is that to stop immune response once the "enemy" has been defeated, thereby avoiding a potential uncontrolled response against self-tissue, i.e., autoimmunity. CTLA-4 is constitutively expressed by regulatory T cells (Tregs) and upregulated in other T cell subtypes, such as CD4+ T cells, after their activation. CTLA-4 mediates its inhibitor function replacing co-stimulatory receptor CD28 for B7 ligands on antigen-presenting cells (APC) in the lymph nodes, thereby indirectly inhibiting proliferation and IL-2 secretion by T cells [39]. CTLA-4 was the first immune checkpoint discovered and targeted for therapy. The anti-CTLA-4 antibodies interpose and prevent the interaction between CTLA-4 and its receptor, inhibiting the completion of the immune response and allowing the maintenance of the anti-tumoral immune activity. This is associated with the increase of the effector T-cells and a dramatic reduction of the intratumor Tregs [40].

Unlike CTLA-4, the main site of action for the PD-1 is in the tumor microenvironment, where it inhibits CD8+ T cells. PD-1 can be upregulated on both circulating tumor-specific T cells and tumor-infiltrating lymphocytes upon stimulation through T cell receptor or exposition to different cytokines (e.g., IL-2, IL-7, IL-15, IL-21). PD-1 ligands are PD-L1 and PD-L2, both expressed by cancer cells or APC within the tumor and upregulated under IFN-γ stimulation [41].

Figure 8.1 illustrates the microenvironment determinants based on the type of response to ICIs.

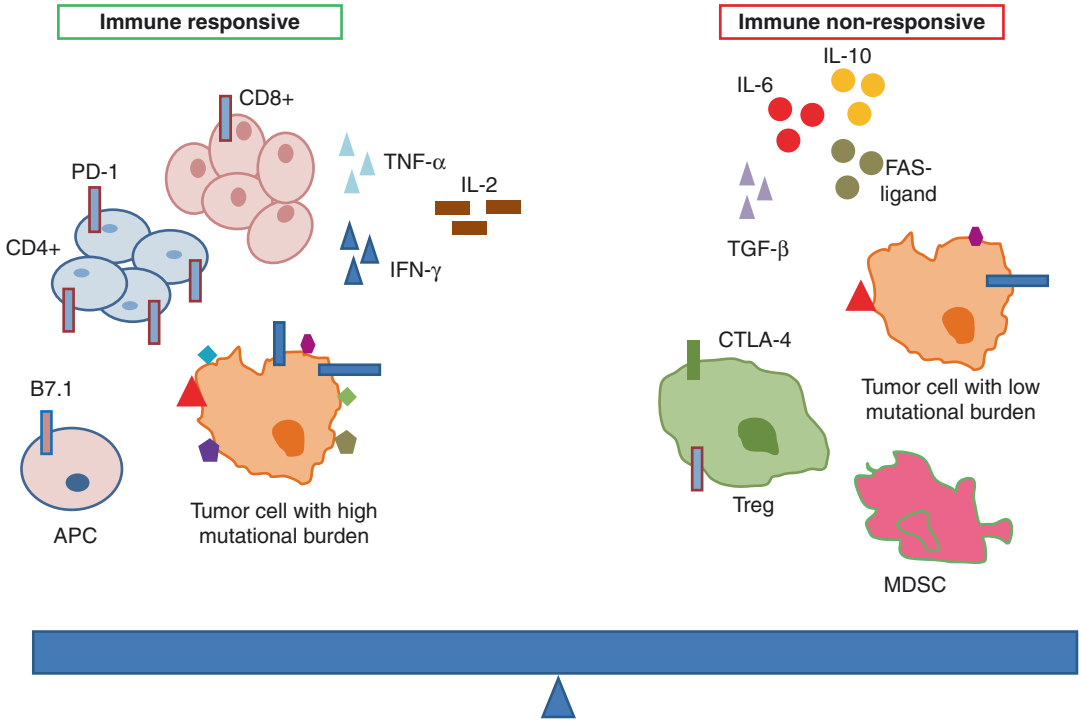

Fig. 8.1 An overview of the microenvironment predominance in case of immune response or not to ICIs

8.4 Assessment of Treatment Response

8.4.1 Anatomic Response Assessment

First imaging response criteria, i.e., World Health Organization (WHO) and Response Evaluation Criteria in Solid Tumors (RECIST), were created to assess tumor response from conventional treatments, such as chemotherapy, radiotherapy, and surgery. In fact, they were essentially based on tumor shrinkage without considering the appearance of new lesions [42, 43]. In 2009, new RECIST 1.1 criteria were established trying to address some of the pitfalls with the previous ones, such as the assessment of lymph nodes, number of lesions evaluated, and the use of new imaging techniques (e.g., CT, MRI) [44]. However, the development of ICI has generated a plethora of new imaging patterns, which are fundamental to recognize when assessing tumor response. As a consequence, the immune-related Response Criteria (irRC), followed by their simplification immune-related RECIST (irRECIST), were developed to standardize treatment evaluation during ICI [45, 46]. irRC consider bidimensional (unidimensional for irRECIST) measurement of lesions and include new lesions in the computation of total tumor burden along with index lesions. Main difference for immune versus traditional response criteria is the definition of progressive disease (PD). In fact, PD needs to be confirmed at least after 4 weeks from first progression report, in addition to an increase of total tumor burden >25%, or progression on non-target lesions, or new lesions. Last morphologic criteria published were those from Seymour and colleagues [47], so-called iRECIST ("*i*" immune), proposed mostly for research purposes

rather than to guide clinical practice. They introduced unconfirmed progressive disease (iUPD) as new response: in case of iUPD that is confirmed on a subsequent scan by a further increase in size of the lesion, the response becomes iCPD (confirmed progressive disease), otherwise iCR (complete response), iPR (partial response), or iSD (stable disease) if tumor regression occurs.

8.4.2 Metabolic Response Criteria

Innovative anticancer agents, such as inhibitors of CTLA-4 or PD-1/PD-L1 pathway, are more cytostatic than cytotoxic. Therefore, tumor response can also be seen by reduction of metabolic activity rather than reduction in size [48]. In 1999, the European Organization for Research and Treatment of Cancer (EORTC) criteria were the first metabolic criteria published, based on percentage change of standardized uptake value (SUV), although number of lesions and minimum SUVmax level were not specified [49]. In immunotherapy setting, EORTC criteria were initially adopted by Sachpekidis et al. [50] in metastatic melanoma. The authors demonstrated that early 18F-FDG PET/CT after two cycles of ipilimumab was highly predictive of the final treatment outcome between patients with progressive and stable metabolic disease. Ten years later, PET Response Criteria in Solid Tumors (PERCIST) have been published to assess treatment response [51]. The main difference with EORTC is the introduction of the standardized uptake value (SUV) corrected for lean body mass (SUL) and the SULpeak, measured within a spherical region of interest of diameter 1.2 cm within the area of highest uptake in the tumor. Furthermore, a threshold of at least 30% of SUVlean reduction was recommended to define partial response (PR), which is higher than that proposed by EORTC (i.e., 25%). PERCIST criteria repeat, in a certain way, RECIST ones, by considering SUL measuring in up to five lesions (up to two per organ) for target lesions.

Afterwards, Cho et al. [52] combined morphologic (RECIST 1.1, irRC) and metabolic criteria (EORTC, PERCIST) to detect early evidence of response during treatment with ICI in advanced melanoma. In particular, in patients with stable disease by RECIST 1.1 at 3–4 weeks, a change of SULpeak threshold of 15.5% of hottest lesion well differentiated patients with and without clinical benefit at 4 months, yielding sensitivity of 100%, specificity of 93%, and overall accuracy of 95%. Thus, such new criteria were termed as PET/CT Criteria for Early Prediction of Response to Immune Checkpoint Inhibitor Therapy (PECRIT).

On the other hand, another paper from German researchers highlighted the importance of the absolute number of new lesions rather than SUV values to predict response to ipilimumab [53]. According the so-called PET Response Evaluation Criteria for Immunotherapy (PERCIMT), a cut-off value of 4 new lesions of any size led to a sensitivity of 84% and a specificity of 100% to correctly predict clinical benefit and no-clinical benefit after four cycles of ipilimumab, respectively. Then, the threshold value was lower for lesions with larger functional diameter (i.e., 3 for lesions >1 cm, and 2 for lesions >1.5 cm).

Recently, Ito and colleagues [54] from Memorial Sloan Kettering Cancer Center proposed a new version of PERCIST, named "immunotherapy-modified" (im) PERCIST. The key point behind these newer criteria is the interpretation of new lesions. In contrast to PERCIST criteria where new lesions always configure a progressive metabolic disease, in imPERCIST progression can be assessed only if the sum of SULpeak of up to 5 target lesions (not necessarily the same lesions identified at baseline) increases by at least 30%. To confirm potential positive impact in clinical practice, imPERCIST was demonstrated the only independent factor associated with OS (HR 3.853, 95%CI 1.498–9.911, p = 0.005).

Table 8.2 summarizes main features of metabolic response criteria.

Figure 8.2 illustrates the stopping rules related to the different anatomical and metabolic criteria.

Table 8.2 Main features of 18F-FDG PET/CT based response criteria

	EORTC [49]	PERCIST [51]	PERCIMT [53]	imPERCIST [54]
CMR	Disappearance of all metabolically active lesions	Disappearance of all metabolically active lesions	No new lesions	Same as PERCIST
PMR	Reduction (15–25%) in SUV after one cycle of chemotherapy, or Reduction (>25%) after more than one treatment cycle	Reduction (>30%, >0.8 unit) in SULpeak in the hottest target lesion	No new lesions	Same as PERCIST
SMD	Increase (<25%) in SUV, or Reduction (<15%) in SUV	Neither PMD nor PMR/CMR	Neither PMD nor PMR/CMR	Same as PERCIST
PMD	Increase (>25%) in SUV, or New metastatic lesions	Increase (>30%, >0.8 unit) in SULpeak in the hottest target lesion, or New ^{18}F-FDG avid lesions	4 or more new lesions (<1 cm in functional diameter), or 3 or more new lesions (>1 cm in functional diameter), or 2 or more new lesions (>1 cm in functional diameter)	Increase (>30%, >0.8 unit) in SULpeak in the hottest target lesion

CMR complete metabolic response, *PMR* partial metabolic response, *SMD* stable metabolic disease, *PMD* progressive metabolic disease, *EORTC* European Organization for Research and Treatment of Cancer, *PERCIST* PET Response Criteria in Solid Tumors, *imPERCIST* immunotherapy-modified PERCIST, *RECIST* Response Evaluation Criteria In Solid Tumors, *PERCIMT* PET Response Evaluation Criteria for Immunotherapy

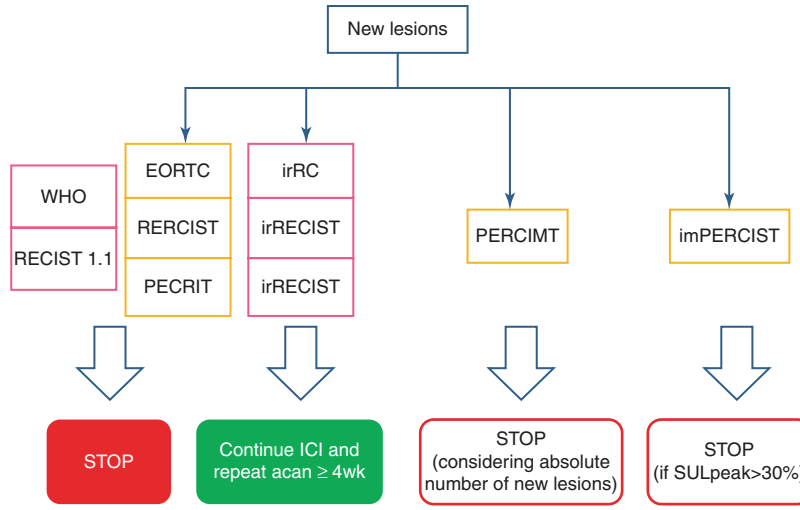

Fig. 8.2 Flowchart of clinical decision based on morphologic or metabolic criteria

8.4.3 Responders Vs. Non-Responders

In spite of the important success of ICI, response rates range from 19% for anti-CTLA-4 to 44% for anti-PD-1 when considered as monotherapies until 56% in the studies where the two agents are in combination [18]. Clinically we can distinguish resistance to ICI in two categories of patients: 1) those that will never respond (innate resistance) and 2) those the initially respond, but actually develop disease progression (acquired resistance) (Fig. 8.3). Therefore, there is a compelling need to identify potential predictive biomarkers for differentiating responders and non-responders [55, 56]. To date several factors have been studied, each with their own strengths and weaknesses, as well as others are under investigation [57, 58] (Fig. 8.4).

As we know, FDA approved pembrolizumab in patients with untreated metastatic NSCLC with PD-L1 expression ≥50%, highlighting its

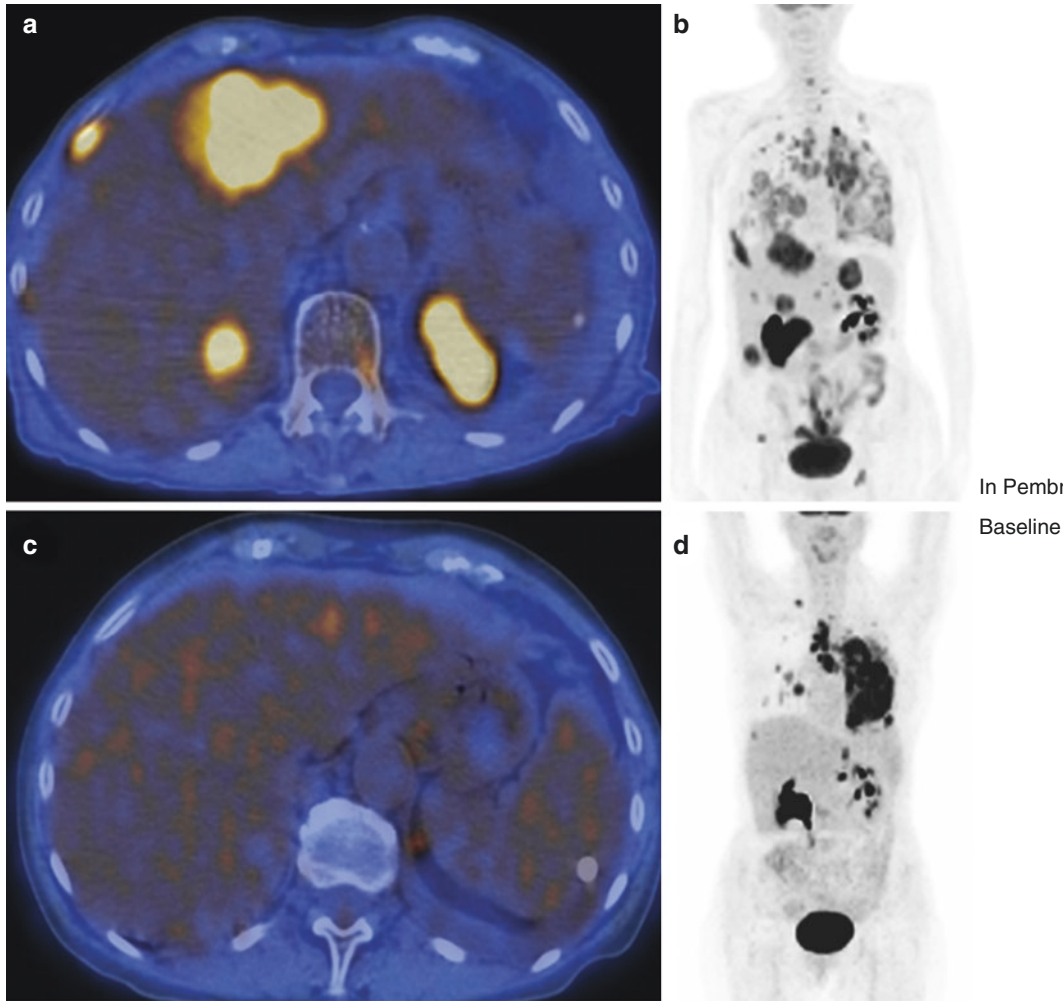

Fig. 8.3 Comparison of FDG PET/CT scans of a NSCLC patient investigated at baseline and after three cycles of pembrolizumab; MIP (maximal intensity projection) images are shown on the right side, while fused axial views on the left illustrate part of the lesions progressing during ICI. Despite a partial metabolic response on the primary left lung mass, overall the patient was in disease progression

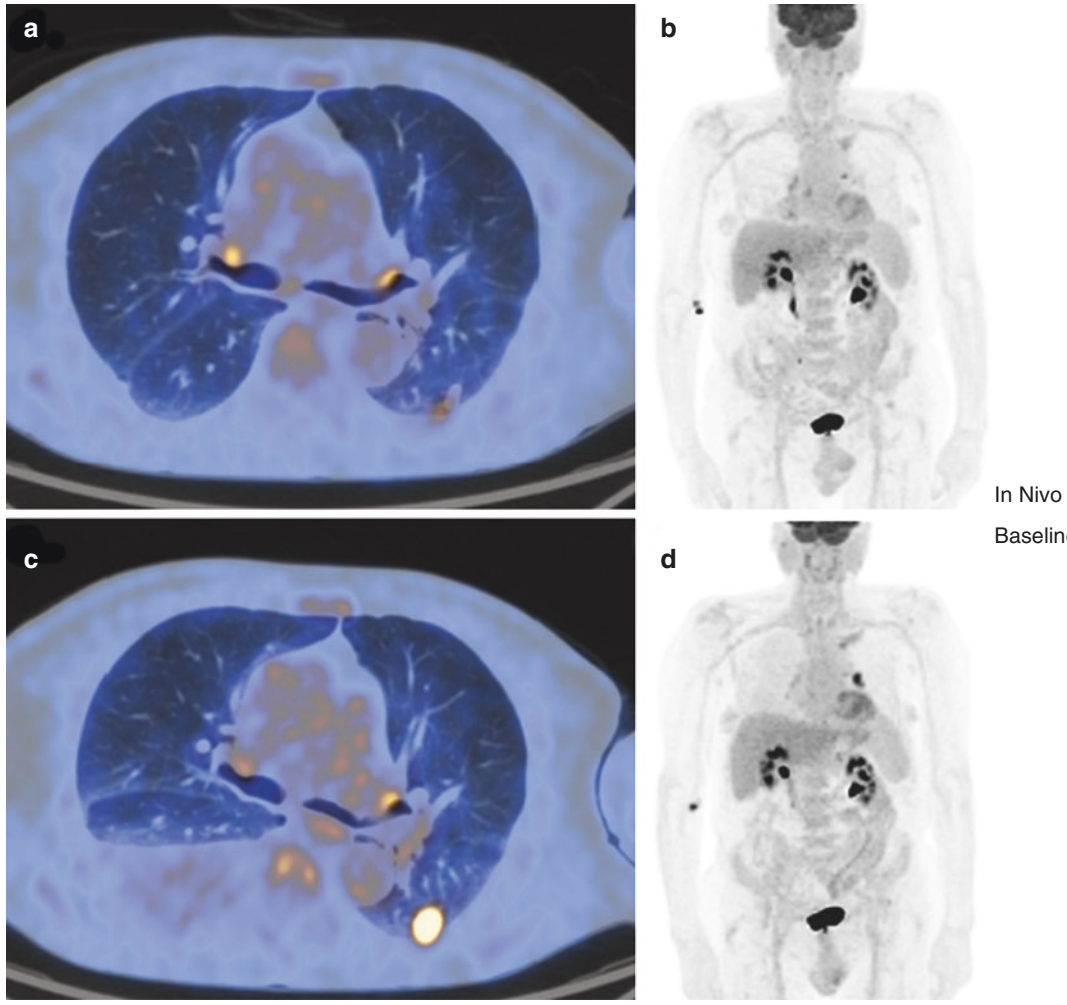

Fig. 8.4 Fused FDG PET/CT and MIP images illustrate herein a NSCLC patient responding to immunotherapy; the scans were performed at baseline and after four cycles of nivolumab. The left lung nodule resulted in partial metabolic and morphological response to ICI

role in patients' selection. Nevertheless, PD-L1 expression as a predictive biomarker in other tumors other than NSCLC is still matter of debate [59]. Beside PD-L1 tumor expression, TILs and other immune cells play an important role in the tumor microenvironment. Several studies have demonstrated that high numbers of TILs, which configure an immune inflamed phenotype, are associated with better clinical outcomes [60]. Among circulating factors, lactate dehydrogenase (LDH) and peripheral immune cell counts were identified as potential predictors of response to ICI [61–63]. Likewise, elevated expression of IFN-γ or IFN-γ-related genes are associated to response to atezolizumab, although in a phase I study. On the other hand, circulating tumor DNA (ctDNA) has been associated with tumor burden and progression in melanoma patients [64, 65].

Melanoma and NSCLC are characterized by great amount of somatic mutations, as well as tumors with deficiency in DNA repair mechanisms, such as colorectal cancers. As a result, these mutations generate novel proteins, so-called neo-antigens, resulting in a higher binding affinity to MHC and TCR, which enhance

immune cells readily to target and to eliminate tumor cells [66, 67].

Finally, immuno-PET is a new non-invasive imaging technique which permits to track CD8+ T cells or to distinguish PD-L1 positive tumors in preclinical models [68, 69]. It is reasonable in an immediate future that immuno-PET will allow to overcome some issues related to tumor tissue heterogeneity.

8.4.4 Pitfalls and beyond (Pseudo-, Hyper-Progression, irAEs, Brain Mets, Cost-Effectiveness)

Owing to their different mechanism of action, ICI have also determined response patterns different from those observed with conventional cytotoxic drugs. Two atypical patterns have been described during treatment with ICI: pseudo-progression (Fig. 8.5) and hyper-progression. The first was defined as an initial tumor increase in metabolic tumor volume or appearance of new lesions followed by their shrinkage in the subsequent evaluations [70]. The pathophysiological mechanism underlying pseudo-progression could be related to a temporary immune cell infiltration within the tumor associated with edema and necrosis or associated to tumor growing until an adequate immune response is generated [70, 71]. Despite pseudo-progression represents a rare phenomenon, ranging between 0.6% and 4.7%, and limited mostly to case reports, oncologists should be aware of such event and in order to discern between true progression and pseudo-progression should consider multiple features, such as performance status along with imaging and, in case, biopsy [47]. On the other hand, the definition of hyper-progression is quite variable among studies. Champiat et al. [72] defined this phenomenon as a progression of the disease at first evaluation according to RECIST 1.1 and an increase of more than twofold of the tumor growth rate, while for Matos et al. [73] hyper-progression was defined based on a time-to-treatment failure <2 months and a minimum increase in measurable lesion of 10 mm plus increase of ≥40% in target tumor burden at baseline or increase of ≥20% with the appearance of multiple new lesions from baseline. In another paper with metastatic head and neck squamous cell carcinoma treated with anti-PD1/PD-L1 therapy, hyper-progression was defined as an increase of more than two times of the tumor growth kinetics rate (ratio between pre and post starting immunotherapy) [74]. However, regardless of definition, patients with hyper-progression showed worse clinical outcome.

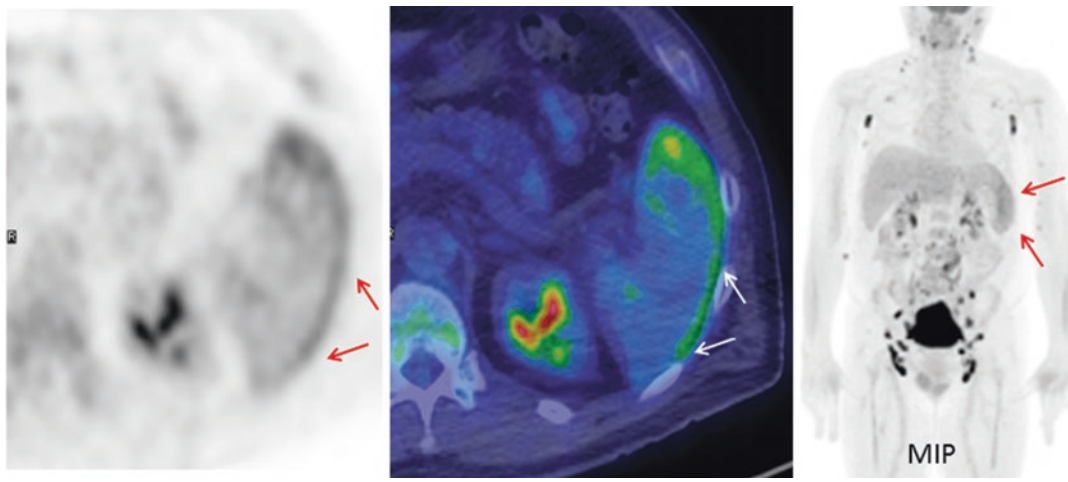

Fig. 8.5 This is the case of a melanoma patient treated with ipilimumab and presenting with diffuse supra- and infra-diaphragmatic adenopathies. Note the appearance of increased spleen uptake during ICI, frequently associated with pseudo-progression

Beside the abovementioned patterns, ICI can also determine peculiar immune-related adverse events (irAEs), which assume double importance. On one hand, they may represent a potential source of error when evaluating 18F-FDG PET/CT images, and on the other hand a late diagnosis and management of severe irAEs can compromise patient's life. These irAEs, essentially caused by a hyperstimulation of T cells, can interest any part of the body [75, 76]. Although irAEs are the same, their incidence rate varies among class of antibodies. A recent meta-analysis showed a higher number of irAEs in patients treated with anti-CTLA-4 (54%) than anti-PD-1 (26%), or anti-PD-L1 (17%) [77]. Moreover, death related to irAEs is quite rare (1%) mostly due to colitis, diarrhea, perforation, or hepatitis. Another potential severe or life-threatening irAE is represented by pneumonitis, mostly seen with anti-PD-1 agents [78]. As a matter of fact, clinicians, especially radiologists and nuclear medicine physicians, must be familiar about the atypical tumor response patterns and common irAEs seen at imaging of patients undergoing treatment with this novel class of drugs.

Another feature that need to be deepened regards the brain metastases. Approximately 15–30% of cancer patients develop brain metastases, with NSCLC as the most common primary tumor followed by melanoma and breast cancer [79]. Nevertheless, as these patients have been excluded for a long time from clinical trials, we still have paucity of evidence for brain metastases with checkpoint inhibitors. One of the main reason of exclusion was the consideration of the blood–brain barrier as cause of non-response for systemic therapies, making brain an immune-privileged site [79, 80]. However, the identification of TILs within brain metastases has induced researchers to test ICI in these subgroup of patients [81]. To date, few ongoing studies are evaluating ICI, alone or in combination with radiotherapy or other agents, for treatment of brain metastases [82–85].

Last but not least drawback associated with ICI treatment is represented by the financial side. In fact, most of clinical trials do not include cost analysis: considering that the mean prices for nivolumab and pembrolizumab are $28.78/mg and $51.79/mg, it is clear that the use of ICI would generate a cost of more than 1 million for patients [86]. A recent systematic review showed that pembrolizumab was cost-effective for recurrent/metastatic NSCLC, while nivolumab would have been cost-effective if PD-L1 cutoffs were applied. Contrary to ipilimumab, either nivolumab or pembrolizumab were cost-effective for melanoma, whereas nivolumab or pembrolizumab was not cost-effective for both head/neck and genitourinary cancers [87].

Pictorial examples of response to ICI are illustrated in Figs. 8.1, 8.2 and 8.3.

Teaching Points

- Consider which type of checkpoint inhibitor (anti-CTLA-4, anti-PD-1, or anti-PD-L1) or their combination has been adopted when evaluating treatment response.
- Take note of the number of cycles and last administration date.
- Focus on the possible presence of symptoms related to the two most severe, potential life-threating, irAEs (e.g., pneumonia, colitis).
- Usually, irAEs are more common with anti-CTLA-4.
- Both traditional morphologic and metabolic criteria have proven some limitations for the assessment during treatment with ICI.
- Although not indicated in the metabolic response criteria, it might be useful to report volumetric PET parameters, such as TLG and MTV.
- Identify the target lesions and their metabolic activity (SULpeak) at baseline and at follow-up scan.
- Take into account that the appearance of new lesions is not synonym of progression disease: only if summed SULpeak in the follow-up scan is ≥30%, progressive disease can be called.
- Refer to baseline PET/CT when irAE is suspected: the early increase of FDG uptake in some organ is often indicative of irAE.
- Evaluate site and distribution of new lesions: diffuse splenic uptake, symmetric hilar and medias-

tinal uptake, sarcoidosis-like signs, increased uptake in organs whose typically are rare site of metastases (e.g., thyroid, pituitary gland).
- Focus on lung parenchyma and colorectal uptake to exclude pneumonia and colitis, respectively.

References

1. Hodi FS, O'Day SJ, McDermott DF, et al. Improved survival with ipilimumab in patients with metastatic melanoma. N Engl J Med. 2010;363:711–23.
2. Raedler LA. Opdivo (nivolumab): second PD-1 inhibitor receives FDA approval for unresectable or metastatic melanoma. Am Health Drug Benefits. 2015;8:180–3.
3. Chuk MK, Chang JT, Theoret MR, et al. FDA approval summary: accelerated approval of pembrolizumab for second-line treatment of metastatic melanoma. Clin Cancer Res. 2017;23:5666–70.
4. Motzer RJ, Escudier B, McDermott DF, et al. CheckMate 025 Investigators. Nivolumab versus everolimus in advanced renal-cell carcinoma. N Engl J Med. 2015;373:1803–13.
5. Balar AV, Galsky MD, Rosenberg JE, et al. IMvigor210 study group. Atezolizumab as first-line treatment in cisplatin-ineligible patients with locally advanced and metastatic urothelial carcinoma: a single-arm, multicentre, phase 2 trial. Lancet. 2017;389:67–76.
6. Armand P, Shipp MA, Ribrag V, et al. Programmed death-1 blockade with pembrolizumab in patients with classical hodgkin lymphoma after brentuximab vedotin failure. J Clin Oncol. 2016;34:3733–9.
7. Ferris RL, Blumenschein G Jr, Fayette J, et al. Nivolumab for recurrent squamous-cell carcinoma of the head and neck. N Engl J Med. 2016;375:1856–67.
8. Brahmer J, Reckamp KL, Baas P, et al. Nivolumab versus docetaxel in advanced squamous-cell non-small-cell lung cancer. N Engl J Med. 2015;373(2):123–35.
9. Borghaei H, Paz-Ares L, Horn L, et al. Nivolumab versus docetaxel in advanced nonsquamous non–small-cell lung cancer. N Engl J Med. 2015;373(17):1627–39.
10. Herbst RS, Baas P, Kim DW, et al. Pembrolizumab versus docetaxel for previously treated, PD-L1-positive, advanced non-small-cell lung cancer (keynote-010): a randomised controlled trial. Lancet. 2016;387:1540–50.
11. Schadendorf D, Hodi FS, Robert C, et al. Pooled analysis of long-term survival data from phase II and phase III trials of ipilimumab in unresectable or metastatic melanoma. J Clin Oncol. 2015;33(17):1889–94.
12. Ascierto PA, Del Vecchio M, Robert C, et al. Ipilimumab 10 mg/kg versus ipilimumab 3 mg/kg in patients with unresectable or metastatic melanoma: a randomised, double-blind, multicentre, phase 3 trial. Lancet Oncol. 2017;18(5):611–22.
13. Hamid O, Puzanov I, Dummer R, et al. Final analysis of a randomised trial comparing pembrolizumab versus investigator-choice chemotherapy for ipilimumab-refractory advanced melanoma. Eur J Cancer. 2017;86:37–45.
14. Robert C, Long GV, Brady B, et al. Nivolumab in previously untreated melanoma without BRAF mutation. N Engl J Med. 2015;372(4):320–30.
15. Robert C, Schachter J, Long GV, et al. Pembrolizumab versus ipilimumab in advanced melanoma. N Engl J Med. 2015;372(26):2521–32.
16. Schachter J, Ribas A, Long GV, et al. Pembrolizumab versus ipilimumab for advanced melanoma: final overall survival results of a multicentre, randomised, open-label phase 3 study (KEYNOTE-006). Lancet. 2017;390(10105):1853–62.
17. Weber JS, D'Angelo SP, Minor D, et al. Nivolumab versus chemotherapy in patients with advanced melanoma who progressed after anti-CTLA-4 treatment (CheckMate 037): a randomised, controlled, open-label, phase 3 trial. Lancet Oncol. 2015;16(4):375–84.
18. Larkin J, Chiarion-Sileni V, Gonzalez R, et al. Combined nivolumab and ipilimumab or monotherapy in untreated melanoma. N Engl J Med. 2015;373(1):23–34.
19. Wolchok JD, Chiarion-Sileni V, Gonzalez R, et al. Overall survival with combined nivolumab and ipilimumab in advanced melanoma. N Engl J Med. 2017;377(14):1345–56.
20. Eggermont AMM, Chiarion-Sileni V, Grob J-J, et al. Prolonged survival in stage III melanoma with ipilimumab adjuvant therapy. N Engl J Med. 2016;375(19):1845–55.
21. Eggermont AMM, Chiarion-Sileni V, Grob JJ, et al. Adjuvant ipilimumab versus placebo after complete resection of high-risk stage III melanoma (EORTC 18071): a randomised, double-blind, phase 3 trial. Lancet Oncol. 2015;16(5):522–30.
22. Weber J, Mandala M, Del Vecchio M, et al. Adjuvant therapy with nivolumab (NIVO) versus ipilimumab (IPI) after complete resection of stage III/IV melanoma: updated results from a phase III trial (CheckMate 238). J Clin Oncol. 2018;36(supplement 15):9502.
23. Eggermont AMM, Blank CU, Mandala M, et al. Adjuvant pembrolizumab versus placebo in resected stage III melanoma. N Engl J Med. 2018;378(19):1789–801.
24. Rothermel LD, Sarnaik AA, Khushalani NI, Sondak VK. Current immunotherapy practices in melanoma. Surg Oncol Clin N Am. 2019;28(3):403–18.
25. Garon EB, Rizvi NA, Hui R, et al. Pembrolizumab for the treatment of non-small-cell lung cancer. N Engl J Med. 2015;372(21):2018–28.
26. Fehrenbacher L, Spira A, Ballinger M, et al. Atezolizumab versus docetaxel for patients with previously treated non-small-cell lung cancer (POPLAR):

a multicentre, open-label, phase 2 randomised controlled trial. Lancet. 2016;387(10030):1837–46.
27. Forde PM, Chaft JE, Smith KN, et al. Neoadjuvant PD-1 blockade in resectable lung cancer. N Engl J Med. 2018;378(21):1976–86.
28. Rosenberg JE, Hoffman-Censits J, Powles T, et al. Atezolizumab in patients with locally advanced and metastatic urothelial carcinoma who have progressed following treatment with platinum-based chemotherapy: a single-arm, multicentre, phase 2 trial. Lancet. 2016;387(10031):1909–20.
29. Massard C, Gordon MS, Sharma S, et al. Safety and efficacy of durvalumab (MEDI4736), an anti-programmed cell death ligand-1 immune checkpoint inhibitor, in patients with advanced urothelial bladder cancer. J Clin Oncol. 2016;34(26):3119–25.
30. Heery CR, O'Sullivan-Coyne G, Madan RA, et al. Avelumab for metastatic or locally advanced previously treated solid tumours (JAVELIN solid tumor): a phase 1a, multicohort, dose-escalation trial. Lancet Oncol. 2017;18(5):587–98.
31. Sharma P, Retz M, Siefker-Radtke A, et al. Nivolumab in metastatic urothelial carcinoma after platinum therapy (CheckMate 275): a multicentre, single-arm, phase 2 trial. Lancet Oncol. 2017;18(3):312–22.
32. Sharma P, Callahan MK, Bono P, et al. Nivolumab monotherapy in recurrent metastatic urothelial carcinoma (CheckMate 032): a multicentre, open-label, two stage, multi-arm, phase 1/2 trial. Lancet Oncol. 2016;17(11):1590–8.
33. Plimack ER, Bellmunt J, Gupta S, et al. Safety and activity of pembrolizumab in patients with locally advanced or metastatic urothelial cancer (KEYNOTE-012): a non-randomised, open-label, phase 1b study. Lancet Oncol. 2017;18(2):212–20.
34. Bellmunt J, de Wit R, Vaughn DJ, et al. Pembrolizumab as second-line therapy for advanced urothelial carcinoma. N Engl J Med. 2017;376(11):1015–26.
35. Balar AV, Castellano D, O'Donnell PH, et al. First-line pembrolizumab in cisplatin-ineligible patients with locally advanced and unresectable or metastatic urothelial cancer (KEYNOTE-052): a multicentre, single-arm, phase 2 study. Lancet Oncol. 2017;18(11):1483–92.
36. Dogan V, Rieckmann T. Mu¨nscher a, et al. current studies of immunotherapy in head and neck cancer. Clin Otolaryngol. 2018;43(1):13–21.
37. Joshi SS, Maron SB, Catenacci DV. Pembrolizumab for treatment of advanced gastric and gastroesophageal junction adenocarcinoma. Future Oncol. 2018;14(5):417–30.
38. Galluzzi L, Buqué A, Kepp O, Zitvogel L, Kroemer G. Immunological effects of conventional chemotherapy and targeted anticancer agents. Cancer Cell. 2015;28(6):690–714.
39. Topalian SL, Drake CG, Pardoll DM. Immune checkpoint blockade: a common denominator approach to cancer therapy. Cancer Cell. 2015;27(4):450–61.
40. Postow MA, Callahan MK, Wolchok JD. Immune checkpoint blockade in cancer therapy. J Clin Oncol. 2015;33:1974–82.
41. Pardoll D. The blockade of immune checkpoints in cancer immunotherapy. Nat Rev Cancer. 2012;12:252–64.
42. Miller AB, Hoogstraten B, Staquet M, Winkler A. Reporting results of cancer treatment. Cancer. 1981;47:207–14.
43. Therasse P, Arbuck SG, Eisenhauer EA, et al. New guidelines to evaluate the response to treatment in solid tumors. J Natl Cancer Inst. 2000;92(3):205–16.
44. Eisenhauer EA, et al. New response evaluation criteria in solid tumours: revised RECIST guideline (version 1.1). Eur J Cancer. 2009;45(2):228–47.
45. Wolchok JD, Hoos A, O'Dav S, Weber JS, Hamid O, Lebbe C, Maio M, Binder M, Bohnsack O, Nichol G, Humphrey R, Hodi FS. Guidelines for the evaluation of immune therapy activity in solid tumors: immune-related response criteria. Clin Cancer Res. 2009;15:7412–20.
46. Nishino M, Giobbie-Hurder A, Gargano M, Suda M, Ramaiya NH, Hodi FS. Developing a common language for tumor response to immunotherapy: immune-related response criteria using unidimensional measurements. Clin Cancer Res. 2013;19:3936–43.
47. Seymour L, Bogaerts J, Perrone A, et al. iRECIST: guidelines for response criteria for use in trials testing immunotherapeutics. Lancet Oncol. 2017;18:e143–52.
48. Aide N, Hicks RJ, Le Tourneau C, et al. FDG PET/CT for assessing tumour response to immunotherapy: report on the EANM symposium on immune modulation and recent review of the literature. Eur J Nucl Med Mol Imaging. 2019;46(1):238–50.
49. Young H, Baum R, Cremerius U, et al. Measurement of clinical and subclinical tumour response using [18F]-fluorodeoxyglucose and positron emission tomography: review and 1999 EORTC recommendations. European Organization for Research and Treatment of cancer (EORTC) PET study group. Eur J Cancer. 1999;35:1773–82.
50. Sachpekidis C, Larribere L, Pan L, Haberkorn U, Dimitrakopoulou-Strauss A, Hassel JC. Predictive value of early 18F-FDG PET/CT studies for treatment response evaluation to ipilimumab in metastatic melanoma: preliminary results of an ongoing study. Eur J Nucl Med Mol Imaging. 2015;42:386–96.
51. Wahl RL, Jacene H, Kasamon Y, Lodge MA. From RECIST to PERCIST: evolving considerations for PET response criteria in solid tumors. J Nucl Med. 2009;50(Suppl 1):122s–50s.
52. Cho SY, Lipson EJ, Im H-J, Rowe SP, Gonzalez EM, Blackford A, Chirindel A, Pardoll DM, Topalian SL, Wahl RL. Prediction of response to immune checkpoint inhibitor therapy using early-time-point 18F-FDG PET/CT imaging in patients with advanced melanoma. J Nucl Med. 2017;58:1421–8.
53. Anwar H, Sachpekidis C, Winkler J, Kopp-Schneider A, Haberkorn U, Hassel JC, Dimitrakopoulou-Strauss A. Absolute number of new lesions on 18F-FDG PET/CT is more predictive of clinical response than SUV changes in metastatic melanoma patients

receiving ipilimumab. Eur J Nucl Med Mol Imaging. 2018;45:376–83.
54. Ito K, Teng R, Schöder H, et al. 18F-FDG PET/CT for monitoring of Ipilimumab therapy in patients with metastatic melanoma. J Nucl Med. 2019;60:335–41.
55. Rossi S, Toschi L, Castello A, et al. Clinical characteristics of patient selection and imaging predictors of outcome in solid tumors treated with checkpoint-inhibitors. Eur J Nucl Med Mol Imaging. 2017;44:2310–25.
56. Rossi S, Castello A, Toschi L, Lopci E. Immunotherapy in non-small-cell lung cancer: potential predictors of response and new strategies to assess activity. Immunotherapy. 2018;10:797–805.
57. Sharma P, Hu-Lieskovan S, Wargo JA, Ribas A. Primary, adaptive, and acquired resistance to cancer immunotherapy. Cell. 2017;168(4):707–23.
58. Seidel JA, Otsuka A, Kabashima K, et al. Anti-PD-1 and Anti-CTLA-4 therapies in cancer: mechanisms of action, efficacy, and limitations. Front Oncol. 2018;8:86.
59. Aguiar PN, et al. The role of PD-L1 expression as a predictive biomarker in advanced non-small-cell lung cancer: a network meta-analysis. Immunotherapy. 2016;8:479–88.
60. Balatoni T, et al. Tumor-infiltrating immune cells as potential biomarkers predicting response to treatment and survival in patients with metastatic melanoma receiving ipilimumab therapy. Cancer Immunol Immunother. 2018;67:141–51.
61. Martens A, et al. Baseline peripheral blood biomarkers associated with clinical outcome of advanced melanoma patients treated with ipilimumab. Clin Cancer Res. 2016;22:2908–18.
62. Delyon J, et al. Experience in daily practice with ipilimumab for the treatment of patients with metastatic melanoma: an early increase in lymphocyte and eosinophil counts is associated with improved survival. Ann Oncol. 2013;24:1697–703.
63. Kelderman S, et al. Lactate dehydrogenase as a selection criterion for ipilimumab treatment in metastatic melanoma. Cancer Immunol Immunother. 2014;63:449–58.
64. Maleki Vareki S, Garrigos C, Duran I. Biomarkers of response to PD-1/PD-L1 inhibition. Crit Rev Oncol Hematol. 2017;116:116–24.
65. Lee JH, Long GV, Boyd S, Lo S, Menzies AM, Tembe V, et al. Circulating tumour DNA predicts response to anti-PD1 antibodies in metastatic melanoma. Ann Oncol. 2017;28(5):1130–6.
66. Schumacher TN, Schreiber RD. Neoantigens in cancer immunotherapy. Science. 2015;348:69–74.
67. Rizvi NA, et al. Mutational landscape determines sensitivity to PD-1 blockade in non–small cell lung cancer. Science. 2015;348:124.
68. Tavare R, et al. An effective immuno-PET imaging method to monitor CD8-dependent responses to immunotherapy. Cancer Res. 2016;76:73–82.
69. Maute RL, et al. Engineering high-affinity PD-1 variants for optimized immunotherapy and immuno-PET imaging. Proc Natl Acad Sci U S A. 2015;112:E6506–14.
70. Chiou VL, Burotto M. Pseudoprogression and immune-related response in solid tumors. J Clin Oncol. 2015;33(31):3541–3.
71. Hodi FS, Hwu WJ, Kefford R, Weber JS, Daud A, Hamid O, Patnaik A, Ribas A, Robert C, Gangadhar TC, Joshua AM, Hersey P, Dronca R, Joseph R, Hille D, Xue D, Li XN, Kang SP, Ebbinghaus S, Perrone A, Wolchok JD. Evaluation of immune-related response criteria and RECIST v1.1 in patients with advanced melanoma treated with Pembrolizumab. J Clin Oncol. 2016;34:1510–7.
72. Champiat S, Dercle L, Ammari S, Massard C, Hollebecque A, Postel-Vinay S, et al. Hyperprogressive disease is a new pattern of progression in cancer patients treated by anti-PD-1/PD-L1. Clin Cancer Res. 2017;23:1920–8.
73. Matos I, Martin-Liberal J, Hierro C, et al. Incidence and clinical implications of a new definition of hyperprogression (HPD) with immune checkpoint inhibitors (ICIs) in patients treated in phase 1 (Ph1) trials. J Clin Oncol. 2018;36(15 Suppl):3032.
74. Saâda-Bouzid E, Defaucheux C, Karabajakian A, et al. Hyperprogression during anti-PD-1/PD-L1 therapy in patients with recurrent and/or metastatic head and neck squamous cell carcinoma. Ann Oncol. 2017;28:1605–11.
75. Michot JM, Bigenwald C, Champiat S, et al. Immune-related adverse events with immune checkpoint blockade: a comprehensive review. Eur J Cancer. 2016;54:139–48.
76. Wong AN, McArthur GA, Hofman MS, et al. The advantages and challenges of using FDG PET/CT for response assessment in melanoma in the era of targeted agents and immunotherapy. Eur J Nucl Med Mol Imaging. 2017;44(Suppl 1):67–77.
77. El Osta B, Hu F, Sadek R, Chintalapally R, Tang SC. Not all immune-checkpoint inhibitors are created equal: meta-analysis and systematic review of immune-related adverse events in cancer trials. Crit Rev Oncol Hematol. 2017;119:1–12.
78. Nishino M, Giobbie-Hurder A, Hatabu H, Ramaiya NH, Hodi FS. Incidence of programmed cell death 1 inhibitor–related pneumonitis in patients with advanced cancer: a systematic review and meta-analysis. JAMA Oncol. 2016;2(12):1607–16.
79. Kourie HR, Kanaan H, Awada G, Awada AH. Checkpoint inhibitors in the treatment of brain metastases of non-small-cell lung cancer and melanoma. Future Oncol. 2017 May;13(12):1097–103.
80. Rossi S, Finocchiaro G, Marchetti S, et al. Checkpoint inhibitors: 'raising the bar' also in brain metastases from non-small-cell lung cancer? Immunotherapy. 2018;10(5):403–10.
81. Harter PN, Bernatz S, Scholz A, et al. Distribution and prognostic relevance of tumor-infiltrating lymphocytes (TILs) and PD-1/PD-L1 immune checkpoints in human brain metastases. Oncotarget. 2015;6(38):40836–49.

82. Margolin K, Ernstoff MS, Hamid O, et al. Ipilimumab in patients with melanoma and brain metastases: an open-label, phase II trial. Lancet Oncol. 2012;13(5):459–65.
83. Di Giacomo AM, Ascierto PA, Pilla L, et al. Ipilimumab and fotemustine in patients with advanced melanoma (NIBIT-M1): an open-label, single-arm phase II trial. Lancet Oncol. 2012;13(9):879–86.
84. Goldberg SB, Gettinger SN, Mahajan A, et al. Pembrolizumab for patients with melanoma or non-small-cell lung cancer and untreated brain metastases: early analysis of a non-randomised, open-label, phase II trial. Lancet Oncol. 2016;17(7):976–83.
85. Kotecha R, Kim JM, Miller JA, et al. The impact of sequencing PD-1/PD-L1 inhibitors and stereotactic radiosurgery for patients with brain metastasis. Neuro Oncol. 2019;21(8):1060–8.
86. Andrews A. Treating with checkpoint inhibitors-figure $1 million per patient. Am Health Drug Benefits. 2015;8:9.
87. Verma V, Sprave T, Haque W, et al. A systematic review of the cost and cost-effectiveness studies of immune checkpoint inhibitors. J Immunother Cancer. 2018;6(1):128.

9 Treatment Response Evaluation of Bone Metastases Using ^{18}F-NaF

Kalevi Kairemo and Homer A. Macapinlac

9.1 Introduction

^{18}F-NaF PET/CT plays essential role in initial staging, detection of suspected first osseous metastasis, suspected progression of osseous metastases, or treatment monitoring in many types of cancer, such as prostate, breast, and lung cancer.

The morphology and extent of osteoblastic bone metastases, especially when widespread throughout the axial and appendicular skeleton, pose a challenge for conventional anatomic imaging (such as CT, MRI) to determine the tumor load and to evaluate objectively response to therapy. Conventional bone scintigraphy (BS) has been consistently proven to be an inaccurate and insensitive imaging tool to assess response to therapy in many metastatic cancers, such as castration resistant prostate cancer (mCRPC). Only with unequivocal new lesions is there a benefit to monitoring therapy with conventional bone scan. Although BS is capable of determining the extent of osteoblastic bone metastases, BS is not a prognostic indicator because the exact extent of tumor load is often underdiagnosed. Additionally, ^{18}F-Fluoride PET/CT has the ability to determine the whole bone tumor burden quantitatively. Even though the evaluation of outcome prior to treatment and response after treatment is challenging and not fully well established with ^{18}F-Fluoride PET/CT, studies have consistently shown that objective quantification seems more promising to monitor therapy when compared to subjective image analysis [1].

Furthermore, a diagnostic radiotracer such as ^{18}F-Fluoride (a bone-seeking radiotracer for diagnosis) has uptake properties similar to a therapeutic radiotracer such as ^{223}Ra (the bone-seeking radiotracer for therapy) has the potential to precisely assess the possibility and efficacy of a treatment (the *Theragnostic* concept).

The Society for Nuclear Medicine has published guidelines for ^{18}F-NaF PET/CT [2]. Bone uptake of ^{18}F-NaF reflects bone remodeling, and the uptake of ^{18}F-NaF is part of the mineralization of bone matrix. ^{18}F- is exchanged for OH^-, so hydroxyapatite bone matrix is transformed into fluoroapatite, indicating that high uptake of ^{18}F-NaF reflects bone reactions to bone metastases, not to cancer itself. Therefore, positive findings with ^{18}F-NaF PET/CT may be due to both benign and malignant bone disorders.

Here, we review the use of ^{18}F-NaF PET/CT in prostate, breast, lung, thyroid, and renal cell

K. Kairemo (✉)
Department of Nuclear Medicine, University of Texas MD Anderson Cancer Center, Houston, TX, USA

Department of Theragnostics, Docrates Cancer Center, Helsinki, Finland

H. A. Macapinlac
Department of Nuclear Medicine, University of Texas MD Anderson Cancer Center, Houston, TX, USA

S. Fanti et al. (eds.), *Atlas of Clinical PET-CT in Treatment Response Evaluation in Oncology*,
https://doi.org/10.1007/978-3-030-68858-5_9

cancer and discuss ^{18}F-NaF PET/CT's capability to monitor therapy, i.e., prior to initiation of therapy (baseline scans), during treatment (interim scans), and after therapy (follow-up scans).

9.2 Management and Types of Treatments

Novel oncologic therapeutic agents, chemotherapy, hormone therapy, immunotherapy, or radionuclide therapies such as ^{223}Ra and ^{177}Lu-PSMA are expensive, and diagnostic test able to predict and monitor response to treatment, avoid overtreatment, and unnecessary costs will improve patient management and guide individualized therapy.

9.2.1 Baseline ^{18}F-Fluoride PET/CT

^{18}F-Fluoride PET/CT has superior sensitivity, specificity, and accuracy, when compared to other imaging modalities, including PET/CT, bone scintigraphy with SPECT/CT, and whole-body MRI, to detect osteoblastic metastases in a variety of cancers [3–5]. This is noteworthy in cancers such as breast [5, 6], prostate [5, 7], lung [8, 9], and renal cell carcinoma [10, 11].

^{18}F-Fluoride PET/CT's higher spatial resolution leads to improved patient management because of the capability to determine, in a timely manner, the proper initial therapy in the early stages of cancers by detecting small osteoblastic metastases. If available, ^{18}F-Fluoride PET/CT should be the image of choice as it leads to improved patient management, as well as reduced waiting time to perform images when compared to conventional bone scans [12]. Another potential advantage of ^{18}F-Fluoride PET/CT is the concurrently acquired CT images, which enable the detection of soft-tissue and/or visceral metastases, consequently increasing specificity.

In addition, baseline ^{18}F-Fluoride PET/CT imaging has been shown to be a prognostic imaging biomarker, helpful in therapy monitoring. Many different parameters are being investigated, the vast majority in prostate cancer.

Further we will discuss ^{18}F-Fluoride PET/CT's capability to monitor therapy in different cancer types.

9.2.1.1 Prostate Cancer

Osteoblastic bone metastases originating from prostate cancer may predominate or be the only site of disease. The assessment of prognosis prior to and during treatment of prostate cancer is crucial to increase the odds of individualized patient management and of better outcome. Some international recommendations already include ^{18}F-NaF as a radiotracer for skeletal imaging [13]. PET/CT technology has exhibited higher spatial resolution and substantially greater sensitivity than conventional gamma cameras, resulting in higher image quality for a skeletal PET than for planar bone scintigraphy or SPECT [7, 14].

^{18}F-NaF has been used for initial staging, detection of newly suspected skeletal metastases, suspected progression of skeletal disease, or assessing treatment response in prostate cancer patients.

The ^{18}F-NaF fluoride PET/CT methodology allows for the simultaneous characterization of the alterations of metastatic bone density and the tracer uptake, which both are well established markers of lesion severity and may be essential in judging the necessity of early implementation of radionuclide therapies for bony pain palliation and treatment. For instance, most lytic lesions are not detectable at bone scintigraphy. It has been reported that in cancer patients with multiple skeletal metastases, an increased ^{18}F-NaF-fluoride uptake is detected both in lesions with sclerotic characteristics on CT and in mixed sclerotic and lytic metastases [15].

There is a small meta-analysis about ^{18}F-NaF PET/CT scans: of 3918 patients, 1289 (33%) had positive scans [16].

Bone metastases occur in nearly all patients with castration-resistant prostate cancer and are the primary cause of disability, impaired quality of life, and death, due to an increased risk of pathologic fractures, spinal cord or nerve root compression, and hypercalcemia of malignancy [17]. In this context, the skeletal involvement from prostate cancer can be assessed using

^{18}F-NaF-Fluoride PET/CT. This imaging modality allows the identification and quantification of bone metastatic lesions [18, 19].

Current drugs for the treatment of bone metastases also include ADT and systemic chemotherapy but monoclonal antibodies, analgesics, EBRT, radiopharmaceuticals, and bisphosphonates specifically target osseous disease alone or in combination. However, ^{18}F-NaF-Fluoride PET/CT is best in the evaluation of bone-targeted therapies and in bone-dominant metastatic prostate cancer.

This ^{18}F-Fluoride PET/CT methodology can be used for assessing the final outcome of many treatments [14]. The Na^{18}F burden data is convincing, because serum markers, such as alkaline phosphatase (AFOS) or prostate-specific antigen (PSA), seldom reflect small changes in the overall cancer burden.

Retrospective and prospective studies have shown that the whole-body skeletal tumor burden on baseline ^{18}F-Fluoride PET/CT is a powerful imaging biomarker, capable of independently evaluating prognosis in prostate cancer patients [15, 20]. The calculation of skeletal tumor burden on baseline ^{18}F-Fluoride PET/CT has been conducted by establishing basically two different SUVmax thresholds: SUVmax = 10 [21] and SUVmax = 15 [22]. Regardless of the quantification method and the threshold levels described above, all are reproducible and have a remarkable prognostic power [1]. Baseline ^{18}F-Fluoride PET/CT estimation of tumor burden may be able to define which prostate cancer patients will benefit from ^{223}Ra therapy. ^{223}Ra is a bone-seeking therapeutic radionuclide that increases overall survival in metastatic castrate-resistant prostate cancer (mCRPC) patients [23]. The ^{18}F-fluoride uptake in osteoblastic bone metastases from prostate cancer measured in baseline ^{18}F-Fluoride PET/CT images has been shown to strongly, significantly, and directly correlate with the corresponding uptake and absorbed dose of ^{223}Ra, and these metrics can help evaluate subsequent lesion response to treatment [24, 25]. Additionally, ^{18}F-Fluoride PET/CT is useful in patients with end-stage disease to monitor the odds of developing bone marrow failure after ^{223}Ra due to extensive bone marrow tumor infiltration [26].

9.2.1.2 Breast Cancer

The skeleton is the major site of distant metastases in breast cancer patients although, unlike prostate cancer, osteolytic and osteoblastic lesions are present. Osseous metastases in breast cancer are approximately 50% osteoblastic, whereas in prostate cancer osteoblastic metastases occur in more than 80% of metastases based on histomorphometry [27]. Even though osteolytic lesions may be present in breast cancer patients, ^{18}F-Fluoride uptake occurs in these osteolytic lesions because of the surrounding osteoblastic response. Figures 9.1 and 9.2 demonstrate the use of ^{18}F-NaF-Fluoride PET/CT in clinical practice of breast cancer patients. It may also be used for assessing the cause of hip pain, i.e., due to malignancy or other etiology.

The largest study in the literature about NaF PET/CT in osseous metastases in breast cancer consisted of 118 patients [6]. In this Dutch study, F-NaF PET/CT detected bone metastases in 42% with an accuracy of 0.93. The scan results led to a change in patient management in 25%. In the evaluation of bone pain, an explanation for pain was found in 71% of the scans, benign pathology in 66%, and bone metastases in 5%. Indications for ^{18}F-NaF PET/CT included primary staging (12%), follow-up (31%), bone pain (52%), abnormal laboratory findings (5%), and evaluation of equivocal osseous lesions on other imaging modalities (3%). Bone metastases were found in 42%, whereas 53% of the scans were negative and 5% yielded equivocal results. Correlation with the reference standard yielded a sensitivity of 0.96, a specificity of 0.91, a positive predictive value of 0.89, a negative predictive value of 0.97, and an accuracy of 0.93 [6].

Monitoring therapy in breast cancer can also be achieved by calculating the skeletal tumor burden on ^{18}F-Fluoride PET/CT [28]. Most importantly, the determination of the skeletal tumor burden in ^{18}F-Fluoride PET/CT images has been shown to be an independent imaging biomarker of prognosis in these patients. This information will lead to proper patient management as there are no laboratory or other imaging biomarkers that, in disease that has affected the skeleton, can independently assess outcome to determine the

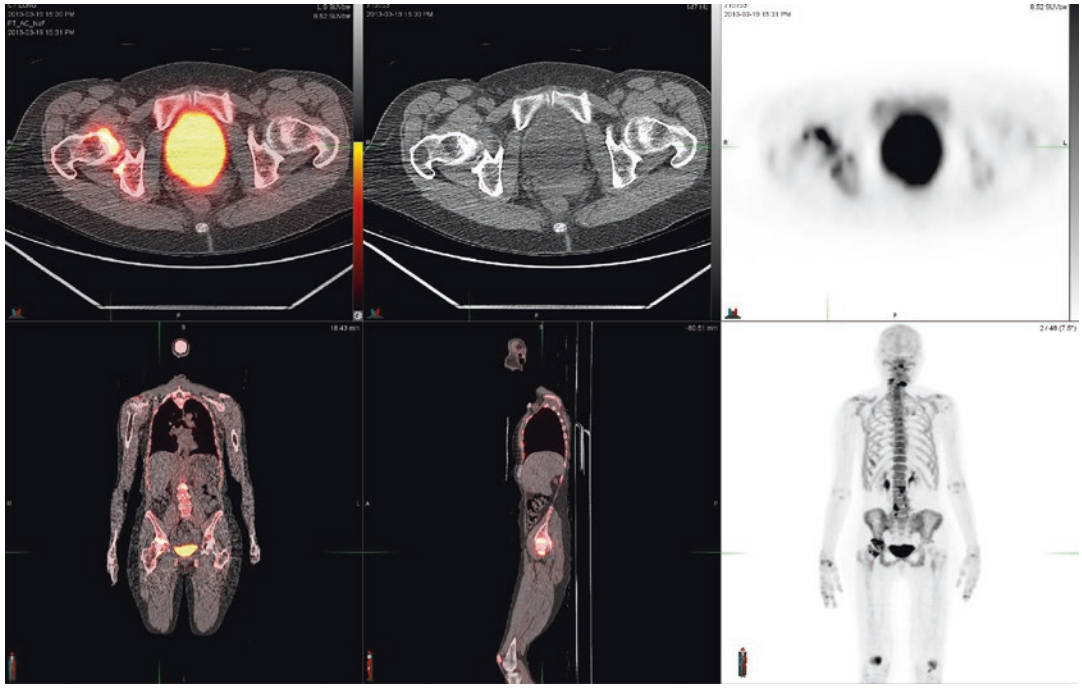

Fig. 9.1 71-year-old female patient with breast cancer treated with multimodality therapy presenting with right hip pain. The NaF PET/CT scan demonstrates severe osteoarthritis of the right hip. CT imaging shows severe joint space narrowing superiorly, with bone-on-bone contact and sclerosis and irregularity of both the femoral and acetabular bone in this location. The fluoride localization on PET/CT scanning localizes along this interface, involving the cortical and subcortical bone at the site of the joint space narrowing

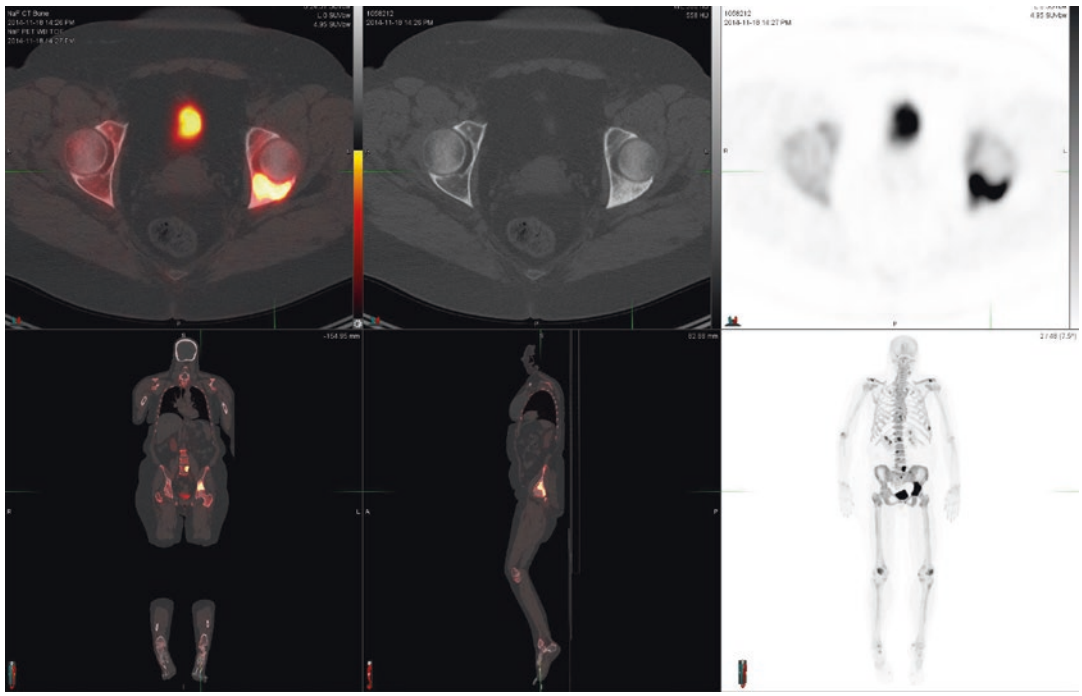

Fig. 9.2 58-year-old woman with breast cancer treated with multimodality therapy presents with left hip and back pain. The NaF PET/CT scans demonstrates multiple osseous metastases. The largest lesion in the left acetabulum is intensely fluoride-avid, with an SUV of 62.1

adequate treatment strategy [28]. In this Brazilian study [28], the skeletal tumor burden (TLF_{10}) on ^{18}F-Fluoride PET/CT images of 107 female breast cancer patients was quantified, 40 for primary staging and the remainder for restaging after therapy. Bone metastases were present in 49 patients, the median follow-up time was 19.5 months. On multivariable analysis, skeletal tumor burden was significantly and independently associated with overall survival ($p < 0.0001$) and progression-free survival ($p < 0.0001$). The simple presence of bone metastases was associated with time to bone event ($p = 0.045$) [28].

There have been some attempts to characterize the ^{18}F-NaF behavior on skeletal metastases of breast cancer in more detailed manner, especially in relation to prognosis and endocrine treatment, but results are very preliminary. ^{18}F-Fluoride metabolic flux to bone mineral (Ki) by positron emission tomography/computed tomography (PET/CT) may provide incremental value in response assessment of bone metastases in breast cancer, because a significant mean percentage increase in Ki from baseline occurred in the 4 patients with clinical progressive disease compared with SUV_{max} (89.7% vs. 41.9; $p < 0.001$) [29]. After 8 weeks of endocrine treatment for bone-predominant metastatic breast cancer, Ki more reliably differentiated disease progression from non-progression: In the 4 patients with clinical progressive disease, mean Ki significantly increased (>25%) in all, whereas in the 8 non-progrediating patients, Ki decreased or remained stable in 7 [29].

Additionally, a prospective study has been performed to test ^{18}F-FDG PET and ^{18}F-NaF PET to predict time to skeletal-related events (tSRE), time-to-progression (TTP), and overall survival (OS) in patients with bone-dominant metastatic breast cancer [30]. Twenty-eight patients were imaged with ^{18}F-FDG PET and ^{18}F-NaF PET prior to new therapy and again approximately 4 months later. Changes in ^{18}F-FDG PET parameters during therapy were predictive of tSRE and TTP, but not OS. Serial ^{18}F-NaF PET was associated with OS, because an increase in the uptake between scans of up to 5 lesions by ^{18}F-NaF PET was associated with longer OS ($P = 0.027$). NaF was not useful for predicting TTP or tSRE in these patients [30].

9.2.1.3 Lung Cancer

The only large study in the literature compared the diagnostic accuracy of F-labeled sodium fluoride (F-NaF) PET/CT with 99 m-technetium methylene diphosphonate (Tc-MDP) single photon emission computed tomography (SPECT) to detect bone metastases (BMs) in patients with preoperative lung cancer [31, 32]. Patients with lung cancer ($n = 181$) were examined with ^{18}F-NaF PET/CT, and another 167 patients with lung cancer were examined with Tc-MDP SPECT [32]. Sensitivity and specificity of PET/CT was significantly better than that of SPECT when equivocal reading was categorized as malignant or benign ($P < 0.05$). Based on lesion-based analysis, SPECT produced 26 equivocal lesions of 333 lesions, but PET/CT produced only 5 equivocal lesions of 991 lesions. PET/CT was significantly better than SPECT in the aspect of producing equivocal patients ($\chi = 58.141$, $P < 0.001$). Sensitivity and specificity of PET/CT was significantly better than that of SPECT when equivocal reading was categorized as malignant or benign ($P < 0.05$). F-NaF PET/CT is a highly sensitive and specific modality for the detection of BM in patients with preoperative lung cancer. It is better than conventional Tc-MDP SPECT in detecting BM in patients with preoperative lung cancer [31].

9.2.1.4 Thyroid Cancer

Two small studies have compared diagnostic performance of ^{18}F-NaF PET/CT with bone scintigraphy or the detection of thyroid cancer bone metastases. In a Korean study of the 17 suspected bone lesions in six (papillary:follicular = 2:4) patients, 10 were metastatic and 7 benign [32]. Compared to BS, bone PET/CT exhibited superior sensitivity (10/10 = 100% vs. 2/10 = 20%, $p = 0.008$) and accuracy (14/17 = 82.4% vs. 7/17 = 41.2%, $p < 0.025$). The specificity (4/7 = 57.1%) of bone PET/CT was not significantly different from that of BS (5/7 = 71.4%, $p > 0.05$) [20].

In a Japanese study, consisting of 11 patients who had been suspected of having bone metastases after total thyroidectomy and were hospitalized to be given ^{131}I therapy [33], metastases were confirmed in 24 (13.6%) of 176 bone segments in 9 of the 11 patients. The sensitivity of ^{18}F-fluoride PET/CT was significantly higher than that of ^{18}F-FDG PET/CT and ^{99m}Tc bone scintigraphy (planar) ($p < 0.05$) [33].

The original study of 35 patients with known or suspected bone metastases from thyroid (papillary:follicular = 9:26) carcinoma evaluated the anatomical distribution and metabolic behavior of bone metastases using bone scintigraphy, whole-body iodine scintigraphy, ^{18}F-NaF PET and CT or MRI [34]. The anatomical distribution of 43 bone metastases found in 18 patients was as follows: spine, 42%; skull, 2%; thorax, 16%; femur, 9%; pelvis, 26%; humerus and clavicle, 5%. All metastases were osteolytic on x-ray and two-thirds (29/43) presented a missing or very limited osteosclerotic bone reaction on ^{18}F-PET. The combination bone scintigraphy and whole-body iodine scintigraphy revealed all the metastases, but neither of them alone. The findings, including a low sensitivity of NaF (33%), are explained by missing or only weak osteosclerotic bone reaction in thyroid cancer bone metastases [34]. Two own cases are shown in Figs. 9.3 and 9.4.

9.2.1.5 Renal Cell Cancer

Two studies have compared diagnostic performance of ^{18}F-NaF PET/CT with bone scintigraphy or the detection of renal cell cancer (RCC) bone metastases. ^{18}F-NaF PET/CT is significantly more sensitive at detecting RCC skeletal metastases than conventional bone scintigraphy or

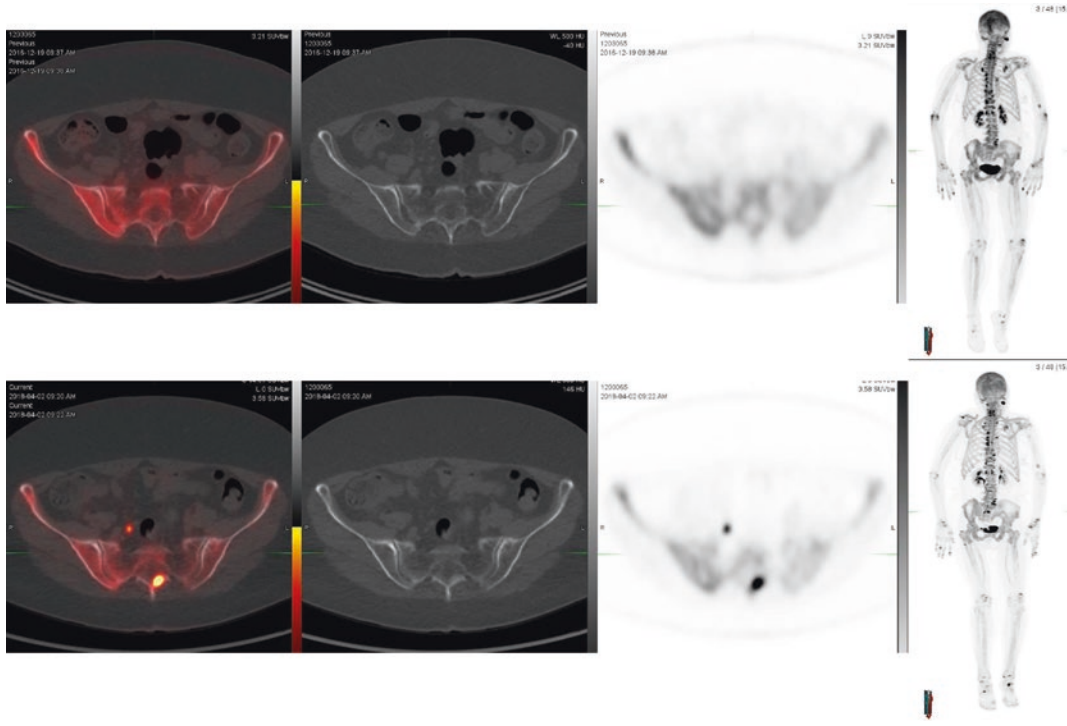

Fig. 9.3 76-year-old female patient with metastatic papillary thyroid cancer, post total thyroidectomy, radioiodine therapy, and lumbar spine metastasis treated with RT. The patient was referred for restaging of RAI refractory osseous metastasis after radiation therapy to the lumbar spine. The upper row of images represent the baseline NaF PET/CT scan demonstrating multifocal metastases in the spine, pelvis, and left zygoma. The lower row restaging after 8 months demonstrating progression in the sacrum. The other metastatic lesions showed stable uptake

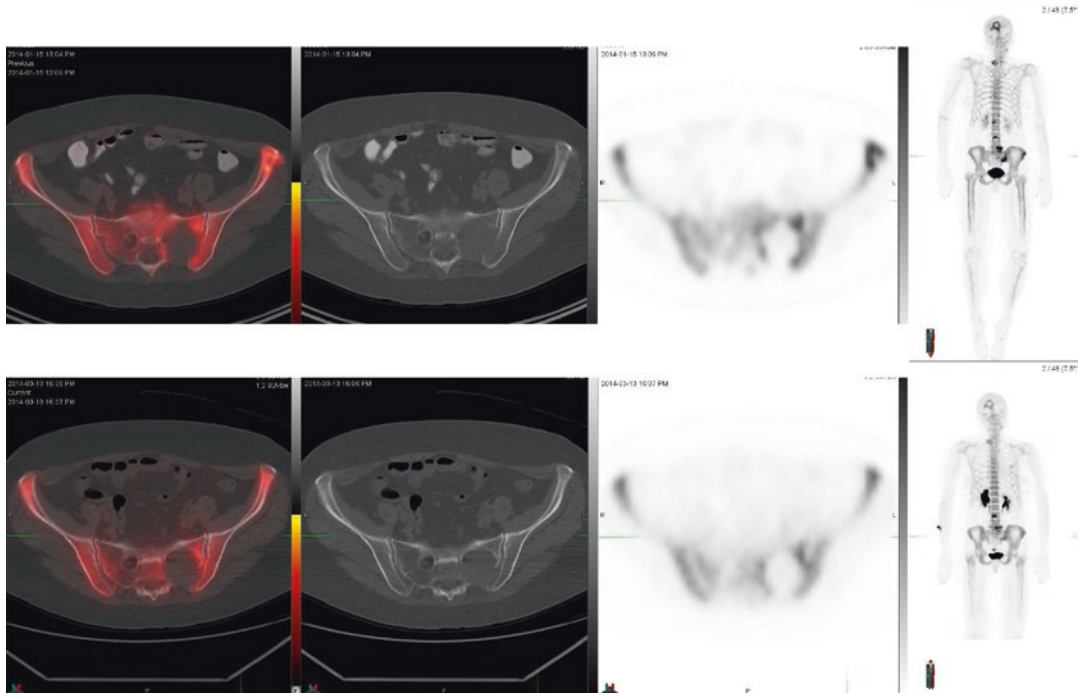

Fig. 9.4 58-year-old female with metastatic thyroid cancer and known osseous metastases referred for baseline evaluation prior to cabozantinib therapy. The upper row demonstrates multifocal osseous metastases in the spine, left pelvis, and calvarium. The post therapy scan in the lower rows shows the large lytic lesions in the left sacral ala and left iliac crest showing resolution of previously noted rim or increased uptake, corresponding to response to treatment

CT. Seventy-seven lesions in ten patients were diagnosed as malignant: 100% were identified by ^{18}F-NaF PET/CT, 46% by CT, and 29% by bone scintigraphy/SPECT [35]. Standard-of-care imaging with CT and bone scintigraphy identified 65% of the metastases reported by ^{18}F-NaF PET/CT. On an individual patient basis, ^{18}F-NaF PET/CT detected more RCC metastases than (99 m)Tc-MDP bone scintigraphy/SPECT or CT alone ($P = 0.007$). The SUV mean and SUVmax of the malignant lesions were significantly greater than those of the benign lesions ($P < 0.001$) [35]. The detection of occult bone metastases could greatly alter patient management, particularly in the context when standard-of-care imaging is negative for skeletal metastases.

Another study reports similar results: Overall, F-fluoride PET/CT showed a sensitivity of 100%, specificity of 94.4%, positive predictive value of 94.7%, negative predictive value of 100%, and accuracy of 97.2% [36]. It demonstrated a total of 134 skeletal lesions, of which 101 were characterized as metastasis and 33 as benign. Corresponding CT changes were seen for 129/134 lesions. The mean SUVmax of the lesions was 30 ± 48. F-Fluoride PET/CT and F-FDG PET/CT showed similar accuracy for visualization of bone metastasis (93.7 vs. 100%; $P = 0.993$). However, F-FDG PET/CT additionally demonstrated extraskeletal metastasis in 6/16 patients. No significant difference was seen between the accuracies of BS and F-fluoride PET/CT for visualization of bone metastasis (93.7 vs. 100%; $P = 0.115$), but the former showed significantly more skeletal lesions (91 vs. 44; $P < 0.0001$). In 4/22 patients (18%) with negative BS, F-Fluoride PET/CT demonstrated skeletal metastases [36].

9.3 Assessment of Treatment Response (Postsurgical, Post Chemotherapy, Post Radiotherapy, Neoadjuvant, and Immunotherapy Settings)

Most scientific evidence about Na^{18}F-PET in the response evaluation is based on the skeletal metastasis treatment by using ^{223}Ra. This has been evaluated quantitively and after different number of treatment cycles. Anecdotally, even response criteria have been developed for primary bone tumors. These are discussed in this section.

9.3.1 Interim ^{18}F-Fluoride PET/CT

The ideal moment to perform ^{18}F-Fluoride PET/CT scan to assess response to treatment is quite unclear. Bone restoration as a consequence of appropriate treatment causes an osteoblastic reaction in order to restore normal bone, increasing ^{18}F-Fluoride uptake, which is known as a flare response [37]. Flare responses may occur as early as the first cycle of therapy, whether with ^{223}Ra for prostate cancer [38] or chemotherapy, monoclonal antibody therapy [39], or hormonal therapy for breast cancer [40]. The flare phenomenon generally peaks and diminishes approximately 2 months after initiation of therapy. This may explain why ^{18}F-Fluoride PET/CT scans performed 3 months after the beginning of therapy is a more reliable measure of tumor response than scans acquired after 2 months [41].

Unfortunately, progression of osteoblastic bone metastases will also cause an increase in osteoblastic reaction and inflammation secondary to tumor-associated growth factors. Therefore, the occurrence of the flare phenomenon reduces the specificity of interim scans to determine response to therapy. Even though the CT portion of the ^{18}F-Fluoride PET/CT scans normally reveals reparative changes noted by the increased extent of the sclerotic lesions, there is no guarantee that this phenomenon is due to reparative changes and not due to progressive disease.

9.3.1.1 Prostate Cancer

Interim ^{18}F-Fluoride PET/CT scan has been performed in prostate cancer patients in the advanced stages as well as in early stages of cancer. The initial small series of 10 mCRPC patients submitted to interim ^{18}F-Fluoride PET/CT scans and demonstrated that the determination of outcome after ^{223}Ra was not possible since increased uptake was noted in responders and in nonresponders [18]. These preliminary results in a larger population (n = 161) submitted to 772 ^{223}Ra cycles [14].

Etchebehere et al. [42] evaluated 68 ^{18}F-Fluoride PET/CT scans of mCRPC submitted to ^{223}Ra therapy to determine if the interim scan could predict overall survival, progression-free survival, or time to a skeletal-related event. None of those outcome measures could be determined by interim ^{18}F-Fluoride PET/CT scans. Additionally, in their study, a finding not described before in the literature was the decrease in ^{18}F-Fluoride uptake on the interim scan compared to the baseline scan in a small group of patients that developed bone marrow failure due to extensive bone marrow infiltration by tumor. On the contrary, in other patients, the increased ^{18}F-Fluoride uptake was due to a flare phenomenon, posing a difficulty in determining which patients were progressing and which were responding. In their study, bone ALP levels had higher specificity than the interim ^{18}F-Fluoride PET/CT scan.

However, while an interim ^{18}F-Fluoride PET/CT scan may not be useful to determine outcome after ^{223}Ra therapy, its use on various chemotherapeutic, tyrosine kinase, and hormonal agents may be impactful. For example, changes in interim ^{18}F-Fluoride PET/CT scans to determine response to dasatinib therapy in 12 mCRPC have been shown to correlate well with bone alkaline phosphatase levels but have a borderline correlation with progression-free survival [43]. Contrary to expected findings, the mCRPC patients with the largest decrease in ^{18}F-Fluoride uptake within the osteoblastic metastases in response to dasatinib had the worst outcomes while those patients with a lower decline or even an increase in osteoblastic activity had the lon-

gest duration of therapy until progression. This may be caused by the properties of dasatinib, promoting osteoblast differentiation and activation thus increasing bone mineralization, comparable to a flare phenomenon seen on ^{18}F-Fluoride PET/CT scans.

In mCRPC patients undergoing chemotherapy or hormonal therapy, a recent study evaluated the ability of baseline and interim (after three cycles of therapy) ^{18}F-Fluoride PET/CT scans to determine outcome of androgen receptor pathway inhibitors ($n = 40$) and chemotherapy ($n = 16$) in 56 mCRPC patients with osteoblastic metastases. The interim ^{18}F-Fluoride PET/CT scan was the strongest univariable predictor of progression-free survival [44].

These different studies have demonstrated that the variation of ^{18}F-Fluoride uptake may be associated with the mechanism of therapeutic reaction within the bone. For example, bone-activating agents (such as ^{223}Ra and dasatinib) may promote a flare response, and thus the increased ^{18}F-Fluoride uptake may be related to better outcome. Quite the reverse, when using therapeutic agents that do not promote bone-activation (such as chemotherapy and hormonal therapy agents), the increase in ^{18}F-Fluoride uptake may be related to worst outcome.

Therefore, it is not possible to extrapolate the ^{18}F-Fluoride uptake results obtained from the evaluation of one drug to all forms of systemic therapy, including secondary hormone therapy, chemotherapy, radiation therapy, monoclonal antibodies, and osteoclast activating inhibitors. The mechanism of action of individual drugs may vary, and the differences in biological behavior of tumor types and effects on the skeleton may also differ.

An evaluation at 12 weeks after initiation of systemic therapy for bone metastases remains at an early enough time point to be clinically relevant in informing clinical management decisions and for measuring early response in clinical trials.

9.3.1.2 Breast Cancer

There are a limited number of studies evaluating the role of interim ^{18}F-Fluoride PET/CT to determine response to therapy in metastatic breast cancer patients.

In one study, the ^{18}F-Fluoride metabolic flux (Ki) measurement calculated after 8 weeks of endocrine treatment for bone-predominant metastatic breast cancer seems more reliable in differentiating progressive disease from nonprogressive disease when compared to semi-quantitative SUV measures. The Ki was better than quantitative SUV measurements since the SUV metrics in general underestimates the ^{18}F-Fluoride clearance from metastatic bone. These initial results, observed in 12 patients, need further prospective validation in larger patient groups under different therapy regimes [29].

Dynamic ^{18}F-Fluoride PET/CT studies demonstrate a decrease of kinetic parameters as response to treatment, reflecting changes at a molecular level before any morphological modifications arise.

9.3.2 Follow-Up ^{18}F-Fluoride PET/CT

9.3.2.1 Prostate Cancer

Unlike the use of interim ^{18}F-Fluoride PET/CT to monitor therapy in which uptake may vary and depend on the type of therapy being applied, the use of ^{18}F-Fluoride PET/CT at the end of therapy has demonstrated better results (see Fig. 9.5 for response and Fig. 9.6 for progression).

^{18}F-Fluoride PET/CT performed at baseline and 6 weeks after the last ^{223}Ra cycle in 10 mCRPC patients demonstrated quantitative reduction of ^{18}F-Fluoride uptake ranging from 7% to 68% was noted in all patients that responded to ^{223}Ra treatment [18]. The quantitative assessment of ^{18}F-Fluoride PET/CT was based on modified PET response criteria, i.e., the sum of the SUVs from two regions [18]. The total skeletal burden such as TLF_{10} [21] is more precise in the follow-up setting. The study which analyzed ^{18}F-Fluoride PET/CT scans to determine outcome of androgen receptor pathway inhibitors ($n = 40$) and chemotherapy ($n = 16$) in mCRPC patients with osseous metastases used actually TLF_{15} as a disease indicator and it turned

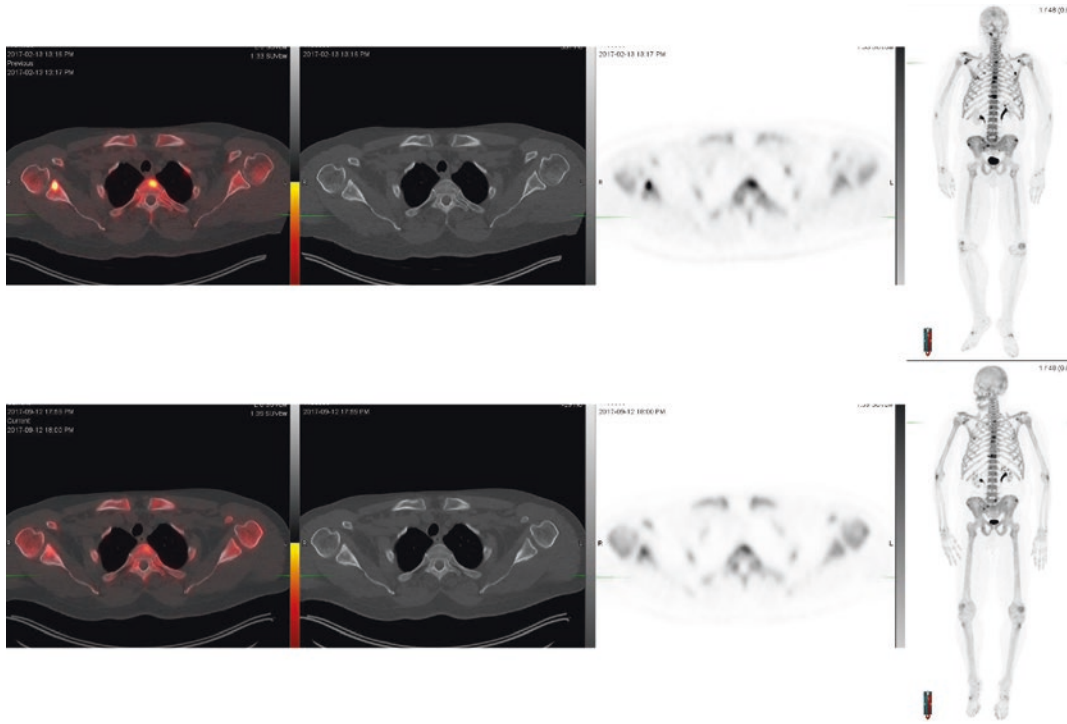

Fig. 9.5 68-year-old male with metastatic castration-resistant prostate cancer referred for ^{223}Ra therapy. The upper row of images represents the baseline NaF PET/CT scan prior to treatment. The lower row of NaF PET/CT scans were acquired after 6 cycles of ^{223}Ra therapy, with the patient demonstrating decrease in PSA levels. The NaF PET/CT scan demonstrates reduction of uptake in a right scapula and T2 vertebral body metastases. The other lesions in the spine and left third rib also showed reduction of activity

out be the strongest parameter to predict progression-free survival [44].

A recent study compared the accuracy of a first generation ^{18}F-labeled prostate-specific membrane antigen (PSMA)-targeted agent (^{18}F-DCFBC PET/CT) and of ^{18}F-Fluoride PET/CT to evaluate treatment response of 28 mCRPC patients submitted to androgen deprivation therapy. In patients on androgen deprivation therapy with early or metastatic castrate sensitive disease (PSA levels below 2 ng/mL), follow-up images after androgen deprivation therapy demonstrated significantly more lesions (residual disease) on ^{18}F-Fluoride PET/CT compared to ^{18}F-DCFBC. However, in patients with advanced mCRPC, the residual number of bone lesions was similar or higher on ^{18}F-DCFBC compared to ^{18}F-Fluoride PET/CT. Therefore, the utility of each radiotracer will depend on patient disease course and treatment status [45].

9.3.2.2 Breast Cancer

A study conducted on 28 patients with breast cancer and metastases to the bone were evaluated with ^{18}F-Fluoride PET/CT performed at a baseline and approximately 4 months after initiation of the therapy. The increase in the ^{18}F-Fluoride uptake between scans was associated with longer overall survival, although they were not predictive of time to skeletal-related events or to time-to-progression [30].

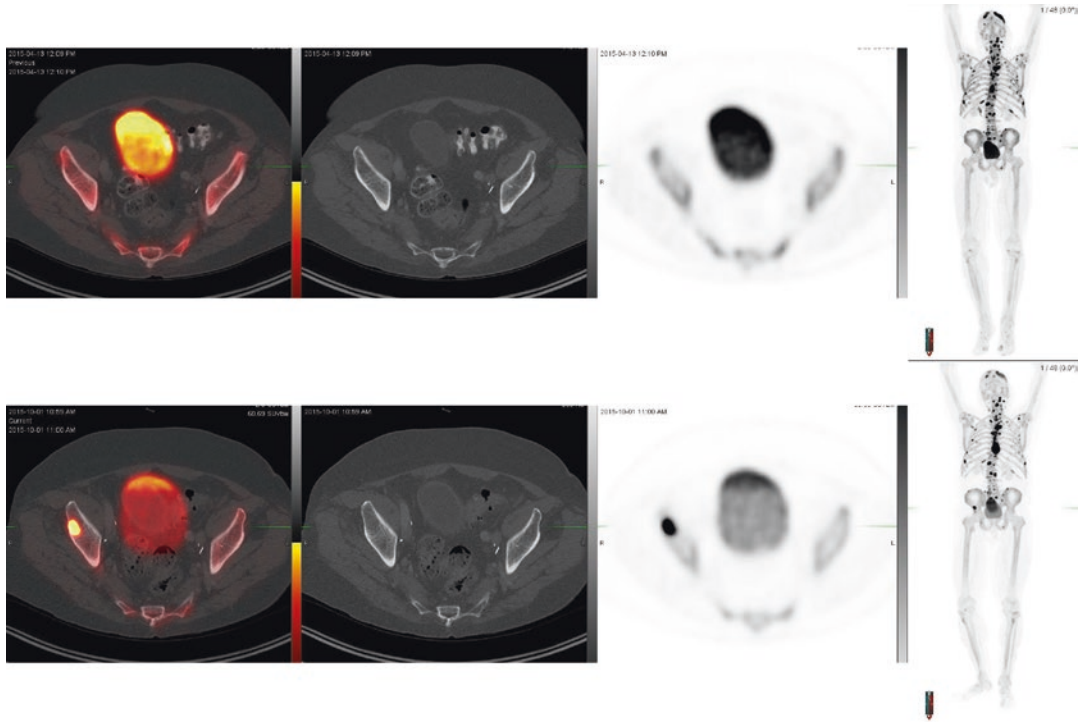

Fig. 9.6 76-year-old male with metastatic castration resistant prostate cancer with known osseous metastases referred for ^{223}Ra therapy. The upper row of images represents the baseline NaF PET/CT scan prior to treatment. The lower row of NaF PET/CT scans were acquired after 6 cycles of ^{223}Ra therapy, with the patient demonstrating increase in PSA levels. The NaF PET/CT scan demonstrates a new metastatic marrowbased lesion in the right ilium. Progression was also noted in the sternal body seen on the MIP image in the rightmost lower row whole-body MIP

9.3.2.3 Multiple Myeloma

In multiple myeloma patients, ^{18}F-Fluoride PET/CT scan does not seem to add significantly to response to therapy. A study evaluating the benefit of ^{18}F-Fluoride PET/CT for treatment response assessment of multiple myeloma in 34 patients undergoing high-dose chemotherapy followed by autologous stem cell transplantation showed that, even though 65% of the patients responded to treatment, 85% of the follow-up ^{18}F-Fluoride PET/CT images were unaltered compared to that of baseline images [46].

9.3.2.4 Metastatic Primary Bone Tumors

^{18}F-NaF PET/CT suits for osteosarcoma diagnostics not just because of its sensitivity in bone lesions but because of its possibility to analyze soft-tissue metastases due to bone formation. We also have developed new criteria (NAFCIST) for staging the disease [47], disease monitoring, and quantitative evaluation of response. These NAFCIST criteria were used successfully in phase I/II.

^{223}Ra trial [48]. The NAFCIST criteria are presented in Table 9.1 and how they differ from

Table 9.1 Positron emission tomography response criteria in primary bone tumors (NAFCIST)

Response category	Criteria
Complete metabolic response	Normalization of all lesions (target and nontarget) to SUL less than mean skeletal SUL and equal to normal surrounding tissue SUL Verification with follow-up study in 1 month if anatomic criteria indicate disease progression
Partial metabolic response	>30% decrease in SUVpeak[a] Verification with follow-up study if anatomic criteria indicate disease progression
Progressive metabolic disease	>30% increase in SUVpeak[a] >75% increase in total NaF burden of the five most active lesions Visible increase in extent of NaF uptake New lesions Verification with follow-up study if anatomic criteria indicate complete or partial response
Stable metabolic disease	Does not meet other criteria

SUL standardized uptake value using lean body mass
[a]Primary outcome determination is measured on the single most active lesion on each scan (not necessarily the same lesion). Secondary outcome determination is the summed activity of up to five most intense lesions (no more than two lesions per organ)

Table 9.2 Comparison of RECIST, PERCIST, and NAFCIST in primary bone tumors

	RECIST	PERCIST	NAFCIST
Characteristics	Anatomic response criteria for soft-tissue disease	Functional response criteria reflecting tumor glucose metabolism	Metabolic response criteria for bone forming disease
Advantages	Commonly used	Response determination is possible Regardless of the location	Response determination is possible regardless of the organ
Disadvantages	Limited to "measurable" soft-tissue disease	Limited to FDG-avid disease	Limited to NaF-avid disease

Modified from Costelloe CM, Chuang HH, Madewell JE, Ueno NT. Cancer response criteria and bone metastases: RECIST 1.1, MDA and PERCIST. J Cancer 2010; 1:80–92

RECIST and PERCIST criteria in Table 9.2. Own patients are shown in Figs. 9.7 and 9.8a, b.

9.3.3 Conclusions

^{18}F-Fluoride PET/CT seems promising in the assessment of therapy as a prognostic imaging biomarker. Quantitative approach by defining skeletal tumor burden provides more accurate assessment of prognosis and response to therapy. Optimal disease evaluation by ^{18}F-Fluoride PET/CT imaging can be performed at baseline, at interim, or/and at the end of therapy, depending on the therapeutic regimen.

In order to properly evaluate response to treatment, it seems reasonable to prefer quantification analyses to subjective qualitative reading to reduce reader-dependent subjectivity, inter and intra-observer variability, to detect subtle tumor regression or progression, and to obtain objective measures of bone metastases response.

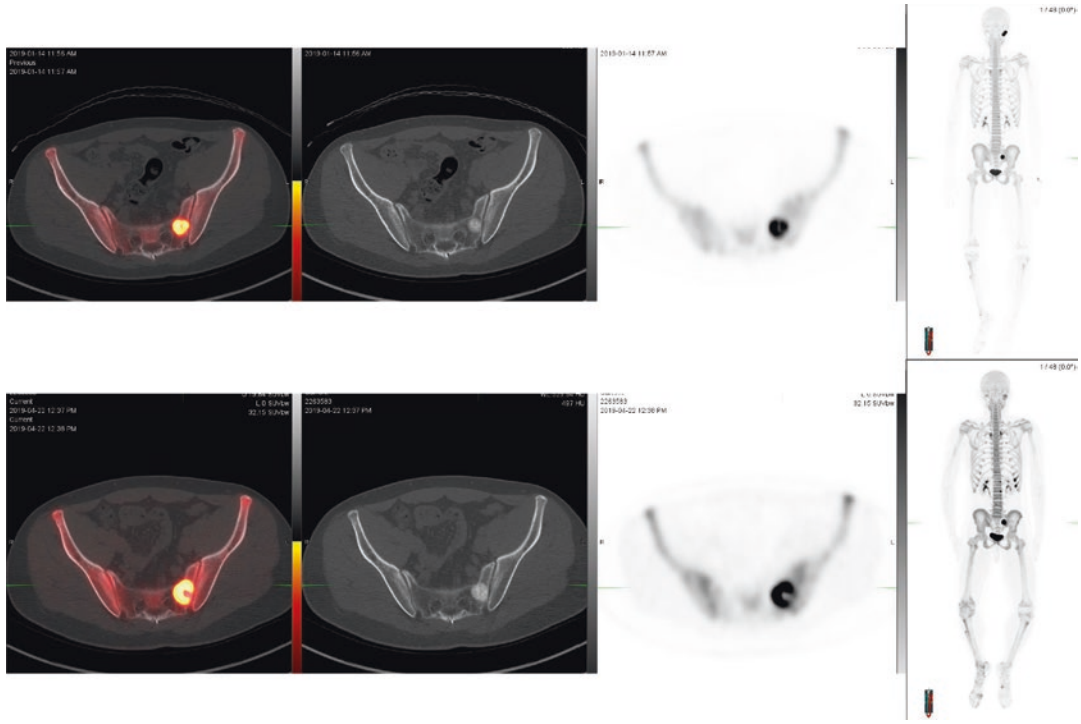

Fig. 9.7 19-year-old male with osteosarcoma of the right fibula post resection, systemic therapy, RT to L1 and left sacrum. The upper row shows NaF PET/CT baseline prior to left mandibular radiation and bottom row shows response of left mandibular metastasis with progression of lest sacral metastasis

9.4 Common Patterns, Pitfalls, Variants, Advantages, and Limitations

Recognition of benign causes of fluoride uptake is essential for overdiagnosis and upstaging. In cases where skeletal disease burden is quantified for purposes of prognosis, care must be taken to differentiate the areas of malignant skeletal involvement from those resulting from benign processes such as fracture repair and inflammation. ^{18}F-Fluoride PET/CT may result in uptake in benign tumors, some of them are listed in Table 9.3.

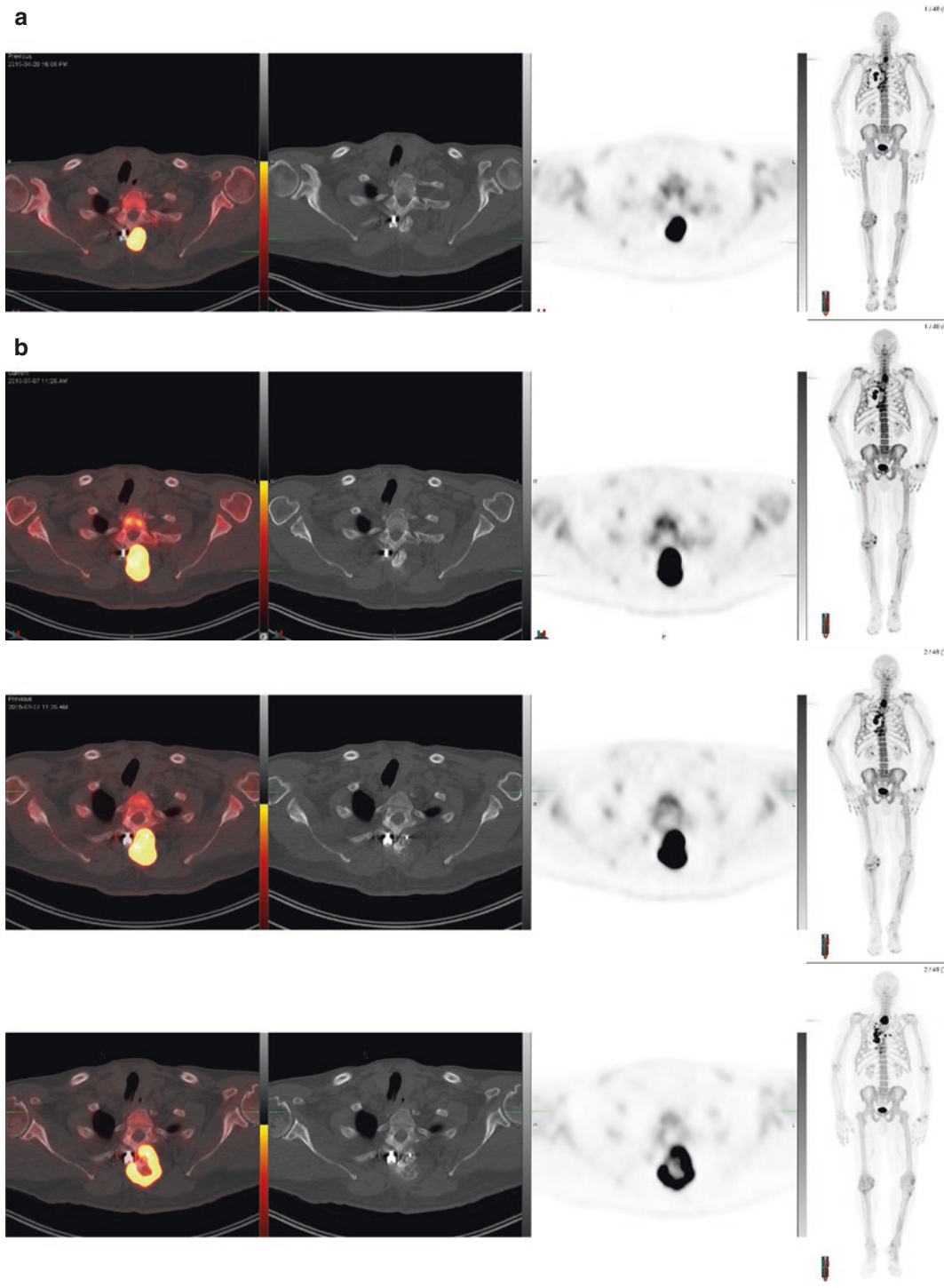

Fig. 9.8 (**a**) 59-year-old male with metastatic osteosarcoma, baseline NaF PET/CT in upper row demonstrating multiple osseous metastases with extraskeletal metastases in the right hemithorax. After 3 cycles of ^{223}Ra therapy on clinical protocol, the majority of the disease is stable but the tumor recurrence dorsal to the upper thoracic spine at the level of T2 is persistently fluoride-avid and has increased slightly in extent since the prior study. (**b**) On follow-up imaging, bottom row shows the majority of the disease is stable but the tumor recurrence dorsal to the upper thoracic spine at the level of T2 is persistently fluoride-avid and has increased in extent since the prior study with the development of central necrosis but greater soft-tissue progression in the paravertebral muscles

Table 9.3 List of benign bone lesions can be found by NaF PET/CT

Fibrous dysplasia
Enchondroma/Eosinophilic granuloma
Giant cell tumor of bone
Nonossifying fibroma
Osteoblastoma
Metastases/myeloma (that can appear benign radiographically)
Aneurysmal bone cyst
Simple (or unicameral) bone cyst
Hyperparathyroidism (brown tumors)
Infection
Chondroblastoma/chondromyxoid fibroma
Paget's disease
Melorheostosis
Gorham-stout disease

References

1. Lin C, Bradshaw T, Perk T, Harmon S, Eickhoff J, Jallow N, et al. Repeatability of quantitative ^{18}F-NaF PET: a multicenter study. J Nucl Med. 2016;57:1872–9.
2. Segall G, Delbeke D, Stabin MG, et al. SNM practice guideline for sodium ^{18}F-fluoride PET/CT bone scans 1.0. J Nucl Med. 2010;51:1813–20.
3. Bortot DC, Amorim BJ, Oki GC, Gapski SB, Santos AO, Lima MC, et al. ^{18}F-fluoride PET/CT is highly effective for excluding bone metastases even in patients with equivocal bone scintigraphy. Eur J Nucl Med Mol Imaging. 2012;39:1730–6.
4. Shen C, Qiu Z, Han T, Luo Q. Performance of ^{18}F-fluoride PET or PET/CT for the detection of bone metastases. A meta-analysis. Clin Nucl Med. 2015;40:103–10.
5. Minamimoto R, Loening A, Jamali M, Barkhodari A, Mosci C, Jackson T, et al. Prospective comparison of 99mTc-MDP Scintigraphy, combined ^{18}F-NaF and ^{18}F-FDG PET/CT, and whole-body MRI in patients with breast and prostate cancer. J Nucl Med. 2015;56:1862–8.
6. Broos W, van der Zant FM, Wondergem M, Knol RJJ. Accuracy of 18F-NaF PET/CT in bone metastasis detection and its effect on patient management in patients with breast carcinoma. Nucl Med Commun. 2018;39:325–33.
7. Even-Sapir E, Metser U, Mishani E, Lievshitz G, Lerman H, Leibovitch I. The detection of bone metastases in patients with high-risk prostate cancer: ^{99m}Tc-MDP planar bone scintigraphy, single- and multi-field-of-view SPECT, ^{18}F-fluoride PET, and ^{18}F-fluoride PET/CT. J Nucl Med. 2006;47:287–97.
8. Kruger S, Buck AK, Mottaghy FM, Hasenkamp E, Pauls S, Schumann C, et al. Detection of bone metastases in patients with lung cancer: 99mTc-MDP planar bone scintigraphy, 18F-fluoride PET or 18F-FDG PET/CT. Eur J Nucl Med Mol Imaging. 2009;36:1807–12.
9. Rao L, Zong Z, Chen Z, Wang X, Shi X, Yi C, et al. ^{18}F-labeled NaF PET-CT in detection of bone metastases in patients with preoperative lung Cancer. Medicine. 2016;95:e3490.
10. Sharma P, Karunanithi S, Chakraborty PS, Kumar R, Seth A, Julka PK, Bal C, Kumar R. ^{18}F-fluoride PET/CT for detection of bone metastasis in patients with renal cell carcinoma: a pilot study. Nucl Med Commun. 2014;35:1247–53.
11. Gerety EL, Lawrence EM, Wason J, Yan H, Hilborne S, Buscombe J, et al. Prospective study evaluating the relative sensitivity of ^{18}F-NaF PET/CT for detecting skeletal metastases from renal cell carcinoma in comparison to multidetector CT and ^{99m}Tc-MDP bone scintigraphy, using an adaptive trial design. Ann Oncol. 2015;26:2113–8.
12. Hillner BE, Siegel BA, Hanna L, Duan F, Quinn B, Shields AF. 18F-fluoride PET used for treatment monitoring of systemic cancer therapy: results from the National Oncologic PET registry. J Nucl Med. 2015;56:222–8.
13. Oyen W, Sundram F, Haug AR, Kairemo K, Maenpaa H, Mottaghy F, et al. Radium-223 dichloride (Ra-223) for the treatment of metastatic castration-resistant prostate cancer: optimizing clinical practice in nuclear medicine centers. J Oncol Pathol. 2015;3:1–25.
14. Kairemo K, Milton DR, Etchebehere E, et al. Final outcome of ^{223}Ra-therapy and the role of ^{18}F-fluoride-PET in response evaluation in metastatic castration-resistant prostate cancer–a single institution experience. Curr Radiopharm. 2018;11:152–7.
15. Etchebehere EC, Araujo JC, Fox PS, Swanston NM, Macapinlac HA, Rohren EM. Prognostic factors in patients treated with 223Ra: the role of skeletal tumor burden on baseline 18Ffluoride PET/CT in predicting overall survival. J Nucl Med. 2015;56:1177–84.
16. von Eyben FE, Kairemo K, Kiljunen T, Joensuu T. Planning of external beam radiotherapy for prostate cancer guided by PET/CT. Curr Radiopharm. 2015;8:19–31.
17. Scher HI, Sawyers CL. Biology of progressive, castration resistant prostate cancer: directed therapies targeting the androgen receptor signaling axis. J Clin Oncol. 2005;23:8253–61.
18. Kairemo K, Joensuu T. Radium-223-dichloride in castration resistant metastatic prostate cancer-preliminary results of the response evaluation using F-18-fluoride PET/CT. Diagnostics (Basel). 2015;5:413–27.
19. Etchebehere E, Brito AE, Rezaee A, et al. Therapy assessment of bone metastatic disease in the era of 223radium. Eur J Nucl Med Mol Imaging. 2017;44(Suppl 1):84–96.
20. Apolo AB, Lindenberg L, Shih JH, Mena E, Kim JW, Park JC, et al. Prospective study evaluating Na18F PET/CT in predicting clinical outcomes and survival in advanced prostate cancer. J Nucl Med. 2016;57:886–92.
21. Rohren EM, Etchebehere EC, Araujo JC, Hobbs BP, Swanston NM, Everding M, et al. Determination of

skeletal tumor burden on 18F-fluoride PET/CT. J Nucl Med. 2015;56:1507–12.
22. Lindgren B, Sadik M, Kaboteh R, Hasani N, Enqvist O, Svärm L, Kahl F, Simonsen J, Poulsen M, Ohlsson M, Høilund-Carlsen P, Edenbrandt L, Trägårdh E. 3D skeletal uptake of ^{18}F sodium fluoride in PET/CT images is associated with overall survival in patients with prostate cancer. EJNMMI Res. 2017;7:15.
23. Parker C, Nilsson S, Heinrich D, Helle SI, O'Sullivan JM, Fossa SD, et al. Alpha emitter radium-223 and survival in metastatic prostate cancer. N Engl J Med. 2013;369:213–23.
24. Letellier A, Johnson AC, Kit NH, Savigny J, Batalla A, Parienti J, Aide N. Uptake of Radium-223 dichloride and early [^{18}F] NaF PET response are driven by baseline [^{18}F]NaF parameters: a pilot study in castration-resistant prostate cancer patients. Mol Imaging Biol. 2018;20:482–91.
25. Murray I, Chittenden SJ, Denis-Bacelar AM, Hindorf C, Parker C, Chua S, Flux GD. The potential of 223Ra and 18F-fluoride imaging to predict bone lesion response to treatment with 223Ra-dichloride in castration-resistant prostate cancer. Eur J Nucl Med Mol Imaging. 2017;44:1832–44.
26. Etchebehere EC, Araujo JC, Milton DR, Erwin WD, Wendt RE 3rd, Swanston NM, et al. Skeletal tumor burden on baseline ^{18}F-fluoride PET/CT predicts bone marrow failure after ^{223}Ra therapy. Clin Nucl Med. 2016;41:268–73.
27. Taube T, Elomaa I, Blomqvist C, Beneton MN, Kanis JA. Histomorphometric evidence for osteoclast-mediated bone resorption in metastatic breast cancer. Bone. 1994;15:161–6.
28. Brito A, Santos A, Sasse AD, Cabello C, Oliveira P, Mosci C, Souza T, Amorim B, Lima M, Ramos CD, Etchebehere E. ^{18}F-Fluoride PET/CT tumor burden quantification predicts survival in breast cancer. Oncotarget. 2017;8:36001–11.
29. Azad G, Siddique MM, Taylor B, et al. Does measurement of ^{18}F-fluoride metabolic flux improve response assessment of breast cancer bone metastases compared with standardised uptake values in ^{18}F-fluoride PET/CT? J Nucl Med. 2018. pii: jnumed.118.208710. https://doi.org/10.2967/jnumed.118.208710.
30. Peterson LM, O'Sullivan J, Wu QV, et al. Prospective study of serial ^{18}F-FDG PET and ^{18}F-fluoride (^{18}F-NaF) PET to predict time to skeletal related events, time-to-progression, and survival in patients with bone-dominant metastatic breast cancer. J Nucl Med. 2018. pii: jnumed.118.211102. https://doi.org/10.2967/jnumed.118.211102.
31. Rao L, Zong Z, Chen Z, et al. ^{18}F-labeled NaF PET-CT in detection of bone metastases in patients with preoperative lung Cancer. Medicine (Baltimore). 2016;95:e3490.
32. Lee H, Lee WW, Park SY, Kim SE. F-18 sodium fluoride positron emission tomography/computed tomography for detection of thyroid Cancer bone metastasis compared with bone scintigraphy. Korean J Radiol. 2016;17:281–8. https://doi.org/10.3348/kjr.2016.17.2.281.
33. Ota N, Kato K, Iwano S, et al. Comparison of ^{18}F-fluoride PET/CT, ^{18}F-FDG PET/CT and bone scintigraphy (planar and SPECT) in detection of bone metastases of differentiated thyroid cancer: a pilot study. Br J Radiol. 2014;87:20130444.
34. Schirrmeister H, Buck A, Guhlmann A, Reske SN. Anatomical distribution and sclerotic activity of bone metastases from thyroid cancer assessed with F-18 sodium fluoride positron emission tomography. Thyroid. 2001;11:677–83.
35. Gerety EL, Lawrence EM, Wason J, et al. Prospective study evaluating the relative sensitivity of ^{18}F-NaF PET/CT for detecting skeletal metastases from renal cell carcinoma in comparison to multidetector CT and 99mTc-MDP bone scintigraphy, using an adaptive trial design. Ann Oncol. 2015;26:2113–8.
36. Sharma P, Karunanithi S, Chakraborty PS, et al. 18F-fluoride PET/CT for detection of bone metastasis in patients with renal cell carcinoma: a pilot study. Nucl Med Commun. 2014;35:1247–53.
37. Rossleigh MA, Lovegrove FT, Reynolds PM, Byrne MJ. Serial bone scans in the assessment of response to therapy in advanced breast carcinoma. Clin Nucl Med. 1982;7:397–402.
38. Castello A, Macapinlac HA, Lopci E, Santos EB. Prostate-specific antigen flare induced by 223RaCl2 in patients with metastatic castration-resistant prostate cancer. Eur J Nucl Med Mol Imaging. 2018. [Epub ahead of print]. https://doi.org/10.1007/s00259-018-4051-y
39. Balasubramanian Harisankar CN, Preethi R, John J. Metabolic flare phenomenon on 18 fluoride-fluorodeoxy glucose positron emission tomography-computed tomography scans in a patient with bilateral breast cancer treated with second-line chemotherapy and bevacizumab. Indian J Nucl Med. 2015;30:145–7.
40. Wade AA, Scott JA, Kuter I, Fischman AJ. Flare response in 18F-fluoride ion PET bone scanning. AJR Am J Roentgenol. 2006;186:1783–6.
41. Cook G Jr, Parker C, Chua S, et al. 18F-fluoride PET: changes in uptake as a method to assess response in bone metastases from castrate-resistant prostate cancer patients treated with 223Ra-chloride (Alpharadin). EJNMMI Res. 2011;1:4.
42. Etchebehere E, Brito AE, Kairemo K, et al. Interim ^{18}F-fluoride PET/CT is not able to predict outcome after radium-223 therapy. Radiol Bras. 2019;52(1):33–40.
43. Yu EY, Duan F, Muzi M, et al. Castration-resistant prostate cancer bone metastasis response measured by ^{18}F-fluoride PET after treatment with dasatinib and correlation with progression-free survival: results from American College of Radiology Imaging Network 6687. J Nucl Med. 2015;56:354–60.
44. Harmon SA, Perk T, Lin C, et al. Quantitative assessment of early [^{18}F] sodium fluoride positron emission

tomography/computed tomography response to treatment in men with metastatic prostate cancer to bone. J Clin Oncol. 2017;35:2829–37.

45. Harmon SA, Bergvall E, Mena E, et al. A prospective comparison of 18F-Sodium Fluoride PET/CT and PSMA-targeted 18F-DCFBC PET/CT in metastatic prostate cancer. J Nucl Med. 2018. pii: jnumed.117.207373. [Epub ahead of print]. https://doi.org/10.2967/jnumed.117.207373
46. Sachpekidis C, Hillengass J, Goldschmidt H, Wagner B, Haberkorn U, Kopka K, Dimitrakopoulou-Strauss A. Treatment response evaluation with 18F-FDG PET/CT and 18F-NaF PET/CT in multiple myeloma patients undergoing high-dose chemotherapy and autologous stem cell transplantation. Eur J Nucl Med Mol Imaging. 2017;44:50–62.
47. Kairemo K, Rohren EM, Anderson PM, et al. Development of sodium fluoride PET response criteria for solid tumours (NAFCIST) in a clinical trial of radium-223 in osteosarcoma: from RECIST to PERCIST to NAFCIST. ESMO Open. 2019;0:e000439. https://doi.org/10.1136/esmoopen-2018-000439.
48. Subbiah V, Anderson PM, Kairemo K, et al. Alpha particle Radium 223 dichloride in high-risk osteosarcoma: a phase I dose escalation trial. Clin Cancer Res. 2019. pii: clincanres.3964.2018. https://doi.org/10.1158/1078-0432.CCR-18-3964.

Reporting Post-Therapy Scans

10

Laura Evangelista and Lea Cuppari

10.1 Introduction

Quantification of tumor burden by medical imaging is often used in our daily clinical practice to assess the effectiveness of various anticancer therapies in soft-tissue tumors.

Computed tomography (CT) represents the most common technique employed for the assessment of response to therapy. Response Evaluation Criteria in Solid Tumors (RECIST) version 1.1 (RECIST1.1) is the currently adopted tumor response criterion in most trials of solid tumors. It uses unidimensional diameters of target lesions and the sum of measurements of all target lesions as a quantitative measure of tumor burden.

Positron emission tomography (PET) has been widely used in clinical practice for the staging, restaging, and the prognosis of patients with oncological disease, by using different radiopharmaceutical agents. However, in the last years, a huge amount of data has been published about its role in evaluating response to therapies, both local and systemic ones. Moreover, ^{18}F-Fluorodeoxyglucose (FDG) PET imaging, which measures functional changes, has shown advantages over anatomic imaging as a response evaluation tool in many malignancies [1–6]. Moreover, a significant association between the response to therapy, assessed by FDG PET/CT and prognosis, has been reported in some solid neoplasia, such as esophageal cancer and non-small-cell lung cancer (NSCLC) [7, 8].

Radiopharmaceuticals such as ^{18}F/11C-Choline, 68Ga-PSMA, or 68Ga-DOTATOC are also used in treatment evaluation response in specific types of cancers such as prostate cancer and neuroendocrine tumor [9, 10]. The present book chapter aims to provide some advice about the standard practices for evaluating response to therapy with PET/CT. More emphasis will be given to FDG, being the commonest radiopharmaceutical agent used in clinical routine.

10.2 Patient Preparation

Before the FDG PET/CT scan, instructions given to the patient aim to reduce tracer uptake in physiologic sites such as myocardium, urinary excretory tract, brown fat, and muscles and optimize accumulation in the tumor tissue with radiation dose as low as reasonably possible.

A checklist for patient preparation should be in place to optimize the imaging quality, particularly for the post-therapy examination.

In Fig. 10.1 example of a checklist.

L. Evangelista (✉) · L. Cuppari
Nuclear Medicine Unit, Veneto Institute of Oncology IOV—IRCCS, Padua, Italy
e-mail: laura.evangelista@iov.veneto.it

S. Fanti et al. (eds.), *Atlas of Clinical PET-CT in Treatment Response Evaluation in Oncology*,
https://doi.org/10.1007/978-3-030-68858-5_10

Fasting for at least 4 hours before PET examination	☐
Reduce as low as possible the carbohydrate the day before PET examination	☐
Diabetes*	☐
Parental nutrition*	☐
Hydratation with 1 liter of water during the 2h prior to PET examination	☐
Avoid physical exercise at least 6 hours before PET examination	☐
Other information: Pregnancy and breastfeeding Medications* Schedule for contrast enhanced CT during PET examination*	 ☐ ☐ ☐

*discuss with the Nuclear Medicine Physician

Fig. 10.1 A checklist for the correct preparation for FDG PET/CT examination

It is essential to maintain a low blood glucose level (lesser than 200 mg/dL, or 160 mg/dL in case of clinical trials), advising patients not to eat for at least four h before injection of FDG. In parenteral nutrition and intravenous fluids containing glucose, it is recommended discontinuing the infusion for at least four h. Adequate hydration is necessary, at least 1 L of water during the two h before injection. Patients must avoid physical exercise, preferably 24 h before PET/CT, to reduce the muscle uptake.

In case of oral hypoglycemic agents or insulin, some advice should be given: (1) metformin should be discontinued for at least 48 h in case of an abdominal neoplasia localization, and (2) insulin infusion should be stopped at least 4 h before the FDG injection and a switch from a long-lasting to short-acting one is recommended.

During the injection of FDG, the patient should remain seated and silent to reduce uptake in muscles and vocal cords, especially for better visualization of the head and neck region. In a young patient and in case of cold temperature, the patient should be kept warm to reduce brown adipose tissue activation that would interfere with imaging interpretation. It is mandatory to exclude claustrophobia and other clinical symptoms that might interfere with not lying still during the PET/CT scan.

Immediately before the PET/CT acquisition, the patient should void the bladder to reduce nonspecific activity in the urinary tract and remove every metallic object.

Table 10.1 Patient preparation for non-FDG tracers

Radiopharmaceutical agent	Preparation
68Ga-PSMA	No fasting Hydrating before the study Voiding before the acquisition (furosemide is recommended in case of a suspicion of prostatic bed recurrence)
^{18}F/11C-Choline	Fasting for at least 6 h Hydrating before the study Voiding before the acquisition (furosemide is recommended in case of a suspicion of prostatic bed recurrence, in case of ^{18}F-Choline)
68Ga-DOTATOC	No special preparation is required

For the evaluation of response to therapy with PET/CT, the instructions given to the patient, the blood sugar level obtained, and the dose of tracer (per kilogram of body weight) should be similar in the first and the subsequent scans, to allow the comparison of visual information and semiquantitative data (i.e., standardized uptake value (SUV)).

The preparations of patients for the other radiopharmaceutical agents are discussed in the table (Table 10.1).

For further details, the readers can refer to the European Association of Nuclear Medicine guidelines (www.eanm.org) or the Society of Nuclear Medicine guidelines (www.snmmi.org).

10.3 Clinical Details

The knowledge of patient clinical information represents the first step for the accurate interpretation of radiological images, as stated by some authors [11–14], in case of incomplete or inadequate history or patient information. It is helpful to discuss with referring physicians and review patient records or notes, and it is recommended.

In Table 10.2, important clinical data which should be collected and the reasons why they are important.

Table 10.2 Clinical details

Clinical data	Reasons
Clinical questions (or clinical indication)	To assess the correct protocol and radiopharmaceutical agent. In case of the evaluation of response to therapy, it is strongly recommended to reproduce the same examinations
The tumor type (also histological information, if available)	Useful to choose the radiopharmaceutical agent
The site of the disease	Useful to choose the protocol acquisition
Previous and/or ongoing treatments for oncological disease	Useful in order to: – Determine the correct time between last treatments and PET/CT scan (see the next paragraph) – Correctly interpret the images
Information useful for the interpretation of the images (i.e., inflammation in specific organs, or infective processes)	Everything that may have relevance to PET/CT interpretation should be mentioned (i.e., sarcoidosis, rheumatoid arthritis, others)
Comorbidities and correlative drugs	To critically evaluate the abnormal tracer distribution and the opportunity to withdraw drugs (i.e., metformin or others)

10.4 Questions to Ask Patient

The discussion with the patient is essential for collecting clinical data, particularly for the post-therapy PET examination. Below are some questions that would support the interpretation of PET images.

1. Have you had any surgery, biopsies, or similar invasive procedures recently? Provide a brief list and the date, as possible.
2. Do you have any prosthetic implants or drainage bags?
3. Have you had any recent infections?
4. Do you suffer any pain at the moment? If so, where?
5. When did you last receive chemotherapy or radiotherapy, or other systemic treatments?

Provide a brief description by giving information about the previous administration, the type of systemic therapy.
6. Are you taking any medicines or tablets? Please list.
7. When was your last menstrual period?

10.5 When to Scan

After local (i.e., radiotherapy or surgery) or systemic treatments, we often encounter different metabolic response patterns or altered biodistribution on the FDG PET/CT scans. These could change the way we interpret the images. A systematic review of the scans in patients undergoing therapy is essential to reduce the rate of false-positive findings (e.g., inflammation, infective, or reparative phenomena) and avoid misinterpretatation.

In Table 10.3 are summarized the optimal timings between therapies and FDG PET imaging.

For the other radiopharmaceuticals, no specific recommendations are suggested. For example, the withdrawal of hormonal therapy and somatostatin analogue therapy for 68Ga-PSMA/radiolabeled choline and 68Ga-DOTATOC, respectively, is under debate.

Table 10.3 Optimal timing of FDG PET/CT and treatments

After treatments	Timing
Chemotherapy	At least 10 days, preferably 3 weeks
Growth factors	At least 2 weeks, it could be long-lasting
Hormonal therapy	No specific evidences are now available. In the majority of cases, the hormonal therapy is chronic or prolonged for more than 2 or 5 or 10 years. Therefore, a complete analysis of risk/benefit should be made prior to withdrawing it
Bisphosphonate drugs	Delayed as long as possible after the previous administration. At least 15 days are suggested
Radiotherapy	8–12 weeks after the end of treatment. However, the time would be less in case of specific clinical need (i.e., in case of whole-body evaluation)
Surgery	Depends on surgery, at least 6 weeks

10.6 What to Look for in the Scans

PET images should be displayed with and without attenuation correction, particularly in case of a suspicion of recurrence close to metallic implants, calcifications, and/or patient motion. The description of the optimal windowing of PET images is beyond the scope of the present chapter; for further details, please refer to Hofman et al. [15].

It is important to have a consistent organizational scheme when reporting imaging findings, in particular, after treatments. Visual criteria represent the most important component of the imaging lecture. Below are some advice for the critical lecture of images:

1. The black and white cine maximum intensity projection (MIP) should be the initial review of PET images.
2. Physiological biodistribution should be considered, especially after treatments in coronal, sagittal, or transverse PET images. Surgery, radiotherapy, and chemotherapy can alter the normal elimination of the tracer. Surgery can change the morphology, and radiotherapy and chemotherapy could temporarily change renal, hepatic, cardiac, and other physiological functions, thus altering the normal kinetic of the tracer.
3. The uptake of radiopharmaceuticals in non-physiological sites should be described, in terms of the intensity of uptake (i.e., low/moderate/high), of the anatomical size, and of the pattern of uptake (i.e., diffuse or focal).
4. The comparison with the previous PET scans should be made by using a specific scheme. For example (1) the images should be viewed over the same dynamic gray scale or color scale range; (2) a comparative information of tracer uptake should be given, in terms of increase, decrease, or stable; (3) an organ of reference should be considered, such as liver

or blood pool, in order to apply specific criteria (see the next paragraph).

10.7 How to Describe, Report Post-Therapy Finding Scores, Criteria, etc. (Post-Surgical, Post-Chemotherapy, Post-Radiotherapy, and Post-Immunotherapy Settings)

The visual analysis of the images would be completed by semiquantitative data. The most common are SUV, in terms of SUVmax, SUVmean, and SUVpeak. The definitions have been extensively reported in literature [16]. However, other semiquantitative information can be added, such as metabolic tumor volume (MTV), TLG (total lesion glycolysis), TLCKA (total lesion choline kinase activity), 68Ga-DOTATOC tumor lesion, and total lesion PSMA (TL-PSMA) [17–20].

For the interpretation of post-therapy PET images, many criteria have been proposed, but only one is now standardized for the clinical practice. The Deauville criteria have been reported in FDG-avid lymphoma patients, and now is employed worldwide for the interim and post-therapy PET evaluation [21]. It is a five-point score criteria that considered blood pool and liver as the reference organs. Score 1 denotes no significant uptake in the index lesion; score 2, an uptake lower than or equal to blood pool; score 3, an uptake higher than blood pool but lower than or equal to liver; score 4, an uptake moderately higher than liver; and score 5, an uptake severely higher than liver or the appearance of new lesions.

The other criteria for the interpretation of PET scan, before and after therapy, are reported in Table 10.4.

An example of a PET report is shown in Fig. 10.2.

Table 10.4 Criteria for the interpretation of images (suggested only for FDG PET examination)

Criteria name, ref	Neoplasia	Therapy	Interpretation
EORTC [22]	Solid tumors	Chemotherapy	CMR: Complete resolution of FDG uptake in all lesions PMR: ≥25% reduction in the sum of SUVmax after more than one cycle of treatment PMD: ≥25% increase in the sum of SUVmax or appearance of new FDG-avid lesions SMD: Not qualify for CMR, PMR, or PMD
PERCIST [23]	Solid tumors	Chemotherapy	CMR: Complete resolution of FDG uptake in all lesions PMR: ≥30% reduction of the SULpeak and an absolute drop of 0.8 SULpeak units PMD: ≥30% increase in the SULpeak of the FDG uptake and an absolute increase of 0.8 SULpeak, or appearance of FDG-avid new lesions SMD: Not qualify for CMR, PMR, or PMD
iPERCIST [24]	Lung cancer	Immunotherapy	CMR: Complete resolution of FDG uptake in all lesions PMR: ≥30% reduction of the SULpeak and an absolute drop of 0.8 SULpeak units PMD: Unconfirmed progressive metabolic disease (UPMD) and confirmed progressive metabolic disease (CPMD) UPMD was a PMD at SCAN-2, and CPMD was an UPMD confirmed 4 weeks later at SCAN-3. In iPERCIST, SCAN-3 is compared to SCAN-2, and patients were classified as CMR, PMR, SMD, or CPMD according to PERCIST recommendations SMD: Not qualify for CMR, PMR, or PMD

(continued)

Table 10.4 (continued)

Criteria name, ref	Neoplasia	Therapy	Interpretation
PECRIT [25]	Melanoma	Immunotherapy	CR: RECIST 1.1 (disappearance of all target lesions; reduction in short axis of target lymph nodes to <1 cm; no new lesions) (clinical benefit) PR: RECIST 1.1 (decrease in target lesion diameter sum >30%) (clinical benefit) SD: Does not meet the other criteria. Change in SULpeak of the hottest lesion of >15% (clinical benefit) Change in SULpeak of the hottest lesion of ≤15% (no clinical benefit) PD: RECIST 1.1 (increase in target lesion diameter sum of >20% and at least 5 mm or new lesions) (no clinical benefit)
PERCIMT [26]	Melanoma	Immunotherapy	CR: Complete resolution of all preexisting 18F-FDG-avid lesions; no new 18F-FDG-avid lesions (clinical benefit) PR: Complete resolution of some preexisting 18F-FDG-avid lesions. No new, 18F-FDG-avid lesions (clinical benefit) SD: Neither PD nor PR/CR (clinical benefit) PD: Four or more new lesions of <1 cm in functional diameter or three or more new lesions of >1.0 cm in functional diameter or two or more new lesions of more than 1.5 cm in functional diameter (no clinical benefit)
PETER MAC [27]	Lung cancer	Radiotherapy and chemotherapy	CR: No tumor FDG uptake or activity in the tumor similar to that in the mediastinum PR: Appreciable reduction in intensity of tumor FDG uptake or tumor volume apparent to the nuclear medicine physician when pre- and post-treatment PET scans were displayed using a standardized method and no disease progression at other sites SD: No appreciable change in intensity of tumor FDG uptake or tumor volume between scans and no new sites of disease PD: Appreciable increase in tumor FDG uptake or volume of known tumor sites or evidence of disease progression at other intrathoracic or distant metastatic sites
IMPeTUs [28]	Multiple myeloma	Chemotherapy	Association of the following parameters: (1) bone marrow state (2) number and site of focal lesions, with or without osteolytic characteristics (3) presence and sites of extra-medullary or para-medullary disease (4) presence of fractures The degree of FDG is usually quantified according to the Deauville criteria
Modified Lugano criteria and LYRIC criteria [29]	Lymphoma	Immunotherapy	CR: PET/CT score 1, 2, or 3 with or without a residual mass on Deauville criteria or on CT, target nodes/nodal masses must regress to <1.5 cm in longest diameter PR: PET/CT score 4 or 5 with reduced uptake Compared with baseline and residual masses Of any size. Or on CT ≥50% decrease in sum of the product of the diameters of up to six target measurable nodes and extranodal sites PD: PET/CT score 4 or 5 with an increase in intensity of uptake from baseline and/or new FDG-avid foci consistent with lymphoma at interim or end-of-treatment assessment. In association with a new category of indeterminate response. For further details, please check Cheson et al. [29]

EORTC European Organisation for Research and Treatment of Cancer, *PERCIST* Positron Emission Tomography Response Criteria in Solid Tumors, *iPERCIST* Immuno Positron Emission Tomography Response Criteria in Solid Tumors, *PECRIT* PET/CT Criteria For Early Prediction Of Response To Immune Checkpoint Inhibitor Therapy, *PERCIMT* PET Response Evaluation Criteria for Immunotherapy, *IMPeTUs* Italian Myeloma criteria for PET USe, *LYRIC* Lymphoma Response to Immunomodulatory therapy Criteria, *CMR* complete metabolic response, *PMR* partial metabolic response, *SMD* stable metabolic response, *PMD* progressive metabolic disease, *CR* complete response, *PR* partial response, *SD* stable disease, *PD* progressive disease

Fig. 10.2 A suggested structure for a PET report

ELEMENT	DESCRIPTION
Clinical details	Indication for study Cancer type and the site of disease Summary of treatment information (insert the last treatment dates)
Technical procedure	Blood glucose level Radiopharmaceutical (name and dose) Time between tracer injection and PET acquisition Precise body region scan PET/CT instrument and characteristics of CT part CT technique (including whether oral or intravenous contrast was used)
Comparison studies	Comparison with prior PET studies, by including date, the scanner type and the name of center (if different)
Findings	Visual analysis (comparison with previous PET scan) Semiquantitative analysis (comparison with previous PET scan) Standardized criteria, if available for the solid tumor Abnormal tracer findings should be correlated with concurrent CT or MRI images, if applicable In addition, incidental findings at PET, CT, and MRI should be described
Impression and conclusions	Clear interpretation of findings: CMR, PMR, SMD, PMD Recommendations for follow-up studies, if applicable

CMR = complete metabolic response; PMR = partial metabolic response; SMD = stable metabolic disease; PMD = progressive metabolic disease

10.8 Common and Less Common Findings

On the PET scan, some benign conditions can mimic persistent disease during or after therapy, particularly with FDG. This radiopharmaceutical is not specific enough, and some conditions, like inflammation, can be associated with a low-moderate tracer uptake at PET images [15, 30]. Therefore, any conditions that can be correlated with adverse events during or after therapy can cause false-positive findings.

In Table 10.5 discuss the major causes of false positives at FDG PET/CT after treatments.

Inflammation and infections can be considered the common false-positive findings in FDG and other metabolic tracers, such as 11C-Choline or ^{18}F-Choline [31]; however, similar data have been reported related to 68Ga-DOTATOC and 68Ga-PSMA [32, 33]. Limited evidence is now available about the role of these agents in the evaluation of response to therapies. Therefore, little data is known about the false positives findings during treatments.

Table 10.5 False-positive causes at PET/CT, after treatments

Treatment	Common	Less common
Chemotherapy	Inflammation (i.e., high and symmetric tonsillar activity post chemotherapy), and/or reactive lymph nodes	Complications due to the therapy (e.g., pneumonitis)
Surgery	Reparative phenomena in the site of surgery (i.e., post talc pleurodesis)	Inflammation and reactive lymph nodes
Radiotherapy	Post-radiotherapy inflammatory change	Reactive lymph nodes, post-actinic effects
Immunotherapy	Immune-related inflammatory response (i.e., diffuse splenic uptake or inflamed lymph nodes)	Immune-related events (i.e., colitis, pneumonitis, sarcoidosis-like syndrome, thyroiditis, etc.)
Hormonal therapy	Granuloma post-injection (i.e., in the gluteus)	Flare phenomenon
Bisphosphonate drugs	None	Mandibular fracture Infection

10.9 How to Interpret the Findings: Dos and Don'ts

10.9.1 What to Do

1. When high metabolic activity is present, one of the primary aims is to ascertain if the etiology is malignant, benign, or inflammatory.
   (a) Malignant uptake is focal, and moderate to intense, and shows a correspondence with an abnormal finding at CT or MRI coregistered images.
   (b) Benign finding is well defined by a low or absent tracer uptake and with a physiological pattern at CT or MRI coregistered images.
   (c) Inflammatory processes are typically linear and track along soft-tissue boundaries such as pleural surfaces or fascial planes.
2. The intensity of uptake in metastases usually parallels that in the primary site of disease. If not, another etiology should be considered. However, some conditions should be evaluated, such as the size of lymph nodes and the proximity of primary tumor. The exception to this concept is tumors with a heterogeneity biology (i.e., follicular lymphoma, chronic lymphocytic leukemia, endocrine tumors). In this case, it is necessary to integrate more radiopharmaceutical agent.
3. Integrating the CT or MRI morphology is crucial to reach an accurate interpretation.
4. In post-therapy examination, it is important to compare all the baseline lesions with the post-scan lesions, both those with and without a significant tracer uptake. Remember that no uptake in a CT lesion is an important prognostic factor.
5. Review of multiple serial MIP images over the course of therapies can enable rapid appreciation of changes, not evident by comparison with the prior study.
6. Suggest any additional procedures, both non-invasive or invasive, in case of unclear or doubtful findings.

10.9.2 What Not to Do

1. Avoid a comparison between images performed too distant, in particular in case of different therapies or settings among the scans.
2. Do not compare two PET scans performed with different radiopharmaceuticals, before and after therapy. In this case, please suggest only the biological behavior and the potential effects in the therapeutic choice.
3. In case of the evaluation of response to therapy, do not use the semiquantitative data in pre- and post-therapy scan, in case of different PET instruments or in case of an intense

extravasation on one of the scans. In this case, only visual assessment is warranted.

4. Avoid to evaluate the response to therapy, by comparing the PET scan with a previous anatomical examination (i.e., MRI or CT). It is strongly recommended to use the same type of examination before, after, and during therapy.

10.10 What to Advise the Referrers

In conclusion, a review of PET images at both baseline and post-therapy evaluation requires good experience and critical analysis. An essential suggestion is to evaluate PET examination, independent of the radiopharmaceuticals, from the clinical data collection to the final report. Discuss indeterminate or unclear findings with the referring physician.

References

1. Wahl RL, Jacene H, Kasamon Y, Lodge MA. From RECIST to PERCIST: evolving considerations for PET response criteria in solid tumors. J Nucl Med. 2009;50(Suppl 1):122S–50S.
2. Mac Manus MP, Hicks RJ, Matthews JP, McKenzie A, Rischin D, et al. Positron emission tomography is superior to computed tomography scanning for response-assessment after radical radiotherapy or chemoradiotherapy in patients with non-small-cell lung cancer. J Clin Oncol. 2003;21:1285–92.
3. Benz MR, Czernin J, Allen-Auerbach MS, Tap WD, Dry SM, et al. FDG-PET/CT imaging predicts histopathologic treatment responses after the initial cycle of neoadjuvant chemotherapy in high-grade soft-tissue sarcomas. Clin Cancer Res. 2009;15:2856–63.
4. Krause BJ, Herrmann K, Wieder H, zum Büschenfelde CM. 18F-FDG PET and 18F-FDG PET/CT for assessing response to therapy in esophageal cancer. J Nucl Med. 2009;50(Suppl 1):89S–96S.
5. Heron DE, Andrade RS, Beriwal S, Smith RP. PET-CT in radiation oncology: the impact on diagnosis, treatment planning, and assessment of treatment response. Am J Clin Oncol. 2008;31:352–62.
6. Brindle K. New approaches for imaging tumour responses to treatment. Nat Rev Cancer. 2008;8:94–107.
7. Lordick F, Ott K, Krause BJ, Weber WA, Becker K, Stein HJ, et al. PET to assess early metabolic response and to guide treatment of adenocarcinoma of the oesophagogastric junction: the MUNICON phase II trial. Lancet Oncol. 2007;8:797–805.
8. Romine PE, Martins RG, Eaton KD, Wood DE, Behnia F, Goulart BHL, et al. Long term follow-up of neoadjuvant chemotherapy for non-small cell lung cancer (NSCLC) investigating early positron emission tomography (PET) scan as a predictor of outcome. BMC Cancer. 2019;19(1):70.
9. Wulfert S, Kratochwil C, Choyke PL, Afshar-Oromieh A, Mier W, Kauczor HU, Schenk JP, Haberkorn U, Giesel FL. Multimodal imaging for early functional response assessment of (90)Y-/ (177)Lu-DOTATOC peptide receptor targeted radiotherapy with DW-MRI and (68)Ga-DOTATOC-PET/CT. Mol Imaging Biol. 2014;16(4):586–94.
10. Gupta M, Choudhury PS, Rawal S, Goel HC, Rao SA. Evaluation of RECIST, PERCIST, EORTC, and MDA criteria for assessing treatment response with Ga68-PSMA PET-CT in metastatic prostate cancer patient with biochemical progression: a comparative study. Nucl Med Mol Imaging. 2018;52:420–9.
11. Berlin L. Accuracy of diagnostic procedures: has it improved over the past five decades? Am J Roentgenol. 2007;188:1173–8.
12. Doubilet P, Herman P. Interpretation of radiographs: effect of clinical history. Am J Roentgenol. 1981;137:1055–8.
13. Leslie A, Jones A, Goddard P. The influence of clinical information on the reporting of CT by radiologists. Br J Radiol. 2000;73:1052–5.
14. Loy CT, Irwig L. Accuracy of diagnostic tests read with and without clinical information: a systematic review. JAMA. 2004;292:1602–9.
15. Hofman MS, Hicks RJ. How we read oncologic FDG PET/CT. Cancer Imaging. 2016;16:35.
16. Kostakoglu L, Chauvie S. Metabolic tumor volume metrics in lymphoma. Semin Nucl Med. 2018;48:50–66.
17. Velikyan I, Sundin A, Sörensen J, Lubberink M, Sandström M, Garske-Román U, et al. Quantitative and qualitative intrapatient comparison of 68Ga-DOTATOC and 68Ga-DOTATATE: net uptake rate for accurate quantification. J Nucl Med. 2014;55:204–10.
18. Schmuck S, von Klot CA, Henkenberens C, Sohns JM, Christiansen H, Wester HJ, et al. Initial experience with volumetric 68Ga-PSMA I&T PET/CT for assessment of whole-body tumor burden as a quantitative imaging biomarker in patients with prostate cancer. J Nucl Med. 2017;58:1962–8.
19. Moskowitz AJ, Schöder H, Gavane S, Thoren KL, Fleisher M, Yahalom J, McCall SJ, et al. Prognostic significance of baseline metabolic tumor volume in relapsed and refractory Hodgkin lymphoma. Blood. 2017;130:2196–203.
20. Guler OC, Torun N, Yildirim BA, Onal C. Pretreatment metabolic tumour volume and total lesion glycoly-

sis are not independent prognosticators for locally advanced cervical cancer patients treated with chemoradiotherapy. Br J Radiol. 2018;91:20170552.
21. Barrington SF, Kluge R. FDG PET for therapy monitoring in Hodgkin and non-Hodgkin lymphomas. Eur J Nucl Med Mol Imaging. 2017;44(Suppl 1):97–110.
22. Kim JH, Kim BJ, Jang HJ, Kim HS. Comparison of the RECIST and EORTC PET criteria in the tumor response assessment: a pooled analysis and review. Cancer Chemother Pharmacol. 2017;80:729–35.
23. Min SJ, Jang HJ, Kim JH. Comparison of the RECIST and PERCIST criteria in solid tumors: a pooled analysis and review. Oncotarget. 2016;7:27848–54.
24. Goldfarb L, Duchemann B, Chouahnia K, Zelek L, Soussan M. Monitoring anti-PD-1-based immunotherapy in non-small cell lung cancer with FDG PET: introduction of iPERCIST. EJNMMI Res. 2019;9:8.
25. Cho SY, Lipson EJ, Im HJ, Rowe SP, Gonzalez EM, Blackford A, et al. Prediction of response to immune checkpoint inhibitor therapy using early-time-point 18F-FDG PET/CT imaging in patients with advanced melanoma. J Nucl Med. 2017;58:1421–8.
26. Anwar H, Sachpekidis C, Winkler J, Kopp-Schneider A, Haberkorn U, Hassel JC, et al. Absolute number of new lesions on 18F-FDG PET/CT is more predictive of clinical response than SUV changes in metastatic melanoma patients receiving ipilimumab. Eur J Nucl Med Mol Imaging. 2018;45:376–83.
27. Mac Manus MP, Hicks RJ, Matthews JP, McKenzie A, Rischin D, Salminen EK, et al. Positron emission tomography is superior to computed tomography scanning for response-assessment after radical radiotherapy or chemoradiotherapy in patients with non-small-cell lung cancer. J Clin Oncol. 2003;21:1285–92.
28. Nanni C, Versari A, Chauvie S, Bertone E, Bianchi A, Rensi M, et al. Interpretation criteria for FDG PET/CT in multiple myeloma (IMPeTUs): final results. IMPeTUs (Italian myeloma criteria for PET USe). Eur J Nucl Med Mol Imaging. 2018;45:712–9.
29. Cheson BD, Ansell S, Schwartz L, Gordon LI, Advani R, Jacene HA, et al. Refinement of the Lugano Classification lymphoma response criteria in the era of immunomodulatory therapy. Blood. 2016;128:2489–96.
30. Culverwell AD, Scarsbrook AF, Chowdhury FU. False-positive uptake on 2-[18F]-fluoro-2-deoxy-D-glucose (FDG) positron-emission tomography/computed tomography (PET/CT) in oncological imaging. Clin Radiol. 2011;66:366–82.
31. Calabria F, Chiaravalloti A, Cicciò C, Gangemi V, Gullà D, Rocca F, et al. PET/CT with 18F-choline: physiological whole bio-distribution in male and female subjects and diagnostic pitfalls on 1000 prostate cancer patients: 18F-choline PET/CT biodistribution and pitfalls. A southern Italian experience. Nucl Med Biol. 2017;51:40–54.
32. Al-Ibraheem A, Bundschuh RA, Notni J, Buck A, Winter A, Wester HJ, et al. Focal uptake of 68Ga-DOTATOC in the pancreas: pathological or physiological correlate in patients with neuroendocrine tumours? Eur J Nucl Med Mol Imaging. 2011;38:2005–13.
33. Shetty D, Patel D, Le K, Bui C, Mansberg R. Pitfalls in Gallium-68 PSMA PET/CT interpretation—a pictorial review. Tomography. 2018;4(4):182–93.

Part II

Therapy Response Evaluation: Clinical Atlas

11 ^{18}F-FDG PET/CT in Treatment Response Evaluation in Head and Neck Cancer

Pierre Lovinfosse and Roland Hustinx

11.1 Case 1

Clinical Details

60-year-old man with a right oropharyngeal moderately differentiated squamous cell carcinoma (HPV-negative, cT3N0M0), which was treated by concomitant radiochemotherapy. Three months after the end of the treatment, the clinical evolution is overall favorable but there remains a slight induration of the right tonsillar region.

Images

Scan Findings

The baseline PET/CT (Fig. 11.1a–d) shows the right oropharyngeal lesion with intense [^{18}F]FDG uptake.

[^{18}F]FDG PET/CT 3 months after the end of concomitant radiochemotherapy (Fig. 11.1e–h). Persistence intense focal uptake in the right tonsillar area, with a low-activity central area (red arrow). There is uptake by the tongue and para-

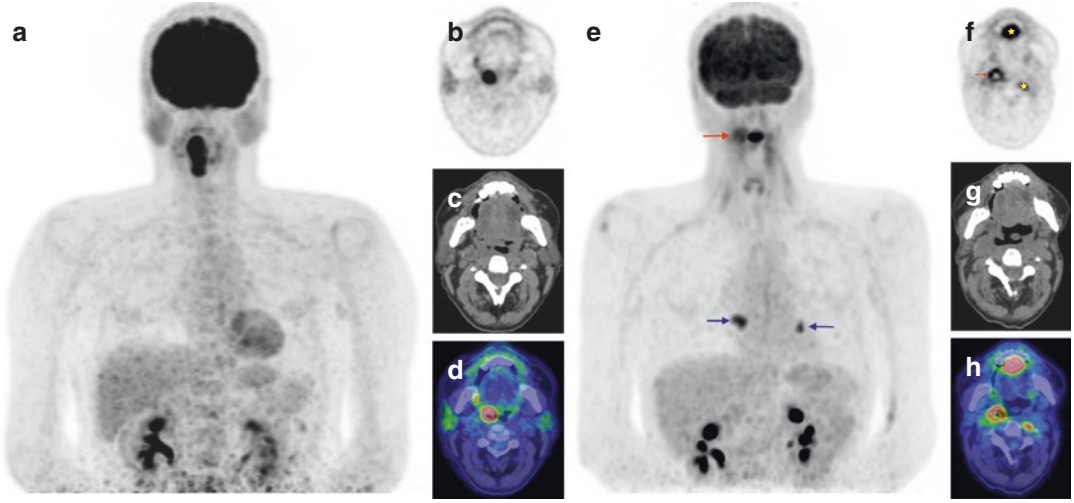

Fig. 11.1

P. Lovinfosse · R. Hustinx (✉)
Division of Nuclear Medicine and Oncological Imaging, University Hospital of Liege, Liege, Belgium
e-mail: rhustinx@chuliege.be

S. Fanti et al. (eds.), *Atlas of Clinical PET-CT in Treatment Response Evaluation in Oncology*,
https://doi.org/10.1007/978-3-030-68858-5_11

vertebral muscle. There are also two new foci in both lungs (blue arrows).

Note: The first three steps of the PET acquisition last 4 min, the others 90 s. The MIP images shown here are reconstructed using a body protocol (pixel size 4 × 4 × 4 mm) whereas the axial slices were extracted from the H&N protocol (pixel size 2 × 2 × 2 mm).

Interpretation

Partial response of the primitive tumor with persistence of a necrotic residual tumoral tissue in the right tonsillar area.

Endoscopy revealed a necrotic lesion of the right tonsil, and biopsy confirms the presence of necrotic tissue with moderately differentiated squamous cell carcinoma infiltration.

Two lung nodules with intense metabolism were deemed consistent with metastases. However, a CT-guided biopsy only showed inflammatory cells.

Teaching Points

Treatment failure is usually easily assessed, but this case serves as a reminder that [^{18}F]FDG uptake is not specific for cancer. The posttreatment scan shows both physiological uptake (muscle) and inflammatory changes (lung lesions). The former needs to be recognized when reading the study, but the later may need pathological correlation.

11.2 Case 2

Clinical Details

27-year-old man with cT2N0M0 squamous cell carcinoma of the left side of the tongue (moderately differentiated and HPV-negative). It was diagnosed in the course of an acute lymphoblastic leukemia treated by chemotherapy and allograft. The patient underwent partial glossectomy and adjuvant radiotherapy, as pathology revealed perinervous infiltration.

Images

Scan Findings

The lesion of the tongue is clearly identified on the baseline scan (Fig. 11.2a–d). Three months after the end of radiotherapy, follow-up [^{18}F]FDG PET/CT showed absence of suspicious lesion (Fig. 11.2e–h). However, 8 months after the end of the radiotherapy, a left lingual lesion clinically developed in the form of an induration, which turned out to be highly hypermetabolic (Fig. 11.2i–l).

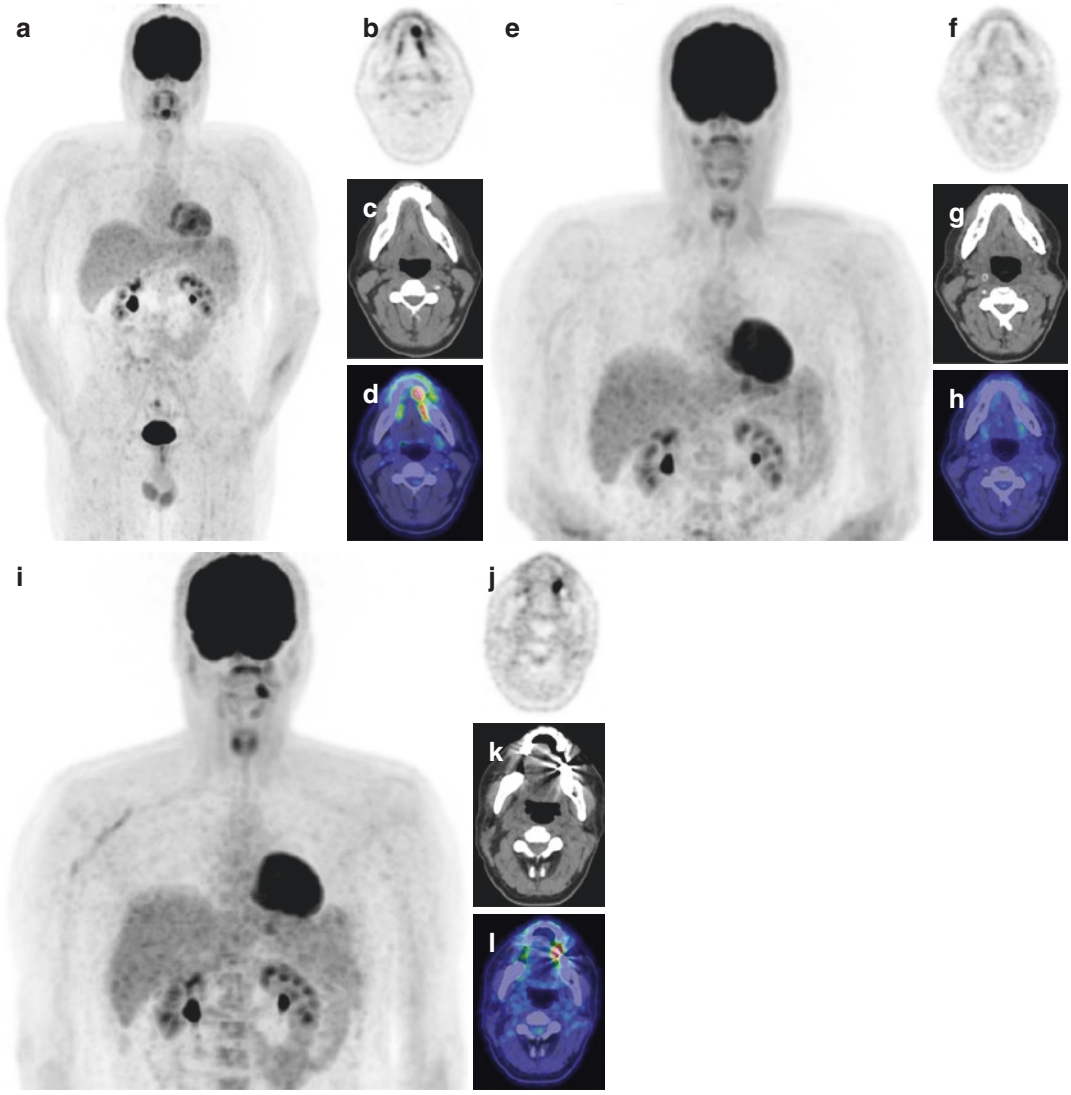

Fig. 11.2

Interpretation

Three months after the end of radiotherapy: complete response.

Eight months after the end of radiotherapy: local recurrence. This was confirmed by a new biopsy.

Teaching Points

Postradiation inflammatory changes are usually easily recognized but they are not systematically present. In this case, they were none whatsoever.

Also, this HPV-negative patient had an early relapse, and this illustrates the capacity of PET/CT for both following up and restaging those patients.

11.3 Case 3

Clinical Details

66-year-old man with a cT2N2c squamous cell carcinoma of the base of the tongue (moderately differentiated, HPV-negative), treated by concomitant radiochemotherapy.

Images

Scan Findings

Baseline [^{18}F]FDG PET/CT (Fig. 11.3a–d):

Intense uptake by the right basal tongue lesion and two ipsilateral adenopathies (cervical area IIa). Very mild uptake in a pericentimetric lymph node in the left cervical area IIa. No distant metastasis.

[^{18}F]FDG PET/CT 3 months after the end of concomitant radiochemotherapy (Fig. 11.3e–h): Mild uptake at the site of primitive tumor and unchanged aspect of the left LN (blue arrow). Furthermore, moderate symmetrical uptake of palatine tonsils. Note that the yellow star indicates paravertebral muscle uptake.

Interpretation

Major response of the primitive tumor with persistence of a moderate hypermetabolism consistent with radiation-induced inflammation. Complete metabolic response of the right cervical adenopathies and no change in the left cervical lymph node, hence considered as equivocal finding according to Mehanna et al. No distant metastasis.

Biopsy of the base of tongue residual metabolism confirmed chronic radiation-induced inflammatory tissues. Exclusive left cervical lymph node dissection showed the absence of lymph node invasion (0/15).

Teaching Points

Assessing residual nodal disease after chemoradiotherapy remains a challenge, as up to one out of four PET/CT studies may be classified as equivocal. Mild uptake in normal size LN is frequently observed in relation with inflammation, in patients who are often smokers or present with impaired oral and dental hygiene. In this case, the absence of evolution was consistent with inflammatory nodes, although it is still recommended to perform LN dissection in such equivocal findings.

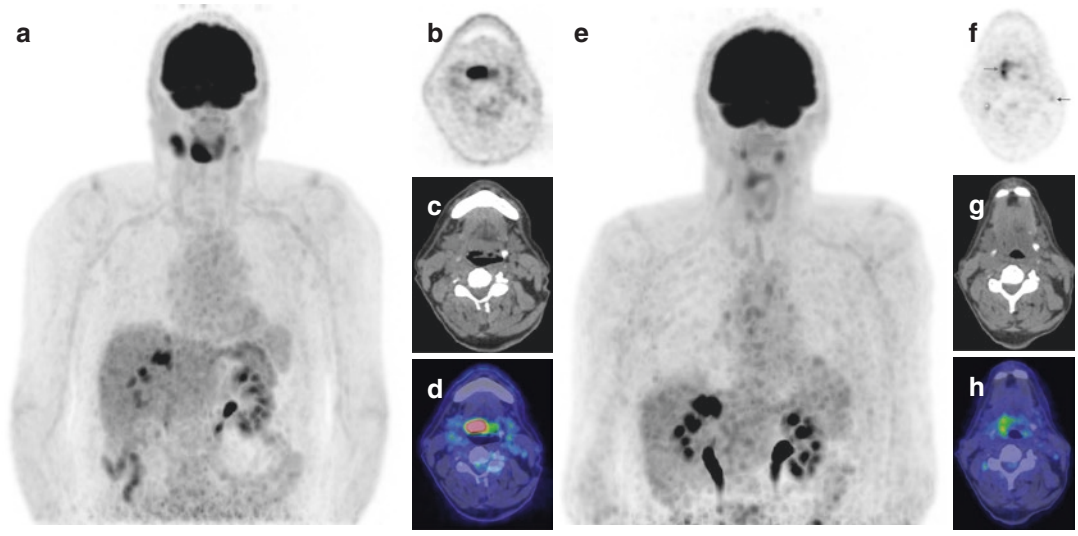

Fig. 11.3

11.4 Case 4

Clinical Details

47-year-old woman with a moderately differentiated cT3N2b squamous cell carcinoma of the right pyriform sinus treated by concomitant radiochemotherapy.

Images

Scan Findings

Baseline [^{18}F]FDG PET/CT (Fig. 11.4a–d): Right pyriform sinus lesion with intense [^{18}F]FDG uptake causing focal lysis of the posterior component of the right lamina of the thyroid cartilage and showing a pre-laryngeal extension. There are also foci of intense uptake in the right cervical areas IIa and III and left cervical area IV and a more moderate focal uptake in the left cervical area III. No distant abnormally.

[^{18}F]FDG PET/CT 3 months after concomitant radiochemotherapy (Fig. 11.4e–h): Very mild uptake at the site of primitive tumor, no residual uptake in the nodal areas. Increased [^{18}F]FDG uptake by the proximal portion of the esophagus. High heterogeneous uptake in the right lower lobe.

Interpretation

Complete response of the primitive tumor and of all lymph node metastasis. Postradiation esophagitis. Right LL bronchopneumonia.

Teaching Points

This illustrates a typical complete tumor response 3 months after RCT. Very mild uptake is often seen and easily identified as postradiation changes.

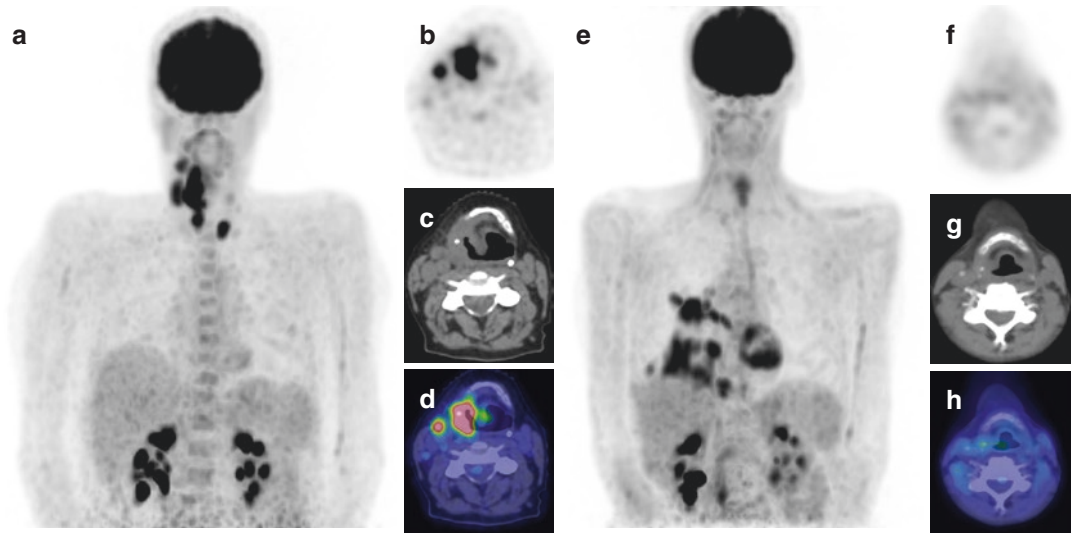

Fig. 11.4

11.5 Case 5

Clinical Details

69-year-old man with a poorly differentiated, HPV-negative cT4N2c squamous cell carcinoma of the left base of the tongue, treated by concomitant radiochemotherapy.

Images

Scan Findings

The baseline scan shows high uptake by the primary, also invading ipsilateral vallecula and tonsil area, along with bilateral cervical lymph nodes (Fig. 11.5a–d).

Three months after the end of treatment, persistence of an intense [^{18}F]FDG uptake regarding the base of tongue and bilateral cervical adenopathies. Additionally, two hypermetabolic pulmonary nodules are seen in the lower left lobe along with a hypermetabolic retroclavicular adenopathy (red arrow, Fig. 11.5e–k).

Interpretation

Partial metabolic response of the primary and left cervical adenopathies and stability of the right cervical adenopathy. Overall, progressive disease (lung metastases and LN).

Teaching Points

Progression of disease is readily identified by PET/CT, including outside the area initially involved.

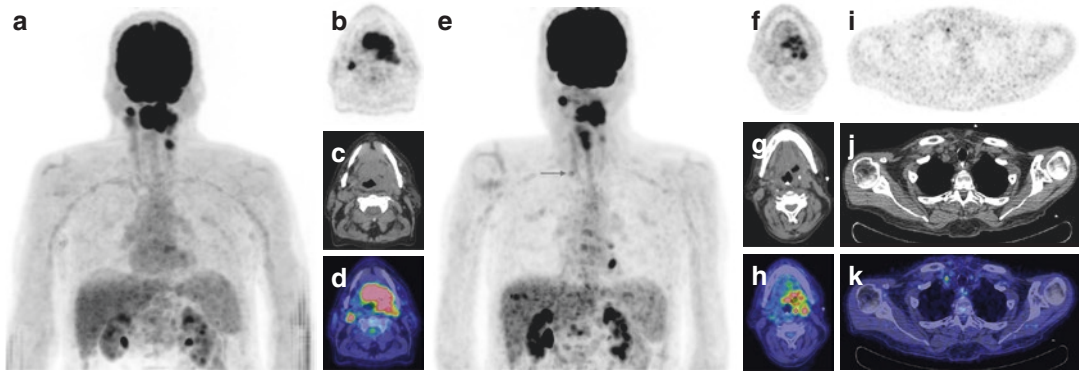

Fig. 11.5

11.6 Case 6

Clinical Details

This patient presented with a left nodal recurrence of a left tongue squamous cell carcinoma, cT4N0M0, treated by exclusive surgery 1 year earlier. Assessment 3 months after the end of radiochemotherapy.

Images

Scan Findings

The baseline scan shows an intense uptake in the nodal recurrence (Fig. 11.6a–d). Three months after the end of treatment (Fig. 11.6e–h), persistence of an intense focal uptake in the left cervical main adenopathy. Mildly increased focal uptake in the right neck. No other suspicious lesion. High, homogeneous esophageal uptake.

Interpretation

Poor partial metabolic and volume response of the large left cervical adenopathy. The infracentimetric right cervical lymph node remains stable consistent with nonspecific inflammatory node (see also Case 3). Diffuse esophagitis.

Teaching Points

Absence of response is readily identified by PET/CT, including as in this case of nodal disease.

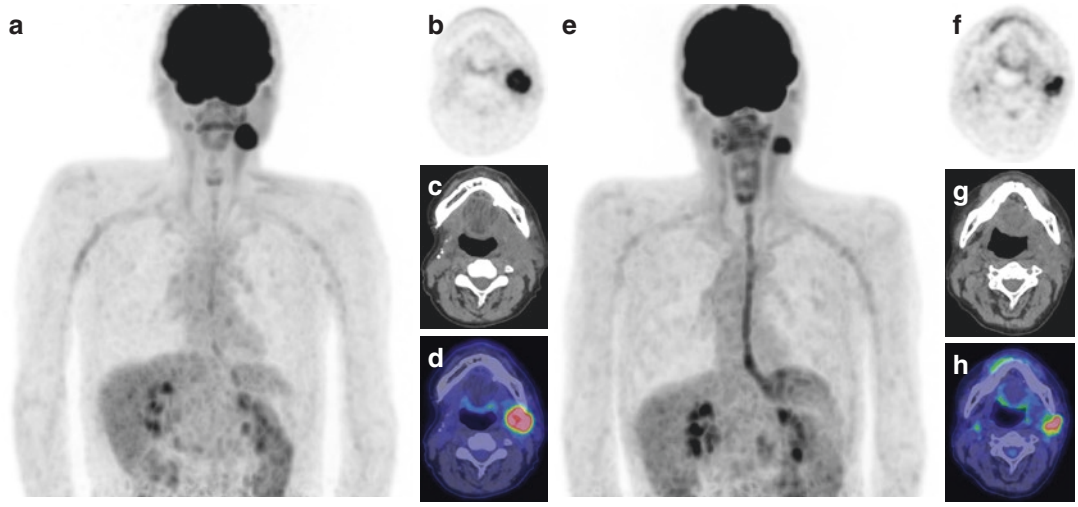

Fig. 11.6

11.7 Case 7

Clinical Details

55-year-old man with a poorly differentiated squamous cell carcinoma of the left submaxillary gland cT3N2bM1 with ipsilateral cervical lymph node metastasis and a single bone metastasis of cervical vertebrae C3. Assessment 3 months after the end of radiochemotherapy.

Images

Scan Findings

High uptake by the primary, multiple invaded lymph nodes and vertebral metastasis (Fig. 11.7a–d). Three months after the end of treatment, only very mild uptake remains in the head and neck area, but there is now an intense focal uptake of [^{18}F]FDG in the left pulmonary hilum (Fig. 11.7e–h).

Interpretation

Complete metabolic response of the primary lymph nodes and bone metastasis. New left pulmonary lesion, highly suspicious of malignity.

Considering the discordant evolution, the pulmonary hilar lesion is biopsied. Pathology reveals an adenocarcinoma.

Teaching Points

Synchronous cancers (lung, esophagus) are not infrequent in HN carcinomas. PET/CT allows for an early detection of such lesions, although in the present case, the primary lung progressed unusually rapidly.

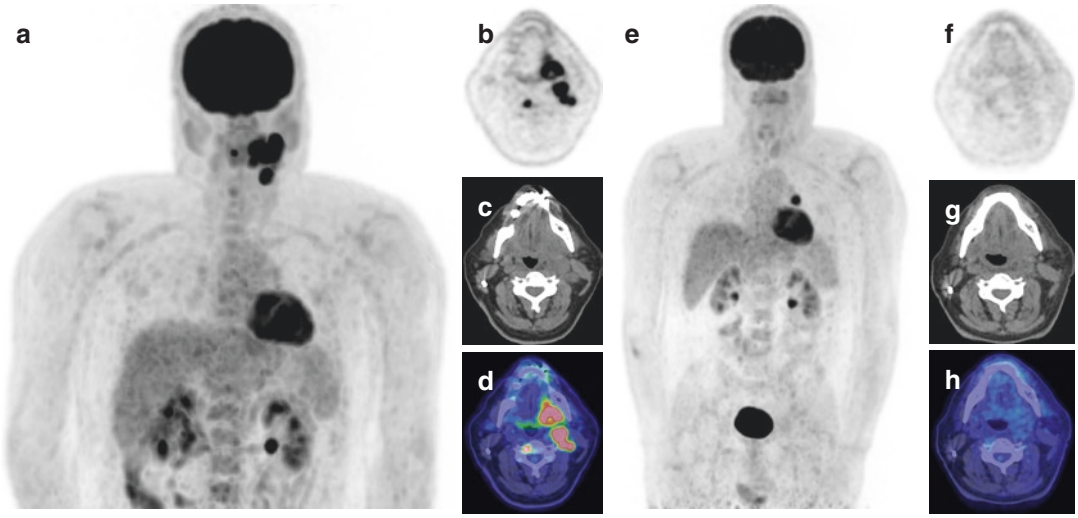

Fig. 11.7

11.8 Case 8

Clinical Details

47-year-old man with a right oropharyngeal squamous cell carcinoma (moderately differentiated, HPV-negative) with bilateral cervical lymph node metastases, classified cT4N2cM0 and treated by concomitant radiochemotherapy.

Images

Scan Findings

The primary and lymph nodes are highly hypermetabolic (Fig. 11.8a–d). Three months after the end of the treatment, there remains only mild uptake in the area of the primary, no abnormal uptake in the nodal areas (Fig. 11.8e–h).

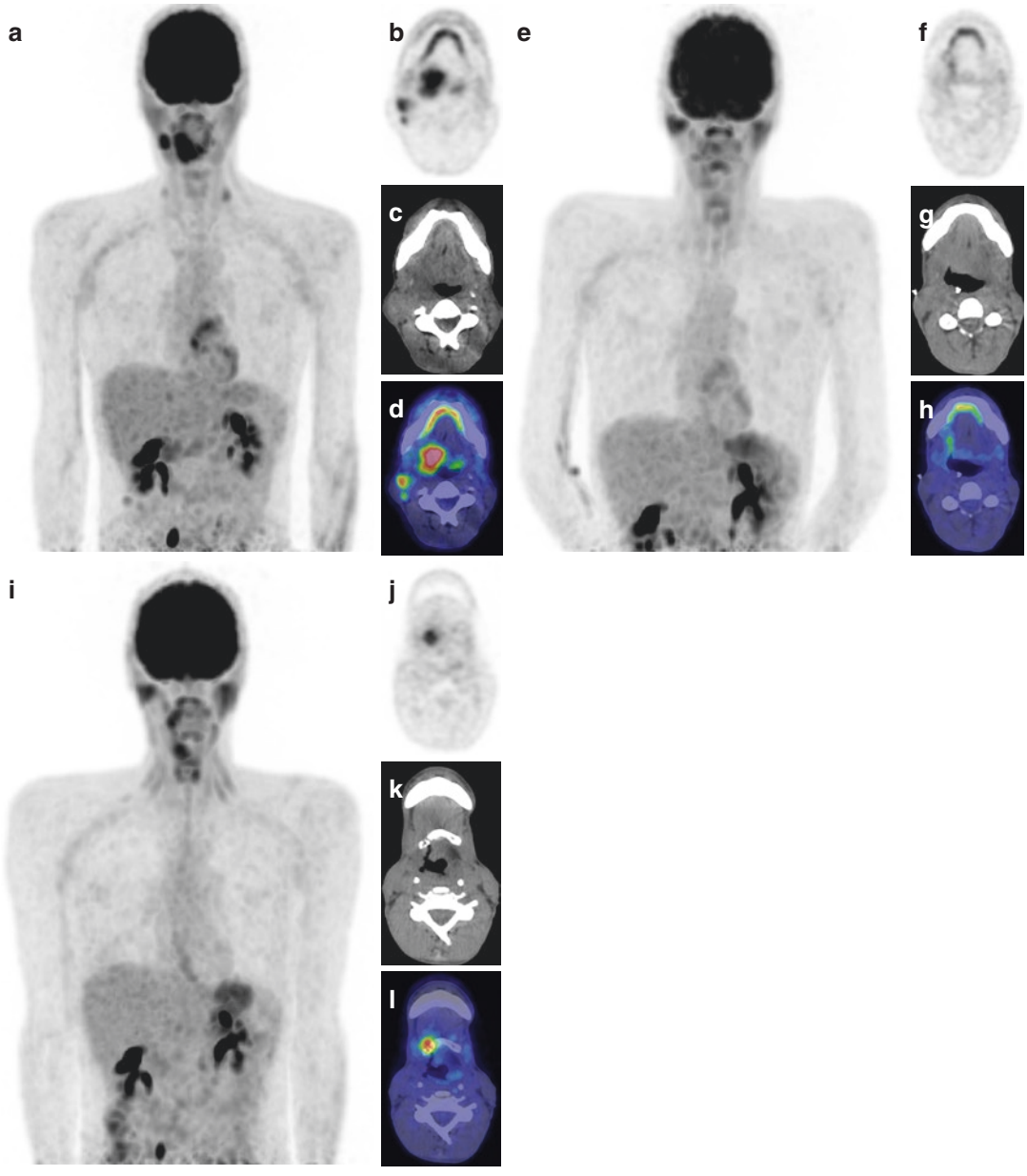

Fig. 11.8

One year later, clinical suspicion of recurrence. PET/CT shows highly increased uptake centered on the right side of the hyoid bone, with corresponding lysis on CT (Fig. 11.8i–l).

Interpretation

Four months after the end of the treatment, complete tumor response with mild postradiation inflammatory changes.

After 1 year, PET/CT consistent with recurrent disease.

However multiple biopsies revealed chronic and subacute inflammatory changes mixed with areas of fibrosis and necrosis. No tumor cells are seen.

Teaching Points

The PET/CT study at 3 months is typical for a complete response, but the clinical course is unusual and the lack of specificity of [^{18}F]FDG makes it impossible for the PET/CT study to distinguish delayed inflammatory changes from recurrence (see also Case 15).

11.9 Case 9

Clinical Details

68-year-old woman with a left oropharyngeal squamous cell carcinoma, treated by surgery (pT2N1M0). Adjuvant radiochemotherapy is administered due to evidence of lymph node capsular effraction at pathology.

Images

Scan Findings

The baseline scan shows highly increased uptake in both the primary and the lymph node (Fig. 11.9a–d). Three months after the end of radiochemotherapy (Fig. 11.9e–h), visualization of a vast hypermetabolic lesion occupying the left lingual floor, crossing the median line, invading the hyoid bone, and extending into the prelaryngeal region and the thyroid gland. There are also bilateral cervical lymph node metastases.

Interpretation

Major locoregional neoplastic progression.

Teaching Points

This represents an unusually rapid progression on treatment, most often seen in HPV-negative/p16 negative oropharyngeal squamous cell carcinoma.

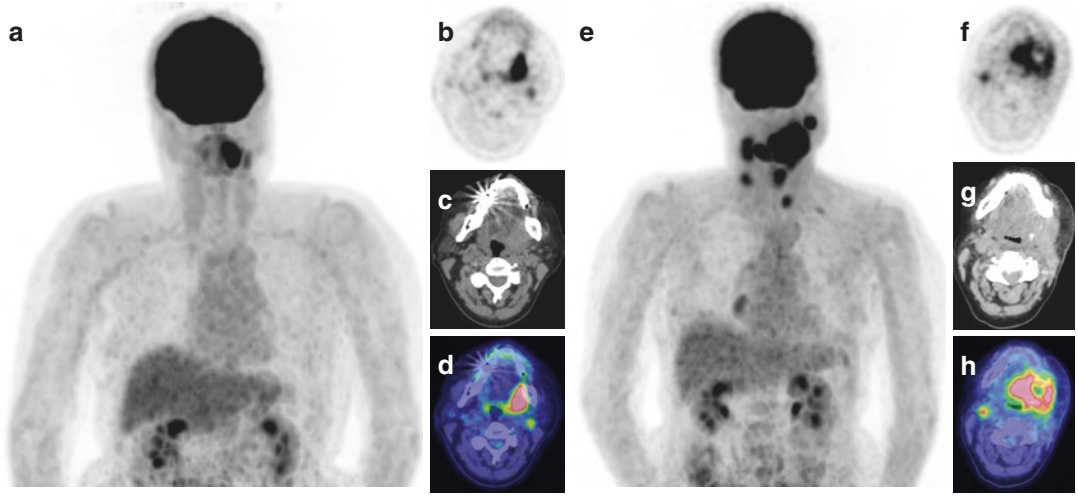

Fig. 11.9

11.10 Case 10

Clinical Details

64-year-old man with a well-differentiated squamous cell carcinoma of the uvula with bilateral cervical lymph node metastasis (cT2N2cM0), treated by local surgery, bilateral cervical lymph node dissection (including parapharyngeal area), and adjuvant radiochemotherapy.

Images

Scan Findings

At baseline, the primary and the adenopathies are highly hypermetabolic (Fig. 11.10a–d). Three months after the end of radiochemotherapy, those lesions are no longer present (Fig. 11.10e). There is increased uptake by the right vocal cord (Fig. 11.10f–h), mild uptake in the right posterior wall of the nasopharyngeal area, distant from the primary location and considered to physiological muscular uptake (Fig. 11.10i–k), and disappearance of all the initial lesions.

Three months later (Fig. 11.10l–o), there is a vast hypermetabolic lesion of the right parapharyngeal area invading the base of the skull. No abnormal laryngeal uptake.

Interpretation

Early recurrent disease mistakenly interpreted as physiological uptake, but became obvious at follow up.

Vocal cords asymmetrical uptake of functional origin (hoarseness at the time of the exam, which spontaneously resolved later on).

Teaching Points

This mild uptake in an area clearly distinct of the primary was misidentified as physiological, although clearly asymmetrical. Sensitivity being the primary strength of [18]FDG cancer imaging, correlative imaging should be performed whenever necessary. In this case, an MRI might have confirmed the recurrence earlier.

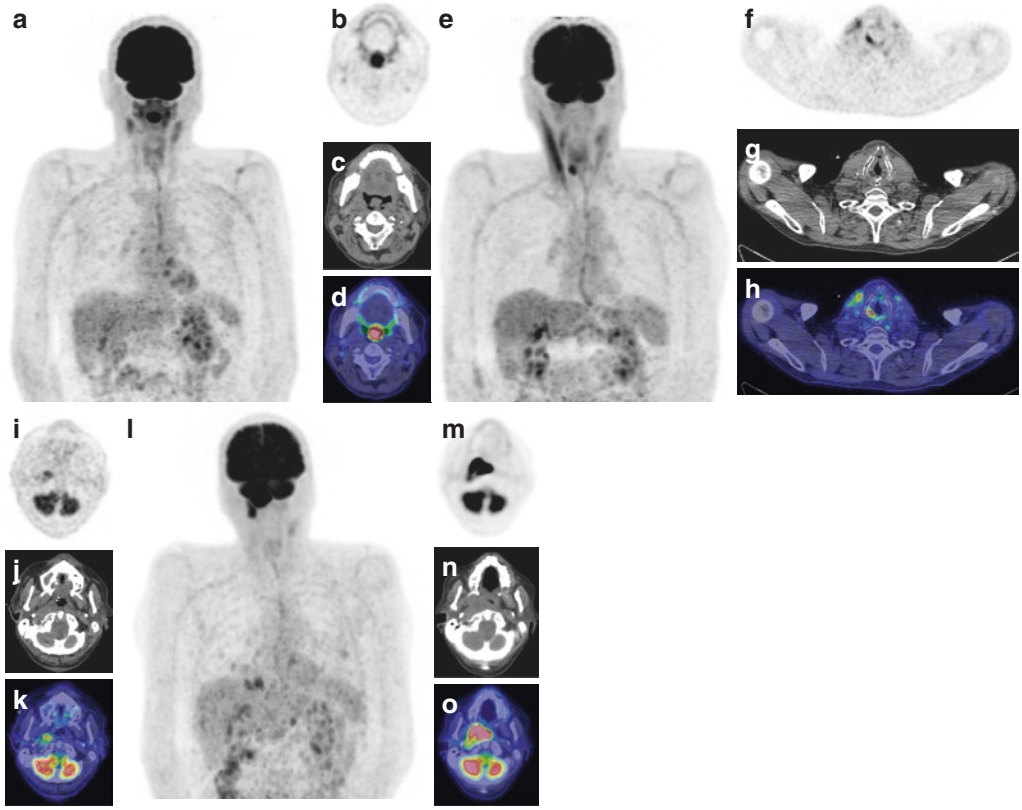

Fig. 11.10

11.11 Case 11

Clinical Details

67-year-old man with a cT2N2c squamous cell carcinoma of the base of the tongue (HPV-negative) treated by concomitant radiochemotherapy, considered in complete remission. Four months after the end of the treatment, the patient develops fatigue with weight loss.

Images

Scan Findings

Highly increased uptake in the right hyo-thyro-epiglottic region, with CT showing the presence of air and a lysis of the hyoid bone. There is also a pulmonary infiltrate of the right upper lobe associated with a moderate [^{18}F]FDG uptake (Fig. 11.11).

Interpretation

The association of the PET and CT findings is consistent with an abscessed collection associated with a hyoid bone fracture, although early tumor recurrence cannot formally be excluded. Right upper lobe bronchopneumonia.

A watch and wait approach was followed, and further imaging showed no changes. Remarkably an [^{18}F]FDG PET/CT study performed 18 months later was totally identical to the first one. A pan-endoscopy was then performed and showed no suspicious lesion. Four-year follow-up shows no recurrence.

Teaching Points

As also illustrated in Case 8, postradiation changes may develop in a spectacular fashion and remain present over long periods of time at PET/CT. Clinical information also need to be integrated. In this case, there was a discordance between the total absence of local symptoms of recurrence and the PET/CT anomalies.

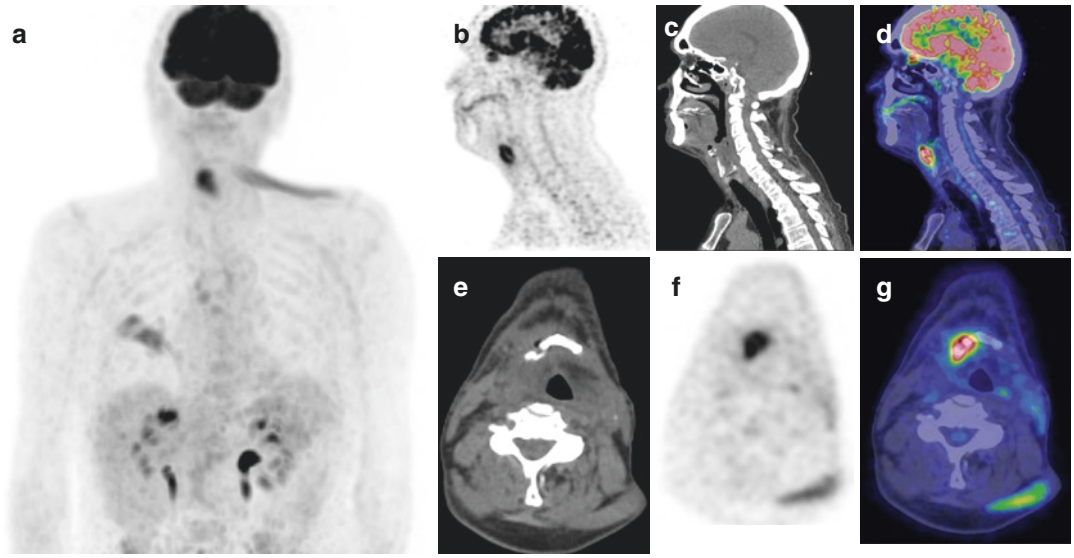

Fig. 11.11

11.12 Case 12

Clinical Details

80-year-old woman with a cT2N2 left oropharyngeal cancer treated by radiotherapy and cetuximab. Three months after completing the treatment, the patient presents with pain in the tongue and oropharyngeal region.

Images

Scan Findings

At baseline, the primary tumor and the lymph nodes are highly hypermetabolic (Fig. 11.12a–d). Three months after the end of treatment, there is high uptake on the left side of the tongue, but without any overlap with the initial tumor area, which is no longer hypermetabolic. There is no abnormal uptake in the nodal area, but two upper left pulmonary lobe hypermetabolic infiltrates, along with a slight asymmetry in the vocal cord uptake.

Interpretation

Post-therapeutic mucositis.

Complete response of the primitive tumor and lymph node metastasis.

Benign inflammatory lung hypermetabolic infiltrates.

Teaching Points

In this case, the postradiation inflammatory changes are correctly identified, as they are located in an area clearly distinct from the primary tumor, and they are also in line with the clinical symptoms (see also Cases 8 and 11).

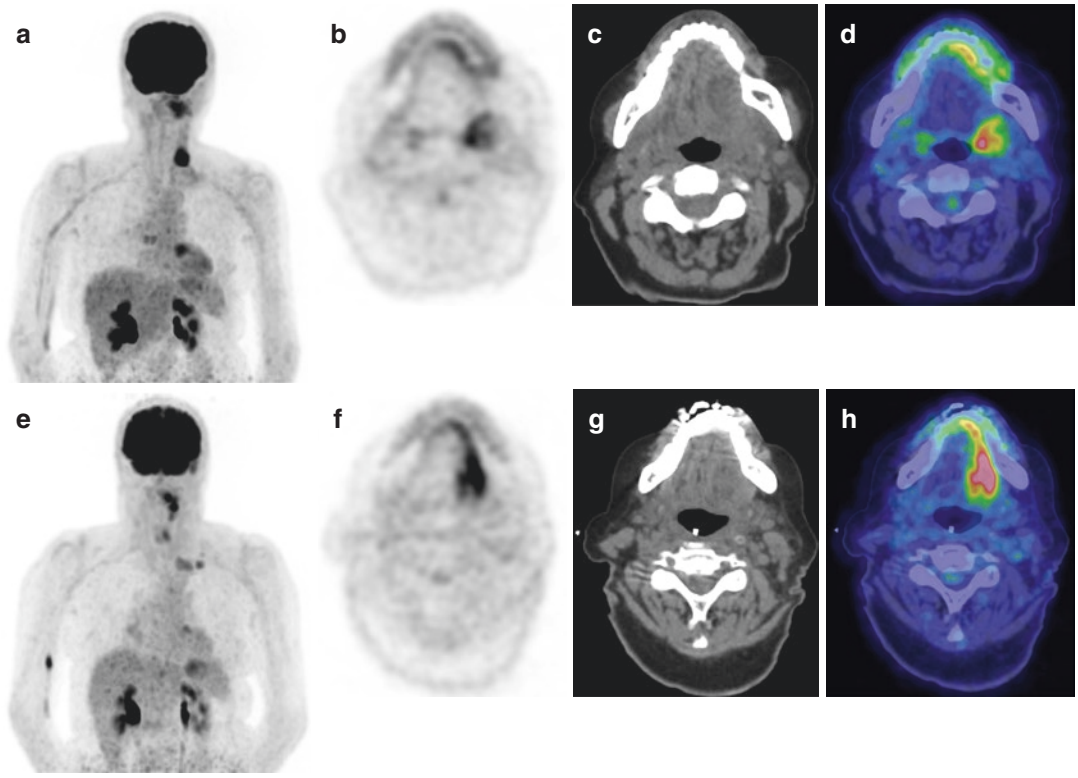

Fig. 11.12

11.13 Case 13

Clinical Details

68-year-old woman with a small cell carcinoma with neuroendocrine differentiation of the right aryepiglottic fold, staged cT2N0 according to CT scan and MRI. She was treated by radiochemotherapy. The baseline [^{18}F]FDG PET/CT was performed 2 weeks after the beginning of the chemotherapy.

Images

Scan Findings

On the baseline PET/CT (Fig. 11.13a–d), the primitive aryepiglottic neoplasia was not hypermetabolic, and there was only a very faint focal uptake in a 10 mm lymph node (right IIa cervical area: red arrow).

Three months after the end of the treatment (Fig. 11.13e–h), the uptake in LN further increases, but its size remains stable. There are no other suspicious lesions.

Interpretation

Progression of the hypermetabolism of the right cervical lymph node, consistent with malignancy. No other suspicious lesion was observed. The patient underwent a modified radical right cervical lymph node dissection. Pathology revealed the presence of three lymph node metastases, including one in the IIa area.

Teaching Points

The baseline PET was performed during chemotherapy, which probably explains why the metabolism was underestimated.

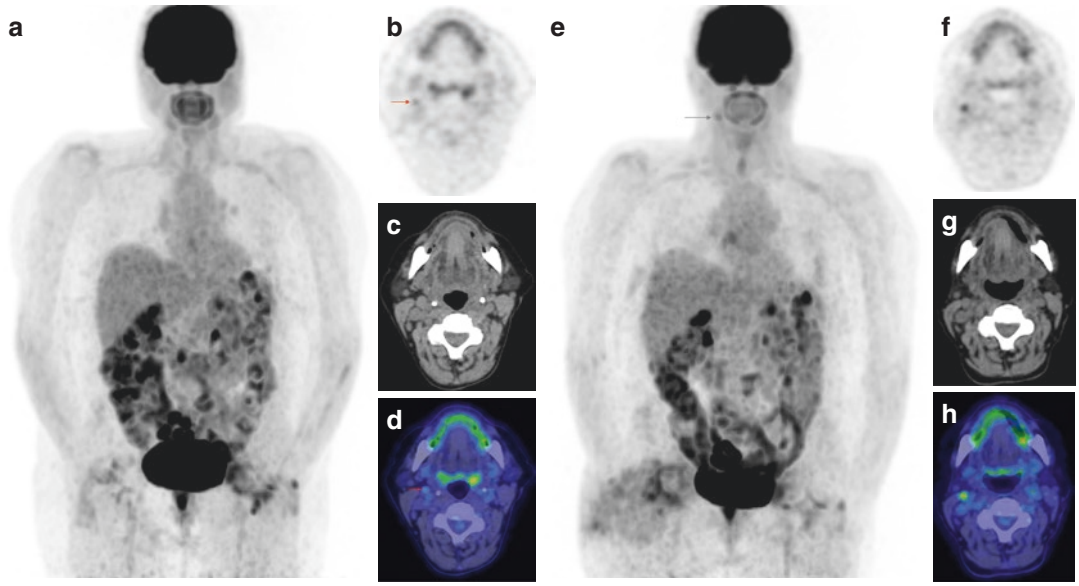

Fig. 11.13

11.14 Case 14

Clinical Details

72-year-old man with a pT4aN2bMx adenoid cystic carcinoma of the right maxillary sinus.

Treatment by extensive surgery with free flap reconstruction and adjuvant radiotherapy.

Images

Scan Findings

The baseline study (Fig. 11.14a–d) shows the primary tumor invading the ipsilateral nasal cavity, pterygopalatine fossa, and subtemporal fossa. There is osteolysis of the anterior and posterior walls of the antrum, of the maxillary and palatal horizontal process, of the posterior part of the alveolar process, and of the lower part of the nasal septum. The floor of the sphenoidal sinus and the right pterygoid process are also involved.

Six months after the end of the radiotherapy, there is no uptake in the fatty flap (Fig. 11.14e–h), but there is a suborbital superficial lesion with intense [[18]F]FDG uptake (Fig. 11.14i–k). Also note a moderate uptake by the left maxillary sinus walls.

Interpretation

No definite evidence of recurrent/residual tumor, focal hypermetabolic lesion close to the bone graft, probably inflammatory. Inflammatory sinusopathy of the left maxillary sinus.

MRI was then performed and was also consistent with a benign inflammatory lesion, which was confirmed at follow up.

Teaching Points

Surgically reconstructed areas may be difficult to interpret as focally increased uptake related to inflammation may often be observed.

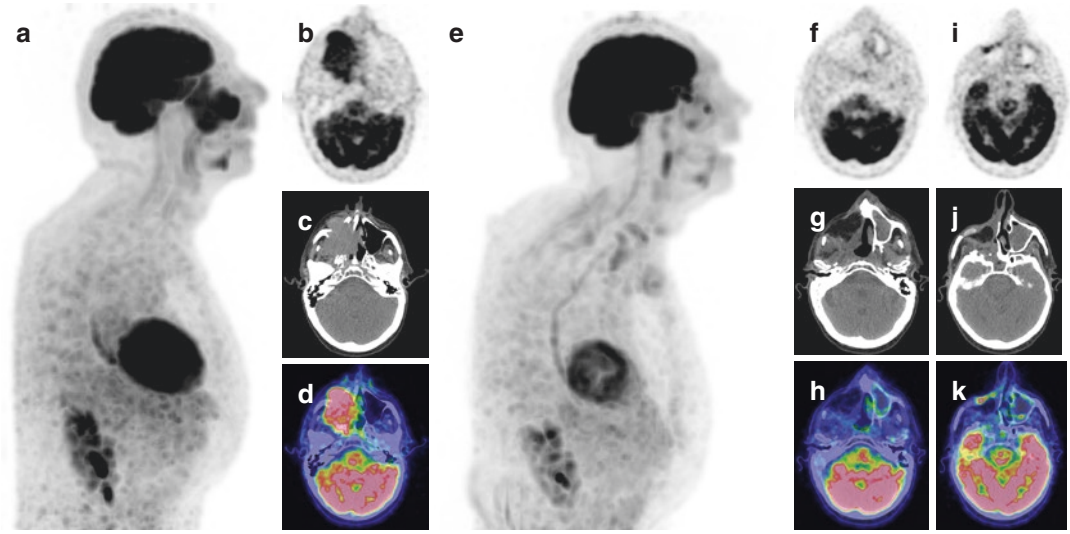

Fig. 11.14

11.15 Case 15

Clinical Details

56-year-old man with a large cT4N2bM0 squamous cell carcinoma of the right oropharynx and lingual floor invading the soft palate and the mandible, associated with bilateral cervical lymph nodes metastases. The patient was treated by radiochemotherapy.

Images

Scan Findings

The baseline PET/CT shows the large highly hypermetabolic primary as well as the bilateral lymph nodes (Fig. 11.15a–d). Three months after the end of the radiochemotherapy (Fig. 11.15e–h), the only remaining abnormality is a moderate uptake centered on an osteolytic area of the mandible.

Sixteen months after the end of the radiochemotherapy, PET/CT was performed due to right oral pain and a purulent skin discharge at the mandibular angle (Fig. 11.15i–l), there is highly increased [^{18}F]FDG uptake in a mass on the right aspect of the floor of the mouth, invading the mandible and extending to the skin.

Interpretation

Three months after the end of the radiochemotherapy, complete metabolic response with persistence of a moderate hypermetabolism due to postradiation inflammatory changes. The CT scan follow-up during the next few months showed the absence of pejorative evolution.

Sixteen months after the end of the radiochemotherapy: local recurrence.

Teaching Points

This case represents a relatively infrequent presentation of initial complete tumor response followed by delayed and rapidly evolving recurrence.

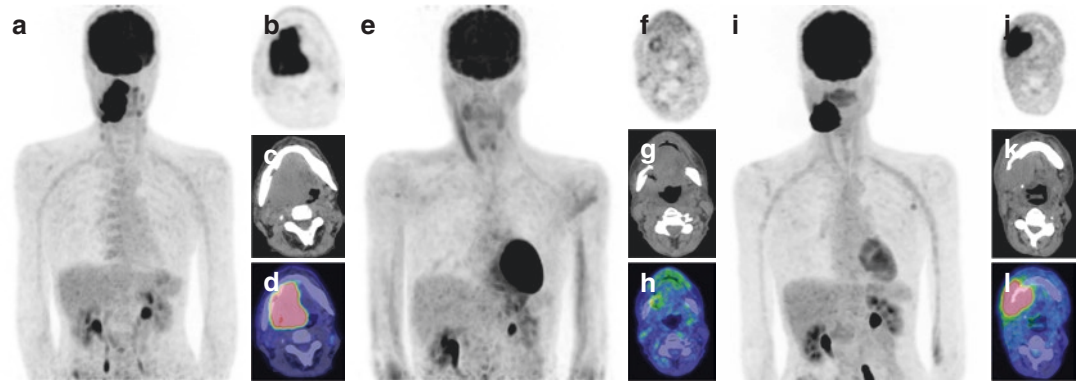

Fig. 11.15

Suggested Reading

Case 3

Mehanna H, Wong WL, McConkey CC et al. PET-CT surveillance versus neck dissection in advanced head and neck cancer. N Engl J Med. 2016;374(15):1444–54.

Risør LM, Loft A, Berthelsen AK et al. FDG-PET/CT in the surveillance of head and neck cancer following radiotherapy. Eur Arch Otorhinolaryngol. 2019 Oct 23.

12 PET/CT in Treatment Response Evaluation: Lung Cancer

Nilendu C. Purandare, Boon Mathew, Ameya D. Puranik, Sneha Shah, Archi Agrawal, and Venkatesh Rangarajan

12.1 Introduction

^{18}F-FDG PET/CT is recommended in the staging and treatment planning of lung cancer [1]. Treatment modalities of lung cancer include surgery, stereotactic body radiotherapy, concurrent chemoradiation therapy, chemotherapy, targeted therapy, and immunotherapy, either alone or in combination depending on the stage of disease. There is no consensus on the optimal imaging modality for assessing response to treatment in lung cancer [2]. However, FDG PET/CT is widely used in assessing response in lung cancer treated with different modalities [3].

Conventional morphological imaging-based size measurements before and post-therapy and response evaluation using WHO criteria and RECIST 1.1 are accepted in clinical trials and routine practice. But these have few problems. Morphological imaging like CT cannot accurately differentiate residual viable tumour from postradiotherapy changes like consolidation, necrosis, and fibrosis. And some tumours respond heterogeneously to radiotherapy which is not apparent on anatomic imaging [4]. CT is not consistent in identifying a histopathologic response post-therapy [5]. CT-based size measurement lag behinds the molecular response to therapy [6]. CT is also limited in assessing tumour response in patients with skeletal metastases [7].

Metabolic response is being evaluated by either the European Organization for Research and Treatment of Cancer (EORTC) criteria or the Positron Emission Tomography Response Criteria in Solid Tumours (PERCIST) criteria. Benefits of using FDG PET/CT in assessing treatment response are manifold. PET/CT can reliably discriminate residual tumour from treatment-related inflammation and fibrosis (Figs. 12.1, 12.2 and 12.3) [4]. Combining CT with PET improves accuracy and allows early assessment of response as the changes in tumour metabolism precedes anatomical response (Figs. 12.4 and 12.5) [8–10]. Whole-body PET/CT can also detect asymptomatic distant failures in patients treated with radical chemoradiation (Fig. 12.6). Assessing tumour response early can guide response adapted therapies improving clinical outcome and limiting unwanted toxicities (Figs. 12.7, 12.8 and 12.9) [11, 12]. Responding skeletal metastases show decrease in FDG uptake similar to soft-tissue metastases and thus avoid the problem of flare phenomenon seen in response (Figs. 12.3 and 12.8) [7]. FDG PET/CT whole-body survey allows better evaluation of response in disseminated metastases (Figs. 12.8 and 12.9). Targeted therapies inhibit growth of tumour cells rather than cell killing. So responders show metabolic changes without change in size, which can

N. C. Purandare (✉) · B. Mathew · A. D. Puranik
S. Shah · A. Agrawal · V. Rangarajan
Department of Nuclear Medicine and Molecular Imaging, Tata Memorial Hospital, Homi Bhabha National University (HBNI), Mumbai, India

S. Fanti et al. (eds.), *Atlas of Clinical PET-CT in Treatment Response Evaluation in Oncology*,
https://doi.org/10.1007/978-3-030-68858-5_12

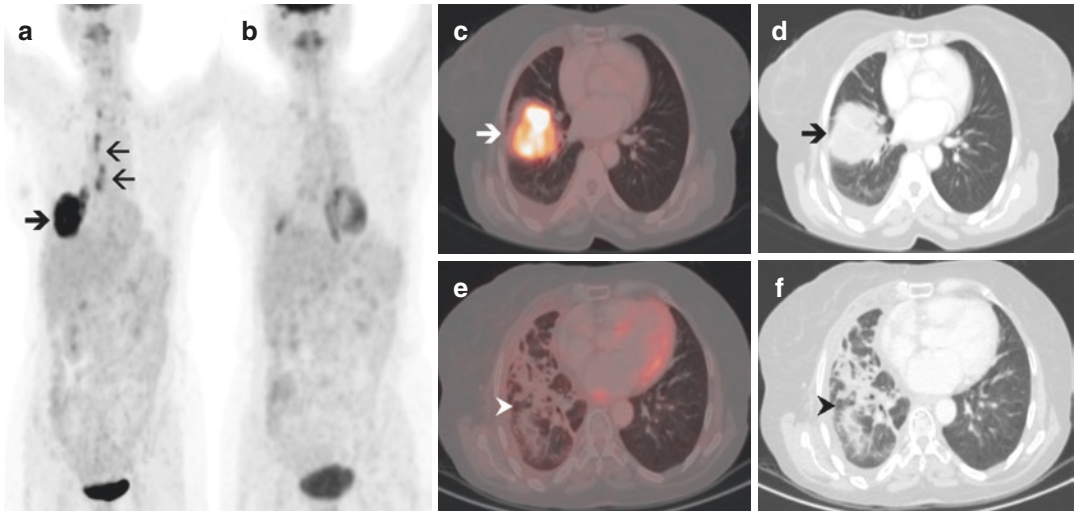

Fig. 12.1 Lung cancer post concurrent chemotherapy and radiotherapy, showing complete response with postradiotherapy changes. Description: A 64-year-old lady with adenocarcinoma of right lung treated with radical concurrent chemotherapy and radiotherapy. Baseline whole-body MIP (**a**), axial fusion (**c**) and axial CT images (**d**) show a right lung mass (thick arrow) with ipsilateral mediastinal nodes (thin arrow). Twelve weeks post-therapy whole-body MIP (**b**), axial fusion (**e**) and axial CT images (**f**) show complete response of the primary and mediastinal nodes with appearance of patchy areas of consolidation, ground glass opacities (arrowheads) suggestive of postradiotherapy changes. Take-home message: PET/CT is an excellent tool in assessing response to concurrent chemotherapy and radiotherapy

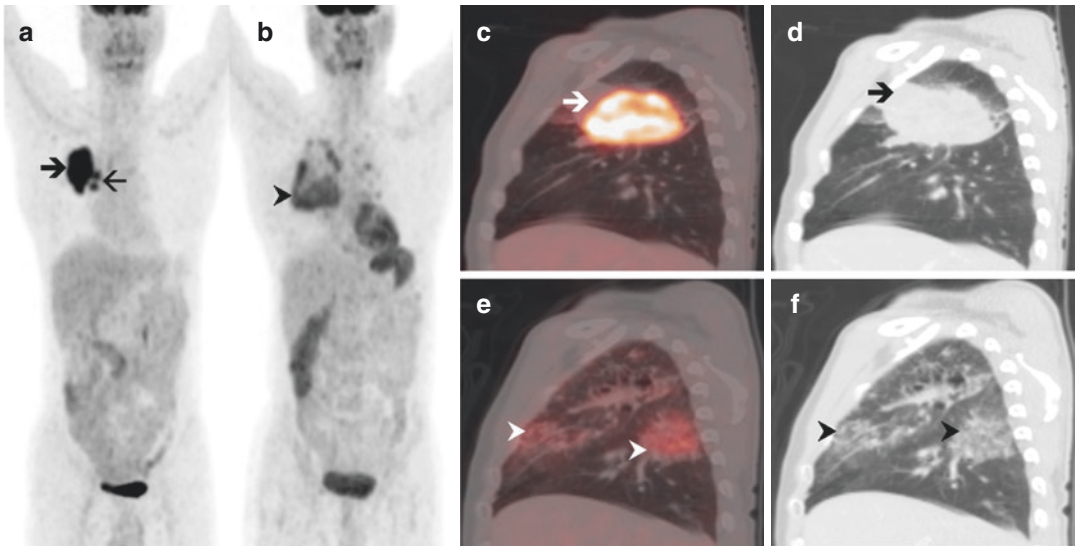

Fig. 12.2 Lung cancer post concurrent chemotherapy and radiotherapy, showing complete response with radiation pneumonitis. Description: A 58–year-old lady with squamous cell carcinoma of right lung treated with concurrent chemotherapy and radiotherapy. Baseline whole-body MIP (**a**), sagittal fusion (**c**) and sagittal CT images (**d**) show a right lung mass (thick arrow) with ipsilateral mediastinal nodes (thin arrow). Ten weeks post-therapy whole-body MIP (**b**), sagittal fusion (**e**) and sagittal CT images (**f**) show complete response of the primary and mediastinal nodes with appearance of FDG avid patchy areas of consolidation with ground glass opacities (arrowheads) around the primary site suggestive of early radiation-induced lung damage. Take-home message: Radiation pneumonitis can show high FDG uptake. Knowing the pattern of lung changes on CT images in the radiation field helps to identify radiation-induced changes from residual or recurrent tumour

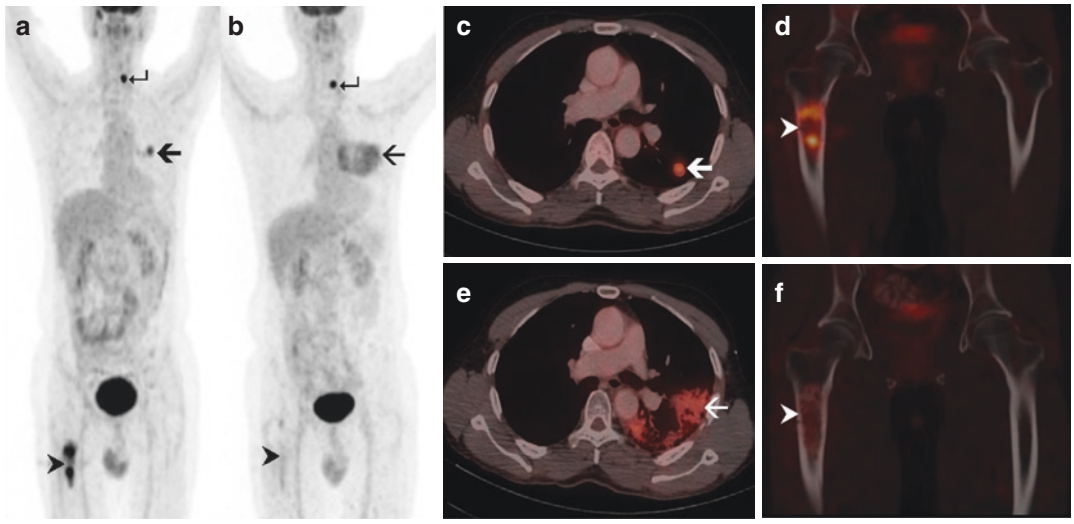

Fig. 12.3 Lung cancer with solitary skeletal metastases, post radical radiotherapy to primary and bone metastases, showing complete response. Description: A 63-year gentleman with adenocarcinoma of left lung with solitary metastases in right femur, treated with radical radiotherapy to primary and bone metastases. Baseline whole-body MIP (**a**), axial fusion (**c**) and coronal fusion images (**d**) show a left lung nodule (thick arrow) and solitary metastases in right femur (arrowhead). Post-therapy whole-body MIP (**b**), axial fusion (**e**) and coronal fusion images (**f**) show complete response of the primary (thick arrow) and bone metastases (arrowhead) with perilesional consolidation in left lung (thin arrow) suggestive of radiation-induced lung damage. Metabolically active biopsy-proven benign thyroid nodule (elbow arrow) is also noted in whole-body MIP images. Take-home message: whole-body PET/CT can assess response to radiotherapy in both primary and distant skeletal metastases

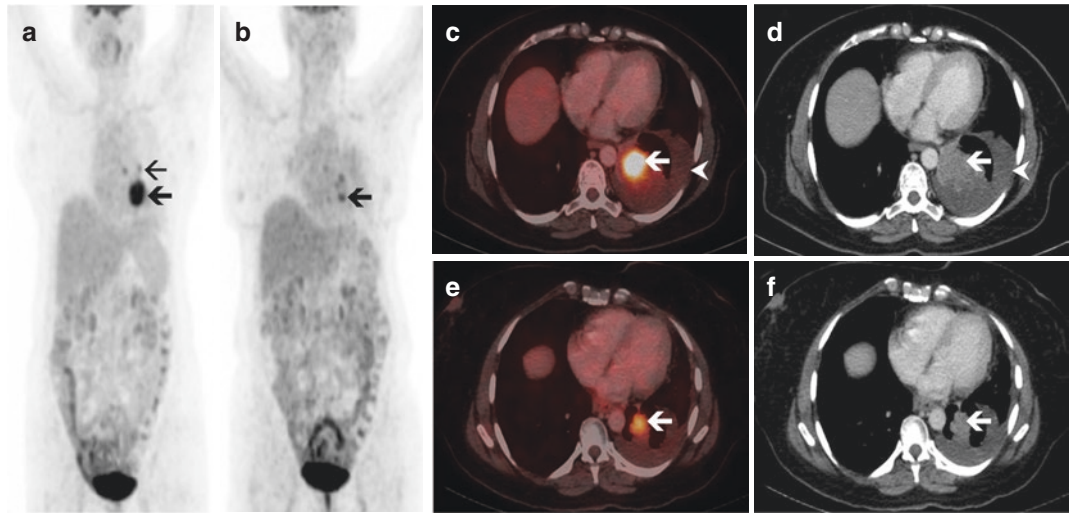

Fig. 12.4 Lung cancer post concurrent chemotherapy and radiotherapy, showing partial response. Description: A 49-year-old lady with adenocarcinoma of left lung treated with concurrent chemotherapy and radiotherapy. Baseline whole-body MIP (**a**), axial fusion (**c**) and axial CT images (**d**) show a left lung mass (thick arrow) with ipsilateral mediastinal nodes (thin arrow) and reactive pleural effusion (arrowheads). Twelve weeks post-therapy whole-body MIP (**b**), axial fusion (**e**) and axial CT images (**f**) show partial regression in metabolism and size of the primary (thick arrow). Take-home message: By evaluating both metabolic and morphological changes, PET/CT can identify nature of response

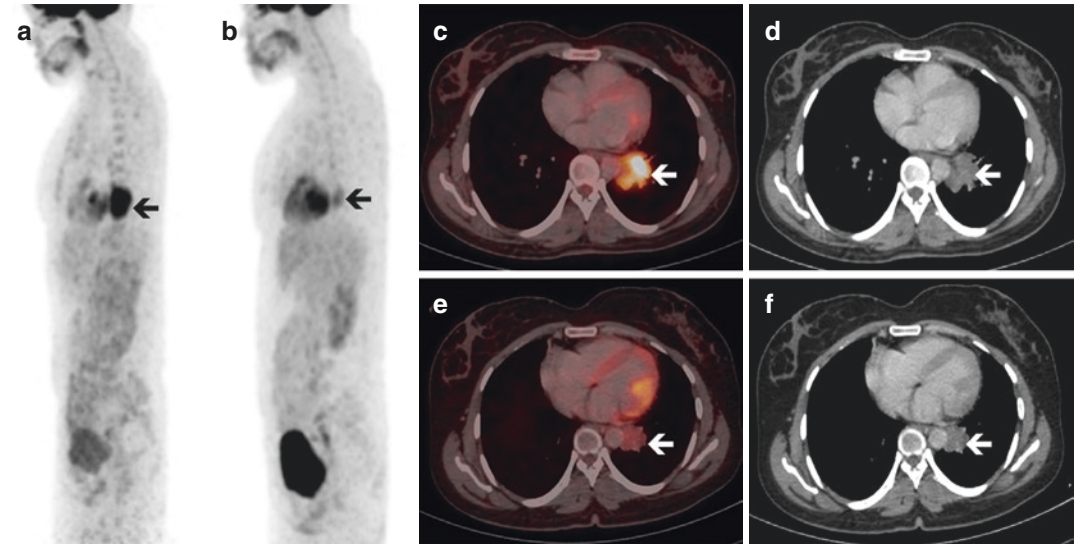

Fig. 12.5 Lung cancer post neoadjuvant chemotherapy, showing partial response. Description: A 28-year-old lady with adenocarcinoma of left lung treated with neoadjuvant chemotherapy prior to surgical resection. Baseline whole-body MIP (**a**), axial fusion (**c**) and axial CT images (**d**) show a left lung mass (thick arrow). Post-therapy whole-body MIP (**b**), axial fusion (**e**) and axial CT images (**f**) show partial regression in the metabolism and size of the primary (thick arrow). Take-home message: PET/CT is used to evaluate response to neoadjuvant chemotherapy to identify eligible candidates for surgery

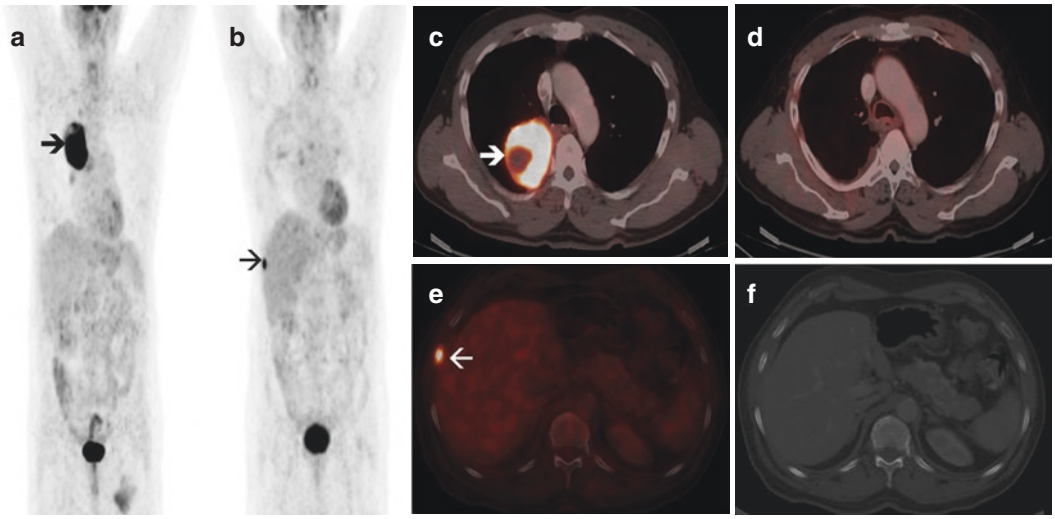

Fig. 12.6 Locally advanced lung cancer post radical chemoradiation, showing complete regression of primary with a solitary distant failure. Description: A 64-year gentleman with squamous cell carcinoma of right lung treated with radical chemoradiation therapy. Baseline whole-body MIP (**a**) and axial fusion (**c**) show a right lung mass (thick arrow). Post-therapy whole-body MIP (**b**) and axial fusion (**d**) show complete response of the primary. However, post-therapy whole-body MIP (**b**) and axial fusion (**e**) image show a solitary metastatic lesion in right 10th rib (thin arrow) with no morphological abnormality seen on axial CT image (**f**). Take-home message: whole-body survey by PET/CT can detect asymptomatic distant failure after radical chemoradiation

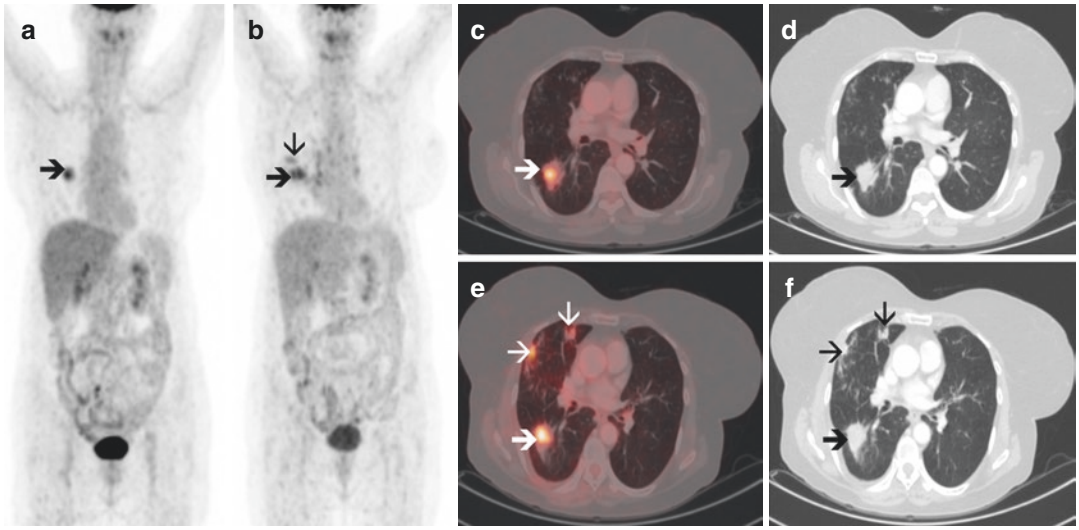

Fig. 12.7 Lung cancer post stereotactic body radiotherapy, showing stable disease. Description: A 59-year-old lady with adenocarcinoma of right lung treated with stereotactic body radiotherapy. Baseline whole-body MIP (**a**), axial fusion (**c**) and axial CT images (**d**) show a right lung lesion (thick arrow). Post-therapy whole-body MIP (**b**), axial fusion (**e**) and axial CT images (**f**) show no response of the primary (thick arrow) with FDG avid nodular areas of post-treatment consolidation in geographically distinct areas of lung (thin arrow). Take-home message: PET/CT can accurately assess response to stereotactic body radiotherapy. It is important to know the appearance and geographic extent of post-SBRT-induced lung changes which are distinct from conventional chemoradiation

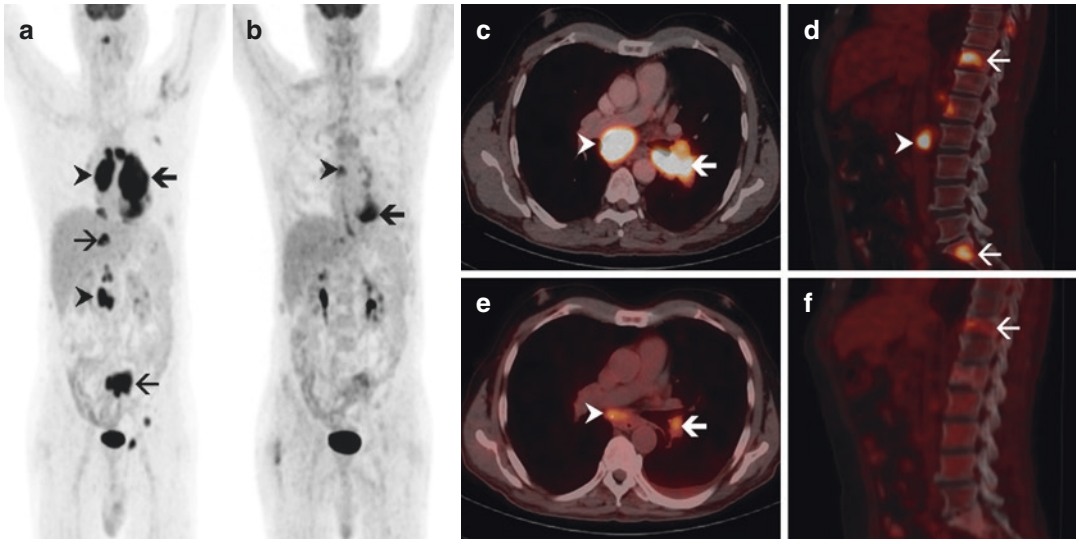

Fig. 12.8 Lung cancer with nodal and skeletal metastases, post 3 cycles of palliative chemotherapy, showing partial response. Description: A 64-year-old man with metastatic small cell carcinoma of left lung treated with palliative chemotherapy. Baseline whole-body MIP (**a**), axial fusion (**c**) and sagittal fusion (**d**) images show left lung mass (thick arrow), nodal metastases (arrowhead) and skeletal metastases (thin arrow). Post-therapy whole-body MIP (**a**), axial fusion (**c**) and sagittal fusion (**d**) images show partial response of the primary (thick arrow), nodal metastases (arrowhead) and skeletal metastases (thin arrow). Take-home message: whole-body PET/CT perform better than CT scan in evaluating response to palliative chemotherapy, especially in skeletal metastases

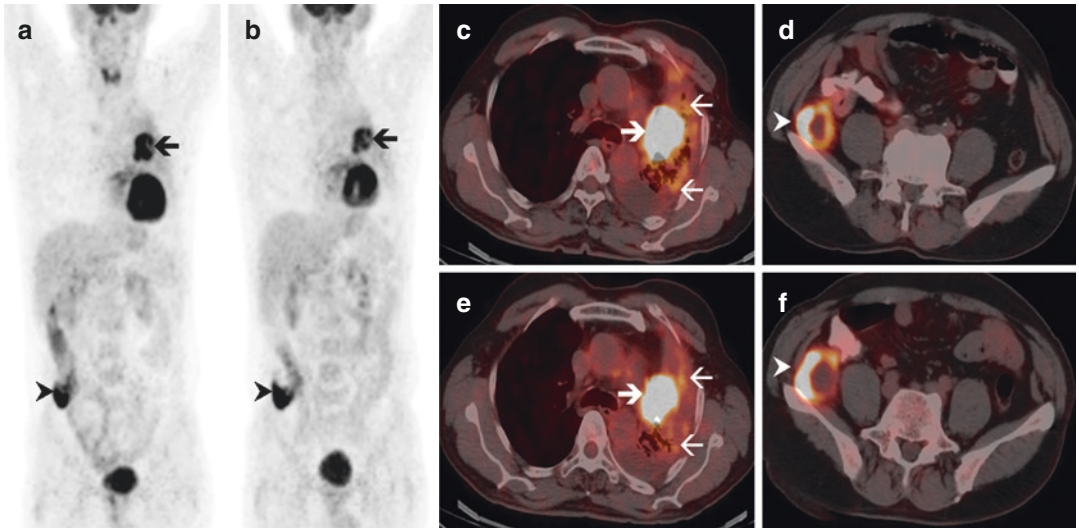

Fig. 12.9 Lung cancer post chemotherapy, showing stable disease. Description: A 71-year-old man with locally advanced squamous cell carcinoma of left lung resistant to concurrent chemoradiation. He is later diagnosed with metastatic peritoneal deposit in right iliac fossa and is treated with palliative chemotherapy. Pre-therapy whole-body MIP (**a**) and axial fusion (**c**, **d**) images show a left lung primary (thick arrow) and metastatic peritoneal deposit (arrowhead). Post-therapy whole-body MIP (**b**) and axial fusion (**e**, **f**) images show no significant response of the primary (thick arrow) and metastatic peritoneal deposit (arrowhead). Peripheral thick consolidation (thin arrow) is noted in left lung suggestive of post-radiotherapy changes. Take-home message: whole-body PET/CT can identify chemoresistance early guiding appropriate treatment

be easily evaluated by FDG PET/CT (Figs. 12.10 and 12.11) [13, 14]. FDG PET/CT has shown potential for assessing response in patients receiving immunotherapy. The value of PET in predicting response was early and significantly higher than CT [15, 16]. PET-based response assessment has additional value in predicting outcomes. Studies have shown the correlation of response with poor progression-free survival and overall survival [17, 18]. Estimation of total lesion glycolysis (TLG) and its change with therapy can further improve outcome prediction [12, 19]. FDG PET/CT, when performed for response assessment, has several advantages over conventional imaging, and the evidences are still evolving.

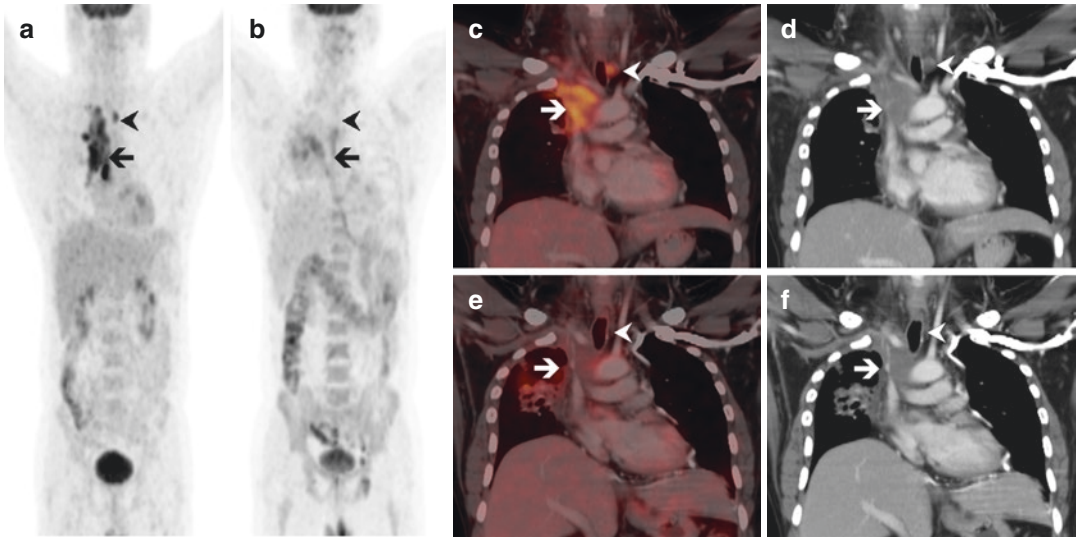

Fig. 12.10 Lung cancer post Crizotinib therapy, showing complete metabolic response. Description: A 33-year-old man with locally advanced adenocarcinoma of right lung resistant to concurrent chemoradiation. He was then treated with ALK-ROS1 inhibitor, Crizotinib. Pre-Crizotinib therapy whole-body MIP (**a**), coronal fusion (**c**) and coronal CT (**d**) images show a right upper lobe mass infiltrating into mediastinum (thick arrow) with discrete lower cervical nodes (arrowhead). Post-therapy whole-body MIP (**b**), coronal fusion (**e**) and coronal CT (**f**) images show complete regression of the primary and neck nodes. Take-home message: Metabolic response measured by PET/CT is early and very reliable in assessing response to targeted therapies which are often cytostatic causing a delayed morphological response

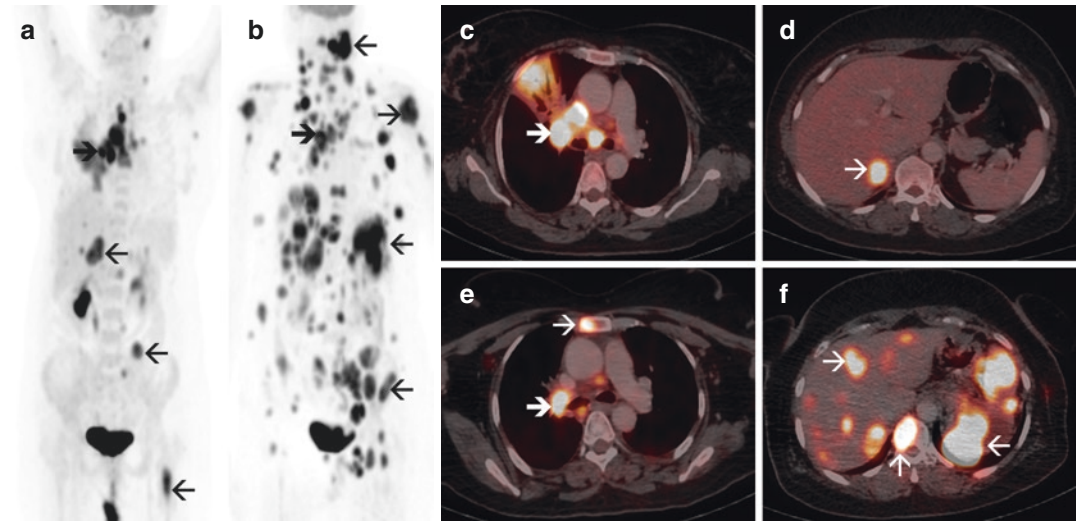

Fig. 12.11 Lung cancer post Crizotinib therapy, showing progressive disease. Description: A 44-year-old lady with adenocarcinoma of right lung treated with ALK-ROS1 inhibitor, Crizotinib. Pre-Crizotinib therapy whole-body MIP (**a**) and axial fusion (**c**, **d**) images show a right lung primary (thick arrow) and metastatic lesions (arrowhead). Post-Crizotinib therapy whole-body MIP (**b**) and axial fusion (**e**, **f**) images show partial response of the primary (thick arrow) and new metastatic lesions (arrowheads). Take-home message: whole-body PET/CT can identify resistance to targeted therapies very early in the disease course

References

1. National Comphrehensive Cancer Network. NCCN Clinical practice guidelines in oncology—Non Small Cell Lung Cancer version 8. 2017 [Internet]. https://www.nccn.org/professionals/physician_gls/f_guidelines.asp. Accessed 30 Aug 2017
2. Colt HG, Murgu SD, Korst RJ, Slatore CG, Unger M, Quadrelli S. Follow-up and surveillance of the patient with lung cancer after curative-intent therapy: diagnosis and management of lung cancer, 3rd ed: American College of Chest Physicians evidence-based clinical practice guidelines. Chest. 2013;143(5 Suppl):e437S–54S.
3. Sheikhbahaei S, Mena E, Yanamadala A, Reddy S, Solnes LB, Wachsmann J, et al. The value of FDG PET/CT in treatment response assessment, follow-up, and surveillance of lung cancer. AJR Am J Roentgenol. 2017;208(2):420–33.
4. Cliffe H, Patel C, Prestwich R, Scarsbrook A. Radiotherapy response evaluation using FDG PET-CT—established and emerging applications. Br J Radiol. 90(1071):20160764. https://www.ncbi.nlm.nih.gov/pmc/articles/PMC5601535/
5. William WN, Pataer A, Kalhor N, Correa AM, Rice DC, Wistuba II, et al. Computed tomography RECIST assessment of histopathologic response and prediction of survival in patients with resectable non-small cell lung cancer after neoadjuvant chemotherapy. J Thorac Oncol. 2013;8(2):222–8.
6. Puranik AD, Purandare NC, Shah S, Agrawal A, Rangarajan V. Role of FDG PET/CT in assessing response to targeted therapy in metastatic lung cancers: morphological versus metabolic criteria. Indian J Nucl Med. 2015;30(1):21–5.
7. Cook GJR, Azad GK, Goh V. Imaging bone metastases in breast cancer: staging and response assessment. J Nucl Med. 2016;57(Suppl 1):27S–33S.
8. Kim JH, Kim BJ, Jang HJ, Kim HS. Comparison of the RECIST and EORTC PET criteria in the tumor response assessment: a pooled analysis and review. Cancer Chemother Pharmacol. 2017;80(4):729–35.
9. Van den Abbeele AD. The lessons of GIST—PET and PET/CT: a new paradigm for imaging. Oncologist. 2008;13(Suppl 2):8–13.
10. Lee DH, Kim S-K, Lee H-Y, Lee SY, Park SH, Kim HY, et al. Early prediction of response to first-line therapy using integrated 18F-FDG PET/CT for patients with advanced/metastatic non-small cell lung cancer. J Thorac Oncol. 2009;4(7):816–21.
11. Sethi A, Dombrowski J, Hong R, Soni Y, Emami B. PET/CT guided adaptive radiotherapy of locally advanced non-small cell lung cancer. Int J Radiat Oncol Biol Phys. 2007;69(3):S650–1.
12. Fledelius J, Winther-Larsen A, Khalil AA, Bylov CM, Hjorthaug K, Bertelsen A, et al. 18F-FDG PET/CT for very early response evaluation predicts CT response in Erlotinib-treated non-small cell lung Cancer patients: a comparison of assessment methods. J Nucl Med. 2017;58(12):1931–7.
13. Yaghmai V, Miller FH, Rezai P, Benson AB, Salem R. Response to treatment series: part 2, tumor response assessment—using new and conventional criteria. AJR Am J Roentgenol. 2011 Jul;197(1):18–27.
14. Lyu L, Wu N, Ying L, Yan F, Xiaomeng L, Ying L. Early predictive and prognostic value of 18F-FDG PET/CT for response assessment in non-small cell lung cancer treated with EGFR-TKI. J Nucl Med. 2017;58(supplement 1):143.
15. Spigel DR, Chaft JE, Gettinger S, Chao BH, Dirix L, Schmid P, et al. FIR: efficacy, safety, and biomarker analysis of a phase II open-label study of Atezolizumab in PD-L1-selected patients with NSCLC. J Thorac Oncol. 2018;13(11):1733–42.
16. Kaira K, Higuchi T, Naruse I, Arisaka Y, Tokue A, Altan B, et al. Metabolic activity by 18F-FDG-PET/CT is predictive of early response after nivolumab in previously treated NSCLC. Eur J Nucl Med Mol Imaging. 2018;45(1):56–66.
17. Ding Q, Cheng X, Yang L, Zhang Q, Chen J, Li T, et al. PET/CT evaluation of response to chemotherapy in non-small cell lung cancer: PET response criteria in solid tumors (PERCIST) versus response evaluation criteria in solid tumors (RECIST). J Thorac Dis. 2014;6(6):677–83.
18. Shang J, Ling X, Zhang L, Tang Y, Xiao Z, Cheng Y, et al. Comparison of RECIST, EORTC criteria and PERCIST for evaluation of early response to chemotherapy in patients with non-small-cell lung cancer. Eur J Nucl Med Mol Imaging. 2016;43(11):1945–53.
19. Ho K-C, Fang Y-HD, Chung H-W, Liu Y-C, Chang JW-C, Hou M-M, et al. TLG-S criteria are superior to both EORTC and PERCIST for predicting outcomes in patients with metastatic lung adenocarcinoma treated with erlotinib. Eur J Nucl Med Mol Imaging. 2016;43(12):2155–65.

13

^{18}F-FDG PET/CT and Non ^{18}F-FDG-PET/CT in Treatment Response Evaluation in Neuro-Oncology

S. Islam, A. S. Mehdi, T. Barwick, D. J. Coope, S. Bisdas, A. D. Waldman, and G. Thompson

13.1 Introduction

Conventional contrast-enhanced magnetic resonance imaging (CE-MRI) remains the reference standard non-invasive diagnostic tool for monitoring patients with primary and secondary brain tumours for a number of reasons, including exceptional soft-tissue contrast, high spatial resolution and widespread availability [1]. Despite these qualities, CE-MRI has limited biological specificity for neoplastic tissue, which can often result in challenges for the radiologist in differentiating neoplastic tissue from non-neoplastic processes. This makes it challenging to delineate tumour extent accurately and precisely, and differentiate treatment-related changes from true recurrent or progressive disease. Significant progress in the use of positron emission tomography (PET) with an array of radiotracers helps to overcome some of these limitations. This particular clinical unmet need has been highlighted by the PET task force of the Response Assessment in Neuro-Oncology (RANO) working group who have suggested that there is benefit for the integration of amino acid PET in glioma imaging compared with CE-MRI alone [2, 3].

There has been significant development in the use of PET imaging for a number of use cases in neuro-oncology, e.g. non-invasive grading of primary brain tumours as well as the prediction of molecular markers [1]. However, for radiologists and clinicians involved in the diagnosis and care of patients with brain tumours, there remain three distinct areas of interest:

1. identification of neoplastic tissue which includes the delineation of tumour extent for further therapeutic management such as surgery and radiotherapy;
2. differentiation of treatment-related changes from tumour progression at follow up and,
3. sensitive and specific treatment response assessment to local and systemic therapies.

S. Islam (✉)
Department of Surgery and Cancer, Imperial College London, London, UK

Department of Radiology, Imperial College Healthcare NHS Trust, London, UK
e-mail: s.islam@imperial.ac.uk

A. S. Mehdi · T. Barwick
Department of Radiology, Imperial College Healthcare NHS Trust, London, UK

D. J. Coope
Department of Neurosurgery, Salford Royal NHS Foundation Trust, Manchester, UK

S. Bisdas
Lysholm Department of Neuroradiology, National Hospital for Neurology and Neurosurgery, London, UK

A. D. Waldman · G. Thompson
Centre for Clinical Brain Sciences, University of Edinburgh, Edinburgh, UK

S. Fanti et al. (eds.), *Atlas of Clinical PET-CT in Treatment Response Evaluation in Oncology*,
https://doi.org/10.1007/978-3-030-68858-5_13

13.2 PET Tracers Used in Neuro-Oncology

[^{18}F]-2-fluoro-2-deoxy-D-glucose (FDG) PET has historically been the workhorse of PET imaging in body oncology; however, the high physiological FDG uptake in healthy brain limits its utility in neuro-oncology for tumour delineation except in cases where progressive tumour or suspected transformation occurs in the context of hypometabolic brain or cystic lesions, or on review of whole-body imaging for malignancy where hypermetabolic brain metastases can exceed grey matter uptake and appropriate windowing can aid conspicuity of lesions on an avid grey matter background [3]. The use of FDG PET in neuro-oncology is further limited by the fact that certain neurological inflammatory processes similarly exhibit increased FDG uptake, thereby reducing diagnostic accuracy [2].

Amino acid (AA) PET has gained particular interest in neuro-oncology because of its high uptake in tumour tissue coupled with relatively low uptake in healthy brain, resulting in superior tumour to background ratio [2, 4]. [^{11}C]-methyl-L-methionine (MET), 3,4-dihydroxy-6-[^{18}F]-fluoro-L-phenylalanine (FDOPA) and O-(2-[^{18}F]-fluoroethyl)-L-tyrosine (FET) are amongst the other commonly used amino acid PET tracers. Neoplastic tissues, e.g., glioma and cerebral metastases often overexpress certain amino acid transporters such as amino acid transporters of the L type (LAT), which are targeted by MET, FDOPA and FET radiotracers. Of note, FDOPA demonstrates physiological uptake in the striatum due to the normal distribution of dopamine transporters, and there is a theoretical limitation when dealing with striatal or subinsular tumours.

Non-FDG and Non-AA tracers for glioma and cerebral metastases also include 3′-deoxy-3′-[^{18}F]-fluorothymidine (FLT) which is an analogue to the DNA nucleoside thymidine required for DNA replication but not RNA transcription and has been developed to image cellular proliferation which is increased in tumour tissue [5]. Choline is an essential component of cell membrane phospholipids and is taken up into cells via choline kinase (CK) transporters. Following a process of phosphorylation and conversion to P-Choline, it then contributes to membrane production and turnover. Brain tumour imaging using either ^{11}C or ^{18}F Choline PET (CHO) has garnered interest due to its low background physiological uptake, and good tumour to background ratio, although there is some uncertainty regarding the degree to which blood–brain barrier disruption and choline metabolism contribute to tracer uptake [6].

The performance characteristics of FDG and AA PET are influenced by increased uptake in certain non-neoplastic conditions such as neuroinflammation, but the combination of PET and structural conventional MRI in the hands of experienced subspecialist radiologists has added value in neuro-oncology.

Targeting the overexpression of somatostatin receptors (SSTR) with radiolabelled SSTR ligands has proven useful in meningioma imaging as the SSTR subtype 2 has been shown to demonstrate 100% expression in meningiomas [7]. SSTR ligands are typically labelled with ^{68}Ga, which includes DOTA-D-Phe1-Tyr3-octreotate (DOTATATE) and DOTA-Tyr3-octreotide (DOTATOC). These tracers demonstrate excellent lesion to background uptake, with minimal uptake in adjacent bone and healthy brain [8, 9]. In addition to meningioma imaging, they are also useful in imaging of neuroendocrine tumours, which also demonstrate overexpression of SSTR [10].

13.3 Case 1

Clinical Details 32-year-old male with a known right temporal low-grade glioma underwent ^{18}F-FDG PET surveillance imaging at 1 year.

Images
(Courtesy of Dr. Teresa Szyszko, Consultant Radiologist, Royal Free Hospital NHS Foundation Trust).

1A Baseline (post biopsy)

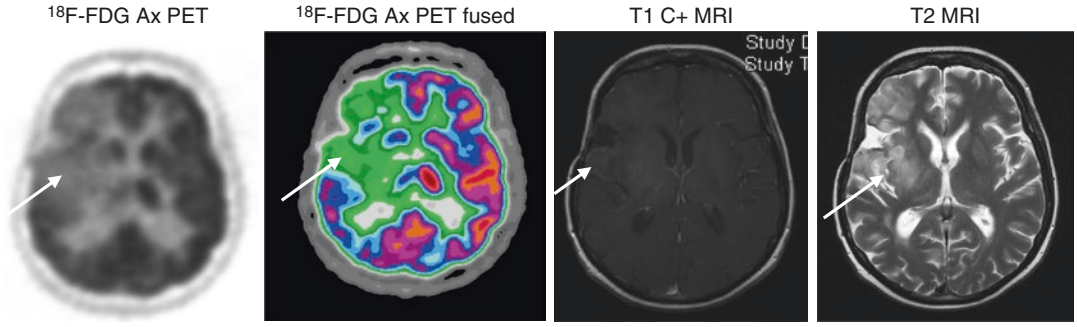

1B (12 months surveillance imaging)

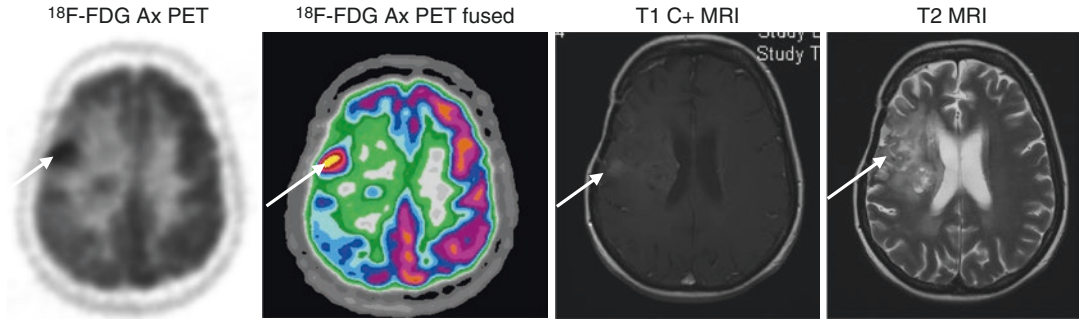

Scan findings and interpretation:
Case 1A (baseline):

Axial ^{18}F FDG PET demonstrates reduced FDG uptake within the right temporal cortex compared to the contralateral left temporal cortex. The corresponding contrast-enhanced axial MRI does not demonstrate significant contrast enhancement. On the T2W-MRI, there is some white matter oedema, and fluid in the biopsy tract.

B (12 months):

There is a focus of increased tracer update within the right temporal cortex which was not present on the previous imaging. On the corresponding T1C+ MRI, there is new contrast enhancement within the posterior edge of the tumour and worsening white matter oedema on the T2 MRI.

Comments on interpretation:

Low-grade gliomas are often 'cold' on ^{18}F-FDG PET, due to low metabolic activity, often lower than the surrounding grey matter. The increase in uptake of FDG 12 months later suggests increased metabolic activity consistent with transformation to a high-grade glioma, one of the indications for FDG in neuro-oncology.

13.4 Case 2

Clinical Details Adult male with a right frontal glioma which was fully resected underwent post-operative surveillance imaging with ^{18}F FDG PET.

Images
2A Post Op imaging

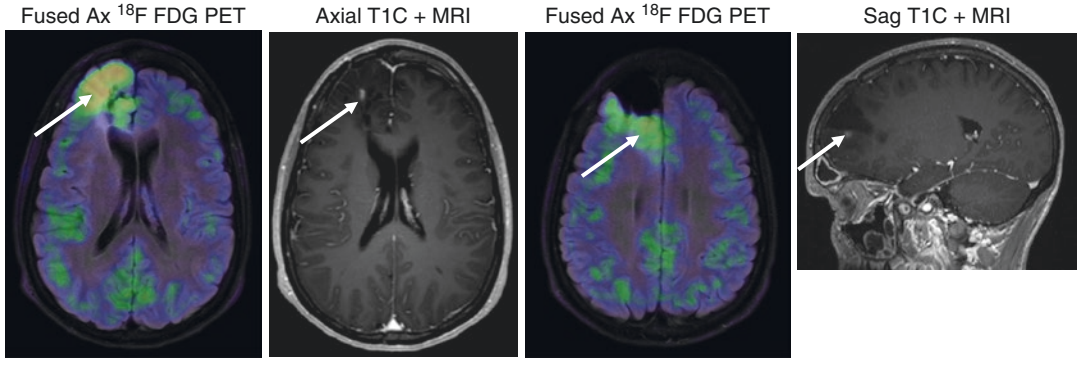

Scan findings and interpretation:

Right frontal resection cavity avid with FDG uptake within the frontal lobe and the posterior margin resection margin. There is only minimal punctate T1C+ enhancement in the peri surgical resection bed.

Comments on interpretation:

The combined PET and MRI findings are consistent with recurrent disease; however, the minimal punctate contrast enhancement grossly underestimates the extent of recurrence.

13.5 Case 3

Clinical Details Young adult who had treatment for a glioma (likely anaplastic pilocytic astrocytoma) as a child including surgery and interstitial brachytherapy within a trial. More than 20 years later, she has increasing enhancement within the surgical cavity on routine follow-up scans, and FDG was used to assess for evidence of late tumour recurrence.

Images

3A Routine surveillance imaging

Cor T1 C+ MRI

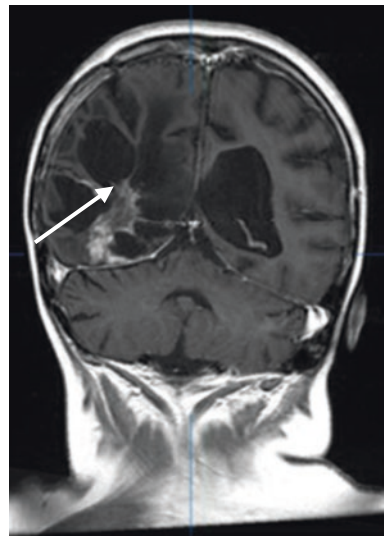

3B PET scan for further characterisation

Fused Cor ^{18}F FDG PET

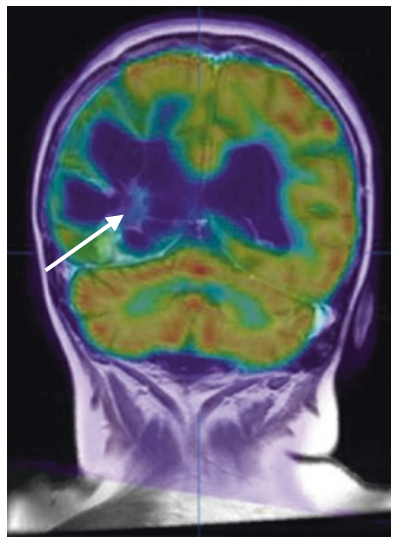

Cor ^{18}F FDG PET

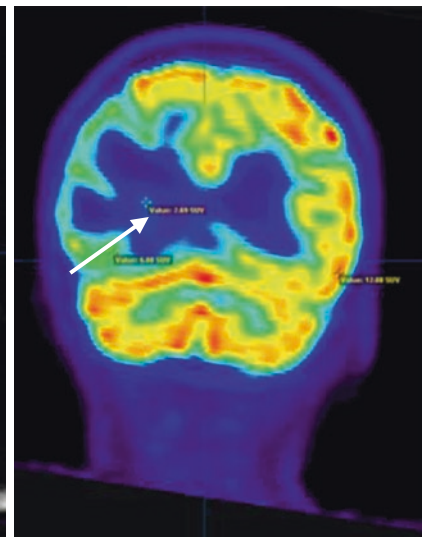

Scan findings and interpretation:

Case 3A Surveillance imaging:

New temporal lobe enhancement within the right surgical resection cavity.

Case 3B:

There is low uptake on FDG imaging within the MRI enhancing regions.

Comments on interpretation:

FDG uptake was low suggestive of delayed post-treatment changes.

13.6 Case 4

Clinical Details 48-year-old female who just completed systemic therapy for primary lung cancer and underwent whole-body ^{18}F-FDG PET/CT re-staging 12 months later.

Images

4A Baseline

Ax ^{18}F FDG PET/CT Thorax Fused

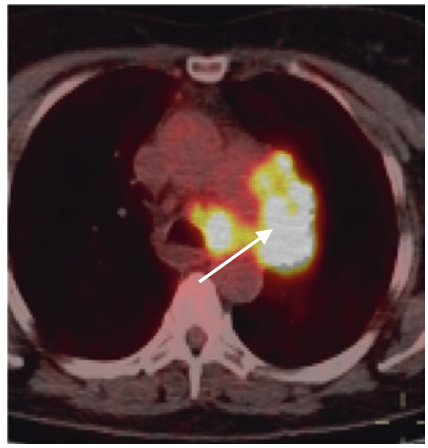

Ax CT Brain Unenhanced

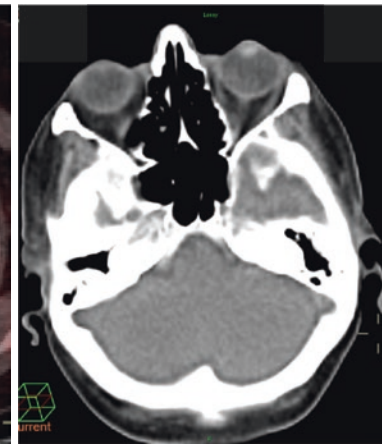

4B 12 months

Ax ^{18}F FDG PET (SUV max 10)

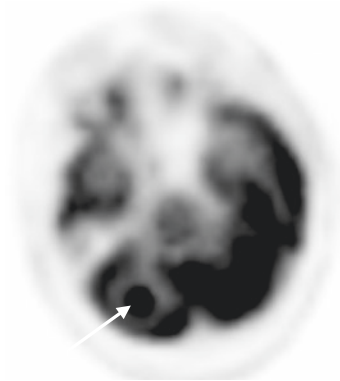

Ax windowed ^{18}F FDG PET (SUV max 20)

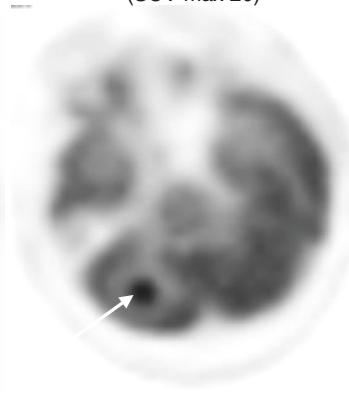

Ax T1 C+ MRI

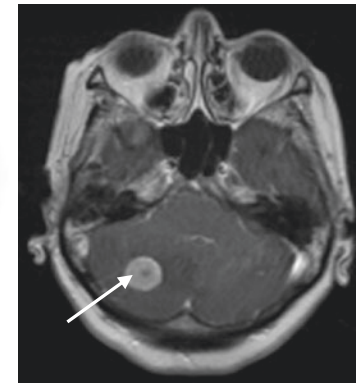

Scan findings and interpretation:

Scan findings Case 4A:

^{18}F-FDG-Fused PET/CT of the thorax shows a primary left-sided hilar and mediastinal malignancy. The CT brain at the time did not show any discernible posterior fossa mass.

Scan findings Case 4B:

12 months later on re-staging, following systemic therapy, there is increased subcortical FDG uptake within the right cerebellar hemisphere on the SUV Max 10 and SUV Max 20 PET imaging. The T1C+ MRI confirmed the presence of a new cerebellar metastasis.

Comments on interpretation:

Due to the high background uptake of FDG within the brain, small lesions can easily be missed when viewing on the window (SUV max 10), especially those close to the cerebral grey matter. It is prudent to widen the window to SUV max 20, when searching for brain lesions on ^{18}F-FDG PET brain imaging.

13.7 Case 5

Clinical Details 65-year-old female with known breast cancer on Bevacizumab developed new neurology and underwent MRI imaging of the brain followed by whole-body ^{18}F-FDG PET.

Images
5A On antiangiogenic therapy

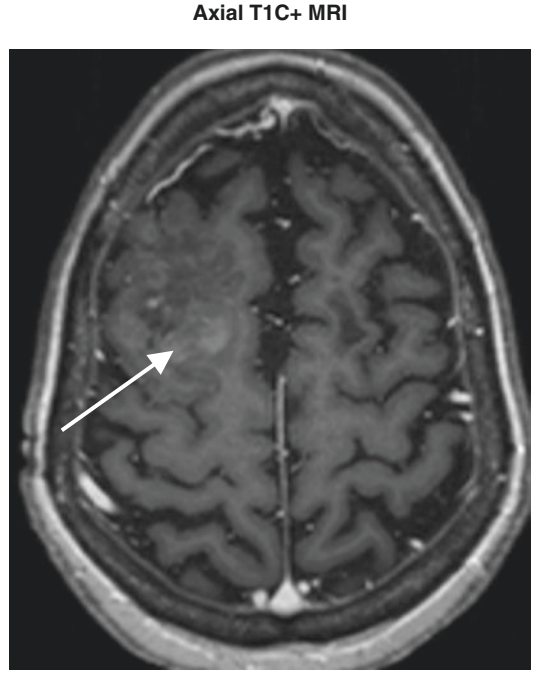

5B (1 month)

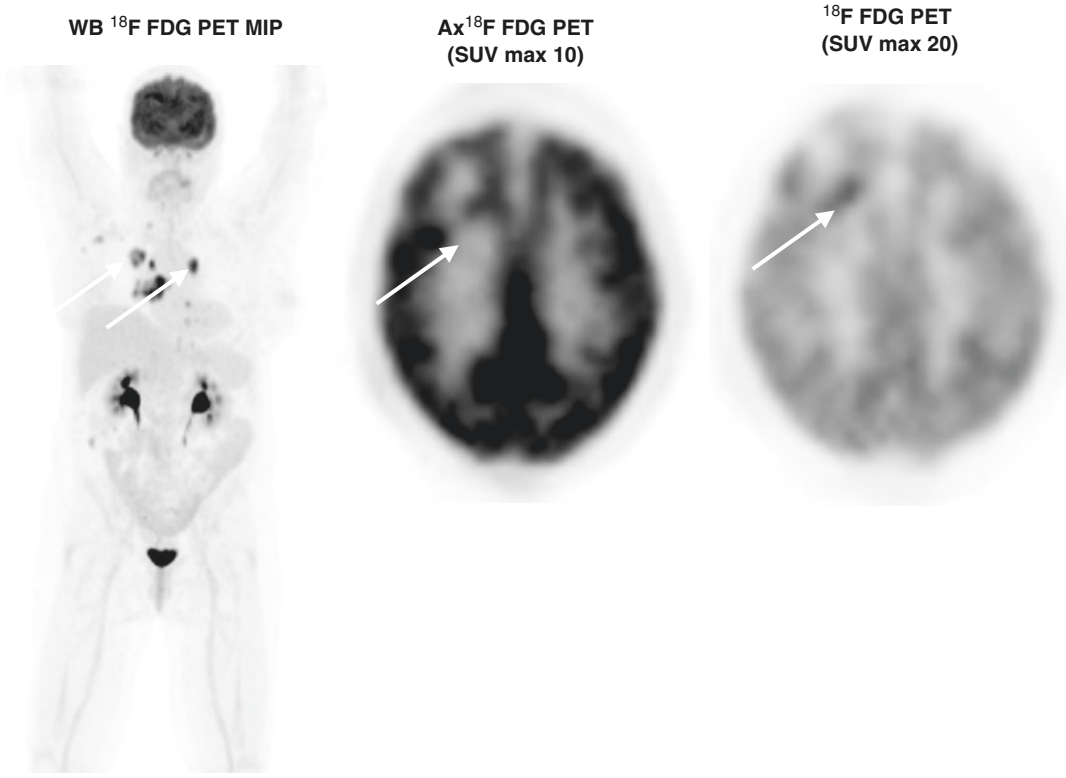

Scan findings and interpretation:

Scan findings Case 5A:

New solid space occupying lesion within the right frontal lobe with some faint enhancement within the posterior margin.

Scan findings Case 5B:

WB FDG PET/CT shows multiple areas of uptake within the thorax in keeping with metastatic lesions. On the Non windowed, PET uptake cannot be appreciated due to high background grey matter uptake. When windowed to SUV 20, true peripheral tumoural uptake is delineated.

Comments on interpretation:

The findings are consistent with a new right frontal metastatic lesion. Caution should be taken when interpreting T1C+ MRI when the patient is on antiangiogenic treatments, as the permeability of the lesion is affected; however, this is not the case on the ^{18}F-FDG PET.

13.8 Case 6

Clinical Details 38-year-old male had a grade II ependymoma fully resected followed by surveillance MRI imaging at 9 months and ^{11}C-MET PET/CT at 18 months.

Images
(Courtesy of Dr. Tilak Das, Consultant Neuroradiologist, Cambridge University Hospitals, UK).

6A Pre- and post-operative imaging

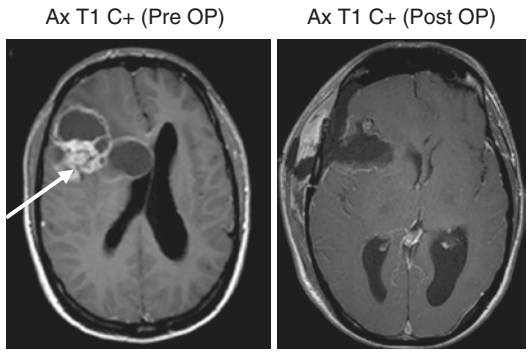

6B. 9 months

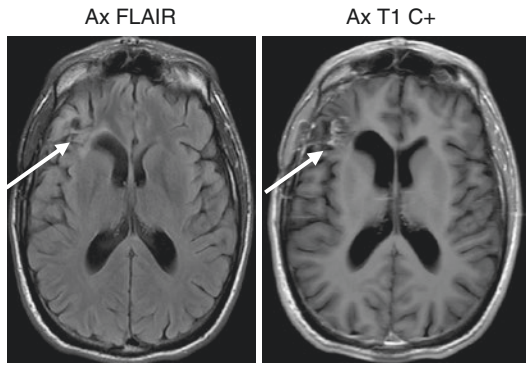

6C 18 months

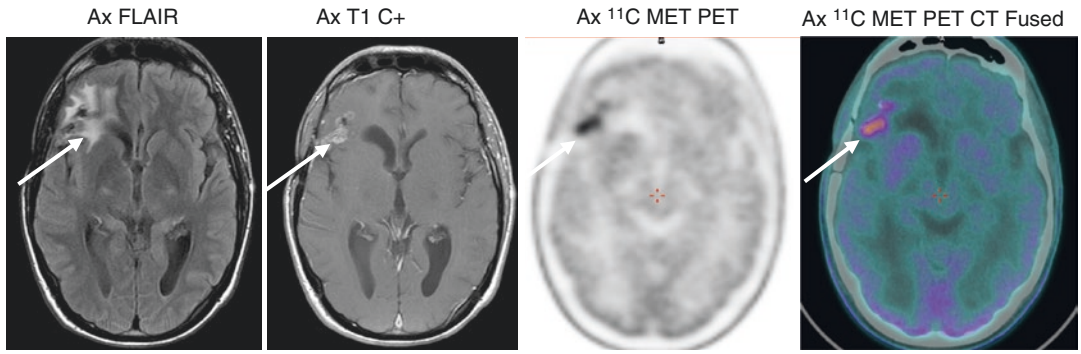

Scan findings and interpretation:

Case 6A

There has been complete resection of the right frontal grade II ependymoma.

Case 6B

There has been increased FLAIR signal in the resection cavity with subtle enhancement on the T1C MRI.

Case 6C

At 18 months, the FLAIR signal gradually worsens with increasing enhancement in the resection cavity. On ^{11}C MET PET, there is an area of avid tracer uptake within the resection cavity in keeping with recurrent disease.

Comments on interpretation:

The gradual changes in the MRI FLAIR signal and contrast enhancement were not specific for recurrent disease and could have represented with the treatment-related changes/necrosis; however, these would not be ^{11}C MET PET avid. The patient had a second resection which confirmed recurrent tumour, followed by PCV chemotherapy.

13.9 Case 7

Clinical Details 34-year-old male who had a resection of a grade II/III right frontal astrocytoma underwent MRI and ^{11}C MET PET to assess for residual disease.

Images
7A

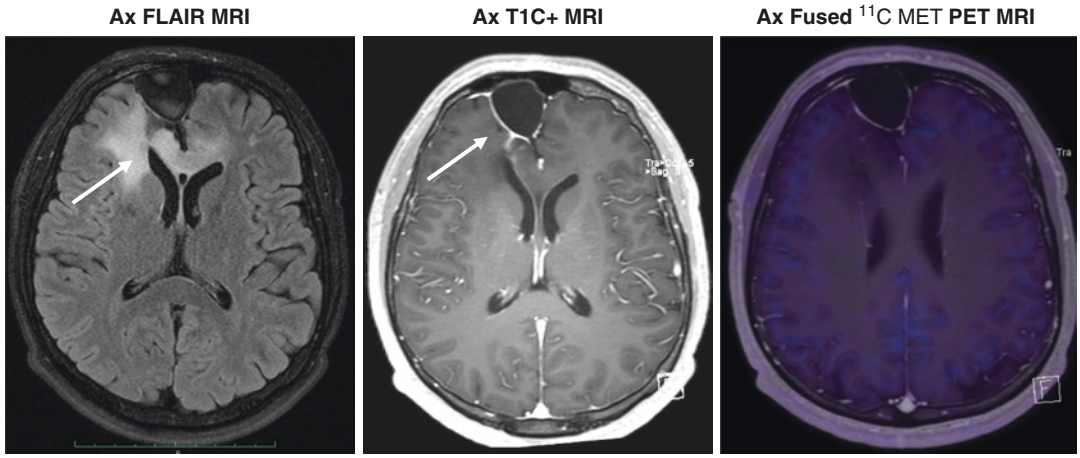

Scan findings and interpretation:
7A:
There is a cystic resection cavity with the right frontal lobe, with surrounding T2 FLAIR signal involving the corpus callosum which extends contralaterally. There is subtle punctate enhancement deep to the resection bed on the T1C+ MRI. There is no appreciable ^{11}C MET PET uptake, especially within the T2 FLAIR signal abnormality regions.

Comments on interpretation:
The imaging features suggest the higher grade component of the tumour (grade III) having been successfully resected with an absence of uptake on the MET imaging, but FLAIR signal changes are concerning for residual lower grade components which are 'cold' on MET imaging.

13.10 Case 8

Clinical Details Adult male with a right parietal GBM had radiotherapy and adjuvant chemotherapy. Underwent ^{11}C MET PET on completion of treatment to assess treatment response.

Images
8A Baseline pre-surgical

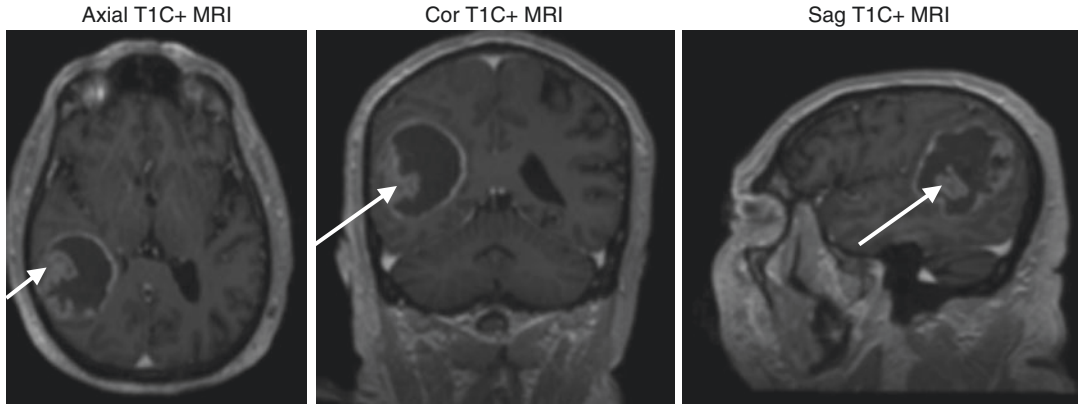

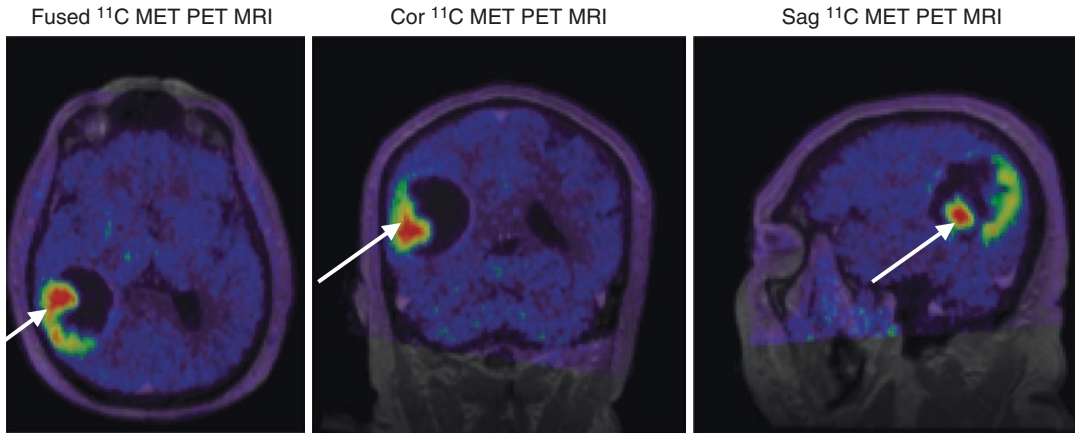

8B. 3 Months Post-Surgery, RT, and Adjuvant Chemotherapy

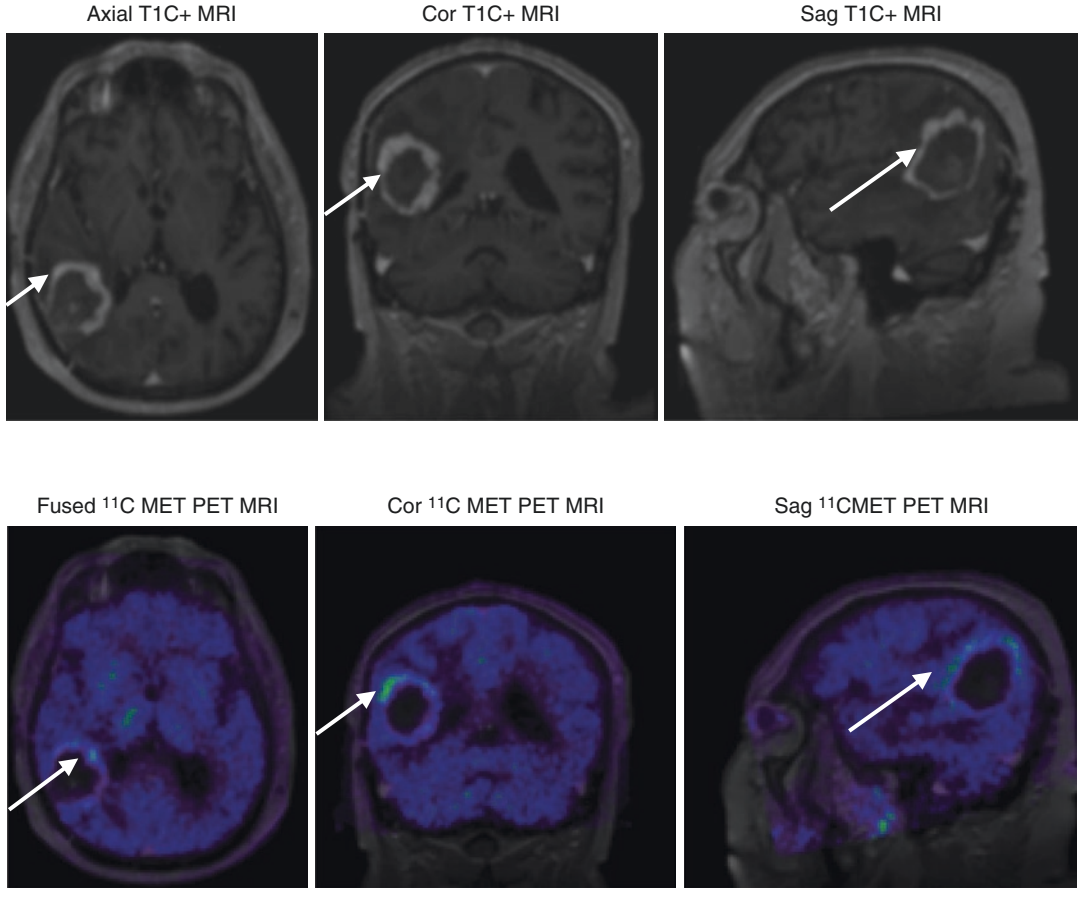

Scan findings and interpretation:

Case 8A: The T1C+ MRI shows an enhancing solid/cystic right parietal lesion. The lateral solid components show avid MET uptake.

Case 8B: Whilst there remains avid enhancement of the peripheral solid components of the tumour, there remains MET uptake in the antero-superior margin of the tumour bed.

Comments on interpretation:

The findings are consistent with partial response to treatment. The residual enhancing tumour on MRI which is not PET avid may be due to treatment effect.

13.11 Case 9

Clinical Details Adult male with right frontal GBM underwent MRI and ^{11}C MET PET imaging to assess response to treatment.

Images

9A Post completion of radiotherapy and adjuvant chemotherapy (temozolomide)

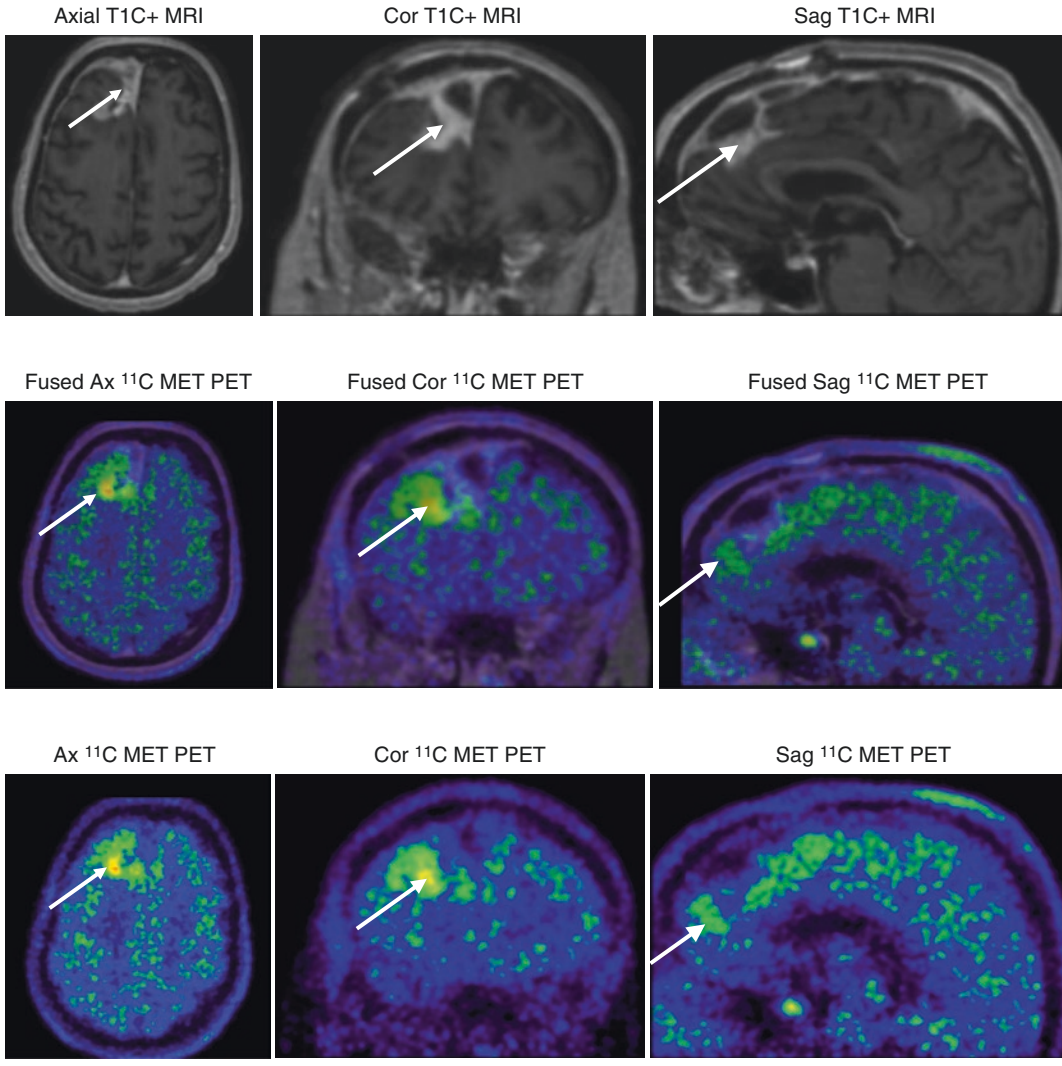

Scan findings and interpretation:

9A Post RT and Adjuvant chemotherapy (Temozolomide): Solid and cystic enhancing right frontal lesion. On the sagittal reformats, the solid enhancing component within the cavity is cold on ^{11}C MET PET.

Comments on interpretation:

Solid enhancement in cavity is 'cold' on methionine and likely inflammatory whereas there is a new focus of parenchymal enhancing tumour which is methionine avid adjacent to the cavity. This demonstrates that treatment-related effects can and often do co-exist with active or progressive disease.

13.12 Case 10

Clinical Details 78-year-old male had completed radiotherapy and adjuvant chemotherapy for a left parietal GBM.

Images
(Courtesy of Dr. Sam Khan, Consultant Radiologist Imperial College Healthcare Foundation Trust).

10A Post radiotherapy

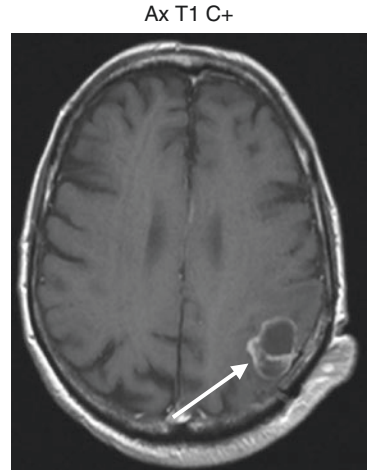

10B 6 Months

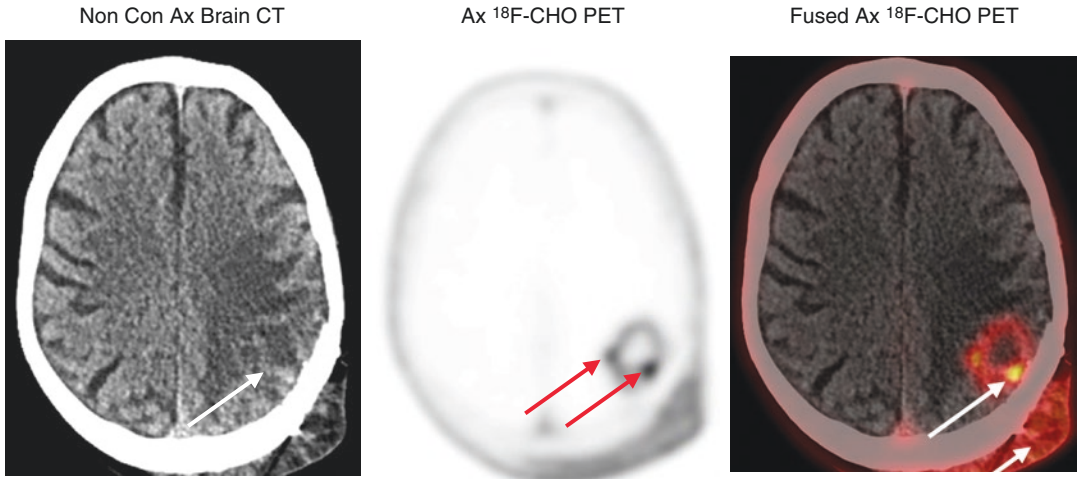

10C 7 Months

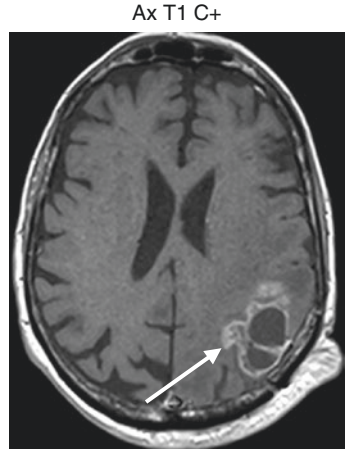

Scan findings and interpretation:

Case 10A

The post radiotherapy MRI demonstrates a necrotic cystic core with peripheral enhancement, which may be treatment-related change.

Scan findings Case 10B:

The axial non contrast CT brain shows oedema within the left parietal lobe. On the corresponding ^{18}F CHO PET, heterogenous peripheral uptake with two foci of avid PET activity. Choline uptake is also noted within soft tissues overlying the craniotomy site.

Scan findings Case 10C:

The subsequent MRI taken a month later shows increasing enhancing solid tissue at the location of the PET avid nidus seen on the CHO PET imaging.

Comments on interpretation:

Enhancement on T1C+ MRI is not specific for disease progression. On the ^{18}F-CHO PET, there is peripheral enhancement in a similar distribution to the MRI which is likely due to a breakdown in blood–brain barrier, but the medial nidus of avid CHO uptake at the posterior border was correlated with sites of progressive disease on subsequent MRI imaging.

13.13 Case 11

Clinical Details 46-year-old male, with a known paraclival meningioma, underwent pre-operative MRI followed by ^{18}F CHO PET to look for residual disease.

Images
11A Pre-op

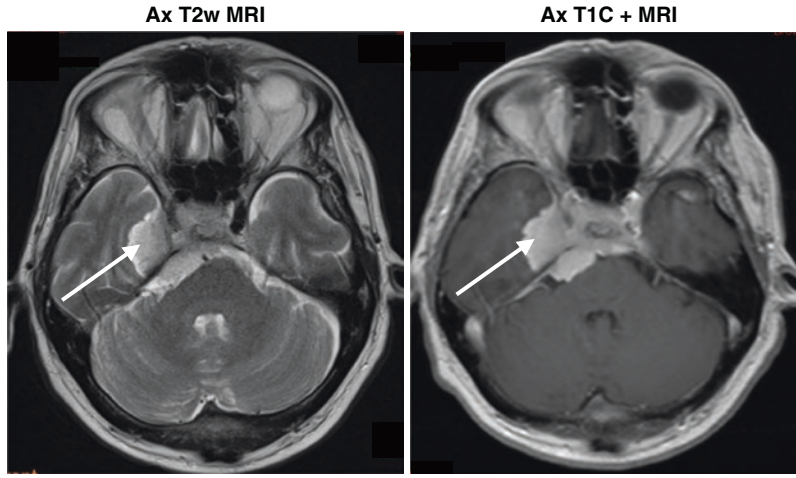

11B Post Op

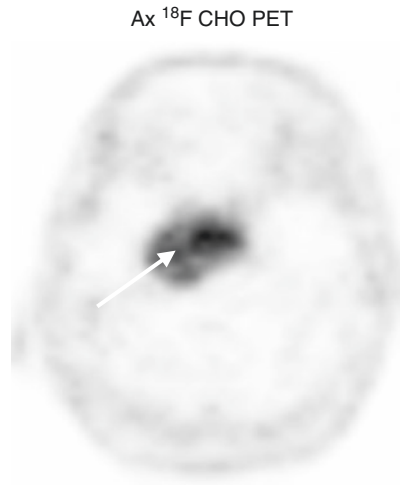

Scan findings and interpretation:

11A Pre-op:

Durally based right paraclival lesion which demonstrated avid gadolinium enhancement on the T1C+ MRI with no significant oedema on the T2W MRI.

11B Post Op:

Avid clival and paraclival ^{18}F CHO uptake in keeping with large burden residual disease.

Comments on interpretation:

^{18}F CHO PET is sensitive to skull base meningioma disease and can be used for longitudinal follow up, but it is non-specific and cannot confidently differentiate between brain metastases, gliomas or meningiomas. The superior tumour/background ratio makes it an ideal tracer to delineate residual disease accurately.

13.14 Case 12

Clinical Details 55-year-old male had undergone treatment for an oligodendroglioma 25 years ago with surgery and radiotherapy. He developed non-specific new neurology followed by MRI and ^{18}F CHO PET scan for evaluation.

Images

(Courtesy of Dr. Sam Khan, Consultant Radiologist Imperial College Healthcare Foundation Trust).

12A Baseline

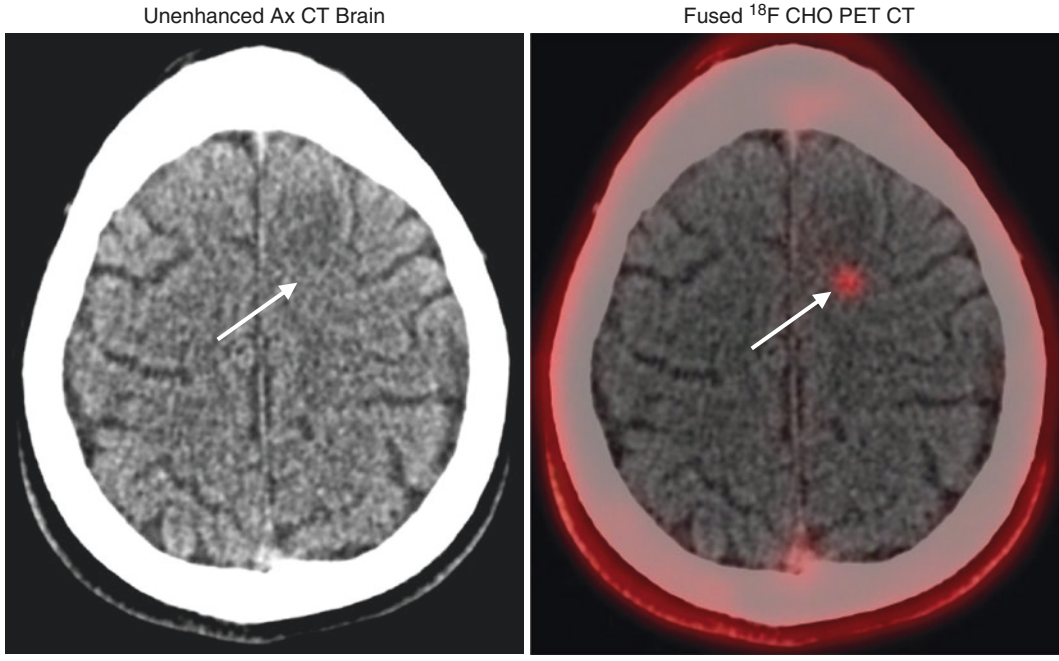

12B 3 months

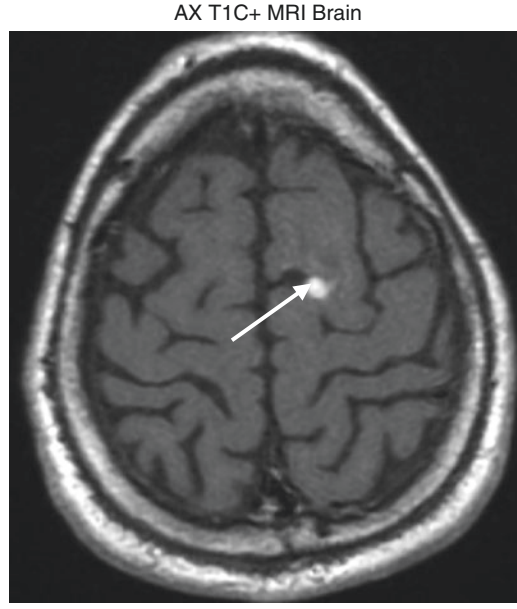

Scan findings and interpretation:

Case 12A

On the unenhanced CT scan, there is no discernible space occupying lesion, but very subtle left frontal vasogenic oedema without mass effect. The fused ^{18}F CHO PET shows a focus of avid uptake within the left frontal lobe.

Case 12B

The T1C+ demonstrates a contrast enhancing lesion within the left frontal lobe at the site of PET avidity.

Comments on interpretation:

In this case, the findings were in keeping with recurrent disease, and high-grade transformation. Although PET avid focus correlates with enhancing disease on the subsequent MRI, it is not clear whether the CHO uptake is truly specific for tumour or a result of breakdown in the blood–brain barrier.

13.15 Case 13

Clinical Details Adult male underwent imaging of a known midline tumour with ^{18}F CHO PET and ^{18}F DOPA PET.

Images

13A Baseline

Ax T2 MRI

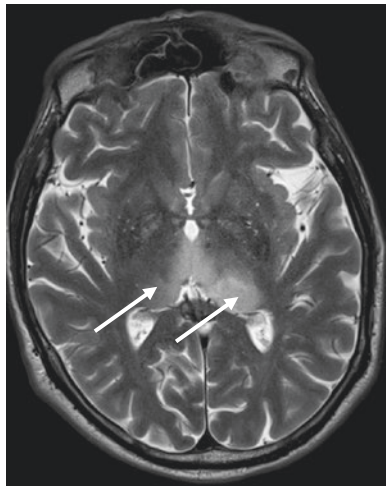

13B 1 Month

Fused ^{18}F CHO PET

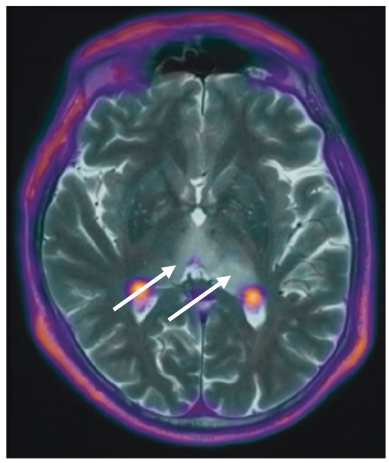

13C 1 Month

Fused ^{18}F DOPA PET MRI

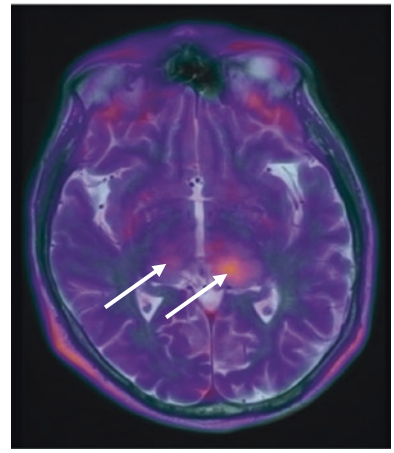

Scan findings and interpretation:

Case 13A Baseline (Ax T2 MRI)

The baseline imaging shows increased signal in the midline and both thalami on the T2 MRI.

Case 13B 1 month (Fused 18F-CHO PET)

The Fused ^{18}F-CHO PET demonstrated no uptake in the midline tumour. Normal physiological uptake is seen in the choroid plexus.

Case 13C 1 month (Fused ^{18}F-DOPA PET)

Fused ^{18}F-DOPA PET MRI identifies DOPA avid hot spots within the tumour, particularly within the left thalamic component. Physiological uptake is seen bilaterally in the striatum, but this is below the uptake seen in the posterior thalamic neoplasia.

Comments on interpretation:

^{18}F DOPA PET has demonstrated increased uptake within the midline tumour, which was cold on CHO PET. The uptake of DOPA helps characterise the tumour in terms of metabolism and grade. Based on the imaging alone, the differential diagnosis would include a histone-mutant midline glioma, which has poor prognosis.

13.16 Case 14

Clinical Details 56-year-old male who has had multiple operations for a right temporal meningioma, underwent ^{68}Ga-DOTATATE PET imaging for assessment of residual disease.

Images

14A Post-surgical MRI and ^{68}Ga-DOTATATE PET

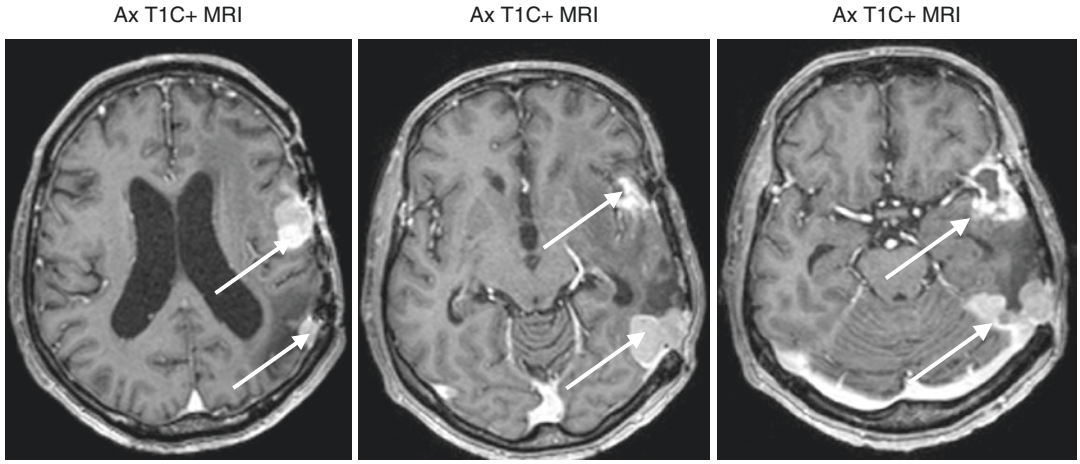

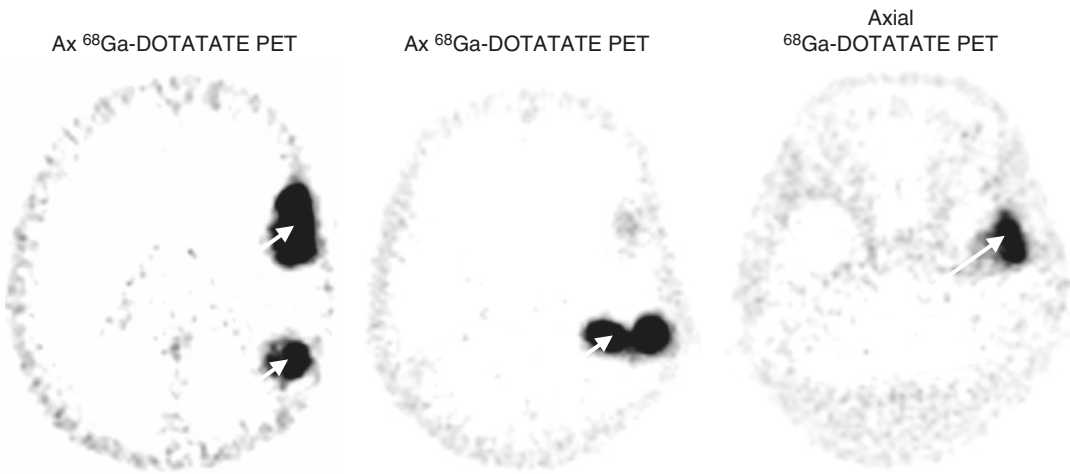

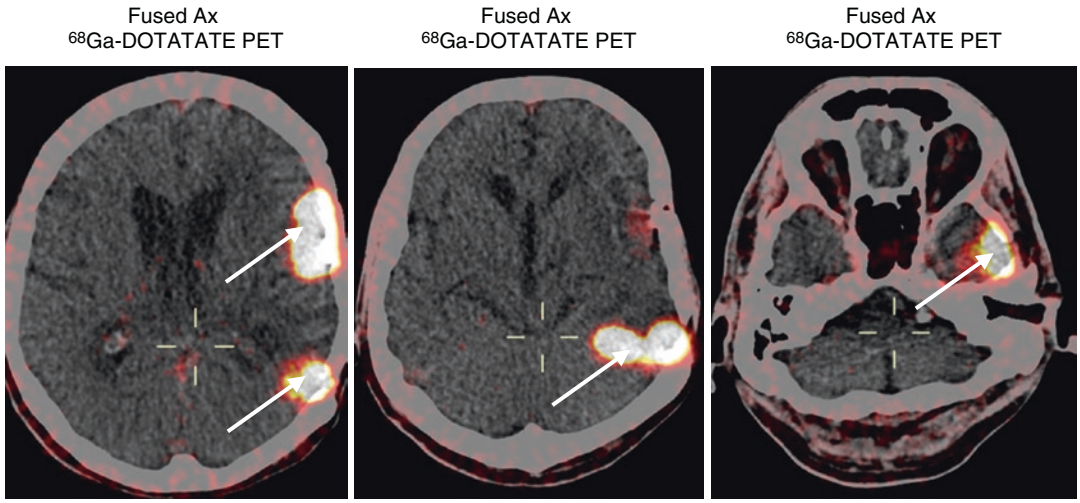

Scan findings and interpretation Case 14A

The T1C+ MRI show large areas of solid tissue which is avidly enhancing and appear to be related to the underlying dura. On the ^{68}Ga-DOTATATE PET and fused ^{68}Ga-DOTATATE PET, these same areas demonstrate avid ^{68}Ga-DOTATATE uptake.

Comments on interpretation:

The findings are suggestive of large volume residual disease. Unlike CHO, DOTATATE specifically targets overexpression of SSTR which is found in meningiomas and paragangliomas, although the latter would be expected to have distinct morphological appearances on structural imaging.

13.17 Case 15

Clinical Details Adult female who underwent resection of a left frontal glioma. She had surveillance imaging with MRI and ^{18}F FET PET to look for disease reoccurrence.

Images

15A Post-operative surveillance imaging

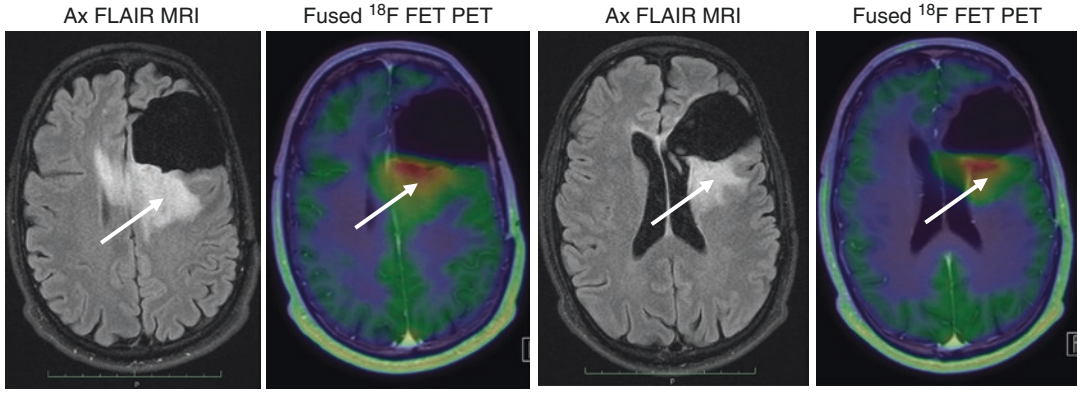

15B. 3 Months

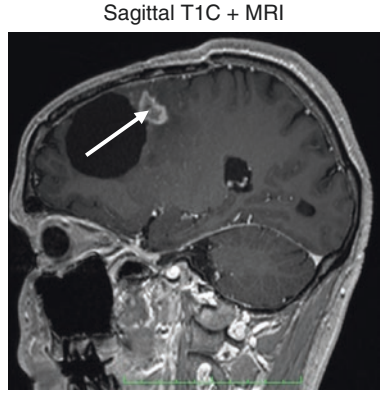

Scan findings and interpretation:

15A: There is a left frontal surgical cavity with increased T2 FLAIR signal at the posterior margin and deep white matter. On the corresponding fused ^{18}F-FET PET, there is increased ^{18}F FET uptake within these areas.

15B: 3 months later on the sagittal T1C+ MRI is new enhancing disease at the posterior margin.

Comments on interpretation:

The PET avidity at the posterior resection margin is in keeping with disease recurrence which was later developed into enhancing disease on the subsequent MRI.

References

1. Galldiks N, Lohmann P, Albert NL, Tonn JC, Langen K-J. Current status of PET imaging in neuro-oncology. Neuro Oncol Adv. 2019;1:1.
2. Langen K-J, Galldiks N, Hattingen E, Shah NJ. Advances in neuro-oncology imaging. Nat Rev Neurol. 2017;13(5):279–89.
3. Albert NL, et al. Response assessment in neuro-oncology working group and European Association for Neuro-Oncology recommendations for the clinical use of PET imaging in gliomas. Neuro Oncol. 2016;18(9):1199–208.
4. Langen K-J, Watts C. Neuro-oncology: amino acid PET for brain tumours—ready for the clinic? Nat Rev Neurol. 2016;12(7):375–6.
5. Shields AF, et al. Imaging proliferation in vivo with [F-18]FLT and positron emission tomography. Nat Med. 1998;4(11):1334–6.
6. Grech-Sollars M, et al. Imaging and tissue biomarkers of choline metabolism in diffuse adult glioma: 18F-Fluoromethylcholine PET/CT, magnetic resonance spectroscopy, and choline kinase alpha. Cancers (Basel). 2019;11(12):1969.
7. Dutour A, et al. Expression of somatostatin receptor subtypes in human brain tumors. Int J Cancer. 1998;76(5):620–7.
8. Rachinger W, et al. Increased 68Ga-DOTATATE uptake in PET imaging discriminates meningioma and tumor-free tissue. J Nucl Med. 2015;56(3):347–53.
9. Afshar-Oromieh A, et al. Detection of cranial meningiomas: comparison of ^{68}Ga-DOTATOC PET/CT and contrast-enhanced MRI. Eur J Nucl Med Mol Imaging. 2012;39(9):1409–15.
10. Johnbeck CB, Knigge U, Kjær A. PET tracers for somatostatin receptor imaging of neuroendocrine tumors: current status and review of the literature. Future Oncol. 2014;10(14):2259–77.

14 PET/CT in the Assessment of Treatment Response in Hepatobiliary, Gall Bladder and Pancreatic Malignancies

Kanhaiyalal Agrawal, Sayak Choudhury, Arvind Suresh, Archi Agrawal, and Gopinath Gnanasegaran

14.1 Introduction

Liver is often affected by metastatic disease from various tumour and is relatively more common than primary hepatocellular cancer (HCC). The management strategy for HCC includes surgical, systemic chemotherapy, surgical cryoablation, chemoembolization, radiofrequency ablation and liver transplantation. Patients with hepatic metastases are often treated with systemic chemotherapy or regional therapy. ^{18}F-FDG PET is reported to be useful in assessing the response to chemotherapy and other regional therapies. Literature evidence suggest ^{18}F-FDG PET imaging is useful in the management of cholangiocarcinoma. In patients with pancreatic cancer, ^{18}F-FDG PET imaging is reported to be useful for the assessment of metabolic tumour response to neoadjuvant therapy and detecting recurrent disease. ^{18}F-FDG PET is helpful in assessing equivocal lesion at the resection bed when CT is indeterminate. FDG PET/CT is reported to be useful in (a) differentiating recurrence from postoperative and post-radiation changes, (b) rising tumor markers and equivocal findings on conventional imaging or work-up and (c) finally in evaluating lesion which are too small or difficult to biopsy. In this chapter, we will illustrate clinical examples related to the role of ^{18}F-FDG in assessment of treatment response in hepatic, pancreatic, biliary tract and gall bladder cancers.

K. Agrawal (✉)
Department of Nuclear Medicine, All India Institute of Medical Sciences (AIIMS), Bhubaneswar, India

S. Choudhury · A. Suresh · A. Agrawal
Department of Nuclear Medicine and Molecular Imaging, Tata Memorial Hospital, Mumbai, India

G. Gnanasegaran
Department of Nuclear Medicine, Royal Free London NHS Foundation Trust, London, UK

S. Fanti et al. (eds.), *Atlas of Clinical PET-CT in Treatment Response Evaluation in Oncology*,
https://doi.org/10.1007/978-3-030-68858-5_14

14.2 Case 1

Rectal cancer with hepatic and extrahepatic metastases on neoadjuvant chemotherapy. FDG PET/CT to assess treatment response and resection of metastases (Fig. 14.1).

Teaching Points

- Metabolic response to systemic therapy is a well-recognized prognostic marker for improved survival.
- RECIST criteria-based morphological response assessment is limited by its low sensitivity for detecting objective response to treatment. Usually, RECIST criteria include necrotic and non-viable components of the lesions, and therefore, precise response evaluation is limited.
- Standard metabolic response assessment using ^{18}F-FDG PET/CT is usually performed 8–12 weeks after therapy initiation, together with a morphology-based imaging test.
- Current evidence justifies the useful role of ^{18}F-FDG PET/CT in metabolic treatment response assessment in patients with colorectal malignancy.
- Studies show that patients who achieved complete metabolic response on ^{18}F-FDG PET/CT have improved clinical outcomes.

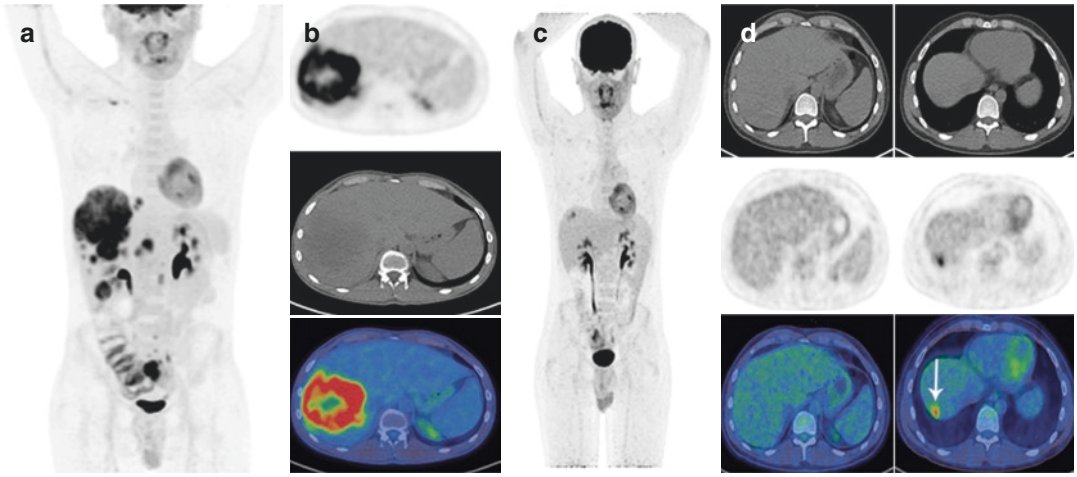

Fig. 14.1 Good partial metabolic response (**a**). MIP images show increased multifocal and increased tracer uptake within the liver, abdominal lymph nodes and in the rectal primary. (**b**) There is intense increased uptake with a large liver metastasis with central necrosis. (**c**, **d**) Post-therapy scan after 6 cycles of Folfoxiri shows significant reduction in tracer activity within the liver with only small focal residual uptake. The tracer uptake in the local lymph nodes has resolved. There is only minor tracer uptake within the rectal primary (MIP, **c**). The scan findings are suggestive good partial metabolic response to treatment with residual disease in the primary and with the liver metastasis

14.3 Case 2

Metastatic colon cancer on chemotherapy. FDG PET/CT scan to assess distant disease for consideration of focal liver treatment (Fig. 14.2).

Teaching Points

- Current evidence suggests FDG PET/CT is sensitive in response detection as soon as after one cycle of treatment and correlates with treatment outcome and identification of non-responding patients.
- ^{18}F-FDG PET/CT has a complementary role to cross-sectional imaging in prognostication, treatment monitoring and planning in patients with colorectal cancer.
- ^{18}F-FDG PET imaging is used to predict the clinical outcome of chemotherapy in patients with advanced colorectal cancer.

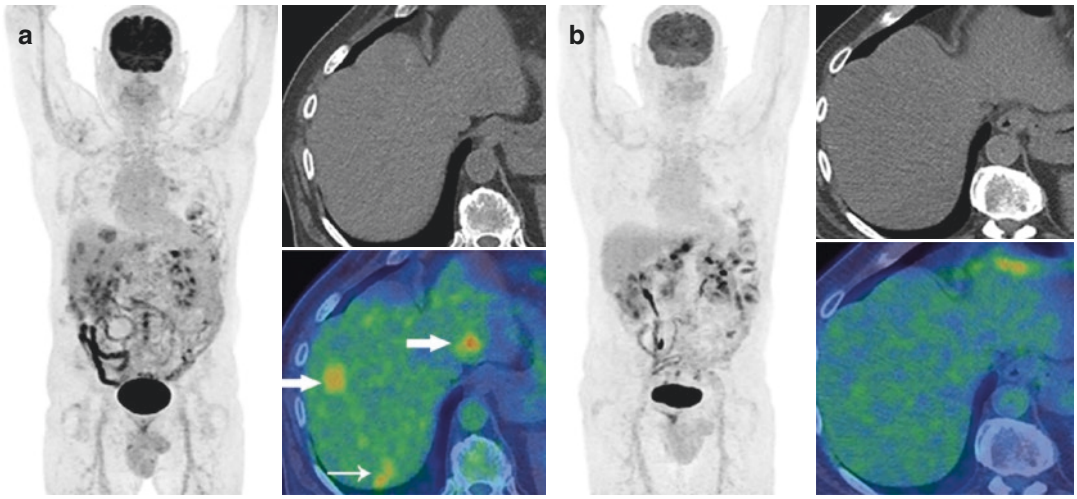

Fig. 14.2 Complete metabolic response. Pretherapy study (**a**). MIP images show multifocal increased tracer uptake within the liver. There is increased uptake with multiple liver metastases (arrows in fused PET/CT images). Post-therapy study (**b**) after chemotherapy shows no abnormal focal tracer activity within the liver. The scan findings are compatible with complete metabolic response to treatment with resolution of metabolic activity in the liver metastases

14.4 Case 3

Metastatic colorectal cancer underwent extended right hemicolectomy and left hepatectomy and chemotherapy for liver metastasis. Rising tumour markers and FDG PET/CT scan to assess recurrent disease (Fig. 14.3).

Teaching Points

- In patients who show symptomatic disease and/or rising carcinoembryonic antigen (CEA) during surveillance after rectal cancer surgery, equivocal CT findings may be aided by FDG PET/CT imaging to improve the detection of a recurrence.
- FDG PET/CT is useful in detecting both short-term and long-term tumour responses, which are either not apparent with CT or precede a significant decrease in tumour size, by weeks or month.
- Conversely, a lack of a metabolic response can indicate (a) primary resistance to therapy and (b) re-emergence of metabolic activity within a tumour site following a period of therapeutic response might indicate secondary resistance.
- Metabolic response to chemotherapy assessed on FDG PET/CT is reported to correlate well with clinical response, tumour biology and disease-free survival in patients with metastatic colorectal cancer.

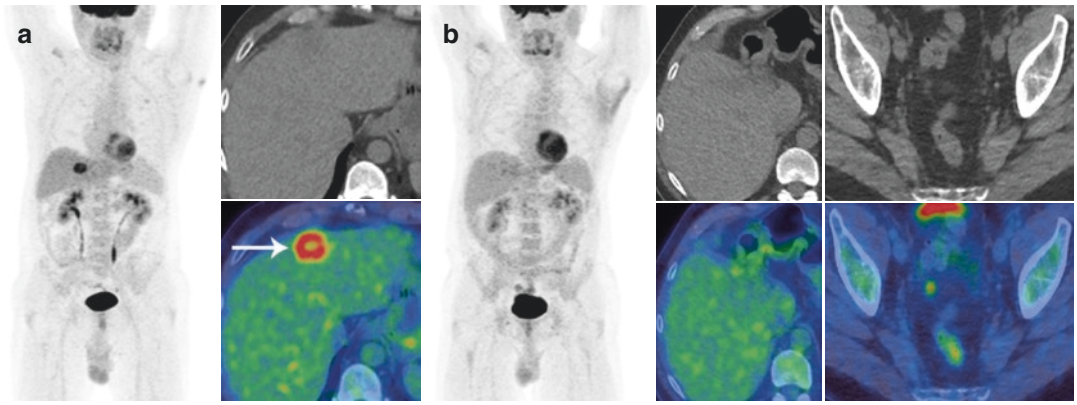

Fig. 14.3 Metastatic colorectal cancer with recurrent disease (**a**) Focal increased tracer uptake in the liver (arrow) in keeping with metastasis and patient underwent left hepatectomy. (**b**) Post left lobe hepatectomy FDG PET: Note is made of previous left hepatectomy. New focal increased tracer uptake in a nodule close to the seminal vesicle in keeping with metastasis

14.5 Case 4

Hepatocellular carcinoma on treatment. ^{18}F-FDG scan for post-therapy assessment (Fig. 14.4).

Teaching Points

- The sensitivity of FDG PET for detecting intrahepatic hepatocellular carcinoma (HCC) lesions is limited.
- ^{18}F-FDG PET/CT is a good predictive tool to assess treatment outcomes of HCC metastasis and for the early identification of treatment failure.
- ^{18}F-FDG PET/CT might be useful in assessing the viability of HCC after transcatheter arterial chemoembolization (TACE) and is reported to be superior to contrast-enhanced CT. In addition, non-attenuation-corrected PET data might be helpful to avoid false-positive results of tracer uptake induced by lipiodol deposition.

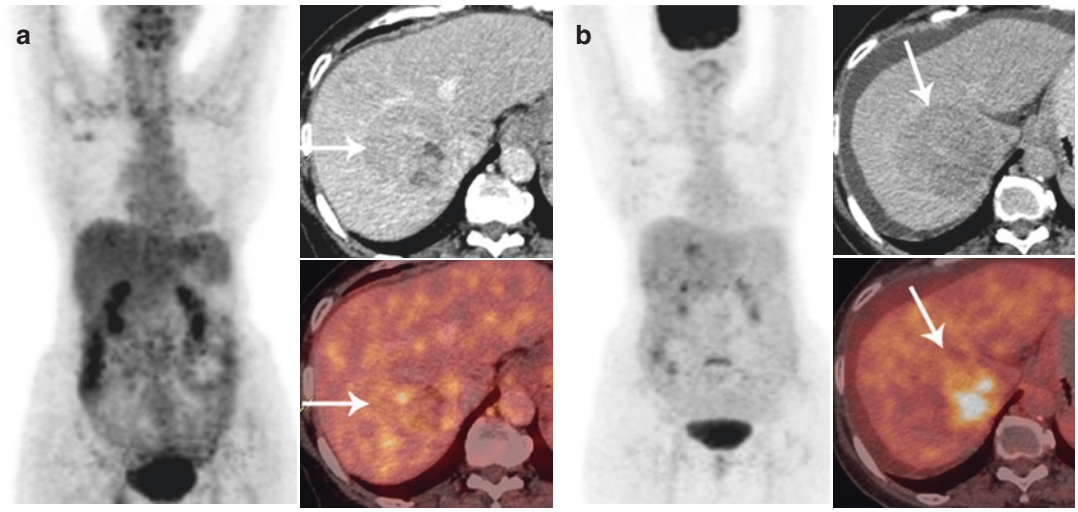

Fig. 14.4 Disease progression (**a**) Staging FDG PET/CT shows a large lesion in the right lobe with no significant FDG uptake (arrows). (**b**) Post-treatment FDG PET/CT shows increase in size and metabolic activity of the lesion in the right lobe of the liver (SUVmax 7.6) with ascites. Scan findings are compatible with disease progression

14.6 Case 5

Metastatic hepatocellular cancer on chemotherapy (Fig. 14.5).

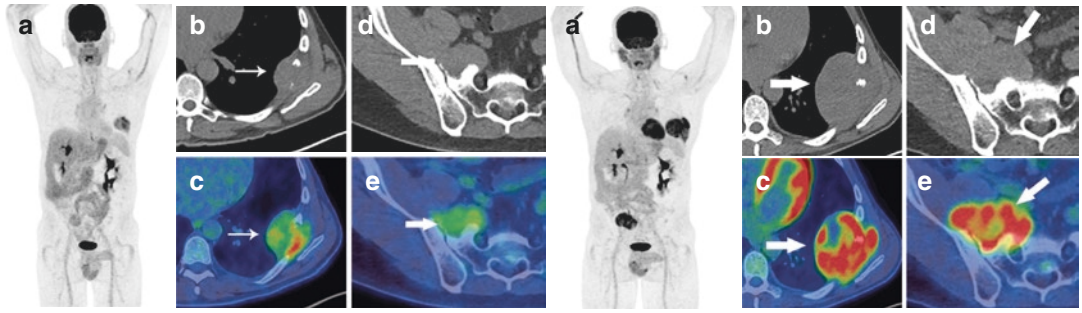

Fig. 14.5 Metastatic hepatocellular cancer with metabolic progression. (**a**) Pre-chemotherapy: There is increased FDG uptake within the left chest wall mass with destruction of the left 7th rib and SUVmax 8.0 (arrow in **b** and **c**), and right sacral ala mass with SUVmax 5.0 (arrow in **d** and **e**). (**b**) Post-chemotherapy: There is continued increased in size and FDG avidity of the left chest wall mass with destruction of the left 7th rib with SUVmax 18.0 (arrow in **b** and **c**). The right sacral ala mass has significantly increased in size and FDG avidity with SUVmax 14.0 (arrow in **d** and **e**). The scan findings are compatible with anato-metabolic progression in the left chest wall and right sacral mass

14.7 Case 6

Pancreatic cancer, ^{18}F-FDG PET/CT to assess treatment response (Fig. 14.6).

Teaching Points

- Necrosis and fibrosis following radiation therapy complicate interpretation of CT imaging.
- ^{18}F-FDG PET is superior to CT in assessing response to treatment in pancreatic cancer.

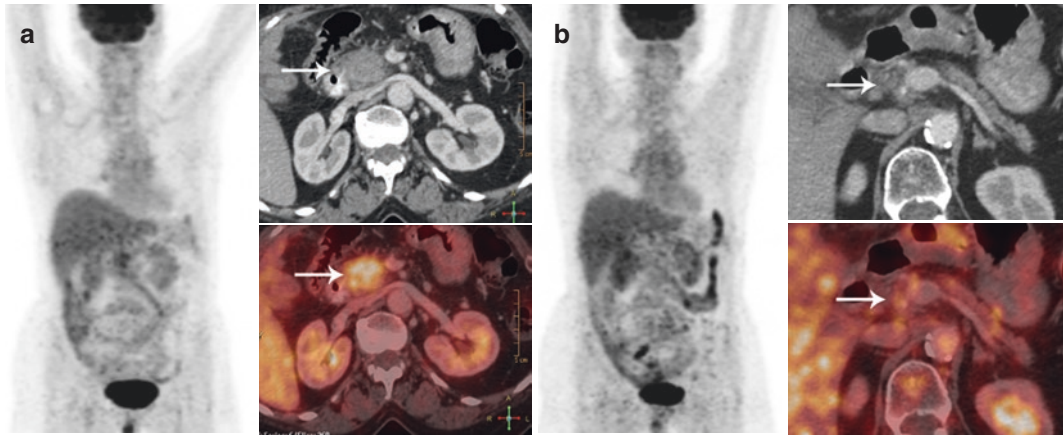

Fig. 14.6 Complete metabolic response: ^{18}F-FDG PET/CT (**a**) Pre-treatment study shows moderate increased tracer uptake within the mass in the head of pancreas with SUVmax 6.2 (arrow). (**b**) Post chemoradiotherapy PET/CT shows complete resolution of metabolic activity with significant regression in size of lesion (arrow) suggestive of complete metabolic response

14.8 Case 7

Pancreatic cancer, ^{18}F-FDG PET/CT for response assessment post completion of chemoradiation therapy (Fig. 14.7).

Teaching Points

- CT assessment of treatment response might delay detection of disease progression and regression.
- The nature of sporadically scattered cancer cells in fibrosis and connective tissue background in pancreatic cancer limits identifying tumour lesions.
- FDG PET is useful in the assessment of treatment response in pancreatic cancer.

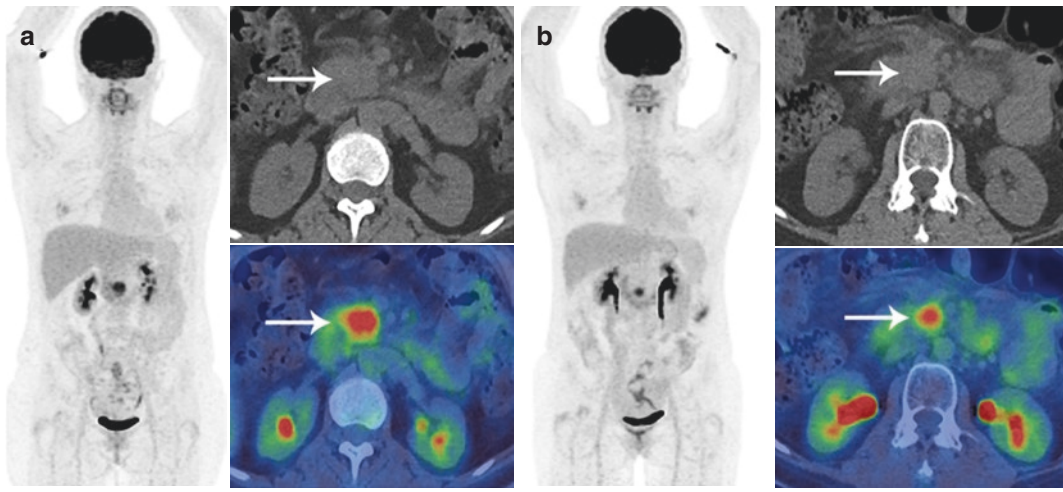

Fig. 14.7 Partial metabolic response: (**a**) Staging PET shows intense FDG uptake in the uncinate process of the pancreas (arrow). (**b**) On the post-therapy scan, there is regression in tracer uptake within the uncinate process of the pancreas compatible with partial metabolic response to treatment (arrows)

14.9 Case 8

Pancreatic cancer, ^{18}F-FDG PET/CT to assess treatment response (Fig. 14.8).

Teaching Points

- Chemoradiotherapy is a standard of care for locally advanced pancreatic cancer, and the local relapse rates are high.
- Several studies have demonstrated the performance of ^{18}F-FDG PET in assessing response to chemotherapy and chemoradiation and predicting clinical outcomes.
- The use of FDG PET/CT during CRT is limited by the inflammation caused by bile duct occlusion.

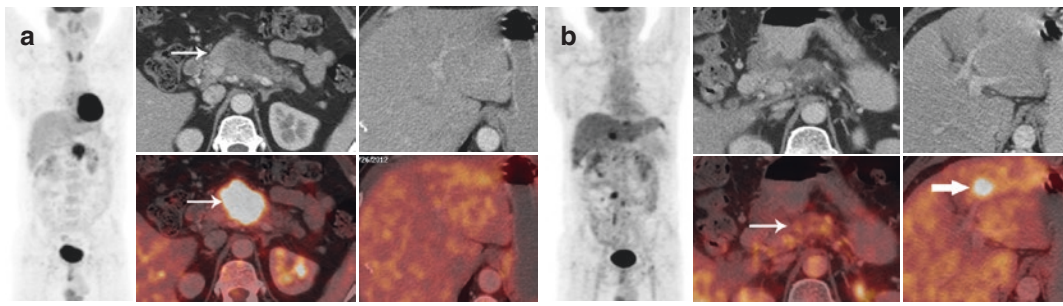

Fig. 14.8 Disease progression: (**a**) Staging FDG PET/CT shows tracer avid soft-tissue mass involving head and neck of pancreas with SUVmax 15 (arrow). There is no pathological lesion in the liver. (**b**) Post chemoradiation PET/CT scan shows complete resolution of metabolic activity with significant regression in size of pancreatic mass (thin arrow), but there is a new metastatic lesion in the liver, suggesting disease progression (thick arrow)

14.10 Case 9

Pancreatic carcinoma with liver metastasis ongoing chemotherapy. ^{18}F-FDG PET/CT for treatment response assessment (Fig. 14.9).

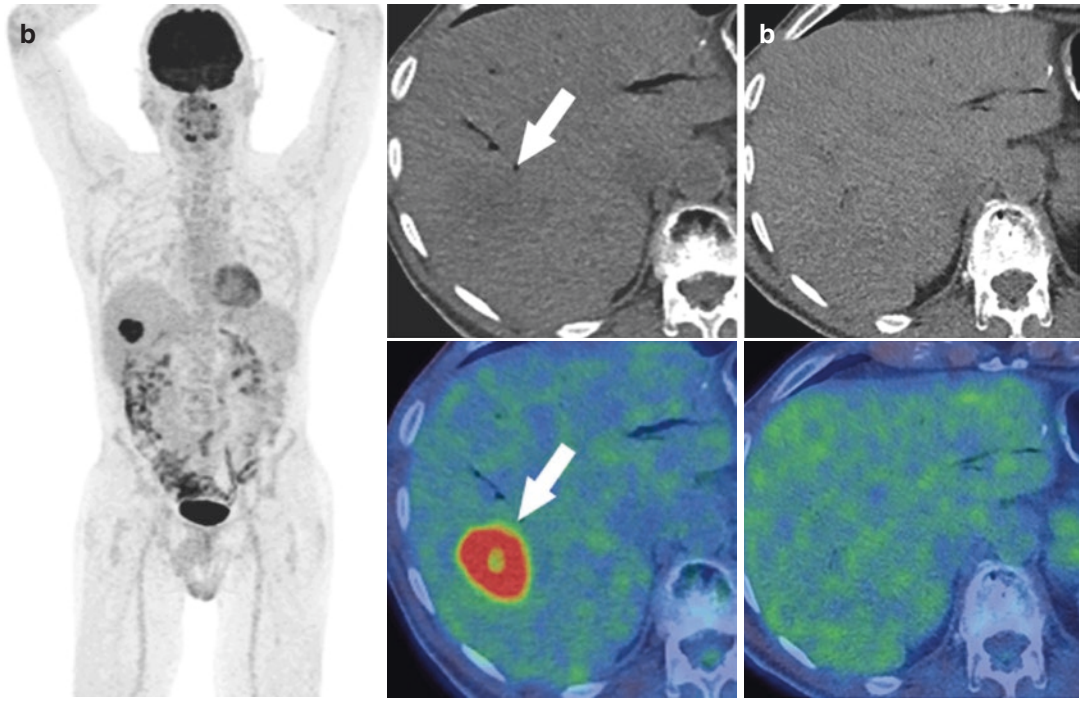

Fig. 14.9 Complete metabolic response: (**a**) There is focal intense tracer uptake within the right lobe of the liver demonstrating peripheral tracer uptake (arrow) and central photon deficiency (SUVmax 17.0). (**b**) On the follow-up scan, there is interval complete resolution of metabolic activity in the liver. The FDG PET/CT scan findings are suggestive of complete metabolic response to treatment

14.11 Case 10

Resected pancreatic cancer with liver and mediastinal node metastases on chemotherapy. FDG PET/CT to assess treatment response (Fig. 14.10).

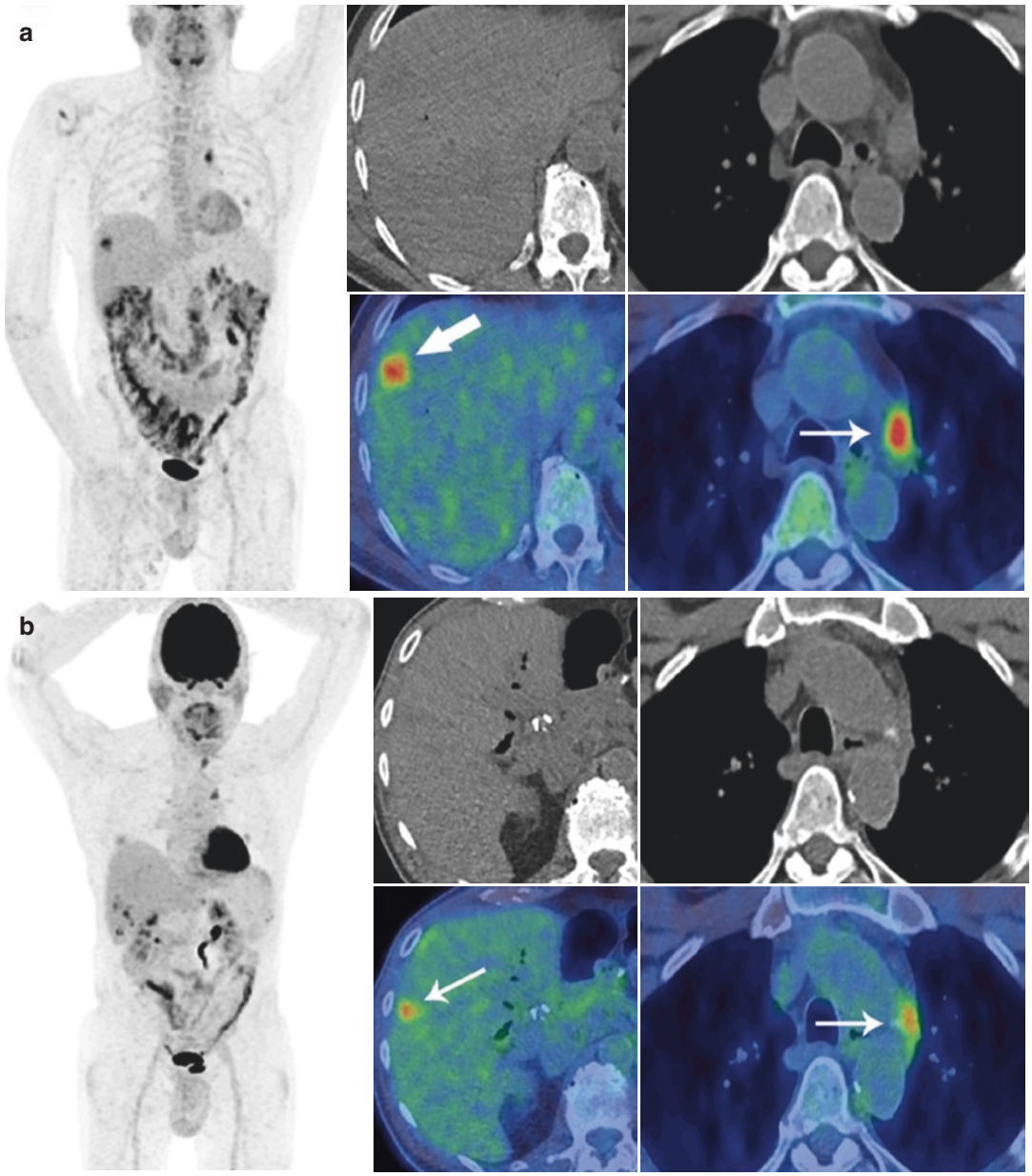

Fig. 14.10 Partial metabolic response to treatment: (**a**) Pretreatment study: There is a focus of intense FDG uptake (SUVmax 9.0) within segment VIII of the liver (thick arrow). FDG uptake noted within the aortopulmonary lymph node with SUVmax 7.0 (thin arrow). (**b**) Post-treatment study: interval regression in FDG uptake within the hepatic lesion (SUVmax 4.0) and aortopulmonary lymph node (SUVmax 4.0) suggesting partial metabolic response to treatment

14.12 Case 11

Suspected cholangiocarcinoma for staging (Fig. 14.11).

Teaching Points

- Pancreatitis is seen as a complication of biliary stenting and radiation therapy.
- Diffuse FDG uptake in combination with inflammatory CT features (pancreatic oedema, peripancreatic stranding and fluid collections) can point towards the diagnosis of pancreatitis.
- Delayed 2 hour scan is often reported to contribute to differentiation between malignant and benign lesions in the pancreas. However, the evidence is still evolving.
- Intense FDG uptake is seen in cholangitis and cholangiocarcinoma. Cholangitic abscess can often be mistaken as metastatic disease.
- Imaging features that can help differentiate inflammation from malignancy: Distribution of the FDG avidity in a linear branching pattern along the biliary radicles and a photopenic fluid filled the centre of an abscess.

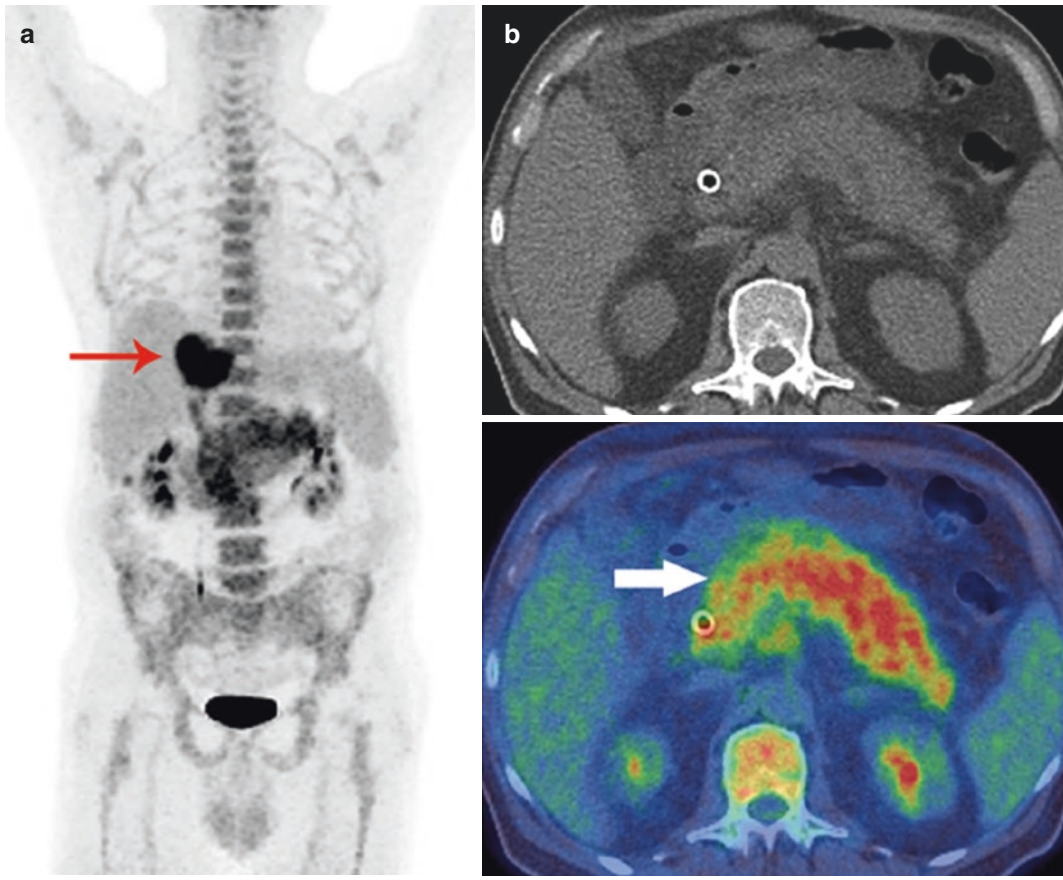

Fig. 14.11 Inflammation: FDG PET/CT study: MIP images show a large mass in the liver (red arrow) and heterogenous uptake in the abdomen. The heterogenous tracer uptake localizes to diffuse increased tracer uptake in the pancreas (white arrow) secondary to recent biliary stenting and ERCP and thus inflammatory in nature

14.13 Case 12

Gall bladder carcinoma, ^{18}F-FDG PET/CT to assess treatment response (Fig. 14.12).

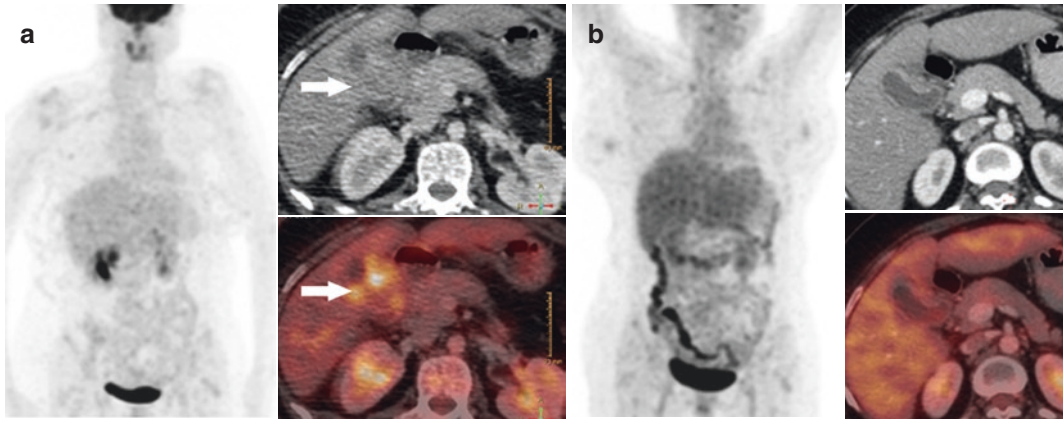

Fig. 14.12 Complete metabolic response: (**a**) Staging FDG PET/CT evaluation shows FDG avid soft-tissue mass in the gall bladder fossa with infiltration of the adjacent liver parenchyma (arrow). Fat planes with the distal end of the stomach, duodenum and hepatic flexure of the colon are effaced (SUVmax 8). (**b**) Post 4 cycles of chemotherapy—there is interval complete resolution of metabolic activity with minimal soft tissue noted involving fundus of gall bladder. The scan findings are compatible with complete metabolic and significant morphological regression of soft-tissue mass in the gall bladder fossa

14.14 Case 13

Gall bladder carcinoma, FDG PET/CT to assess treatment response (Fig. 14.13).

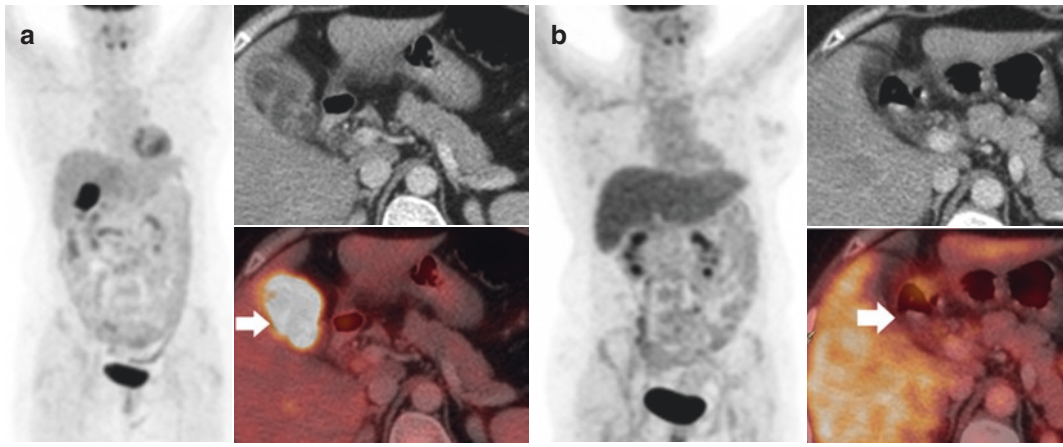

Fig. 14.13 Complete metabolic response: Staging ^{18}F-FDG PET/CT (**a**) shows intensely FDG avid soft-tissue mass involving the gall bladder (arrow). The mass is infiltrating the adjacent liver parenchyma (SUVmax 16.0). (**b**) Post chemoradiotherapy treatment response scan shows no perceptible FDG avid lesion in the gall bladder fossa (arrow) suggestive of complete metabolic response

14.15 Case 14

Gall bladder carcinoma, ^{18}F-FDG PET/CT to assess treatment response (Fig. 14.14).

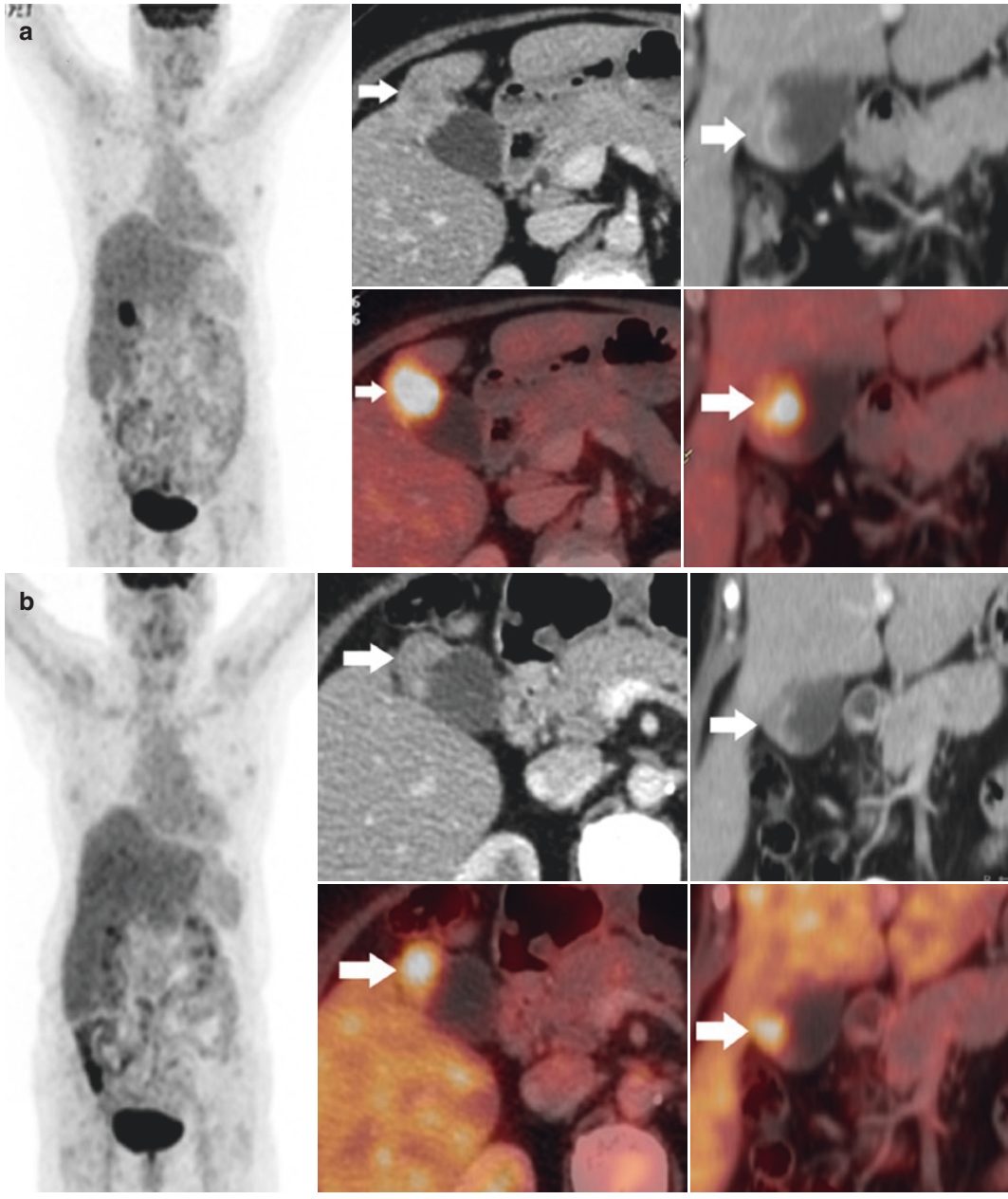

Fig. 14.14 Carcinoma of gall bladder with partial metabolic response. (**a**) Staging FDG PET/CT scan—FDG avid wall thickening arising from fundus of gall bladder (arrows) with adjacent hepatic parenchymal infiltration (SUVmax 14.0). (**b**). FDG PET/CT scan post 3 cycles of chemotherapy for treatment response evaluation shows FDG avid soft-tissue lesion in the fundus of the gall bladder (arrows) with minimal adjacent liver parenchymal infiltration (SUVmax 6). Scan findings are compatible with partial response to treatment

14.16 Case 15

Carcinoma of gall bladder. ^{18}F-FDG PET/CT for assessment of treatment (Fig. 14.15).

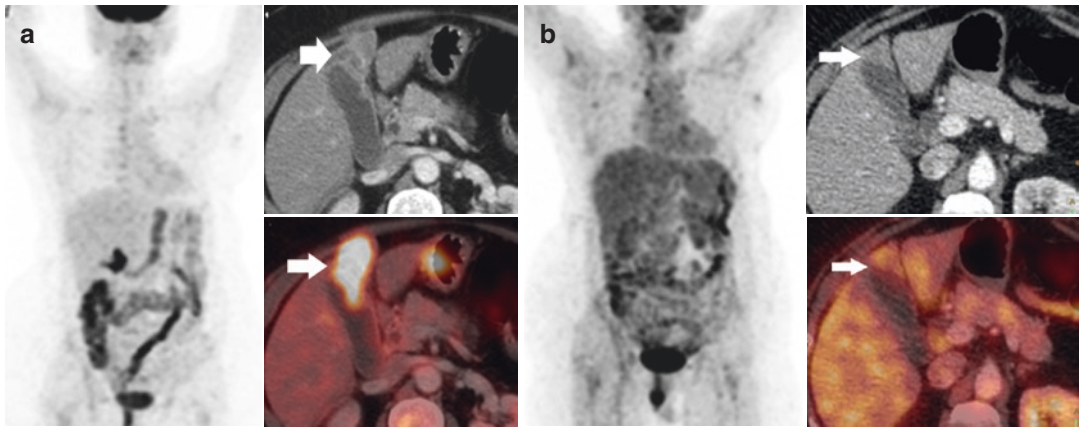

Fig. 14.15 Partial metabolic response. ^{18}F-FDG PET/CT (**a**) Staging scan shows FDG avid wall thickening in the fundus and body of gall bladder, involving parenchyma of adjacent right lobe of liver (SUVmax 13). (**b**) Post 4 cycles of chemotherapy, there is low-grade FDG avid lesion in the gall bladder (SUVmax 3), and there is subtle residual disease evident on the axial PET and CECT images. Scan findings are compatible with favourable partial metabolic response

14.17 Case 16

Cholangiocarcinoma, Klatskin tumor. ^{18}F-FDG PET/CT to assess treatment response (Fig. 14.16).

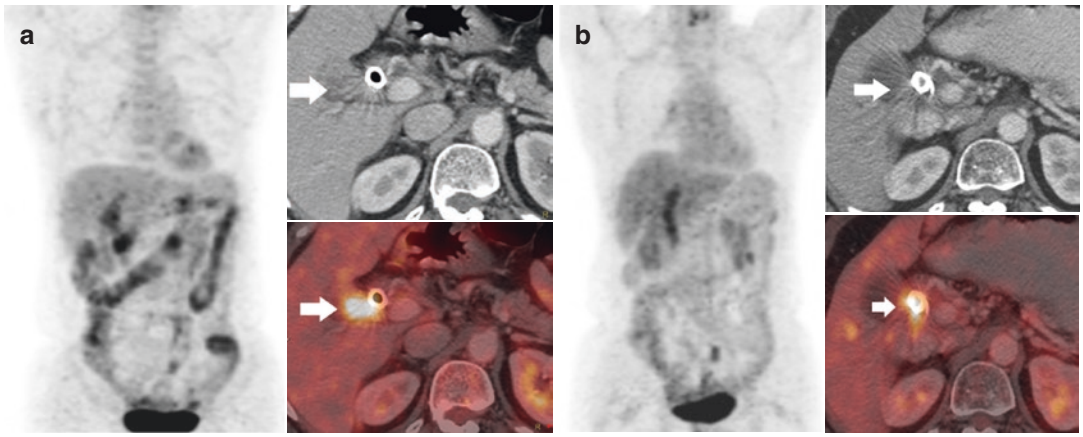

Fig. 14.16 Partial metabolic response (**a**) Baseline scan—FDG avid soft-tissue mass is noted measuring 4.0 cm × 3.2 cm × 2.3 cm with SUVmax 11.0 at the porta hepatis with involvement of the proximal common bile duct, common hepatic duct and confluence. (**b**) Post chemoradiotherapy study shows significant interval reduction in the metabolic activity and size of mass at the porta hepatis, compatible with partial metabolic response. Non attenuation corrected images are helpful for evaluation of metabolic activity at the site of metallic stents/implants

14.18 Case 17

Cholangiocarcinoma, post percutaneous transhepatic biliary drainage. ^{18}F-FDG PET/CT scan to assess treatment response (Fig. 14.17).

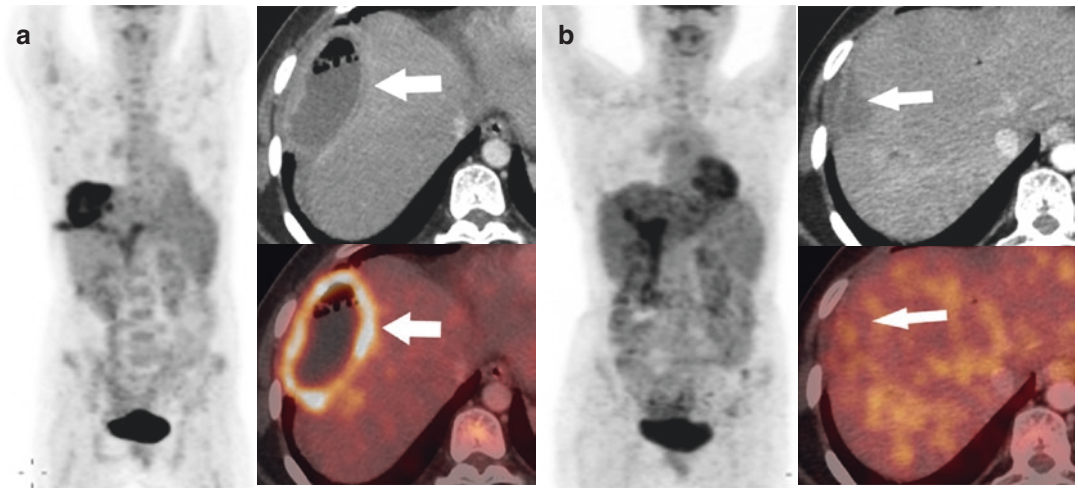

Fig. 14.17 Complete metabolic response: (**a**) Peripheral increased FDG tracer uptake is noted in thick-walled cystic lesion in the right lobe of the liver (segment VIII) measuring 7.8 × 4.2 cm and SUVmax 9.0. The lesion shows air pockets within it, suggestive of liver abscess (arrows). (**b**) Follow-up PET/CT post drainage of the abscess shows complete resolution of metabolic activity and significant morphologic regression (arrows)

14.19 Case 18

Cholangiocarcinoma, on chemotherapy. ^{18}F-FDG PET/CT to assess treatment response (Fig. 14.18).

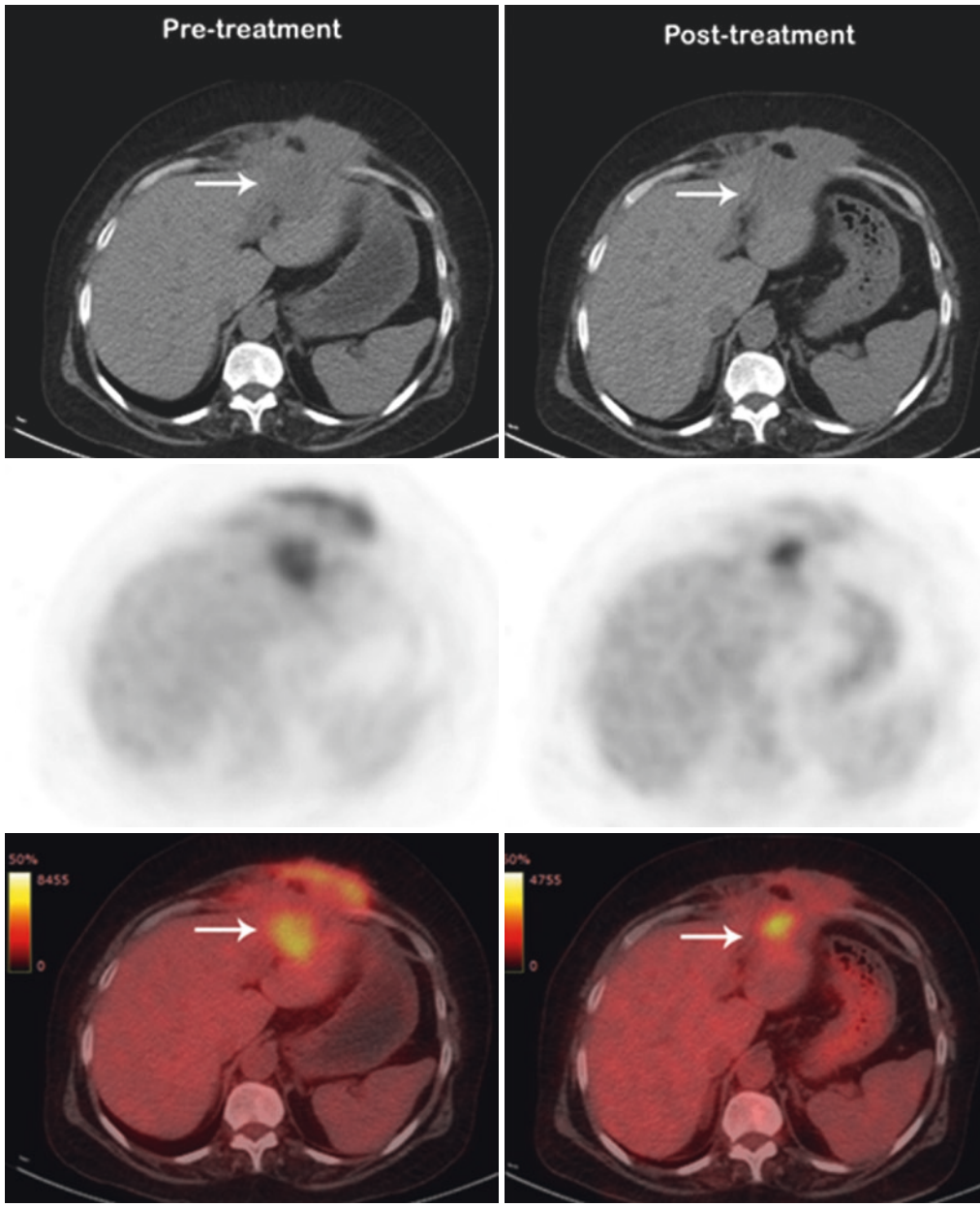

Fig. 14.18 Partial metabolic response: A case of cholangiocarcinoma presented with hepatic mass infiltrating anterior abdominal wall. The pre-treatment PET/CT on the left panel shows heterogeneously increased FDG uptake in the ill-defined soft-tissue mass measuring 10.5 cm × 6.8 cm and SUVmax 8.1. Post chemotherapy repeat PET/CT after 3 months shows minimal regression in size of mass measuring 10.0 cm × 6.6 cm with SUVmax 5.4. There is no significant regression in size of lesion and anatomically stable disease; however, as there is approx. 33% reduction in SUVmax and most of the tumour is metabolically inactive except a small part, suggestive of partial metabolic response

Suggested Reading

Introduction

Delbeke D, Martin WH. Update of PET and PET/CT for hepatobiliary and pancreatic malignancies. HPB (Oxford). 2005;7(3):166–79.

Keiding S, Hansen SB, Rasmussen HH, Gee A, Kruse A, Roelsgaard K, et al. Detection of cholangiocarcinoma in primary sclerosing cholangitis by positron emission tomography. Hepatology. 1998;28:700–6.

Rose DM, Delbeke D, Beauchamp RD, Chapman WC, Sandler MP, Sharp KW, Richards WO, Wright JK, Frexes ME, Pinson CW, et al. 18Fluorodeoxyglucose—positron emission tomography (18FDG—PET) in the management of patients with suspected pancreatic cancer. Ann Surg. 1998;229:729–38.

Case 1

Chiu KWH, Lam K, An H, et al. Long-term outcomes and recurrence pattern of 18F-FDG PET-CT complete metabolic response in the first-line treatment of metastatic colorectal cancer: a lesion-based and patient-based analysis. BMC Cancer. 2018;18:776.

Liu FY, Yen TC, Wang JY, Yang TS. Early prediction by 18F-FDG PET/CT for progression-free survival and overall survival in patients with metastatic colorectal cancer receiving third-line cetuximab-based therapy. Clin Nucl Med. 2015;40:200–5.

Van den Abbeele AD. The lessons of GIST—PET and PET/CT: a new paradigm for imaging. Oncologist. 2008;13:8–13.

Woff E, Hendlisz A, Garcia C, et al. Monitoring metabolic response using FDG PET-CT during targeted therapy for metastatic colorectal cancer. Eur J Nucl Med Mol Imaging. 2016;43(10):1792–801.

Case 2

Chiu, K.W.H., Lam, K., An, H. et al. Long-term outcomes and recurrence pattern of 18F-FDG PET-CT complete metabolic response in the first-line treatment of metastatic colorectal cancer: a lesion-based and patient-based analysis. BMC Cancer. 2018;18:776.

Engelmann BE, Loft A, Kjaer A, Nielsen HJ, Gerds TA, von Benzon E, et al. Positron emission tomography/computed tomography and biomarkers for early treatment response evaluation in metastatic colon cancer. Oncologist. 2014;19:164–72.

de Geus-Oei LF, van Laarhoven HWM, Visser EP, Hermsen R, van Hoorn BA, Kamm YJL, et al. Chemotherapy response evaluation with FDG-PET in patients with colorectal cancer. Ann Oncol. 2008;19:348–52.

Hendlisz A, Golfinopoulos V, Garcia C, Covas A, Emonts P, Ameye L, et al. Serial FDG–PET/CT for early outcome prediction in patients with metastatic colorectal cancer undergoing chemotherapy. Ann Oncol. 2012;23:1687–93.

Liu FY, Yen TC, Wang JY, Yang TS. Early prediction by 18F-FDG PET/CT for progression-free survival and overall survival in patients with metastatic colorectal cancer receiving third-line cetuximab-based therapy. Clin Nucl Med. 2015;40:200–5.

Woff E, Hendlisz A, Garcia C, et al. Monitoring metabolic response using FDG PET-CT during targeted therapy for metastatic colorectal cancer. Eur J Nucl Med Mol Imaging. 2016;43(10):1792–801.

Case 3

Gauthé M, Richard-Molard M, Cacheux W, Michel P, Jouve J, Mitry E. Role of fluorine 18 fluorodeoxyglucose positron emission tomography/computed tomography in gastrointestinal cancers. Dig Liver Dis. 2015;47:443–54.

Gollub M, Schwartz LH, Akhurst T. Update on colorectal cancer imaging. Radiol Clin N Am. 2007;45:85–118.

Van den Abbeele AD. The lessons of GIST—PET and PET/CT: a new paradigm for imaging. Oncologist. 2008;13:8–13.

Van Cutsem E, Verheul HM, Flamen P, et al. Imaging in colorectal cancer: progress and challenges for the clinicians. Cancers (Basel). 2016;8(9):81.

Case 4

Choi SH, Chang JS, Jeong YH, Lee Y, Yun M, Seong J. FDG-PET predicts outcomes of treated bone metastasis following palliative radiotherapy in patients with hepatocellular carcinoma. Liver Int. 2014;34:1118–25.

Lu RC, She B, Gao WT, et al. Positron-emission tomography for hepatocellular carcinoma: Current status and future prospects. World J Gastroenterol. 2019;25(32):4682–95.

Song HJ, Cheng JY, Hu SL, Zhang GY, Fu Y, Zhang YJ. Value of 18F-FDG PET/CT in detecting viable tumour and predicting prognosis of hepatocellular carcinoma after TACE. Clin Radiol. 2015;70:128–37.

Case 6

Kadhim LA, Dholakia AS, Herman JM, et al. The role of 18F-fluorodeoxyglucose positron emission tomography in the management of patients with pancreatic adenocarcinoma. J Radiat Oncol. 2013;2:341–52.

Case 7

Bang S, Chung HW, Park SW, Chung JB, Yun M, Lee JD, Song SY. The clinical usefulness of 18-fluorodeoxyglucose positron emission tomography in the different diagnosis, staging, and response evaluation after concurrent chemoradiotherapy for pancreatic cancer. J Clin Gastroenterol. 2006;40:923–29.

Dalah E, Tai A, Oshima K, Hall WA, Erickson B, Li XA. PET-based treatment response assessment for neoadjuvant chemoradiation in pancreatic adenocarcinoma: an exploratory study. Transl Oncol. 2018;11(5):1104–9.

Orlando LA, Kulasingam SL, Matchar BD. Meta-analysis: the detection of pancreatic malignancy with positron emission tomography. Aliment Pharmacol Ther. 2004;20:1063–70.

Yoshioka M, Sato T, Furuya T, Shibata S, et al. Role of positron emission tomography with 2-deoxy-2[18F] fluoro-d-glucose in evaluating the effects of arterial infusion chemotherapy and radiotherapy on pancreatic cancer. J Gastroenterol. 2004;39:50–5.

Zhao B, Schwartz LH, Larson SM. Imaging surrogates of tumor response to therapy: anatomic and functional biomarkers. J Nucl Med. 2009;50:239–49.

Case 8

Cliffe H, Patel C, Prestwich R, Scarsbrook A. Radiotherapy response evaluation using FDG PET-CT—established and emerging applications. BJR. 2017;90:1071.

Kadhim LA, Dholakia AS, Herman JM, et al. The role of 18F-fluorodeoxyglucose positron emission tomography in the management of patients with pancreatic adenocarcinoma. J Radiat Oncol. 2013;2:341–52.

Topkan E, Parlak C, Kotek A, et al. Predictive value of metabolic 18FDG-PET response on outcomes in patients with locally advanced pancreatic carcinoma treated with definitive concurrent chemoradiotherapy. BMC Gastroenterol. 2011;10:123.

Case 11

Kato K, Nihashi T, Ikeda M, Abe S, Iwano S, Itoh S, Shimamoto K, Naganawa S. Limited efficacy of (18) F-FDG PET/CT for differentiation between metastasis-free pancreatic cancer and mass-forming pancreatitis. Clin Nucl Med. 2013;38(6):417–21.

Nakamoto Y, Higashi T, Sakahara H, Tamaki N, Kogire M, Doi R, Hosotani R, Imamura M, Konishi J. Delayed (18)F-fluoro-2-deoxy-d-glucose positron emission tomography scan for differentiation between malignant and benign lesions in the pancreas. Cancer. 2000;89(12):2547–54.

Santhosh S, Mittal BR, Bhasin D, Rana SS, Bhattacharya A, Srinivasan R, Nada R, Gupta R. Dual-phase 18F-FDG PET/CT imaging in the characterization of pancreatic lesions: does it offer prognostic information? Nucl Med Commun. 2014;35(10):1018–25.

15

^{18}F-FDG PET/CT in Treatment Response Evaluation: Gastroesophageal Cancer

Archi Agrawal, M. V. Manikandan, Nilendu C. Purandare, Sneha Shah, Ameya D. Puranik, and Venkatesh Rangarajan

15.1 Introduction

Esophageal cancer has high mortality rate with poor 5-year overall survival of 17% [1]. There are two main histological subtypes—adenocarcinoma and squamous carcinoma. Surgery is the mainstay of treatment for locoregional disease. Approximately 20–30% of patients with locally advanced disease have distant metastatic disease at presentation [2]. Combined chemo-radiotherapy (CTRT) and neoadjuvant chemotherapy (NACT) prior to surgery are some of the approaches used to improve local control. These approaches help to downstage the disease, increase the resection rates, and also treat micro-metastases, not detected on imaging [3, 4].

^{18}F-FDG PET/CT is the modality of choice to identify treatment responders from nonresponders. FDG PET/CT can distinguish viable from nonviable disease, but false positives do occur because of posttreatment (CTRT) inflammatory changes due to uptake of FDG in macrophages and activated leukocytes. PET cannot distinguish between microscopic residual disease from complete response. In spite of these issues, PET/CT is more accurate than any other imaging modality, e.g., CT, EUS, in identifying responders from nonresponders [5–7].

Pathological complete response after neoadjuvant chemotherapy with or without radiotherapy is associated with lower recurrence rates and longer survival [8–12]. Few meta-analyses have shown improved 3-year survival in patients who received neoadjuvant CTRT as compared to those who underwent surgery alone [13, 14]. Patients with complete metabolic response on imaging may at times benefit from wait and watch policy [12].

We hereby present multiple case scenarios in response assessment of esophageal and gastric malignancy.

A. Agrawal (✉) · M. V. Manikandan · N. C. Purandare
S. Shah · A. D. Puranik · V. Rangarajan
Department of Nuclear Medicine and Molecular Imaging, Tata Memorial Hospital, Homi Bhabha National Institute, Mumbai, India

S. Fanti et al. (eds.), *Atlas of Clinical PET-CT in Treatment Response Evaluation in Oncology*,
https://doi.org/10.1007/978-3-030-68858-5_15

15.2 Case No. 1: Radiation-Induced Esophagitis

Clinical Details 62-year male; a case of squamous carcinoma of middle esophagus. Received CTRT, response study was done 2 months after completion of treatment (Fig. 15.1).

Interpretation Low-grade diffuse uptake in the esophagus in the irradiated region represents posttreatment inflammatory changes. This was confirmed by a posttreatment biopsy which revealed no residual disease.

Teaching Point

- Low-grade diffuse metabolic activity in the esophagus represents radiation-induced inflammatory changes suggestive of esophagitis [15, 16].

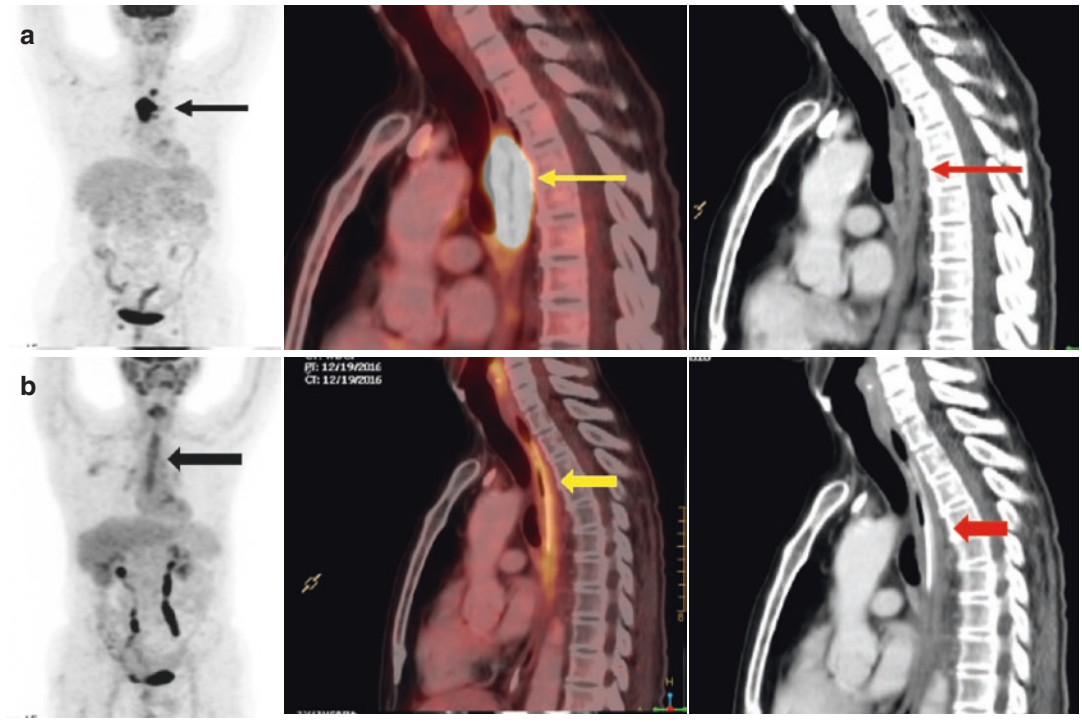

Fig. 15.1 (**a**) Upper row shows FDG-avid circumferential thickening involving the middle esophagus (arrow). (**b**) Lower row shows low-grade diffuse FDG uptake in the esophagus (block arrow) with no mass lesion in the esophagus

15.3 Case No. 2: Radiation-Induced Pneumonitis

Clinical Details 62-year male with moderately differentiated squamous cell carcinoma (MDSCC) of middle esophagus. Staging and post CTRT scan done 10 months after completion of RT (Fig. 15.2).

Interpretation Post radiotherapy to the esophagus, paramediastinal inflammatory changes are seen in both the lungs. This is because the radiation port includes minimal lung tissue. Ground glass opacities are typically seen in the early phase and traction bronchiectasis in the late stage. These are referred to as radiation-induced lung injury or radiation pneumonitis.

Teaching Points

- Posttreatment inflammatory changes should not be mistaken as disease to the lung or lymphangitis.
- Radiation pneumonitis is inflammatory reaction of the pulmonary parenchyma which is affected by radiation.
- Acute changes are seen 6–12 weeks after radiotherapy. Chronic changes in the form of fibrosis are seen 6–12 months after RT and can last for 2 years [17, 18].

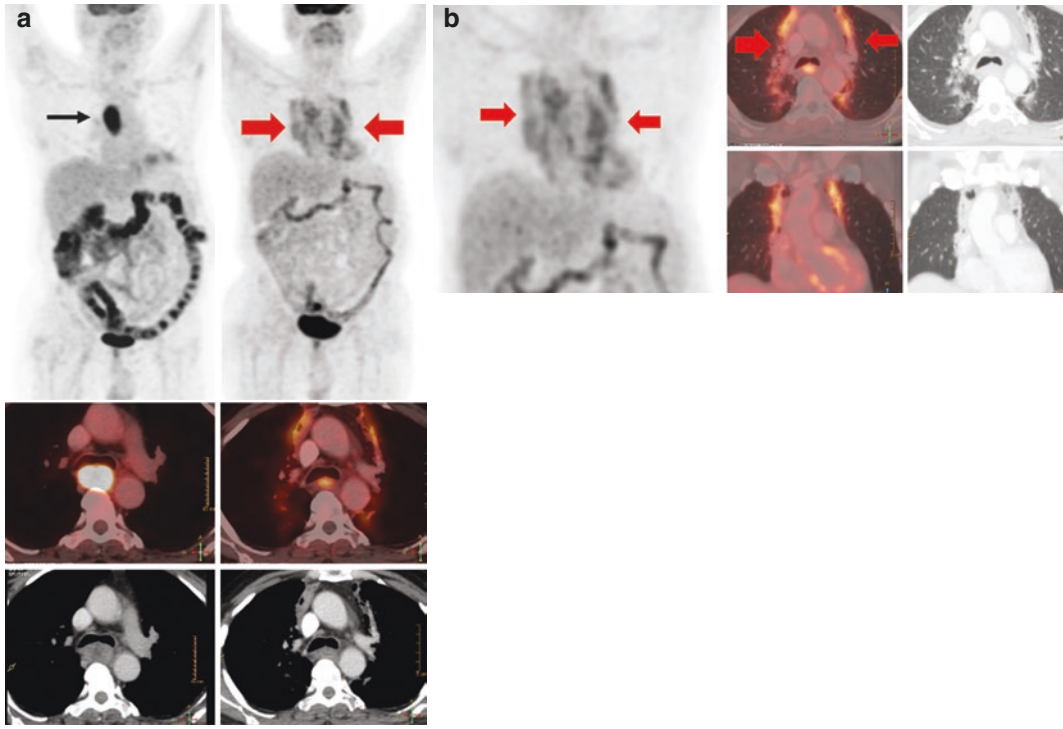

Fig. 15.2 (**a**) FDG-avid concentric wall thickening involving the middle esophagus (arrow). The MIP and the axial image on the right show increased FDG uptake in the paramediastinal region of the lungs (block arrows). (**b**) Increased FDG uptake is noted in ground glass opacities in the paramediastinal lung (block arrow)

15.4 Case No. 3: Post Transthoracic Esophagectomy (TTE) Appearance

Clinical Details A. 50 years, female, a case of poorly differentiated SCC of middle third esophagus. Post NACT and TTE.

B. 42 years, male, a case of moderately differentiated SSC of the lower esophagus. Post CTRT and TTE (Fig. 15.3).

Interpretation These are normal appearances post transthoracic esophagectomy (TTE).

Teaching Point

- The mobilized gastric tube is placed in the prevertebral space of posterior mediastinum (commonest) or in the right paravertebral or in the substernal space of anterior mediastinum. One should be aware of the post TTE appearance on PET/CT [19].

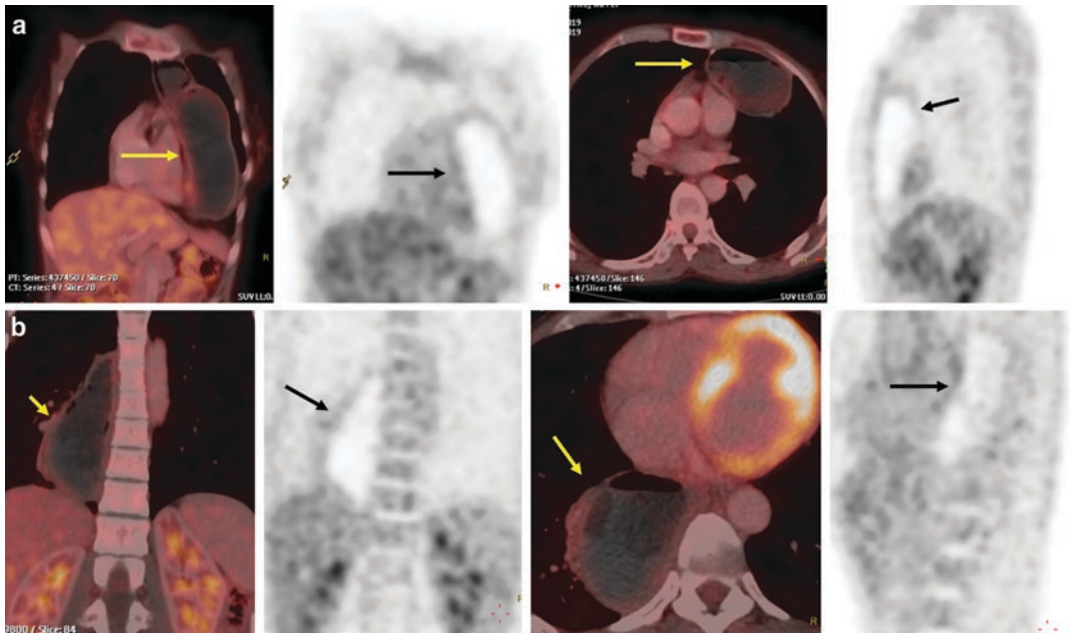

Fig. 15.3 (**a**) PET/CT scan shows the mobilized gastric tube in the substernal space of the mediastinum (arrows), with no increased FDG uptake. (**b**) PET/CT scan shows the mobilized gastric tube in the right paravertebral space (arrows), with no increased FDG uptake

15.5 Case No. 4: Aspiration Pneumonia

Clinical Details 55 years male, a case of poorly differentiated SCC of the middle and lower esophagus. Staging scan (Fig. 15.4).

Interpretation These changes in the left lung are due to aspiration pneumonia.

Teaching Points

- Tracheoesophageal and bronchoesophageal fistulas are seen in 5–10% of patients with advanced esophageal cancer. The prognosis is poor in such patients.
- Pulmonary consolidation may involve one or both the lungs. The radiologic findings are usually nonspecific. Aspiration pneumonia should be suspected in patients with esophageal malignancy who present with recurrent pneumonia [20].

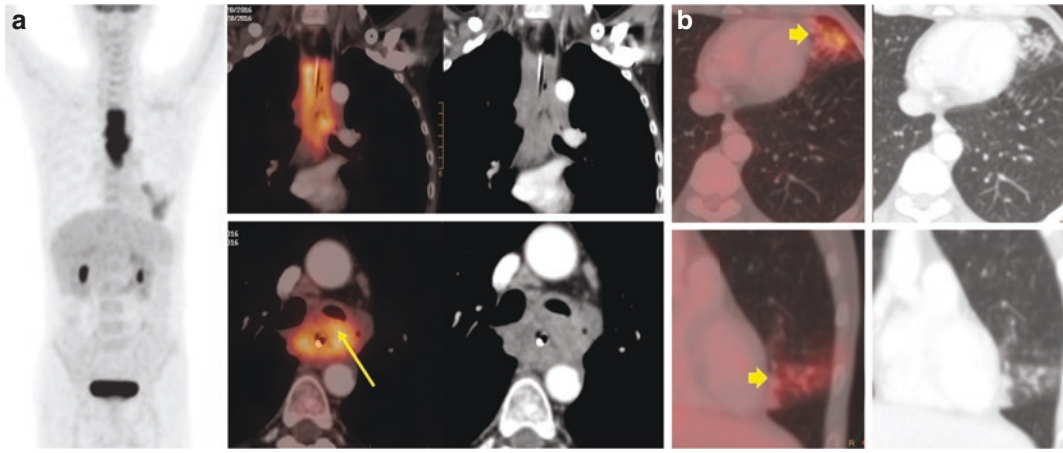

Fig. 15.4 (**a**) FDG PET/CT image shows FDG-avid in the middle and lower esophageal mass. The mass encases the left main bronchus with possible infiltration (arrow). (**b**) FDG-avid branching opacities in the lower lobe of left lung (block arrow)

15.6 Case No. 5: Recurrent Aspiration Pneumonia

Clinical Details 55 years male, a case of poorly differentiated SCC of the middle and lower esophagus. Received NACT and chemotherapy. (same patient as in Case No. 4) (Fig. 15.5).

Interpretation These changes are due to recurrent aspiration pneumonia.

Teaching Point

Recurrent pneumonia is common in patients with locally advanced esophageal malignancy [20].

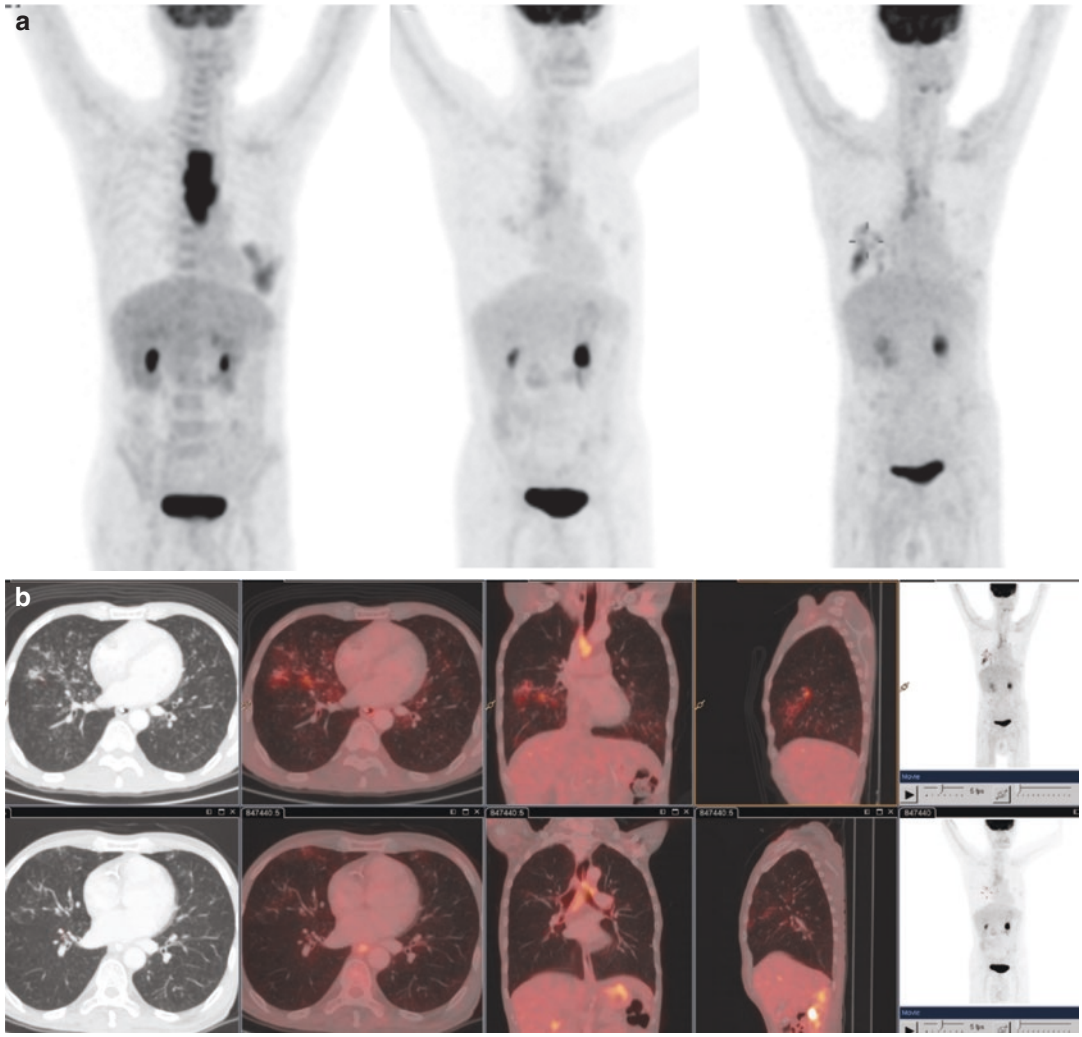

Fig. 15.5 (**a**) FDG PET/CT image shows FDG-avid middle and lower esophageal mass. (**b**, **c**) FDG PET/CT study done post NACT (2 months after the first study) and post palliative chemotherapy (6 months after the first study) shows FDG-avid branching opacities in both the lungs. The opacities have increased in **c**

15.7 Case No. 6: Tracheoesophageal Fistula (TOF)

Clinical Details 68 years, male, case of MDSCC. Received CTRT (Fig. 15.6).

Interpretation The scans show progressive disease and the presence of a bronchoesophageal fistula.

Teaching Point

- Locally advance esophageal malignancy may invade the trachea, bronchus, or at times the lung, resulting in a fistula formation between the esophagus and the trachea-bronchial tree. This carries poor prognosis [21].

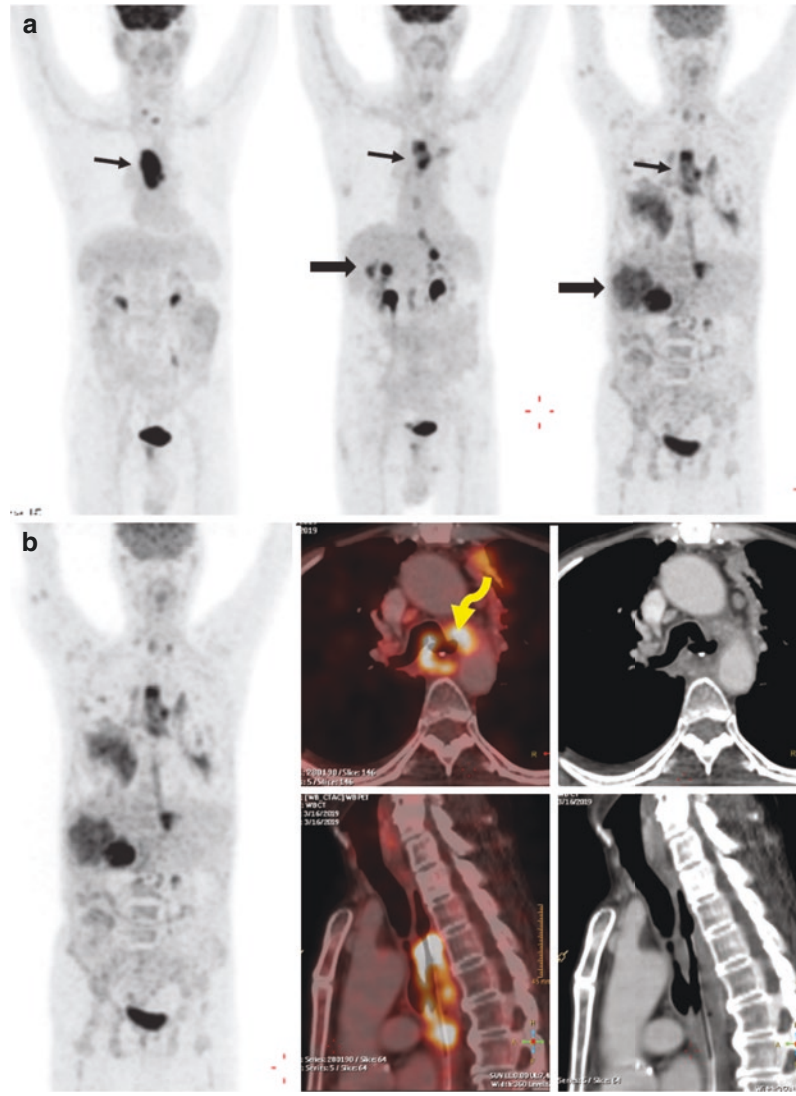

Fig. 15.6 (**a**) Staging scan: FDG-avid middle esophageal mass (arrow). (*Ai*) Post CTRT: Partial response in the esophageal mass (arrow) with appearance of new metabolically active liver lesion (block arrow) suggestive of metastases and disease progression. (**b**) Study done 6 months after the post CTRT scan: Increase in the size of the FDG-avid esophageal mass (arrow) and the liver lesion (block arrow). FDG-avid aspiration pneumonia is noted in both the lungs. (*Bi*) The esophageal mass is invading into the left main bronchus with formation of bronchoesophageal fistula (curved arrow)

15.8 Case No. 7: Upper Esophageal Mass with Complete Response Post CTRT

Clinical Details 47 years' male, case of SCC of upper esophagus. PET/CT done after three cycles of NACT and post CTRT (Fig. 15.7).

Interpretation Both the response scans done after NACT and post CT RT show complete response to treatment. These findings are suggestive of complete response (CR) to treatment.

Teaching Point

- FDG PET/CT is the better than all imaging modalities for assessment of response post chemo-radiotherapy [5, 7].

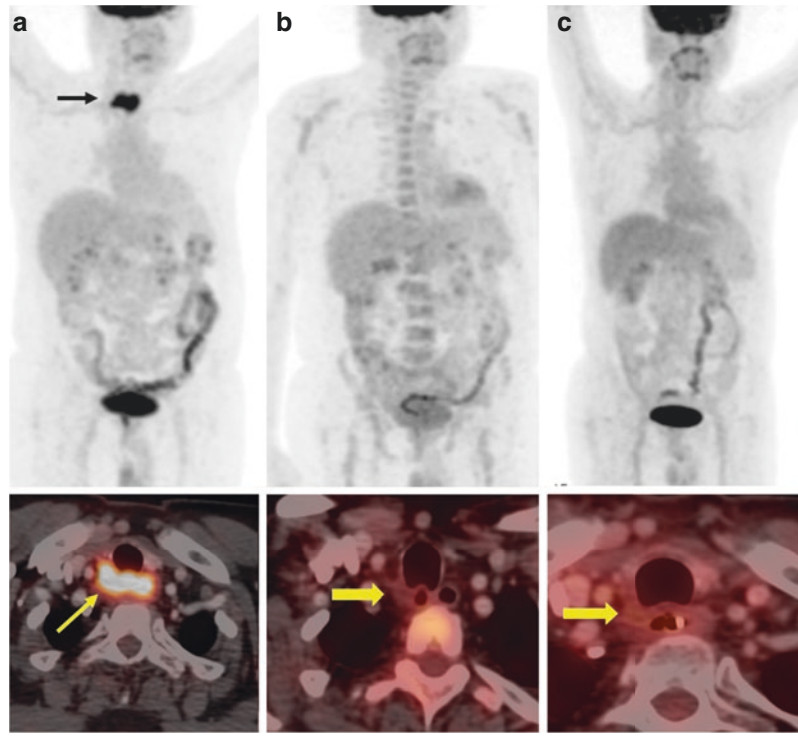

Fig. 15.7 (**a**) Staging scan: FDG PET CT image showing hypermetabolic circumferential thickening involving the upper esophagus (arrow). (**b**) Scan post NACT: No FDG-avid lesion seen in the upper esophagus in the scan (block arrow). (**c**) Post CTRT scan: No FDG-avid lesion seen in the upper esophagus in the scan done after 2 months of completion of CTRT (block arrow)

15.9 Case No. 8: Post CTRT Complete Response with Inflammatory Changes in the Esophagus

Clinical Details 75 years, male, a case of MDSCC. Staging and post CTRT scan (Fig. 15.8).

Interpretation Low-grade diffuse FDG uptake in the posttreatment scan represents posttreatment inflammatory changes, confirmed by histopathology. Biopsy done after CTRT showed chronic inflammatory exudate suggestive of post-treatment changes.

Teaching Point

- Radiation esophagitis is seen after 2 weeks of completion of CTRT and is commonly seen with high radiation doses in range of 40 Gy and above [22].

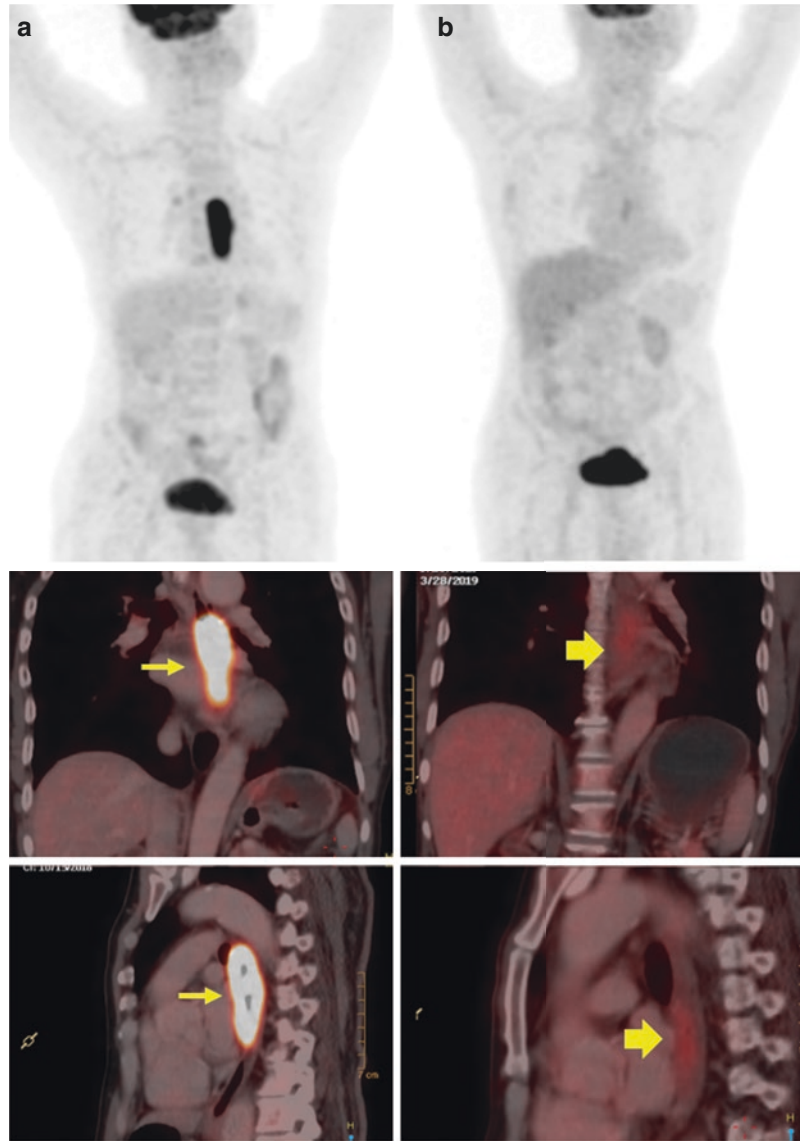

Fig. 15.8 (**a**) Staging study: FDG-avid (maxSUV 24.22) circumferential thickening noted in the middle and lower esophagus (arrow). (**b**) Response assessment scan done post CT RT: No FDG-avid mass in esophagus. Only low-grade diffuse FDG uptake [maxSUV 3.26] is noted in the mid and lower esophagus (block arrow)

15.10 Case No. 9: Complete Response on PET/CT with Microscopic Residual Disease on Histopathology

Clinical Details 69 years male. A case of MDSCC of the lower esophagus. Pretreatment and post NACT scans (Fig. 15.9).

Interpretation Complete metabolic response is seen in the esophageal lesion post three cycles of NACT. The patient underwent TTE after NACT which revealed residual MDSCC. The bulky adrenal was benign.

Teaching Point

- Though PET/CT is the best modality for response assessment, it cannot pick microscopic residual disease [5, 7].

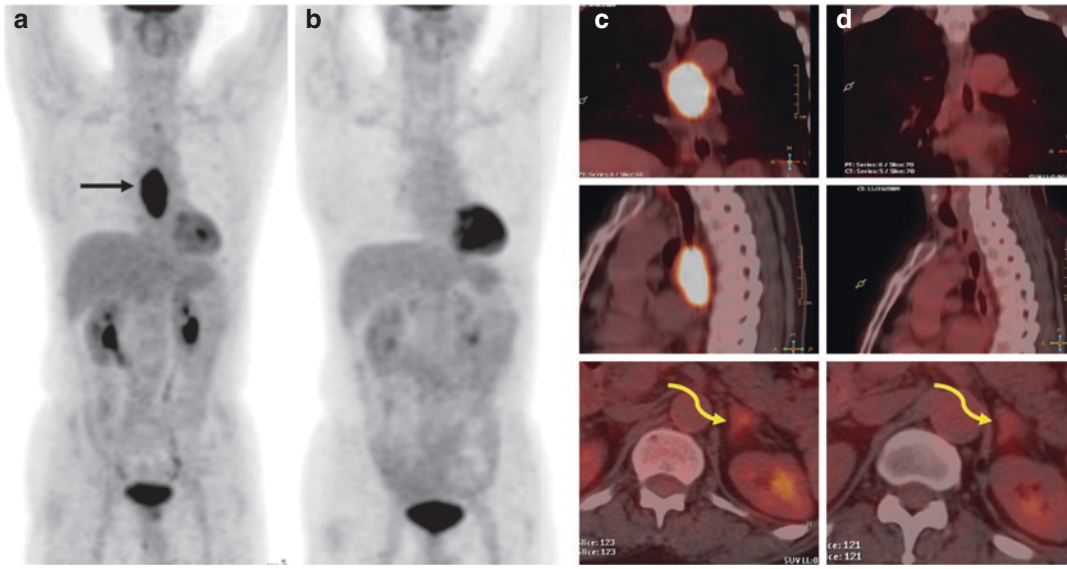

Fig. 15.9 (**a** and **c**) Staging scan: FDG-avid mass in the lower esophagus (arrow). Low-grade FDG-avid bulky left adrenal (maxSUV 2.9) (curved arrow). (**b** and **d**) Post NACT response scan: No FDG-avid lesion in the esophagus. The bulky left adrenal is unchanged (curved arrow)

15.11 Case No. 10: Posttreatment Changes Vs. Residual Disease

Clinical Details 60-year-old male, case of MDSCC. Staging scan and post CTRT scan (Fig. 15.10).

Interpretation Low-grade metabolic activity in the minimal soft-tissue thickening in the middle esophagus. This finding is indeterminate. This could represent either residual disease or post-treatment changes. This patient underwent TTE which showed no residual disease.

Teaching Point

- It is at times difficult to differentiate between inflammatory posttreatment changes in the esophagus and minimal residual disease.

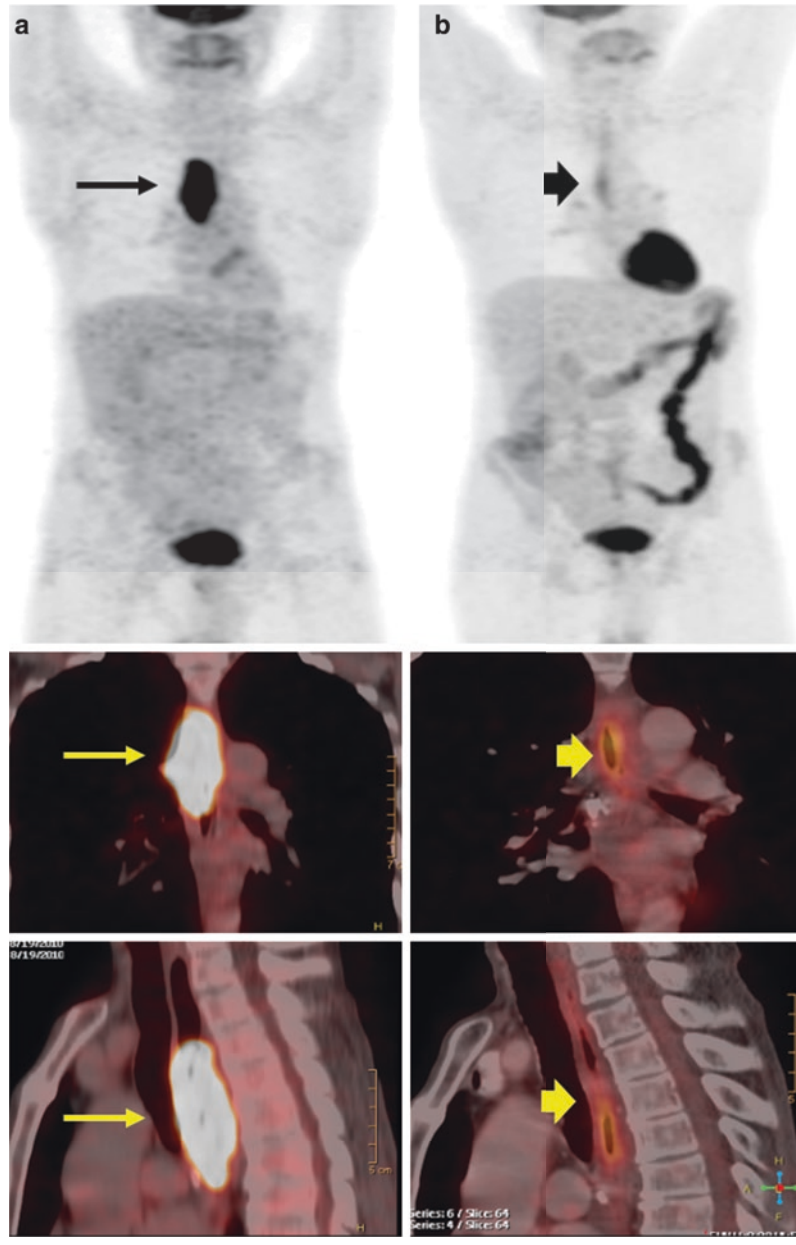

Fig. 15.10 (**a**) Staging scan: FDG-avid mass (maxSUV 14.1) in the middle third esophagus (arrow). (**b**) Response assessment scan post CT RT: Low-grade diffuse FDG uptake (maxSUV 3.5) with minimal soft-tissue thickening is noted in the middle esophagus (block arrow)

15.12 Case No. 11: Partial Response to Treatment

Clinical Details 54 years, male. A case of poorly differentiated SCC. Staging and post CTRT scan (Fig. 15.11).

Interpretation Partial response post CTRT. Post TTE revealed PDSCC with residual viable disease with metastatic node with perinodal extension.

Teaching Point

- Demonstration of partial response.

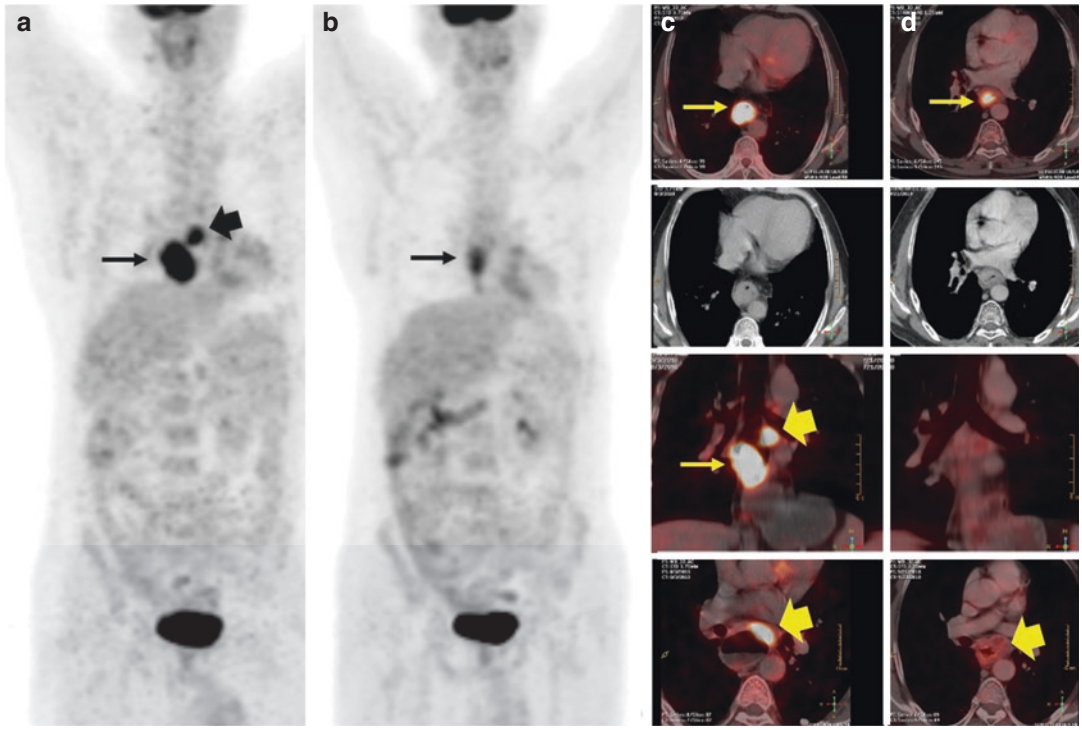

Fig. 15.11 (**a** and **c**) Staging scan: FDG-avid mass lesion is noted in the lower esophagus (arrow) and FDG-avid paraesophageal node (block arrow). (**b** and **d**) Post CTRT scan: FDG-avid lesion seen in the lower esophagus with decrease in size and metabolic activity of the esophageal lesion and the paraesophageal node

15.13 Case No. 12: Stable Disease with Radiation-Induced Esophagitis

Clinical Details 54 years, female. Case of PD SCC. Received three cycles of NACT and underwent TTE (Fig. 15.12).

Interpretation These findings suggest stable disease post NACT along with inflammatory esophagitis. This patient underwent TTE which revealed residual viable poorly differentiated squamous carcinoma with tumor regression grade (TRG) 4/5.

Teaching Point

- Residual disease may coexist with radiation-induced esophagitis.

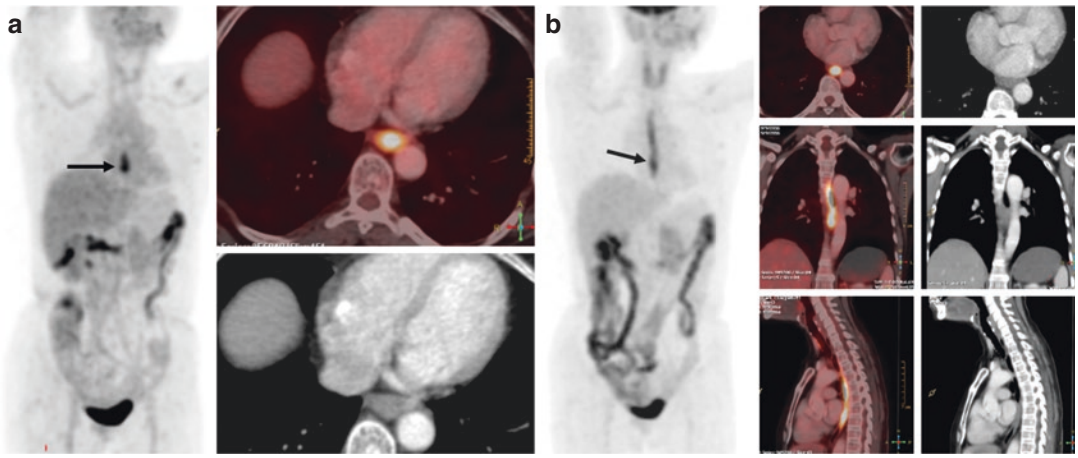

Fig. 15.12 (**a**) Staging scan: FDG-avid mass (maxSUV 10.93) is noted in the lower esophagus (arrow). (**b**) Post NACT scan: FDG-avid mass in the lower esophagus with minimal decrease in thickness and no significant change in metabolic activity (maxSUV 9.56). Diffuse FDG uptake is seen along the esophagus

15.14 Case No. 13: GE Junction Mass with Partial Response

Clinical Details 35 years' male, a case of poorly differentiated adenocarcinoma. Staging and post four cycles of chemotherapy scan (Fig. 15.13).

Interpretation Though there is significant resolution of the metabolic activity and the soft-tissue mass involving the lower esophagus and GE junction, there is still persistence of residual disease. This is partial response. The patient underwent TTE which revealed: scanty residual, viable poorly differentiated adenocarcinoma with tumor regression grade (TRG) 2/5.

Teaching Point

- Due to physiological uptake in the GE junction, prediction of response may be difficult on PET/CT at times.

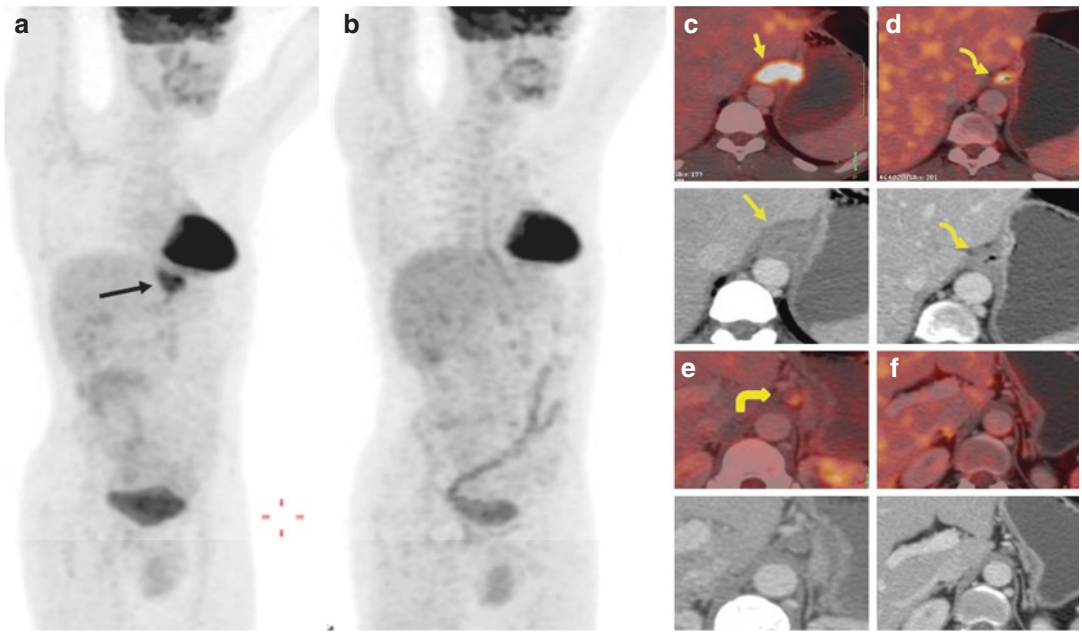

Fig. 15.13 (**a**, **c**, **e**) Staging scan: FDG-avid mass is noted in the distal esophagus extending into the gastroesophageal junction (arrow). 6-mm-sized FDG-avid gastrohepatic node is noted as E (block arrow). (**b**, **d**, **f**) Response assessment scan: Low-grade FDG uptake (curved arrow) with minimal soft-tissue thickening is noted in the GE junction. There is complete resolution of the gastrohepatic node

15.15 Case No. 14: Complete Response

Clinical Details 55 years' male, a case of poorly differentiated SCC of the middle and lower esophagus. Staging scan and Post NACT study (Fig. 15.14).

Interpretation Complete metabolic and morphologic response in the esophageal mass.

Teaching Point

- Demonstration of complete response.

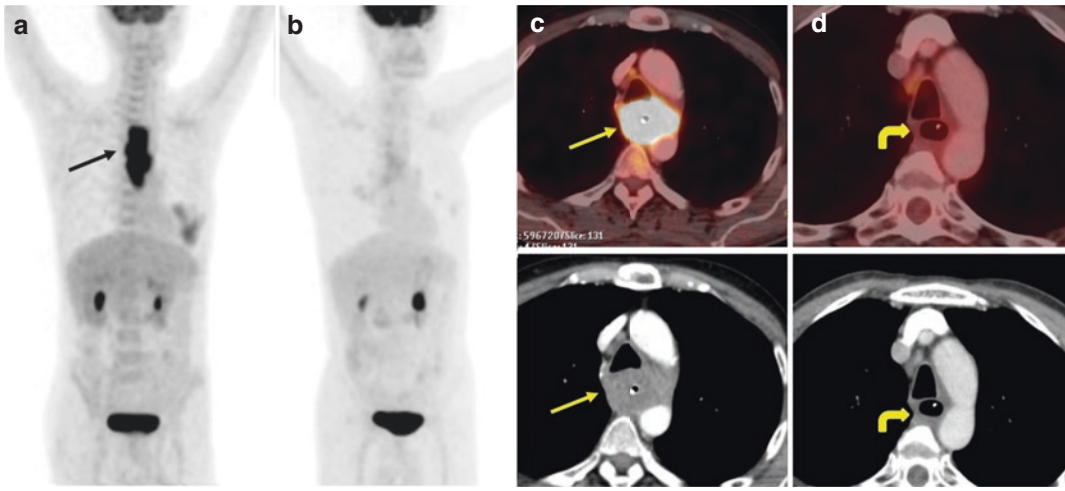

Fig. 15.14 (**a** and **c**) FDG-avid large mass in the mid and lower esophagus (arrow). Also noted is aspiration pneumonia in the lower lobe of left lung. (**b** and **d**) No FDG-avid mass in the esophagus (block arrow)

15.16 Case No. 15: Coexisting Malignancy and Granulomatous Infection

Clinical Details 48 years' male, a case of carcinoma of GE junction. Scan done at staging and post four cycles of NACT (Fig. 15.15).

Interpretation Partial response is seen in the primary. The right supraclavicular node is marginally increased in size after NACT. This node was biopsied which showed granulomatous infection. Tuberculosis is one of the commonest infections in this part of the world (India).

Teaching Point

- Malignancy and tuberculosis can coexist. SUVs do not help differentiate between the two. Biopsy is the way forward.

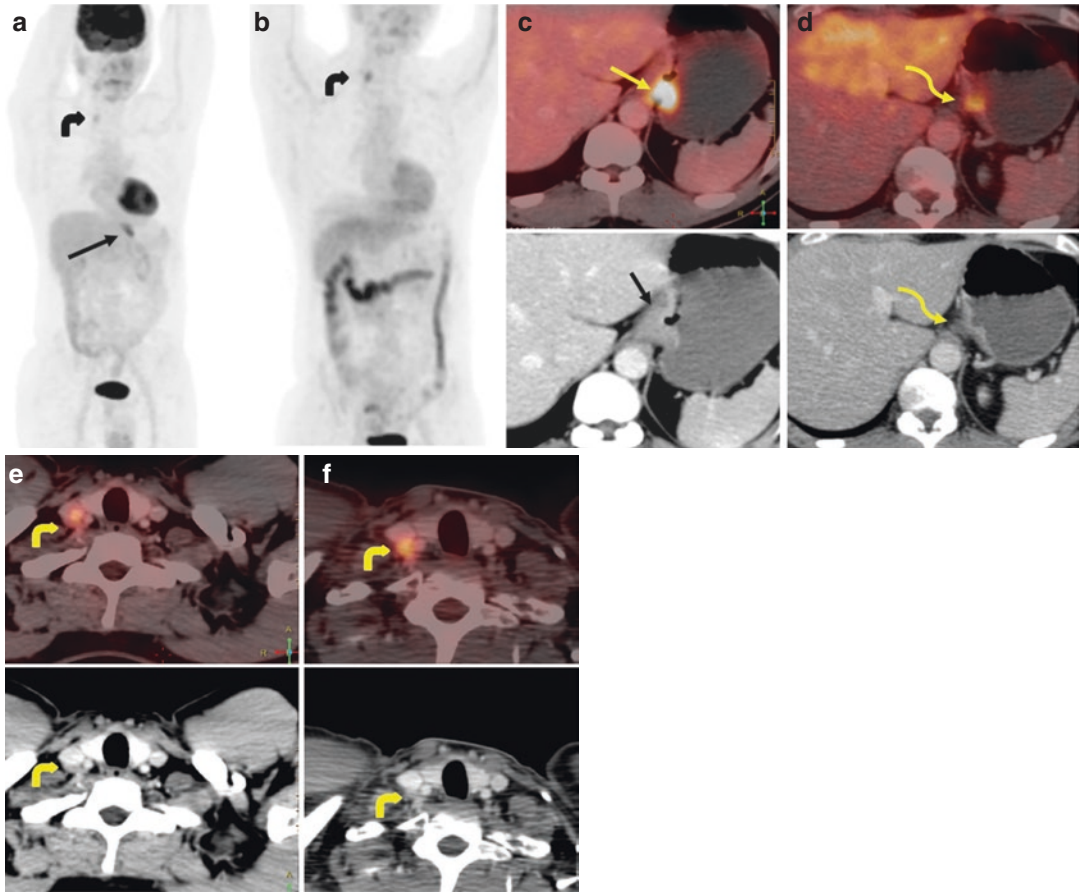

Fig. 15.15 (**a** and **c**) Staging scan: FDG-avid wall thickening is noted involving the GE junction and lesser curvature of stomach (arrow). (**b** and **d**) Post NACT response assessment scan: Significant decrease in the size and metabolic activity of the GE junction and lesser curvature of stomach mass (curved arrow). (**a**, **b**, **e**, **f**) FDG-avid right supraclavicular node is noted in both the staging (maxSUV 3.74) and post NACT scan (maxSUV 5.67) (block arrow). Though response is noted in the primary mass, there is increase in the size and metabolic activity of the right supraclavicular node

15.17 Case No. 16: Esophageal Primary with Coexisting Tuberculous Infection in the Lungs

Clinical Details 44 years old female, case of MDSCC. Received CTRT (Fig. 15.16).

Interpretation Metabolically active primary esophageal mass with coexisting tuberculosis involving the lungs. The patient was treated with CTRT and anti koch's therapy.

Teaching Point

- Tree-in-bud branching opacities are hallmark of infective etiology and should not be mistaken for metastatic disease.

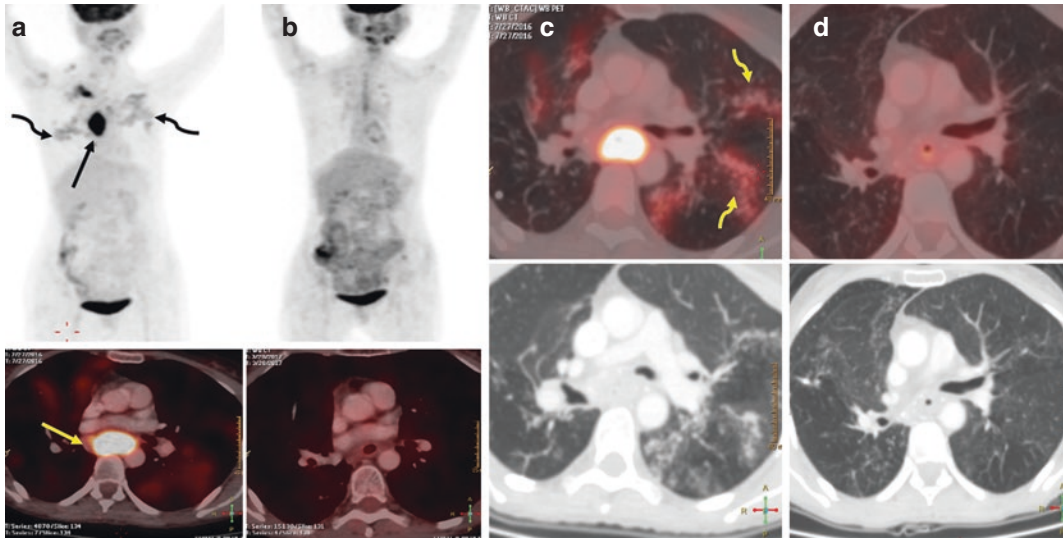

Fig. 15.16 (**a** and **c**) FDG-avid mass in the distal esophagus (arrow). Also seen are multiple branching tree-in-bud and nodular opacities in both the lungs (maxSUV 11.82) (curved arrow). (**b** and **d**) Complete response noted in the esophageal lesion as well as the lungs opacities

15.18 Case No. 17: GE Junction and Proximal Stomach Mass with Partial Response

Clinical Details 32 years, male with poorly differentiated adenocarcinoma of the GE junction and proximal stomach (Fig. 15.17).

Interpretation These findings are suggestive of partial response.

Teaching Point

- Demonstrate of partial response.

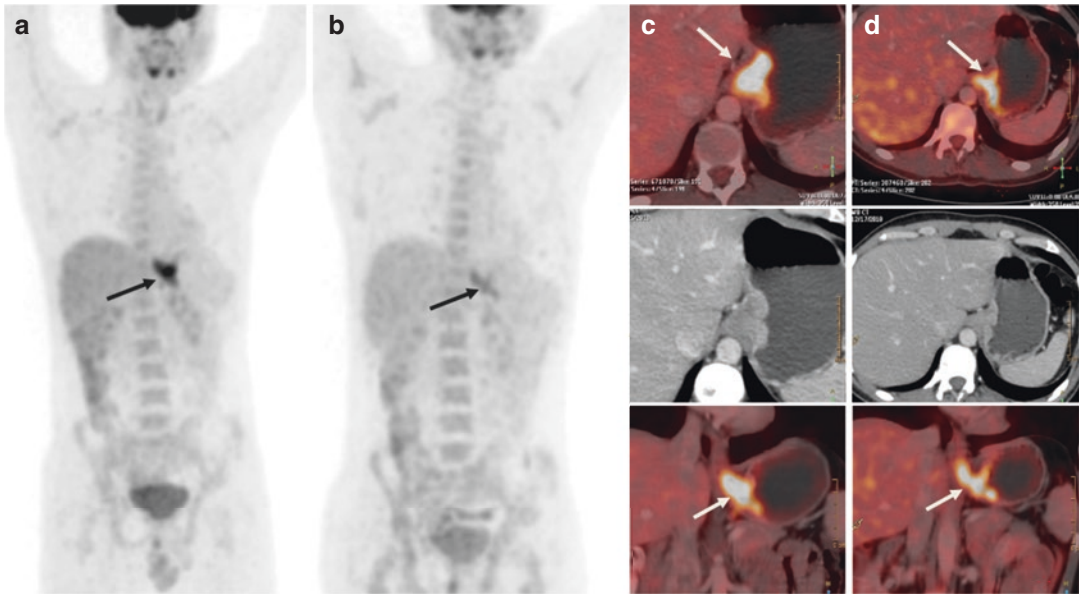

Fig. 15.17 (**a**, **c**) Staging scan: FDG-avid mass in the GE junction and proximal stomach (arrow). (**b**, **d**) Post three cycles of NACT: There is minimal decrease in soft-tissue thickening and metabolic activity of the GE junction and proximal stomach mass

15.19 Case No. 18: Complete Response in Esophageal Primary with Marrow Hyperstimulation Post Chemotherapy

Clinical Details 50 years' male, case of SCC of the middle esophagus. Staging and post two cycles of NACT scan (Fig. 15.18).

Interpretation Intense marrow uptake is due to post chemotherapy marrow hyperstimulation.

Teaching Point

- Marrow hyperstimulation is common after chemotherapy, may look intense and patchy at times, and should not be mistaken for disease involvement.

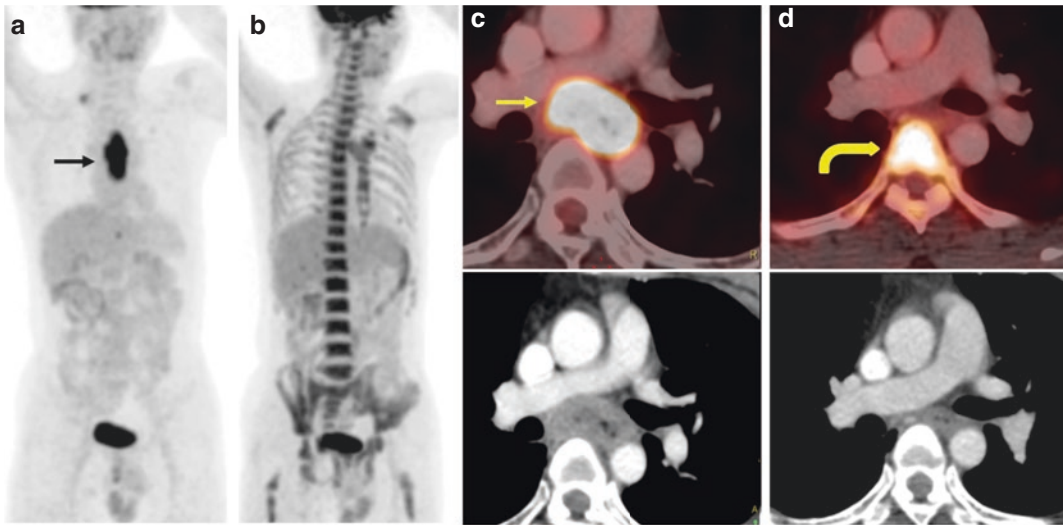

Fig. 15.18 (**a**, **c**) Staging scan: FDG-avid mass in the mid esophagus (arrow). (**b**, **d**) No FDG-avid mass is noted in the esophagus implying complete response post chemotherapy. Intense marrow uptake is noted in the axial and appendicular skeleton (block arrow)

15.20 Case No. 19: Progressive Disease

Clinical Details 65 years, male, case of SCC. Staging scan and Post CTRT scan (Fig. 15.19).

Interpretation Partial response in the primary lesion in the distal esophagus. Appearance of new hypermetabolic metastatic supraclavicular and para-aortic nodes. Biopsy from the supraclavicular node was consistent with metastases from squamous cell cancer.

Teaching Point

- Though the primary mass shows partial response, new metastatic disease lesions suggest disease progression.

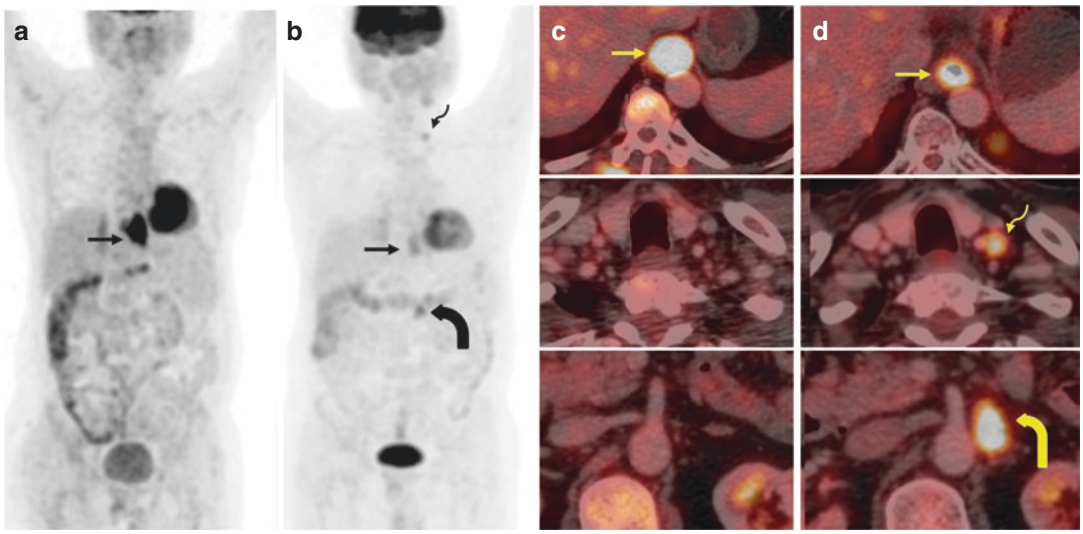

Fig. 15.19 (**a**, **c**) Staging scan: FDG-avid mass in the distal esophagus and GE junction (arrow). (**b**, **d**) Post CTRT scan: Decrease in size and metabolic activity of the esophageal mass (arrow). New metastatic left supraclavicular (curved arrow) and paraaortic nodes (curved block arrow) are noted

15.21 Case No. 20: Post TTE Recurrence

Clinical Details 43 years, male, case of SCC. Underwent TTE. Developed recurrent disease 2 years after the surgery (Fig. 15.20).

Interpretation Recurrent disease in the TO groove post TTE.

Teaching Points

- FDG PET has a sensitivity of 94% and specificity of 82% for detection of recurrent esophageal cancer.
- More than 50% of patients will develop recurrence within 3 years of definitive treatment.
- The prognosis of recurrent esophageal cancer is poor [23–25].

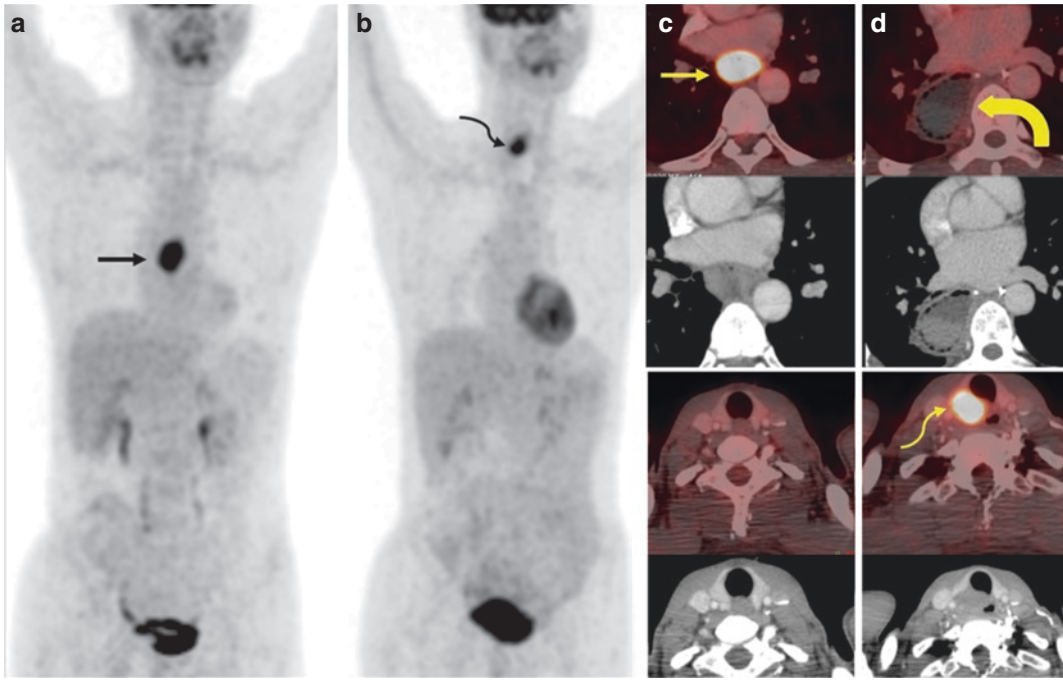

Fig. 15.20 (**a**, **c**) Staging scan: FDG-avid mass in the lower esophagus (arrow). (**b**, **d**) Scan done 2 years post TTE: FDG-avid mass is noted in the right tracheaesophageal (TO) groove (curved arrow), suggesting recurrent disease. The gastric pull-up is seen in **d** (block arrow)

15.22 Case No. 21: Recurrent Disease Post CTRT

Clinical Details 74 years male, case of MD SCC of the middle esophagus. 14 months post CTRT developed recurrence (Fig. 15.21).

Interpretation Recurrent disease in the lower esophagus after 14 months of completion of CTRT.

Teaching Points

- Recurrences are common after definitive CTRT.
- Approximately 40–60% of patients receiving definitive CTRT will develop locoregional recurrence. The treatment in this condition is usually salvage surgery [26].

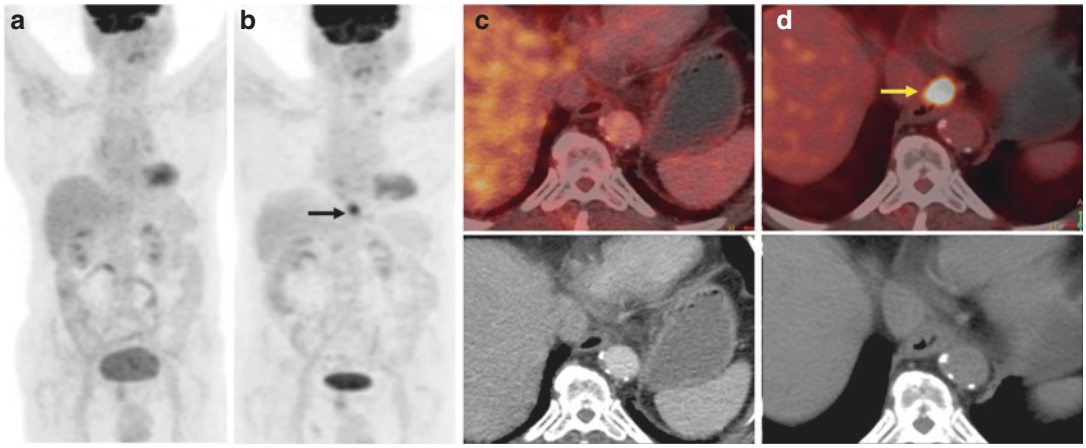

Fig. 15.21 (**a** and **c**) Post CTRT study: No metabolically active disease in the study. (**b** and **d**) On follow-up after 14 months of completion of CTRT: FDG-avid mass in the lower esophagus (arrow)

15.23 Case No. 22: Recurrence and Then Progressive Disease

Clinical Details 56 years male, case of SCC of mid and lower esophagus, and was treated with NACT and CTRT. Showed complete response. Developed recurrence, esophageal stenting was done with a self-expanding metallic tube (SEMS) for esophageal stricture. Six months later, the patient developed disease progression (Fig. 15.22).

Interpretation Recurrence post CTRT and then unequivocal disease progression.

Teaching Point

- Recurrences are common after definitive CTRT. Approximately 40–60% of patients receiving definitive CTRT will develop locoregional recurrence [26].

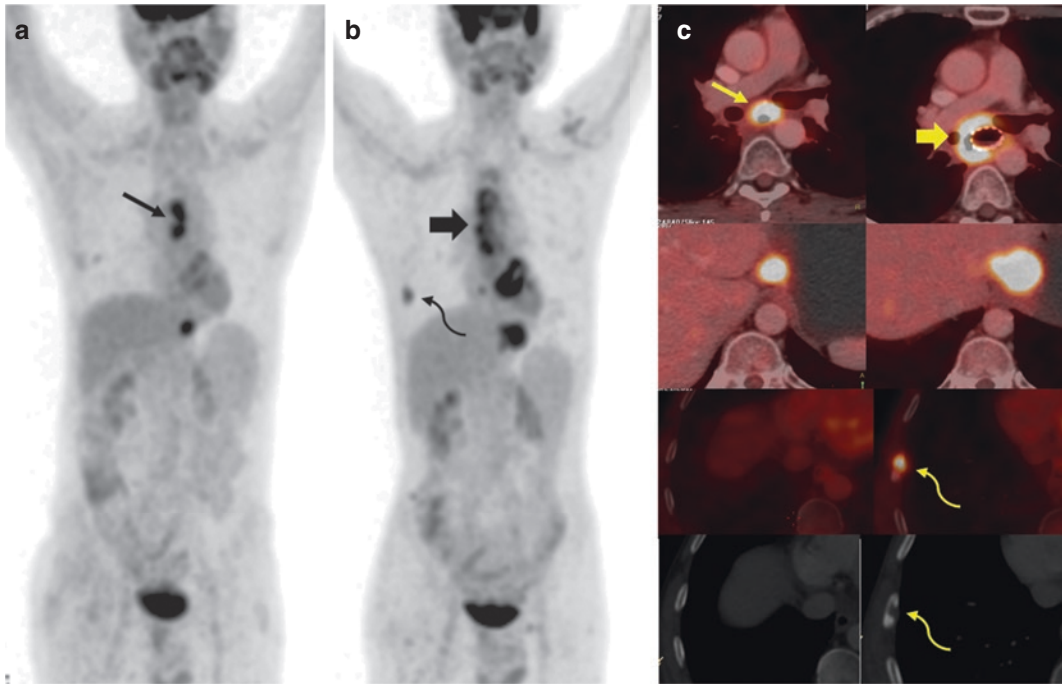

Fig. 15.22 (**a** and **c**) Post CTRT study: FDG-avid recurrent mass in the middle and lower esophagus (arrow). (**b** and **d**) Follow up study: Increase in extent and metabolic activity of the esophageal mass in the middle and lower esophagus around the esophageal stent (block arrow). Increase in size of the gastrohepatic node. New FDG-avid lytic lesion in the right seventh rib (curved arrow)

15.24 Case No. 23: Post CTRT Recurrence

Clinical Details 66 years, male, a case of SCC of mid third esophagus. Received CTRT and had complete response. Developed recurrent disease 6 months post CTRT (Fig. 15.23).

Interpretation Recurrent disease in the middle esophagus.

Teaching Point

- Recurrent disease after definitive treatment has poor prognosis. Salvage surgery may be considered if the disease is localized.

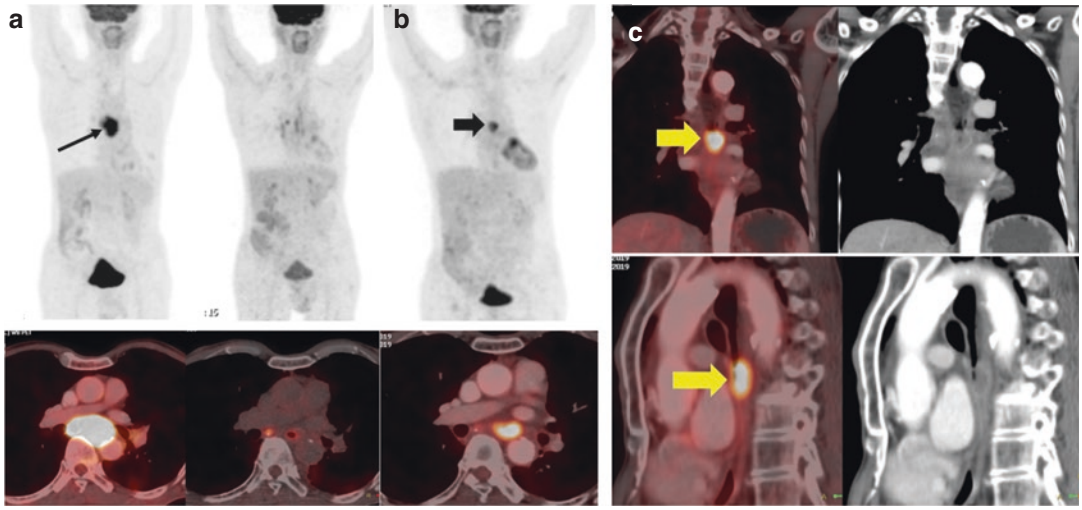

Fig. 15.23 (**a**) Staging scan: FDG-avid mass in the middle esophagus (arrow). (*Ai*) Post CTRT response scan: No FDG-avid mass in the esophagus, suggesting complete response. (**b** and **c**) Follow-up scan: FDG-avid mass in the middle esophagus (block arrow)

15.25 Case No. 24: Post TTE Metastatic Disease

Clinical Details 65-year-old lady, case of SCC of the esophagus. Received NACT and underwent TTE. Eight months post TTE developed metastatic disease (Fig. 15.24).

Interpretation The liver lesion is suggestive of metastatic disease. It was proven by biopsy.

Teaching Point

- Recurrences are common after curative esophagectomy. The survival of patients with metastatic disease in such scenarios is extremely poor.

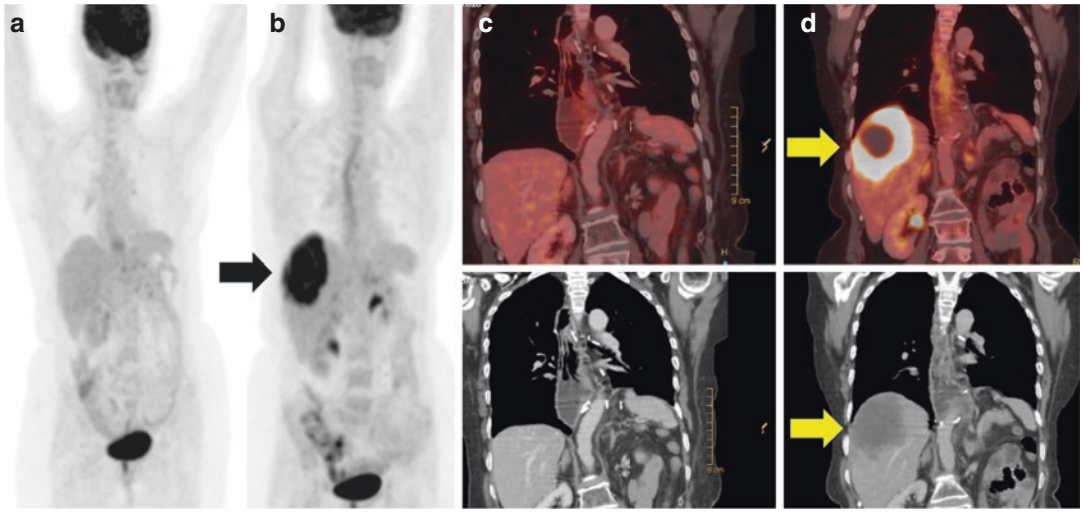

Fig. 15.24 (**a** and **c**) Scan done 2 months after TTE: No FDG-avid disease. Gastric pull-up is seen. (**b** and **d**) Large FDG-avid hypodense mass in the liver (block arrow)

15.26 Case No. 25: Adenocarcinoma Stomach with Complete Metabolic Response

Clinical Details 58-year-old lady, case of moderately differentiated adenocarcinoma involving the distal esophagus and proximal stomach. Received three cycles of NACT and underwent esophagogastrectomy (Fig. 15.25).

Interpretation There is complete metabolic response on the mass with residual morphological thickening in the lesser curvature.

Patient underwent surgery, the histopathology revealed only scanty dysplastic glands and no invasive carcinoma.

Teaching Point

- Of all imaging modalities, FDG PET/CT is the best for response assessment.

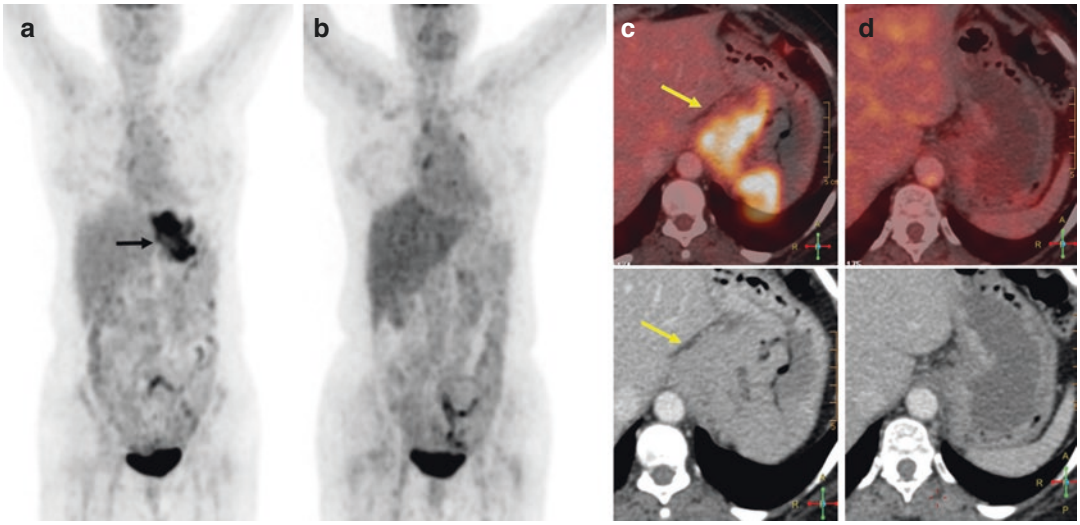

Fig. 15.25 (**a** and **c**) Staging scan: FDG-avid mass involving the lesser curvature of stomach and GE junction (arrow). (**b** and **d**) Complete metabolic and significant morphological response is noted the mass in the lesser curvature of stomach and GE junction

References

1. Siegel R, Naishadham D, Jemal A. Cancer statistics, 2012. CA Cancer J Clin. 2012;62:10–29.
2. Flanagan FL, Dehdashti F, Siegel BA, et al. Staging of esophageal cancer with 18F-fluorodeoxyglucose positron emission tomography. AJR Am J Roentgenol. 1997;168:417–24.
3. Ra J, Paulson EC, Kucharczuk J, et al. Postoperative mortality after esophagectomy for cancer: development of a preoperative risk prediction model. Ann Surg Oncol. 2008;15:1577–84.
4. Shah RD, Cassano AD, Neifeld JP. Neoadjuvant therapy for esophageal cancer. World J Gastrointest Oncol. 2014;6(10):403–6.
5. Swisher SG, Maish M, Erasmus JJ, Correa AM, Ajani JA, Bresalier R, Komaki R, Macapinlac H, Munden RF, Putnam JB, Rice D, Smythe WR, Vaporciyan AA, Walsh GL, Wu TT, Roth JA. Utility of PET, CT, and EUS to identify pathologic responders in esophageal cancer. Ann Thorac Surg. 2004;78(4):1152–60; discussion 1152–60. Review.
6. Bakheet SM, Saleem M, Powe J, et al. F-18 fluorodeoxyglucose chest uptake in lung inflammation, and infection. Clin Nucl Med. 2000;25:273–8.
7. Weber WA, Ott K, Becker K, et al. Prediction of response to preoperative chemotherapy in adenocarcinomas of the esophagogastric junction by metabolic imaging. J Clin Oncol. 2001;19:3058–65.
8. Van Hagen P, Hulshof MC, van Lanschot JJ, et al. Preoperative chemoradiotherapy for esophageal or junctional cancer. N Engl J Med. 2012;366(22):2074–84.
9. Shapiro J, van Lanschot JJB, Hulshof MCCM, et al. Neoadjuvant chemoradiotherapy plus surgery versus surgery alone for oesophageal or junctional cancer (CROSS): long-term results of a randomized controlled trial. Lancet Oncol. 2015;16(9):1090–8.
10. Van Hagen P, Wijnhoven BP, Nafteux P, et al. Recurrence pattern in patients with a pathologically complete response after neoadjuvant chemoradiotherapy and surgery for oesophageal cancer. Br J Surg. 2013;100(2):267–73.
11. Zanoni A, Verlato G, Giacopuzzi S, et al. Neoadjuvant concurrent chemoradiotherapy for locally advanced esophageal cancer in a single high-volume center. Ann Surg Oncol. 2013;20(6):1993–9.
12. Beukinga RJ, Hulshoff JB, Mul VEM, Noordzij W, Kats-Ugurlu G, Slart RHJA, Plukker JTM. Prediction of response to Neoadjuvant chemotherapy and radiation therapy with baseline and restaging (18)F-FDG PET imaging biomarkers in patients with esophageal Cancer. Radiology. 2018;287(3):983–92.
13. Urschel JD, Vasan H. A meta-analysis of randomized controlled trials that compared neoadjuvant chemoradiation and surgery to surgery alone for resectable esophageal cancer. Am J Surg. 2003;185:538–43.
14. Fiorica F, Di Bona D, Schepis F, et al. Preoperative chemoradiotherapy for oesophageal cancer: a systematic review and meta-analysis. Gut. 2004;53:925–30.
15. Seol KH, Lee JE. PET/CT planning during chemoradiotherapy for esophageal cancer. Radiat Oncol J. 2014;32(1):31–42.
16. Bhargava P, Reich P, Alavi A, et al. Radiation-induced esophagitis on FDG PET imaging. Clin Nucl Med. 2003;28:849–50.
17. Choi YW, Munden RF, Erasmus JJ, Park KJ, Chung WK, Jeon SC, Park CK. Effects of radiation therapy on the lung: radiologic appearances and differential diagnosis. Radiographics. 2004;24(4):985–97; discussion 998. Review.
18. Demirev AK, Kostadinova ID, Gabrovski IR. (18) F-FDG PET/CT in patients with parenchymal changes attributed to radiation pneumonitis. Mol Imaging Radionucl Ther. 2018;27(3):107–12.
19. Kim TJ, Lee KH, Kim YH, Sung SW, Jheon S, Cho SK, Lee KW. Postoperative imaging of esophageal cancer: what chest radiologists need to know. Radiographics. 2007;27(2):409–29. Review
20. Giménez A, Franquet T, Erasmus JJ, Martínez S, Estrada P. Thoracic complications of esophageal disorders. Radiographics. 2002;22:S247–58. Review.
21. Gschossmann JM, Bonner JA, Foote RL, Shaw EG, Martenson JA Jr, Su J. Malignant tracheoesophageal fistula in patients with esophageal cancer. Cancer. 1993;72(5):1513–21.
22. Bruzzi JF, Munden RF, Truong MT, Marom EM, Sabloff BS, Gladish GW, Iyer RB, Pan TS, Macapinlac HA, Erasmus JJ. PET/CT of esophageal cancer: its role in clinical management. Radiographics. 2007;27(6):1635–52. Review.
23. Flamen P, Lerut A, Van Cutsem E, et al. The utility of positron emission tomography for the diagnosis and staging of recurrent esophageal cancer. J Thorac Cardiovasc Surg. 2000;120:1085–92.
24. Dresner SM, Griffin SM. Pattern of recurrence following radical oesophagectomy with two-field lymphadenectomy. Br J Surg. 2000;87:1426–33.
25. Mariette C, Balon JM, Piessen G, Fabre S, Van Seuningen I, Triboulet JP. Pattern of recurrence following complete resection of esophageal carcinoma and factors predictive of recurrent disease. Cancer. 2003;97:1616–23.
26. Pennathur A, Gibson MK, Jobe BA, Luketich JD. Oesophageal carcinoma. Lancet. 2013;381:400–12.

16 PET-CT in Treatment Response Evaluation in Lymphoma

Thomas Wagner

16.1 Introduction

FDG PET/CT is now the main imaging tool to assess response to treatment in avid lymphoma. Its value is highest at the end of treatment and the degree of uptake at the end of treatment correlates with survival. Interim assessment is being used more and more and is particularly useful in patients with Hodgkin lymphoma. Research is now focusing on quantitative measures to define prognosis at initial staging and in assessment of response at interim. A number of clinical trials are using FDG PET/CT-guided therapy with the degree of response on the interim scan determining the course of treatment. These clinical trials are looking at escalating treatment in poor responders with poor prognosis to improve survival; and at de-escalating treatment in good responders with good prognosis to reduce side effects of treatment. It is now essential for Nuclear Medicine physicians and radiologists to be familiar with the Deauville score, a visual tool to assess the degree of uptake, and with various clinical scenarios and imaging findings in patients with lymphoma (Figs. 16.1, 16.2, and 16.3). This chapter presents common findings in assessment of response in lymphoma patients.

T. Wagner (✉)
Department of Nuclear Medicine, Royal Free London NHS Foundation Trust, London, UK
e-mail: thomas.wagner@nhs.net

S. Fanti et al. (eds.), *Atlas of Clinical PET-CT in Treatment Response Evaluation in Oncology*,
https://doi.org/10.1007/978-3-030-68858-5_16

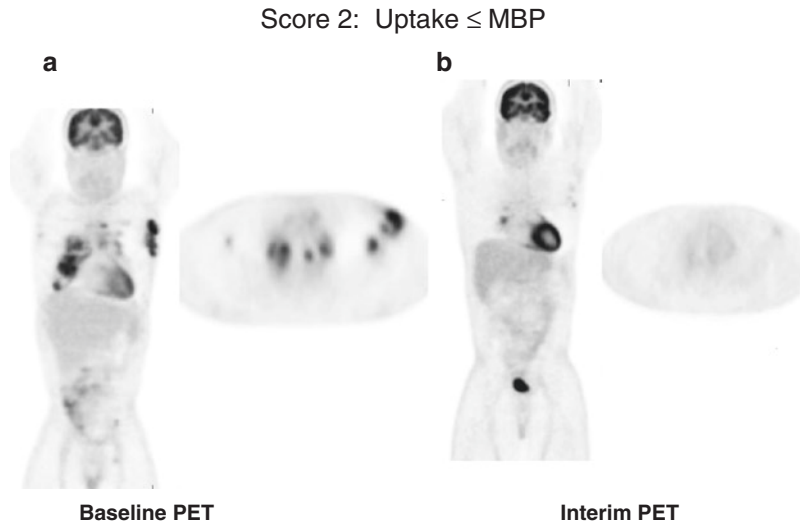

Fig. 16.1 Score 2: Uptake ≤ MBP. FDG PET scan: (**a**) Baseline and (**b**) Interim PET

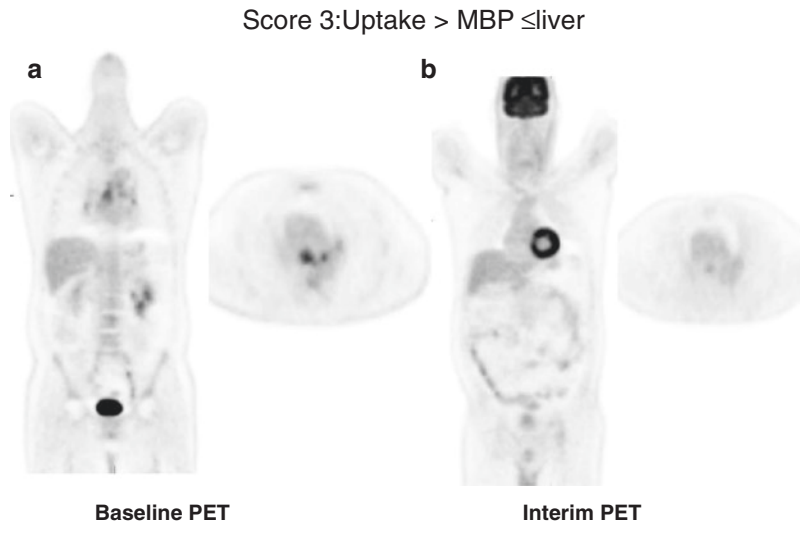

Fig. 16.2 Score 3: Uptake > MBP ≤ liver. FDG PET scan: (**a**) Baseline and (**b**) Interim PET

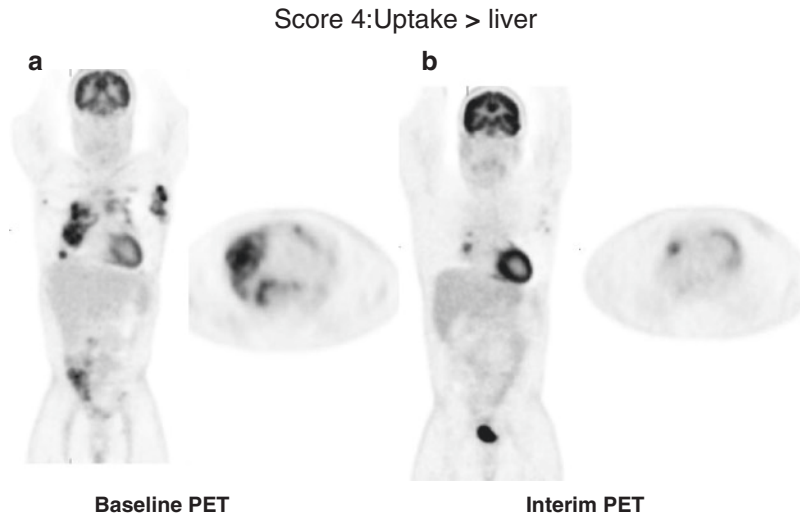

Fig. 16.3 Score 4: Uptake > liver. FDG PET scan: (**a**) Baseline and (**b**) Interim PET

16.2 Case 1 (Fig. 16.4)

Teaching point:

– It is important to locate the smaller nodes post-treatment and measure their uptake against liver background and mediastinal blood pool (Table 16.1).

Table 16.1 Interim PET criteria

Score	PET-CT scan result
1	No uptake above background
2	Uptake ≤ mediastinum
3	Uptake > mediastinum but ≤ liver
4	Uptake moderately increased compared to the liver at any site
5	Uptake markedly increased compared to the liver at any site
X	New areas of uptake unlikely to be related to lymphoma

Deauville criteria = Five-point scale

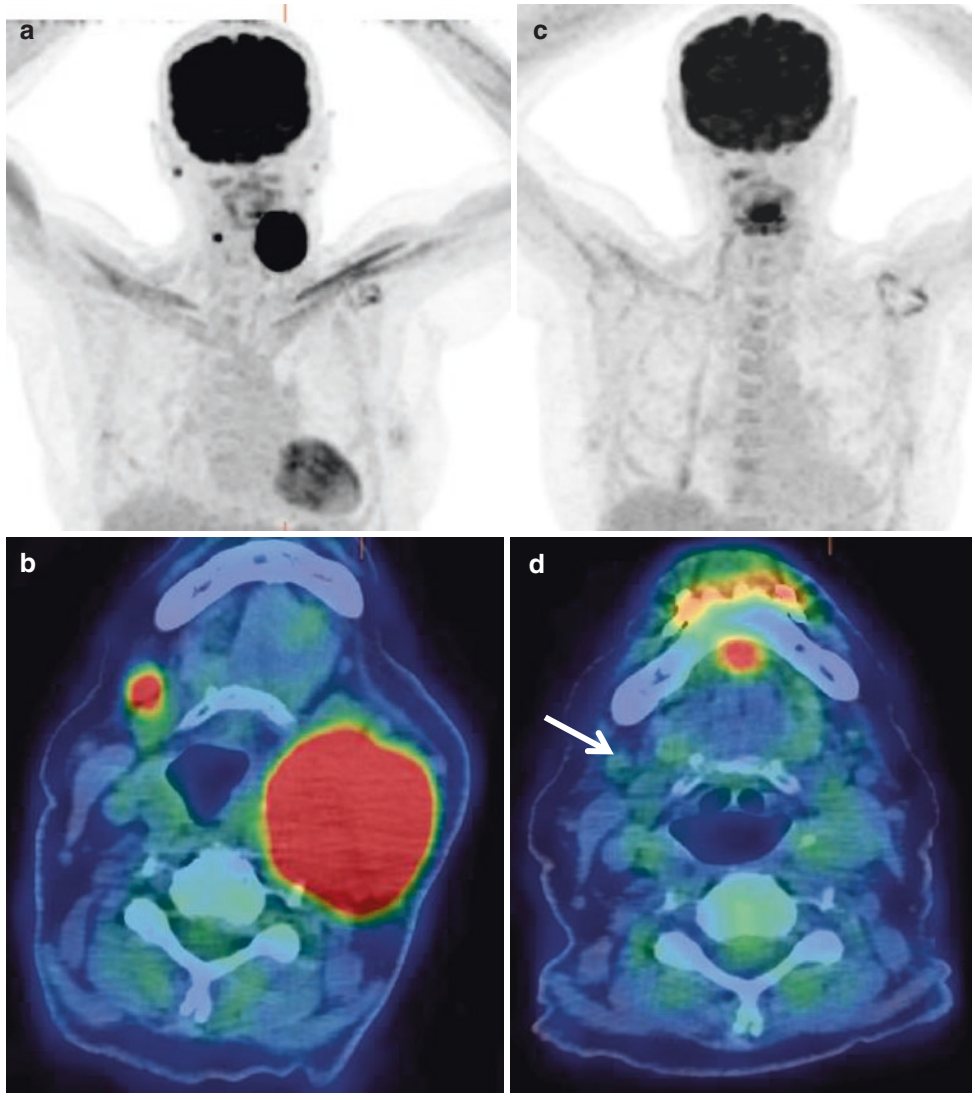

Fig. 16.4 An 83-year-old female presented with DLBCL stage IIA. 18F-FDG Baseline PET/CT scan shows intense uptake in enlarged left submandibular nodal mass and intense uptake in small right submandibular node (**a**, **b**). End of treatment scan demonstrates complete metabolic response of the left submandibular nodal mass and residual low-grade uptake in the right submandibular node, greater than mediastinal blood pool and less than liver background (**c**, **d**). Complete metabolic response, Deauville 3 in right submandibular node

16.3 Case 2 (Fig. 16.5)

Teaching point:

– Intensity of uptake can be variable in low-grade B cell lymphomas but most will show avidity and FDG PET/CT can be used for staging and response assessment.

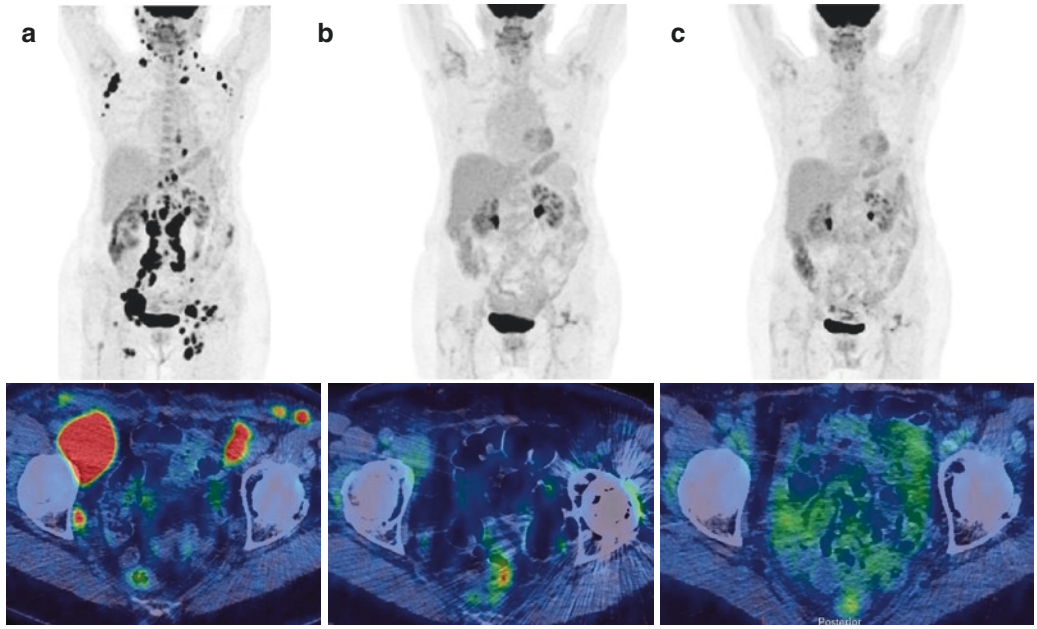

Fig. 16.5 A 73-year-old female presented with marginal zone lymphoma stage 3A. 18F-FDG Baseline PET/CT scan (**a**) showed intense uptake in nodes above and below the diaphragm. Interim PET (**b**) showed complete metabolic response, Deauville 3. End of treatment PET (**c**) showed further reduction in size, Deauville 3

16.4 Case 3 (Fig. 16.6)

Teaching points:

- Intensely avid bone lesion can become cold after treatment as normal bone marrow cells are initially replaced by lymphoma and then by fibrotic tissue after treatment.
- Post-GCSF PET shows diffuse moderate to intense uptake in the bone marrow and in the spleen.

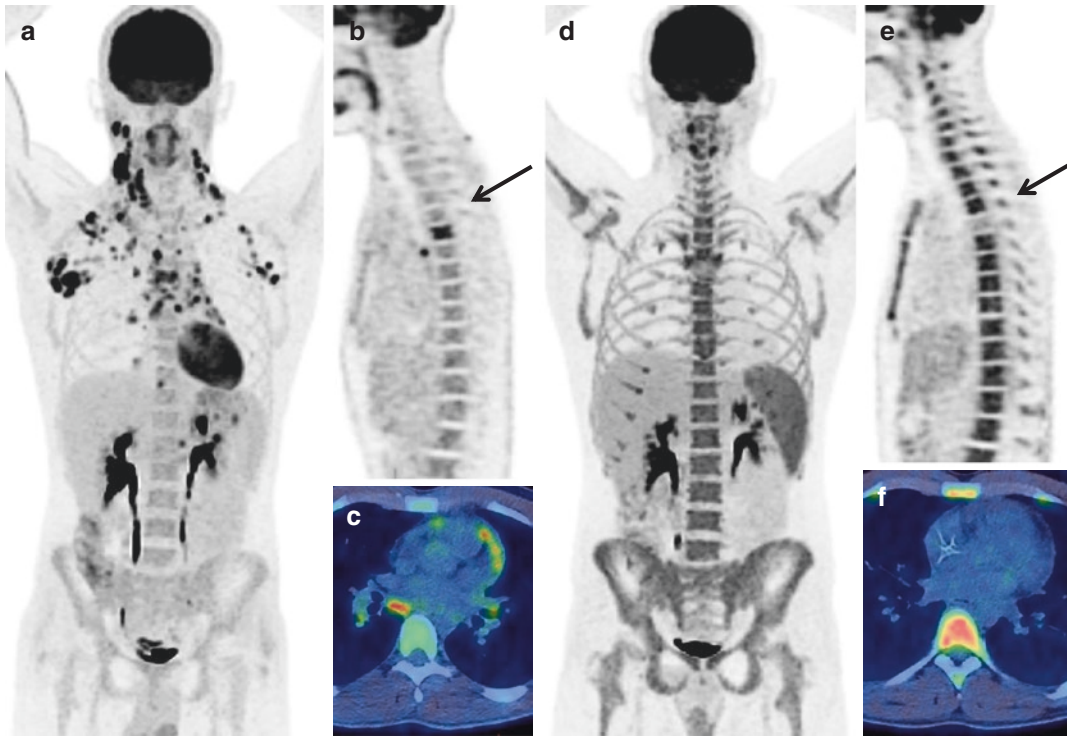

Fig. 16.6 A 23-year-old male presented with hodgkin lymphoma stage IV. 18F-FDG PET/CT. (**a**) Involving T5 (**b**) and the pericardium (**c**). Interim PET (**d, f**) showed complete metabolic response. Post-GCSF finding with diffuse intense BM and splenic uptake on interim PET (**d**). Mirror image of T5 lesion post-treatment (**b**, **e**, arrows). Complete metabolic response of abnormal pericardial uptake

16.5 Case 4 (Fig. 16.7)

Teaching points:

- Brown fat uptake is a common finding which can make interpretation difficult in patients with lymphoma as the areas of brown fat uptake are close to areas where there can be enlarged and avid nodes, especially in the neck. Good knowledge of the many variants of brown fat uptake and good correlation with CT findings are essential.
- Large masses can remain after treatment and show low-grade uptake.

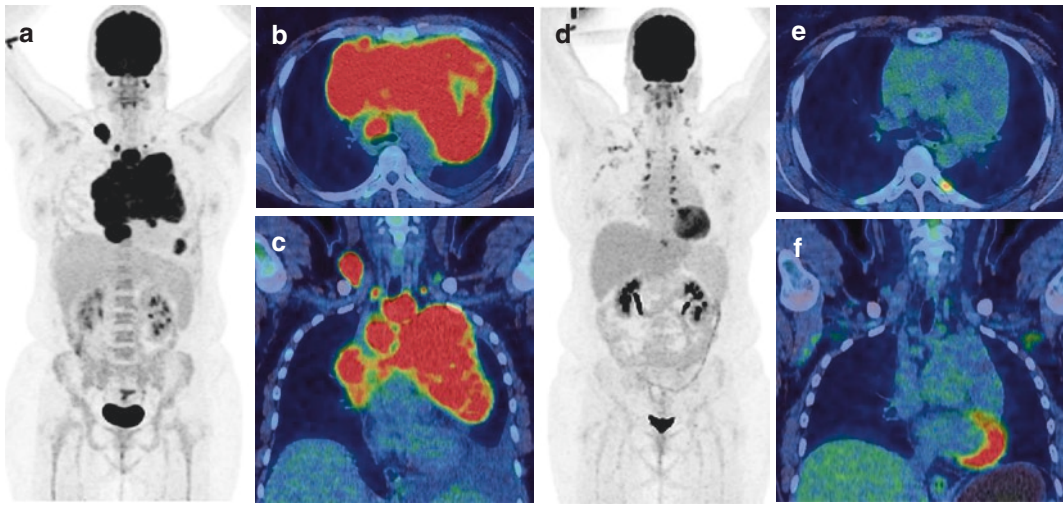

Fig. 16.7 A 42-year-old female presented with hodgkin lymphoma stage 2 with bulky disease with a maximum diameter of 18 cm. 18F-FDG PET/CT staging scan shows a large intensely avid anterior mediastinal mass (**a–c**). Interim PET post two cycles of ABVD shows as residual large mass of 11 cm of maximal diameter with uptake greater than mediastinal blood pool and less than liver background, Deauville 3, in keeping with complete metabolic response (**d–f**). Note the brown fat uptake on MIP and transaxial view with a typical distribution of posterior neck, axillae and costovertebral regions

16.6 Case 5 (Fig. 16.8)

Teaching points:

– High-grade transformation is a complication of low-grade lymphoma. It is suspected when uptake is particularly intense, there is rapidly progressive disease or there is extranodal involvement.

– Post-pleurodesis there is intense uptake in areas of high-density material in the pleura. This can persist for many years. PET appearances are very similar to mesothelioma and careful correlation with clinical history and CT findings is very important.

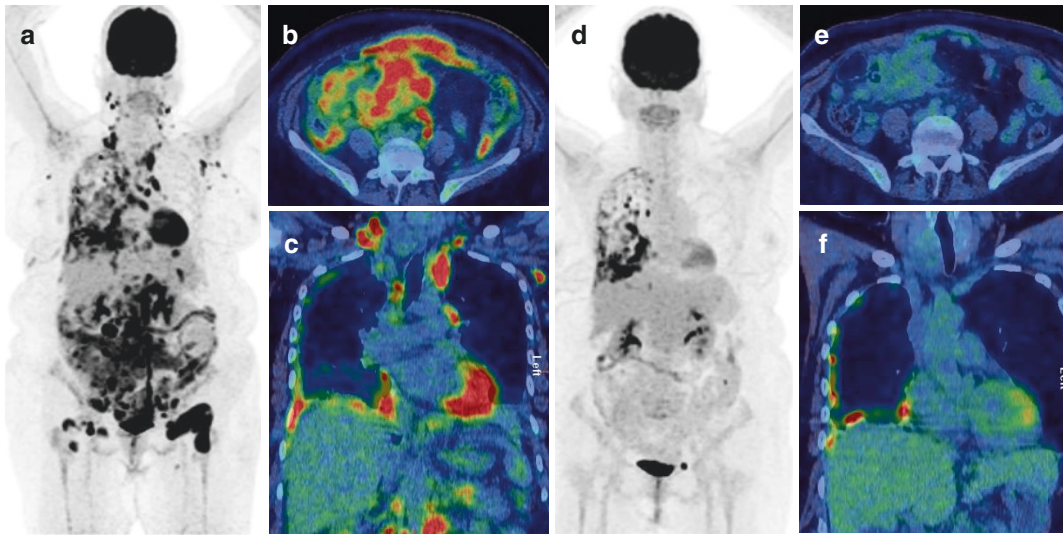

Fig. 16.8 Case 5: A 61-year-old female presented with ffollicular lymphoma stage IVB with suspicion of high-grade transformation, not biopsy proven. Staging 18F-FDG PET/CT shows extensive disseminated large volume disease with bone marrow, small bowel and right pleural involvement with nodal disease above and below the diaphragm and a mesenteric mass (**a–c**). End of treatment PET after six cycles of G-CHOP shows complete metabolic response, Deauville 3. Residual uptake in the mesenteric mass is greater than mediastinal blood pool and less than liver background (**d–f**). Pleural involvement was proven with VATS and pleurodesis was performed. Note residual intense heterogeneous uptake in the right pleura with areas of high density in keeping with previous pleurodesis

16.7 Case 6 (Fig. 16.9)

Teaching point:

– Diffuse intense uptake in the thyroid usually related to thyroiditis.

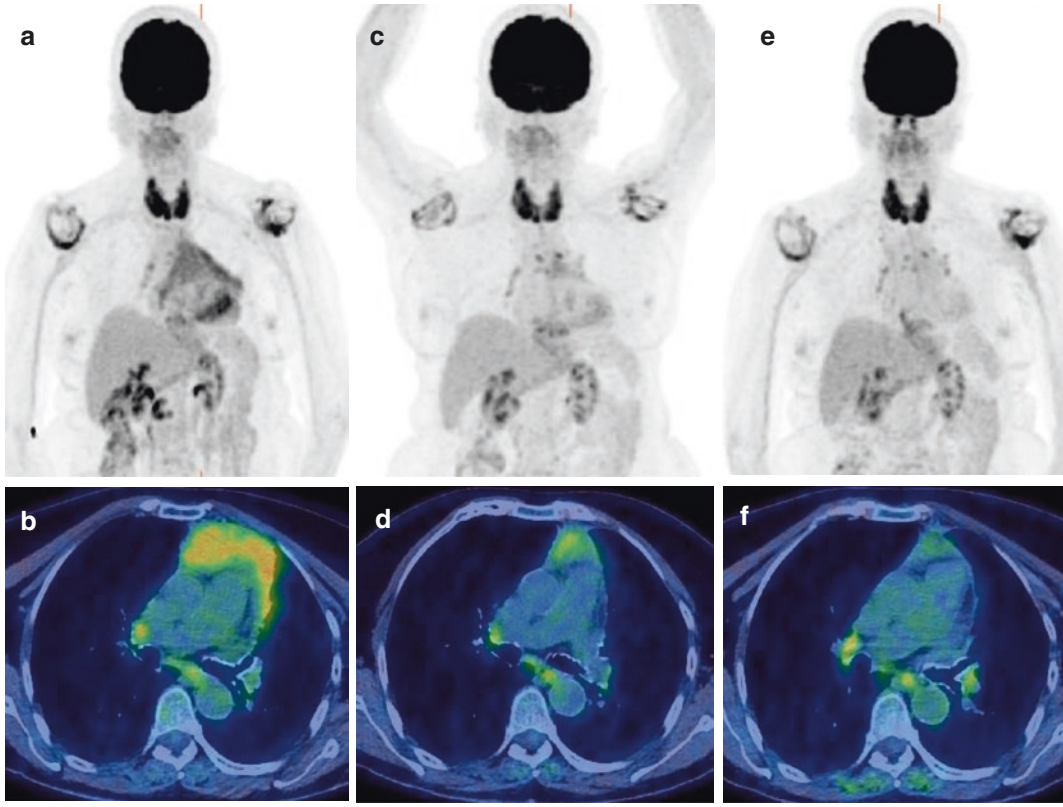

Fig. 16.9 A 78-year-old female presented with marginal zone lymphoma. Staging 18F-FDG PET/CT shows moderate diffuse uptake in an anterior mediastinal mass (**a**, **b**). Interim PET shows partial metabolic response with a decrease in size and intensity of uptake and residual uptake greater than liver background, Deauville 4 (**c**, **d**). End of treatment PET (**e**, **f**) shows further reduction in size and intensity of uptake. Uptake is less than liver background, Deauville 3, consistent with complete metabolic response. Note diffuse persistent stable intense thyroid uptake and shoulder uptake, unrelated and likely representing thyroiditis and inflammatory changes in the shoulder joints

16.8 Case 7 (Fig. 16.10)

Teaching point:

– Bowel perforation is a rare and serious complication of treatment in patients with large volume bowel involvement.

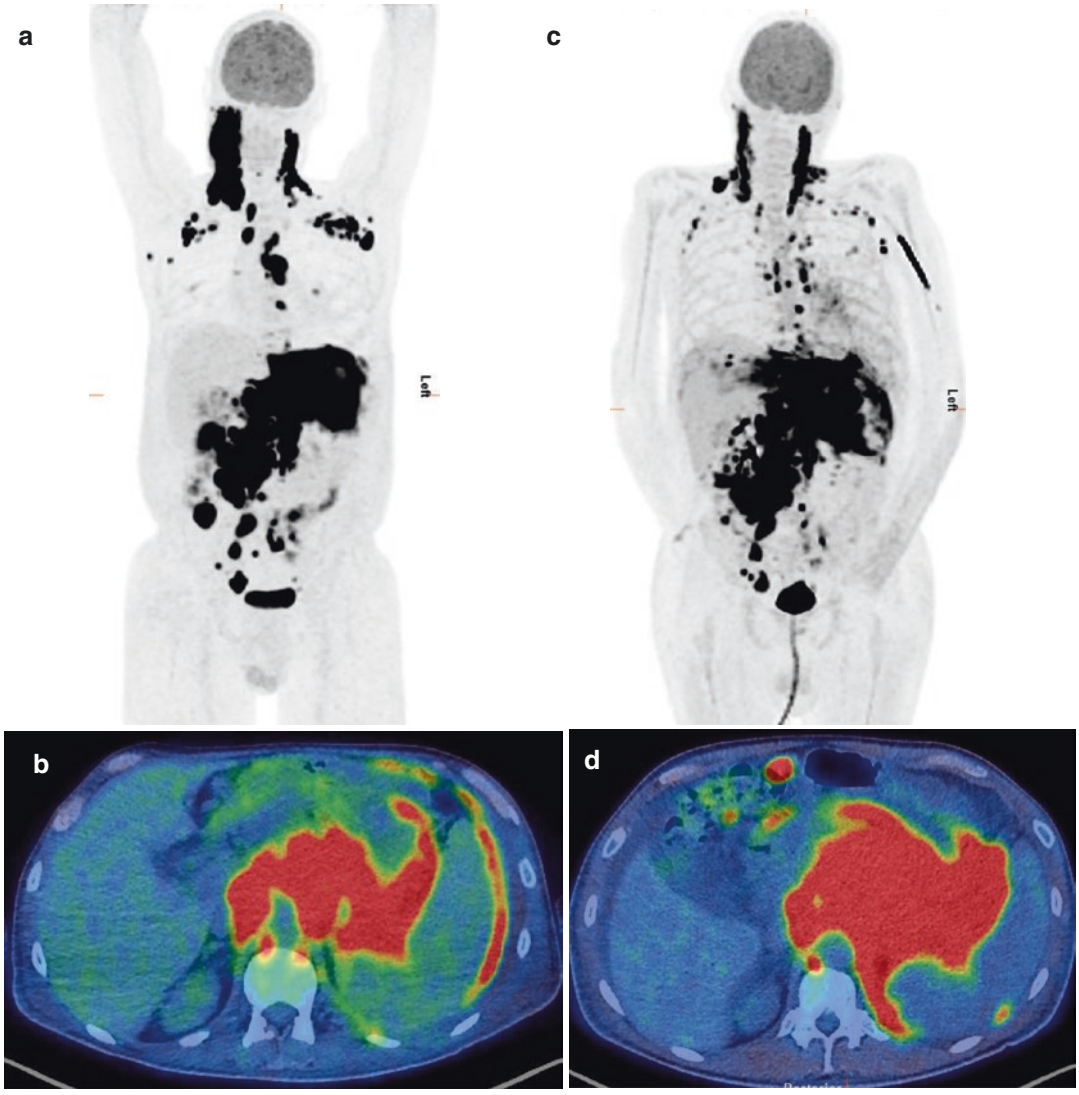

Fig. 16.10 A 61-year-old male presented with DLBCL stage IV. Staging 18F-FDG PET/CT demonstrates multiple extranodal sites of disease: small bowel, stomach, pancreas, left adrenal (**a**, **b**). The patient had bowel perforation following first cycle of chemotherapy. PET for response assessment post three cycles of R mini CHOP shows intensely residual avid large volume disease, Deauville 5 (**c**, **d**)

16.9 Case 8 (Fig. 16.11)

Teaching points:

– In patients being treated for multiple malignancies, it is important to understand the treatments of the malignancies and the natural course of disease.
– In this patient there is partial response to chemotherapy in the lymphoma-related lesions and stable disease in the lung metastases from the thyroid malignancy.

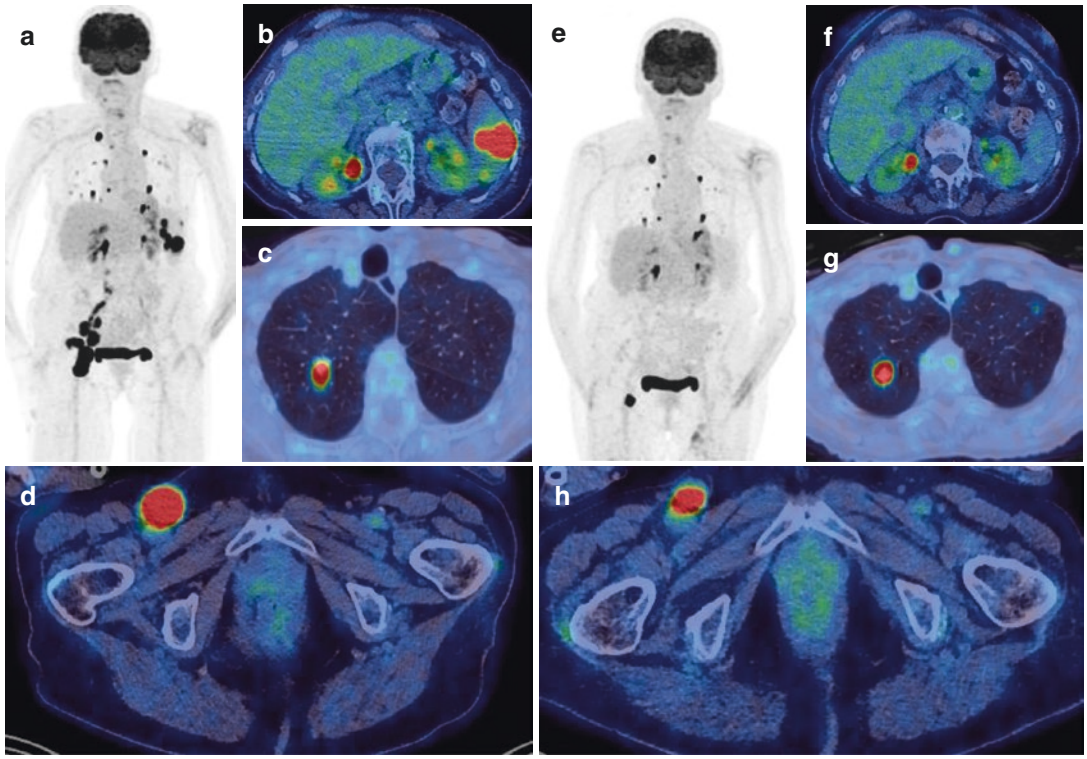

Fig. 16.11 An 84-year-old female presented with DLBCL stage II with splenic involvement. Staging 18F-FDG PET/CT shows intense uptake in the spleen and in an enlarged right inguinal node. Intensely avid lung metastases are seen related to metastatic thyroid cancer (**a–d**).End of treatment PET after six cycles of R-miniCHOP demonstrates residual intense uptake in the right inguinal node which has decreased in size, Deauville 5. Complete metabolic response in the splenic lesion. Stable intensely avid lung metastases from thyroid cancer (**e–h**)

Suggested Reading

Introduction

Barrington SF, Kluge R. FDG PET for therapy monitoring in Hodgkin and non-Hodgkin lymphomas. Eur J Nucl Med Mol Imaging. 2017;44:97–110. https://doi.org/10.1007/s00259-017-3690-8.

Case 1

Barrington SF, Kluge R. FDG PET for therapy monitoring in Hodgkin and non-Hodgkin lymphomas. Eur J Nucl Med Mol Imaging. 2017;44(Suppl 1):97–110. https://doi.org/10.1007/s00259-017-3690-8.

Barrington SF, Mikhaeel NG, Kostakoglu L, Meignan M, Hutchings M, Müeller SP, Schwartz LH, Zucca E, Fisher RI, Trotman J, Hoekstra OS, Hicks RJ, O'Doherty MJ, Hustinx R, Biggi A, Cheson BD. Role of Imaging in the staging and response assessment of lymphoma: consensus of the International Conference on Malignant Lymphomas Imaging Working Group. J Clin Oncol. 2014;32(27):3048–58.

Cheson BD, Fisher RI, Barrington SF, Cavalli F, Schwartz LH, Zucca E, Lister TA. Recommendations for initial evaluation, staging, and response assessment of hodgkin and non-Hodgkin lymphoma: The Lugano classification. J Clin Oncol. 2014;32(27):3059–67.

17 ^{18}F-FDG PET/CT in Treatment Response Evaluation: Breast Cancer

Joan Duch Renom

17.1 Introduction

Since 1989, when Minn and Soini were the first authors to study breast cancer patients with FDG PET, the technique has been widely used for staging, monitoring therapy response, and relapse of breast cancer.

There are some components of tumor biology that are related to FDG uptake, and the following ones are related to a higher FDG uptake: Invasive ductal breast carcinoma, triple-negative breast cancer, primary grade 3 carcinomas, and high Ki-67.

Early-stage breast cancer patients do not benefit from FDG PET/CT, and the technique has demonstrated poor overall sensitivity for the detection of axillary nodal metastases (surgical sampling by sentinel lymph node biopsy remains the method of choice for staging the axilla).

But the technique can reveal additional N3 nodal disease (infra-supraclavicular or internal mammary nodes) not usually diagnosed by the rest of techniques, and this finding leads to a change in therapeutic decisions. Moreover, with metastatic disease, FDG PET/TC has better sensitivity and specificity than conventional imaging (especially useful in locally advanced breast cancer, associated with a higher rate of distant metastases).

Identifying early responder patients in neoadjuvant treatment is important, and FDG PET/CT is useful in imaging therapy response, as changes in FDG metabolism often precede morphologic changes in tumor.

The technique is also useful for identifying the site of relapse, especially when traditional imaging methods are equivocal, and for confirming isolated locoregional relapse or isolated metastatic lesions.

FDG PET/CT has become a standard modality for initial staging of advanced local breast cancer, evaluation of treatment response, and in detection of disease recurrence.

J. D. Renom (✉)
Department of Nuclear Medicine, Hospital de la Santa Creu i Sant Pau, Barcelona, Spain
e-mail: jduchr@santpau.cat

S. Fanti et al. (eds.), *Atlas of Clinical PET-CT in Treatment Response Evaluation in Oncology*,
https://doi.org/10.1007/978-3-030-68858-5_17

17.2 Clinical Examples

17.2.1 Case 1: Staging of Locally Advanced Breast Cancer

Clinical details: Staging of locally advanced breast cancer in a 56-year-old woman. Breast MRI showed a multifocal lesion of 30 × 50 mm in right upper outer quadrant, with some axillary lymph nodes (Fig. 17.1).

Teaching points:

- Knowledge of the distribution of metabolic activity of the disease can improve the accuracy for a better staging, compared to other techniques.
- PET/CT could diagnose pathologic adenopathies with normal size, or located outside the field of MRI technique.

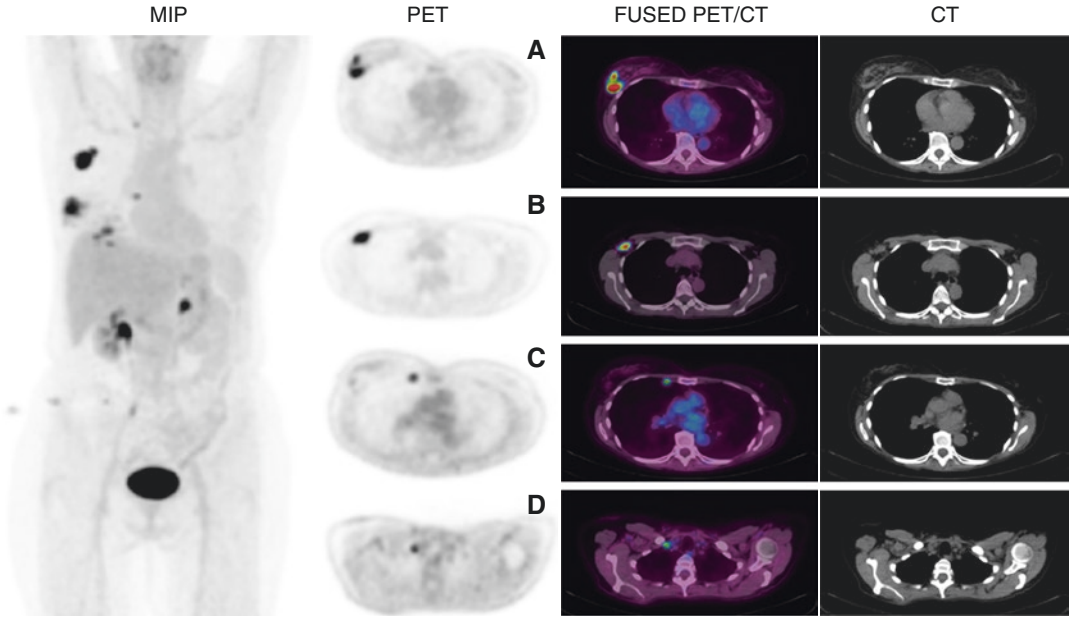

Fig. 17.1 Scan findings: Right breast multicentric lesions with abnormal FDG uptake (SUVmax 12), located in outer quadrants (row A), associated with ipsilateral axillary adenopathies (row B), internal mammary chain adenopathies (row C), and supraclavicular adenopathies and (row D)

17.2.2 Case 2: Staging Metastatic Breast Cancer

Clinical details: Staging of breast cancer in a 49-year-old woman. Breast MRI showed left 26 × 15 mm lesion in upper inner quadrant and some ipsilateral axillary adenopathies (Fig. 17.2).

Teaching points:

- FDG PET/CT is useful for staging locally advanced breast cancer, in order to detect non suspected metastatic lesions.
- The technique has better accuracy than conventional imaging techniques in metastatic disease.

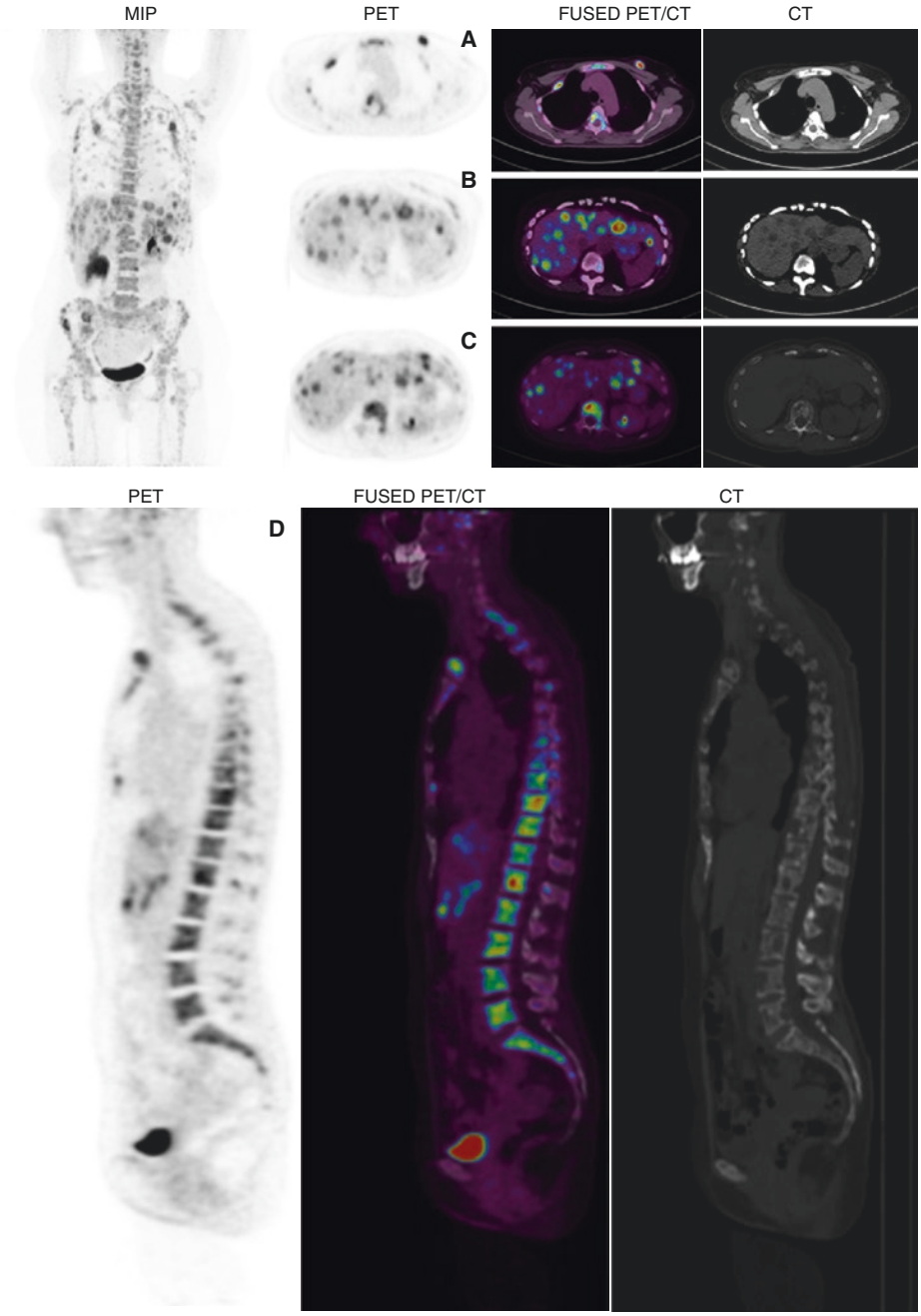

Fig. 17.2 Scan findings: Left breast lesion with increased FDG uptake (row A), axillary lymph node adenopathies and multiple liver (row B), and bone metastasis (row C). Multiple skeletal metastases in the spine (row D)

17.2.3 Case 3: Coexistence of Infiltration and Inflammation/Infection Disease

Clinical details: 52-year-old woman recently diagnosed of breast cancer and referred to a PET/CT study for staging purpose (Fig. 17.3).

Teaching points:

- As the inflammatory/infectious processes can show an increase in FDG uptake, be aware that sometimes FDG uptake can be related to an inflammatory disease.

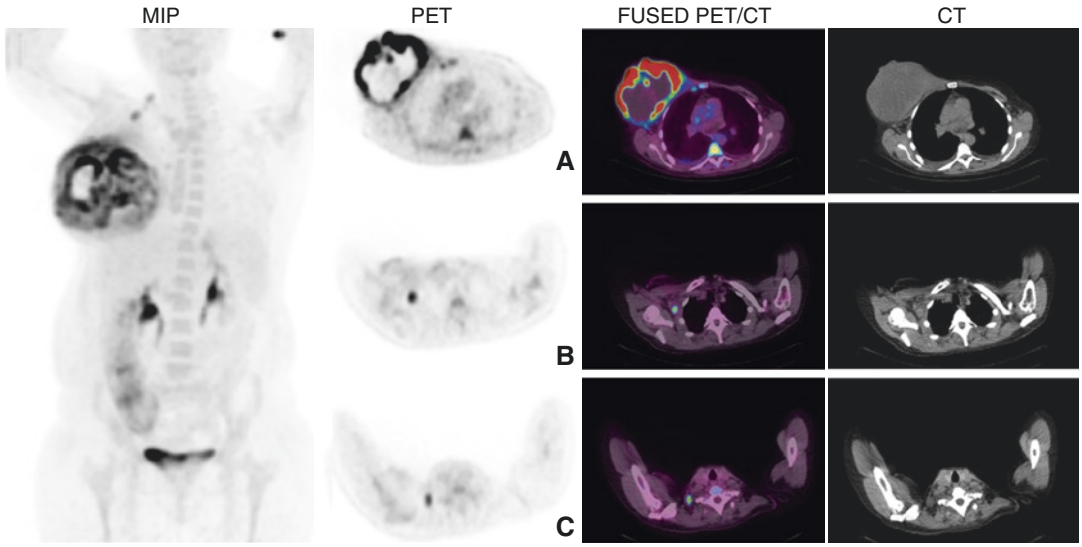

Fig. 17.3 Scan findings: Right breast mass with an heterogenous FDG uptake (row A), associated with some liquid collection in the posterior wall of the lesion, compatible with the primary tumor associated with an infection (abscess). Some axillary (row B), supraclavicular, and cervical lymph nodes (row C) are also seen with an increase in FDG uptake. The etiology of these adenopathies remains unclear between metastatic and inflammation due to abscess

17.2.4 Case 4: Prediction of Response to Treatment

Clinical details: 41-year-old woman diagnosed of locally advanced breast cancer and referred to a PET/CT study for early monitoring response to chemotherapy, prior to surgery (Figs. 17.4 and 17.5).

Teaching points:

- PET/CT technique allows early prediction of the response to treatment with chemotherapy.
- This information is useful to prevent ineffective treatment with chemotherapy and allows not only a change in chemotherapy plan but also an early surgical procedure.

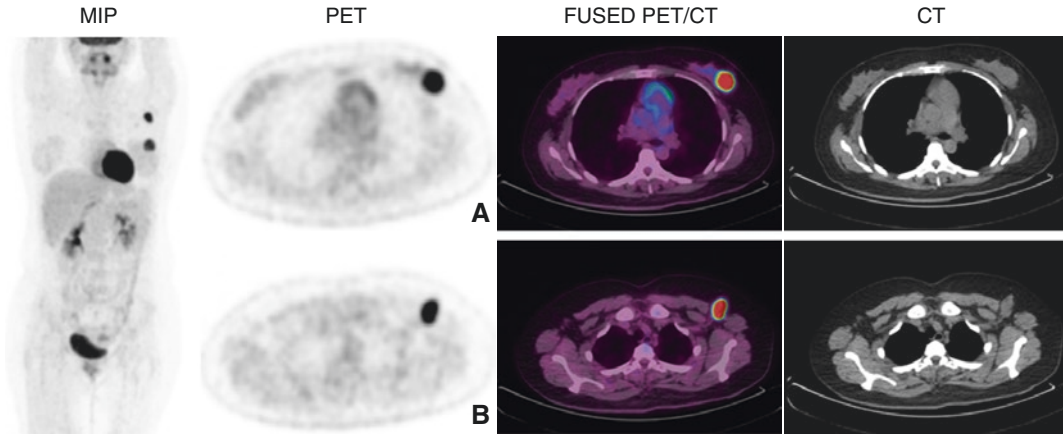

Fig. 17.4 Scan findings: Initial PET/CT study shows left breast mass with increased FDG uptake (row A), and a single axillary hypermetabolic ipsilateral adenopathy (row B), without any sign of metastatic spread. The second study was done after two cycles of chemotherapy (early prediction of response to treatment)

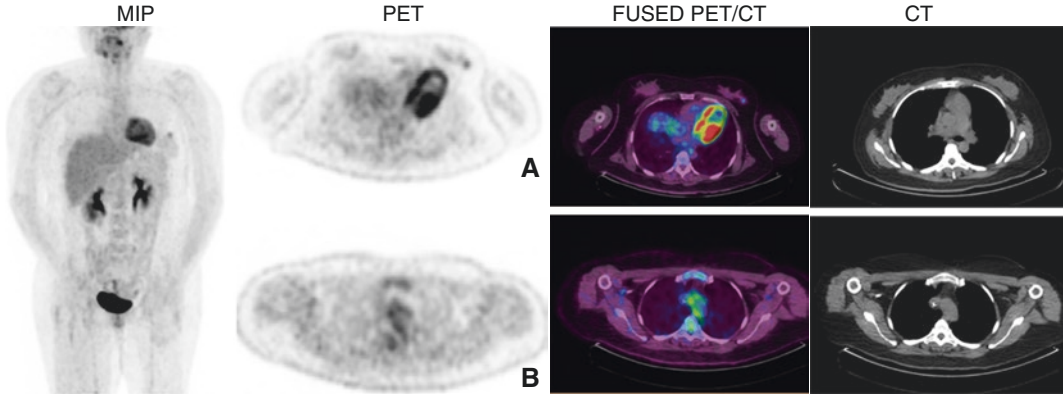

Fig. 17.5 A significant decrease in FDG uptake in the primary breast lesion (row A) and no signs of axillary locoregional infiltration (row B)

17.2.5 Case 5: Monitoring Response to Treatment in Bone Metastatic Disease

Clinical details: 67-year-old woman diagnosed of stage III breast cancer and treated with radical mastectomy 2 years before. Patient referred chest pain and serum increased tumoral markers were confirmed. A first PET/CT study confirmed relapse, and a second PET/CT was performed for response assessment (Figs. 17.6 and 17.7).

Teaching points:

- PET/CT technique allows monitoring treatment response in metastatic disease.
- This information is especially useful in bone disease, as changes in bone marrow tissue due to reparative phenomena can be depicted in bone scintigraphy as an active lesion (as well as flare phenomenon), but are clearly seen in FDG PET/CT studies as residual non-active lesions.

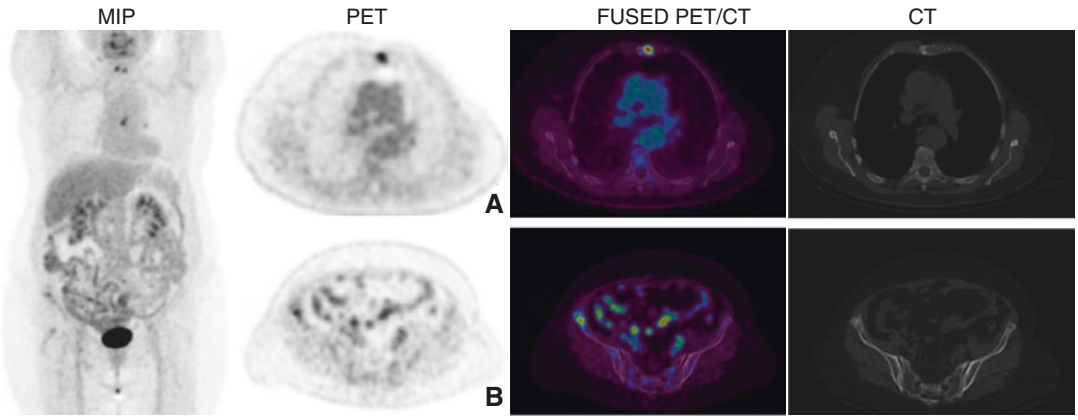

Fig. 17.6 Scan findings: Initial PET/CT study shows bone lytic lesions located in the sternum (row A) and right iliac bone (row B), associated with an increase in FDG uptake

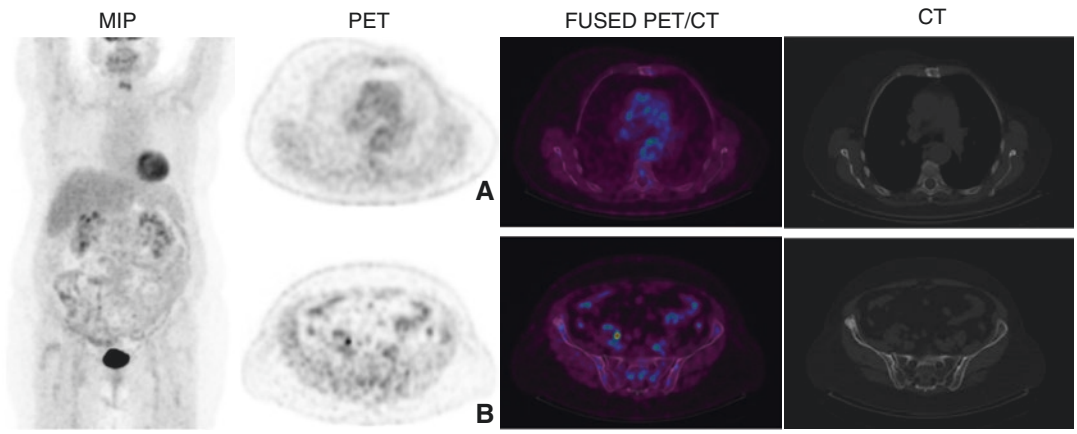

Fig. 17.7 After systemic treatment with chemotherapy, the second study showed an increase of sclerotic changes (A, B) and no FDG uptake, due to bone marrow reparative changes

17.2.6 Case 6: Progression and Potential Pitfalls

Clinical details: 57-year-old woman with a metastatic breast cancer with relapse and was referred to evaluate response to treatment (Fig. 17.8 and 17.9).

Teaching points:

- FDG PET/CT is useful in order to evaluate response to treatment, especially with the cases associated with progression, and can help to decide a change in the treatment management.

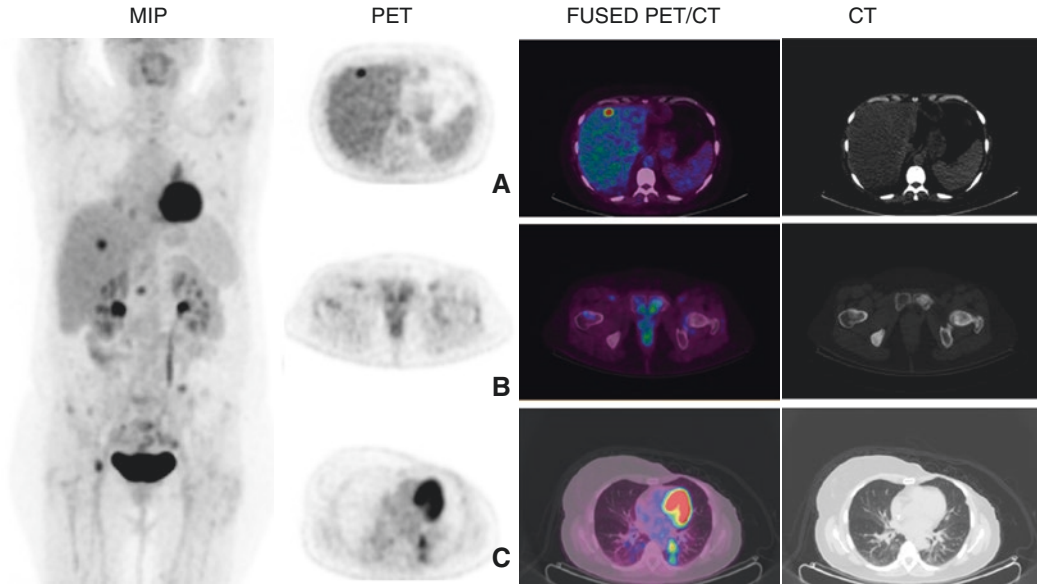

Fig. 17.8 Scan findings: Baseline study shows a hepatic metastasis (fourth segment; row A) and bone metastasis in left humerus, body of third dorsal vertebrae and pelvic bones (row B), and inflammatory opacities in lung due to chemotoxicity (row C)

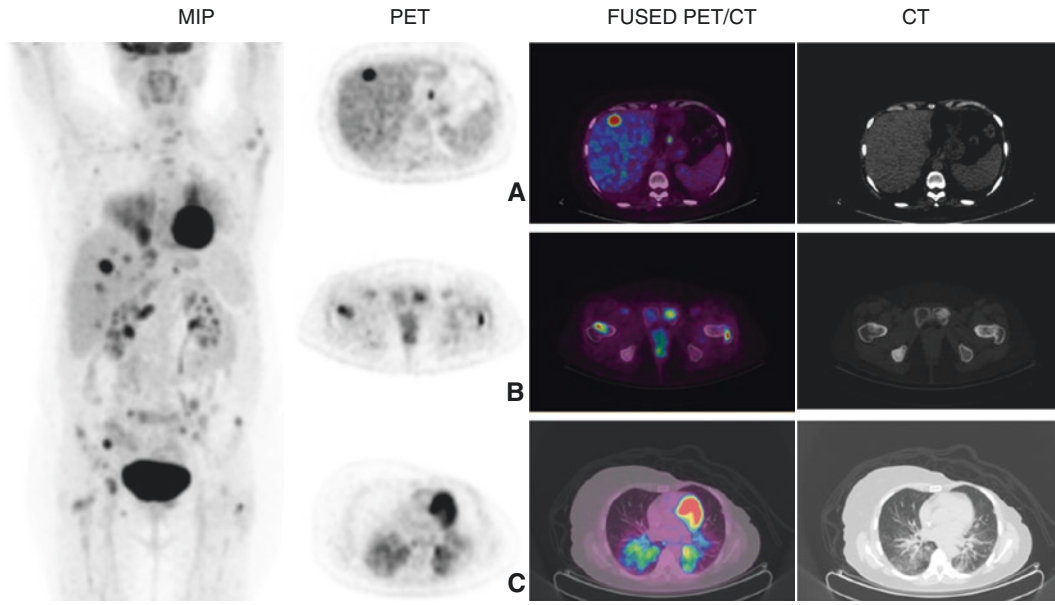

Fig. 17.9 In the second study, 2 months later, several new bone and hepatic lesions were seen, and the known lesions show increased FDG uptake. Moreover, the lung chemotoxicity has progressed (row C)

17.2.7 Case 7: Early Metastatic Spread

Clinical details: 33-year-old woman with a history of breast cancer 2 years ago, with complete response to treatment. A control PET/CT was planned prior to a plastic surgery reconstruction (Fig. 17.10).

Teaching points:

- Early metastatic spread can be diagnosed with FDG PET/CT, before morphological changes are done in the tissue.

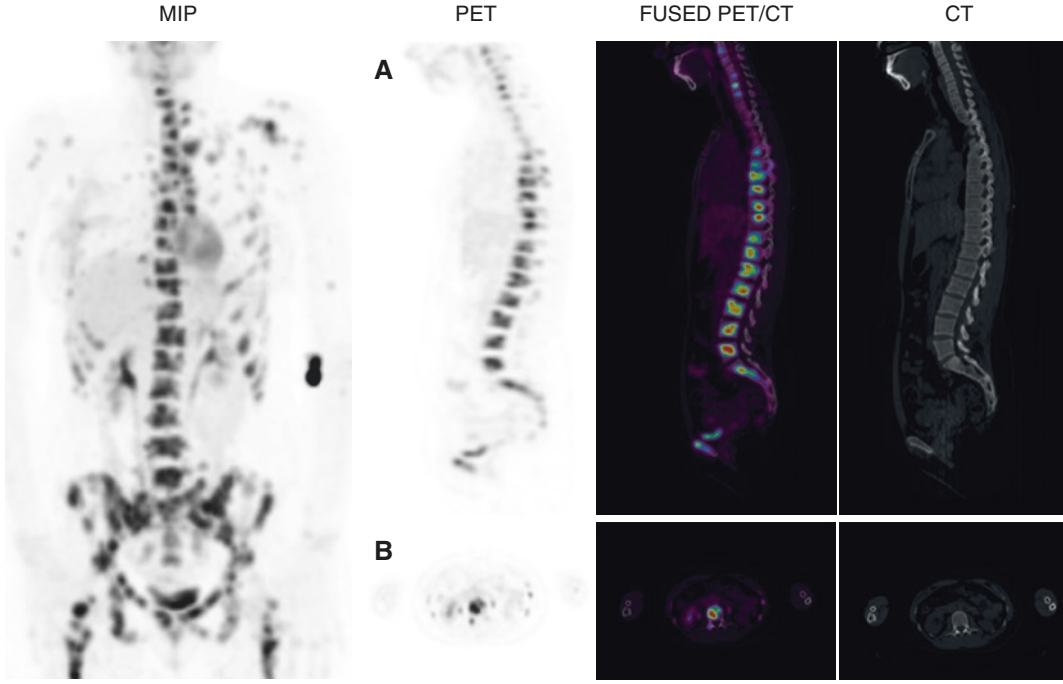

Fig. 17.10 Scan findings: Multiple intramedullary bone lesions in both the axial and the extra-axial skeleton, without morphological changes, due to an early-phase of bone metastatic spread (row A and B)

17.2.8 Case 8: Atypical Relapse

Clinical details: 67-year-old woman with a high-risk breast cancer history. Actually with a suspicion of a relapse, due to an increase in tumoral markers and some cutaneous lesions suspicious of skin metastases (Figs. 17.11 and 17.12).

Teaching points:

- Breast cancer relapse can be often in bone, liver, and lung tissue and also in other infrequent tissues, like in the uterus or the ovarian.
- Skin metastases are usually not seen in FDG PET/CT studies, due to the superficial localization and smaller size.

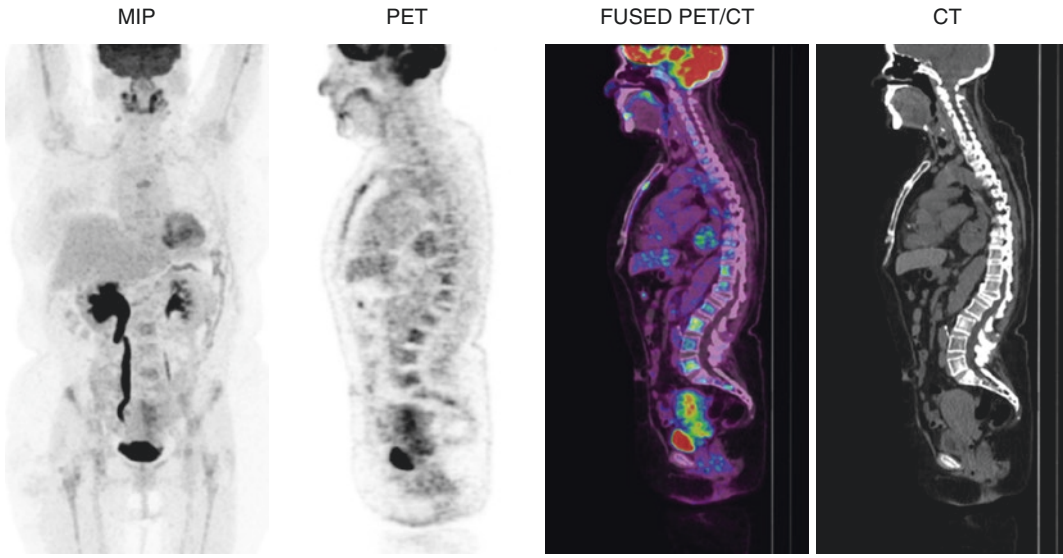

Fig. 17.11 Scan findings: Multiple bone metastases are seen (e.g., sternum, vertebral bodies, and sacral bone)

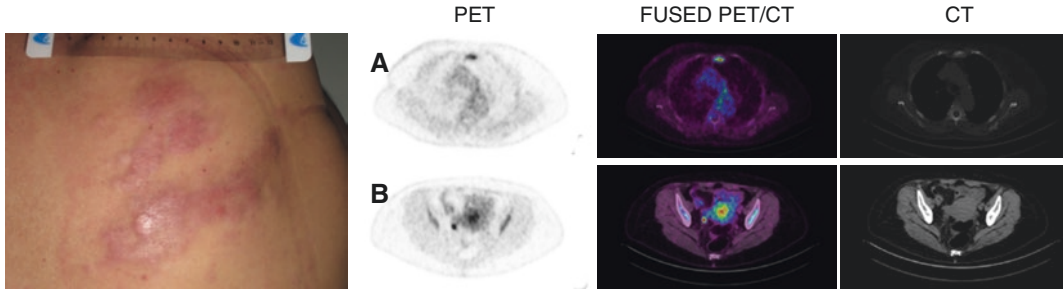

Fig. 17.12 Increased uterine cavity with diffuse FDG uptake that compromises the right ureter (row B). The biopsy confirmed breast cancer infiltration of uterine tissue. Moreover, the known skin metastases were not detected in the study

17.2.9 Case 9: False-Negative Findings

Clinical details: 27-year-old patient with a locally advanced right breast cancer and referred for staging. Biopsy revealed a mixed ductal/lobular carcinoma, grade 1, positive estrogen receptors, no overexpression of c-erbB-2, and a Ki-67 index of 5% (Fig. 17.13).

Teaching points:

- FDG uptake is related to tumor characteristics.
- Lobular histology type, low-grade, positive estrogen receptors, and a low Ki-67 are usually related to a have less FDG uptake.

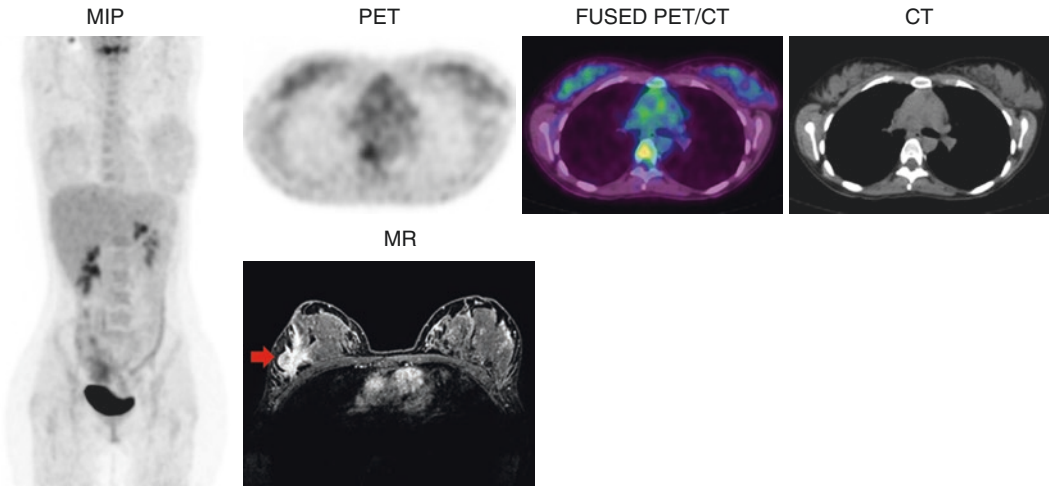

Fig. 17.13 Scan findings: Breast MR shows a lesion of 52 × 30 mm in the right upper outer quadrant (red head arrow). FDG PET/CT showed no significant uptake in the known lesion

17.2.10 Case 10: False-Positive Case

Clinical details: 68-year-old patient with a local relapse of right breast cancer and referred to our department for restaging (Fig. 17.14).

Teaching points:

- Be aware of possible false-positive issues, like the presence of breast prosthesis.

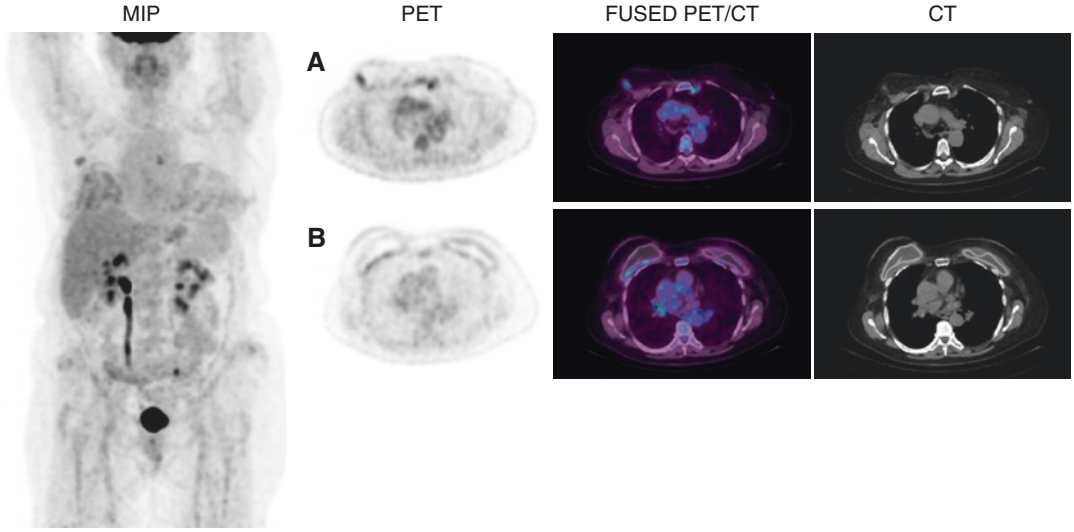

Fig. 17.14 Scan findings: Left internal mammary lymph node is seen, with an SUVmax of 4 and 13 mm of diameter (row A). This adenopathy was related to the presence of dysfunctional breast prothesis and not related to a lymph node spread. Right breast lesion is also seen, associated with an increased FDG uptake, and related to the local relapse (row B)

Suggested Reading

Case 1

Groheux D, Giacchetti S, Delord M, et al. 18 F-FDG PET/CT in staging patients with locally advanced or inflammatory breast cancer: comparison to conventional staging. J Nucl Med. 2013;54:5–11.

Case 2

Caresia Aroztegui AP, García Vicente AM, Alvarez Ruiz S et al. Oncology Task Force of the Spanish Society of Nuclear Medicine and Molecular Imaging. 18F-FDG PET/CT in breast cancer: evidence-based recommendations in initial staging Tumour Biol. 2017;39(10).
Groheux D, Cochet A, Humbert O, et al. ^{18}F-FDG PET/CT for staging and restaging of breast cancer. J Nucl Med. 2016;57(Suppl 1):17S–26S.
Fuster D, Duch J, Paredes P, et al. Preoperative staging of large primary breast cancer with [18F]fluorodeoxyglucose positron emission tomography/computed tomography compared with conventional imaging procedures. J Clin Oncol. 2008;26(29):4746–51.

Case 3

Bakheet SM, Powe J, Kandil A, et al. F-18 FDG uptake in breast infection and inflammation. Clin Nucl Med. 2000;25(2):100–3.

Case 4

Duch J, Fuster D, Muñoz M, et al. 18F-FDG PET/CT for early prediction of response to neoadjuvant chemotherapy in breast cancer. Eur J Nucl Med Mol Imaging. 2009;36(10):1551–7.
Grapin M, Coutant C, Riedinger JM, et al. Combination of breast imaging parameters obtained from 18F-FDG PET and CT scan can improve the prediction of breast-conserving surgery after neoadjuvant chemotherapy in luminal/HER2-negative breast cancer. Eur J Radiol. 2019;113:81–8.
Groheux D, Mankoff D, Espié M, et al. 18F-FDG PET/CT in the early prediction of pathological response in aggressive subtyper of breast cancer: review of the literature and recommendations for use in clinical trials. Eur J Nucl Med Mol Imaging. 2016;43(5):983–93.

Case 5

Cook GJ, Azad GK, Goh V. Imaging bone metastases in breast cancer: staging and response assessment. J Nucl Med. 2016;57(Suppl 1):27S–33S.

Case 6

Groheux D. Role of fludeoxyglucose in breast cancer: treatment response. PET Clin. 2018;13(3):395–414.

Case 7

Al-Muqbel KM. Bone marrow metastasis is an early stage of bone metastasis in breast cancer detected clinically by F18-FDG-PET/CT imaging. Biomed Res Int. 2017;2017:9852632.
Evangelista L, Panunzio A, Polverosi R, et al. Early bone marrow metastasis detection: the additional value of FDG-PET/CT vs. CT imaging. Biomed Pharmacother. 2012;66(6):448–53.

Case 8

Akhtar A, Ratra A, Puckett Y, et al. Synchronous uterine metastases from breast cancer: case study and literature review. Cureus. 2017;9(11):e1840.

Case 9

Kitajima K, Fukushima K, Miyoshi Y, et al. Association between 18F-FDG uptake and molecular subtype of breast cancer. Eur J Nucl Med Mol Imaging. 2015;42:1371–7.
Groheux D, Giacchetti S, Moretti JL, et al. Correlation of high (18)F-FDG uptake to clinical, pathological and biological prognostic factors in breast cancer. Eur J Nucl Med Mol Imaging. 2011;38:426–35.

Case 10

D'hulst L, Nicolaij D, Beels L, et al. False-positive axillary lymph nodes due to silicone adenitis on (18) F-FDG PET/CT in an oncological setting. J Thorac Oncol. 2016;11(6):e73–5.

18F-Choline, 68Ga-PSMA-11 and 18F-FDG PET/CT in Treatment Response Evaluation: Prostate Cancer

18

Giulia Polverari, Alessandro Lambertini, Stefano Fanti, and Francesco Ceci

18.1 Introduction

PET/CT imaging represents, at the moment, one of the most useful diagnostic procedures for investigating prostate cancer (PCa). Over the last decade, PET/CT with 11C-Choline or 18F-Choline proved its role for investigating PCa. Particularly, choline PET/CT proved to be a better diagnostic tool for restaging PCa patients presenting biochemical recurrence (BCR), as compared with radiological imaging. Furthermore, choline PET/CT demonstrated its usefulness for staging high-risk PCa, with high PSA levels and Gleason Scores, before the primary treatment. However, over the last years, new probes able to provide better performances when compared with choline PET/CT were developed. PSMA is a molecular probe targeting the prostate-specific membrane antigen (PSMA), a glutamate carboxypeptidase II, that is a membrane-bound metallopeptidase physiologically expressed in several tissues. Due to its selective overexpression in 90–100% of PCa lesions, PSMA is a reliable tissue marker for PCa and is considered an ideal target for tumor-specific imaging and therapy. According to the results published in literature, PSMA PET imaging showed a promising accuracy to stage PCa prior to curative treatment but the main application remains the restaging of the disease. In this setting, PET imaging could help physicians by addressing patients to the most tailored salvage therapies (e.g., salvage radiotherapy or salvage lymph node dissection). PSMA can also serve as a theranostics agent for treating metastatic castrate-resistant PCa (mCRPC). In this context, PSMA-based PET imaging can play a crucial role addressing mCRPC patients to the most appropriate therapies (e.g., 223Ra or 177Lu-PSMA-617 radioligand therapy). Finally, PSMA PET could be considered as a valuable tool to assess the response to treatment after radioligand therapy.

G. Polverari (✉) · A. Lambertini · F. Ceci
Nuclear Medicine, Department of Medical Sciences, University of Turin, Turin, Italy

S. Fanti
Nuclear Medicine, Sant'Orsola Hospital, Bologna, Italy

S. Fanti et al. (eds.), *Atlas of Clinical PET-CT in Treatment Response Evaluation in Oncology*,
https://doi.org/10.1007/978-3-030-68858-5_18

18.2 Case 1: 11C-Choline PET/CT: Biodistribution and Variants

Clinical details: This is a case of a 58-year-old PCa patient treated with radical prostatectomy (RP) and lymph node dissection (PLND) in 2009 (Gleason Score (GS) = 4 + 3; T2c,N0,M0,R0, initial PSA=5.7 ng/mL). BCR occurred in December 2012 with a PSA value of 0.8 ng/mL.

Patient was referred to 11C-Choline PET/CT to restage the disease. No salvage radiotherapy was already administrated.

Images:

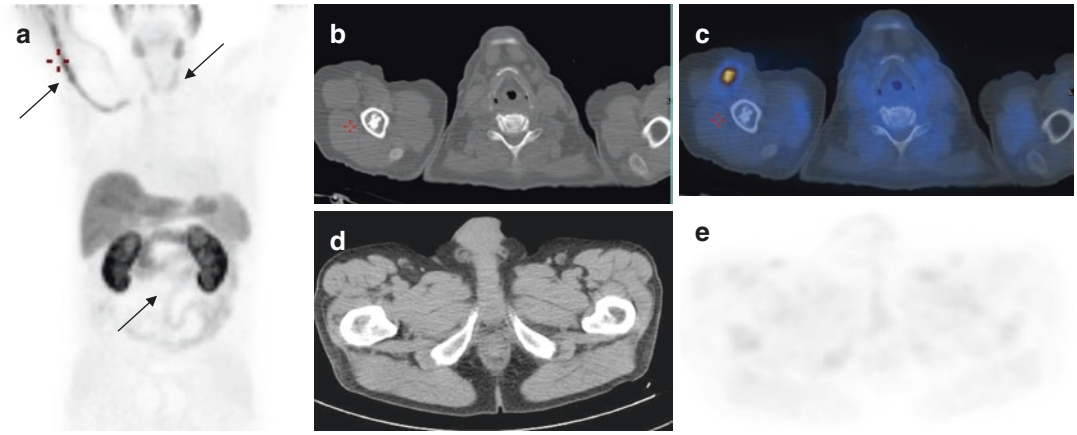

Scan findings: 11C-Choline PET/CT does not show any pathological lesions from PCa. Physiological tracer uptake is seen in salivary glands, liver, spleen, and kidneys (A: Maximum Intensity Projection; MIP image). 11C-Choline uptake in the thyroid is variable and could be faint or mild and without focal uptake does not deserve further investigation (A: black arrow). The vascular uptake in the right arm is also physiological and it is due to the site of injection (A: black arrow; B: CT image; C: PET and CT-fused images). 11C-Choline uptake in the bowel can be faint to mild or intense and without focal uptake should be considered physiological. In this case, morphologically reactive inguinal lymph nodes were also seen on low-dose CT showing mild uptake at 11C-Choline PET/CT (D: CT image; E: PET image).

Teaching points:

- Knowledge of the biodistribution of a tracer is essential to recognize physiological variants or diagnostic pathological lesions.
- This case shows several variants of 11C-Choline such as the site of injection, thyroid, and bowel [1, 2].
- 11C-Choline uptake can occur in reactive inguinal lymph nodes and should not be interpreted falsely as secondary uptake. In fact, inguinal lymph nodes are very uncommon sites of PCa, and they should be suspected mostly in advanced patients with diffused systemic disease.

18.3 Case 2: 11C-Choline PET/CT Pitfalls: Paget's Disease

Clinical details: a 68-year-old patient with PCa (initial PSA 12.5 ng/mL, GS 4+4, staging cT3aNxMx) was treated with radiation therapy as primary treatment in 2013. In 2015, PSA rised up to 3.96 ng/mL, and 11C-Choline PET/CT was performed to restage the disease. Patient was asymptomatic at the time of the scan.

Images:

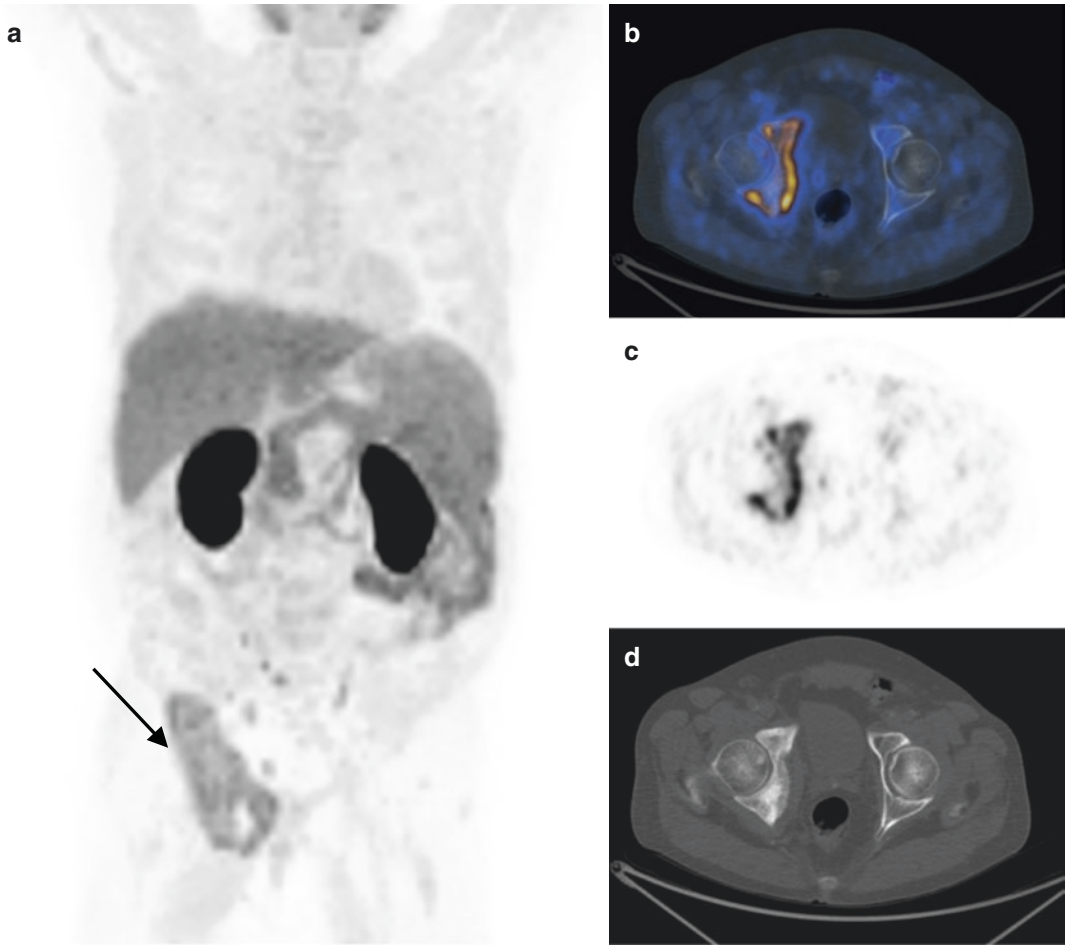

Scan findings: 11C-Choline PET/CT showed several small lymph nodes with tracer uptake in the bilateral internal and external iliac region. Together with these findings, a diffuse area of moderate 11C-Choline uptake was observed in the right-sided pelvic bones (A: black arrow). CT demonstrated coarsened and bloated pelvic bones with diffuse sclerotic process (D). No other distant lesions with tracer uptake were observed. A: MIP image; B: PET and CT-fused transaxial image; C: PET transaxial image; D: low dose CT transaxial image.

Interpretation: The internal and external iliac lymph nodes were considered suspicious for PCa secondary lesions. Considering CT morphology and diffuse uptake pattern, the right-sided pelvis finding was suggestive for Paget's disease.

Teaching points:

- Paget's disease is a common disorder affecting up to 3% of senior adults, characterized by hypertrophic and abnormally structured remodeling of bone [3].
- Usually, patients are asymptomatic, whereas others suffer from pain, nerve compression, or even pathologic factures [3, 4].
- Paget's disease could show faint, mild, or intense 11C-Choline uptake, and this should be taken into consideration during workup of patients with PCa in order to avoid pitfalls in PET/CT image interpretation.

18.4 Case 3: 18F-Choline PET/CT: Biodistribution and Pitfalls

Clinical details: This is a case of a 63-year-old PCa patient treated with RP and PLND in May 2015 (GS = 4 + 3; T3a,N0,M0; initial PSA = 7.9 ng/mL). BCR occurred in April 2016 with a PSA value of 0.32 ng/mL and a PSAdt of 9.3 months. No salvage radiotherapy was administrated.

Images:

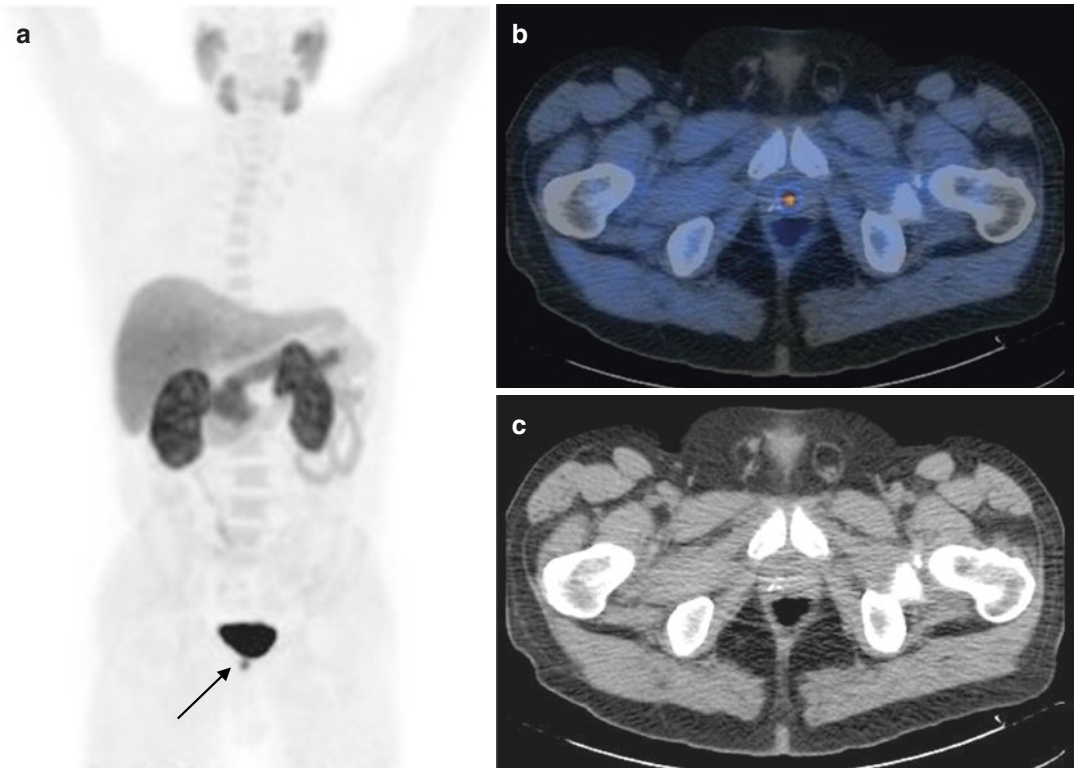

Scan findings: 18F-Choline PET/CT demonstrated a central, small, and focal uptake right under the bladder. No other suspected lesions were observed. A: MIP image; B: CT and PET-fused transaxial image; C: low-dose CT transaxial image.

Interpretation: This finding could be suspicious for a local relapse but considering the central position, the high SUVmax value (SUVmax = 13.4) and the biodistribution of 18F-Choline, this was considered as radioactive urine. This focal uptake became more faint in the late scan performed after 20 min confirming the presence of radioactive urine.

Teaching points:

- The knowledge of the biodistribution of a tracer is essential to recognize physiologic variants or diagnostic pitfalls.
- The biodistribution of 18F-Choline is similar to 11C-Choline except from the presence of the bladder activity [5].
- A potential pitfall of 18F-Choline is the central focal uptake under the bladder due to the presence of radioactive urine. This is important to know to avoid misinterpretation of the images.

18.5 Case 4: 11C-Choline PET/CT: Staging

Clinical details: This is a case of a 73-year-old patient with a recent diagnosis of PCa (initial PSA 30.7 ng/mL, GS 4 + 4, clinical staging cT3bNxMx). Pelvic MRI with endo-coil does not show any suspected lymph nodes metastasis. Patient was referred to bone scintigraphy to exclude the presence of bone metastasis prior to RP. Bone scan observed a faint uptake in the proximal epiphysis of the right humerus. Subsequently patient was referred to 11C-Choline PET/CT due to the high-risk disease.

Images:

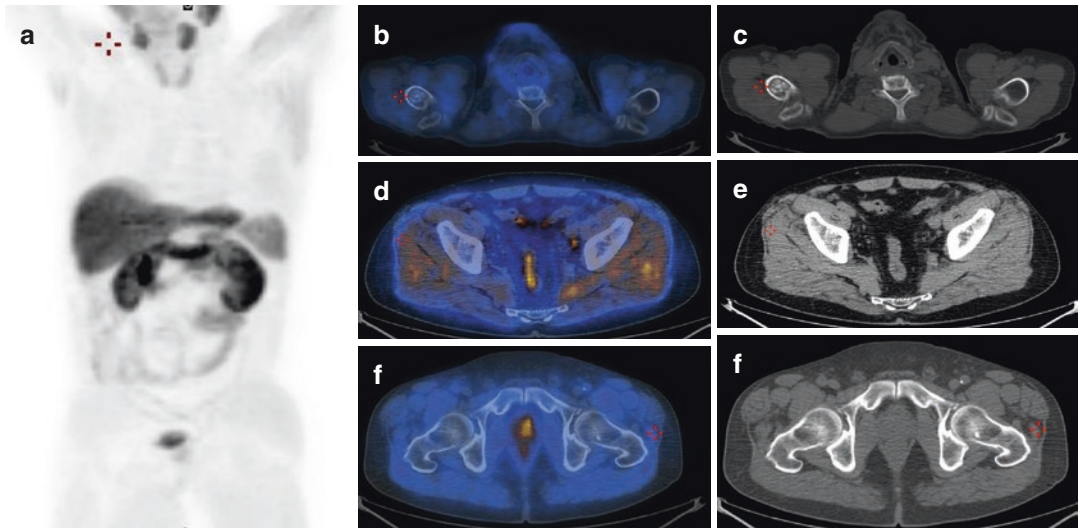

Scan findings: 11C-Choline PET/CT demonstrated a focal uptake in prostate gland (SUV-max = 9.4) and a small left external iliac lymph node with focal tracer uptake (D: red arrow). The bone lesion (right humerus) did not show any significant uptake of 11C-Choline. A: MIP image; B, C: PET and CT-fused transaxial image and low-dose transaxial image of the right humerus bone lesion; D, E: PET and CT-fused image and low-dose CT transaxial image of the left external iliac lymph node (red arrow); F, G: PET and CT-fused image and low-dose CT transaxial image of the intraprostatic lesion.

Interpretation: The focal prostate gland uptake is referable to intraprostatic PCa lesion. Despite the small dimension external iliac lymph node chain is a very common site of metastasis and should be suspected in high-risk PCa. The bone lesion was considered a benign disease. MRI confirmed the presence of osteonecrosis of the proximal epiphysis of the right humerus.

Teaching points:

- In benign bone lesions such as osteonecrosis or degenerative disease, 11C-Choline PET/CT usually presents very faint uptake.
- 11C-Choline PET/CT for staging the disease might have a role in high/very high-risk PCa patients (GS 9–10 regardless PSA values; GS 8 with PSA > 10 ng/mL; young patients with long life expectancy) [6, 7].
- In case of PET positive lymph nodes, 11C-Choline PET/CT could guide the PLND and/or could extend the planning target volume (PTV), including lymph nodes that are not usually removed with standard PLND or included in the PTV of external beam radiotherapy (EBRT) [6, 7].
- In case of distant metastasis, 11C-Choline PET/CT could address patients with high surgical risk (age, comorbidity) to palliative therapies (less invasive approach) instead of curative treatment (RP and EBRT) [6, 7].

18.6 Case 5: 11C-Choline PET/CT: Mediastinal Lymph Nodes

Clinical details: This is the case of a 67-year-old patient with a recent diagnosis of PCa (initial PSA = 11.2 ng/mL, GS = 4 + 3, clinical staging: cT2CNxMx) referred to 11C-Choline PET/CT for staging the disease prior to RP.

Images:

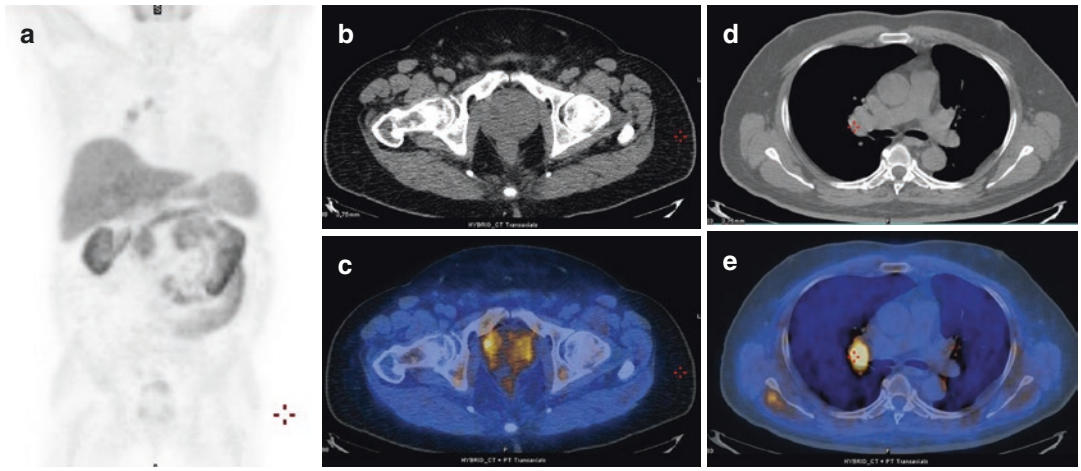

Scan findings: 11C-Choline PET/CT revealed a in-homogenous uptake in both lobes of the prostate gland (C). Focal tracer uptake was also seen in two mediastinal lymph nodes: right peribronchial and right pulmonary hilar lymph nodes with an SUVmax of 8.7 (E). No other areas of focal uptake were observed. A: MIP image; B, C: CT and PET/CT-fused images of prostate gland; D, E: CT and PET/CT-fused images of the right peribronchial lymph node.

Interpretation: The prostate gland uptake is referable to intraprostatic PCa lesion. Mediastinal lymph nodes were reported as undetermined but not related to PCa. Further follow-up confirmed the inflammatory nature of these findings.

Teaching points:

- Mediastinal lymph node uptake of choline is frequently observed and usually is related to inflammation; thus, interpretation of positive mediastinal lymph node uptake should be done carefully [8].
- 11C-Choline PET/CT might have a role in intermediate-high-risk patient excluding the presence of distant or local metastases and addressing PCa patient to RP with curative intent [9].

18.7 Case 6: 11C-Choline PET/CT: Biochemical Recurrence

Clinical details: This is a case of a 67-year-old patient treated with RP (T3b,Nx,M0,R0), ISUP Group 4, and initial PSA of 5.4 ng/dL. BCR occurred 8 months after surgery. Patient was addressed to 11C-Choline PET/CT with PSA of 1.3 ng/dL and PSAdt of 3 months. He also underwent a bone scan with negative result.

Images:

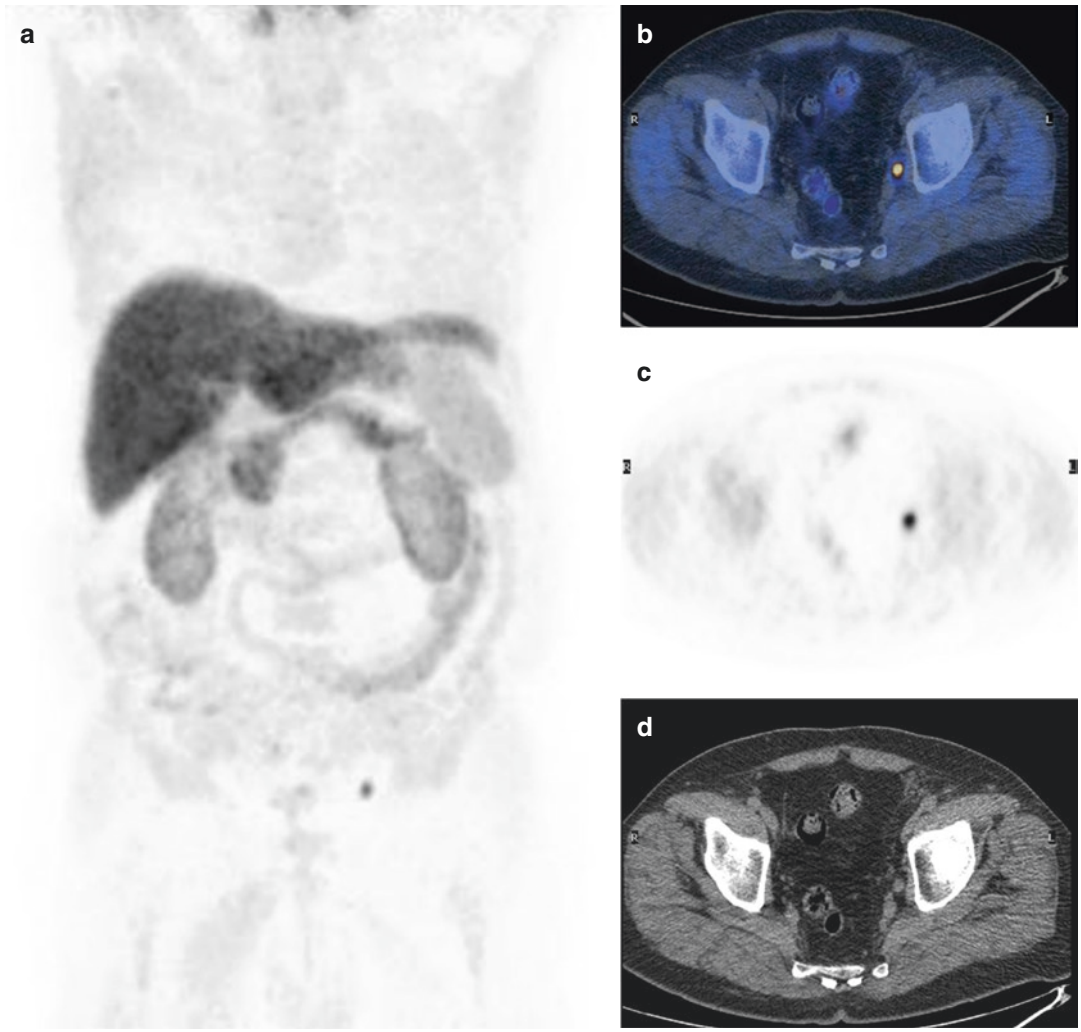

Scan findings: 11C-Choline PET/CT revealed a small but focal and intense uptake in a left obturator lymph node (SUVmax = 8.7). No other lesions with significant uptake were observed. A: MIP image; B: CT and PET fused transaxial image; C: PET transaxial image; D: CT transaxial image.

Interpretation: Considering the high and focal uptake and the very common site of metastasis of the obturator lymph node chain, a PCa lymph node lesion was suspected.

Teaching points:

- Recurrence of PCa is suspected when an increase in the prostate-specific antigen level is detected after radical treatment.
- The recurrence could be local relapse, distant relapse, or both. Differentiation between the two patterns of relapse is critical for choosing the proper treatment strategy.
- 11C-Choline PET/CT could be of help in discriminating patients with local, lymph node, and bone recurrences, thus having an impact on patient management [10–12].

18.8 Case 7: 18F-Choline PET/CT: Biochemical Recurrence

Clinical details: a 60-year-old patient treated with RP (T3a,N0,M0,R0), ISUP Group 4, and initial PSA of 11.2 ng/dL experienced BCR 12 months after surgery. He was addressed to 18F-Choline PET/CT with a PSA of 0.9 ng/dL. He also underwent a bone scan with negative result.

Images:

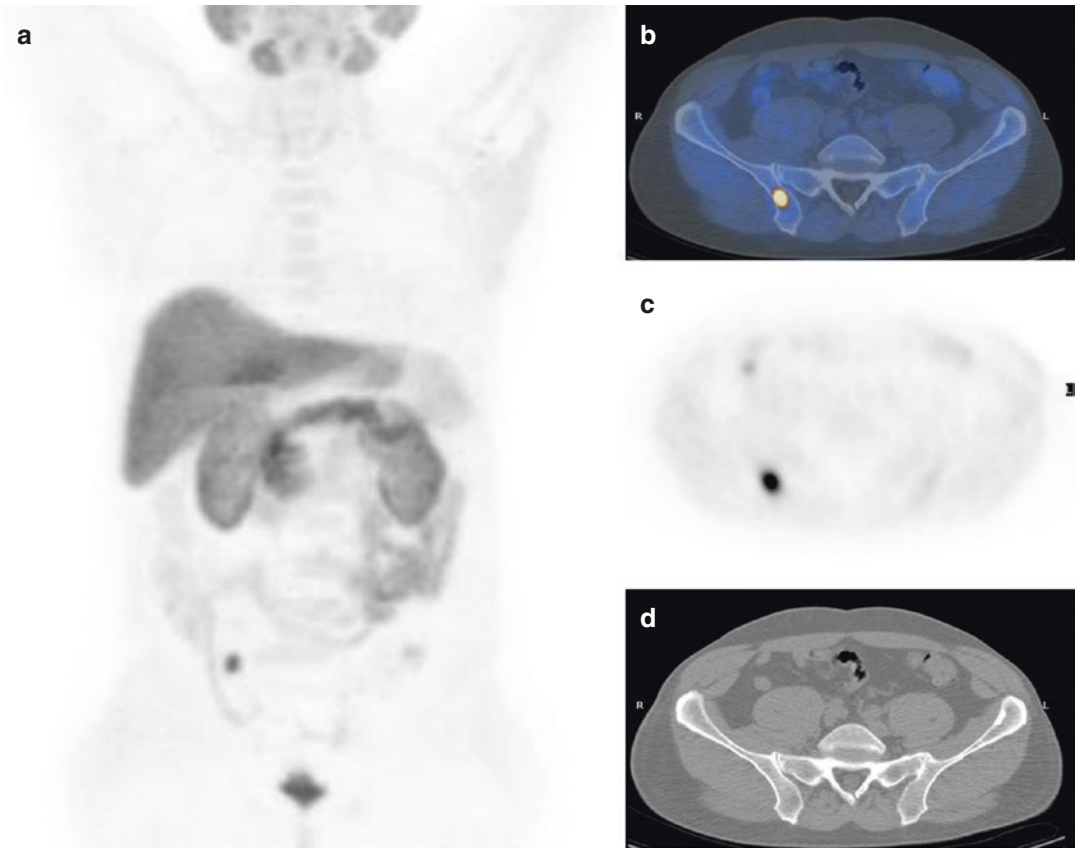

Scan findings: 18F-Choline PET/CT shows a focal and intense uptake (SUVmax: 7.0) in the right iliac bone. To note that CT does not show any significant morphological alteration. No other bone lesions were observed. A: MIP image; B: CT and PET fused transaxial image; C: PET transaxial image; D: CT transaxial image.

Interpretation: Despite the lack of CT correlatives, the focal and intense tracer uptake in the right iliac bone is highly suggestive for PCa bone metastasis.

Teaching points:

- As 11C-Choline PET/CT also 18F-Choline is widely used in PCa patient, especially in BCR setting [13].
- 18F-Choline PET/CT proved to be a useful tool to localize the sites of occult BCR, leading to an adequate management change in PCa patients [14].

18.9 Case 8: 18F-Choline PET/CT During Androgen Deprivation Therapy (ADT)

Clinical details: a 73-year-old patient was treated with RP and PLND dissection in 2007 (GS 4 + 3, initial PSA 8.6 ng/mL). BCR occurred in April 2011 with PSA 1.4 ng/mL. 18F-Choline was performed to restage the disease. The scan revealed some small pelvic lymph nodes (right external iliac) suspected for PCa relapse. Faint uptake in T12 uncertain for metastasis was also observed. Patient was subsequently treated with ADT with a decrease of PSA (<0.02 ng/mL). After 2 years of continuous treatment, PSA raised up to 0.6 ng/mL. Patient was addressed to 18F-Choline to restage the disease.

Images:

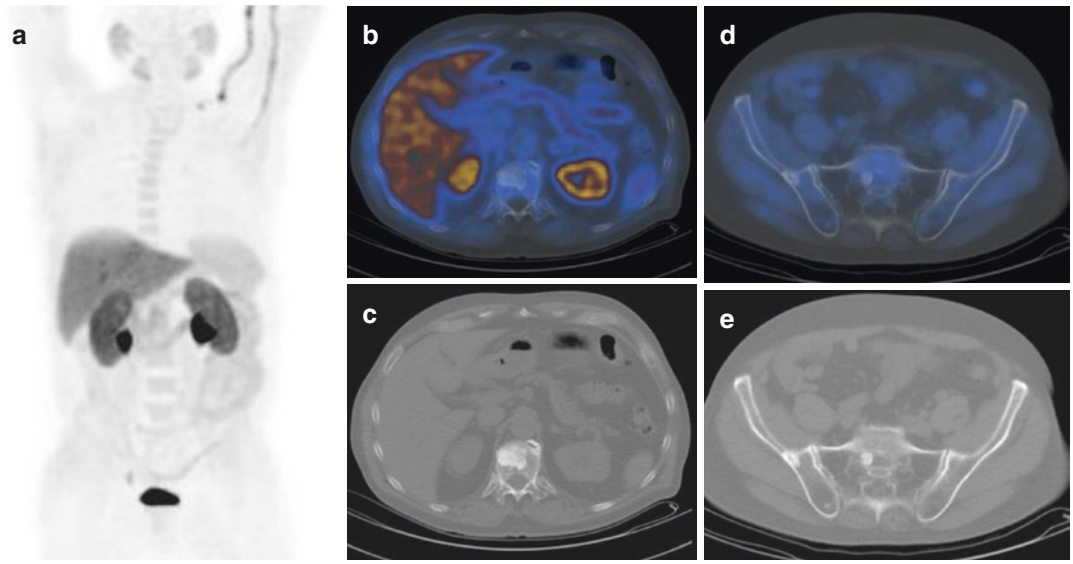

Scan findings: 18F-Choline shows several sclerotic bone lesions visible on low-dose CT without tracer uptake. No other lesions were described. A: MIP image; B: CT and PET-fused transaxial image; C: CT transaxial image; D: CT and PET-fused transaxial image; E: CT transaxial image.

Interpretation: Bone lesions show rsponse to treatment. The presence of bone metastases is radiologically confirmed by the CT.

Teaching points:

- Hormonal responsive lesions from PCa may not show 18F-Choline uptake.
- In patients with ADT on-going, it is possible to have some active lesions (not responding to ADT) with choline uptake together with other lesion responding to ADT and choline negative [15, 16].

18.10 Case 9: 11C-Choline PET/CT: Oligometastatic Patient

Clinical details: This is a case of a 59-year-old patient treated with RP + PLND in 2009 for PCa (GS 4 + 5; T3bN0Mx R0). BCR occurred in October 2014 with a PSA of 1.4 ng/mL (PSAdt = 4.3 months). Patient was referred to 11C-Choline PET/CT to restage the disease.

Images: pre-therapy 11C-Choline PET/CT

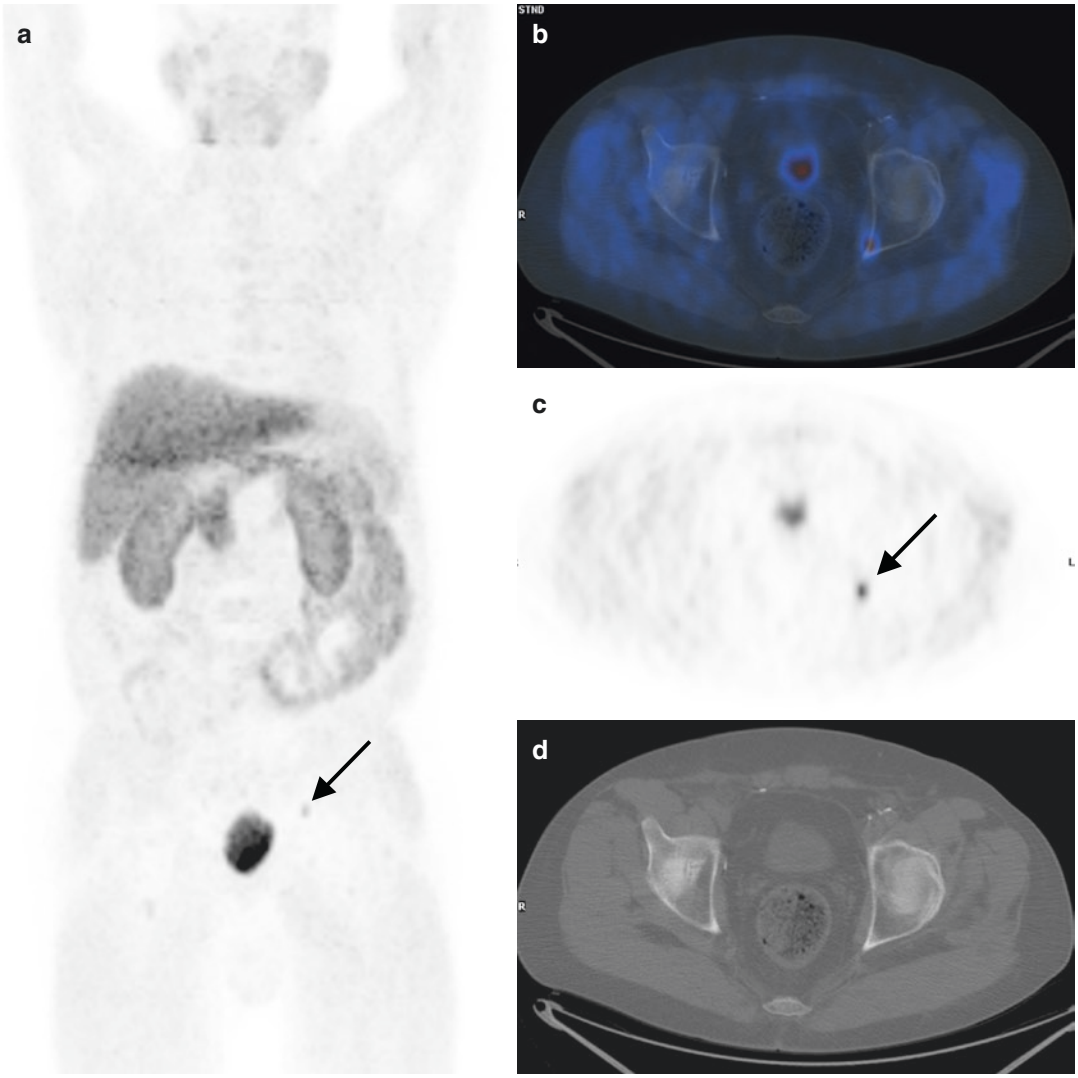

Scan findings: 11C-Choline PET/CT shows a small but intense and focal uptake in the left acetabulum (black arrows) with SUVmax of 6.8. The low-dose CT showed very faint bone rehash. Faint uptake was observed in bilateral inguinal lymph nodes with reactive morphology on low-dose CT. No other findings were seen. A: MIP image; B: PET and CT-fused image; C: PET image; D: CT transaxial image.

Interpretation: Despite the small dimension of the finding, the left acetabulum uptake was reported as PCa metastasis due to the location, focal uptake, and initial bone alteration on CT.

Bilateral inguinal lymph nodes were reported as reactive due to their symmetry, faint uptake, CT morphology, and unusual localization of metastasis in non-advanced PCa patient. Patient was subsequently addressed to stereotactic-body RT on the bone lesion together with ADT. After treatment, PSA reached undetectable level. 11C-Choline PET/CT was subsequently performed to assess response to therapy.

Images: post-therapy 11C-Choline PET/CT

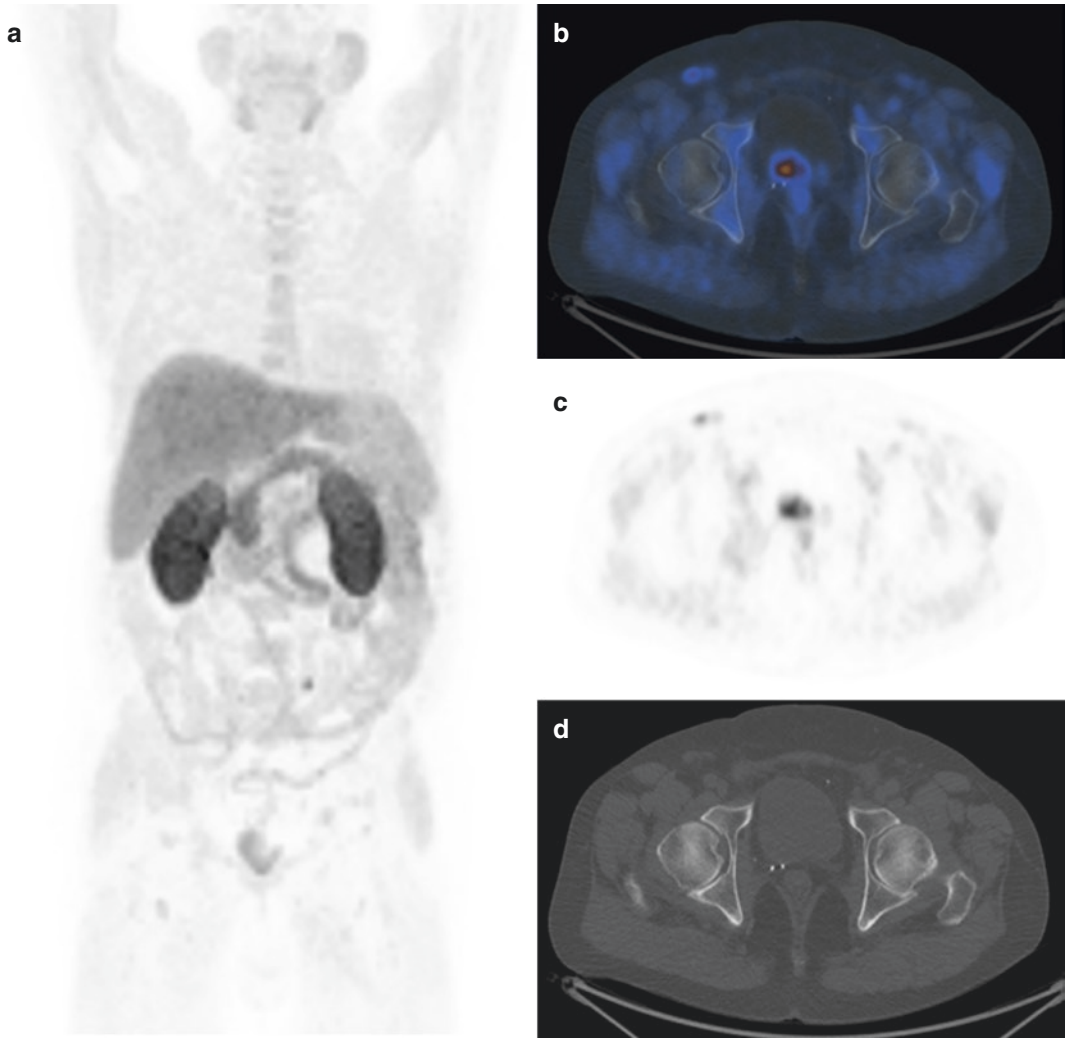

Scan interpretation: 11C-Choline PET/CT showed no significant uptake in the left acetabulum. No other findings were seen. A: MIP image; B: PET and CT-fused image; C: PET image; D: CT transaxial image.

Teaching points:

- Patients with recurrent PCa limited to a small number of active metastatic lesions are named "oligometastatic patients."
- Patients with oligometastatic disease could eventually be managed by treating all the active lesions with a local metastasis-directed therapy (MDT) [17, 18].
- Choline PET/CT could have a role in detecting PCa active lesions and selecting patients who could benefit from MDT [17, 18].

18.11 Case 10: 11C-Choline PET/CT: Metastatic Castration-Resistant Prostate Cancer (mCRPC)

Clinical details: This is a case of a patient of 63-year-old treated with radiotherapy as radical treatment in 2007 (stage cT3aNxMx; GS 4 + 3). BCR occurred in 2013 and 11C-Choline PET/CT was performed with negative result. Patient was subsequently addressed to ADT. After 3 years of good response, patient experienced rapid increase in serum PSA and was referred to 11C-Choline PET/CT to restage the disease (PSA value at the time of PET/CT scan = 16.6 ng/mL).

Images:

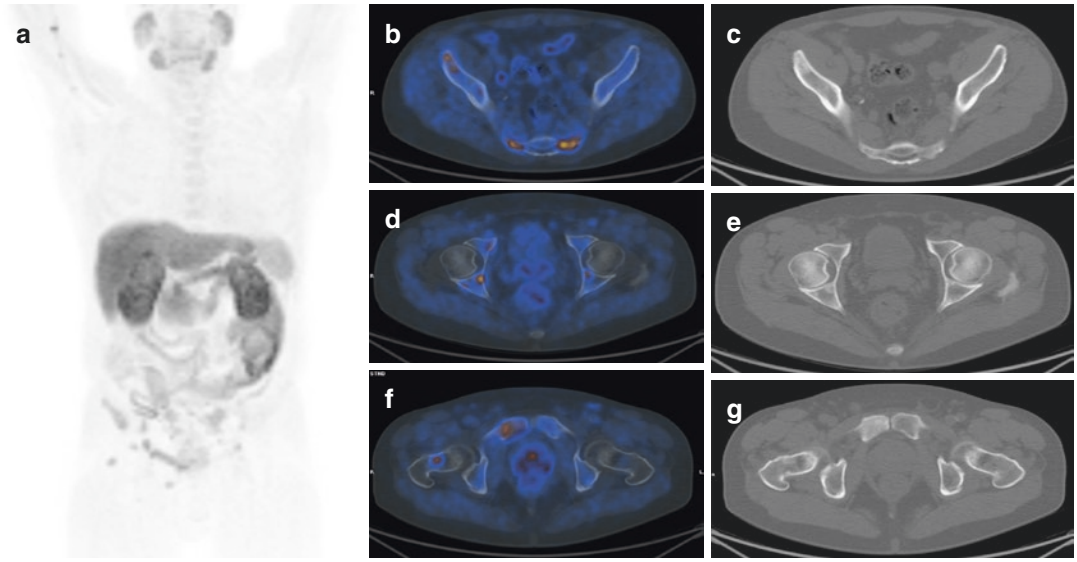

Scan findings: The scan shows in-homogenous tracer uptake in prostate gland (SUVmax = 6.9) extended to seminal vesicles together with several bilateral external and internal iliac lymph nodes (SUVmax of the highest in right external iliac region = 7.7) and multiple sclerotic bone lesions with high tracer uptake in the pelvis (SUVmax of the right acetabulum = 9.9) and in the right femur. A: MIP image; B, D, F: PET/CT-fused transaxial images; C, E, G: low dose CT images.

Interpretation: All PET/CT findings were reported as lesions from PCa. Patient was considered as mCRPC and subsequently he was addressed to an androgen-receptor (AR) targeted therapy. After six cycles of enzalutamide, PSA dropped to 5.46 ng/mL, and a further 11C-Choline PET/CT was performed to assess response to therapy.

Images:

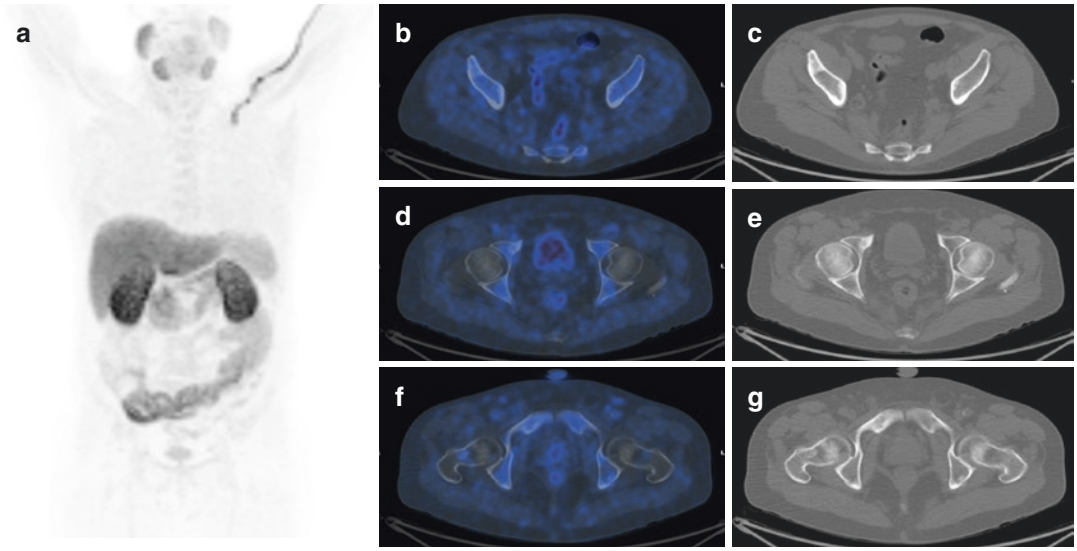

Scan Findings: 11C-Choline PET/CT demonstrated significant reduction of uptake in prostate gland and in seminal vesicles (SUVmax = 4.8), the metabolic normalization of the pelvic lymph nodes, and the presence of in-homogenous uptake without significant focality in the skeletal segment examined.

Interpretation: The PET/CT scan showed a partial response to therapy, and AR-targeted therapy was continued.

Teaching points:

- Metastatic castration-resistant prostate cancer (mCRPC) is defined as evidence of rising tumor marker in spite of androgen blockade [19].
- Under these conditions, massive spread to the skeletal tissue frequently occurs and this process can significantly contribute to morbidity and mortality [19].
- Patients with this condition are benefiting from an increasing number of treatment options. However, assessing therapy response in patients with multiple localizations might be challenging.
- 11C-Choline PET/CT, as metabolic tracer, is generally considered a good diagnostic procedure to assess response to systemic therapy in mCRPC [20, 21].

18.12 Case 11: 68Ga-PSMA-11: Biodistribution and Variants

Clinical details: This is a case of a 67-year-old PCa patient treated with RP + PLND in May 2012 (GS 4 + 4; T3aN1Mx R0). BCR occurred in July 2015, and 11C-Choline PET/CT was performed with negative result (PSA at the time of the scan = 0.48 ng/mL). Six months later, the patient was referred to 68Ga-PSMA-11 PET/CT for restaging the disease during BCR (PSA at the time of the scan 0.57 ng/mL; PSAdt = 10.9 months).

Images:

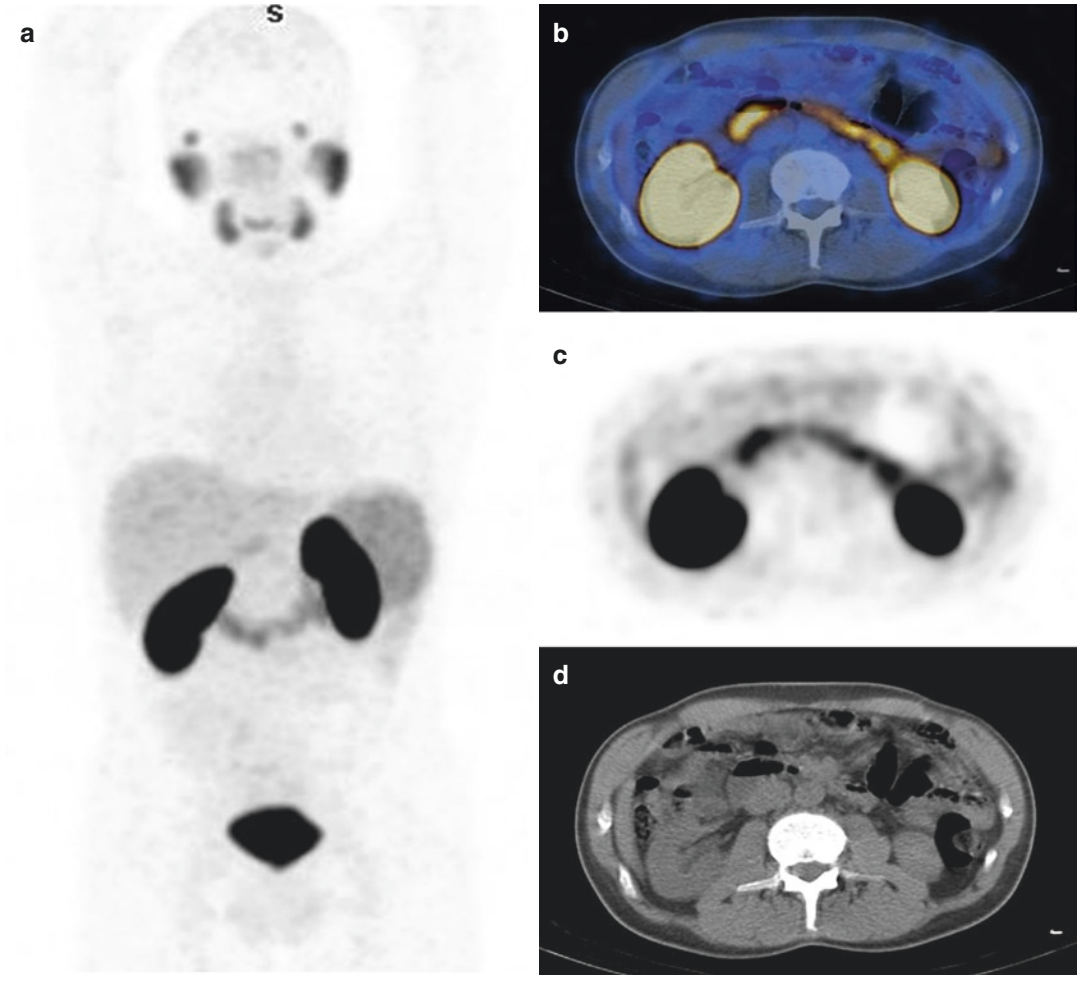

Scan findings: 68Ga-PSMA-11 PET/CT does not show any pathological lesions from PCa. Physiological tracer uptake is seen in salivary glands, liver, spleen, jejunum, kidneys, and bladder.

Kidneys and bladder uptake is variable and could be mild or more intense due to patient's hydration status. 68Ga-PSMA PET/CT uptake in jejunum can be faint to mild or intense and without focal uptake should be considered physiological. A: MIP image; B transaxial PET and CT-fused image; C. PET image; D: low-dose CT image.

Teaching points:

- An accurate characterization of PSMA-positive findings can be accomplished only if one is aware of the normal distribution pattern, physiological variants of radiotracer uptake, and potential sources of false-positive and false-negative imaging findings [22, 23].
- Knowledge of these limitations is necessary to increase the confidence of interpreting physicians and avoid images misinterpretation.

18.13 Case 12: 68Ga-PSMA-11 PET/CT Pitfalls: Ganglia

Clinical details: This is a case of a 68-year-old PCa patient treated with RP in 2012 (GS = 5 + 4; T3bNxMx R1). Adjuvant radiation therapy was administrated together with ADT (bicalutamide) up to December 2014. BCR occurred in May 2016, and patient was referred to 68Ga-PSMA to restage the disease (PSA at the time of the scan = 0.8 ng/mL).

Images:

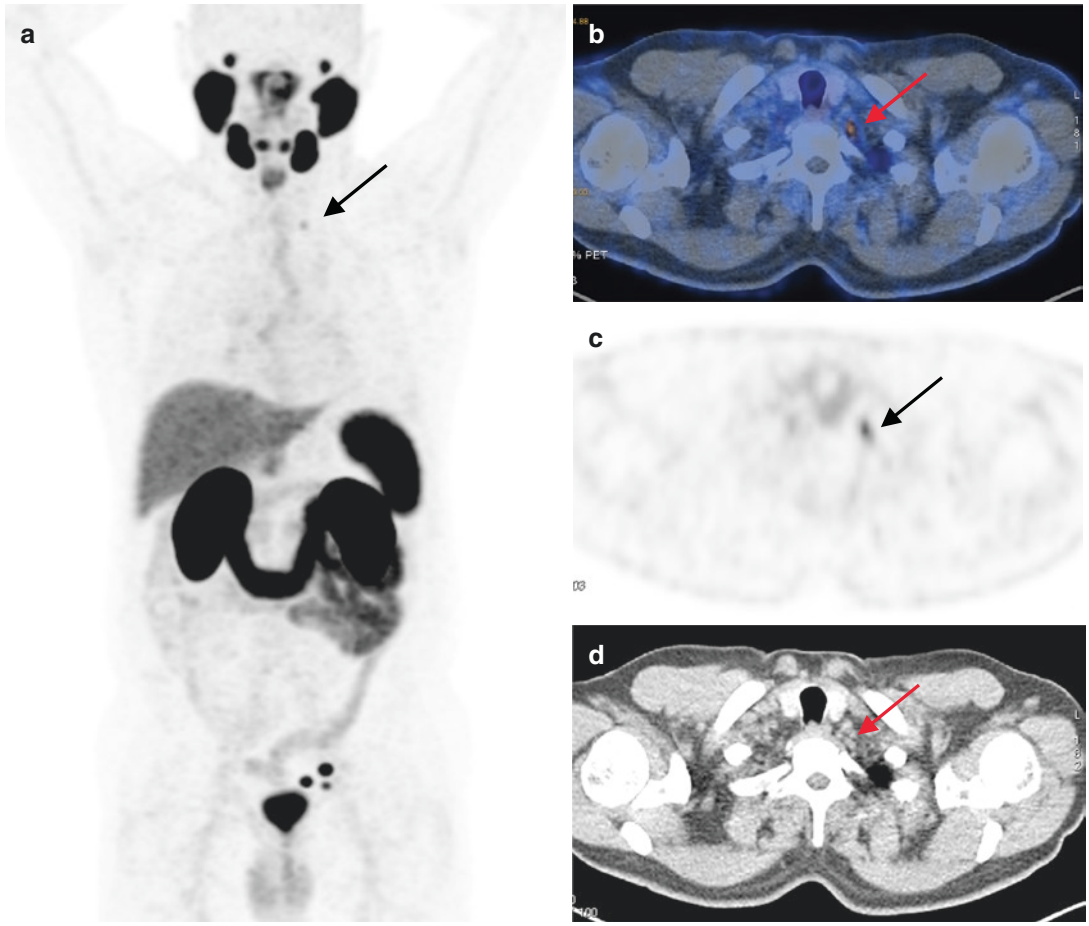

Scan findings: 68Ga-PSMA PET/CT shows three areas of intense and focal uptake in the left external iliac region (SUVmax = 9.8). A small area of tracer uptake was also seen in the left supraclavicular region (black and red arrows). No other findings with tracer uptake were observed. A: MIP image; B: PET and CT-fused image; C: PET image; D: low-dose CT image.

Interpretation: The three left external iliac lymph nodes with very high and focal uptake were reported as metastasis from PCa. The left supraclavicular finding was difficult to interpretate, but considering location, CT morphology, and faint uptake, it was reported as cervical ganglion. Patient was subsequently addressed to salvage radiation therapy on the left iliac fossa.

Teaching points:

- 68Ga-PSMA-11 uptake in ganglia along the sympathetic trunk represents an important pitfall in prostate cancer PET imaging [24].
- For the differentiation between lymph node metastases and sympathetic ganglia, both intensity of ^{68}Ga-PSMA uptake and exact localization and configuration of the respective lesion should be examined carefully.
- Usually ganglia exhibit a band-shaped or a teardrop configuration and only rarely a nodular configuration. Conversely, lymph node metastases are only rarely band-shaped, but more often show teardrop or nodular appearance [24].

18.14 Case 13: 68Ga-PSMA-11 PET/CT Pitfall: Paget's Disease

Clinical details: This is a case of a 72-year-old PCa patient treated with RP + PLND in 2011 (GS = 4 + 3; T2bN0Mx R0). BCR occurred 3 years later, and patient was investigated with pelvic MRI with negative result. Subsequently patient was referred to 68Ga-PSMA-11 PET/CT (PSA at the time of the scan = 0.98 ng/mL; PSAdt = 10.3 months).

Images:

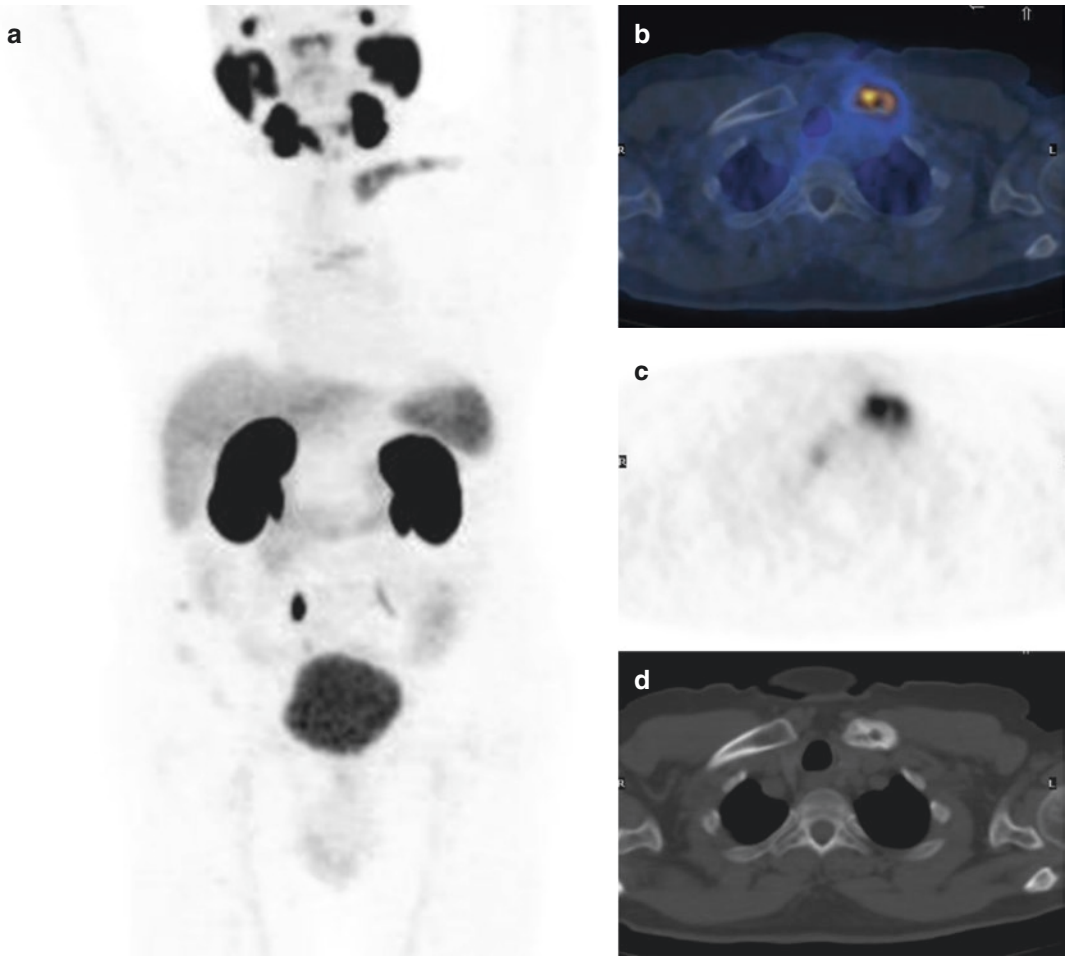

Scan findings: 68Ga-PSMA PET/CT scan shows diffuse uptake in the left clavicle with coarsened and bloated bone and diffuse sclerotic process on low-dose CT image. No other lesions with tracer uptake were seen. A: MIP image; B: PET and CT-fused image; C: PET image; D: low-dose CT image.

Interpretation: Considering the diffuse pattern of tracer uptake and the CT characteristics of left clavicle, Paget's disease was suspected. Subsequently patient was subject to biopsy, and the clavicle finding was histopathologically proven to be Paget's disease.

Teaching points:

- Paget's disease is a common disorder affecting up to 3% of senior adults, characterized by hypertrophic and abnormally structured remodeling of bone [25].
- Usually patients are asymptomatic, whereas others suffer from pain, nerve compression, or even pathologic factures [25, 26].
- Paget's disease could show faint, mild, or intense 68Ga-PSMA-11 uptake, and this should be taken into consideration during workup of patients with PCa in order to avoid pitfalls in PET/CT image interpretation.

18.15 Case 14: 68Ga-PSMA-11 PET/CT: Staging

Clinical details: This is a case of a 69-year-old patient with a recent diagnosis of PCa (GS = 4 + 3) with an initial PSA of 26 ng/mL. Patient was referred to 68Ga-PSMA PET/CT to stage the disease prior to radical therapy.

Images:

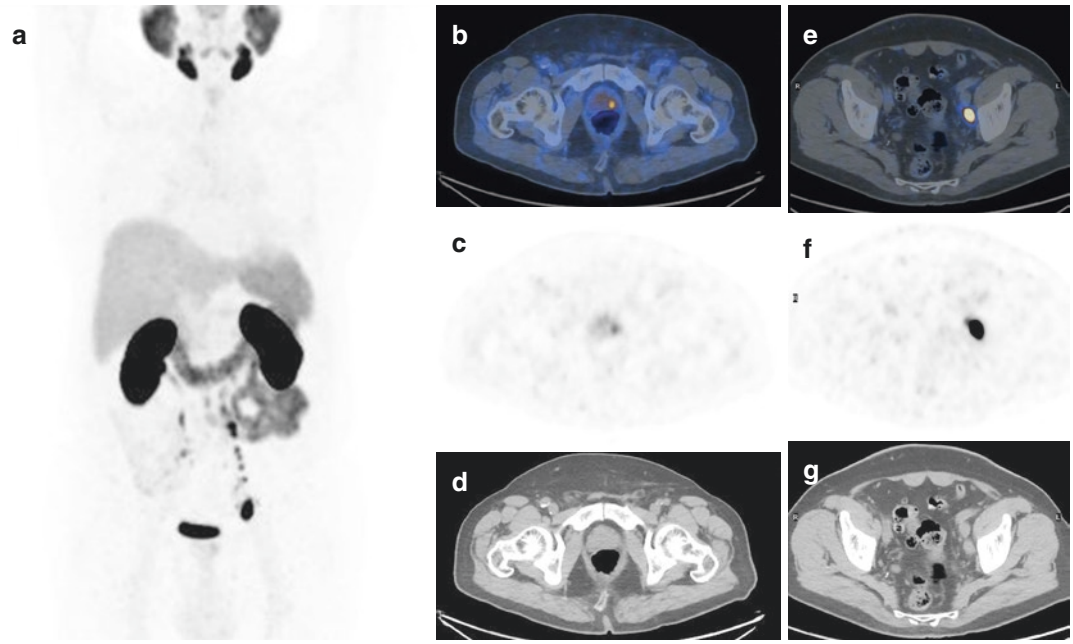

Scan findings: 68Ga-PSMA-11 PET/CT demonstrated the presence of focal uptake in the left lobe of prostate gland (SUVmax = 4.3) together with several left internal, external, and obturator lymph nodes with intense and focal uptake (SUVmax of the left obturator lymph node = 13.9). A: MIP image; B–D: transaxial PET/CT-fused image, PET image, and CT image of the prostate gland; E–G: transaxial PET/CT-fused image, PET image, and CT image of the left obturator lymph node.

Interpretation: PET/CT demonstrated the presence of intraprostatic PCa lesion and multiple lymph nodes metastasis. Patient was subsequently addressed to RP + PLND which confirmed the pathological nature of lymph nodes (T3a,N1,Mx,R0). Considering the high-risk disease, patient was also initiated to ADT.

Teaching points:

- 68Ga-PSMA PET/CT might have a role in staging high-risk PCa patient, since it can evaluate the presence of distant or local metastases and address patient to the most appropriate therapy [27, 28].
- In case of positive lymph nodes, PET/CT could guide PLND and in case of distant metastases PET/CT could address patients with high surgical risk (age, comorbidity) to systemic therapies instead of radical treatment (RP and EBRT) [27, 28].

18.16 Case 15: 68Ga-PSMA-11 PET/CT in Biochemical Recurrence: Local Relapse

Clinical details: A 60-year-old patient was treated with RP as primary treatment for PCa (T3a,N0,Mx, ISUP Group 4, initial PSA = 8.9 ng/mL). After 1 year from surgery, BCR occurred (PSA = 0.34 ng/mL, PSADT 5 months). Patient was referred to 68Ga-PSMA-11 PET/CT to restage the disease.

Images:

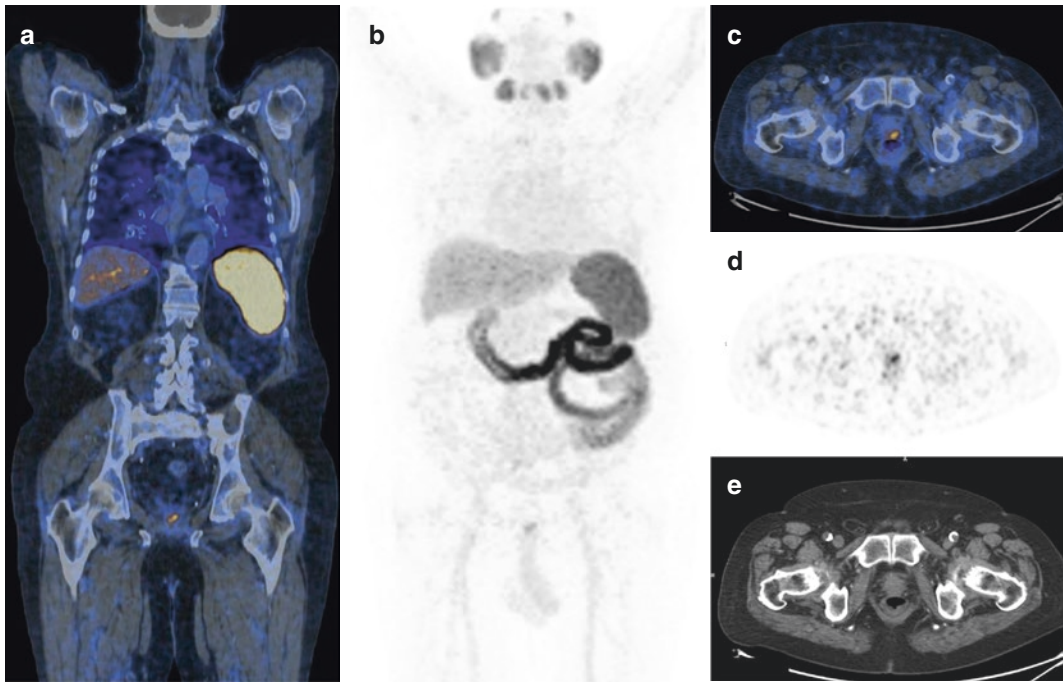

Scan findings: 68Ga-PSMA PET/CT showed a small paramedian focal uptake (SUVmax 3.7) in prostate bed. A lesion on low-dose CT (nodule or tissue) was not observed. No other findings were seen. A: Fused coronal PET/CT image; B: MIP projection image; C–E: Fused PET and CT images, PET image, and CT image of the prostate bed finding.

Interpretation: The uptake in the prostate bed was reported as suspicious for local relapse due to the focal and paramedian uptake. Subsequently the finding was further investigated, and patient performed a TRUS-guided biopsy. The presence of PCa relapse was confirmed by histology.

Teaching points:

- Recurrence of PCa is suspected when an increase in the prostate-specific antigen level is detected after radical treatment and takes place in 20–30% of patients within 10 years after RP [29].
- Numerous studies have shown the advantage of early intervention in BCR when disease burden is low [29–31].
- 68Ga-PSMA-11 PET/CT could be of help in discriminating patients with local, lymph node, and bone recurrences, thus having an impact on patient management [29–31].

18.17 Case 16: 68Ga-PSMA-11 PET/CT in Biochemical Recurrence: Bone Metastasis

Clinical details: This is a case of a 68-year-old PCa patient (T3b,N0,Mx, ISUP Group 5) treated with RP and PLND as primary treatment followed by adjuvant RT. BCR occurred 2 years after radical therapy, and patient was referred to 68Ga-PSMA PET/CT to restage the disease. PSA at the time of the scan was = 2.1 ng/ml (PSAdt = 4 months), and the patient was receiving bicalutamide.

Images:

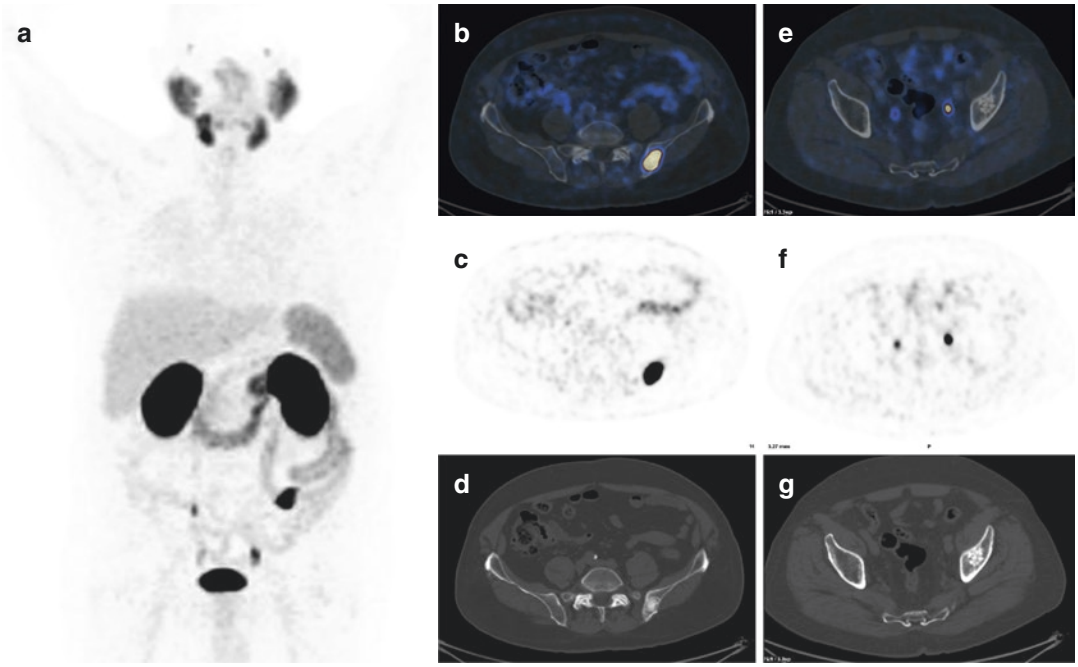

Scan findings: 68Ga-PSMA PET/CT showed an intense focal uptake (SUVmax = 13.1) in the left iliac bone. On CT, an osteoblastic left iliac bone lesion was observed together with an area of bone rehash in the left iliac crest without significant PSMA uptake. A: MIP projection; B–D: Fused PET/CT image, PET image, and CT image of the left iliac bone lesion; E–G: Fused PET/CT image, PET image, and CT image of the left iliac crest benign lesion.

Interpretation: The left iliac finding with high and focal uptake was referable to PCa bone metastasis while the left iliac crest finding was reported as benign bone lesion due to CT morphology and PSMA negativity. Pelvic MRI confirmed the benign nature of the lesion.

Teaching point:

- In benign bone lesions such as osteonecrosis or degenerative disease, 68Ga-PSMA PET/CT usually do not present significant uptake [32].

18.18 Case 17: 68Ga-PSMA-11 PET/CT in Biochemical Recurrence: Distant Lymph Nodes

Clinical details: This is a case of a 62-year-old PCa patient (T3b,Nx,Mx, GS 4+5 ISUP Group 5) treated with RP as primary treatment in 2008. BCR occurred in 2014, and patient was treated with salvage PLND. PSA raised up again in 2016 and an extended radiation therapy was performed (prostate bed, retroperitoneal, and bilateral iliac lymph nodes). The patient was also treated with ADT (continuous scheme). In December 2018, PSA raised up to 0.18 ng/ml and the patient was referred to 68Ga-PSMA PET/CT to restage the disease.

Images:

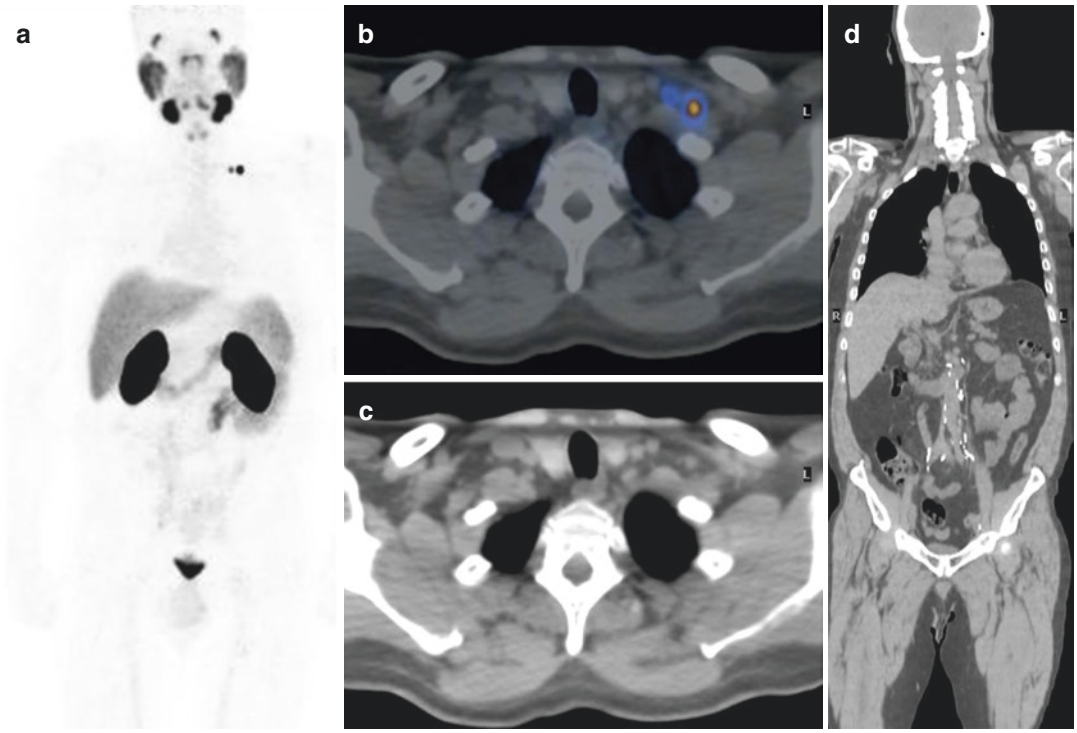

Scan findings: 68Ga-PSMA PET/CT showed two small left sovraclavicular lymph nodes with focal uptake (SUVmax of the biggest lymph node = 9.1). No other lesions with tracer uptake were observed. A: MIP projection; B: Fused PET/CT image; C: trans-axial CT image; D: coronal CT image.

Interpretation: The left sovraclavicular lymph nodes were reported as suspicious for PCa metastases subsequently confirmed by histology.

Teaching points:

- The incidence of sovraclavicular or mediastinal PCa lymph nodes metastases is not common [33].
- However, it should be suspected in case of diffused disease, concurrent retroperitoneal lymph nodes, or retroperitoneal lymph nodes at the diagnosis [33].
- In this case, patient performed radiation therapy in an extended PTV (prostate bed, retroperitoneal, and bilateral iliac lymph nodes), thus the risk of distant lesions was very high.

18.19 Case 18: Biochemical Persistence After Radical Therapy: 11C-Choline vs. 68Ga-PSMA-11 PET/CT

Clinical details: This is a case of a 50-year-old patient with PCa (T3b,N1,M0, ISUP Group 5, iPSA 34 ng/ml). Pelvic MRI, CT, and bone scan were performed to stage the disease. Conventional imaging did not reveal the presence of PCa metastasis. Patient was subsequently treated with RP in December 2018 as primary treatment. PSA nadir was 0.32 ng/ml in January 2019, and patient was addressed to ADT from January 2019. Due to the fast rising of PSA (PSA 3.1 ng/ml in February 2019), the patient was referred to 11C-Choline PET/CT. The scan revealed no significant areas of focal uptake reliably referred to PCa metastases. Due to the high-risk disease and the doubting result of 11C-Choline PET/CT, 1 week later, patient was referred to 68Ga-PSMA PET/CT.

Images:

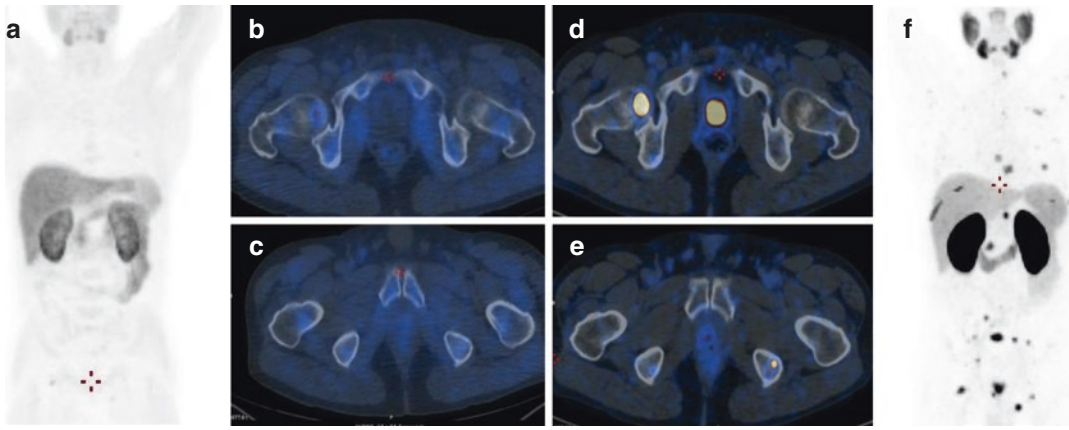

Scan findings: 11C-Choline PET/CT shows only faint and in-homogenous uptake in several bone without significant focal uptake and no CT correlatives (A: 11C-Choline MIP projection; B, C: 11C-Choline PET and CT-fused images). 68Ga-PSMA-11 PET/CT showed multiple bone lesions with high and focal uptake (D, E: 68Ga-PSMA-11 PET and CT-fused images; F: 68Ga-PSMA-11 MIP projection).

Interpretation: All PSMA-positive lesions were reported as PCa metastases, and patient was subsequently addressed to systemic therapy.

Teaching points:

- In PCa patients with biochemical failure after therapy, current imaging techniques have a low detection rate at the PSA levels at which targeted salvage therapy is effective.
- 11C-Choline and 18F-fluoromethylcholine, though widely used, have poor sensitivity at low PSA levels [34].
- In several studies, 68Ga-PSMA-11 demonstrated a higher detection rate than [18] F-fluoromethylcholine [35, 36].

18.20 Case 19: 68Ga-PSMA-11 PET/CT: mCRPC

Clinical details: This is a case of a 74-year-old patient treated with RP for PCa (GS = 4 + 5, T3bN1(2/24)MxR0, PSAi = 12.1 ng/mL). BCR occurred 11 months after surgery, with rising PSA levels (PSA 4.1 ng/mL). Patient was addressed to ADT with continuous scheme (bicalutamide + LH-RH inhibitor), experiencing PSA response (PSA values <0.2 ng/mL). After 1 year, BCR occurred with rising PSA levels during ADT. Patient was subsequently referred to 68Ga-PSMA-11 PET/CT with PSA value of 1.98 ng/mL.

Images:

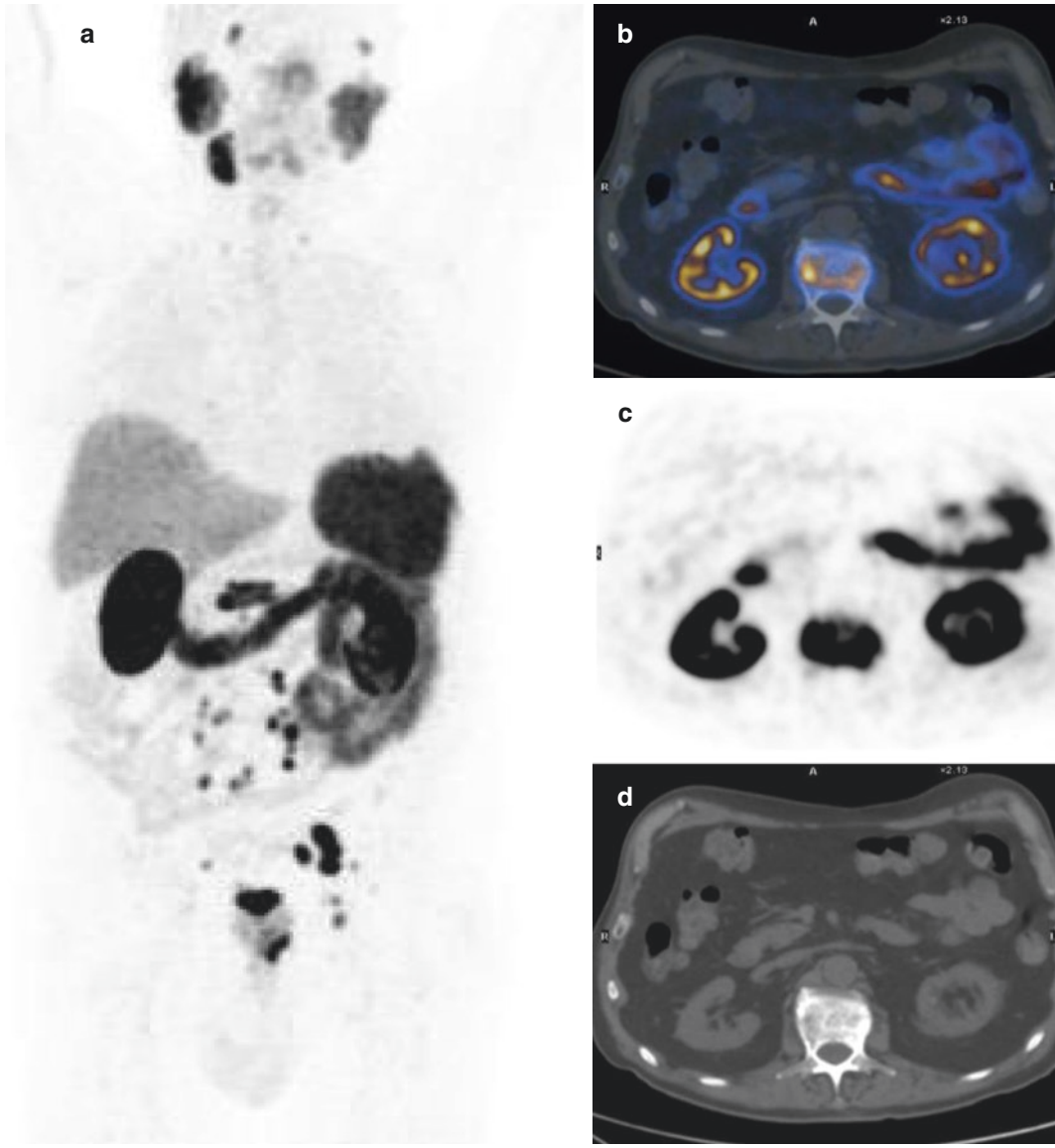

Scan findings: 68Ga-PSMA-11 PET/CT showed one bone metastasis (L1) together with lymph node relapse (bilateral common, internal, and external iliac lymph nodes). A: MIP projection; B: Fused PET/CT image; C: PET transaxial image; D: low-dose CT image.

Interpretation: Patient was addressed to EBRT on L1 and androgen-receptor (AR)-targeted therapy according to the diffuse metastatic spread revealed by 68Ga-PSMA-11 PET/CT. After six cycles of enzalutamide, PSA rapidly raised up to 14.3 ng/mL and 68Ga-PSMA-11 PET/CT was newly performed to restage the disease.

Images:

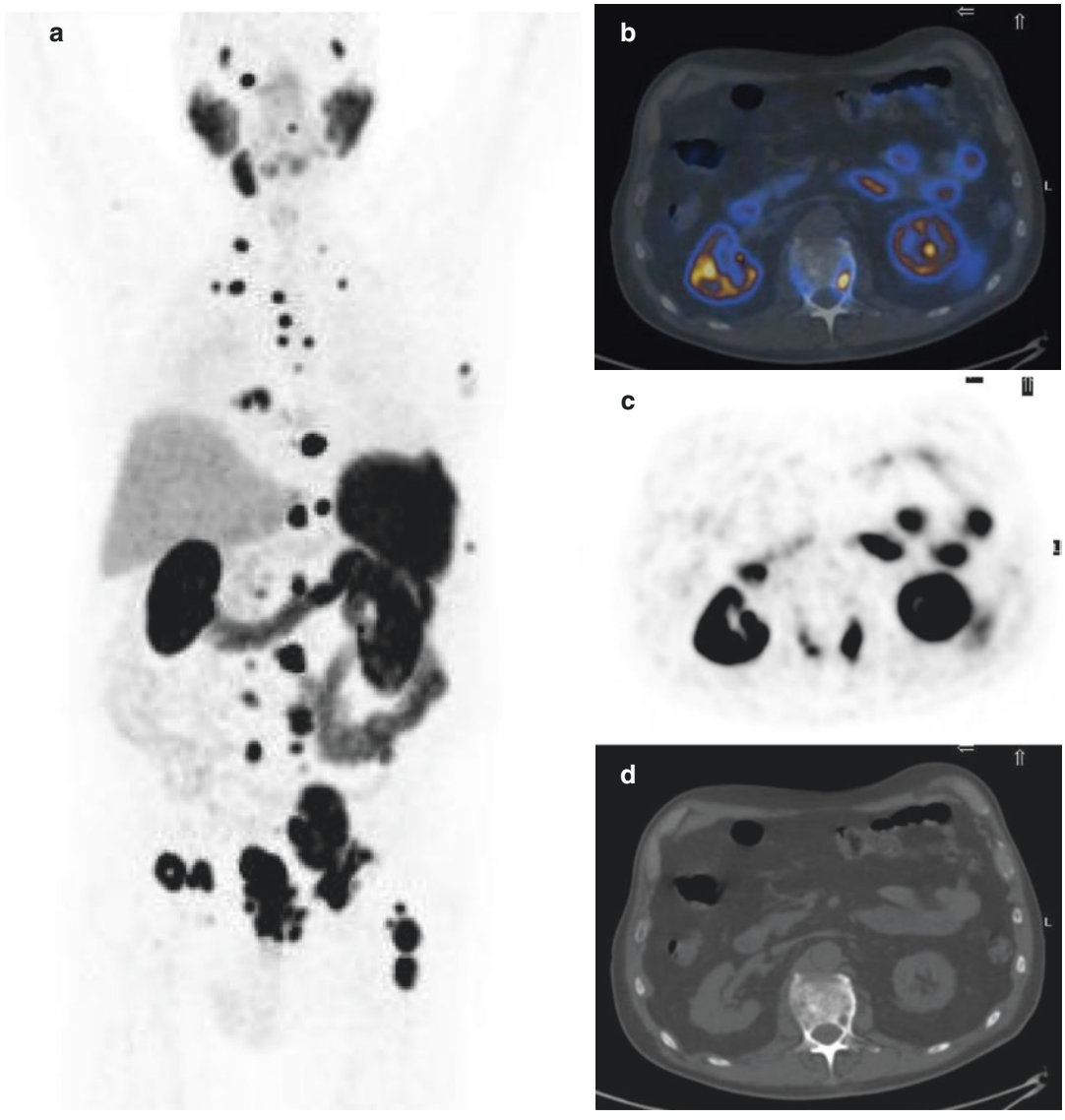

Scan findings: 68Ga-PSMA-11 PET/CT revealed a massive spread to lymph nodes (lomboaortic and mediastinal lymph nodes) and to the skeletal tissue (pelvis, left femur, spine, and ribs). A: MIP projection; B: Fused PET/CT image; C: PET transaxial image; D: low-dose CT image.

Interpretation: According to the diffuse metastatic spread revealed by 68Ga-PSMA-11 PET/CT, patient was addressed to chemotherapy (Docetaxel). 223Ra treatment was excluded due to the presence of lymph nodes bigger than 3 cm.

Teaching points:

- Defining an optimal therapeutic approach in mCRPC patients in advanced stages is still challenging in routine clinical practice.
- Patients with this condition are benefiting from an increasing number of treatment options such as AR-targeted therapy, chemotherapy, 223Ra, and PSMA radioligand therapy (177Lu-PSMA-617 or 225Ac-PSMA-617).
- However, assessing therapy response in patients with multiple localizations might be challenging.
- 68Ga-PSMA-11 PET/CT could be a good diagnostic procedure to assess response to systemic therapy in mCRPC, especially to evaluate PSMA radioligand therapy response [37, 38].

18.21 Case 20: 18F-FDG PET/CT in PCa

Clinical details: This is a case of a patient with a recent diagnosis of PCa (GS = 4 + 4 on 7/12 biopsy samples). During diagnostic work-up, patient performed a CT revealing multiple abdominal adenopathy. Patient was referred to 18F-FDG PET/CT to exclude the presence of other malignancies prior to PCa radical therapy.

Images:

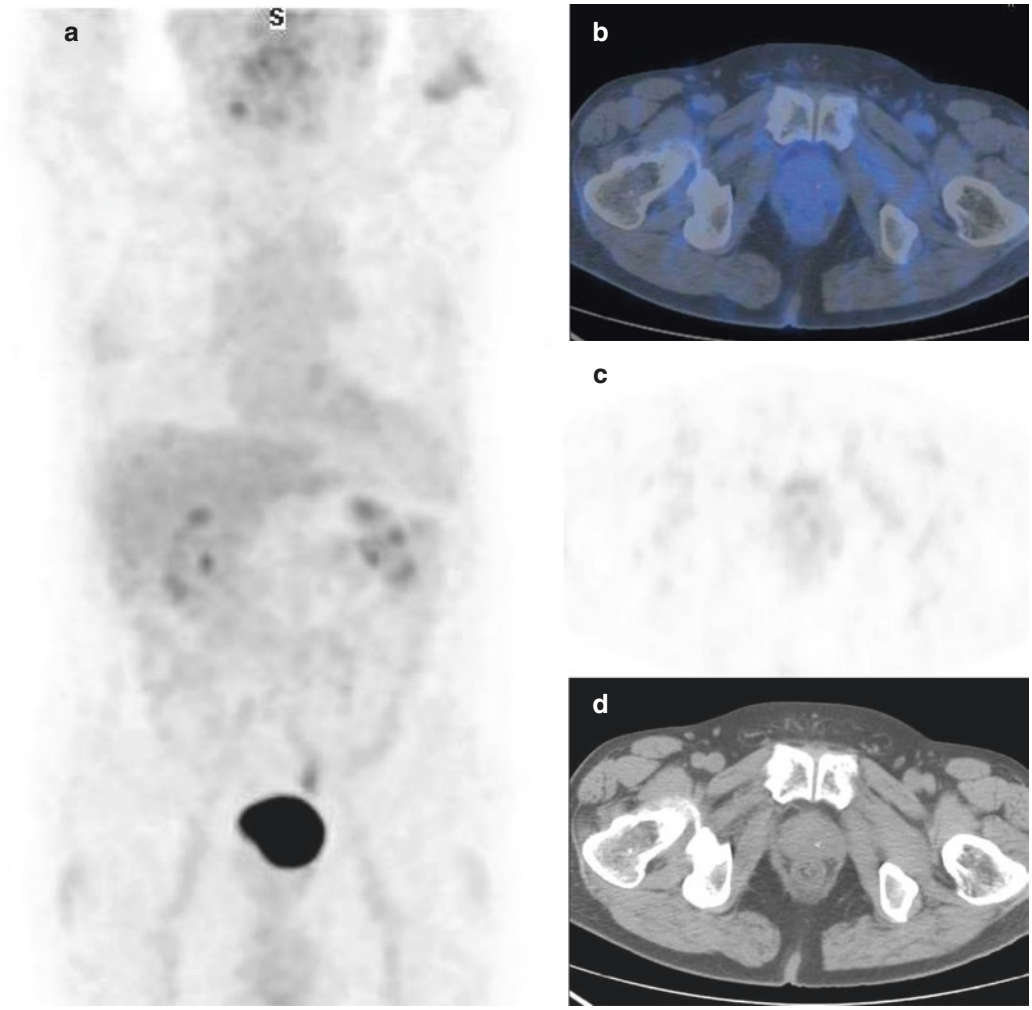

Scan findings: 18F-FDG PET/CT did not show any significant areas of tracer uptake. The multiple abdominal lymph nodes showed no significant FDG uptake. Prostate gland did not demonstrate any focal uptake. A: MIP projection; B: PET and CT-fused image; C: PET image; D: CT image of prostate gland.

Teaching points:

- While the utility of 18F-FDG PET/CT in many cancers is relatively well established, its role in PCa is controversial [39, 40].
- Overall, the level of FDG accumulation can overlap in normal prostate, benign prostate hyperplasia (BPH), and PCa tissues, which often coexist altogether in a heterogeneous pattern [39, 40].
- Occasionally, incidental high FDG uptake may be seen in the prostate gland of patients who undergo 18F-FDG PET/CT for a condition unrelated to known prostate pathology [41].
- In this context, it has been suggested that incidental prostate uptake on FDG PET scans should not be ignored and at least a serum PSA measurement should be considered [41, 42].

References

Case 1

1. Calabria F, Schillaci O. The biodistribution of the radiolabeled kinds of choline in male patients, assessed by PET/CT. Nucl Med Commun. 2016;37(3):329–30.
2. Haroon A, Zanoni L, Celli M, Zakavi R, Beheshti M, Langsteger W, et al. Multicenter study evaluating extraprostatic uptake of 11C-choline, 18F-methylcholine, and 18F-ethylcholine in male patients: physiological distribution, statistical differences, imaging pearls, and normal variants. Nucl Med Commun. 2015;36(11):1065–75.

Case 2

3. Delmas PD, Meunier PJ. The management of Paget's disease of bone. N Engl J Med. 1997;336(8):558–66. Review.
4. Giovacchini G, Samanes Gajate AM, Messa C, Fazio F. Increased C-11 choline uptake in pagetic bone in a patient with coexisting skeletal metastases from prostate cancer. Clin Nucl Med. 2008;33(11):797–8.

Case 3

5. Calabria F, Chiaravalloti A, Cicciò C, Gangemi V, Gullà D, Rocca F, et al. PET/CT with (18)F-choline: physiological whole bio-distribution in male and female subjects and diagnostic pitfalls on 1000 prostate cancer patients: (18)F-choline PET/CT biodistribution and pitfalls. A southern Italian experience. Nucl Med Biol. 2017;51:40–54.

Case 4

6. Evangelista L, Guttilla A, Zattoni F, Muzzio PC, Zattoni F. Utility of choline positron emission tomography/computed tomography for lymph node involvement identification in intermediate- to high-risk prostate cancer: a systematic literature review and meta-analysis. Eur Urol. 2013;63(6):1040–8.
7. Schiavina R, Bianchi L, Mineo Bianchi F, Borghesi M, Pultrone CV, Dababneh H, et al. Preoperative staging with (11)C-choline PET/CT is adequately accurate in patients with very high-risk prostate cancer. Clin Genitourin Cancer. 2018;16(4):305–312.e1.

Case 5

8. Rietbergen DD, van der Hiel B, Vogel W, Stokkel MP. Mediastinal lymph node uptake in patients with prostate carcinoma on F18-choline PET/CT. Nucl Med Commun. 2011;32(12):1143–7.
9. Evangelista L, Guttilla A, Zattoni F, Muzzio PC, Zattoni F. Utility of choline positron emission tomography/computed tomography for lymph node involvement identification in intermediate- to high-risk prostate cancer: a systematic literature review and meta-analysis. Eur Urol. 2013;63(6):1040–8.

Case 6

10. Fanti S, Minozzi S, Castellucci P, Balduzzi S, Herrmann K, Krause BJ, et al. PET/CT with (11)C-choline for evaluation of prostate cancer patients with biochemical recurrence: meta-analysis and critical review of available data. Eur J Nucl Med Mol Imaging. 2016;43(1):55–69.
11. Krause BJ, Souvatzoglou M, Tuncel M, Herrmann K, Buck AK, Praus C, et al. The detection rate of [11C]choline-PET/CT depends on the serum PSA-value in patients with biochemical recurrence of prostate cancer. Eur J Nucl Med Mol Imaging. 2008;35(1):18–23.
12. Mapelli P, Incerti E, Ceci F, Castellucci P, Fanti S, Picchio M. 11C- or 18F-choline PET/CT for imaging evaluation of biochemical recurrence of prostate cancer. J Nucl Med. 2016;57(Suppl 3):43S–8S.

Case 7

13. Mapelli P, Incerti E, Ceci F, Castellucci P, Fanti S, Picchio M. 11C- or 18F-choline PET/CT for imaging evaluation of biochemical recurrence of prostate cancer. J Nucl Med. 2016;57(Suppl 3):43S–8S.
14. Gillebert Q, Huchet V, Rousseau C, Cochet A, Olivier P, Courbon F, et al. 18F-fluorocholine PET/CT in patients with occult biochemical recurrence of prostate cancer: detection rate, impact on management and adequacy of impact. A prospective multicentre study. PLoS One. 2018;13(2):e0191487.

Case 8

15. Beheshti M, Haim S, Zakavi R, Steinmair M, Waldenberger P, Kunit T, et al. Impact of 18F-choline PET/CT in prostate cancer patients with biochemical recurrence: influence of androgen deprivation ther-

apy and correlation with PSA kinetics. J Nucl Med. 2013;54(6):833–40.
16. Evangelista L, Zattoni F, Guttilla A, Basso U, Zattoni F. The effects of androgen deprivation therapy on the 18F-Chcoline uptake in prostate cancer patients undergoing neoadjuvant treatment. Q J Nucl Med Mol Imaging. 2019;63(3):278–83.

Case 9

17. Ost P, Reynders D, Decaestecker K, Fonteyne V, Lumen N, De Bruycker A, et al. Surveillance or metastasis-directed therapy for oligometastatic prostate cancer recurrence: a prospective, randomized, multicenter phase II trial. J Clin Oncol. 2018;36(5):446–53. https://doi.org/10.1200/JCO.2017.75.4853.
18. Pasqualetti F, Panichi M, Sainato A, Matteucci F, Galli L, Cocuzza P, et al. [(18)F]Choline PET/CT and stereotactic body radiotherapy on treatment decision making of oligometastatic prostate cancer patients: preliminary results. Radiat Oncol. 2016;11:9.

Case 10

19. Heidenreich A, Bastian PJ, Bellmunt J, Bolla M, Joniau S, van der Kwast T, et al. EAU guidelines on prostate cancer. Part II: Treatment of advanced, relapsing, and castration-resistant prostate cancer. Eur Urol. 2014;65:467–79.
20. Ceci F, Castellucci P, Graziani T, Schiavina R, Renzi R, Borghesi M, et al. (11)C-Choline PET/CT in castration-resistant prostate cancer patients treated with docetaxel. Eur J Nucl Med Mol Imaging. 2016;43(1):84–91.
21. Caroli P, De Giorgi U, Scarpi E, Fantini L, Moretti A, Galassi R, et al. Prognostic value of 18F-choline PET/CT metabolic parameters in patients with metastatic castration-resistant prostate cancer treated with abiraterone or enzalutamide. Eur J Nucl Med Mol Imaging. 2018;45(3):348–54.

Case 11

22. Keidar Z, Gill R, Goshen E, Israel O, Davidson T, Morgulis M, et al. 68Ga-PSMA PET/CT in prostate cancer patients - patterns of disease, benign findings and pitfalls. Cancer Imaging. 2018;18(1):39.
23. Afshar-Oromieh A, Malcher A, Eder M, Eisenhut M, Linhart HG, Hadaschik BA, et al. PET imaging with a [68Ga]gallium-labelled PSMA ligand for the diagnosis of prostate cancer: biodistribution in humans and first evaluation of tumour lesions. Eur J Nucl Med Mol Imaging. 2013;40(4):486–95.

Case 12

24. Rischpler C, Beck TI, Okamoto S, Schlitter AM, Knorr K, Schwaiger M, et al. (68)Ga-PSMA-HBED-CC uptake in cervical, celiac, and sacral ganglia as an important pitfall in prostate cancer PET imaging. J Nucl Med. 2018;59(9):1406–11.

Case 13

25. Delmas PD, Meunier PJ. The management of Paget's disease of bone. N Engl J Med. 1997;336(8):558–66. Review.
26. Keidar Z, Gill R, Goshen E, Israel O, Davidson T, Morgulis M, et al. 68Ga-PSMA PET/CT in prostate cancer patients - patterns of disease, benign findings and pitfalls. Cancer Imaging. 2018;18(1):39.

Case 14

27. Wu SY, Boreta L, Shinohara K, Nguyen H, Gottschalk AR, Hsu IC, et al. Impact of staging (68)Ga-PSMA-11 PET scans on radiation treatment plans in patients with prostate cancer. Urology. 2019;125:154–62.
28. Hirmas N, Al-Ibraheem A, Herrmann K, Alsharif A, Muhsin H, Khader J, et al. [(68)Ga]PSMA PET/CT improves initial staging and management plan of patients with high-risk prostate cancer. Mol Imaging Biol. 2018;21:574–81.

Case 15

29. Bashir U, Tree A, Mayer E, Levine D, Parker C, Dearnaley D, et al. Impact of Ga-68-PSMA PET/CT on management in prostate cancer patients with very early biochemical recurrence after radical prostatectomy. Eur J Nucl Med Mol Imaging. 2019;46(4):901–7.
30. Ceci F, Castellucci P, Graziani T, Farolfi A, Fonti C, Lodi F, et al. (68)Ga-PSMA-11 PET/CT in recurrent prostate cancer: efficacy in different clinical stages of PSA failure after radical therapy. Eur J Nucl Med Mol Imaging. 2019;46(1):31–9.
31. Fendler WP, Calais J, Eiber M, Flavell RR, Mishoe A, Feng FY, et al. Assessment of 68Ga-PSMA-11 PET accuracy in localizing recurrent prostate cancer:

a prospective single-arm clinical trial. JAMA Oncol. 2019;5:856–63.

Case 16

32. Keidar Z, Gill R, Goshen E, Israel O, Davidson T, Morgulis M, et al. 68Ga-PSMA PET/CT in prostate cancer patients - patterns of disease, benign findings and pitfalls. Cancer Imaging. 2018;18(1):39.

Case 17

33. Bhattar R, Maheshwari A, Yadav SS, Tomar V. Unusual Presentation of Prostate Carcinoma: A Case Report. J Clin Diagn Res. 2017;11(2):PD06–7.

Case 18

34. Emmett L, Metser U, Bauman G, Hicks RJ, Weickhardt A, Davis ID, et al. A prospective, multi-site, international comparison of F-18 fluoro-methyl-choline, multi-parametric magnetic resonance and Ga-68 HBED-CC (PSMA-11) in men with high-risk features and biochemical failure after radical prostatectomy: clinical performance and patient outcomes. J Nucl Med. 2018. pii: jnumed.118.220103.
35. Morigi JJ, Stricker PD, van Leeuwen PJ, Tang R, Ho B, Nguyen Q, et al. Prospective comparison of 18F-fluoromethylcholine versus 68Ga-PSMA PET/CT in prostate cancer patients who have rising PSA after curative treatment and are being considered for targeted therapy. J Nucl Med. 2015;56(8):1185–90.
36. Schwenck J, Olthof SC, Pfannenberg C, Reischl G, Wegener D, Marzec J, et al. Intention to treat analysis of (68)Ga-PSMA and (11)C-choline PET/CT versus CT for prostate cancer recurrences after surgery. J Nucl Med. 2019. pii: jnumed.118.224543.

Case 19

37. Rahbar K, Boegemann M, Yordanova A, Eveslage M, Schäfers M, Essler M, et al. PSMA targeted radioligandtherapy in metastatic castration resistant prostate cancer after chemotherapy, abiraterone and/or enzalutamide. A retrospective analysis of overall survival. Eur J Nucl Med Mol Imaging. 2018;45(1):12–9.
38. Heinzel A, Boghos D, Mottaghy FM, Gaertner F, Essler M, von Mallek D, Ahmadzadehfar H. (68) Ga-PSMA PET/CT for monitoring response to (177) Lu-PSMA-617 radioligand therapy in patients with metastatic castration-resistant prostate cancer. Eur J Nucl Med Mol Imaging. 2019;46(5):1054–62.

Case 20

39. Salminen E, Hogg A, Binns D, Frydenberg M, Hicks R. Investigations with FDG-PET scanning in prostate cancer show limited value for clinical practice. Acta Oncol. 2002;41(5):425–9. PubMed PMID: 12442917.
40. Jadvar H. Is there utility for FDG PET in prostrate cancer? Semin Nucl Med. 2016;46(6):502–6.
41. Sahin E, Elboga U, Kalender E, et al. Clinical significance of incidental FDG uptake in the prostate gland detected by PET/CT. Int J Clin Exp Med. 2015;8:10577–85.
42. Brown AM, Lindenberg ML, Sankineni S, et al. Does focal incidental 18F-FDG uptake in the prostate gland have significance? Abdom Imaging. 2015;40:3222–9.

19 FDG PET/CT in Treatment Response Evaluation of Gynecological Malignancies

Shelvin Kumar Vadi and Bhagwant Rai Mittal

19.1 Role of FDG PET/CT in Treatment Response Evaluation of Cervical Carcinoma

19.1.1 Introduction

Primary carcinoma of the cervix is the second most common malignancy in women worldwide and a leading cause for mortality [1]. FDG PET/CT has been extensively evaluated in all settings of disease management in cervical cancer [2]. In staging of cervical cancer, although MRI is the gold standard in evaluating locoregional extension of the primary tumor. FDG PET/CT is reported as a useful diagnostic and prognostic [3, 4] modality in identifying lymph nodal as well as distant metastatic spread in initial evaluation [5]. FDG PET/CT is also evaluated for its role in precisely dosing image-guided adaptive radiotherapy [6].

In line with the management of other gynecological malignancies, surgery, radiotherapy, and chemotherapy remain the mainstay of management of cervical cancer, depending on the specific stage. FDG PET/CT has shown good diagnostic utility in the evaluation of treatment response by several studies. Studies have shown that FDG uptake finding in the post-therapy study is predictive of patient survival outcome over and above that to the pretreatment lymph nodal status [7]. The 3-year survival also correlated with the metabolic response pattern of the post therapeutic FDG PET/CT study with progressive metabolic disease in the post therapeutic FDG PET/CT resulting in 0% 3-year survival rate [8]. Posttreatment response and lymph nodal status were the only predictors of progression-free survival in this study. FDG PET/CT is also reported as a promising modality in the prediction of response even at early phase as well as at the completion of chemotherapy [9]. The incorporation of FDG PET/CT in the treatment response evaluation has resulted in alteration of management options in one-third of patients and helped in significantly reducing cost and in guiding accurate surgical intervention [8].

The utility of FDG PET/CT is not without limitations and pitfalls. Postoperative infectious/inflammatory processes, pelvic bowel and urinary activity, postradiation fibrosis, etc., still possess diagnostic challenges in treatment evaluation scenario. Careful evaluation of these physiological/benign findings should be done to avoid the possibility of false-positive interpretations and pitfalls.

S. K. Vadi · B. R. Mittal (✉)
Department of Nuclear Medicine, PGIMER, Chandigarh, India

S. Fanti et al. (eds.), *Atlas of Clinical PET-CT in Treatment Response Evaluation in Oncology*,
https://doi.org/10.1007/978-3-030-68858-5_19

19.1.2 Case 1: Metastatic Carcinoma Cervix with Near-Complete Metabolic Response in FDG PET/CT

Clinical summary: Thirty-one-year female was a known case of carcinoma cervix post four cycles of chemotherapy and adjuvant radiotherapy. She developed chest pain with sudden onset of breathlessness and cough after 6 months of completion of treatment. An FDG PET/CT was done for disease status/recurrence evaluation (Figs. 19.1, 19.2 and 19.3).

Interpretation: FDG PET/CT showed recurrent distant metastatic lesions in a treatment completed patient of carcinoma cervix. After confirming the metastatic nature of the lesion, repeated FDG PET/CT post six cycles of chemotherapy showed near-complete metabolic response. The persistence of FDG uptake in the pelvic ascites prompted in giving two more cycles of chemotherapy.

Teaching points:

1. Pulmonary metastasis from cervical cancer can be isolated or in the form of multiple nodules with or without cavitation and usually is symptom free. An FDG-avid pulmonary lesion in the setting of carcinoma cervix warrants confirmation of the nature of the pulmonary lesion to differentiate it from primary lung malignancy/metastasis from carcinoma cervix or any benign infectious/inflammatory process [10].
2. The presence of minimal residual disease post-treatment completion helped in giving two more cycles as consolidation chemotherapy.

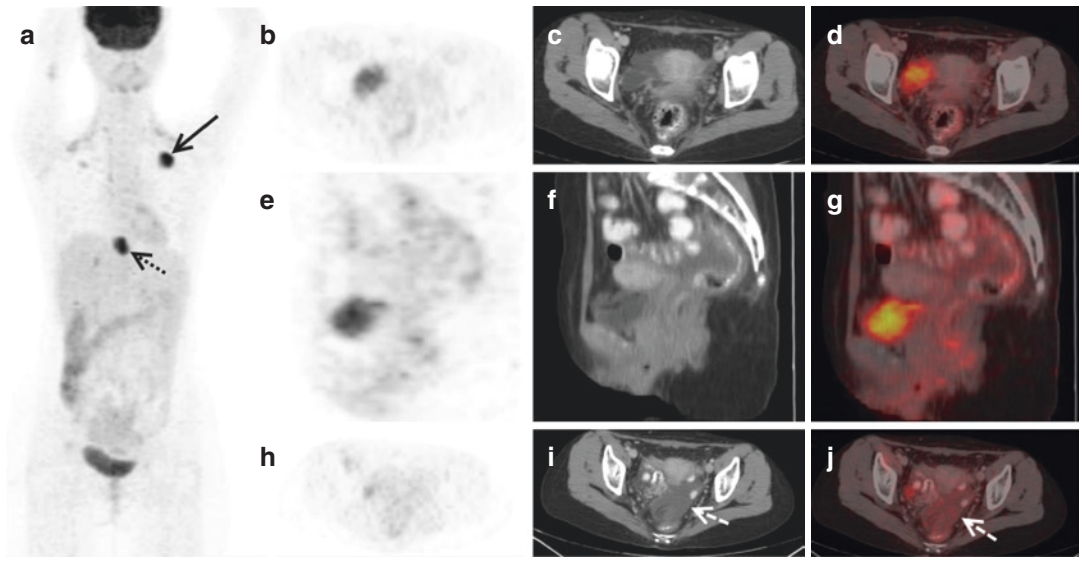

Fig. 19.1 FDG PET/CT in a 31-year female, presenting with chest pain and cough, 6 months posttreatment completion. Abnormal foci of FDG uptake were noted in the chest region in the MIP (**a**; arrows). There was no abnormal FDG uptake/lesion in the uterus and cervix as seen in the axial (**b–d**) and sagittal (**e–g**) PET, CT, and fused PET/CT images, respectively. However, low-grade FDG-avid pelvic ascites were noted (**h–j**; broken arrows)

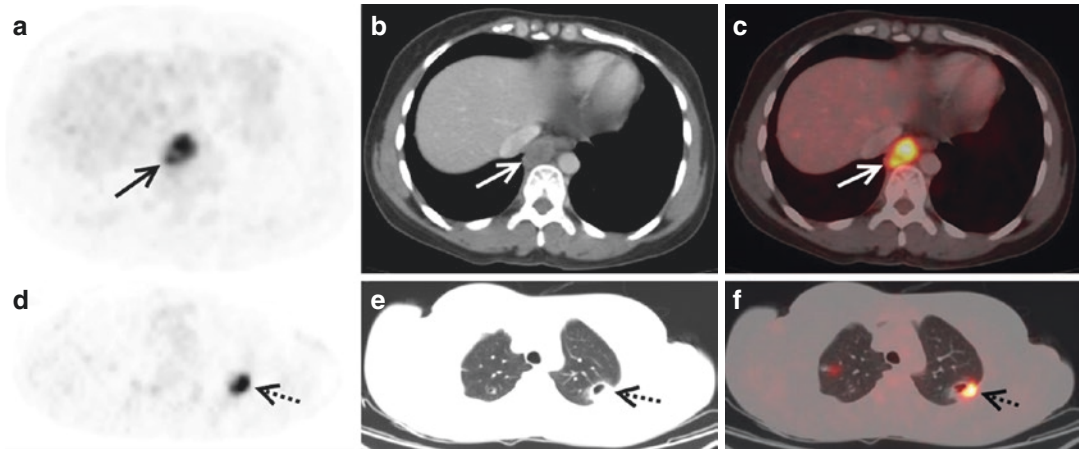

Fig. 19.2 The abnormal foci of increased FDG uptake in the chest region in the MIP image were localized to an enlarged thoracic paraesophageal lymph node (solid arrow; **a–c**) and in the FDG-avid cavitary lesion in the both lung apices (dotted arrows; **d–f**). Fine-needle aspiration of the lung lesion suggested metastatic squamous cell carcinoma

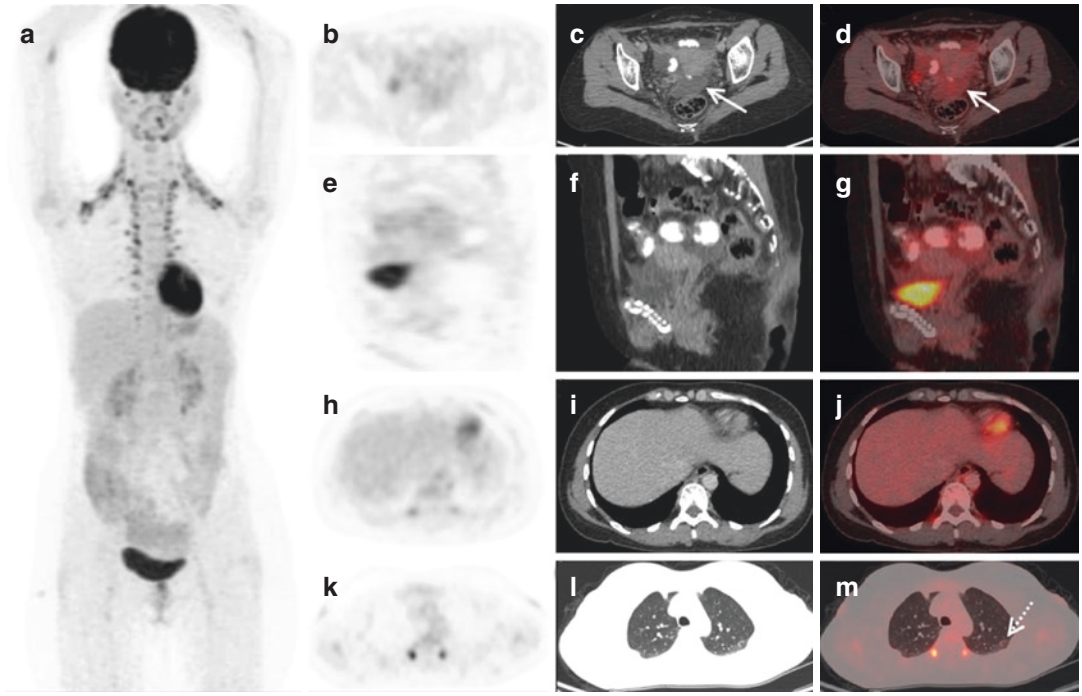

Fig. 19.3 The patient received six cycles of chemotherapy considering the recurrent distant metastatic lesions. FDG PET/CT was repeated for treatment evaluation after 4 weeks of completion of chemotherapy, which showed minimal residual disease in the form of faintly FDG-avid pelvic ascites (**b–g**; solid arrows). There was complete resolution of the FDG-avid thoracic paraesophageal lymph node and the bilateral lung lesions (**h–m**). Symmetrical uptake in the supraclavicular and paravertebral brown adipose tissue FDG uptake can be noted in the MIP (**a**)

19.1.3 Case 2: Vesicovaginal and Rectovaginal Fistulas Complicating Response Evaluation in a Treatment Completed Cervix Carcinoma

Clinical Summary: Fifty-six-year female, a known case of squamous cell carcinoma of cervix underwent total abdominal hysterectomy and bilateral salpingo-oophorectomy with adjuvant chemotherapy. After 2 years of completion of treatment, she presented with per vaginal pus discharge. Biopsy and histopathological analysis from the vaginal stump showed poorly differentiated squamous cell carcinoma. She was treated with six more cycles of chemotherapy and loop colostomy. FDG PET/CT was done for evaluation after treatment (Figs. 19.4 and 19.5).

Images:

Interpretation: FDG PET/CT in this patient showed a well-defined nodular deposit overlaying the right rectus abdominis in the upper pelvis. In the current clinical context, it was suggestive of metastatic deposit, and histopathological correlation was suggested. The increased FDG uptake in the vaginal vault and lumen with contiguous uptake in the bladder and rectosigmoid along with delayed contiguous filling of the contrast was suggestive of the presence of vesicovaginal and rectovaginal fistulas in this patient which was confirmed on retrospective history and examination.

Teaching points:

1. Fistulas may develop in gynecological malignancies as a complication to radiation therapy or radical surgeries involving complex surgical fields/prior irradiated field, and the annual incidence of radiotherapy-induced vesicovaginal fistulas is ~1–5%. Vesicovaginal and enterovaginal fistulas are the most common types seen in association with gynecologic malignancies [11, 12].

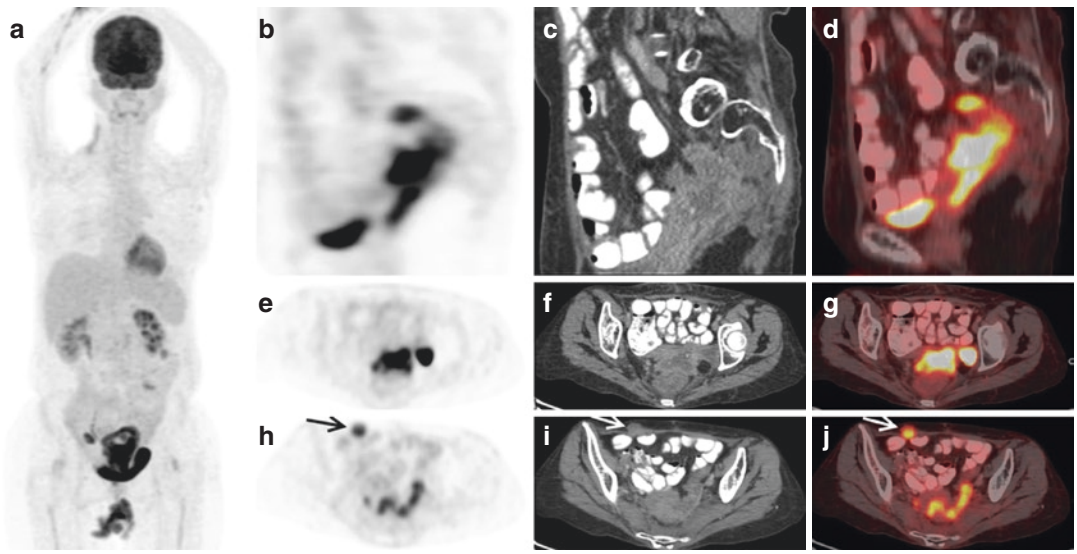

Fig. 19.4 FDG PET/CT post six cycles of chemotherapy for disease recurrence after 2 years of treatment completion, in a 46-year female with squamous cell carcinoma cervix. Maximum intensity projection (**a**) showed abnormal foci of increased tracer uptake in the pelvis and physiological tracer uptake elsewhere. The abnormal tracer uptake was localized to the vaginal stump and vaginal lumen and continuing with the rectosigmoid loops and urinary bladder tracer activity as seen in the sagittal and axial PET, CECT, and fused PET/CT images (**b–g**). A focus of increased FDG uptake was also noted in a well-defined nodular deposit overlaying the rectus abdominis muscle on right side in the pelvis (highlighted with arrow; **h–j**)

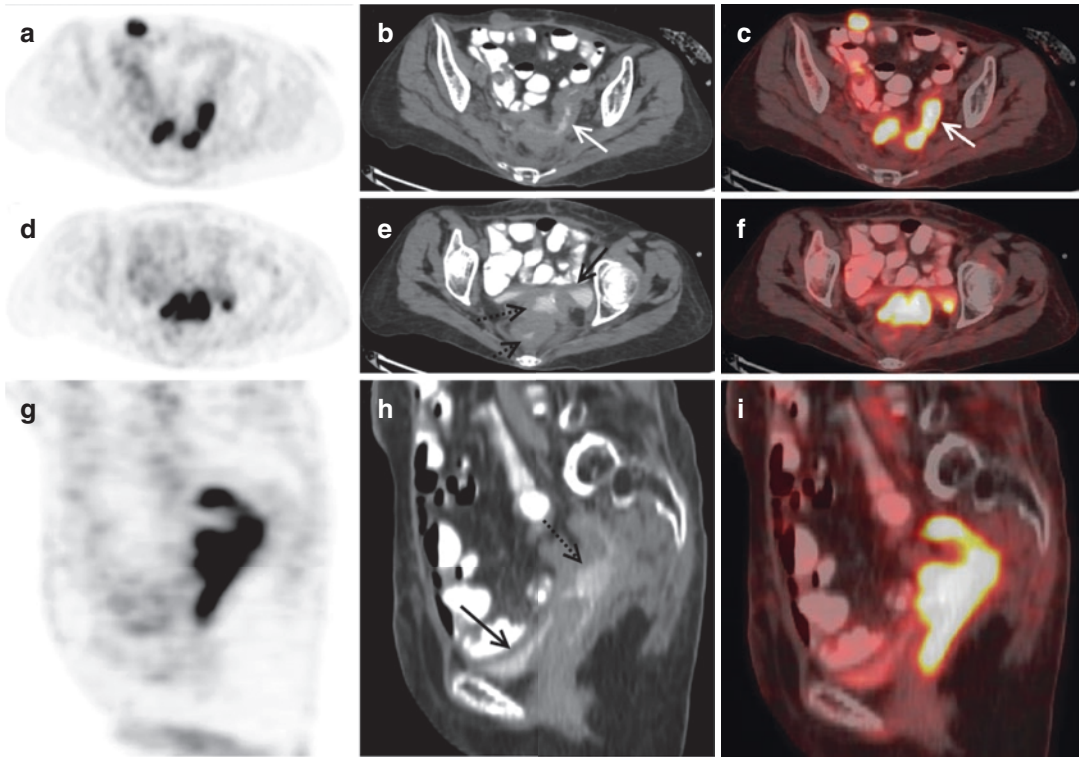

Fig. 19.5 Delayed images (dual time point) of the pelvis were also acquired (**a–i**) which showed increased FDG activity in the rectosigmoid (white arrows **b** and **c**), vaginal vault contiguous with the urinary bladder (solid arrow; **e** and **h**) along with intraluminal contrast filling in the vaginal vault and rectum (dotted arrows in **e** and **h**) on delayed images

2. Fistulation with contamination from urinary FDG excretion can lead to an overestimation of activity within malignant disease or, conversely, may mask disease. Therefore, care should be taken when assessing these patients, with close correlation with recent clinical history, physical examination, and conventional imaging [13].
3. False-positive urinary tracer uptake of FDG in the fistulous tract complicates the interpretation, and a delayed CECT image helps in showing excretion of intravenous contrast material into the vagina in approximately 60% of patients. Furthermore, there may be air or fluid in the vagina [14, 15].

19.1.4 Case 3: FDG PET/CT Showing Complete Metabolic Response to EBRT and ICA in Carcinoma Cervix

Clinical summary: Forty-five-year female developed menorrhagia for 6 months. She was evaluated with endocervical and endometrial curettage and biopsy. The histopathological analysis confirmed poorly differentiated cervical carcinoma. FDG PET/CT was done for initial staging (Figs. 19.6 and 19.7).

Images:

Interpretation: FDG PET/CT in this patient of carcinoma cervix ruled out extracorporeal disease spread and showed complete metabolic response to EBRT+ICA.

Teaching points:

1. Apart from International Federation of Gynecology and Obstetrics (FIGO) staging, additional imaging at diagnosis can provide valuable information to guide prognosis, determine management, and assist in treat-

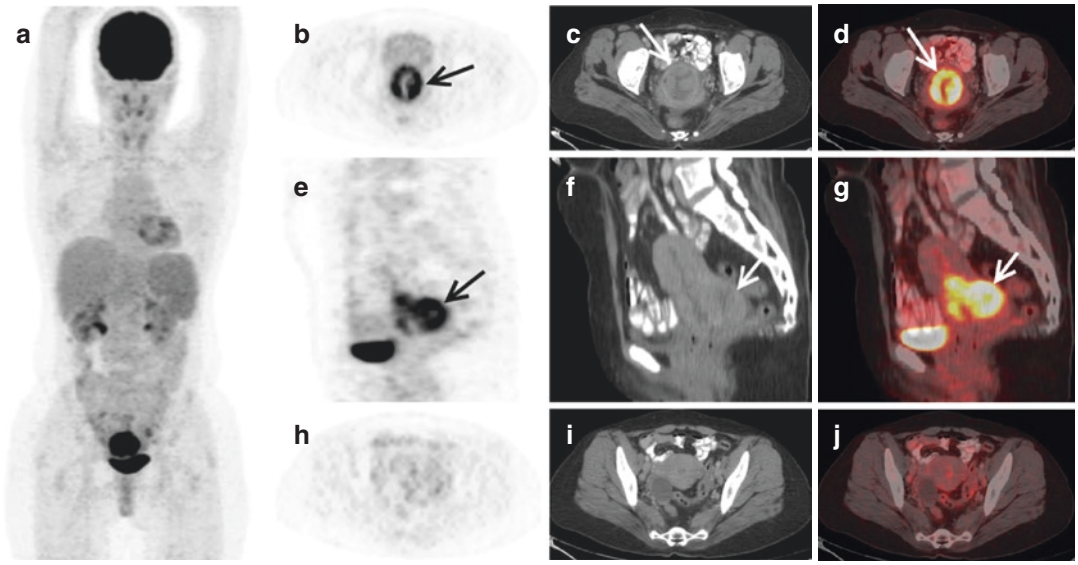

Fig. 19.6 FDG PET/CT done for initial staging in a case of poorly differentiated carcinoma cervix. Abnormal FDG uptake is noted in the pelvis which was localized to the heterogeneously enhancing mass lesion in the cervix with endo-luminal components and myometrial invasion as seen in the MIP (**a**), axial (arrows; **b–d**) and corresponding sagittal (arrows; **e–g**) PET, CECT, and fused PET/CT images. A non FDG-avid cystic lesion was also noted in the right adnexa (**h–j**). No other foci of abnormal FDG uptake were noted elsewhere in the body as seen in the MIP (**a**) image. Patient was managed with 25# (55 Gy) of EBRT followed by two sittings of intracavitary brachytherapy (ICA). FDG PET/CT was repeated after 3 months

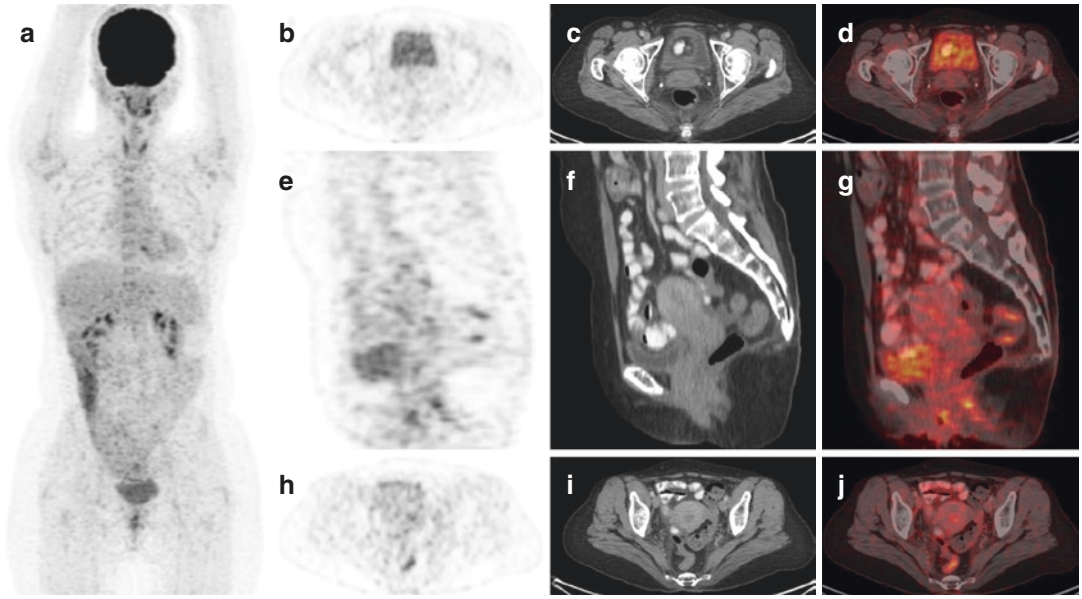

Fig. 19.7 FDG PET/CT done for treatment response evaluation after EBRT and ICA showing complete metabolic response with resolution of FDG uptake and size of the previously seen cervical lesion shown in MIP (**a**) and axial and sagittal PET, CECT, and fused PET/CT images (**b–g**). The cystic lesion in the right adnexa also resolved in the posttreatment PET/CT (**h–j**)

ment planning in carcinoma cervix [16]. For locally advanced disease, pelvic magnetic resonance imaging (MRI) and positron emission tomography/computed tomography (PET/CT) should be obtained at diagnosis when possible [17].

2. PET/CT helps in ruling out pelvic as well as extra-pelvic lymph nodal metastasis and has prognostic value in predicting response to therapy, independent of FIGO stage [18].
3. Post radiotherapy PET/CT FDG uptake and SUVmax have significant prognostic values and predictive powers for progression-free survival [2].

19.1.5 Case 4: FDG PET/CT in Treatment Evaluation in Metastatic Carcinoma Cervix—End of Treatment Assessment

Clinical summary: Fifty-four-year female, a known case of squamous cell carcinoma cervix underwent ^{18}F-FDG PET/CT for initial staging which showed FDG-avid soft-tissue lesion in the cervix along with pelvic lymph nodes. She received four cycles of chemotherapy followed by pelvic external beam radiotherapy as well as brachytherapy. Pelvic MRI done at the end of treatment was suggestive of bulky cervix likely due to posttreatment sequelae/residual disease. ^{18}F-FDG PET/CT done at the end of treatment for response evaluation showed a complete metabolic response, and the patient was then on follow up without additional therapy. An FDG PET/CT was also done after 14 months of follow up which again showed no interval change (Figs. 19.8 and 19.9).

Images:

Interpretation:

^{18}F-FDG PET/CT done for initial staging localized the disease in the pelvis by ruling out distal metastases. The patient was then managed with only four cycles of systemic chemotherapy and pelvic external beam radiotherapy and brachytherapy to cervix. The pelvic MRI could not rule out the possibility of residual disease likely due to posttreatment scarring/induration. ^{18}F-FDG PET/CT done posttreatment showed the complete metabolic response in this patient. The patient was put on follow up and remained disease-free which was confirmed with FDG PET/CT done at 14 months posttreatment completion.

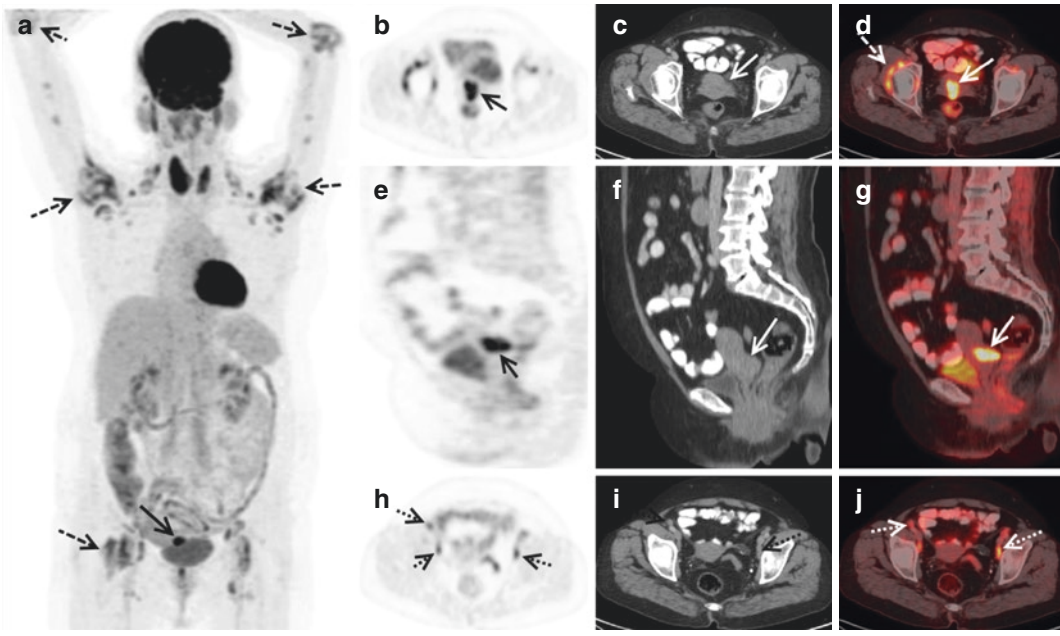

Fig. 19.8 ^{18}F-FDG PET/CT done for initial staging in a 54-year female with squamous cell carcinoma of the cervix. The maximum intensity projection (MIP) image (**a**) and the axial and corresponding sagittal PET (**b** and **e**), contrast-enhanced CT (**c** and **f**), and fused PET/CT (**d** and **g**) showing focally FDG-avid hypermetabolic soft-tissue lesion in the cervix (solid arrows). In addition, there was FDG-avid enlarged external iliac lymph nodes on both sides shown in the axial PET (**h**), CECT (**i**), and fused PET/CT (**j**) images further highlighted with dotted arrows. Heterogeneously increased FDG uptake is noted in the elbows, shoulders, and hip joints (highlighted with dashed arrows in MIP and axial fused PET/CT (**d**)) due to active arthritis. Diffusely increased FDG uptake was also noted in the both lobes of thyroid (**a**)

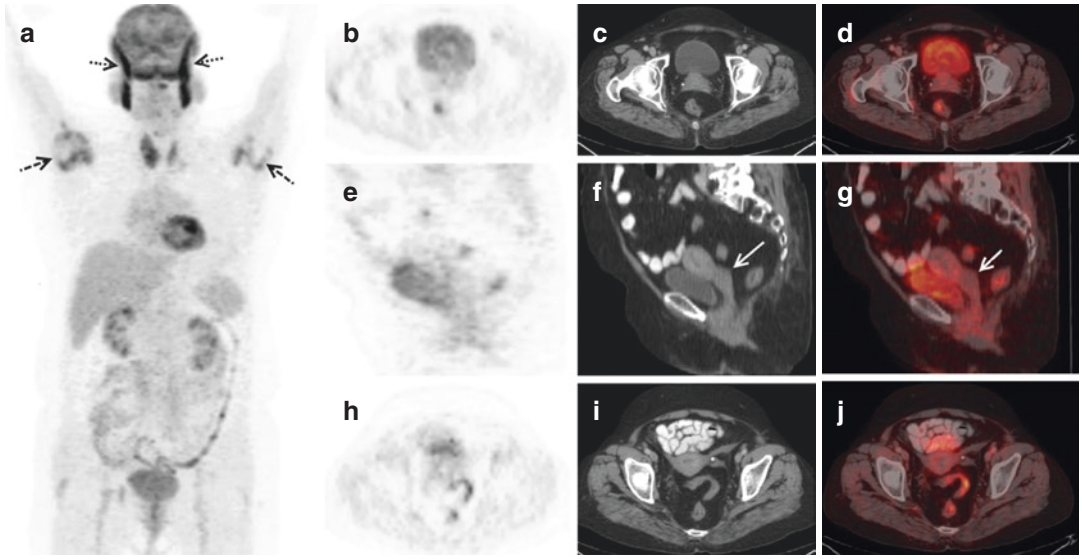

Fig. 19.9 ^{18}F-FDG PET/CT was done again for response evaluation post four cycles of chemotherapy followed by pelvic external beam radiotherapy and selective brachytherapy to cervix. The maximum intensity projection (MIP) image (**a**) and the axial and corresponding sagittal PET (**b** and **e**), contrast-enhanced CT (**c** and **f**), and fused PET/CT (**d** and **g**) showing resolution of the previously FDG-avid soft-tissue lesion in the cervix (solid arrows). The MIP (**a**) as well as the axial PET (**h**), CECT (**i**), and corresponding fused PET/CT (**j**) images showing resolution of the previously seen FDG-avid pelvic lymph nodes also. Persistence of FDG uptake in the shoulders (dashed arrows in MIP) can be seen due to arthritis. Intense FDG uptake was also noted in the masticatory muscles in the MIP (**a**; dotted arrows). Patient was kept on follow up considering the complete metabolic disease response

Teaching points:

1. FDG PET/CT at initial staging helped in ruling out the distant metastases and tailoring the therapy options.
2. Posttreatment scarring/ induration, fibrosis, and necrosis at the local sites make it challenging for pelvic MRI to rule out the presence of residual disease [19, 20]. FDG PET/CT being a functional/structural hybrid imaging can decrease the false positivity in this regard as in the index case.
3. Posttreatment complete metabolic response is a good prognostic predictor in case of carcinoma cervix [8].

19.1.6 Case 5: FDG PET/CT Showing Complete Metabolic Response in an Advanced Metastatic Cervix Cancer After Prior Disease Progression

Clinical summary: Forty-seven-year female presented with deep venous thrombosis on right side along with pelvic lymphadenopathy. CECT of the pelvis showed thrombus involving the right femoral, external iliac, and common iliac veins along with pelvic lymphadenopathy. USG-guided fine-needle aspiration cytology of the right sided pelvic lymph node was suggestive of metastatic squamous cell carcinoma. PET/CT done as part of carcinoma of unknown primary evaluation showed FDG-avid lesion in the uterine cervix with pelvic lymphadenopathy. Biopsy and histopathology from cervical lesion showed squamous cell carcinoma of cervix. She received external beam radiotherapy for the pelvis. FDG PET/CT was done post 3 months of completion of radiotherapy (Figs. 19.10, 19.11, 19.12 and 19.13).

Images:

Interpretation: The patient developed disease progression in the form of distant metastatic spread in the post-therapy FDG PET/CT which helped in the initiation of systemic chemotherapy and the repeat FDG PET/CT for treatment response evaluation showed a complete metabolic response.

Teaching points:

1. Distant metastatic spread can occur anytime in the course of management of cervical cancer as metastasis can occur both by lymphatic and by hematogenous spread [21]. This patient was offered local pelvic radiotherapy at first due to the restriction of the disease in the pelvic cavity in the form of primary and regional lymph nodes. Although the radiotherapy yielded complete metabolic response in the pelvis, distant sites of lymph nodal and peritoneal/omental deposits were detected in the post radiotherapy PET/CT. These could have been easily missed if conventional anatomical modalities were used to see the status of pelvis alone as disease was initially localized within the pelvic cavity. The whole-body imaging from PET/CT helped in initiating systemic chemotherapy in this patient with complete metabolic response post 6 months.
2. Outside radiotherapy field, recurrences are predominant in patients who underwent primary radiotherapy for locally advanced carcinoma cervix, and reducing distant metastatic spread is a challenge in carcinoma cervix [22]. The need for consolidation chemotherapy in selected patients of locally advanced cervix cancer patients has been addressed, and this case also conforms to the same need [23]. Whole-body FDG PET/CT will be great useful in these cases of locally advanced carcinoma cervix for treatment response evaluation.
3. Post-therapy complete metabolic response (CMR) in FDG PET/CT is a good prognostic sign with studies showing 78% 3-year survival in CMR group while 0% in the disease progression group [8]. This patient also did not develop any recurrence in the follow-up till 14 months.

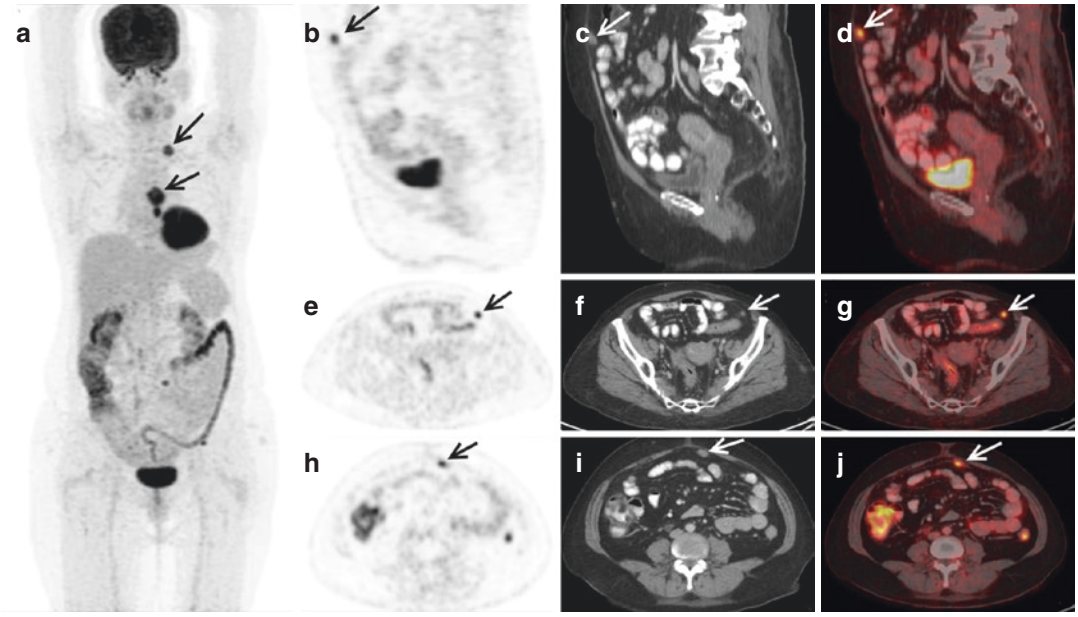

Fig. 19.10 FDG PET/CT post 3 months of completion of external beam radiotherapy in a known case of carcinoma cervix. The MIP (**a**), sagittal PET (**b**), corresponding CECT (**c**), and fused PET/CT (**d**) showing no abnormal FDG uptake/lesion in the uterus and cervix. However, FDG-avid omental/peritoneal deposits are noted in the abdomen as seen in the sagittal (**b–d**) and axial (**e–j**) PET, corresponding CECT, and fused PET/CT images further highlighted with arrows. Foci of increased FDG uptake were also noted in the mid thorax and lower neck in the MIP (**a**, arrows)

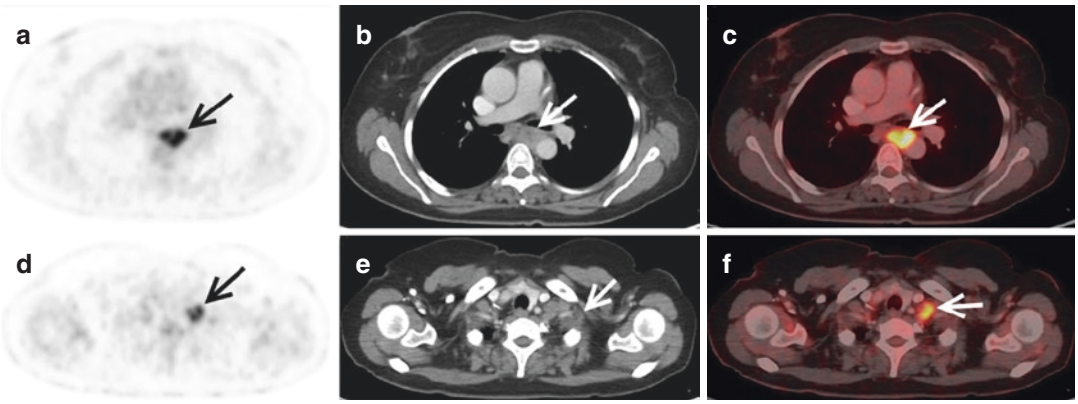

Fig. 19.11 The abnormal FDG uptake in the thorax and neck were localized to FDG-avid enlarged posterior mediastinal and left supraclavicular lymph nodes highlighted with arrows in the axial PET (**a** and **d**), CECT (**b** and **e**), and fused PET/CT (**c** and **f**) images. Post radiotherapy PET/CT showed complete metabolic response in the pelvis with the appearance of FDG-avid omental/peritoneal deposits as well as enlarged mediastinal and left supraclavicular lymph nodes suggestive of disease progression

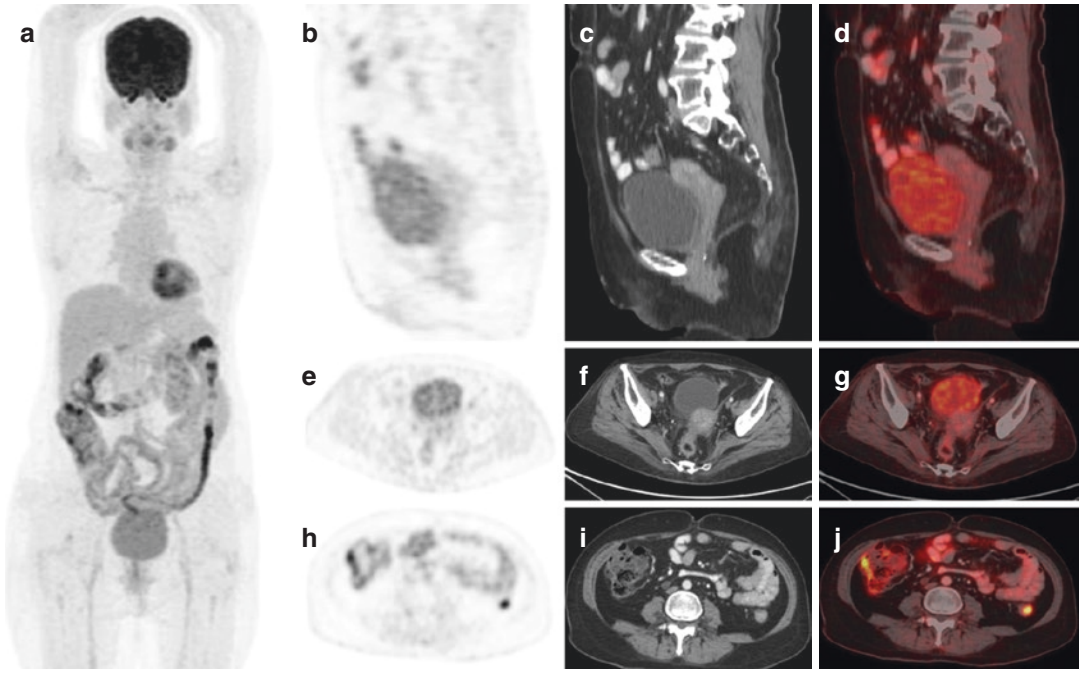

Fig. 19.12 Considering disease progression with distant spread, patient was treated with six cycles of chemotherapy. PET/CT repeated after 8 weeks of chemotherapy showed no abnormal FDG uptake/lesion in the pelvis as well as the distant sites, with resolution of FDG uptake and size of previously seen lesions prior to chemotherapy as seen in the MIP (**a**) and sagittal (**b–d**) and axial (**e–j**) PET, CT, and fused PET/CT images

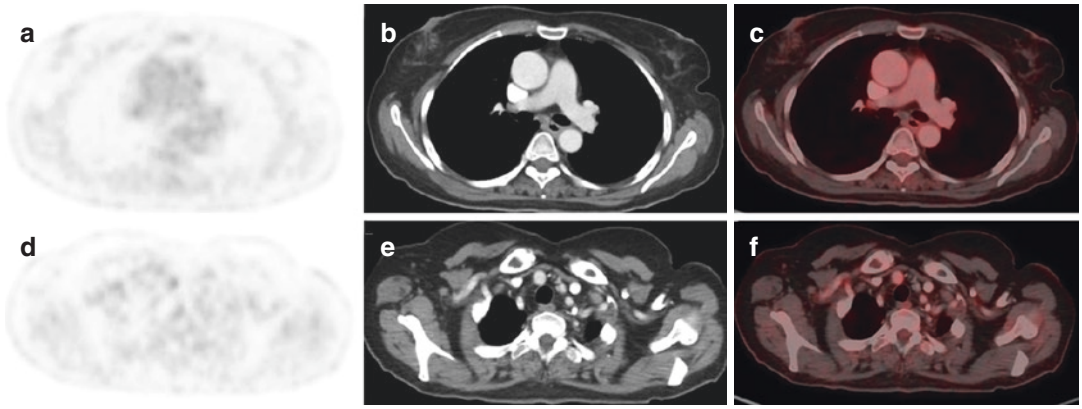

Fig. 19.13 Axial PET (**a** and **d**), corresponding CECT (**b** and **e**), and fused PET/CT (**c** and **f**) images showing complete resolution of the pre-chemotherapy mediastinal and left supraclavicular lymph nodes

19.2 Role of FDG PET/CT in Treatment Response Evaluation of Endometrial Carcinoma

19.2.1 Introduction

Recent data suggest that endometrial carcinoma is the most common gynecological malignancy among developed nations, and the incidence is expected to increase by 1–2% annually [24]. Treatment modalities depend on the stage of the disease, and surgery (hysterectomy and bilateral salpingo-opherectomy) remains the mainstay of treatment. The role of sentinel lymph node mapping and lymphadenectomy along with surgery is still a debatable topic in the primary treatment of endometrial carcinoma. Adjuvant chemotherapy or radiotherapy alone or in combination is given depending on the stage and pathology.

FDG PET/CT is reported to play a useful diagnostic and prognostic role in initial staging of endometrial carcinoma with moderate sensitivity in prediction of lymph nodal metastasis and still having superior diagnostic utility than CT and MRI alone [25–27]. Similarly, many studies show a definitive diagnostic supremacy of FDG PET/CT in evaluation of suspected recurrence/relapse in endometrial carcinoma over conventional CT and MRI [28–30]. The role of FDG PET/CT in treatment evaluation setting is not much studied, and limited studies done specifically on this indication show that early treatment response by FDG PET/CT is indeed beneficial in predicting radiological progression as well as response [31]. Reduction in the uptake value of FDG after neoadjuvant chemotherapy correlated better with histological response after surgery than with that of MRI [32]. Another study reported that the change in FDG accumulation was associated with treatment response, with a sensitivity of 90% and specificity of 80% for differentiating responders from nonresponders using a cutoff based on the percentage change in SUV after treatment [33]. The post therapeutic SUV is reported as a predictive factor for survival and found to have an inverse relationship with progression-free survival. Multivariate analysis showed that posttreatment SUV_{max} (p = 0.001, hazard ratio = 1.199) and serous adenocarcinoma histology (p = 0.028, HR 5.594) predicted recurrence [34]. Further studies to evaluate the association of post therapeutic FDG uptake and prognostication are needed to establish its role as a definitive marker of therapeutic response.

19.2.2 Case 1: FDG PET/CT Showing Near-Complete Metabolic Response in Endometrial Adenocarcinoma Post Chemotherapy

Clinical summary: Forty-six-year female, a known case of carcinoma endometrium underwent modified radical hysterectomy with bilateral salpingo-opherectomy and pelvic lymphadenectomy. ^{18}F-FDG PET/CT done for restaging after surgery showed local recurrence in the vaginal vault and multiple FDG-avid lung nodules in both lung fields suggesting metastatic disease to the lungs. She underwent CT-guided fine-needle aspiration of the lung nodule, and the cytology report showed metastatic adenocarcinoma. The patient underwent six cycles of chemotherapy. ^{18}F-FDG PET/CT was done again for response evaluation (Figs. 19.14 and 19.15).

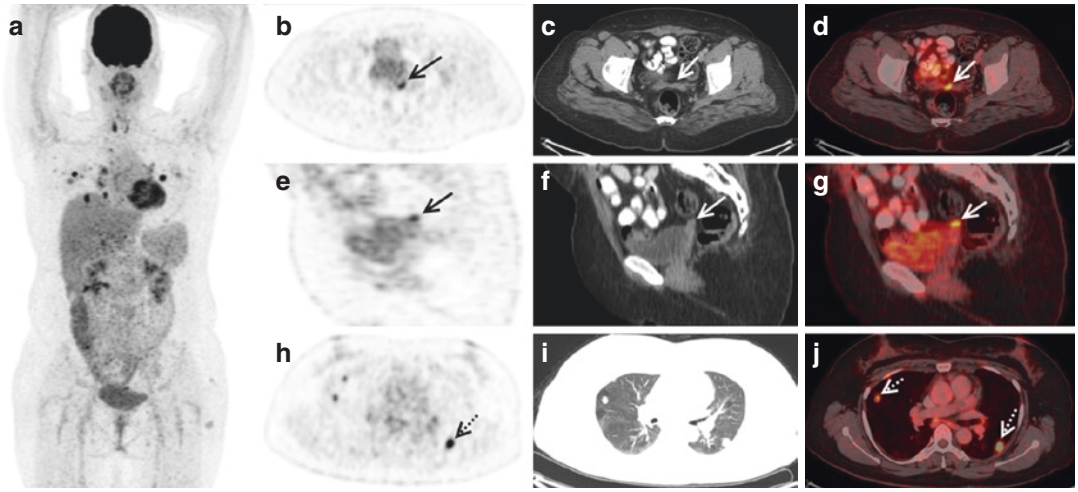

Fig. 19.14 ^{18}F-FDG PET/CT in a 40-year female with carcinoma endometrium post modified radical hysterectomy with bilateral salpingo-opherectomy and pelvic lymphadenectomy. The maximum intensity projection (MIP) image (**a**) and the axial and corresponding sagittal PET (**b** and **e**), contrast-enhanced CT (**c** and **f**), and fused PET/CT (**d** and **g**) images showing focally FDG-avid hypermetabolic focus in a nodular deposit in the vaginal vault (solid arrows). In addition, the MIP (**a**) and the axial PET (**h**), CECT (**i**), and corresponding fused PET/CT (**j**) images showed multiple FDG-avid parenchymal nodules in the both lung fields (dotted arrows). FNAC of the lung nodule confirmed metastatic origin

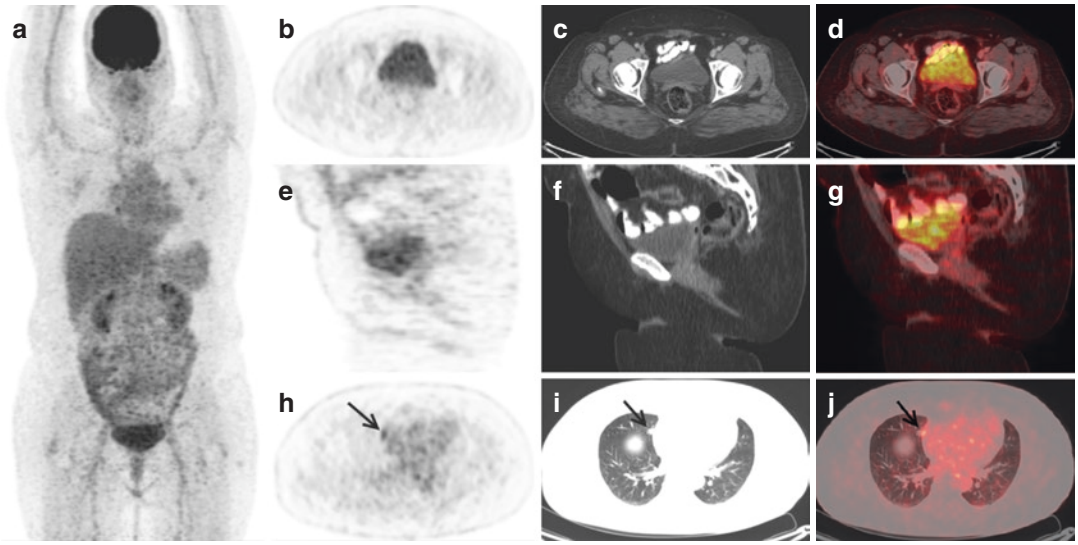

Fig. 19.15 ^{18}F-FDG PET/CT was done again for response evaluation post six cycles of chemotherapy. The maximum intensity projection (MIP) image (**a**) and the axial and corresponding sagittal PET (**b** and **e**), contrast-enhanced CT (**c** and **f**), and fused PET/CT (**d** and **g**) showing resolution of the nodular deposit in the vaginal vault. The MIP (**a**) as well as the axial PET (**h**), CECT (**i**), and corresponding fused PET/CT (**j**) images showing resolution of the most of the pulmonary nodules except an FDG-avid pleural-based subcentimetric nodule in the middle lobe of right lung (solid arrows) suggestive of residual disease

Images:

Interpretation: The initial PET/CT post-surgery in this patient of endometrial adenocarcinoma showed local recurrence at vaginal vault as well as pulmonary metastases. Post six cycles of chemotherapy, FDG PET/CT showed near-complete metabolic response in the form of resolution of the vaginal vault as well as most of the pulmonary nodules with residual disease in a pulmonary nodule in right lung. The patient is planned for two more cycles of chemotherapy considering the favorable response with minimal residual disease.

Teaching points:

1. ^{18}F-FDG PET/CT being a whole-body modality could localize both local (vaginal vault) and distant (pulmonary) metastases in this patient. The FDG-avid nodular vaginal vault lesion, being small in size, could have been easily missed in the conventional modalities like CT and MRI. The resolution of the lesion post chemotherapy also confirms the pathologic nature of the lesion. Studies also conform to the superior sensitivity and specificity of FDG PET/CT with that of conventional imaging modalities [29, 35].
2. ^{18}F-FDG PET/CT done for treatment evaluation post six cycles of chemotherapy showed complete minimal residual metastatic disease in the lung which prompted the continuation of two more cycles of chemotherapy for this patient. ^{18}F-FDG PET/CT thus play a pivotal role in knowing about the metabolic response and in tailoring the chemotherapy dosing in these patients.

19.3 FDG PET/CT in Treatment Response Evaluation of Fallopian Tube Carcinoma

19.3.1 Introduction

Fallopian tube carcinomas are rare subgroup accounting for 0.14–1.8% of the gynecological malignancies [36, 37]. Identification of isolated fallopian tube lesion without presence of ovarian lesion in the primary surgery is a distinguishing feature of fallopian tube malignancy [38]. The incidence of primary fallopian tube carcinoma is reported to be on the rise. The similar clinical presentations, histopathological features, elevation of CA-125 level, etc., make primary fallopian tube malignancies indistinguishable from ovarian cancer. The anatomical proximity also makes mutual invasion form both carcinoma possible in the early course of disease itself making it indistinguishable from ovarian cancer and underestimating the true incidence of this malignancy. Tubal malignancies spread primarily by transcoelomic seeding similar to ovarian carcinoma, and approximately 80% of the metastatic spread is confined within the peritoneal cavity. However, literature shows that distant metastases and retroperitoneal lymphatic spread are more common in tubal carcinoma as compared to ovarian malignancies. Aggressive cyto-reductive surgical removal with additional pelvic and paraaortic lymphadenectomy is the initial treatment of choice. Adjuvant radiotherapy is an option in early-stage patients. In advanced disease, combination chemotherapy is the modality of choice.

Peritoneal implants being a common mode of spread of this malignancy, the accuracy of CT and MRI in detecting the same is not conclusive, and the diagnostic accuracy in these setting is still debatable. PET/CT with high FDG uptake can outperform anatomical imaging in diagnosing these peritoneal implants. The role of FDG PET/CT in this rare malignancy is limited to case reports in the literature. The available literature shows that FDG PET/CT has shown good diagnostic role in identifying the distant spread/recurrence of this malignancy. There are reports of PET/CT outperforming conventional CT in two cases of treatment completed fallopian tube carcinoma in detecting distant hepatic, peritoneal sub-diaphragmatic as well as splenic lesions even at low CA125 levels [39–41]. Some authors have reported isolated cases of usefulness of FDG PET/CT in primary evaluation also [42, 43].

The precise role of FDG PET/CT in the treatment evaluation has been not evaluated till now. However, the available experience on the role of FDG PET/CT in ovarian carcinoma which resemble the mode of spread promises a diagnostic superiority over conventional imaging owing to the low volume structural disease in the peritoneum, greater rate of distant metastasis, and lymph nodal spread seen in tubal malignancy.

19.3.2 Case 1: FDG PET/CT Showing Disease Progression in a Treatment Completed Case of Bilateral Fallopian Tube Carcinoma

Clinical summary: Forty-seven-year female, a known case of bilateral fallopian tube carcinoma underwent total abdominal hysterectomy and bilateral salpingo-opherectomy and omentectomy. Postoperative histopathology revealed papillary adenocarcinoma of bilateral fallopian tubes. Peritoneal fluid analysis was suspicious for malignancy. She received 14 cycles of chemotherapy and 30 fractions of pelvic external beam radiotherapy. After 3 months of completion of radiotherapy, her CA-125 level was 53.6 U/ml which was borderline elevated. PET/CT was done for disease evaluation (Figs. 19.16, 19.17, and 19.18).

Images:

Interpretation: The PET/CT done post radical surgery and adjuvant chemo-radiotherapy in this patient showed disease progression despite the aggressive surgical and medical treatment received. PET/CT could show FDG-avid lymph nodes on both sides of the diaphragm as well as omental deposits.

Teaching points:

1. CA-125 is a useful marker for post-treatment follow-up in fallopian tube carcinoma also. It is an early and sensitive marker for tumor progression during follow-up [44, 45]. It has been reported that the lead time (elevated serum CA-125 levels prior to clinical or radiological diagnosis of recurrence) is 3 months (range, 0.5–7 months) [46]. Literature also shows that lymphatic spread through retroperitoneal lymphatic channels is more common in fallopian tube carcinoma than in ovarian carcinoma [38].
2. ^{18}F-FDG PET/CT was done on the suspicion of residual/recurrent disease post aggressive treatment with elevation of CA-125 level. Being a whole-body functional imaging, FDG PET/CT could show residual/recurrent lymph nodal disease on both sides of the diaphragm. Conventional imaging like CT may fail to demonstrate the mediastinal and supraclavicular lesions as in most settings they are done for the abdomino-pelvic regions. Prior reports of PET/CT outperforming conventional CT in cases of treatment completed fallopian tube carcinoma in detecting distant metastatic lesions even at low CA 125 levels also reinforce the same [39–41].

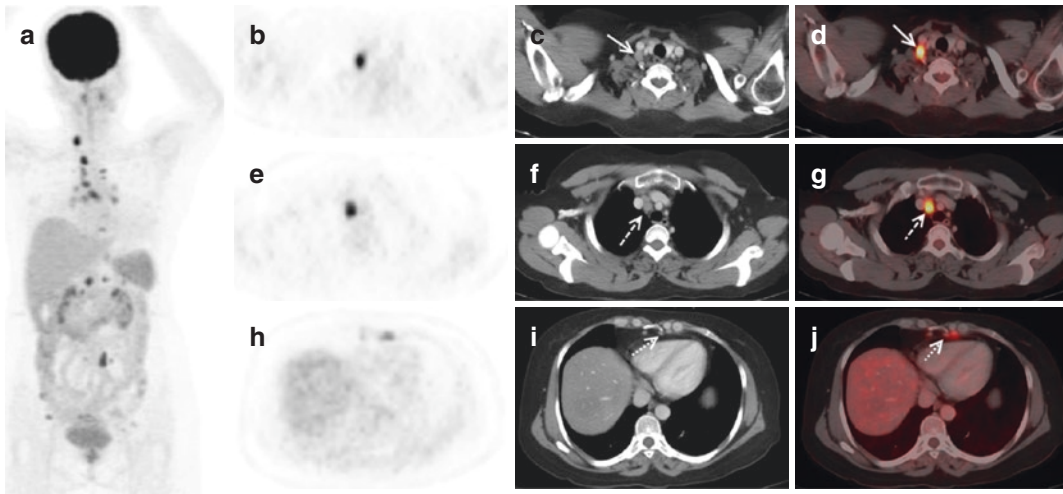

Fig. 19.16 ^{18}F-FDG PET/CT in a 47-year female with bilateral fallopian tube carcinoma post TAH+BSO+omentectomy and adjuvant chemo and radiotherapy. The maximum intensity projection image (**a**) and the axial PET (**b**, **e**, and **h**), corresponding axial CECT (**c**, **f**, and **i**), and the fused axial PET/CT (**d**, **g**, and **j**) showing focal FDG uptake in the right supraclavicular (solid arrows), right lower paratracheal (broken arrows), and paracardiac (dotted arrows) lymph nodes

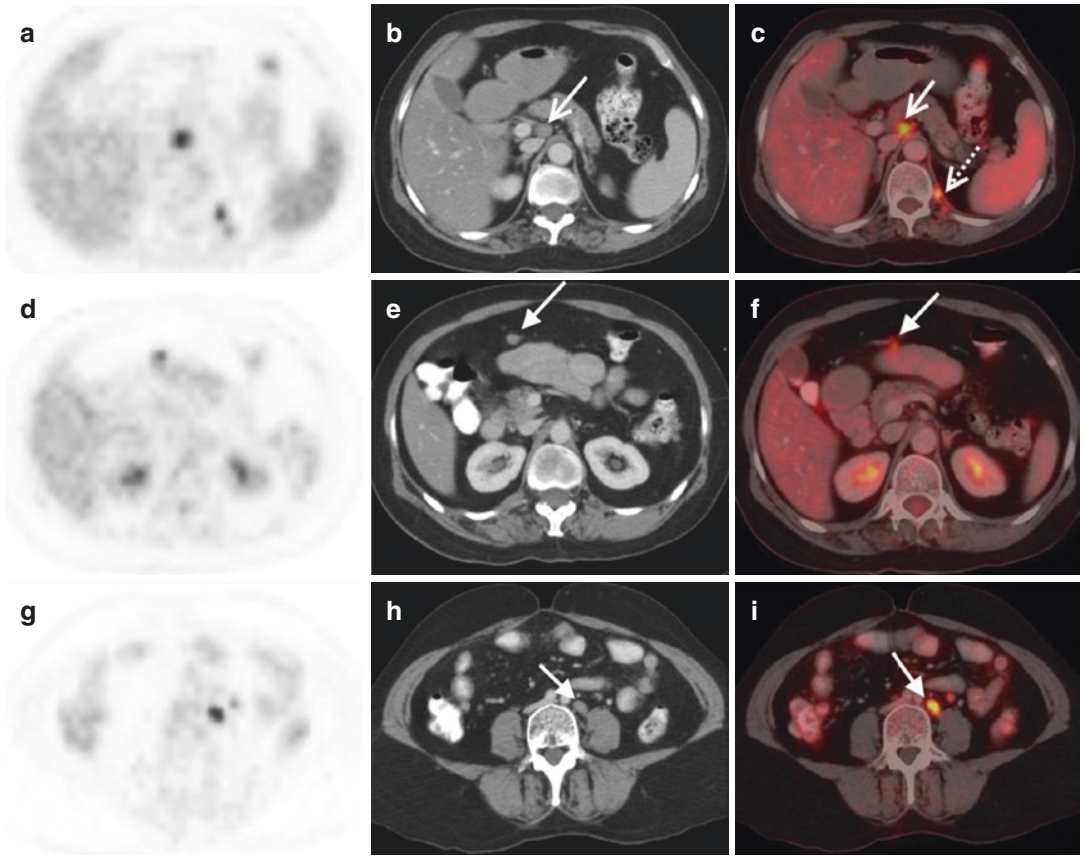

Fig. 19.17 ^{18}F-FDG PET/CT also showed FDG-avid enlarged portocaval (**b** and **c** solid arrows), left subcrural (dotted arrow **c**) lymph nodes, FDG-avid omental deposits (**e** and **f** solid arrows) and left common iliac lymph node (**h** and **i** solid arrows)

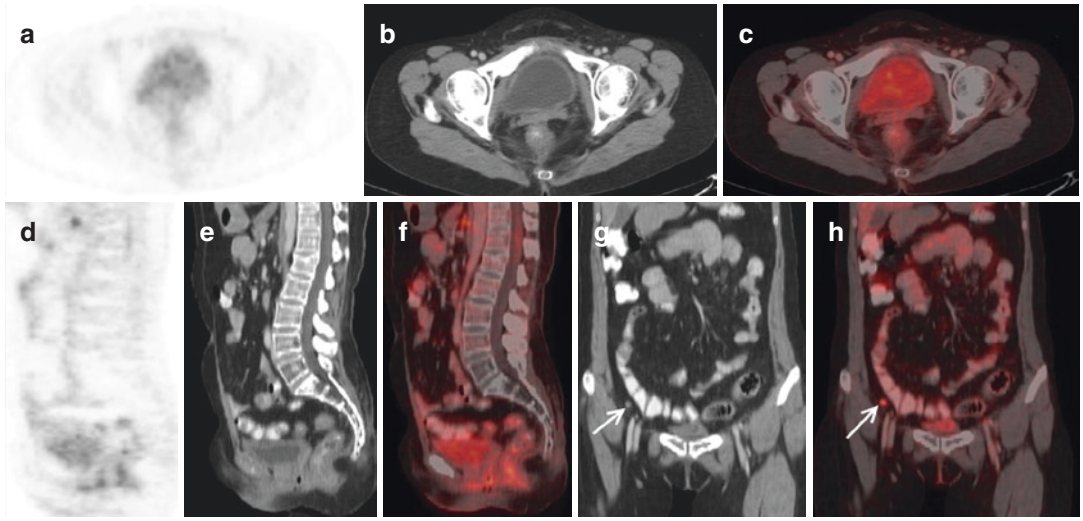

Fig. 19.18 There was no FDG uptake/structural lesion in the vaginal stump as seen in the axial PET (**a**), CT (**b**), and fused axial PET/CT (**c**) as well as the corresponding sagittal images (**d–f**, respectively). However, an FDG-avid right external iliac lymph node was noted (**g** and **h** solid arrows)

19.3.3 Case 2: FDG PET/CT Showing Disease Progression in Form of Hepatic and Serosal Metastases in a Treatment Completed Bilateral Fallopian Tube Carcinoma

Case summary: Fifty-six-year female post pan hysterectomy (uterus + cervix + fallopian tubes and both ovaries) for bilateral high-grade serous carcinoma of bilateral fallopian tubes. Patient also received nine cycles of adjuvant chemotherapy. CA-125 level post 2 months of completion of chemotherapy was 72.20 U/ml which was elevated. An FDG PET/CT was done for treatment response evaluation (Figs. 19.19 and 19.20).

Images:

Interpretation: FDG PET/CT showed distant hepatic, lymph nodal, and serosal metabolically active metastatic disease in this patient of treatment completed bilateral carcinoma of fallopian tube.

Teaching points:

1. Elevated CA-125 level post-therapy indicates residual/recurrent disease in a case of fallopian tube carcinoma also. The distribution of metastases may be similar to that of ovarian carcinoma, but there appears to be a higher propensity to spread outside the peritoneal cavity [39] as in the index case. Considering this fact, early/interim assessment of treatment response and more aggressive follow-up is needed in the context of fallopian tube carcinoma.
2. FDG PET/CT shows good diagnostic utility even in borderline or mildly elevated CA-125 levels in showing distant metastatic sites. Previous reports suggest good FDG uptake in the metastatic sites despite low CA-125 levels [39, 41].

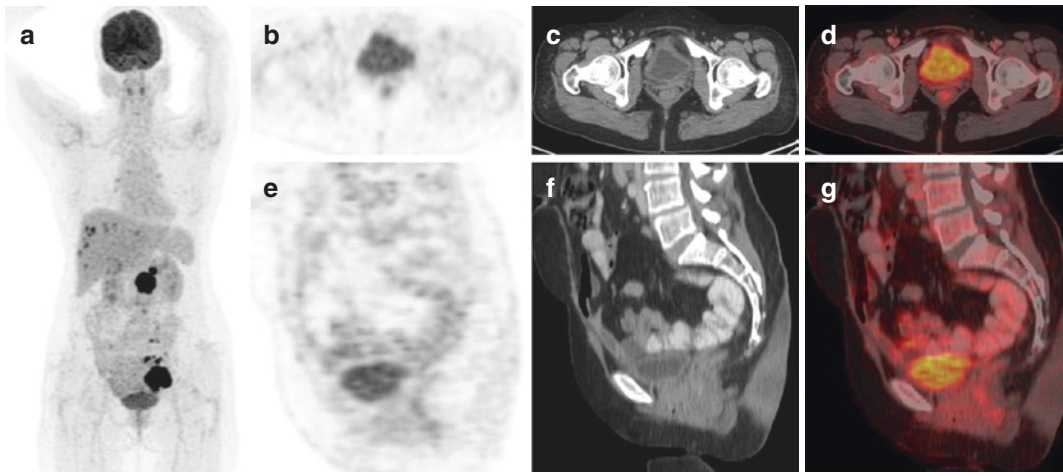

Fig. 19.19 FDG PET/CT done in this 56-year female post-surgery and chemotherapy showing no residual disease in the surgical uterine bed as well as in the vaginal stump suggested by the axial PET (**b**), CT (**c**), and fused PET/CT (**d**) and corresponding coronal (**e–g**, respectively) images. However, the maximum intensity projection image (**a**) showed abnormal foci of FDG uptakes in the pelvis, mid abdominal region, and liver

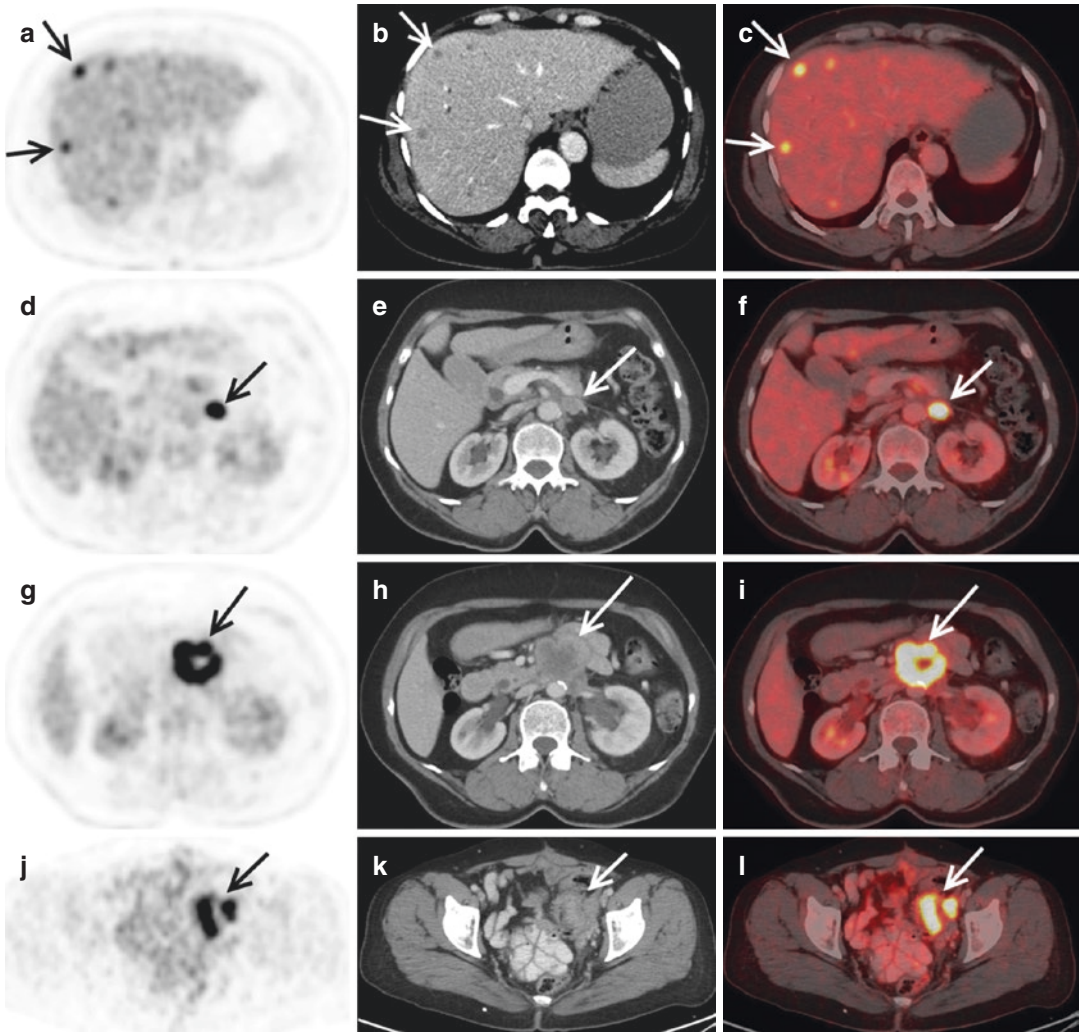

Fig. 19.20 The abnormal foci of FDG uptakes in the abdominal region were localized to multiple hypodense lesions in the liver (**a–c** arrows), enlarged left paraaortic lymph node (**d–f** arrows), FDG avid necrotic deposits in the serosa of duodenum with infiltration (**g–i** arrows), and serosal deposit in the sigmoid colon (**j–l**) suggesting metabolically active metastatic disease

19.4 FDG PET/CT in Treatment Response Evaluation of Vaginal Carcinoma

19.4.1 Introduction

Vaginal carcinomas constitute a rare malignancy accounting for up to 2% of all gynecological cancers [47]. ^{18}F-FDG PET/CT has emerged as an important diagnostic as well as prognostic tool among the more common gynecological malignancies like ovarian and cervical malignancies. FDG PET/CT promises to be of similar potential in vaginal cancer owing to the comparable epidemiological and histological findings of vaginal malignancies with that of cervical cancer [48, 49].

The role of FDG PET/CT in vaginal malignancies is very less known owing to the rarity of the disease and the limited published data on the same. Among the limited published research, Lamoreaux et al. reported that FDG PET/CT outperforms conventional CT in detecting primary lesion as well as pelvic lymph nodal metastasis in vaginal cancer [50]. Robertson et al., in their study, suggested that FDG PET/CT may be a valuable tool in prognostication as well as management of vaginal and vulvar malignancies [51]. The precise role of FDG PET/CT in the posttreatment evaluation of vaginal cancer is still unexplored. Given the high avidity of FDG in vaginal malignancies, FDG PET/CT has the potential to become a key noninvasive diagnostic tool in tailoring the treatment options in vaginal cancer in harmony with other malignancies like ovarian and cervical malignancies. Till date, there is no available literature on the role of FDG PET/CT in treatment evaluation for this rare malignancy. Considering the fact that surgery, radiotherapy, and concurrent chemo-radiotherapy being the mainstay management modalities in vaginal cancer also, FDG PET/CT can be extrapolated as an imaging biomarker for treatment response in this gynecological malignancy too.

Vaginal cancer possesses significant challenges on account of its anatomical location in the setting of treatment evaluation. Post-surgical/radiotherapy scarring and fibrosis, risk of development of superadded infection and inflammation posttreatment, reactive lymphadenopathy in the pelvis and inguinal regions, etc., make the response evaluation challenging for both conventional structural and functional PET/CT imaging. The close proximity with the urinary system and the greater risk of urinary contamination warrant careful scrutiny of the FDG uptake in these regions to avoid false-positive interpretations. The use of FDG PET/CT post radiotherapy treatment evaluation suffers from the pitfall of false-positive inflammatory uptake making it challenging to differentiate between residual or recurrent active tumor and inflammation.

In pelvic malignancies especially in setting of treatment evaluation, additional measures are to be taken to avoid false interpretations. The use of delayed (dual time point) imaging, use of intravenous contrast agents, etc., may help in increasing the specificity of the study. The incorporation of vaginal catheter has been documented to increase the diagnostic power by accurately localizing the hypermetabolic foci in vaginal and paravaginal areas [52]. Dynamic PET/CT images can also differentiate between pathological and benign uptake. The use of dynamic images, intravenous contrast, etc., are documented to identify vesicovaginal fistulas (causing false interpretation) which may develop after radical surgical/RT procedures in these patients [53]. In spite of these limitations, the whole-body assessment and functional nature of the study make it a powerful tool in distinguishing treatment response, early identification of progression, or the development of a distant site metastasis.

Non-FDG PET tracer like ^{18}F-Fluorothymidine (FLT) has been used to overcome these challenges and pilot study with FLT PET/CT for treatment evaluation for vaginal and cervical cancer after external beam radiation shows that FLT uptake is not affected by the superadded inflammation and has the potential of being a more specific alternative to FDG PET/CT in the setting of treatment evaluation [54].

19.4.2 Case 1: FDG PET/CT Showing Near-Complete Metabolic Response After Chemotherapy in Vaginal Carcinoma and predicts Long-Term Remission

Case summary: Forty-three-year female presented with history of low back ache for 10 months. On examination, she was found to have tenderness of the lower lumbar vertebrae. Evaluation with pelvic MRI showed altered signal intensity at the L5 vertebra with destructive change and a large soft-tissue mass suggestive of skeletal metastasis. Histopathology from the vertebral lesion suggested metastatic squamous cell carcinoma. FDG PET/CT was done to identify the unknown primary (Figs. 19.21, 19.22, and 19.23).

Images:

Interpretation: FDG PET/CT done for carcinoma of unknown primary revealed primary site in the vagina with FDG-avid skeletal and retroperitoneal lymph nodal metastasis. PET/CT done for treatment evaluation post chemotherapy showed favorable disease response. The follow-up PET/CT also showed no metabolically active disease even after 2 years of treatment completion.

Teaching points:

1. FDG PET/CT shows high metabolic activity in primary cancer of the vagina and shows a good diagnostic utility in identifying primary lesion as well as metastatic sites [50].
2. Gynecological malignancies are an uncommon primary site for skeletal metastasis with unknown primary. The near-complete metabolic response after chemotherapy in this patient also predicted long-term remission in this patient.
3. FDG PET/CT is reported to change the prognostic impression as well as management algorithm in a significant proportion of cases with vulval and vaginal carcinoma [51].

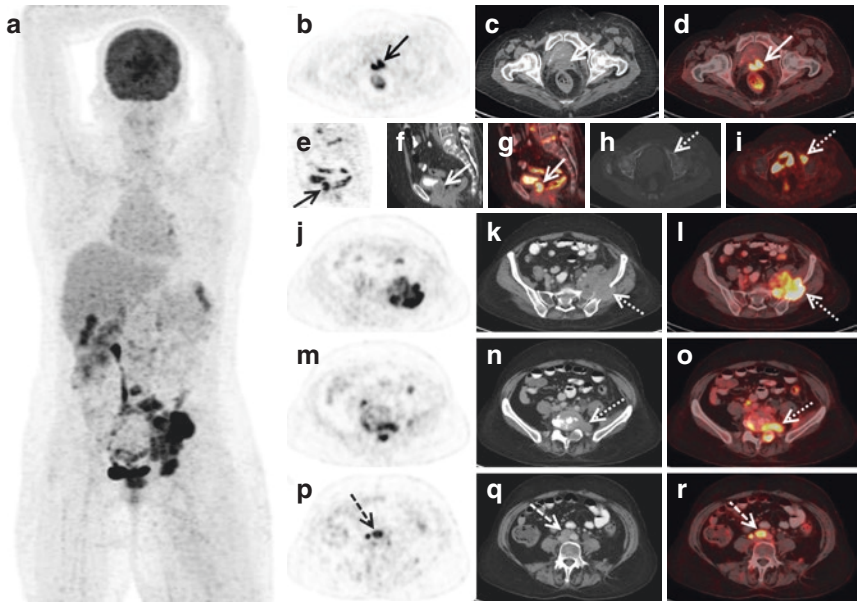

Fig. 19.21 FDG PET/CT in a 43-year female with metastatic lesion in the L5 vertebra for unknown primary. The whole-body MIP images (**a**) showing abnormal areas of FDG uptake in the lower abdomen and pelvic regions. Abnormal FDG uptake was noted in the thickening in the upper vagina including vault as shown in the axial (**b–d**) and corresponding sagittal (**e–g**) PET, CECT, and fused PET/CT, respectively. FDG-avid lytic skeletal lesions were noted in the anterior lip of left acetabulum (dotted arrows; **h** and **i**), lytic destructive lesion in the left iliac blade with soft tissue extending to adjoining pelvic muscles (dotted arrows; **j–l**), and L5 vertebra with associated soft-tissue component (dotted arrows; **m–o**). FDG-avid retroperitoneal lymph nodes were also noted in the aortocaval location (broken arrows; **p–r**). Biopsy from the upper third of vagina revealed squamous cell carcinoma, poorly differentiated. She was managed with chemotherapy, and FDG PET/CT was repeated after five cycles of chemotherapy

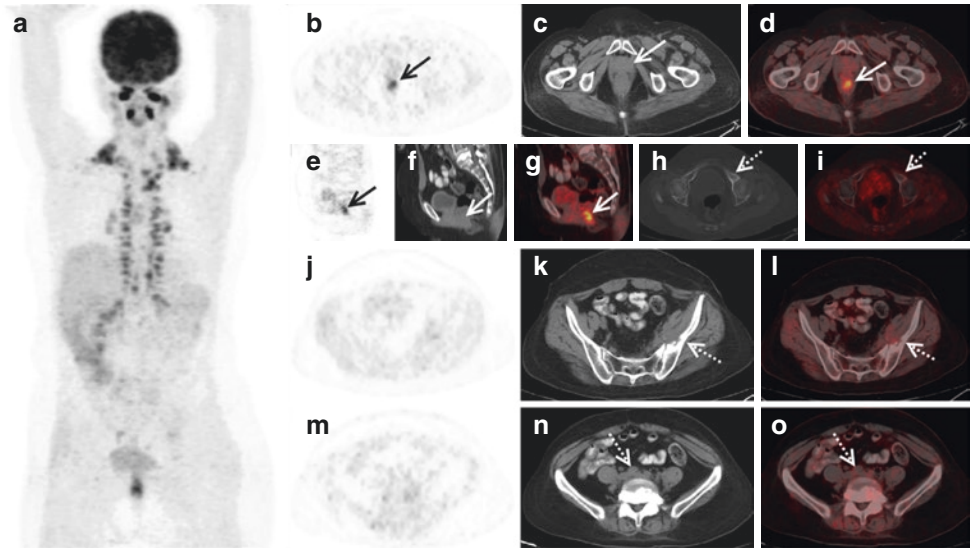

Fig. 19.22 FDG PET/CT post five cycles of chemotherapy for treatment response evaluation. Significant reduction in FDG uptake and size of the pre-existing lesions were noted as seen in the MIP (**a**). Mild FDG uptake is noted in the residual lesion in the vagina (arrows; **b–g**). Resolution in FDG uptake with appearance of sclerosis is noted in the lytic lesion in the left acetabulum (dotted arrows; **h** and **i**). Resolution in FDG uptake with significant reduction in soft-tissue component and appearance of sclerosis noted in the left iliac blade lesion (dotted arrows; **j–l**). Resolution in FDG uptake was noted in the aortocaval lymph node also (dotted arrows; **m–o**). Considering the near-complete metabolic response in metastatic sites and favorable disease response, she was given one more cycle of chemotherapy and was on routine follow-up. FDG PET/CT was repeated after 2 years of follow-up

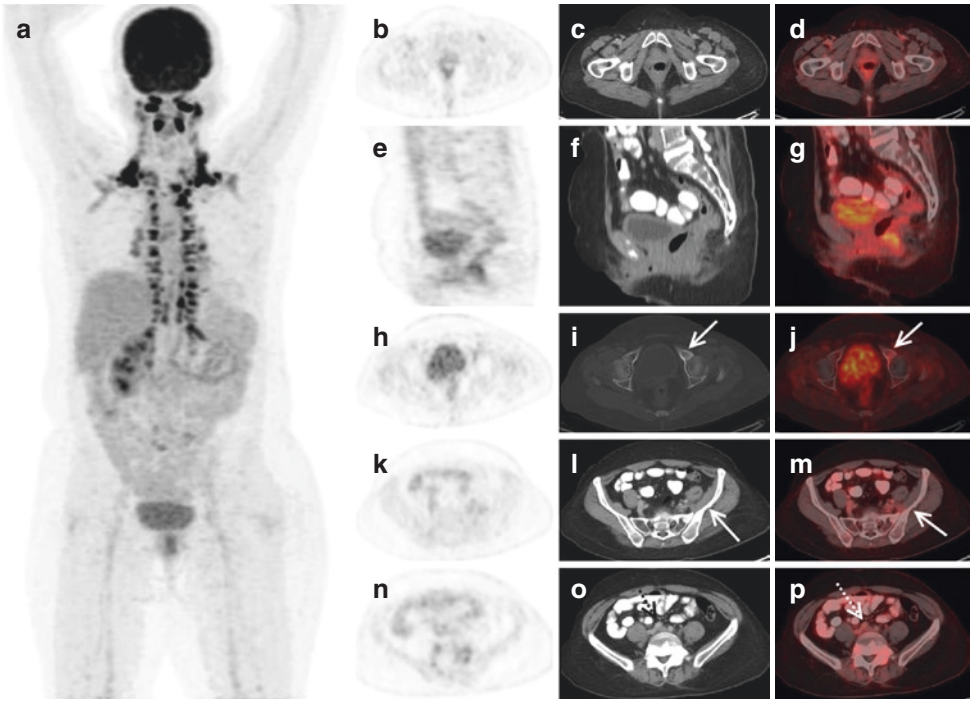

Fig. 19.23 FDG PET/CT during follow-up and after 2 years of treatment completion. The MIP (**a**) image and the axial (**b–d**) and sagittal (**e–g**) PET, CECT, and fused PET/CT images showed no abnormal FDG uptake/lesion in the primary site in vagina. No increase in FDG uptake was also noted in the metastatic sites in the left acetabulum (**h–j**), left iliac blade (**k–m**) and the aortocaval lymph node (**n–p**)

19.5 Role of FDG PET/CT in Treatment Response Evaluation in Vulval Carcinoma

19.5.1 Introduction

Carcinoma of the vulva is a rare malignancy in the women with an overall incidence rate of 1.5–2.4 per 100,000 women per year and accounting to ~4% of all gynecological malignancies in India [55–57]. Despite being more incident in the elderly postmenopausal women, there is a rising trend in the younger women likely due to the insurgence of human papilloma virus, immunodeficiency, etc. [58–60]. Radical resection followed by inguino-femoral lymphadenectomy is the primary treatment modality in case of vulval squamous cell carcinoma which accounts for up to 90% of all vulval carcinomas. Radiation therapy has also emerged as a major role in the treatment armamentarium mainly in the adjuvant setting and also in the neoadjuvant and definitive treatment scenarios. Concurrent chemoradiation is the alternative for those patients with large tumors in whom primary surgical resection is not feasible [61–63].

The role of ^{18}F-FDG PET/CT in the management of vulval cancer is a lesser exploited zone given the limited studies on the topic and rarity of the disease. Given the fact that 90% of the vulval cancers are squamous cell carcinomas and show good FDG uptake, few study reports suggest its usage for staging the disease [64], and the National Comprehensive Cancer Network also recommends consideration for whole-body FDG PET/CT in staging of vulval cancer with T2 or more stage with suspicion for metastases [65]. Most of the available literature on the role of FDG PET/CT in vulval cancer focuses on its potential to identify locoregional lymph nodes, sentinel nodal mapping, or staging prior to definitive management [66–71]. The impact of FDG PET/CT in the assessment of treatment response as well as recurrence evaluation posttreatment is lesser explored and is mostly adapted from the studies on their more evaluated counterparts like ovarian and cervical cancers.

Pelvic lymph nodal status is the best predictor of prognosis in a pretreated vulval cancer, however in the setting of posttreatment, this scenario changes. Treatment response evaluation is a keystone to any oncological management setting, and the limited studies on the role of treatment evaluation for vulval cancer with FDG PET/CT reports that residual/recurrent metabolic disease on FDG PET/CT posttreatment is a more significant adverse predictor of disease outcome [72]. Early identification of metabolic progression will entail the patient to opt for other salvage modalities at the earliest. Being a functional imaging armamentarium, FDG PET/CT outscore other conventional structural imaging like CT and MRI in signifying the malignant potential of the residual structural disease which is quite challenging in the post-surgical/radiotherapy changes like fibrosis. Besides, being a whole-body imaging, new progressive distant metastasis developing in the setting of locoregional-directed therapies can be early identified. However, like in other pelvic pathologies, FDG PET/CT suffers from the inherent limitations of false-positive findings with respect to urinary activity in the pelvis, posttreatment inflammation, reactive pelvic as well as mediastinal lymphadenopathies, development of complications like post-surgical fistulas and infections, etc. Careful and cautious interpretation of the FDG PET/CT findings in these scenarios and delayed imaging to alleviate some of these and a histopathological confirmation to rule out/in the true nature of the disease is still warranted.

19.5.2 Case 1: FDG PET/CT Showing Early Disease Progression Post Chemotherapy in Relapsed Case of Carcinoma Vulva

Clinical summary: Fifty-two-year female presented with ulcerated lesion at the vulva involving left labia and subsequently diagnosed as a case of squamous cell carcinoma (SCC) vulva stage IIIA. She was managed with radical vulvectomy and bilateral pelvic lymphadenectomy. She also received 50 Gy of external beam pelvic radiotherapy as adjuvant treatment. On follow-up, she presented with left inguinal lymphadenopathy. An FDG PET/CT was done for recurrence evaluation (Figs. 19.24 and 19.25).

Images:

Interpretation: FDG PET/CT in this patient showed disease recurrence in the pelvis, and after histopathological confirmation, PET/CT was repeated post two cycles of chemotherapy. There was increase in FDG uptake and size of the recurrent primary as well as metastatic lymph nodal lesions with appearance of new nodal metastasis suggestive of disease progression.

Teaching points

1. Recurrence can occur in vulval cancer in approximately 24% of patient population after primary treatment with surgery with or without adjuvant radiation [55]. FDG PET/CT helps in detection of recurrence owing to high metabolic activity and to rule out presence of distant metastases.
2. FDG PET/CT helped in identifying disease progression in index patient even in early phase of chemotherapy schedule and in constituting alternative management options/regimen. The posttreatment response on FDG PET/CT is also associated with locoregional control and overall survival [56].

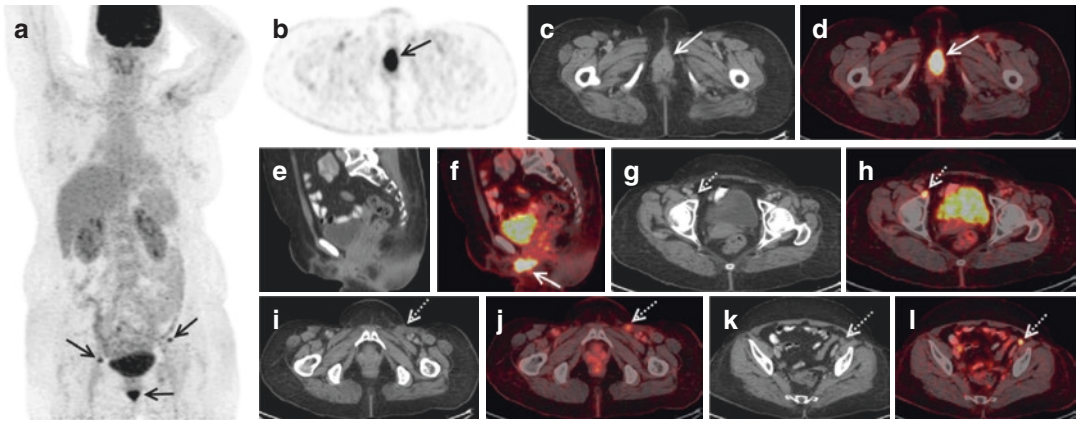

Fig. 19.24 FDG PET/CT in a 52-year female, a known case of vulval squamous cell carcinoma, post radical surgery, and pelvic lymphadenectomy with adjuvant pelvic radiotherapy for suspected recurrence in follow-up. The MIP image (**a**) showed few abnormal foci of FDG uptake in the pelvis (arrows; **a**) which were localized to the highly FDG-avid lesion (arrows) in the lower third of vagina and vulval base region as shown in the axial PET (**b**), CECT (**c**), and fused PET/CT (**d**) and corresponding sagittal CT (**e**) and fused PET/CT (**f**). In addition, FDG-avid lymph nodes were also noted in the bilateral external iliac and left inguinal region highlighted with dotted arrows (**g–l**). FNA from left inguinal lymph node revealed metastatic SCC and biopsy from vulval lesion suggested SCC recurrence

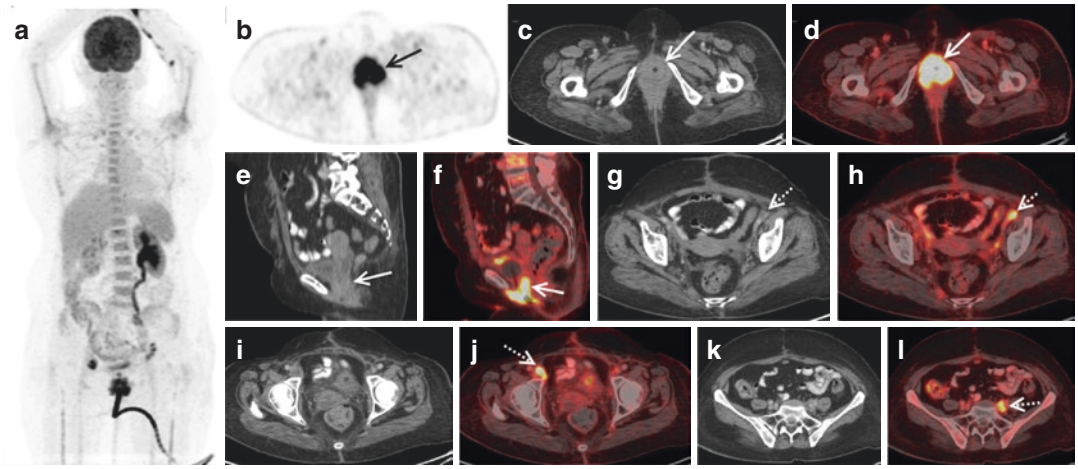

Fig. 19.25 Patient was planned for chemotherapy for relapsed disease, and FDG PET/CT was repeated after two cycles of chemotherapy with urinary catheter in situ (MIP; **a**). FDG PET/CT showed increase in extent and FDG uptake of the lesion in the vulva and extension into lower vaginal third (arrows; **b–f**). FDG-avid bilateral external iliac lymph nodes were also noted which showed increase in size and FDG uptake (**g–j**; dotted arrows). In addition, FDG-avid left common iliac lymph node (new lesion) was also noted (dotted arrow; **k** and **l**). Marrow activation with diffuse increased FDG uptake can be noted in the MIP (**a**) image likely due to reactive changes to chemotherapy with sparing of the pelvic bone marrow (post local radiotherapy) as appreciated in the sagittal (**e** and **f**) images

19.6 Role of FDG PET/CT in Treatment Response Evaluation of Ovarian Carcinoma

19.6.1 Introduction

Ovarian carcinoma accounts for 2.5% of all malignancies in women but due to late presentation and late stage at the time of diagnosis, accounts for ~5% of cancer-driven deaths in women [73, 74]. The average lifetime risk for developing ovarian cancer is 1.3%, the equivalent of 1 in 78 women. Epithelial ovarian cancer predominates in all racial groups accounting for up to 90% followed by germ cell and sex cord stromal tumors [73].

FDG PET/CT has shown good diagnostic utility in detection as well as staging of primary ovarian malignancy even with some pitfalls like benign and physiological uptake, urinary tracer activity and ovarian cyst, pelvic inflammatory disease, etc., resulting in false-positive results [75–77]. The most convincing role of FDG PET/CT in ovarian carcinoma is in the detection of suspected recurrence in setting of elevated or even normal CA-125 and negative conventional imaging modalities [78–80].

FDG PET/CT is reported to be more reliable than morphologic imaging in the prediction of treatment response, since the metabolic response precedes structural changes [81, 82]. Majority of the ovarian cancer present at advanced disease and neoadjuvant chemotherapy is used for debulking before definitive surgery. The early prediction of treatment response to neoadjuvant chemotherapy will help in identifying nonresponders at an early phase [83–85]. In the response evaluation post-therapy, sequential imaging with PET has been shown to predict response as early as after one cycle of neoadjuvant chemotherapy. PET has also shown more prognostic accuracy than histopathologic criteria or CA-125 level in predicting response [86]. The percentage decrease in SUV from baseline after neoadjuvant chemotherapy is also reported to predict pathological responders [87]. PET/CT is also been shown as a predictor of response to novel therapeutic options including temsirolimus. Metabolic parameters like SUVmax and total lesion glycolysis are shown to predict radiological response as well as disease progression in this setting [88]. A negative PET/CT study at the end of treatment completion correlates significantly with a higher progression-free as well as 4-year overall survival [89]. Despite these study results emphasizing the role in assessment/predicting tumor response to therapies, there are still challenges in accurately evaluating oligometastases which are small and beyond limitation of spatial resolution as well as many pitfalls in evaluating pelvic pathologies, which are yet to be addressed.

19.6.2 Case 1: FDG PET/CT Showing Favorable Response to Second-Line Chemotherapy Regimen in a Case of Platinum-Resistant Metastatic Ovarian Carcinoma

Clinical summary: Fifty-nine-year female, completed treatment (total abdominal hysterectomy + bilateral salpingo-opherectomy and adjuvant pelvic radiotherapy) for ovarian carcinoma. She was suspected with disease recurrence in the form of elevated CA-125 levels 6 months after completion of treatment. An FDG PET/CT done at that time for suspected recurrence revealed metabolically active mediastinal and abdomino-pelvic lymph nodes suggestive of metastatic disease. She was treated with six cycles of platinum-based chemotherapy. FDG PET/CT was repeated 4 weeks after completion of chemotherapy for disease response assessment (Figs. 19.26 and 19.27).

Images:

Interpretation: FDG PET/CT post six cycles of platinum-based chemotherapy for disease relapse after primary treatment in a known case of metastatic ovarian carcinoma showed disease progression despite chemotherapy. She was managed with second-line chemotherapy regimen. FDG PET/CT post four cycles showed favorable response in the form of resolution of most of the preexisting lesions with residual disease in the abdominal and retroperitoneal lymph nodes.

Teaching points:

1. Platinum-based chemotherapy remains the mainstay for treatment of recurrent ovarian carcinoma. Platinum resistance, defined as

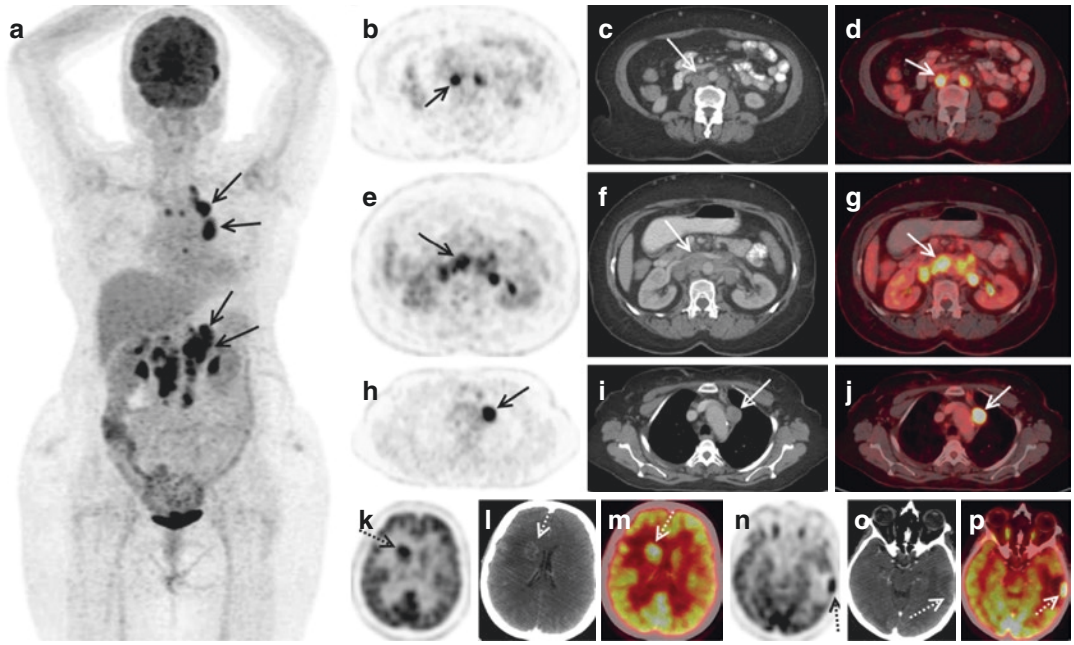

Fig. 19.26 FDG PET/CT post six cycles of chemotherapy given for disease recurrence in a treatment completed case of ovarian carcinoma. The MIP image (**a**) showed abnormal tracer uptake in the abdominal and mediastinal regions (arrows) localizing to FDG-avid enlarged multiple abdominal and retroperitoneal lymph nodes (**b–g**) highlighted with arrows. There was FDG-avid enlarged mediastinal lymph nodes also (**h–j**; arrows). FDG-avid multiple enhancing lesions are also noted in the brain with perilesional edema on CT (**k–p**) highlighted with dotted arrows. In the context of metastatic disease in the abdomen, mediastinum, and new brain lesions, the patient was offered with four cycles of alternate second-line chemotherapy, and FDG PET/CT was repeated for treatment response assessment

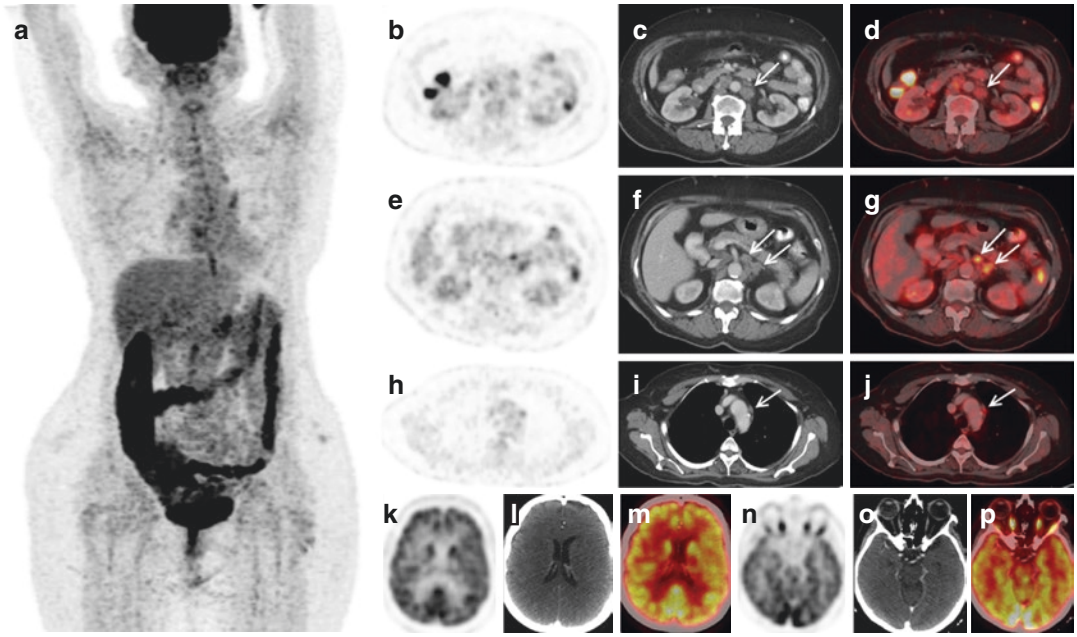

Fig. 19.27 FDG PET/CT after four cycles of alternate second-line chemotherapy in this platinum-resistant ovarian carcinoma. The MIP image (**a**) showing resolution of most of the abnormal FDG uptake in the abdomen and mediastinum. However, low-grade FDG-avid residual disease was noted in the retroperitoneal and abdominal lymph nodes (**b–g**; arrows). Significant resolution in FDG uptake and size was noted in the mediastinal lymph nodes (**h–j**; arrows). Complete resolution in FDG uptake and size of the brain lesions were also noted (**k–p**). The patient is on additional two cycles of chemotherapy

tumor progression during or within 6 months after completion of prior platinum therapy, is common in recurrent disease [90, 91].

2. In advanced metastatic and platinum-resistant ovarian carcinoma, early response evaluation would have helped in this patient in advocating alternate chemo-regimen at an earlier phase.
3. FDG PET/CT showed disease progression as well as favorable disease response to second-line regimen at interim evaluation including complete response in the metastatic sites in the brain which is usually challenging with physiological FDG uptake in the brain. Ovarian cancer is a rare cause of brain metastasis and only ~1–2% of patients are reported to have brain metastases in the reported literature, though the prevalence is found to be increasing [92].

19.6.3 Case 2: FDG PET/CT Showing Treatment Failure to Bevacizumab-Based Chemotherapy in Ovarian Carcinoma

Clinical summary: Thirty-nine-year female was diagnosed with carcinoma of left ovary (papillary serous adenocarcinoma). She was managed aggressively with total abdominal hysterectomy + bilateral salpingo-opherectomy + infra-colic omentectomy and pelvic lymphadenectomy. CECT abdomen done at end of treatment showed mildly enhancing soft tissue in surgical site and soft-tissue deposit in pelvis with suspicion of residual/recurrence disease. An FDG PET/CT was done to restage the disease after radical surgical treatment (Figs. 19.28, 19.29, and 19.30).

Images:

Interpretation: FDG PET/CT showed residual disease in the form of pre-sacral deposit and pelvic lymph nodes after radical surgery. Post adjuvant chemotherapy, there was favorable response in the pre-existing lesions but appearance of new lymph node at the aortic bifurcation was suggestive of disease progression. Patient was managed with bevacizumab-based chemotherapy but post six cycles of therapy FDG PET/CT showed disease progression in the form of pelvic serosal, lymph nodal, pulmonary, and lytic skeletal lesions suggesting new sites of metastatic disease and failure to the chemotherapy.

Teaching points:

1. Despite advances in early diagnosis, ovarian carcinoma is usually detected at a very advanced stage, and prognosis remains unsatisfactory

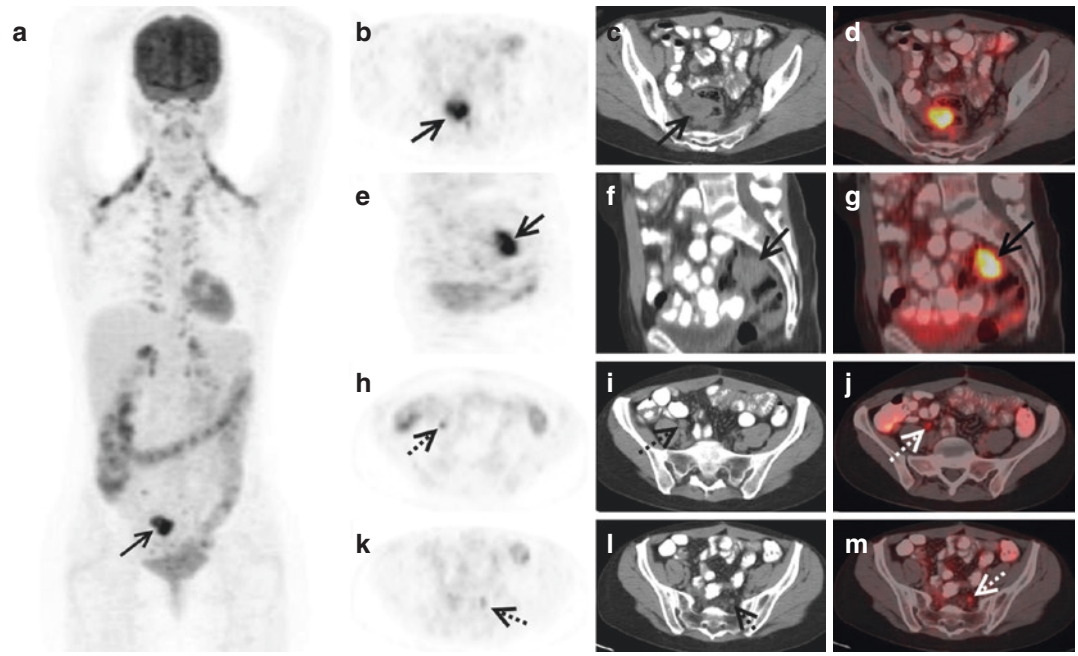

Fig. 19.28 FDG PET/CT after primary treatment in a known case of ovarian carcinoma post radical surgery and adjuvant chemotherapy. There is FDG-avid pre-sacral serosal soft-tissue deposit abutting sigmoid colon highlighted with arrows in the MIP (**a**) axial and corresponding sagittal PET, CT, and fused PET/CT images (**b–g**). In addition, faintly FDG-avid subcentimetric pelvic mesenteric lymph nodes are also noted (highlighted with dotted arrows in axial sections of PET, CT, and fused PET/CT images; **h–m**). In view of the FDG-avid residual disease, patient was given six cycles of adjuvant chemotherapy

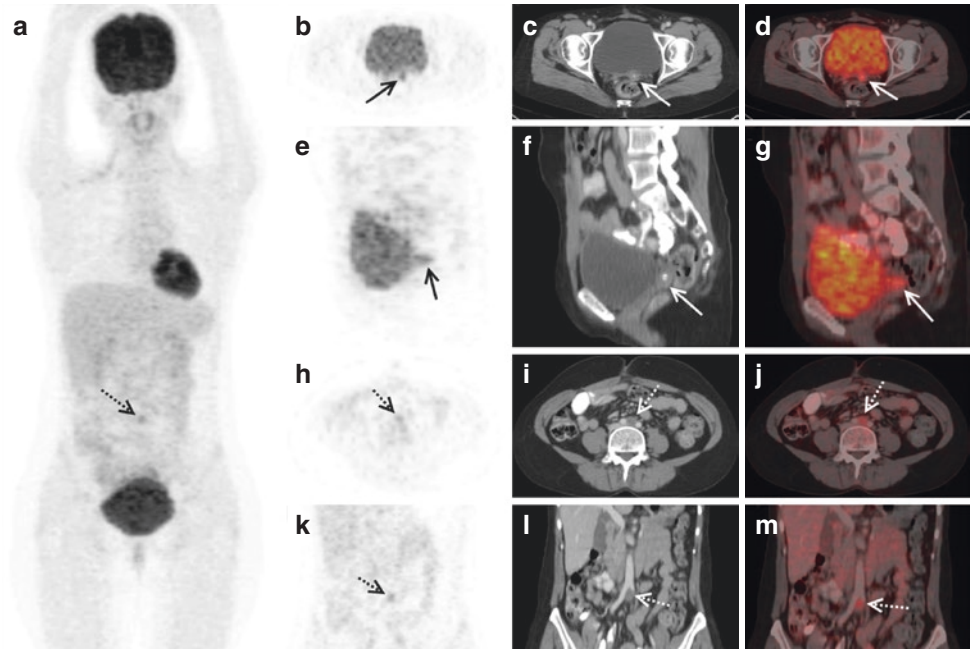

Fig. 19.29 Post six cycles of adjuvant chemotherapy, FDG PET/CT done for response evaluation showed FDG-avid ill-defined enhancing nodular density in the vaginal vault abutting urinary bladder anteriorly and the rectum posteriorly, as seen in the axial (**b–d**) and corresponding sagittal (**e–g**) PET, CECT, and fused PET/CT images (highlighted with arrows). Additionally, a low-grade FDG avid lymph node (~1.2 cm in short axis diameter; SUVmax 2.3) is noted just below the aortic bifurcation, highlighted with dotted arrows in the MIP (**a**), axial (**h–j**), and corresponding coronal (**k–m**) images. FDG PET/CT showed favorable response in all the sites except presence of new lymph node at aortic bifurcation suggestive of disease progression. The patient was offered six cycles of alternate regimen chemotherapy (bevacizumab based). FDG PET/CT was repeated after six cycles for treatment response

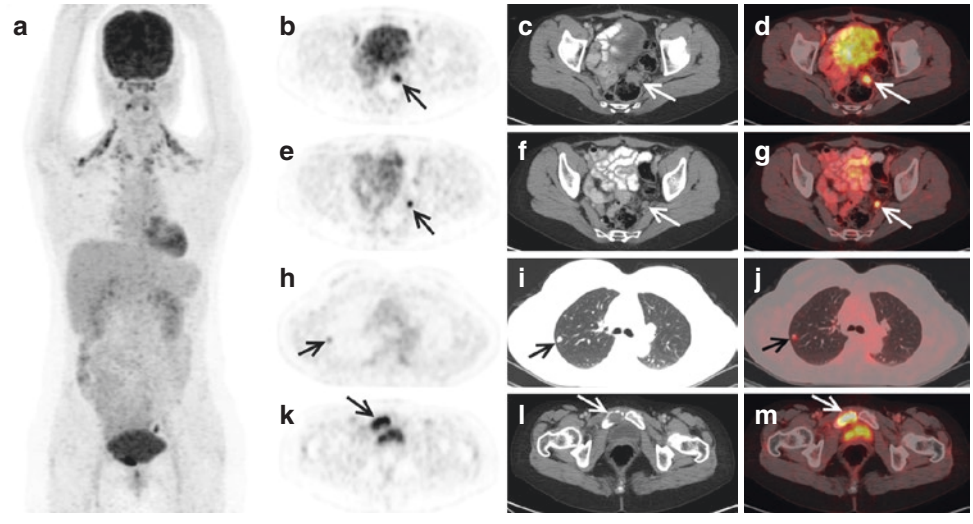

Fig. 19.30 FDG PET/CT post six cycles of bevacizumab-based chemotherapy show FDG-avid serosal deposit along the sigmoid colon in the pelvis (arrows; **b–d**), left-sided pelvic lymph node (arrows; **e–g**), FDG-avid parenchymal nodule in the right lung (arrows; **h–j**), and FDG-avid lytic lesion with soft-tissue component in the right pubic bone near symphysis (arrows; **k–m**) suggesting disease progression

with poor survival rates, despite the current availability of many active and emerging drugs.
2. A large number of patients experience disease progression, and FDG PET/CT has the potential to identify new sites of disease despite favorable response in other preexisting lesions [93, 94]. FDG PET/CT should be introduced early at the course of chemotherapy to predict early response, so that shifting into an alternate regimen is possible at an earlier phase.
3. Bevacizumab is a humanized monoclonal antibody targeting vascular endothelial growth factor, and it is the first molecular-targeted agent to be used for the treatment of ovarian cancer. Several trials show variable results in different settings in the management of ovarian carcinoma [94, 95]. FDG PET/CT in this patient has shown disease progression and failure to chemotherapy by showing new sites of metastatic disease.

Funding: There is no financial disclosure
Conflict of interest: None

References

Cervical Carcinoma

1. Parkin DM, Bray F, Ferlay J, et al. Global cancer statistics, 2002. CA Cancer J Clin. 2005;55:74–108.
2. Mirpour S, Mhlanga JC, Logeswaran P, et al. The role of PET/CT in the management of cervical cancer. AJR Am J Roentgenol. 2013;201:W192–205.
3. Son H, Kositwattanarerk A, Hayes MP, et al. PET/CT evaluation of cervical cancer: spectrum of disease. Radiographics. 2010;30:1251–68.
4. Park W, Park YJ, Huh SJ, et al. The usefulness of MRI and PET imaging for the detection of parametrial involvement and lymph node metastasis in patients with cervical cancer. Jpn J Clin Oncol. 2005;35:260–4.
5. Grigsby PW. The prognostic value of PET and PET/CT in cervical cancer. Cancer Imaging. 2008;8:146–55.
6. Lin LL, Yang Z, Mutic S, et al. FDG-PET imaging for the assessment of physiologic volume response during radiotherapy in cervix cancer. Int J Radiat Oncol Biol Phys. 2006;65:177–81.
7. Grigsby PW, Siegel BA, Dehdashti F, et al. Posttherapy [18F] fluorodeoxyglucose positron emission tomography in carcinoma of the cervix: response and outcome. J Clin Oncol. 2004;22:2167–71.
8. Schwarz JK, Siegel BA, Dehdashti F, et al. Association of posttherapy positron emission tomography with tumor response and survival in cervical carcinoma. JAMA. 2007;298:2289–95.
9. Schwarz JK, Grigsby PW, Dehdashti F, et al. The role of 18F-FDG PET in assessing therapy response in cancer of the cervix and ovaries. J Nucl Med. 2009;50(Suppl 1):64S–73S.
10. Ki EY, Lee KH, Park JS, et al. A clinicopathological review of pulmonary metastasis from uterine cervical cancer. Cancer Res Treat. 2016;48:266–72.
11. Emmert C, Kohler U. Management of genital fistulas in patients with cervical cancer. Arch Gynecol Obstet. 1996;259:19–24.
12. Narayanan P, Nobbenhuis M, Reynolds KM, et al. Fistulas in malignant gynecologic disease: etiology, imaging, and management. Radiographics. 2009;29:1073–83.
13. Lakhani A, Khan SR, Bharwani N, et al. FDG PET/CT pitfalls in gynecologic and genitourinary oncologic imaging. Radiographics. 2017;37:577–94.
14. Yu NC, Raman SS, Patel M, et al. Fistulas of the genitourinary tract: a radiologic review. Radiographics. 2004;24:1331–52.
15. Kashyap R, Agrawal K, Singh H, et al. Disease- and treatment-related complication on F-18-fluorodeoxyglucose positron emission tomography/computed tomography in oncology practice: a pictorial review. Indian J Nucl Med. 2017;32:304–15.
16. Haie-Meder C, Potter R, Van Limbergen E, et al. Recommendations from Gynaecological (GYN) GEC-ESTRO Working Group (I): concepts and terms in 3D image based 3D treatment planning in cervix cancer brachytherapy with emphasis on MRI assessment of GTV and CTV. Radiother Oncol. 2005;74:235–45.
17. Banerjee R, Kamrava M. Brachytherapy in the treatment of cervical cancer: a review. Int J Womens Health. 2014;6:555–64.
18. Kidd EA, Siegel BA, Dehdashti F, et al. Lymph node staging by positron emission tomography in cervical cancer: relationship to prognosis. J Clin Oncol. 2010;28:2108–13.
19. Vincens E, Balleyguier C, Rey A, et al. Accuracy of magnetic resonance imaging in predicting residual disease in patients treated for stage IB2/II cervical carcinoma with chemoradiation therapy : correlation of radiologic findings with surgicopathologic results. Cancer. 2008;113:2158–65.
20. Fields EC, Weiss E. A practical review of magnetic resonance imaging for the evaluation and management of cervical cancer. Radiat Oncol. 2016;11:15.
21. Stehman FB, Bundy BN, DiSaia PJ, et al. Carcinoma of the cervix treated with radiation therapy. I. A multi-variate analysis of prognostic variables in the Gynecologic Oncology Group. Cancer. 1991;67:2776–85.
22. Kobayashi R, Yamashita H, Okuma K, et al. Details of recurrence sites after definitive radiation therapy for cervical cancer. J Gynecol Oncol. 2016;27:e16.
23. Tangjitgamol S, Katanyoo K, Laopaiboon M, et al. Adjuvant chemotherapy after concurrent chemoradiation for locally advanced cervical cancer. Cochrane Database Syst Rev. 2014;(12):CD010401.

Endometrial Carcinoma

24. Tran AQ, Gehrig P. Recent advances in endometrial cancer. F1000Res. 2017;6:81.
25. Kitajima K, Murakami K, Yamasaki E, et al. Accuracy of 18F-FDG PET/CT in detecting pelvic and paraaortic lymph node metastasis in patients with endometrial cancer. AJR Am J Roentgenol. 2008;190:1652–8.
26. Nakamura K, Hongo A, Kodama J, et al. The measurement of SUVmax of the primary tumor is predictive of prognosis for patients with endometrial cancer. Gynecol Oncol. 2011;123:82–7.
27. Crivellaro C, Signorelli M, Guerra L, et al. Tailoring systematic lymphadenectomy in high-risk clinical early stage endometrial cancer: the role of 18F-FDG PET/CT. Gynecol Oncol. 2013;130:306–11.
28. Sharma P, Kumar R, Singh H, et al. Carcinoma endometrium: role of 18-FDG PET/CT for detection of suspected recurrence. Clin Nucl Med. 2012;37:649–55.
29. Ozcan Kara P, Kara T, Kaya B, et al. The value of FDG-PET/CT in the post-treatment evaluation of endometrial carcinoma: a comparison of PET/CT findings with conventional imaging and CA 125 as

a tumour marker. Rev Esp Med Nucl Imagen Mol. 2012;31:257–60.
30. Chung HH, Kang WJ, Kim JW, et al. The clinical impact of [(18)F]FDG PET/CT for the management of recurrent endometrial cancer: correlation with clinical and histological findings. Eur J Nucl Med Mol Imaging. 2008;35:1081–8.
31. Boers-Sonderen MJ, de Geus-Oei LF, Desar IM, et al. Temsirolimus and pegylated liposomal doxorubicin (PLD) combination therapy in breast, endometrial, and ovarian cancer: phase Ib results and prediction of clinical outcome with FDG-PET/CT. Target Oncol. 2014;9:339–47.
32. Yoshida Y, Kurokawa T, Kawahara K, et al. Metabolic monitoring of advanced uterine cervical cancer neoadjuvant chemotherapy by using [F-18]-fluorodeoxyglucose positron emission tomography: preliminary results in three patients. Gynecol Oncol. 2004;95:597–602.
33. Nishiyama Y, Yamamoto Y, Kanenishi K, et al. Monitoring the neoadjuvant therapy response in gynecological cancer patients using FDG PET. Eur J Nucl Med Mol Imaging. 2008;35:287–95.
34. Chung HH, Kim JW, Kang KW, et al. Post-treatment [(1)(8)F]FDG maximum standardized uptake value as a prognostic marker of recurrence in endometrial carcinoma. Eur J Nucl Med Mol Imaging. 2011;38:74–80.
35. Colombo N, Preti E, Landoni F, et al. Endometrial cancer: ESMO Clinical Practice Guidelines for diagnosis, treatment and follow-up. Ann Oncol. 2013;24(Suppl 6):vi33–8.

Fallopian Tube Carcinoma

36. Sedlis A. Primary carcinoma of the fallopian tube. Obstet Gynecol Surv. 1961;16:209–26.
37. Brown MD, Kohorn EI, Kapp DS, et al. Fallopian tube carcinoma. Int J Radiat Oncol Biol Phys. 1985;11:583–90.
38. Pectasides D, Pectasides E, Economopoulos T. Fallopian tube carcinoma: a review. Oncologist. 2006;11:902–12.
39. Patel PV, Cohade C, Chin BB. PET-CT localizes previously undetectable metastatic lesions in recurrent fallopian tube carcinoma. Gynecol Oncol. 2002;87:323–6.
40. Karlan BY, Hoh C, Tse N, et al. Whole-body positron emission tomography with (fluorine-18)-2-deoxyglucose can detect metastatic carcinoma of the fallopian tube. Gynecol Oncol. 1993;49:383–8.
41. Makhija S, Howden N, Edwards R, et al. Positron emission tomography/computed tomography imaging for the detection of recurrent ovarian and fallopian tube carcinoma: a retrospective review. Gynecol Oncol. 2002;85:53–8.
42. van Leeuwen BL, Pruim J, Gouw AS, et al. Liver metastasis as a first sign of fallopian tube carcinoma and the role of positron emission tomography in preoperative diagnosis. Scand J Gastroenterol. 2002;37:1473–4.
43. Takanami K, Kaneta T, Yamada S, et al. F-18 FDG PET/CT findings of primary carcinoma of the fallopian tube. Clin Nucl Med. 2009;34:377–8.
44. Lootsma-Miklosova E, Aalders JG, Willemse PH, et al. Levels of CA 125 in patients with recurrent carcinoma of the fallopian tube: two case histories. Eur J Obstet Gynecol Reprod Biol. 1987;24:231–5.
45. Hefler LA, Rosen AC, Graf AH, et al. The clinical value of serum concentrations of cancer antigen 125 in patients with primary fallopian tube carcinoma: a multicenter study. Cancer. 2000;89:1555–60.
46. Ajithkumar TV, Minimole AL, John MM, et al. Primary fallopian tube carcinoma. Obstet Gynecol Surv. 2005;60:247–52.

Vaginal Carcinoma

47. Beller U, Sideri M, Maisonneuve P, et al. Carcinoma of the vagina. J Epidemiol Biostat. 2001;6:141–52.
48. Pisani P, Parkin DM, Munoz N, et al. Cancer and infection: estimates of the attributable fraction in 1990. Cancer Epidemiol Biomarkers Prev. 1997;6:387–400. 49. Hemminki K, Li X, Vaittinen P. Time trends in the incidence of cervical and other genital squamous cell carcinomas and adenocarcinomas in Sweden, 1958-1996. Eur J Obstet Gynecol Reprod Biol. 2002;101:64–9.
50. Lamoreaux WT, Grigsby PW, Dehdashti F, et al. FDG-PET evaluation of vaginal carcinoma. Int J Radiat Oncol Biol Phys. 2005;62:733–7.
51. Robertson NL, Hricak H, Sonoda Y, et al. The impact of FDG-PET/CT in the management of patients with vulvar and vaginal cancer. Gynecol Oncol. 2016;140:420–4.
52. Ucak Semirgin S, Basoglu T, Atmaca Saglik B, et al. Diagnostic value of additional 18F-FDG PET/CT imaging using a vaginal catheter in patients with paravaginal malignant lesions. Nucl Med Commun. 2016;37:1260–6.
53. Ishibashi N, Maebayashi T, Aizawa T, et al. Vaginal tumor-vesical fistula detected by dynamic fluorodeoxyglucose-positron emission tomography/computed tomography: A case report. Clin Imaging. 2017;46:113–5.
54. Cho LP, Kim CK, Viswanathan AN. Pilot study assessing (18)F-fluorothymidine PET/CT in cervical and vaginal cancers before and after external beam radiation. Gynecol Oncol Rep. 2015;14:34–7.

Vulval Carcinoma

55. Howlader N, Noone AM, Krapcho M, et al. SEER cancer statistics review, 1975–2013. National Cancer Institute website. http://seer.cancer.gov/

csr/1975_2013/. Updated April 2016. Accessed 28 Feb 2018.
56. Bayne L, Butler J, Colombo N, et al. Gynaecological Cancer in Europe, facts and figures in 2015. http://www.asociacionasaco.es/wp-content/uploads/2015/10/Facts-datos-y-figures-estadisticas-2015-imprimible.pdf. Updated September 2015. Accessed 8 May 2018.
57. Consolidated report of hospital based cancer registries 2001-3, National Cancer Registry Program. New Delhi: Indian Council of Medical Research; 2007.
58. Hampl M, Deckers-Figiel S, Hampl JA, Rein D, Bender HG. New aspects of vulvar cancer: changes in localization and age of onset. Gynecol Oncol. 2008;109:340–5.
59. Howlander N, Noone A, Krapcho M, Garshell J, Miller D, Altekruse S. SEER cancer statistics review 1975-2012. National Cancer Institute; 2015.
60. Madsen BS, Jensen HL, van den Brule AJC, Wohlfahrt J, Frisch M. Risk factors for invasive squamous cell carcinoma of the vulva and vagina–population-based case-control study in Denmark. Int J Cancer. 2008;122:2827–34.
61. Koh WJ, Greer BE, Abu-Rustum NR, et al. Vulvar cancer, version 1.2017, NCCN clinical practice guidelines in oncology. J Natl Compr Canc Netw. 2017;15:92–120.
62. Katz A, Eifel PJ, Jhingran A, Levenback CF. The role of radiation therapy in preventing regional recurrences of invasive squamous cell carcinoma of the vulva. Int J Radiat Oncol Biol Phys. 2003;57:409–18.
63. Beriwal S, Coon D, Heron DE, et al. Preoperative intensity-modulated radiotherapy and chemotherapy for locally advanced vulvar carcinoma. Gynecol Oncol. 2008;109:291–5.
64. Alt C, Brocker KA, Eichbaum M, et al. Imaging of female pelvic malignancies regarding MRI, CT, and PET/CT. Strahlenther Onkol. 2011;187:705–14.
65. Koh WJ, Greer BE, Abu-Rustum NR, et al. Vulvar cancer, version 1.2017, NCCN Clinical Practice Guidelines in Oncology. J Natl Compr Canc Netw. 2017;15:92–120.
66. Cohn DE, Dehdashti F, Gibb RK, et al. Prospective evaluation of positron emission tomography for the detection of groin node metastases from vulvar cancer. Gynecol Oncol. 2002;85:179–84.
67. Kamran MW, O'Toole F, Meghen K, et al. Whole-body [18F]fluoro-2-deoxyglucose positron emission tomography scan as combined PET-CT staging prior to planned radical vulvectomy and inguinofemoral lymphadenectomy for squamous vulvar cancer: a correlation with groin node metastasis. Eur J Gynaecol Oncol. 2014;35:230–5.
68. Lin G, Chen CY, Liu FY, et al. Computed tomography, magnetic resonance imaging and FDG positron emission tomography in the management of vulvar malignancies. Eur Radiol. 2015;25:1267–78.
69. Dolanbay M, Ozcelik B, Abdulrezzak U, et al. F-18 fluoro-D-glucose (FDG)-positron emission tomography (PET)/computed tomography (CT) in planning of surgery and sentinel lymph node screening in vulvar cancers. Arch Gynecol Obstet. 2016;293:1319–24.
70. Peiro V, Chiva L, Gonzalez A, et al. Utility of the PET/CT in vulvar cancer management. Rev Esp Med Nucl Imagen Mol. 2014;33:87–92.
71. Crivellaro C, Guglielmo P, De Ponti E, et al. 18F-FDG PET/CT in preoperative staging of vulvar cancer patients: is it really effective? Medicine (Baltimore). 2017;96(38):e7943.
72. Rao YJ, Hassanzadeh C, Chundury A, Hui C, et al. Association of post-treatment positron emission tomography with locoregional control and survival after radiation therapy for squamous cell carcinoma of the vulva. Radiother Oncol. 2017;122:445–51.

Ovarian Carcinoma

73. Torre LA, Trabert B, DeSantis CE, et al. Ovarian cancer statistics, 2018. CA Cancer J Clin. 2018;68:284–96.
74. Siegel RL, Miller KD, Jemal A. Cancer statistics, 2018. CA Cancer J Clin. 2018;68:7–30.
75. Risum S, Hogdall C, Loft A, et al. The diagnostic value of PET/CT for primary ovarian cancer--a prospective study. Gynecol Oncol. 2007;105:145–9.
76. Prakash P, Cronin CG, Blake MA. Role of PET/CT in ovarian cancer. AJR Am J Roentgenol. 2010;194:W464–70.
77. Park T, Lee S, Park S, et al. Value of (18)F-FDG PET/CT in the detection of ovarian malignancy. Nucl Med Mol Imaging. 2015;49:42–51.
78. Palomar Munoz A, Cordero Garcia JM, Talavera Rubio MDP, et al. Value of [18F]FDG-PET/CT and CA125, serum levels and kinetic parameters, in early detection of ovarian cancer recurrence: influence of histological subtypes and tumor stages. Medicine (Baltimore). 2018;97:e0098.
79. Palomar A, Nanni C, Castellucci P, et al. Value of FDG PET/CT in patients with treated ovarian cancer and raised CA125 serum levels. Mol Imaging Biol. 2012;14:123–9.
80. Cengiz A, Koc ZP, Ozcan Kara P, et al. The role of (18)F-FDG PET/CT in detecting ovarian cancer recurrence in patients with elevated CA-125 levels. Mol Imaging Radionucl Ther. 2019;28:8–14.
81. Ben-Haim S, Ell P. 18F-FDG PET and PET/CT in the evaluation of cancer treatment response. J Nucl Med. 2009;50:88–99.
82. Avril NE, Weber WA. Monitoring response to treatment in patients utilizing PET. Radiol Clin North Am. 2005;43:189–204.
83. Avril N, Gourtsoyianni S, Reznek R. Gynecological cancers. Methods Mol Biol. 2011;727:171–89.
84. Sironi S, Messa C, Mangili G, et al. Integrated FDG PET/CT in patients with persistent ovarian cancer: correlation with histologic findings. Radiology. 2004;233:433–40.

85. Vallius T, Peter A, Auranen A, et al. 18F-FDG-PET/CT can identify histopathological non-responders to platinum-based neoadjuvant chemotherapy in advanced epithelial ovarian cancer. Gynecol Oncol. 2016;140:29–35.
86. Avril N, Sassen S, Schmalfeldt B, et al. Prediction of response to neoadjuvant chemotherapy by sequential F-18-fluorodeoxyglucose positron emission tomography in patients with advanced-stage ovarian cancer. J Clin Oncol. 2005;23:7445–53.
87. Nishiyama Y, Yamamoto Y, Kanenishi K, et al. Monitoring the neoadjuvant therapy response in gynecological cancer patients using FDG PET. Eur J Nucl Med Mol Imaging. 2008;35:287–95.
88. Boers-Sonderen MJ, de Geus-Oei LF, Desar IM, et al. Temsirolimus and pegylated liposomal doxorubicin (PLD) combination therapy in breast, endometrial, and ovarian cancer: phase Ib results and prediction of clinical outcome with FDG-PET/CT. Target Oncol. 2014;9:339–47.
89. Caobelli F, Alongi P, Evangelista L, et al. Predictive value of (18)F-FDG PET/CT in restaging patients affected by ovarian carcinoma: a multicentre study. Eur J Nucl Med Mol Imaging. 2016;43:404–13.
90. Gore ME, Fryatt I, Wiltshaw E, et al. Treatment of relapsed carcinoma of the ovary with cisplatin or carboplatin following initial treatment with these compounds. Gynecol Oncol. 1990;36:207–11.
91. Matsuo K, Lin YG, Roman LD, et al. Overcoming platinum resistance in ovarian carcinoma. Expert Opin Investig Drugs. 2010;19:1339–54.
92. Pakneshan S, Safarpour D, Tavassoli F, et al. Brain metastasis from ovarian cancer: a systematic review. J Neurooncol. 2014;119:1–6.
93. Francis J, Coakley N, Elit L, et al. Systemic therapy for recurrent epithelial ovarian cancer: a clinical practice guideline. Curr Oncol. 2017;24:e540–6.
94. Cortez AJ, Tudrej P, Kujawa KA, et al. Advances in ovarian cancer therapy. Cancer Chemother Pharmacol. 2018;81:17–38.
95. Rossi L, Verrico M, Zaccarelli E, et al. Bevacizumab in ovarian cancer: a critical review of phase III studies. Oncotarget. 2017;8:12389–405.

[18F]FDG PET/CT in Treatment Response Evaluation: Colorectal Cancer

20

F. A. Vuijk, L. Heijmen, M. J. Roef, A. I. J. Arens, A. L. Vahrmeijer, E. L. van Persijn van Meerten, D. E. Hilling, and L. F. de Geus-Oei

20.1 Introduction

With an incidence of 1.8 million and nearly 900,000 deaths in 2018, colorectal cancer has the third highest cancer incidence and ranks second among common causes of cancer death worldwide [1]. As (neo)adjuvant treatment regimens have been adopted into treatment guidelines for both colon and rectal cancer (neoadjuvant short-course radiotherapy and long course chemoradiotherapy for rectal cancer, adjuvant chemotherapy for colon cancer), treatment response monitoring has become of evident importance.

Currently, response monitoring is performed using computed tomography (CT) imaging combined with colonoscopy and magnetic resonance (MR) and digital rectal examination in rectal cancer patients. Up to now, the use of positron emission tomography (PET) has not been adopted into colorectal guidelines for response monitoring purposes yet.

[18F]Fluorodeoxyglucose (FDG) PET has the potential to provide metabolic information on tumor cells as indicated by the increased uptake and metabolism of glucose. This provides additional information compared to conventional CT or MR imaging alone. While hybrid PET/CT is a common and widely available technique, developments toward optimizing combined PET/MR scanners are still ongoing but show great promise.

In addition to the combination of PET with CT and MR, much progress is also being made in optimizing PET scanner hardware and software. Most recently, the introduction of the digital PET scanner shows promise to further increase the diagnostic abilities of PET.

Previous research and concurrent clinical experience have reported additional value of the use of FDG PET in initial staging of recurrent colorectal cancer and metastases, localizing recurrent disease in patients with unexplained elevation of serum CEA, and in the assessment of residual cancerous masses after treatment. However, the use of FDG PET for response monitoring of colorectal cancer is still cumbersome. As this technique provides metabolic data, FDG PET can detect intratumoral changes preceding anatomical alterations. The technique shows promise in monitoring, but also in predicting response to given therapy, thereby creating

F. A. Vuijk (✉) · A. L. Vahrmeijer · D. E. Hilling
Department of Surgery, Leiden University Medical Center, Leiden, The Netherlands
e-mail: F.A.Vuijk@lumc.nl

L. Heijmen · E. L. van Persijn van Meerten
L. F. de Geus-Oei
Department of Radiology, Leiden University Medical Center, Leiden, The Netherlands

M. J. Roef
Department of Nuclear Medicine, Catharina Hospital, Eindhoven, The Netherlands

A. I. J. Arens
Department of Radiology and Nuclear Medicine, Radboud University Medical Center, Nijmegen, The Netherlands

S. Fanti et al. (eds.), *Atlas of Clinical PET-CT in Treatment Response Evaluation in Oncology*,
https://doi.org/10.1007/978-3-030-68858-5_20

options to establish personalized patient treatment. As PET can not only provide qualitative data, but also quantitative data on multiple lesions simultaneously, monitoring lesions can be performed quantitatively over time.

As (neo)adjuvant therapies thrive and become adopted into standard care, the need for accurate response monitoring increases. This is clearly demonstrated by a subgroup of locally advanced rectal cancer patients, who receive neoadjuvant chemoradiation. A proportion of these patients show a complete remission of tumor and/or pathological lymph nodes after treatment. By accurately selecting these patients, surgery can be omitted, and its associated morbidity and mortality avoided. Current imaging modalities including endoscopy and MR imaging provide reasonable evaluation of residual tumor and/or lymph nodes. However, not all patients with a complete response can be detected. In addition, early detection of nonresponders could prevent futile treatment (and its associated side effects) and unnecessary postponing of inevitable surgical resection.

This chapter regarding response monitoring of colorectal cancer using FDG PET/CT illustrates potential clinical examples in which FDG PET/CT might complement conventional diagnostic imaging modalities in time to come. Further research is however warranted to define the exact situations in which FDG PET/CT can be of additional value. The following clinical cases include response monitoring during neoadjuvant chemoradiation, local treatment of liver metastases, neoadjuvant treatment of recurrent rectal cancer, and palliative systemic treatment of hepatic and extrahepatic disease.

20.2 Clinical Case 1: Colorectal Liver Metastasis

Clinical details: A 55-year-old male with a history of a sigmoid resection for a pT2N0M0 sigmoid carcinoma and metastasectomy for a metachronous liver lesion in segment IVa 3 years later. Three months after the metastasectomy, radiofrequency ablation (RFA) was performed on a second lesion in segment III. Now, 6 years after resection of the primary tumor, serum CEA is elevated, and no metastases were detected prospectively on CT imaging of the chest and abdomen.

Scan findings: A solitary FDG avid lesion is detected in the caudate liver lobe. Also, a photopenic area from the metastasectomy is observed in segment IVa. No evidence of disease recurrence is seen at the anastomosis site (Fig. 20.1).

Interpretation: Suspected solitary liver metastasis in the caudate liver lobe.

Teaching points:

1. FDG PET/CT has a higher sensitivity for detecting colorectal liver metastases compared to contrast-enhanced CT [2].
2. FDG PET/CT can be helpful to localize recurrent disease in case of elevated CEA and undetectable disease on CT [3].

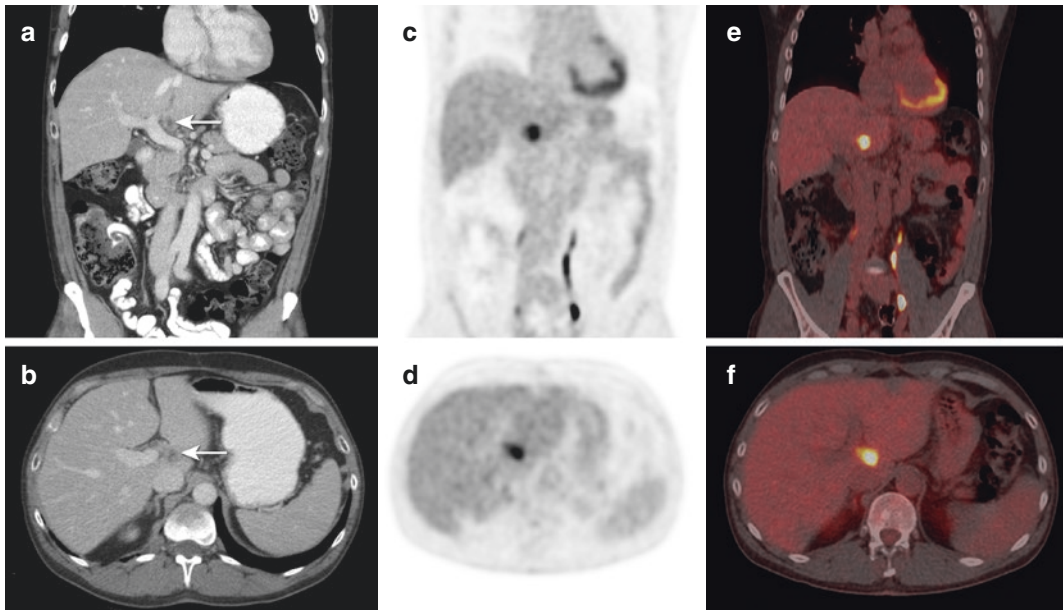

Fig. 20.1 Solitary liver metastasis. Coronal (**a**, **c**, **e**) and axial (**b**, **d**, **f**) images of a solitary liver metastasis in the caudate liver lobe (segment I). Representative images of CT (**a**, **b**), PET (**c**, **d**), and PET/CT (**e**, **f**)

20.3 Clinical Case 2: Colorectal Liver Metastasis

Clinical details: A 55-year-old male with a history of a coecum carcinoma for which a right hemicolectomy was performed developed multiple metachronous liver metastases 6 years later. Left hemihepatectomy and multiple metastasectomies were performed. One year later, RFA was performed on a recurrent liver metastasis. One year after the RFA, thus 8 years after primary diagnosis, at least three suspicious new liver lesions were found on FDG PET/CT (Fig. 20.2a, b) and deemed unresectable. Systemic treatment consisting of capecitabine, oxaliplatin, and bevacizumab was initiated.

Scan findings: Complete remission of the liver metastases (Fig. 20.2c, d). No evidence of other (extra) hepatic metastases.

Interpretation: Complete response of liver metastasis after therapy.

Teaching point:

1. FDG PET/CT can reliably monitor response of liver metastases to systemic treatment.

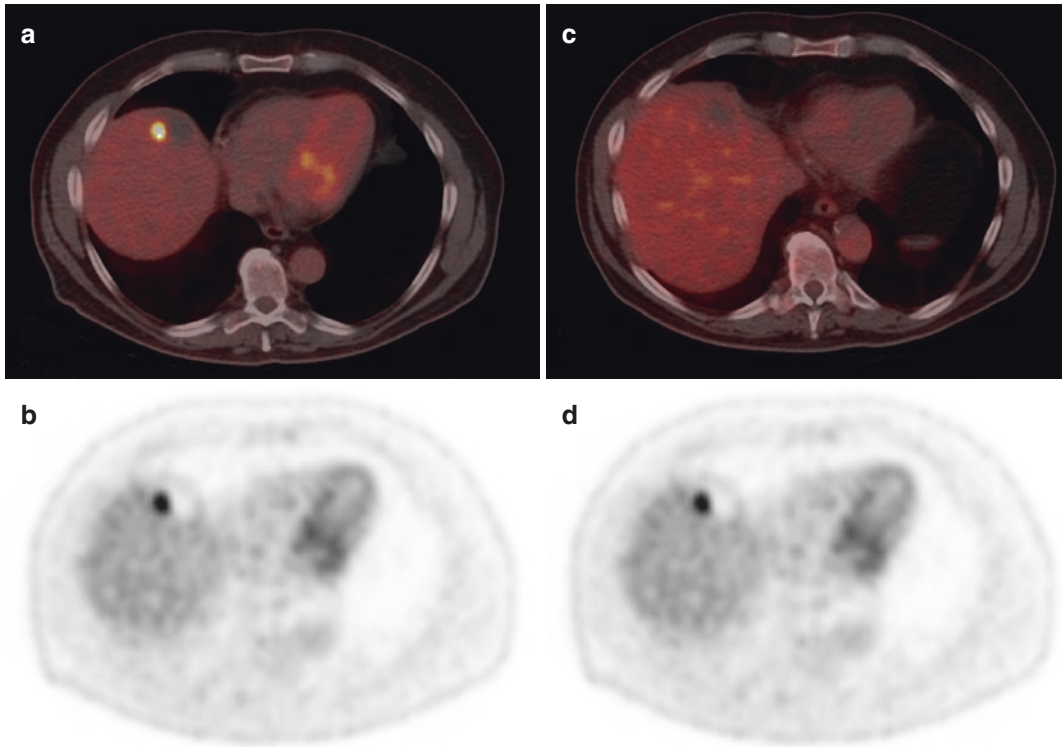

Fig. 20.2 Response monitoring liver metastasis. Images of PET/CT (**a**, **c**) and PET (**b**, **d**) before (**a**, **b**) and after six cycles of therapy (**c**, **d**)

20.4 Clinical Case 3: Sequel to Case 2

Clinical details: Four years after therapy, recurrent liver metastases were detected. Capecitabine monotherapy was restarted and FDG PET/CT was used for response monitoring.

Scan findings: A persistent strong FDG-avid metastasis is seen in segment 6/7 (Fig. 20.3a, e, i), SUV_{max} remains unchanged, however metabolic volume increases. FDG PET/CT shows no changes in the highly active lesion in segment 8 (Fig. 20.3c, g, k).

Interpretation: Stable disease in liver segment 8; slight increase in metabolic volume in segment 6/7. As previous experience in this patient showed stabilizing and eventually decreasing disease with continuous capecitabine treatment, treatment is continued, and evaluation is scheduled after three cycles.

Teaching point:

1. Serial SUV_{max} measurements can monitor therapy response of liver metastases to chemotherapy.

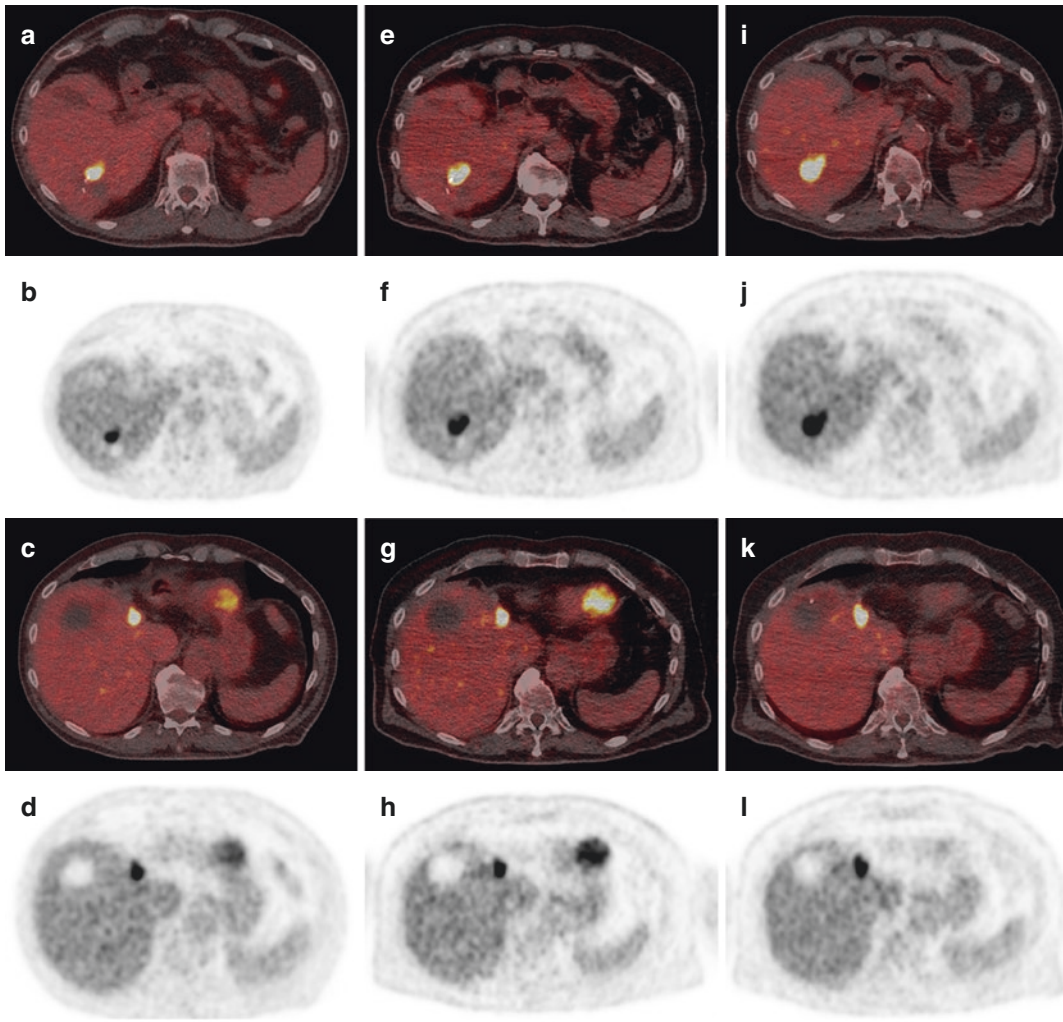

Fig. 20.3 Response monitoring liver metastases. PET/CT (**a**, **c**, **e**, **g**, **i**, **k**) and PET (**b**, **d**, **f**, **h**, **j**, **l**) images before (**a–d**), after three cycles (**e–h**), and after six cycles (**i–l**) of capecitabine treatment

20.5 Clinical Case 4: Response Monitoring of Liver Metastases

Clinical details: A 74-year-old female with colon cancer and multiple synchronous liver metastases was treated with combination therapy consisting of capecitabine and bevacizumab. Treatment was terminated after two cycles due to liver failure, likely due to progressive liver metastases. Four weeks after termination of the treatment, the patient passed away.

The patient participated in a clinical trial, during which PET/CT imaging was performed. The research objective was to evaluate the predictive value of pretreatment PET/CT measurements and early changes 1 week after the start of therapy [4].

Scan findings: Mean SUV_{max} (of five lesions) was 15 before treatment, and 13 after 1 week of treatment. Total lesion glycolysis (TLG) in the same five lesions increased slightly from 3450 to 3565 (Fig. 20.4).

Interpretation: Progressive disease is observed as metabolic volume has increased.

Teaching point:

1. FDG PET can identify patients not responding to therapy, thereby aiding in the decision to terminate treatment when no benefit is expected. Early response monitoring is challenging using CT, and only useful 8 weeks after start of treatment.

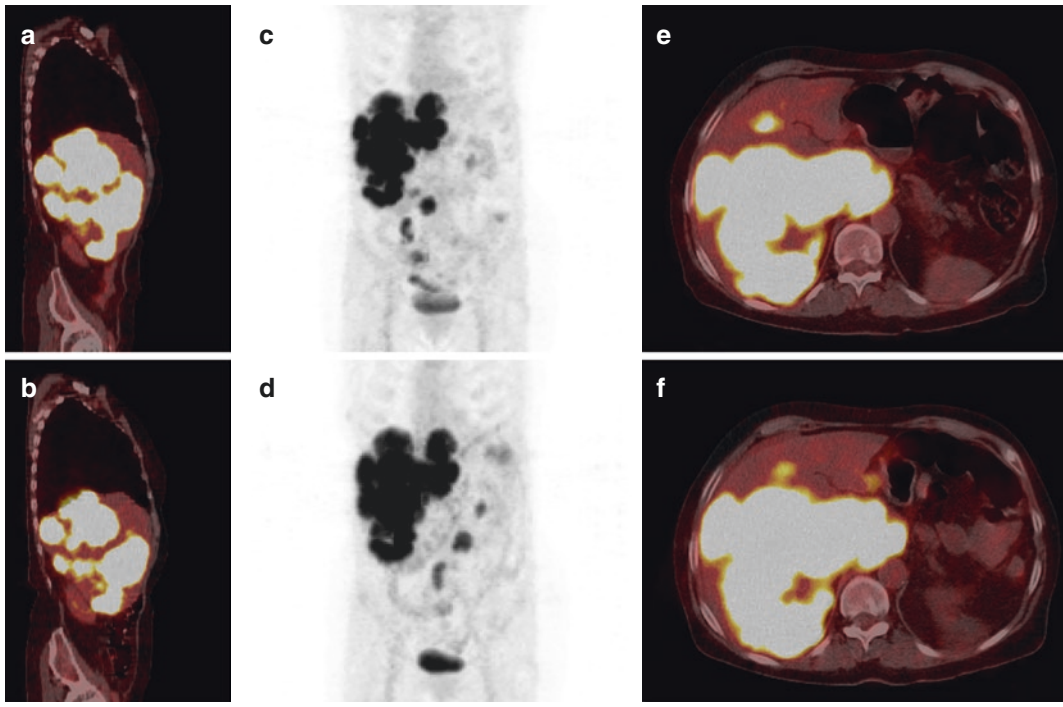

Fig. 20.4 Response monitoring of liver metastases. Images of PET/CT (**a**, **b**, **e**, **f**) and the maximum intensity projection (**c**, **d**) before (**a**, **c**, **e**) and after (**b**, **d**, **f**) treatment

20.6 Clinical Case 5: Response Monitoring of Liver Metastases

Clinical details: A 56-year-old male with colon cancer and synchronous liver metastases is treated with systemic therapy, a combination of capecitabine, oxaliplatin (CAPOX), and bevacizumab.

Scan findings: Mean SUV_{max} (of five lesions) was 7.0 before treatment, 7.0 one week into treatment, and 6.8 after three cycles. TLG decreased from 320 before treatment to 230 after 1 week, and further to 100 after three cycles (Fig. 20.5).

Interpretation: Partial response after three cycles of antitumor treatment.

Teaching point:

1. Serial FDG PET/CT measurements can monitor therapy response of liver metastases to combination therapy (chemotherapy and anti-angiogenic treatment).

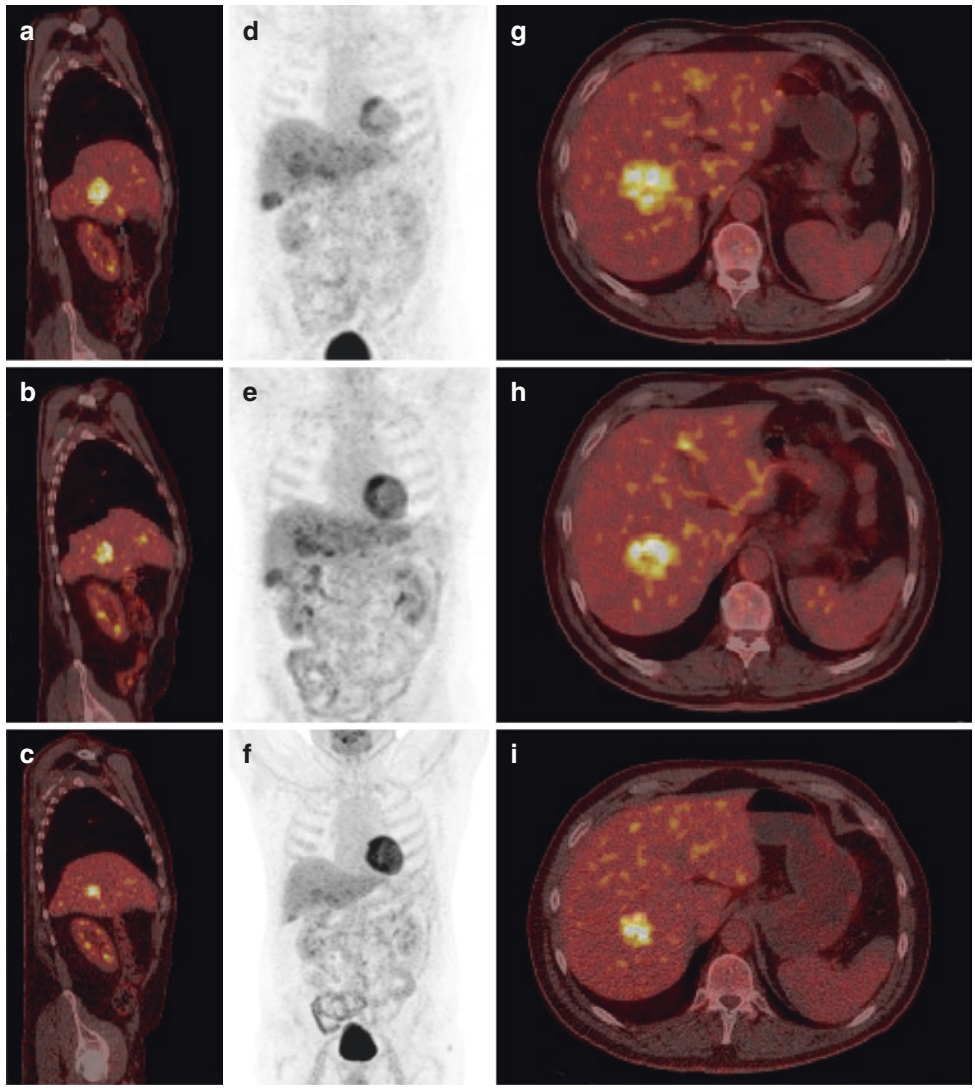

Fig. 20.5 Response monitoring of liver metastases. PET/CT (**a–c**, **g**, **h**, **i**) and maximum intensity images (MIP) (**d–f**) before (**a**, **d**, **g**), after 1 week of therapy (**b**, **e**, **h**), and after three cycles (**c**, **f**, **i**)

20.7 Clinical Case 6: Response Monitoring of Liver and Other Metastases

Clinical details: A 65-year-old male with colon cancer and synchronous liver and lung metastases was treated with neoadjuvant therapy, a combination of CAPOX and bevacizumab.

Scan findings: Mean SUV_{max} of the three liver lesions was 8.4 before treatment, 7.4 after 1 week, and 4.2 after three cycles. TLG of the liver lesions was 950 before treatment, 680 after 1 week, and 95 after three cycles (Fig. 20.6).

Interpretation: Partial response to chemotherapy of the primary tumor, liver metastases, and lung metastases.

Teaching point:

1. Early response monitoring is feasible using FDG PET/CT.

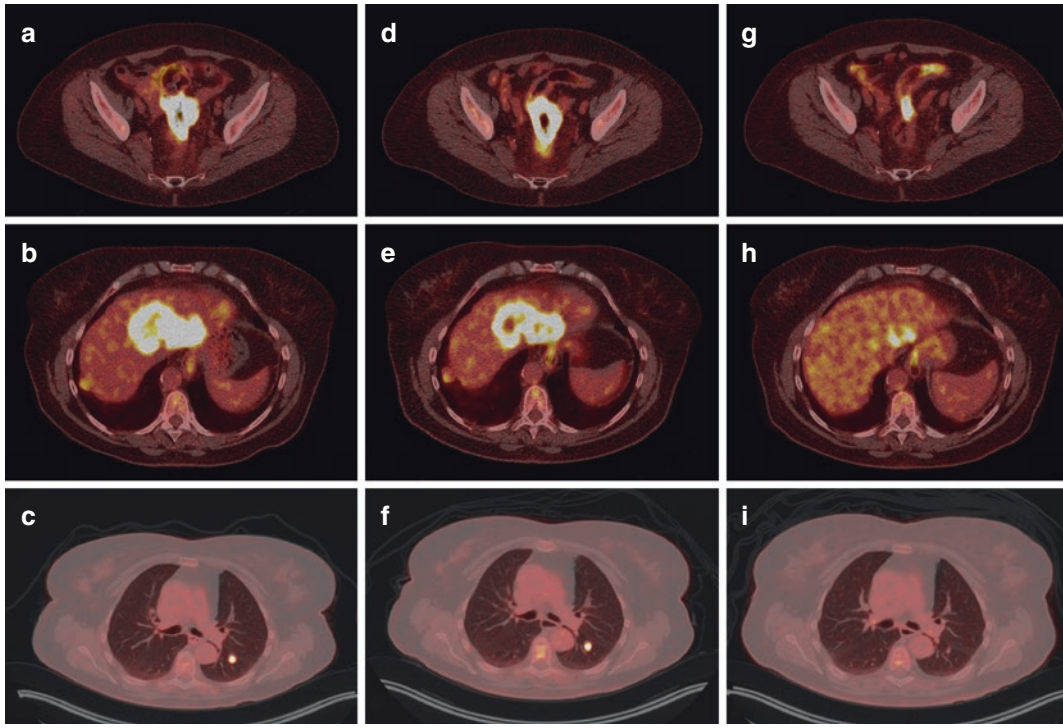

Fig. 20.6 Response monitoring of liver metastases. PET/CT images before treatment (**a–c**), 1 week into treatment (**d–f**), and after three cycles (**g–i**) of respectively the primary tumor, liver metastases, and lung metastases

20.8 Clinical Case 7: Response Monitoring of Liver Metastases

Clinical details: A 75-year-old male with colon cancer and synchronous liver metastases was treated with a combination of neoadjuvant CAPOX and bevacizumab to increase the chance of resectability of the liver metastases.

Scan findings: As the first three scans were part of research, SUV_{max} and TLG analysis was performed. SUV_{max} was 11 before treatment, 9 after 1 week of treatment, and 7 after three cycles (9 weeks). Total lesion glycolysis decreased from 1200 before start of treatment to 500 after 1 week of therapy and decreased further to 220 after three cycles (Fig. 20.7).

Interpretation: Partial response of liver lesions after three cycles, as well as after six cycles. Hereafter, the patient underwent metastasectomy. After this, no evidence of residual or recurrent disease was observed during 24 months of follow-up.

Teaching point:

1. Current response monitoring is performed using the RECIST criteria by evaluating the size of lesions 8–9 weeks after treatment. Metabolic response to antitumor treatment can be visualized earlier.

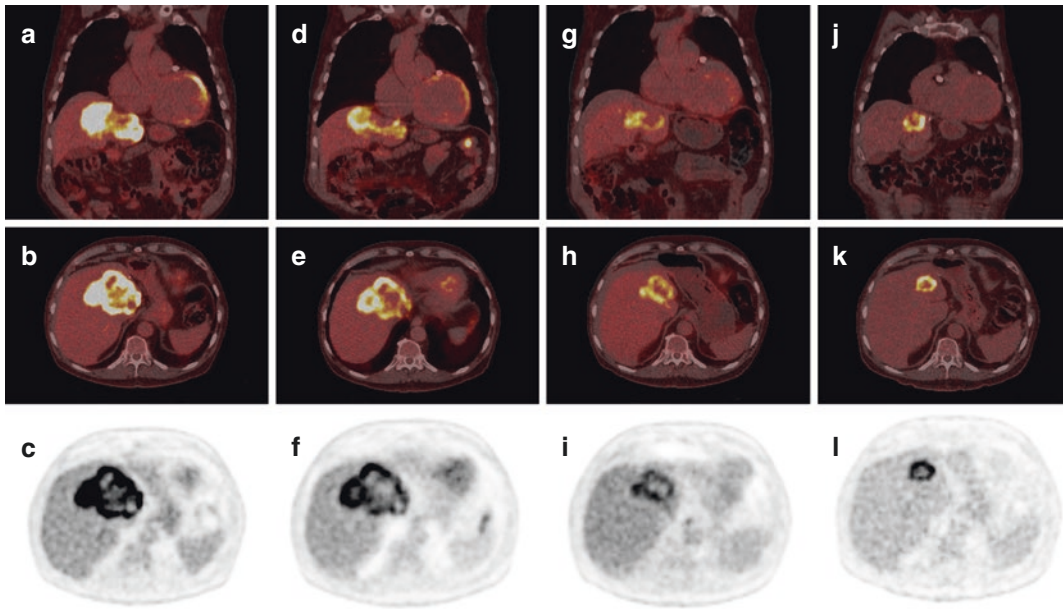

Fig. 20.7 Response monitoring of liver metastases. PET/CT (**a**, **b**, **d**, **e**, **g**, **h**, **j**, **k**) and PET (**c**, **f**, **i**, **l**) before treatment (**a–c**), 1 week into treatment (**d–f**), after three cycles (**g–i**), and after six cycles (**j–l**)

20.9 Clinical Case 8: Residual Disease After Liver Metastasectomy?

Clinical details: A 60-year-old male with rectal cancer and a solitary metachronous liver metastasis for which neoadjuvant short-course radiotherapy was administered and resection was performed. No previous systemic treatment has been given. PET/CT is performed before and 4 days after surgical metastasectomy.

Scan findings: SUV_{max} prior to resection is 7. After resection, slight diffuse uptake is seen along the edge of the resection cavity (Fig. 20.8).

Interpretation: No evidence of residual disease. Postoperative changes are appreciated at the edge of the resection cavity.

Teaching point:

1. Physiologic mild diffuse uptake along the edge of metastasectomy can be seen in the first days to weeks after metastasectomy.

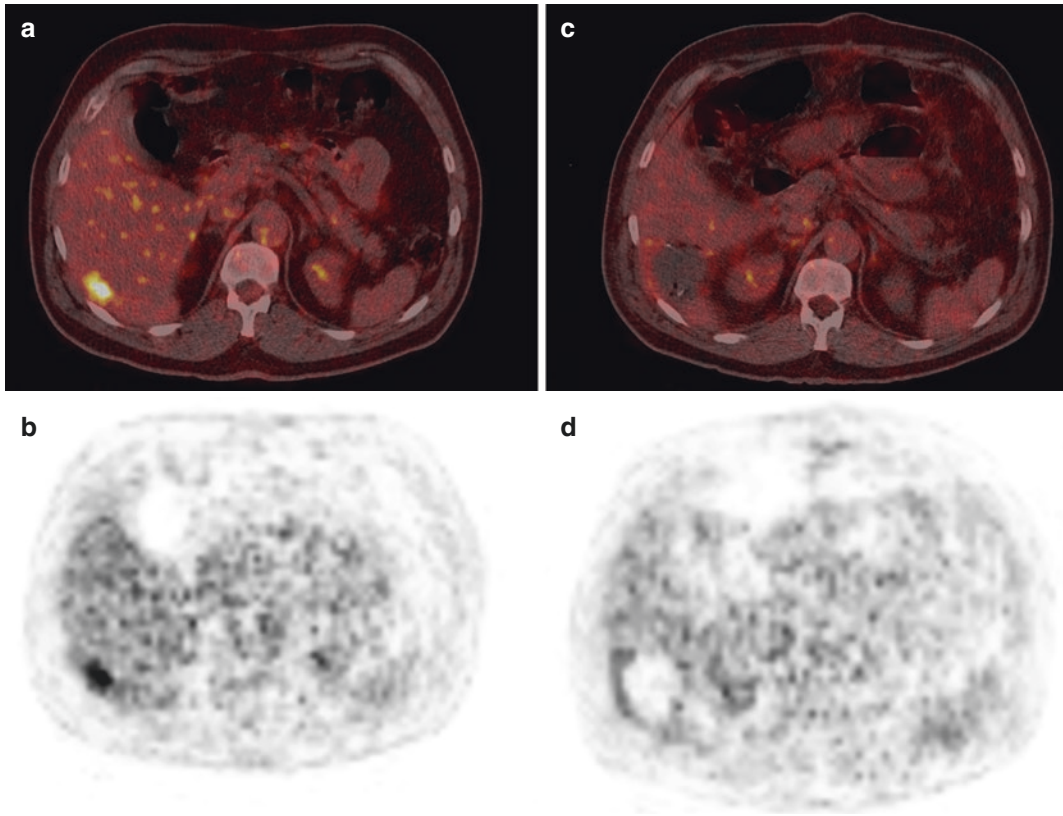

Fig. 20.8 Evaluation after liver metastasectomy. PET/CT (**a**, **c**) and PET (**b**, **d**) images before (**a**, **b**) and 4 days after metastasectomy (**c**, **d**)

20.10 Clinical Case 9: Palliative Treatment of Liver Metastases of Rectal Cancer

Clinical details: A 63-year-old male with rectal cancer in whom two synchronous liver metastases were detected. The patient was treated with palliative chemotherapy consisting of tegafur and uracil, as no curative options were available. CT imaging showed stable disease after three cycles according to RECIST.

Scan findings: Mean SUV_{max} of the two liver lesions was 8.0 before treatment, 9.0 after 1 week (+13%), and 9.4 after three cycles of treatment (+18%). Total lesion glycolysis was 34 before treatment, 46 after 1 week (+35%), and 40 (+18%) after three cycles (Fig. 20.9).

Interpretation: Stable disease on PET/CT (PERCIST).

Teaching point:

1. Fractional changes in tumor glucose metabolism on FDG PET/CT can stratify patients into groups with different survival probabilities [5].

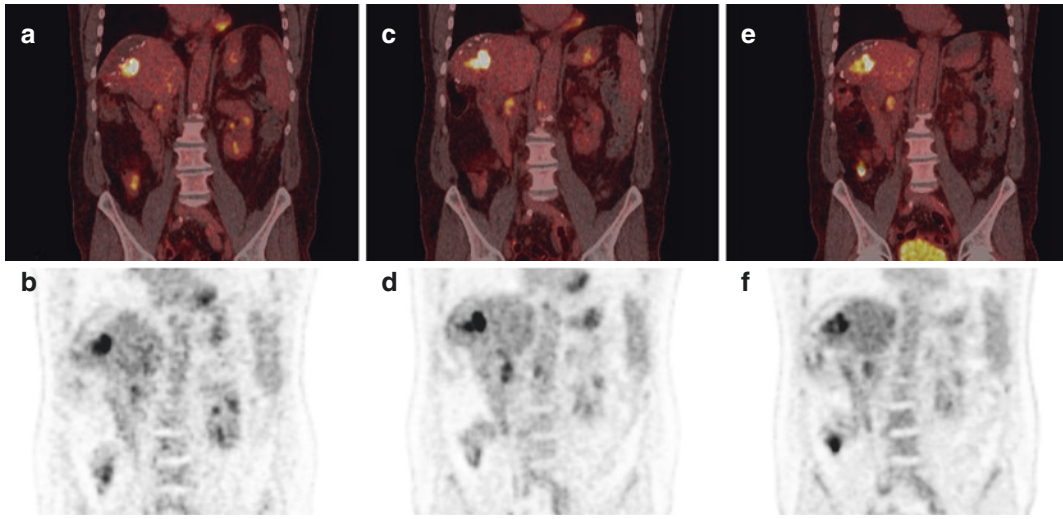

Fig. 20.9 Response monitoring palliative rectal cancer. Representative PET/CT (**a**, **c**, **e**) and PET (**b**, **d**, **f**) images before treatment (**a**, **b**), 1 week into treatment (**c**, **d**), and after three cycles of treatment are depicted (**e**, **f**)

20.11 Clinical Case 10: Recurrent Disease After Liver Microwave Ablation (MWA)

Clinical details: A 75-year-old male with a history of pT3N0M0 sigmoid cancer which was laparoscopically resected. Four years later, CEA was elevated, and a liver metastasis was detected in segment VIII on CT, which was treated with MWA (5 min, 100 W). Routine follow-up CT imaging 3 months after MWA showed no evidence of residual or recurrent disease. Five months later, CEA is again elevated and a lesion suspicious for recurrent metastasis was observed on FDG PET/CT (Fig. 20.10d). Subsequent MR imaging (1 week later) confirmed a solitary recurrent liver metastasis (Fig. 20.10c).

Scan findings: A high metabolically active focus is located mediodorsal of the MWA area, cranial in segment VIII. The focus corresponds to the hypodense lesion as seen on CT and MRI.

Interpretation: Scan findings suspicious for local recurrence of liver metastasis in segment 8 after MWA.

Teaching points:

1. FDG PET/CT is accurate in detecting residual or recurrent disease immediately after local ablative therapy [6].
2. Focal and multifocal uptake is suspicious for recurrent disease already in the first months after local therapy.

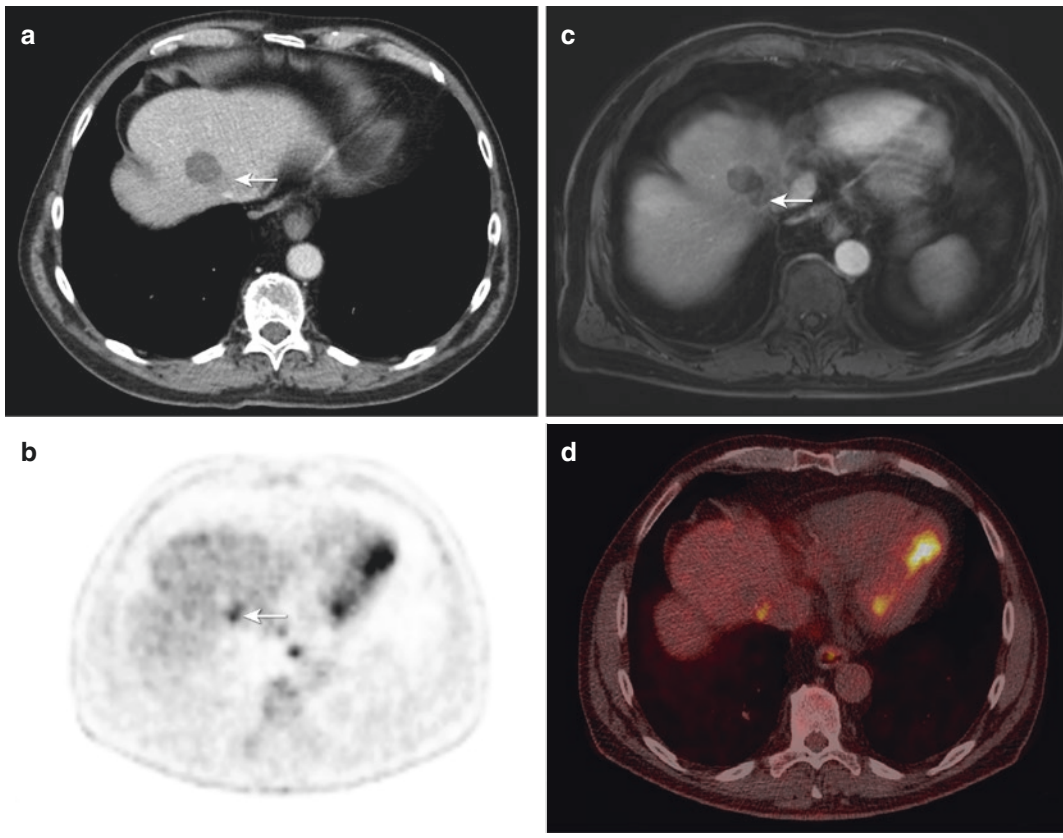

Fig. 20.10 Recurrent disease after liver MWA. Images of contrast-enhanced CT (**a**), PET (**b**), contrast-enhanced MRI (**c**), and PET/CT (**d**) are depicted

20.12 Clinical Case 11: Recurrent Disease After Liver RFA

Clinical details: A 75-year-old male with cT3N2M1 sigmoid carcinoma with multiple synchronous liver metastases in segment VII and VIII. Induction combination chemotherapy consisting of folinic acid, fluorouracil, and oxaliplatin (FOLFOX) was given. Following systemic therapy, the liver lesions decreased in size but were still present. Both the primary tumor and liver metastases were resected or ablated using radiofrequency. Eighteen months later, serum CEA was rising; however, recurrent disease could not be localized on CT of the chest and abdomen.

Scan findings: Status after sigmoid resection, segment resection of segment 8 and RFA in segment 8/5. Focal FDG avidity is seen along the medial edge of the RFA area. No evidence of other metastases (Fig. 20.11).

Interpretation: The FDG avidity in the liver lesion is suspicious for recurrent liver metastasis along the edge of the previous RFA.

Teaching points:

1. FDG PET/CT is more accurate during surveillance after RFA compared to contrast-enhanced CT and MRI [7, 8].
2. Response evaluation after RFA can be performed by FDG PET/CT, as responding lesions become photopenic immediately following RFA [9].
3. Focal and multifocal uptake is suspicious for recurrent disease following local therapy.

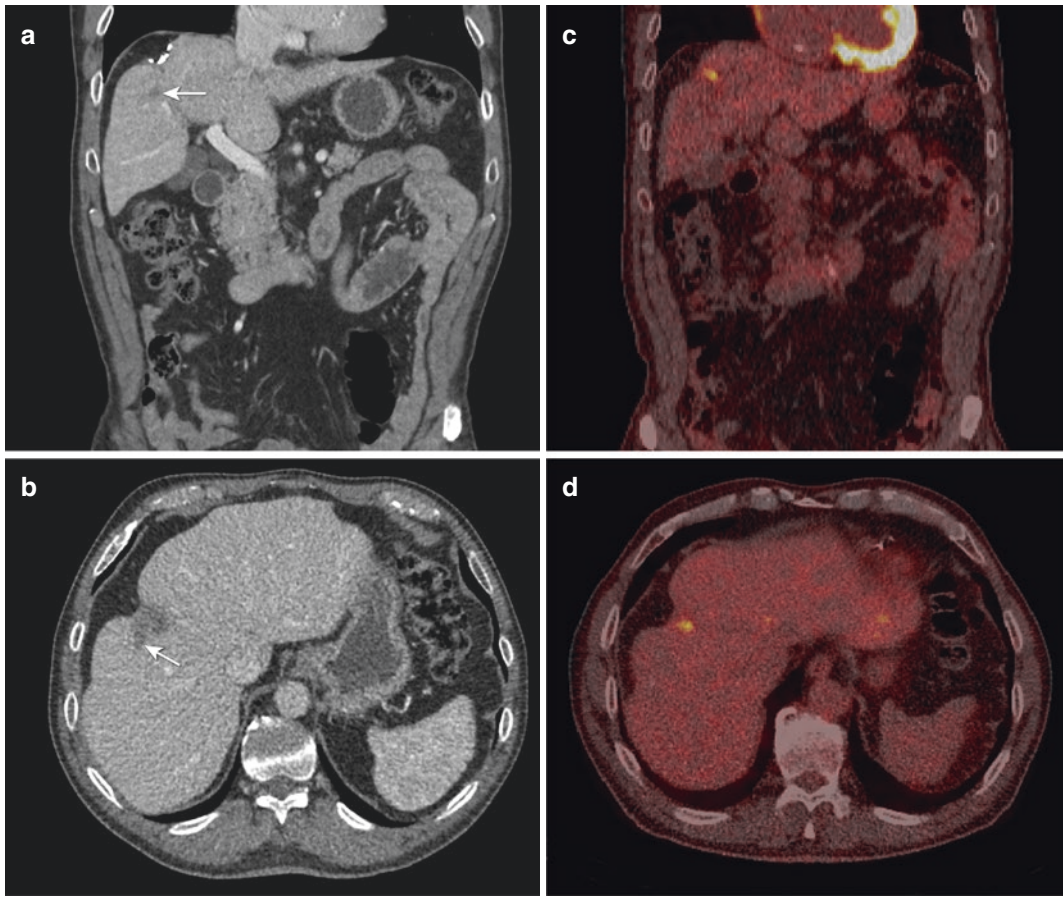

Fig. 20.11 Recurrent disease after liver RFA. Images of CT (**a**, **b**) and PET/CT (**c**, **d**)

20.13 Clinical Case 12: Recurrent Disease After Liver RFA

Clinical details: A 60-year-old male with pT1N1M1 colon carcinoma with a synchronous liver metastasis. The colon carcinoma was resected, after which the solitary liver metastasis in segment seven was ablated using radiofrequency (RFA). Eight months later, a recurrent liver lesion is seen along the ablated site in segment VII on FDG PET/CT (Fig. 20.12d). Subsequent MR imaging confirmed a solitary liver metastasis in segment VII.

Scan findings: High FDG avidity is seen cranially in segment 7/8, corresponding to the lesion as seen on MRI located dorsolateral on the right side adjacent to the RFA cavity. No other FDG accumulation is observed in the liver parenchyma.

Interpretation: FDG uptake is highly suspicious for local recurrent disease dorsolateral along the RFA region, corresponding to the lesion observed on MRI. No other metastases are detected.

Teaching points:

1. FDG PET/CT is more accurate during surveillance after RFA compared to contrast-enhanced CT or MRI [7, 8].
2. FDG PET shows promise in identifying very early response after local ablative treatment (within 24 h post-ablation) [9].
3. Focal and multifocal uptake is suspicious for recurrent disease following local therapy.

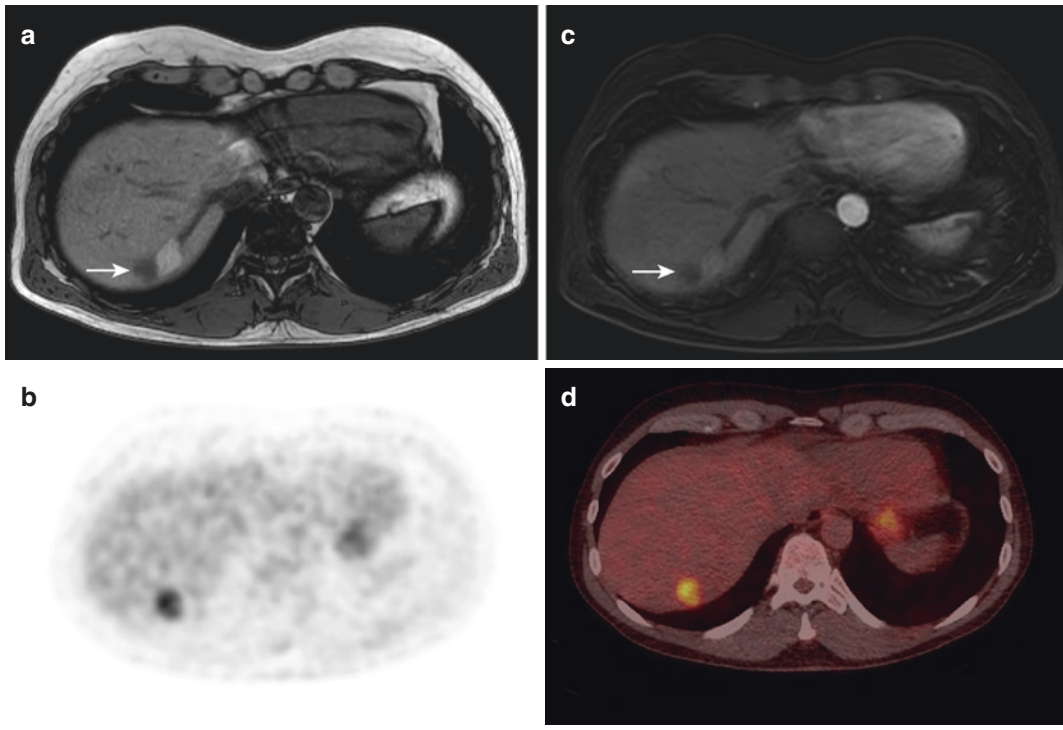

Fig. 20.12 Recurrent disease after liver RFA. Images of T1-weighted MRI before contrast (**a**), PET (**b**), contrast-enhanced MRI (**c**), and PET/CT (**d**)

20.14 Clinical Case 13: Pulmonary Metastases

Clinical details: An 80-year-old woman underwent laparoscopic sigmoid resection 7 years ago for a pT3N0M0 sigmoid carcinoma. Three years after resection, local recurrence and multiple liver and lung metastases were detected and treated in the following years. Three lung metastases were treated with stereotactic radiotherapy. Five months later, CT imaging reveals progression of the known apical consolidation after radiotherapy in the left lower lobe and progression of a lung nodule in the right upper lobe. FDG PET/CT also shows moderate uptake in the progressive area; however uptake may be due to post-radiation inflammation. Now, 18 months after stereotactic radiotherapy (STRT), another FDG PET/CT is performed.

Scan findings: Diffuse mild FDG uptake is observed in the area in the right upper lobe after STRT. However, avid FDG uptake is seen in three lung nodules 18 months after STRT. Two of these nodules are in the right upper lobe (one in and the other located dorsally from the radiation area, Fig. 20.13c, d) and one nodule in the left lower lobe.

Interpretation: Status after stereotactic radiotherapy of two pulmonary metastases. However, three new lung metastases are seen 18 months after STRT. Two in the right lung and one in the left. No evidence of other metastases or local recurrence.

Teaching points:

1. As few patients with pulmonary oligometastases from colorectal origin are eligible for local therapy, early detection is crucial.
2. The sensitivity and specificity of FDG PET/CT for detecting pulmonary metastases from colorectal cancer are respectively 57.1% and 99.1% [10]. This is mainly due to the small size and partial volume effect.
3. Although CT has higher sensitivity compared to FDG PET/CT in detecting lung nodules (90% vs. 57–76%), FDG PET/CT provides higher specificity (75–99% vs. 50%) [10, 11]. However, serial CT imaging probably provides high specificity as well, as is seen in common practice. Such approach, however, is not useful when early specific diagnosis is crucial.

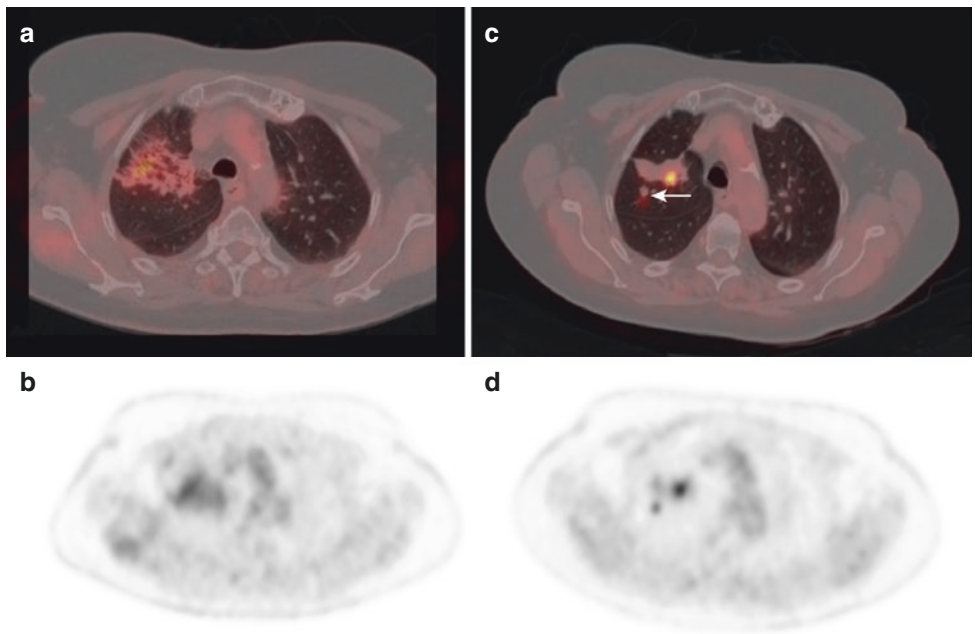

Fig. 20.13 Lung metastasis. Images of PET/CT (**a**, **c**) and PET (**b**, **d**) 11 months after STRT (**a**, **b**) compared to 18 months after STRT (**c**, **d**). Note a location mismatch between PET and CT imaging is visible in the smaller nodule, as indicated by the arrow due to differences in respiration

20.15 Clinical Case 14: Lymph Node Metastases

Clinical details: A 65-year-old woman with a history of breast cancer, to whom after resection, adjuvant chemo- and radiotherapy were given. Six years later, the patient presents with cT3N2M0 sigmoid carcinoma for which sigmoid resection was performed, followed by adjuvant chemotherapy (three cycles of capecitabine). Ten months later, two liver metastases from the sigmoid carcinoma (segment VI and VIII) were resected. In the same period, two para-aortal lymph nodes were resected. Now, 3 years after liver metastasectomy, new enlarged lymph nodes are detected. The patient is treated with three cycles of capecitabine.

Scan findings: As compared to the first scan, no significant change in size and metabolic activity of the left para aortal and mediastinal lymph node metastasis is measured. Note that the hypermetabolic mediastinal lymph node is not enlarged (Fig. 20.14).

Interpretation: Stable lymph node metastases is seen after three cycles.

Teaching points:

1. As treatment decisions depend on presence of hepatic and extrahepatic metastases, FDG PET/CT can aid in providing accurate staging, leading to more effective patient management decisions [12].
2. FDG PET/CT can alter staging for assessing extrahepatic disease in up to 20% of patients [12].
3. FDG PET/CT can identify additional metastatic lymph nodes that are missed on CT imaging [11].
4. Caution is warranted in SUV quantification of lymph nodes because of the possible partial volume effect.

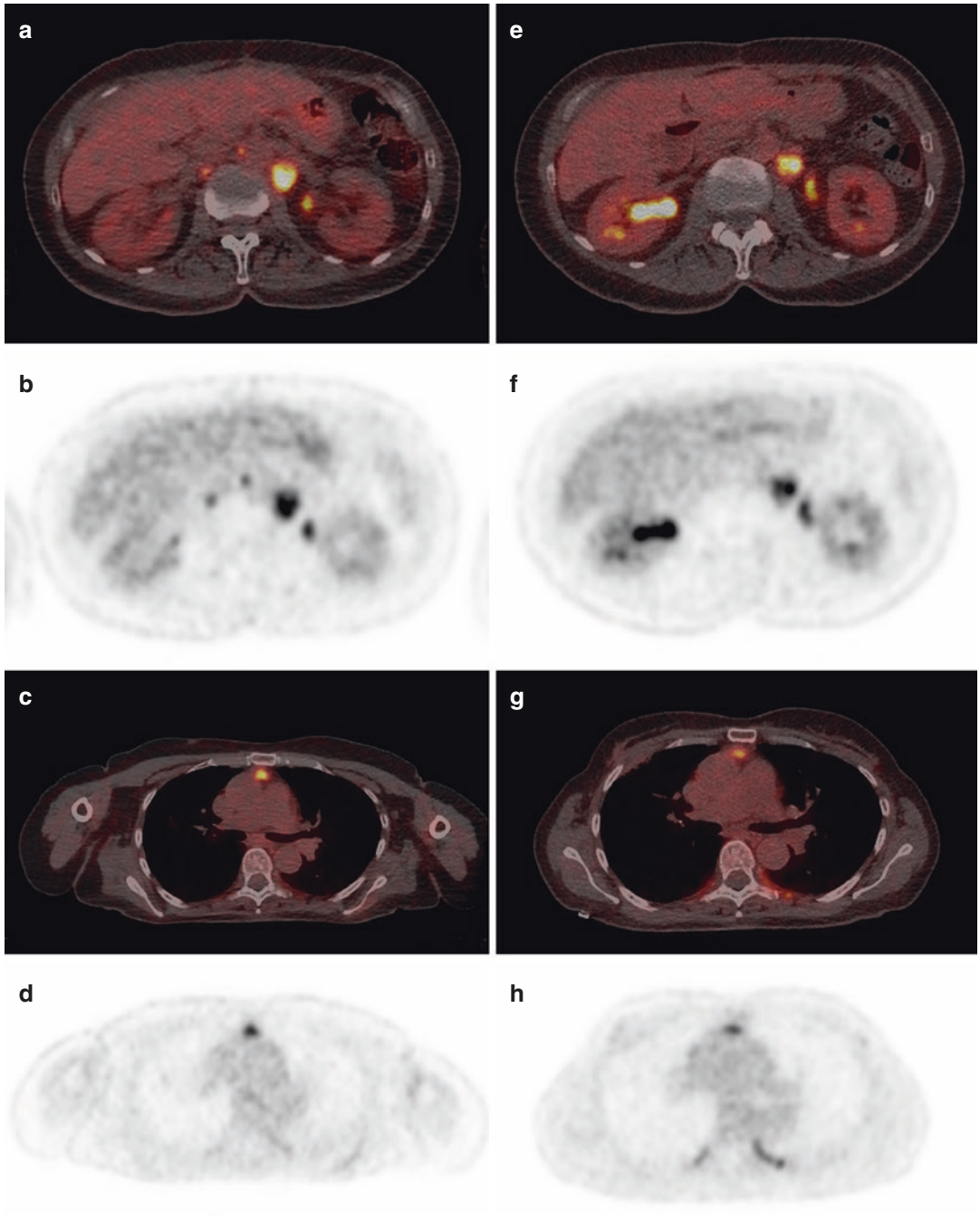

Fig. 20.14 Response monitoring lymph node and pulmonary metastases. PET/CT (**a**, **c**, **e**, **g**) and PET (**b**, **d**, **f**, **h**) images before (**a–d**) and after (**e–h**) three cycles of capecitabine

20.16 Clinical Case 15: Response Monitoring to Neoadjuvant Chemoradiotherapy

Clinical details: A 60-year-old male with cT3N2M0 locally advanced rectal carcinoma for which neoadjuvant chemoradiation (25 × 2 Gy and concurrent capecitabine) was given. After neoadjuvant therapy, abdominoperineal resection was performed. The resection specimen showed ypT1N0 rectal adenocarcinoma on pathological examination. Response monitoring was performed using FDG PET/CT.

Scan findings: FDG accumulation in the primary rectal carcinoma decreased during neoadjuvant therapy. SUV_{max} at staging was 27, decreased to 21 two weeks into treatment and to 8.5 eight weeks after neoadjuvant treatment. No enlarged or avid lymph nodes were visible (Fig. 20.15).

Interpretation: Partial response of the primary tumor.

Teaching points:

1. FDG PET/CT can predict (early) tumor response to therapy. However, thresholds derived from large clinical trials are still lacking [13].
2. In the future, by monitoring early tumor response, neoadjuvant treatment can be adjusted and/or futile chemo(radio)therapy can be avoided in nonresponding patients.

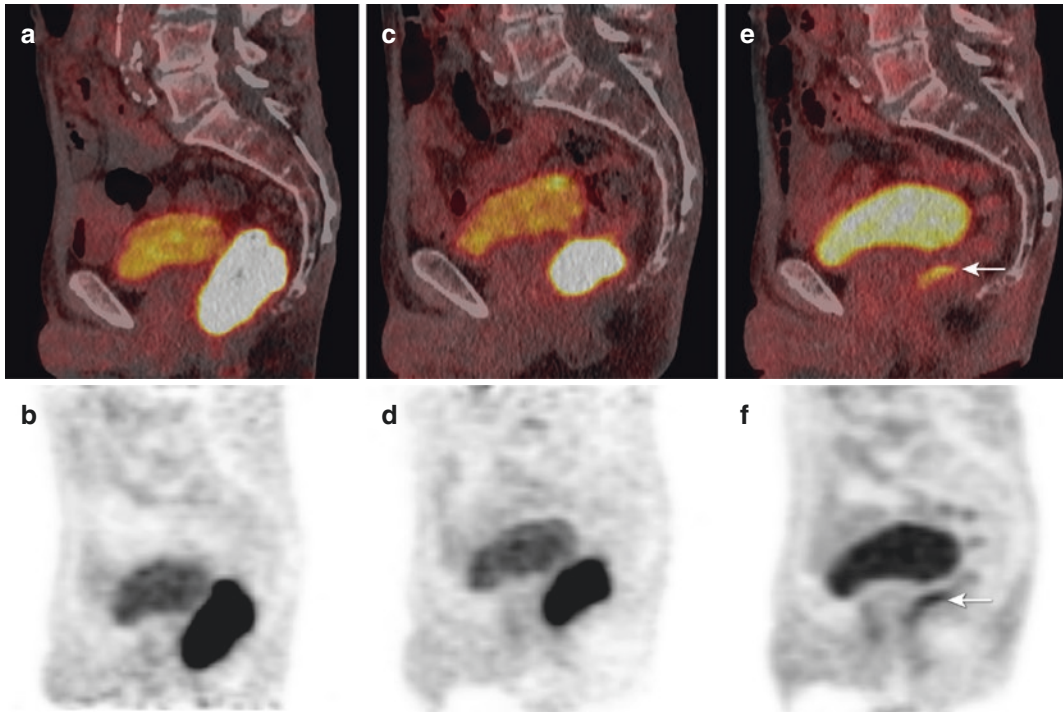

Fig. 20.15 Response monitoring locally advanced rectal cancer. Images show PET/CT (**a**, **c**, **e**) and PET (**b**, **d**, **f**) images before (**a**, **b**), 2 weeks into treatment (**c**, **d**), and 6–8 weeks after neoadjuvant treatment (**e**, **f**)

20.17 Clinical Case 16: Monitoring Response to Neoadjuvant Chemoradiotherapy

Clinical details: A 60-year-old male with cT3N2M0 locally advanced rectal carcinoma for which neoadjuvant chemoradiotherapy (25 × 2 Gy and concurrent capecitabine) was started, followed by total mesorectal excision (TME) resection. The resection specimen showed ypT3N1 rectal adenocarcinoma. Response monitoring was performed using FDG PET/CT.

Scan findings: SUV_{max} at baseline was 26, it decreased to 12 two weeks into treatment, and 8 weeks after neoadjuvant treatment SUV_{max} further decreased to five (Fig. 20.16).

Interpretation: A strong metabolic response is observed.

Teaching points:

1. FDG PET/CT can predict (early) tumor response to therapy. However, thresholds derived from large clinical trials are still lacking [13].
2. In the future, by monitoring early tumor response, neoadjuvant treatment can be adjusted and/or futile chemo(radio)therapy can be avoided in nonresponding patients.

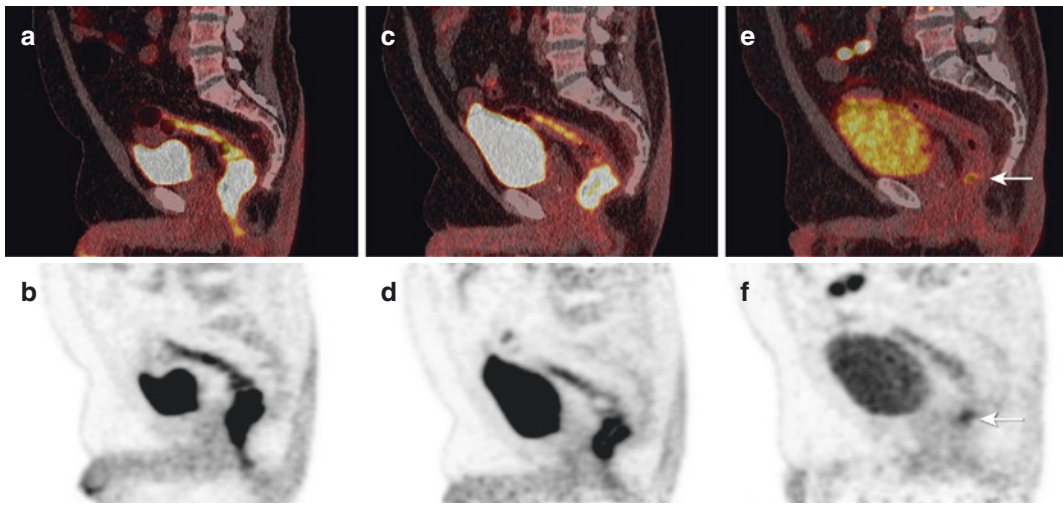

Fig. 20.16 Response monitoring rectal cancer. Images show PET/CT (**a**, **c**, **e**) and PET (**b**, **d**, **f**) images before (**a**, **b**), 2 weeks into treatment (**c**, **d**), and 6–8 weeks after neoadjuvant treatment (**e**, **f**)

20.18 Clinical Case 17: Recurrent Colorectal Cancer

Clinical details: A 60-year-old male with cT3N0M0 proximal rectal cancer for which neoadjuvant chemoradiotherapy was given, followed by TME resection. Nine months later, recurrent rectal cancer was diagnosed, and the patient was treated with one cycle CAPOX followed by re-chemoradiation (15 × 2 Gy in combination with capecitabine) and three additional cycles of CAPOX, followed by resection. Two FDG PET scans were performed: one during the first cycle of CAPOX, the second during the last cycle of CAPOX, 2 months later.

	During first cycle	During third cycle
SUV_{max}	11.6	11.2
Metabolic volume	77.3	67.8

Scan findings: No change in the intense FDG accumulation in the dorsal rectal wall above the anastomosis is seen. A large tumor strand is observed on the right side, cranially along the mesorectum (Fig. 20.17).

Interpretation: Unchanged recurrent rectal tumor in the presacral area with strand cranial along the mesorectum. No signs of lymph node metastases. Subsequently, pelvic exenteration was performed. Three months after resection, recurrent disease was diagnosed, and palliative chemotherapy was initiated.

Teaching point:

1. FDG PET/CT might aid in detecting recurrent rectal cancer patients not responding to therapy.

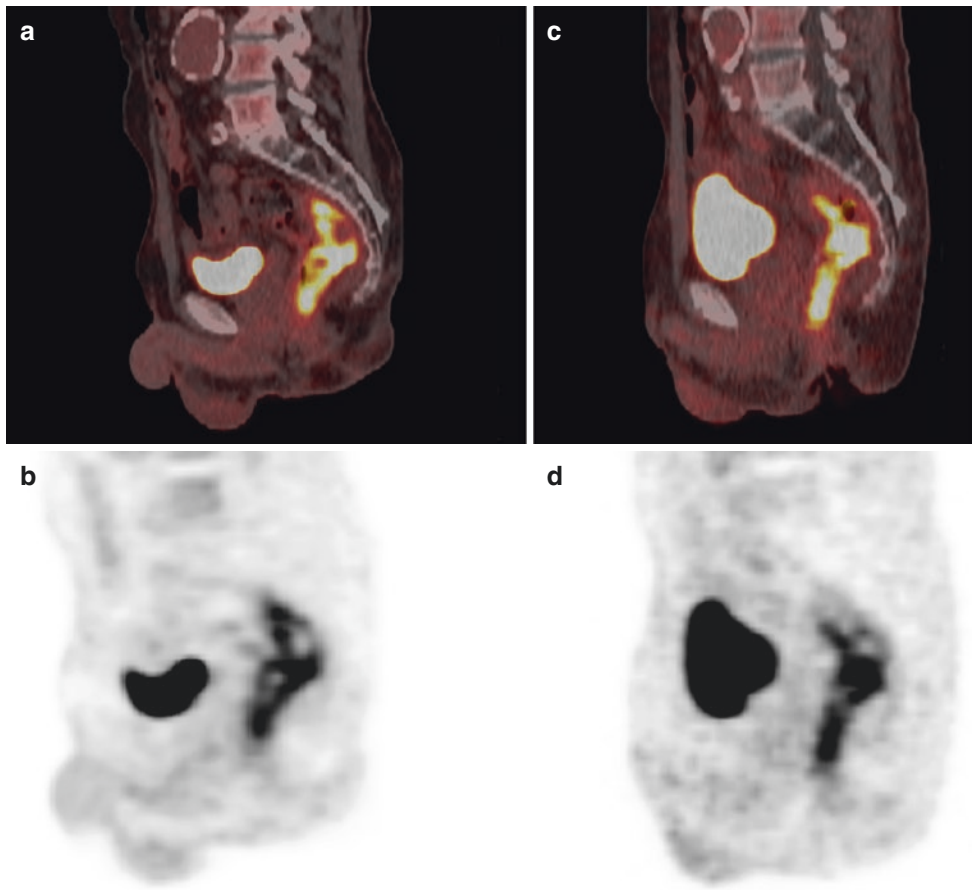

Fig. 20.17 Response monitoring recurrent rectal cancer. Representative images of PET/CT (**a**, **c**) and PET (**b**, **d**) 1 week into treatment (**a**, **b**) and during the third cycle of treatment (**c**, **d**)

20.19 Clinical Case 18: Recurrent Colorectal Cancer

Clinical details: A 65-year-old male with pT3N2M0 sigmoid tumor who underwent sigmoid resection. The patient received eight cycles of adjuvant CAPOX; oxaliplatin was terminated after the fourth cycle due to toxicity. Two months after the last cycle, serum CEA was elevated.

Scan findings: High FDG uptake is seen at the anastomosis site (Fig. 20.18e). Also, high uptake is observed in a possible peritoneal metastasis more proximal along the sigmoid (Fig. 20.18f). High uptake is appreciated in a left parailiacal lymph node (dotted white arrow, Fig. 20.18a). FDG avid foci are seen in the pararenal fascia (black arrow Fig. 20.18a) and peritoneum (white arrows Fig. 20.18a).

Interpretation: Scan findings are suspicious for recurrent disease at the anastomosis site with metastases to the peritoneum, lymph nodes, omentum, and right pararenal fascia.

Teaching points:

1. Detection of local recurrence on CT and MRI can be challenging due to altered anatomy after oncologic resection.
2. FDG PET/CT has a high sensitivity (84–100%), specificity (80–100%), and accuracy (74–94%) in detecting local recurrence of colorectal cancer [14]. Therefore, PET/CT has been adopted into colorectal guidelines for detection of local recurrence.

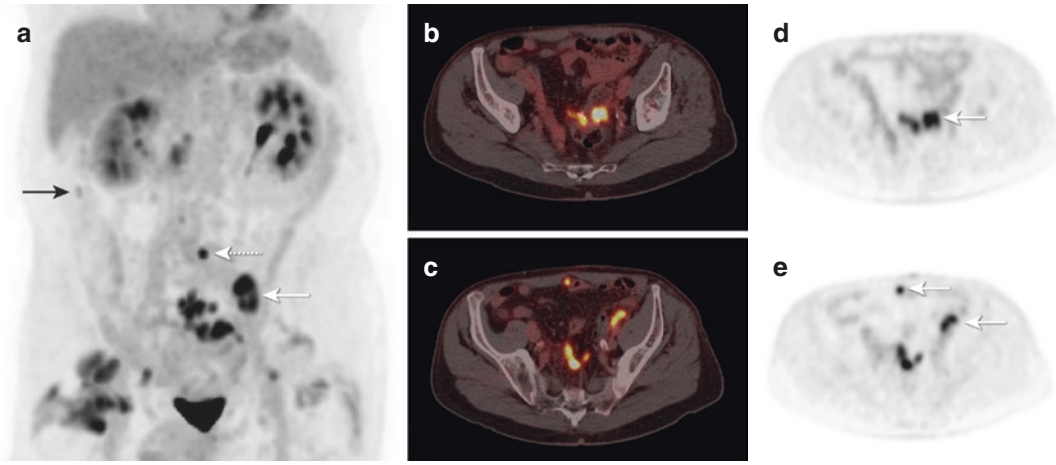

Fig. 20.18 Local recurrence sigmoid tumor. Images of the maximum intensity projection (MIP, **a**), CT (**b**), PET/CT (**c**, **d**), and PET (**e**, **f**) are depicted. The recurrent tumor is indicated by the arrow in **d**, whereas the peritoneal metastases are indicated by the arrows in **e**

20.20 Clinical Case 19: Response Monitoring of Neoadjuvant Treatment of Local Recurrent Rectal Cancer

Clinical details: A 70-year-old male with pT3N2M1 rectal carcinoma and a synchronous solitary liver metastasis. The liver metastasis was treated with three neoadjuvant courses of CAPOX, after which RFA was performed. Following this, abdominoperineal resection of the primary rectal cancer was performed. Two years after resection, local recurrent disease was detected in a lymph node and was treated with four courses of induction chemotherapy (FOLFIRI) followed by chemoradiotherapy (capecitabine in combination with 15 × 2 Gy). FDG PET/CT was performed to monitor response.

Scan findings: Partial metabolic response was visualized on the interim scan after neoadjuvant chemotherapy (2 months later). A complete metabolic response was observed right after neoadjuvant chemoradiotherapy (5 months later) (Fig. 20.19).

Interpretation: A complete metabolic response is seen on the last scan, as was confirmed by the resection specimen showing a pathological complete response. Following neoadjuvant treatment, debulking surgery and intraoperative radiotherapy were performed. The resection specimen showed a pathological complete response to neoadjuvant therapy.

Teaching point:

1. FDG PET/CT can provide additional information on the decision to give consolidation therapy between neoadjuvant therapy and surgery.

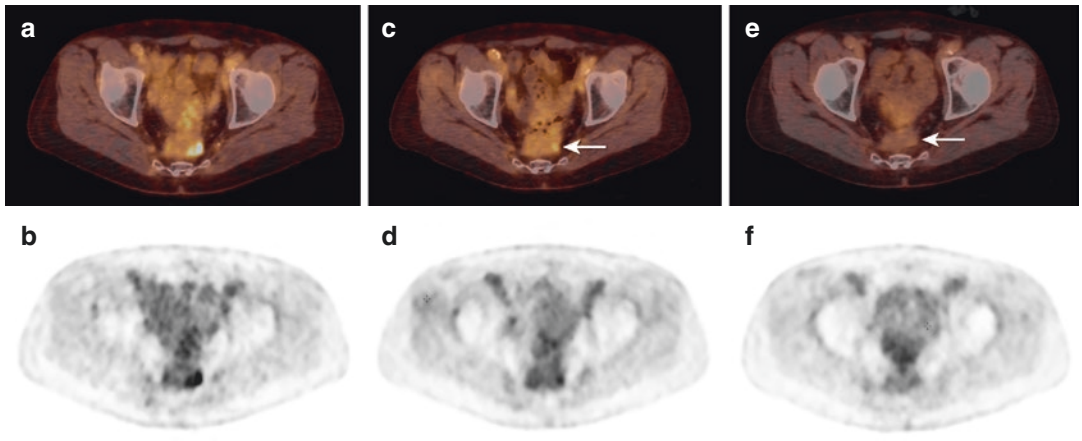

Fig. 20.19 Response monitoring neoadjuvant treatment local recurrence. Representative PET/CT and PET images before treatment (**a**, **b**), after neoadjuvant chemotherapy (**c**, **d**), and after neoadjuvant chemoradiation (**e**, **f**) are depicted

20.21 Clinical Case 20: Response Monitoring of Neoadjuvant Treatment of Local Recurrent Rectal Cancer

Clinical details: A 60-year-old male with locally advanced rectal carcinoma was treated with neoadjuvant chemoradiotherapy, followed by TME resection. Eighteen months later, local recurrent disease was detected and treated with induction chemotherapy (one course CAPOX, then switched to three courses FOLFIRI due to toxicity) followed by chemoradiotherapy (capecitabine in combination with 15 × 2 Gy). Response monitoring was performed by FDG PET/CT.

Scan findings: No changes in FDG avidity is observed after neoadjuvant chemotherapy or after neoadjuvant chemoradiotherapy (Fig. 20.20).

Interpretation: Stable disease was observed after neoadjuvant chemotherapy (2 months later) and immediately after neoadjuvant chemoradiotherapy (4 months later). Following treatment, surgical resection was planned.

Teaching point:

1. FDG PET/CT can provide additional information on the decision to give consolidation therapy between neoadjuvant therapy and surgery.

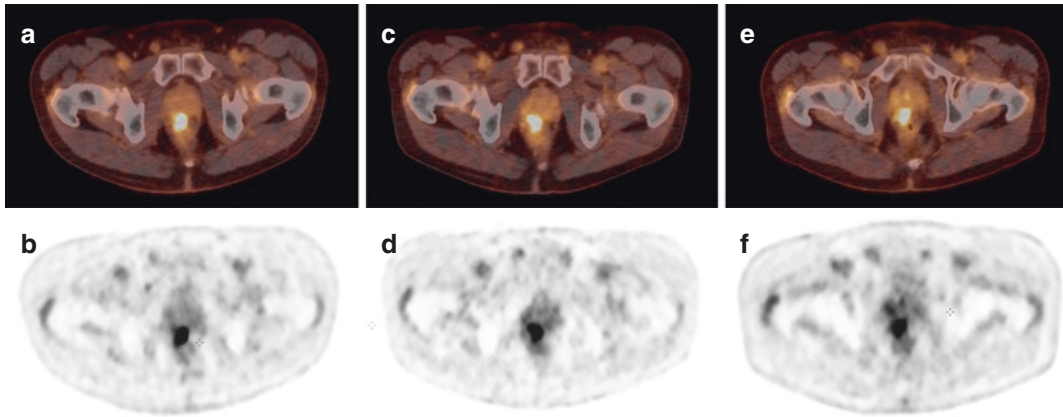

Fig. 20.20 Response monitoring neoadjuvant treatment local recurrence. Representative PET/CT and PET images before treatment (**a**, **b**), after neoadjuvant chemotherapy (**c**, **d**), and after neoadjuvant chemoradiation (**e**, **f**) are depicted

References

1. Bray F, et al. Global cancer statistics 2018: GLOBOCAN estimates of incidence and mortality worldwide for 36 cancers in 185 countries. CA Cancer J Clin. 2018;68:394–424.
2. Sivesgaard K, et al. Diagnostic accuracy of CE-CT, MRI and FDG PET/CT for detecting colorectal cancer liver metastases in patients considered eligible for hepatic resection and/or local ablation. Eur Radiol. 2018;28:4735–47.
3. Grassetto G, et al. Additional value of FDG-PET/CT in management of 'solitary' liver metastases: preliminary results of a prospective multicenter study. Mol Imaging Biol. 2010;12:139–44.
4. Heijmen L, et al. Multimodality imaging to predict response to systemic treatment in patients with advanced colorectal cancer. PLoS One. 2015;10:e0120823.
5. de Geus-Oei LF, et al. Chemotherapy response evaluation with FDG–PET in patients with colorectal cancer. Ann Oncol. 2008;19:348–52.
6. Romanato J, et al. 18F-FDG PET/CT performed immediately after percutaneous ablation to evaluate outcomes of the procedure: preliminary results. Radiol Bras. 2019;52:24–32.
7. Veit P, et al. Detection of residual tumor after radiofrequency ablation of liver metastasis with dual-modality PET/CT: initial results. Eur Radiol. 2006;16:80–7.
8. Aarntzen EHJG, Heijmen L, Oyen WJG. 18F-FDG PET/CT in local ablative therapies: a systematic review. J Nucl Med. 2018;59:551–6.
9. Liu Z-Y, Chang Z-H, Lu Z-M, Guo Q-Y. Early PET/CT after radiofrequency ablation in colorectal cancer liver metastases: is it useful? Chin Med J (Engl). 2010;123:1690–4.
10. Bamba Y, Itabashi M, Kameoka S. Value of PET/CT imaging for diagnosing pulmonary metastasis of colorectal cancer. Hepatogastroenterology. 2011;58:1972–4.
11. Lopez-Lopez V, et al. Role of 18F-FDG PET/CT vs CT-scan in patients with pulmonary metastases previously operated on for colorectal liver metastases. Br J Radiol. 2017;91:20170216.
12. Lake E, et al. The influence of FDG PET-CT on the detection of extrahepatic disease in patients being considered for resection of colorectal liver metastasis. Ann R Coll Surg Engl. 2014;96:211–5.
13. Maffione AM, Marzola MC, Capirci C, Colletti PM, Rubello D. Value of (18)F-FDG PET for predicting response to neoadjuvant therapy in rectal cancer: systematic review and meta-analysis. AJR Am J Roentgenol. 2015;204:1261–8.
14. de Geus-Oei L-F, Vriens D, van Laarhoven HWM, van der Graaf WTA, Oyen WJG. Monitoring and predicting response to therapy with 18F-FDG PET in colorectal cancer: a systematic review. J Nucl Med. 2009;50(Suppl 1):43S–54S.

18F-FDG PET in Treatment Response Evaluation: Soft Tissue Sarcomas

21

Emanuela Palmerini, Andrea Paccagnella, and Stefano Fanti

21.1 Introduction

Soft tissue sarcomas are of mesenchymal origin, and they account for less than one percent of adult cancers [1, 2]. 18F-FDG PET/CT is reported to be a useful imaging tool in the evaluation of patients with soft tissue sarcomas, especially in patients with high-grade lesions [3]. In general, sarcomas are highly 18F-FDG-avid tumors [4]. 18F-FDG PET/CT imaging has been used for the guiding site of biopsy, assessment of treatment response, staging, surveillance etc. [5–10]. 18F-FDG PET/CT is reported to have higher specificity compared with other conventional imaging such as CT and MRI in the detection of local disease recurrence [11, 12]. Traditional imaging modalities have limited accuracy for routine surveillance secondary to post-therapy changes such as fibrosis and scarring [12]. There are several advantages and limitations of using 18F-FDG PET/CT in assessing treatment response.

E. Palmerini (✉)
IRCCS Istituto Ortopedico Rizzoli, Bologna, Italy
e-mail: emanuela.palmerini3@unibo.it

A. Paccagnella · S. Fanti
Nuclear Medicine, Sant'Orsola Hospital, Bologna, Italy

S. Fanti et al. (eds.), *Atlas of Clinical PET-CT in Treatment Response Evaluation in Oncology*,
https://doi.org/10.1007/978-3-030-68858-5_21

21.2 Case 1: Progression

Clinical Details A 59-year-old patient was diagnosed with Grade 2 myxofibrosarcoma of the upper right arm. Preoperative RT on primary lesion was performed and later underwent excision surgery. The patient had adjuvant chemotherapy with epirubicin and ifosfamide. A CT scan detected a new nodular lesion in the inferior left lobe during follow-up, and it was resected histology confirmed metastasis from myxofibrosarcoma. Post-metastasectomy chemotherapy was given; however, the patient developed a new lung metastasis in the inferior left lobe.

Scan Findings and Interpretation An FDG PET as a re-staging tool was performed (Fig. 21.1). The scan showed mild uptake of the tracer in the left lung nodule and the presence of a doubtful uptake in the left lower leg. The patient underwent left leg lesion excision followed by further chemotherapy, and the histology was Schwannoma.

The follow-up PET/CT showed the presence of a peri-splenic nodule with low tracer uptake (SUVmax = 2.5) and a hypermetabolic solid tissue (SUVmax = 4.3) at the left thoracic wall, posterior to the VII left rib. There was low uptake of the radiopharmaceutical (SUVmax = 2.7) at the level of the left lower leg (recent surgery?)

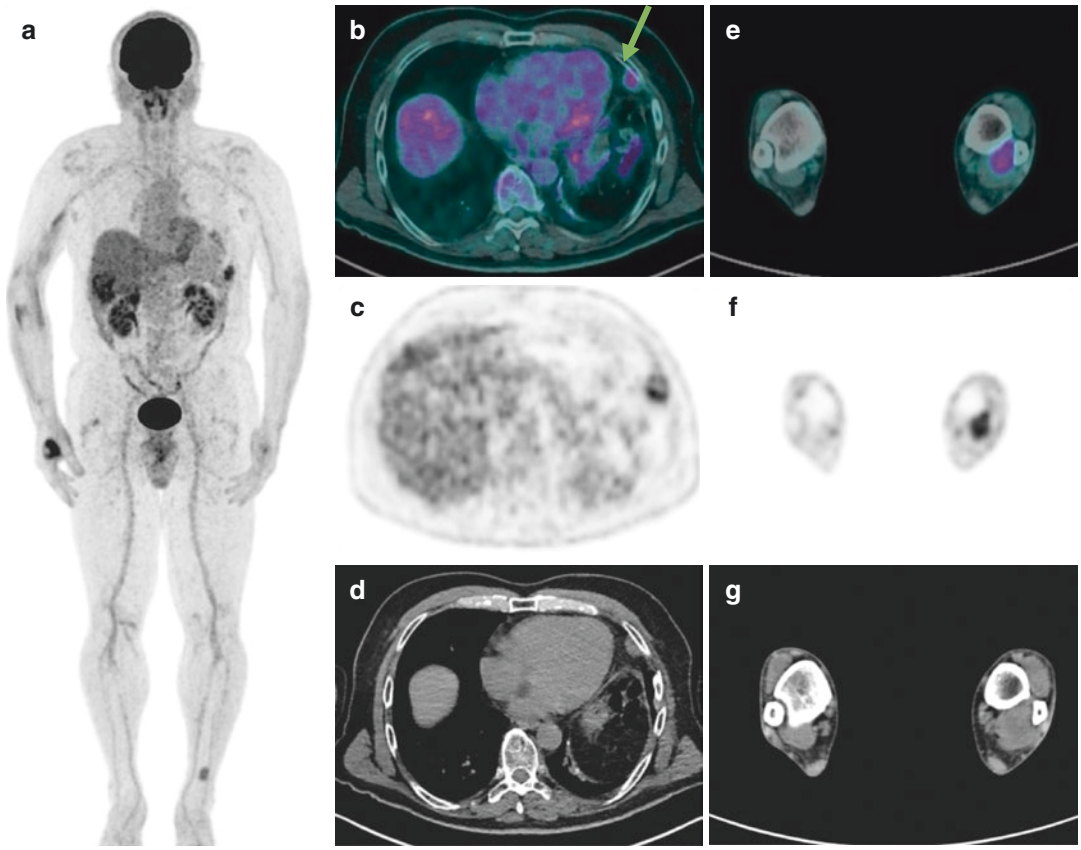

Fig. 21.1 (**a**) Re-staging PET/CT, following myxofibrosarcoma 2° lung relapse: There is mild uptake of the radiopharmaceutical in a left lower lung nodule (**b**–**d**) and presence of a doubtful tracer uptake in the left lower leg distally (**e**–**g**)

(Fig. 21.2). CT to assess treatment response showed a reduction in the size of both peri-splenic and thoracic (posterior to VII left rib) lesions (RECIST 1.1 partial response).

Repeat FDG PET showed low-grade persistent uptake in both the peri-splenic (SUVmax = 2.7) and the left thoracic wall lesions (SUVmax = 2.9); persistence of low uptake of the radiotracer at the level of the left lower leg (SUVmax = 3.1 vs. 2.7) (Fig. 21.3). The patient underwent stereotaxic radiotherapy for the thoracic and para-splenic lesions. The latest CT scan with contrast media showed the pleural nodule progression, with a relapse-free interval of 7 months.

Teaching Points

Myxofibrosarcoma is one of the most common sarcomas in elderly adults, characterized by "infiltrative pattern" (so-called tail sign in MRI), and it arises in the extremities in most cases [13]. Myxofibrosarcomas were reclassified in the 2013 WHO classification and are defined as gelatinous nodules with a noncohesive spindle or stellar tumor cells within a myxoid matrix [14]. The myxoid part of the tumor usually represents at least 50% of the total surface [14], and no specific molecular alteration was demonstrated for this histotype. No metabolic studies in these specific entities were conducted, but hypermetabolic myxofibrosarcoma was described [15].

- Myxofibrosarcoma histologic diagnosis is evolving and challenging.
- No prospective data are available on the metabolic activity in these lesions.
- PET/CT scans are not routinely performed in this subtype.

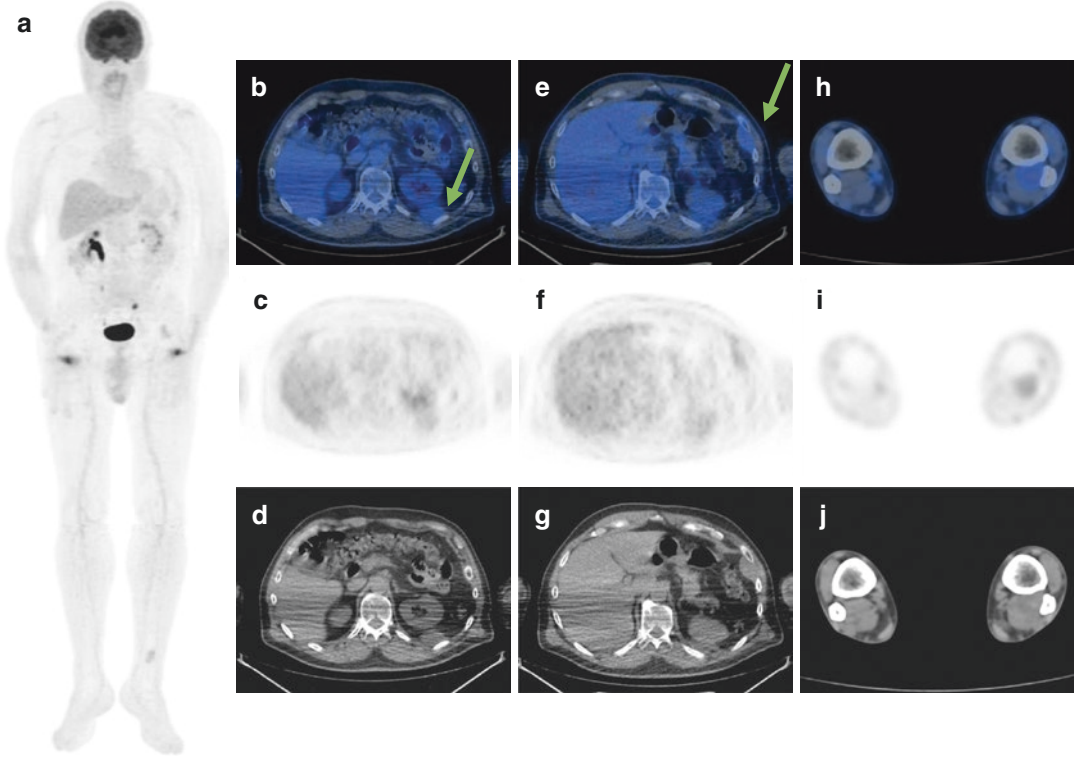

Fig. 21.2 (**a**) PET/CT after second left lung metastasectomy: The peri-splenic nodule shows low-grade tracer uptake (SUVmax = 2.5, with SUVmean liver = 2.3; **b**–**d**) and a new hypermetabolic solid tissue of the thoracic left wall, posterior to the VII left rib (SUVmax = 4.3; **e**–**g**); low-grade uptake of the tracer (SUVmax = 2.7; **h**–**j**) at the level of the left lower leg (recent surgery?)

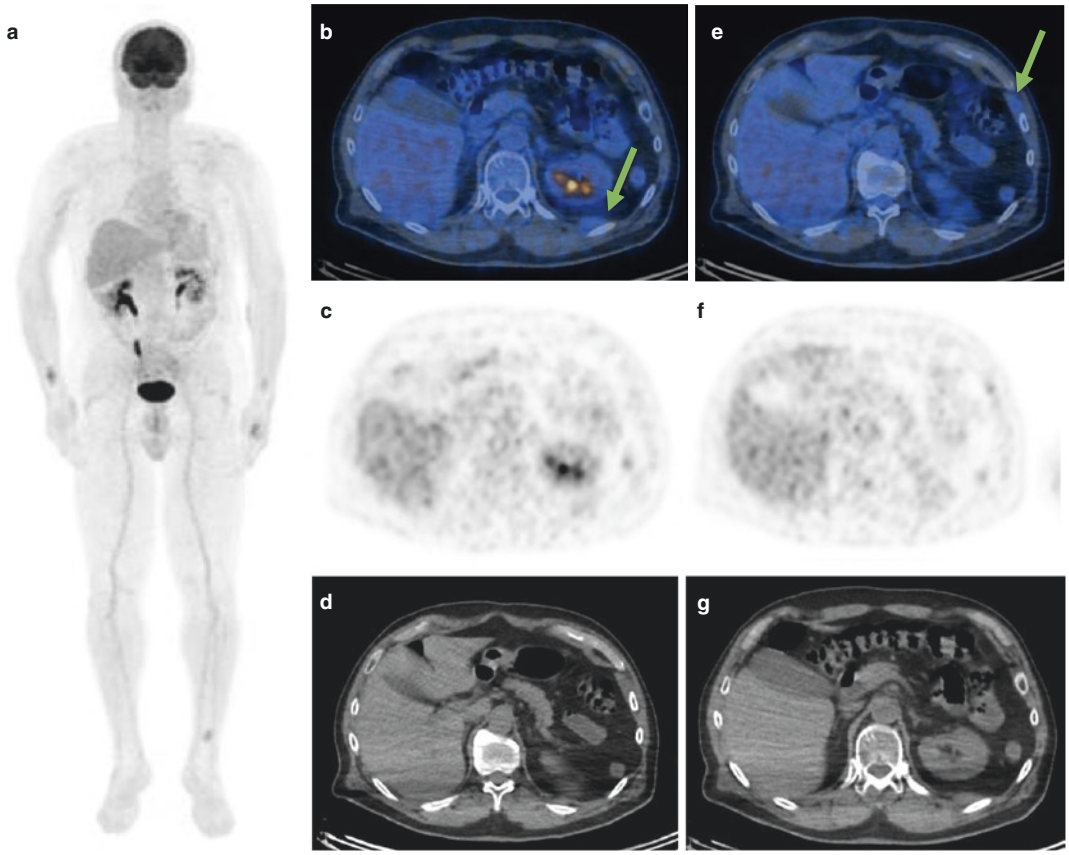

Fig. 21.3 (**a**) Re-staging PET/CT after chemotherapy: There is persistence of very low uptake of both the perisplenic (SUVmax = 2.7; SUVmean liver=3 vs. 2.3) (**b**–**d**) and the left thoracic wall lesions (SUVmax = 2.9; **e**–**g**); persistence low-grade uptake of the tracer (SUVmax = 3.1 vs. 2.7) at the level of left lower leg

21.3 Case 2: Good Response to Treatment

Clinical Details Patient with highly malignant myxoid round cell liposarcoma (MRCL) of the left leg and the lesion was measuring 9 cm in the largest diameter. Staging procedures (chest and abdomen CT scan with contrast medium) were negative for distant secondary locations.

Scan Findings and Interpretation Figure 21.4: PET with FDG showed low-grade tracer uptake (SUVmax = 2.8) of the left leg tumor. The patient had neoadjuvant chemotherapy treatment with Epirubicin and Ifosfamide and later neoadjuvant RT. Figure 21.5: The re-staging FDG PET showed reduced size and uptake in the lower left leg lesion (SUVmax = 2.2). An MRI scan demonstrated size reduction (from 9 to 6 cm) and the adipocytic component's disappearance, with an isointense signal. He underwent excision surgery: margins were wide, and only posttreatment necrosis was seen with no hypercellular component left. A follow-up scan was unremarkable.

Teaching Points

Despite optimum local treatment, about 50% of patients with localized adult-type soft tissue

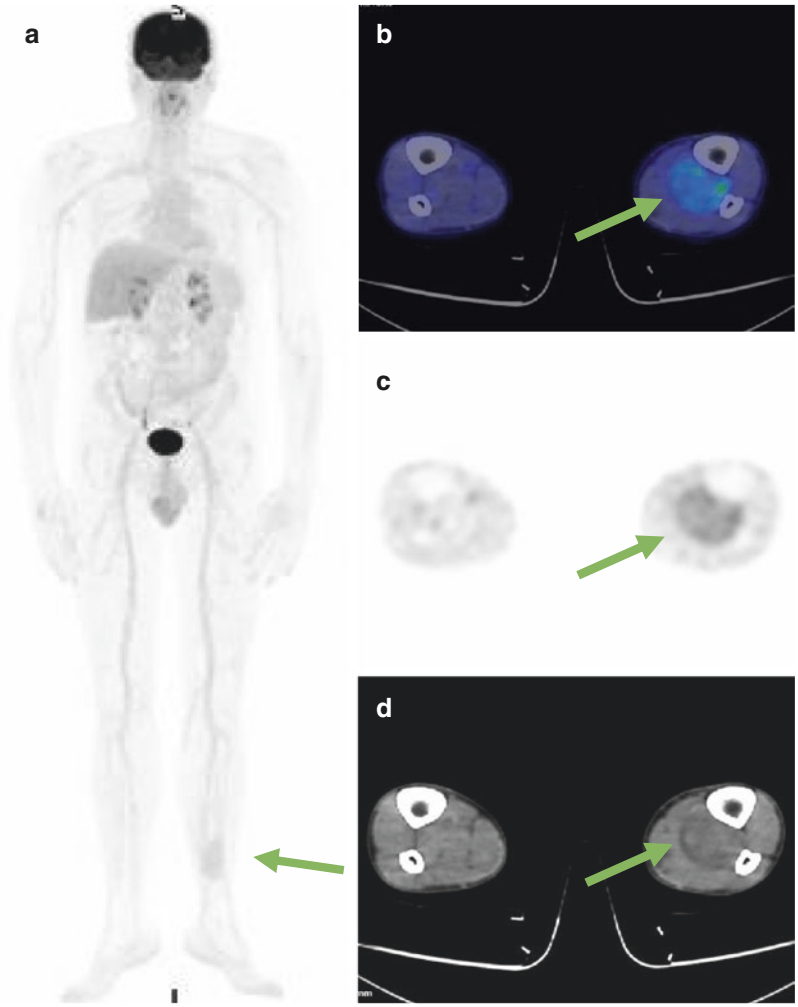

Fig. 21.4 Staging FDG PET/CT: There is low-grade tracer uptake (SUVmax = 2.8) in the right leg tumor (**a**–**d**)

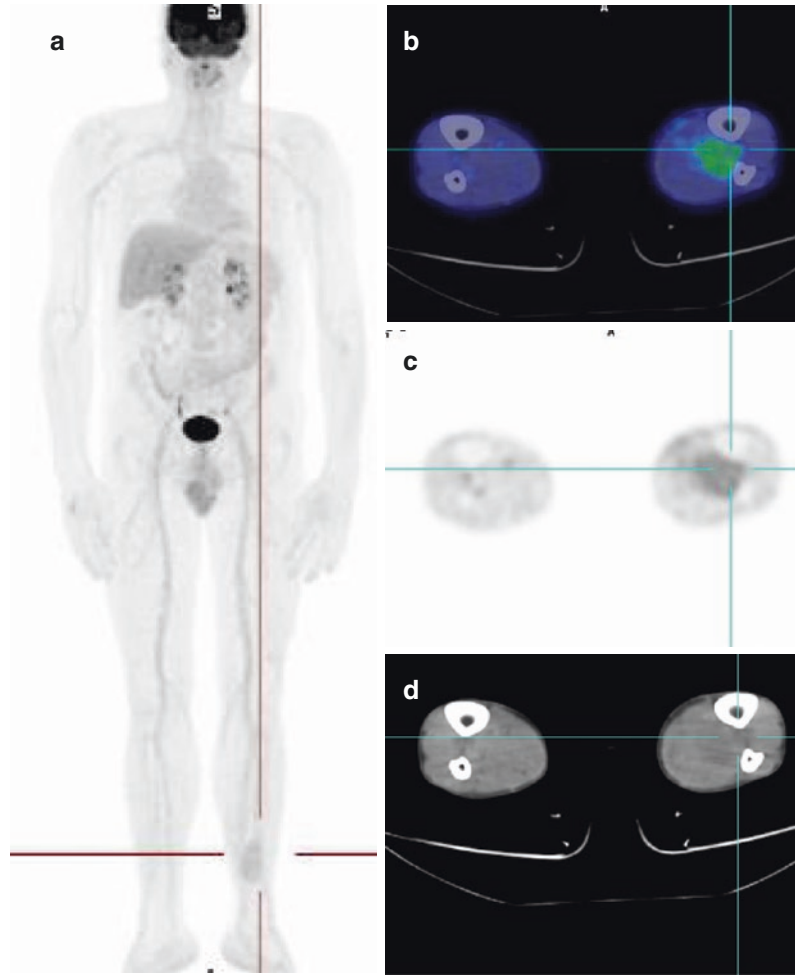

Fig. 21.5 Re-staging 18F-FDG PET/CT after neoadjuvant chwemotherapy and radiotherapy shows reduced size and minimally reduced uptake in the left lower leg lesion (SUVmax = 2.2); no other abnormal findings (**a**–**d**)

sarcoma of the extremities and trunk will develop distant metastases and die of metastatic disease [16]. For this reason, sarcoma guidelines [17] recommend a patient-doctor shared decision on adjuvant chemotherapy in high-grade, deep, >5 cm, limbs sarcoma. The round cells represent the high-grade counterpart of myxoid liposarcoma (MLPS), lying on the poorly differentiated end of the spectrum, with a predominance of round cells. There is evidence of a common translocation abnormality, t(12;16) (q13;p11). MRCL is sensitive to both radiotherapy and chemotherapy. The most active drugs in this entity include antracyclins, trabectedin, eribulin and gemcitabine and taxotere [17]. Epirubicin and ifosfamide combination, and trabectedin, are also proposed in the neoadjuvant setting [16]. Low uptake at FDG PET was demonstrated in this case, as reported in the literature [18].

- Neoadjuvant chemotherapy and radiotherapy might be useful in MRCL.
- No additional information on response to treatments is derived by the use of FDG PET compared to standard morphological imaging (MRI with CM).

21.4 Case 3: Disease Progression

Clinical Details Patient with clear cell sarcoma of the left foot, with soft tissue and lymph node metastases.

Scan Findings and Interpretation Staging FDG PET/CT scan (Fig. 21.6) showed intense glucose uptake in the left foot (SUVmax=15), presence of left popliteal (SUVmax = 14), and inguinal hypermetabolic lymph nodes (SUV = 8). Preoperative radiotherapy was delivered on the foot, and surgical excision of the primary lesion and inguinal and popliteal lymphadenectomy was performed. A re-staging FDG PET/CT (Fig. 21.7) showed hypermetabolic nodule of the plantar lateral area of the right foot (SUVmax = 6.9) (contralateral to the primary tumor) and an area of focal uptake in the right anterior tibial muscle, multiple bilateral hypermetabolic pulmonary nodules which were more evident on the left side (SUVmax = 4.6). Comibination of sunitinib and nivolumab has shown sme activity in clear cell sarcoma [20]. Due to delayed wound healing nivolumab monotherapy was was started at this point. Follow-up FDG PET (Fig. 21.8) showed metabolic uptake stability, with the persistence of hypermetabolic nodule of the plantar lateral area of the right foot (SUVmax = 4.8 vs. 6.9) and an area of focal uptake in the right anterior tibial muscle. In the lungs, PET showed persistence of multiple bilateral hypermetabolic pulmonary nodules, with a minimum increase in metabolic gradient (SUVmax = 5.5 vs. 4.6). Sunitinib was then added to nivolumab. FDG PET/CT (Fig. 21.9) showed progressive disease (new hypermetabolic left popliteal lymph node (SUVmax = 12)) and increased metabolic activity in the lung nodule in the left lung (SUVmax = 8.5 vs. 3.6) and within ipsilateral pulmonary hilum

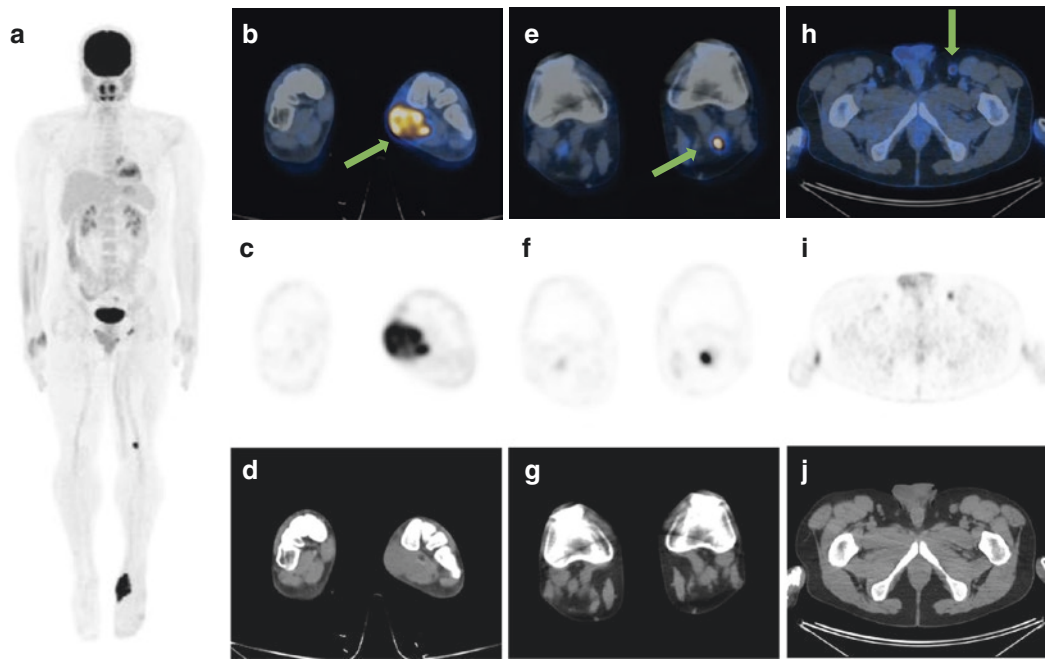

Fig. 21.6 (**a**) Staging FDG PET/CT scan: Mass characterized by abnormal increased uptake at the left foot (SUVmax = 15; **b**–**d**) and within popliteal (SUVmax = 14; **e**–**g**) and inguinal (SUVmax = 8; **h**–**j**) hypermetabolic adenopathy

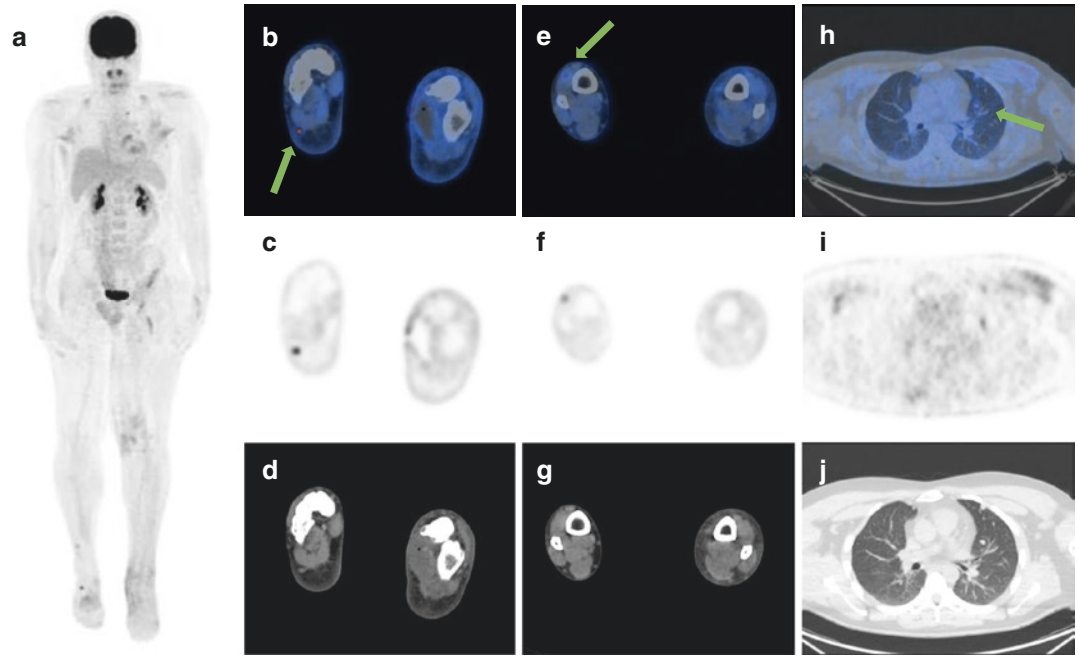

Fig. 21.7 Maximum intensity projection (MIP) (**a**) FDG PET/CT scan after radiotherapy and surgery: Hypermetabolic nodule of the plantar lateral area of the right foot (SUVmax = 6.9; **b**–**d**) and in the right anterior tibial muscle (**e**–**g**); multiple bilateral hypermetabolic pulmonary nodules, more evident on the left side (SUVmax = 4.6; **h**–**j**)

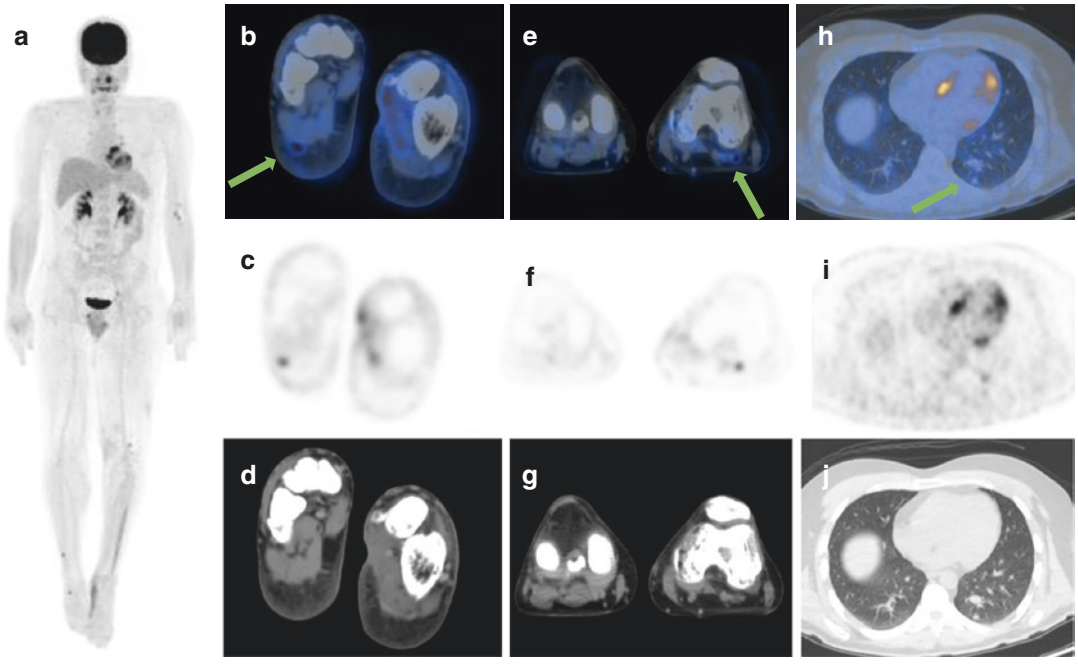

Fig. 21.8 Maximum intensity projection (MIP) (**a**) FDG PET/CT scan after nivolumab shows persistence of hypermetabolic nodule of the plantar lateral area of the right foot (SUVmax = 4.8 vs. 6.9; **b**–**d**) and in the right anterior tibial muscle. There is persistent multiple bilateral hypermetabolic pulmonary nodules, with increased metabolic activity (SUVmax = 5.5 vs. 4.6 at the inferior left lobe; **h**–**j**) and a new left lung nodule. New popliteal (**e**–**g**) and left external-iliac hypermetabolic lymph nodes (reactive? disease?)

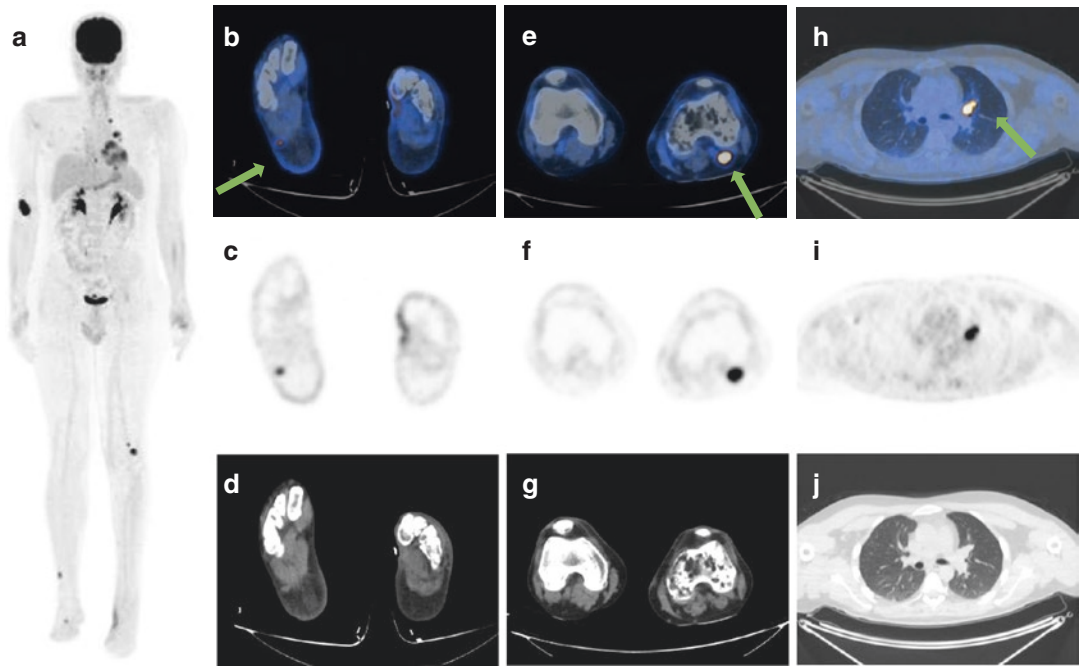

Fig. 21.9 Maximum intensity projection (MIP) (**a**) FDG PET/CT scan after sunitinib and nivolumab: There is a new hypermetabolic left popliteal lymph node (SUVmax = 12.1; **e**–**g**), and increased uptake within lung nodule in the left lung (SUVmax=8.5 vs. 3.6) and in the ipsilateral pulmonary hilar (SUVmax=10.5 vs. 4.5; **h**–**j**). The known hypermetabolic bilateral pulmonary nodules and lesion in the right foot (**b**–**d**) and in distal part of the right leg were stable

(SUVmax = 10.5 vs. 4.5). The known hypermetabolic bilateral pulmonary nodules and the uptake in the right foot and distal part of the right leg were stable. As discussed at a multidisciplinary meeting, stereotactic radiotherapy was planned (only progressing nodules), continuing the combination of sunitinib and nivolumab.

Teaching Points

Clear cell sarcoma is a rare translocation-related sarcoma. Surgery is the gold standard treatment for both primary and metastatic lesions. Conventional chemotherapy has minimal activity documented by the response rate (RR) of 4% and median progression-free survival of 11 weeks in a retrospective series [19]. Recent soft tissue sarcoma studies showed a RR of up to 50% in pretreated patients. The present case demonstrates that PET/CT could detect all metastases sites and is a vital tool to assess treatment response in patients with multiple-site metastases, including lungs and lymph nodes. The activity of a combination of checkpoint inhibitor and tyrosine kinase inhibitor in this patient was low [20].

- Clear cell sarcoma is a rare translocation-related sarcoma
- Conventional chemotherapy has minimal activity in clear cell sarcoma
- Checkpoint (PD-1/PD-L1 axis) inhibitors have relevant activity in clear cells sarcoma as compared to other high-grade soft tissue sarcoma
- FDG PET is a crucial tool to assess the activity of systemic treatment in metastatic clear cell sarcoma

21.5 Case 4: Mixed Response with Disease Progression

Clinical Details Patient with multifocal high-grade angiosarcoma of the left foot with multiple nodules along left lower limb. Considering the age of the patient and the histology. The first-line treatment with weekly gemcitabine 900 mg/m^2 was performed, with a clinical and radiological response. The patient refused amputation, and gemcitabine was continued. Later in 2019 patient underwent left leg and lower thigh amputation. In July 2019, chest CT confirmed new multiple pulmonary metastases. A re-challenge with weekly gemcitabine was started.

Scan Findings and Interpretation Baseline FDG PET (Fig. 21.10) demonstrated multiple areas of abnormally increased tracer uptake (SUVmax = 22.7) in the left foot (soft tissues of the toes and laterally in the heel) and multiple hypermetabolic skin and subcutaneous nodules in the left lower leg (SUVmax = 13); another area of low tracer uptake (SUVmax = 2.4) in subcutaneous tissues near the left sartorius muscle.

FDG PET/CT scan (Fig. 21.11) after eight cycles demonstrated metabolic response (reduction in the number and tracer uptake of the hypermetabolic lesions previously described) in the left lower leg and persistence of multiple areas of uptake in the soft tissue of the left foot (SUVmax = 23.9).

FDG PET repeated after 12 cycles (Fig. 21.12) showed a complete metabolic response in the leg nodules. However, there were persistent uptake areas in soft tissue in the left foot (SUVmax = 20.7 vs. 23.9 with hepatic SUVmean = 2.1 vs. 2). A new small hypermetabolic lesion in the plantar area and near the first metatarsal bone was seen. MRI scan showed a slight quantitative reduction of the forefoot's various neoplastic nodules and a new pathological nodule above the second intermetatarsal space. A follow-up FDG PET scan (Fig. 21.13) showed new hypermetabolic adenopathy at left pulmonary hilum (SUV 18.3), celiac and para-aortic lymph nodes above the bifurcation (SUVmax = 4), and multiple hypermetabolic lymph nodes in the left iliac and inguinal-femoral chains (SUVmax = 16.6). Compared

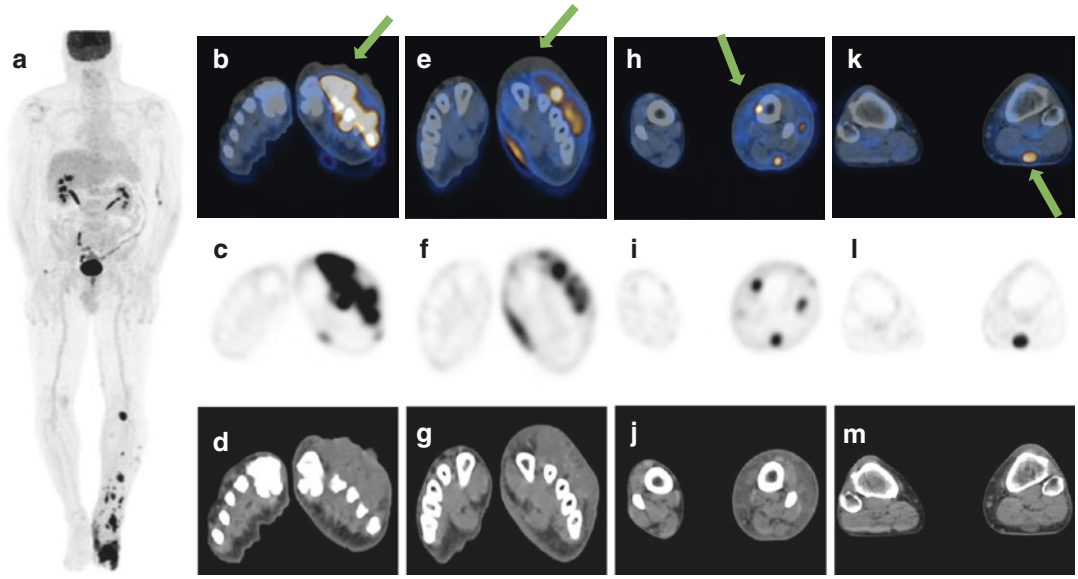

Fig. 21.10 (**a**) Staging FDG PET/CT scan (May 2018): There are multiple areas of increased uptake of the tracer (SUVmax = 22.7) in the left foot (soft tissues of the toes and laterally in the heel; **b**–**g**) and multiple hypermetabolic skin and subcutaneous nodules in the left lower leg (SUVmax = 13; **h**–**j**); and low-grade tracer uptake (SUVmax = 2.4; **k**–**m**) in subcutaneous tissue near the left Sartorius muscle

with the previous FDG PET/CT scan, most of the earlier findings have been resolved. However, two new splenic hypermetabolic lesions and two lung nodules were seen (Fig. 21.14).

Teaching Points

Angiosarcoma (AS) is an ultra-orphan and aggressive tumor of the soft tissue of vascular origin affecting older patients. The incidence is approximately 1000 patients per year in the United States and a similar number in Europe. The standard regimens for unresectable advanced AS include chemotherapy (taxanes, anthracyclines, and gemcitabine) and pazopanib, an inhibitor of multiple receptor tyrosine kinases including vascular endothelial growth factor receptors (VEGFR) [21]. Tumor control of metastatic disease with these therapies is short-lived, with median progression-free survival (PFS) ranging from 3.0 to 6.6 months and median overall survival (OS) of approximately 8–11 months [21]. In this case, the activity of chemotherapy was demonstrated. FDG PET/CT was able to detect all visceral metastases and might be considered an optimal tool for monitoring response in this histotype [22]. It is also essential to underscore the role of surgery and radiotherapy in the setting of pauci-progressive, metastatic disease.

- Angiosarcoma (AS) is an aggressive tumor of the soft tissue of vascular origin, affecting older patients.
- Standard regimens for unresectable advanced AS include chemotherapy as well as pazopanib.
- FDG PET was able to detect all of the metastases and to evaluate the response to treatment.

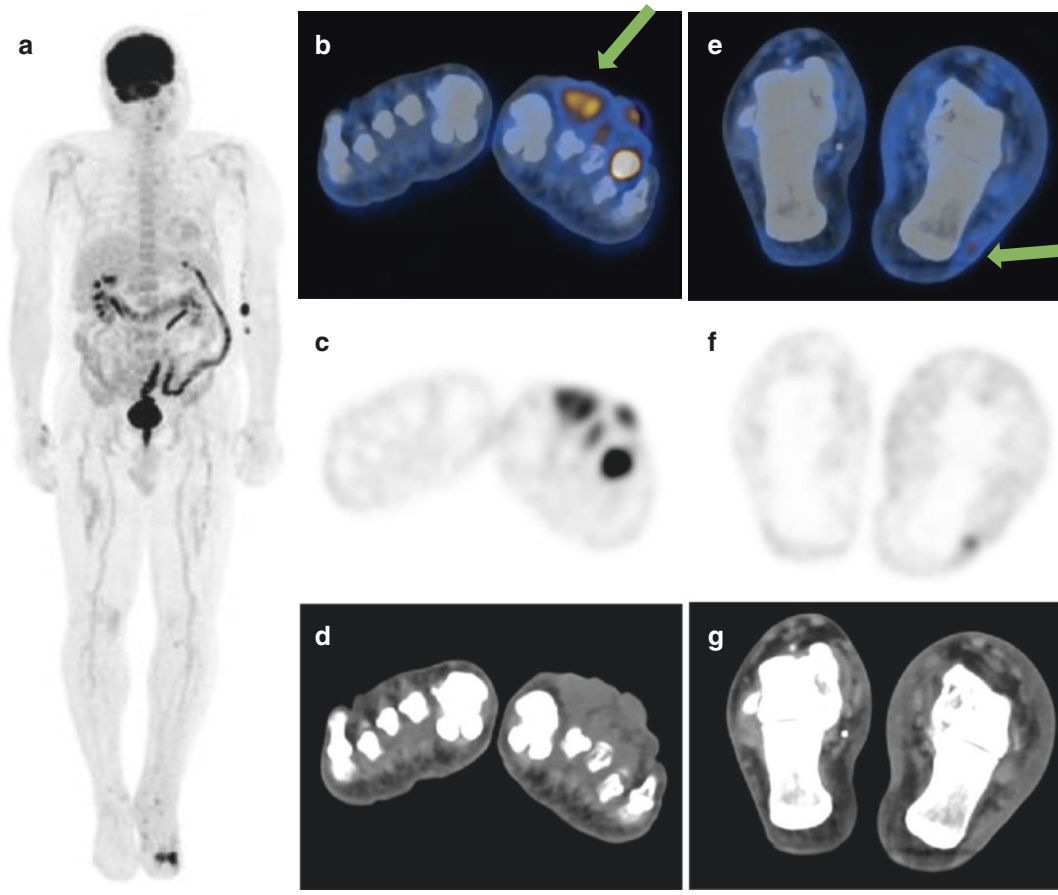

Fig. 21.11 (**a**) FDG PET/CT after gemcitabine (October 2018): There is reduction in number and tracer uptake in the hypermetabolic lesions previously described in the left lower leg with persistent increased uptake within multiple areas in soft tissue of the left foot (SUVmax = 23.9; **b**–**g**)

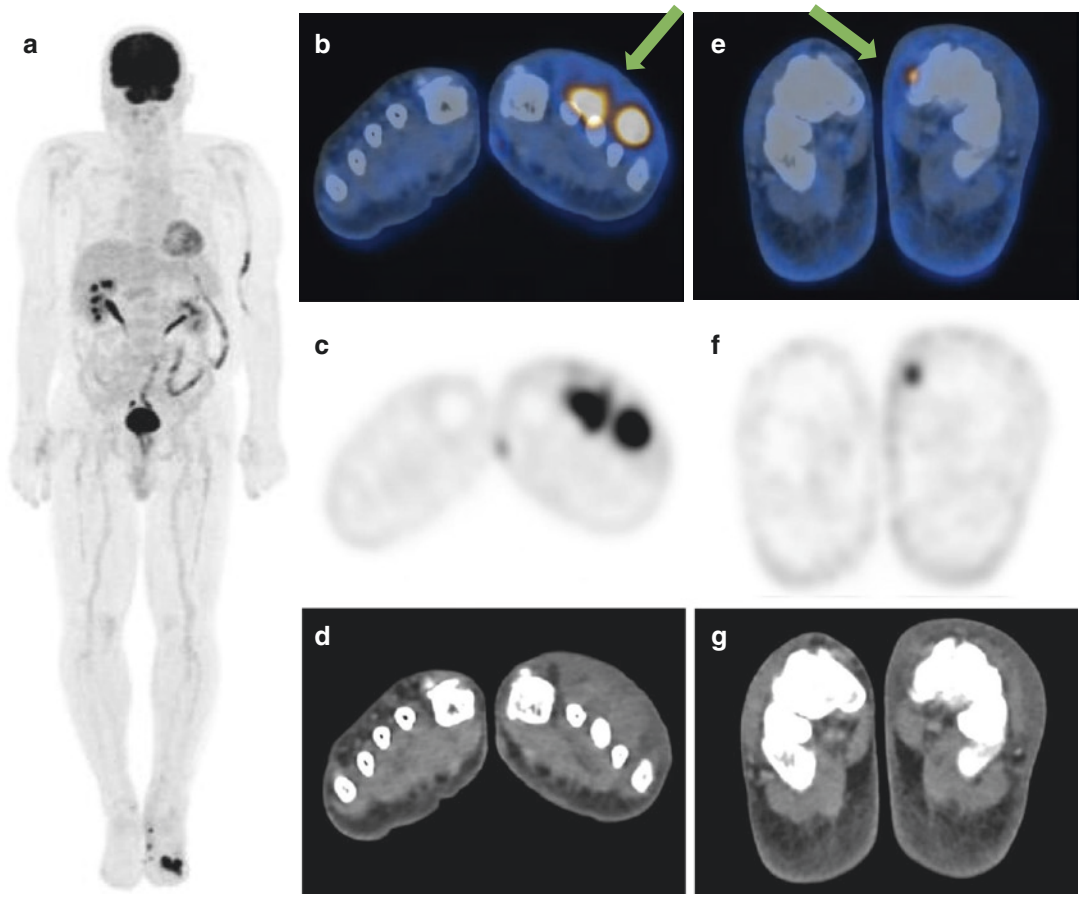

Fig. 21.12 (**a**) FDG PET/CT scan after gemcitabine (Feb 2019): There is persistence of multiple areas of uptake in soft tissue of second, third, and fourth toes of the left foot (SUVmax = 20.7 vs. 23.9 with hepatic SUVmean = 2.1 vs. 2; **b**–**d**). There are new small hypermetabolic lesions in the plantar area and near the first metatarsal bone (**e**–**g**). There is presence of some non-hypermetabolic adenopathy in the left groin

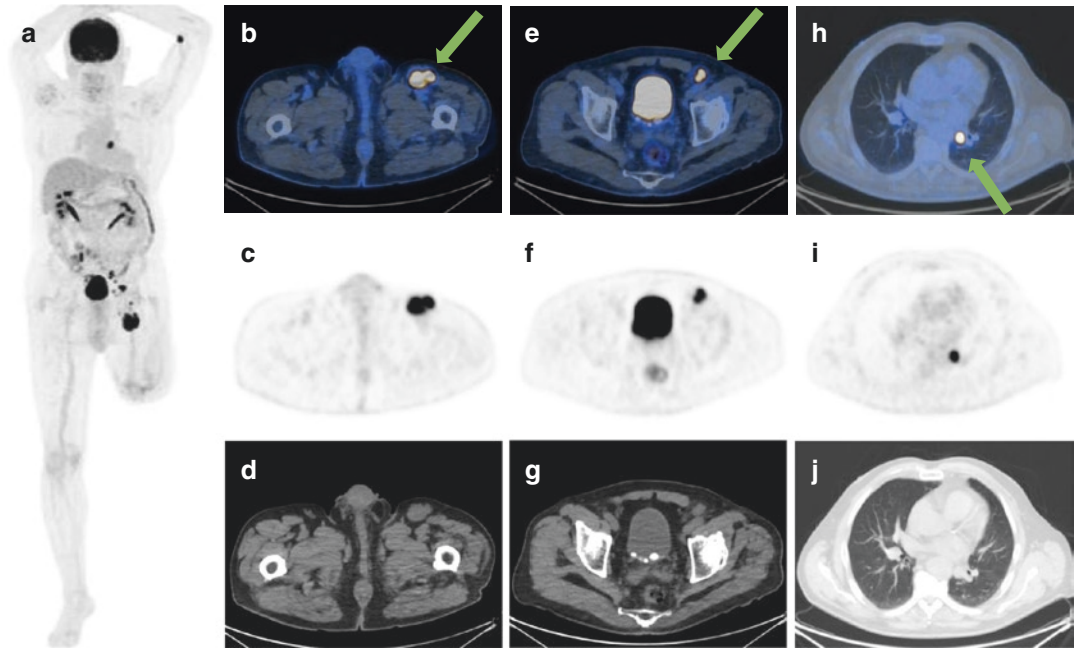

Fig. 21.13 (**a**) FDG PET/CT scan after amputation surgery of lower left leg (July 2019): There is a new hypermetabolic adenopathy in the left pulmonary hilum (SUV 18.3; **h**–**j**), uptake in celiac and para-aortic lymph nodes above the bifurcation (SUVmax = 4), and multiple hypermetabolic lymph nodes in the left iliac and inguinofemoral chains (SUVmax = 16.6; **b**–**g**)

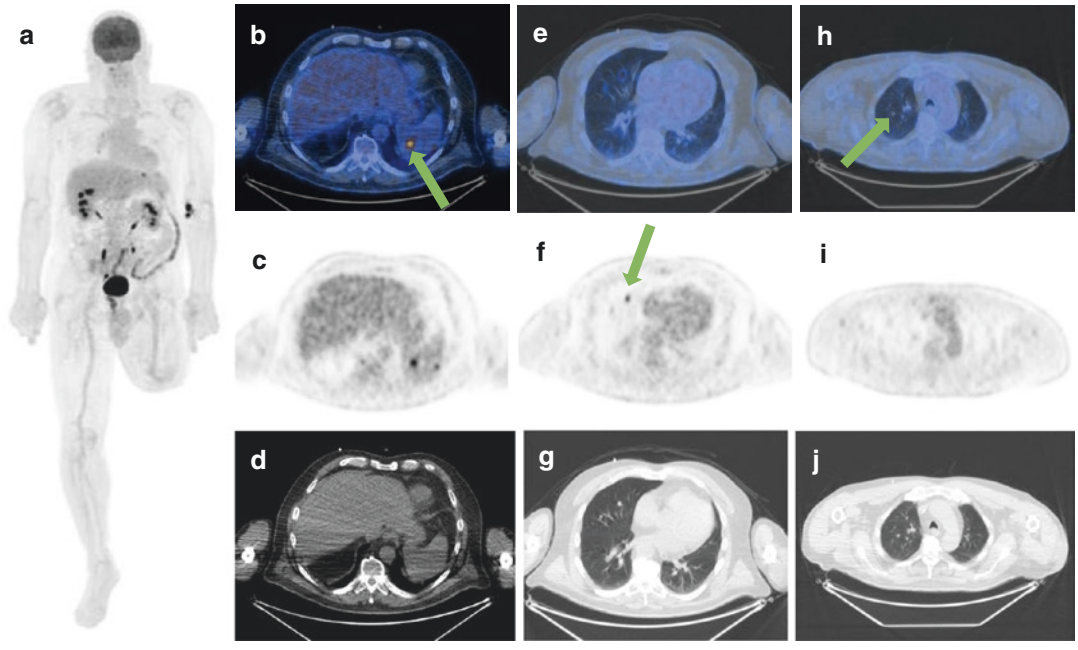

Fig. 21.14 (**a**) FDG PET/CT scan after taxol (Dec 2019): Most of the previous hypermetabolic findings are not visualized in the current study. There are two new splenic hypermetabolic lesions (SUVmax = 6.8; **b**–**d**) and two mild hypermetabolic lung nodules (**e**–**j**)

21.6 Case 5: Disease Progression

Clinical Details A patient with dermatofibrosarcoma protuberans with sarcomatous changes of the left thoracic/abdominal wall underwent local recurrence excision. He developed local recurrence of dermatofibrosarcoma protuberans with sarcomatous changes. The patient had surgical excision with wide margins of the lesion followed by postoperative radiotherapy. Chest and abdominal CT showed the presence of pulmonary nodules and suspected hepatic metastasis, which PET/CT confirmed.

Scan Findings and Interpretation Re-staging FDG PET/CT (Fig. 21.15) showed two areas of focal uptake of the metabolic tracer in the liver, one in VIIs (SUVmax = 6.3) and the other one in VIIIs (SUVmax = 3.8); one hypermetabolic nodule (SUVmax = 3.3) in the superior lobe of the left lung. Follow-up FDG PET/CT (Fig. 21.16) confirmed progressive disease with increased size and uptake of the hepatic lesions.

Teaching Points

Dermatofibrosarcoma protuberans (DFSP) is a low-grade malignant mesenchymal tumor that typically arises in the dermis of the trunk and proximal extremities [23]. DFSP represents 1–6% of all soft tissue sarcomas (STS), and its frequency of detection slowly has increased over time. DFSP is characterized by slow infiltrative growth and a high rate of local recurrence if not adequately treated. When dedifferentiated areas represent more than 5% of tumor tissue, the lesion is classified as fibrosarcomatous ("high-grade") dermatofibrosarcoma protuberans (FS-DFSP) [23]. The distant and local relapse rate for FS-DFSP ranges from 8% to 28% and 20% to 58%, respectively [23]. The activity of anti-tyrosine kinase inhibitor imatinib was described [24]

We report a case with a long history (about 8 years) of local recurrences from FS-DSFP. After visceral metastases, all detected by PET/CT scan [25], the patient experienced a rapid progression resistant to imatinib.

- There are two forms of dermatofibrosarcoma protuberans, based on the presence of dedifferentiated areas.
- Fibrosarcomatous dermatofibrosarcoma protuberances have aggressive behavior, with lung and visceral metastatic spread.
- PET-TC is an optimal tool to restage dermatofibrosarcoma protuberans when they progress to fibrosarcomatous counterpart.

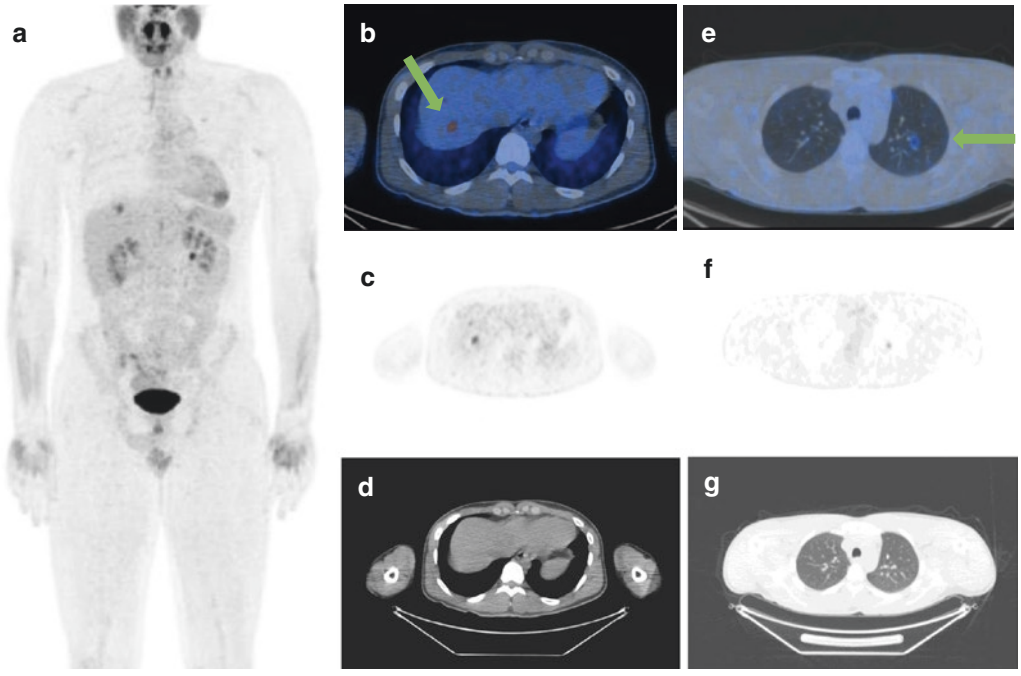

Fig. 21.15 (**a**) PET/CT after surgery and RT: There are two areas of focal uptake of the metabolic tracer in the liver, one in VIIs (SUVmax = 6.3) and the other one in VIIIs (SUVmax = 3.8) (**b**–**d**); another hypermetabolic nodule (SUVmax = 3.3) in the superior lobe of the left lung (**e**–**g**)

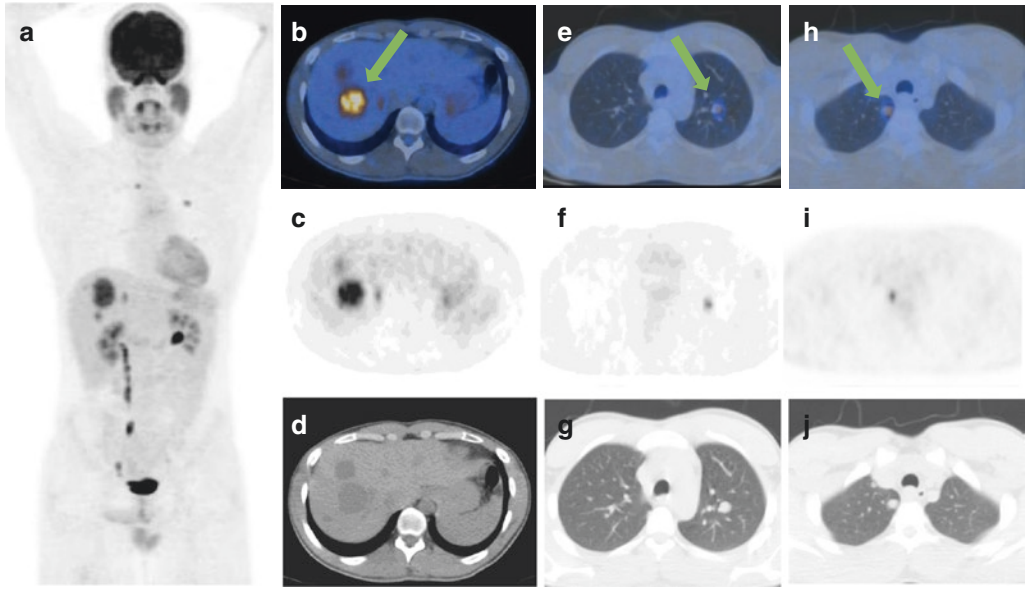

Fig. 21.16 (**a**) PET/CT after imatinib: There has been an increase in size, uptake, and number of the hepatic lesions at VIIs (SUVmax = 9.6 vs. 6.3), VIIIs (SUVmax = 4.3 vs. 3.8), and IVs (SUVmax = 5.7) (**b**–**d**); increased size, uptake, and number of pulmonary nodules at superior left lobe (SUVmax = 4.4 vs. 3.3; **e**–**g**) and superior right lobe (SUVmax = 4.9; **h**–**j**)

21.7 Case 6: Mixed Metabolic Response

Clinical Details Patient with Syt-SSX1 positive biphasic synovial sarcoma of the left tight; the patient underwent surgery and adjuvant chemotherapy (5-cycles Epirubicin/Ifosfamide) and postoperative radiotherapy. The local recurrence was treated with surgery followed by chemotherapy with Ifosfamide.

Scan Findings and Interpretation FDG PET/CT (Fig. 21.17) showed the presence of new hypermetabolic tissue in the upper right phrenic region between the right diaphragmatic pillar, the aorta, and the esophagus (SUVmax = 5.3); the presence of two soft tissue thickenings located between the diaphragm and the posterior part of the right ninth and eleventh ribs (SUVmax = 5.7); and tracer uptake with some right lung nodules (SUVmax = 3.1 in the middle lobe). Follow-up FDG PET/CT (Fig. 21.18) showed metabolic progression with increased size and metabolic uptake in the right upper phrenic region mass, extending to L1. Follow-up FDG PET/CT post-therapy showed (Fig. 21.19) mixed response was described (reduction of the extent and metabolic gradient of the upper right phrenic region mass, SUVmax = 5 vs. 13.1 and new lesions in the right chest wall, the largest located between ribs.

Teaching Points

Synovial sarcoma comprises approximately 8% of all soft tissue sarcomas [26]. Although relatively rare, synovial sarcoma is the third most common extremity soft tissue sarcoma. It affects mostly young adults, with a median age of 35 years [26]. Three histologic subtypes of SS are described: monophasic, entirely composed of spindle cells; biphasic, consisting of both spindle cells and epithelial cells; and poorly differentiated subtypes [26]. Synovial sarcoma contains a

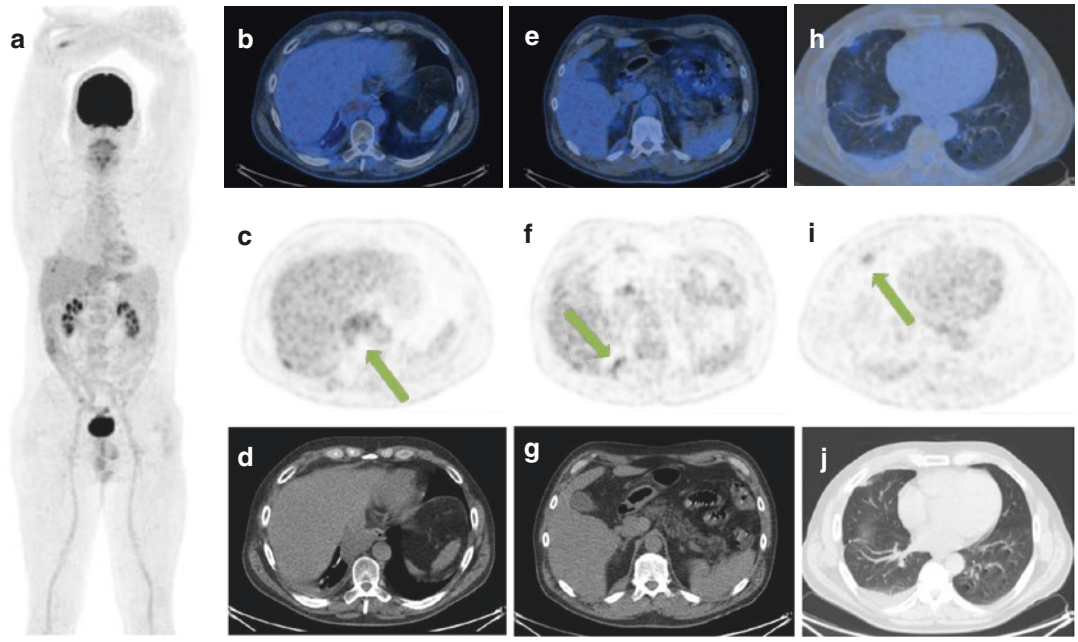

Fig. 21.17 (**a**) September 2017 FDG PET/CT scan: There are increased tracer uptake within several new hypermetabolic foci in the upper right phrenic region between the right diaphragmatic pillar, the aorta, and the esophagus (SUVmax = 5.3; **b**–**d**); presence of two tissue thickenings located between the diaphragm and the posterior part of the ninth and eleventh right ribs (SUVmax = 5.7; **e**–**g**); presence of radiopharmaceutical uptake of some right lung nodules (SUVmax = 3.1 in the middle lobe; **h**, **i**)

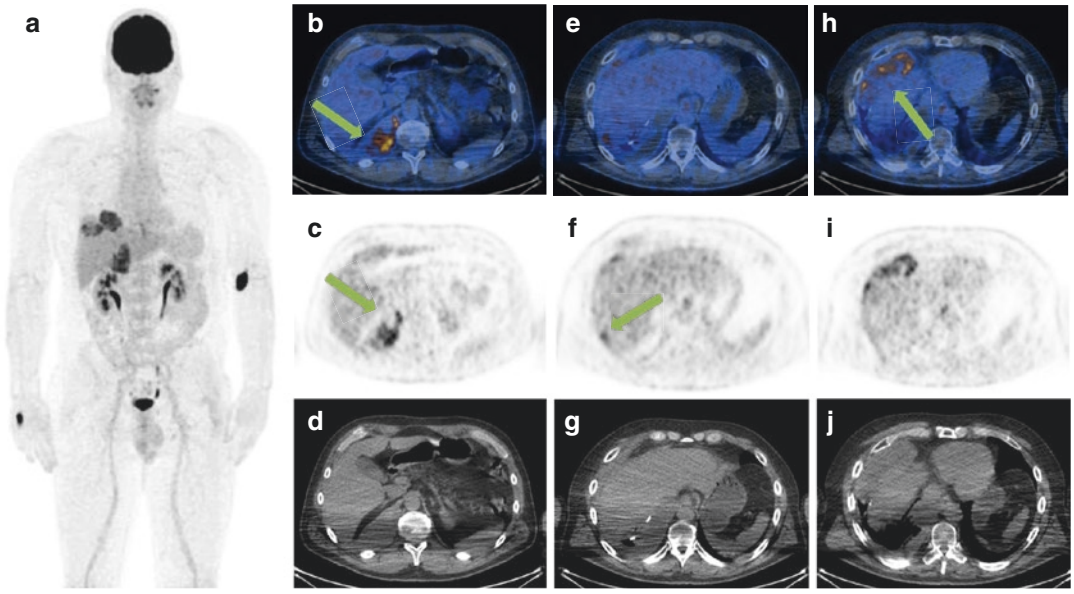

Fig. 21.18 (**a**) August 2018: FDG PET scan: There is persistent increased metabolic uptake and extension of the known tissue located in right upper phrenic region (SUVmax = 13.1; **b**–**d**); persistence of hypermetabolic tissue thickening between the diaphragm and the posterior part of the ninth right rib (**e**–**g**); appearance of an area of inhomogeneous uptake of the tracer in the lower right anterior pleura (SUVmax = 9.7; **h**–**j**)

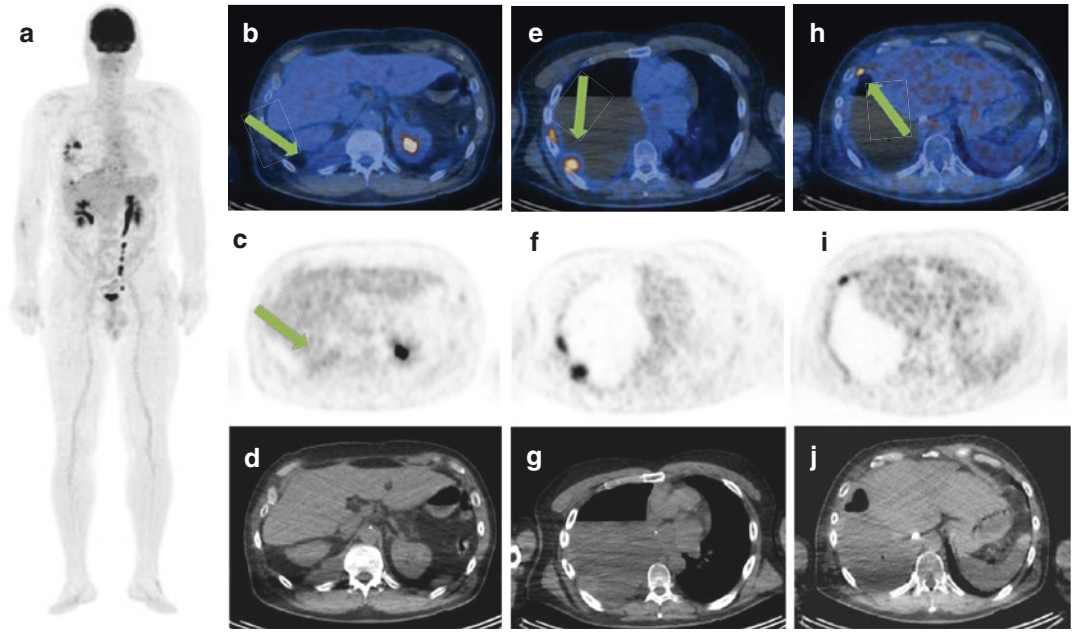

Fig. 21.19 (**a**) May 2019: FDG PET scan: There is reduction of the extent and metabolic gradient of the tissue previously described in the upper right phrenic region (SUVmax = 5 vs. 13.1; **b**–**d**); at least four new foci of hypermetabolic lesions in the right chest wall, of which the largest respectively between V and VI right ribs (SUVmax = 8.7) and between VI and VII ribs (SUVmax = 13.1) (**e**–**g**); disappearance of the inhomogeneous fixation at the level of the anterior right pleural implant, of which only remains a small area near the Glisson's capsule (SUVmax = 7.4; **h**–**j**); no longer appreciable hypermetabolic tissue previously described at the level of the posterior part of the ninth rib (surgical resection?)

characteristic translocation (X;18)(p11;q11), representing the fusion of SYT on chromosome 18 with either SSX1, SSX2, or rarely SSX4 (all on chromosome X). Several prognostic factors, such as age, size, surgical margins, histologic grade, histologic subtype, p53 overexpression, Ki-67 proliferative index, and SYT-SSX fusion type, have been identified. However, the relative prognostic value of each of these factors remains controversial [26].

The standard treatment of primary tumor is the wide surgical removal of the lesion with or without radiotherapy. Adjuvant chemotherapy might be offered to patients with large (>5 cm), deep, localized tumors, with equal benefit from three or five cycles of epirubicin and Ifosfamide [27]. For patients with recurrent disease, no standard treatment strategies have been reported. Still, palliative chemotherapy should be regarded as a standard treatment option, with approximately half of the patients deriving clinical benefit.

This patient had increased survival, with a combination of surgery, radiotherapy, and chemotherapy, with Ifosfamide and pazopanib representing options in this scenario [28]. New treatments for this tumor, including other tyrosine kinase inhibitors, are emerging [29].

Due to the considerable heterogeneity of soft tissue sarcoma, there are no synovial specific reports on FDG PET. Nonetheless, translocation-related soft tissue sarcomas such as synovial sarcoma, Ewing sarcoma, and alveolar rhabdomyosarcoma present with high SUVmax, similarly to bone sarcomas, and studies on the potential role of FDG PET in this subset are warranted [30].

- In 2003, standard adjuvant chemotherapy was five cycles of epirubicin and Ifosfamide, while nowadays three cycles are deemed equally effective.
- Synovial sarcoma is specifically sensitive to high-dose Ifosfamide.
- PALLETTE study showed that pazopanib, an anti-VEGF/anti-PDGF receptor inhibitor, is an active drug in second-line treatment in all non-adipocytic liposarcomas, particularly in synovial sarcoma.
- FDG PET might be informative in metastatic synovial sarcoma, especially in the case of non-visceral metastases (bone, soft tissue).

References

1. Weitz J, Antonescu CR, Brennan MF. Localized extremity soft tissue sarcoma: improved knowledge with unchanged survival over time. J Clin Oncol. 2003;21:2719–25.
2. Siegel R, Ward E, Brawley O, et al. Cancer statistics, 2011: the impact of eliminating socioeconomic and racial disparities on premature cancer deaths. CA Cancer J Clin. 2011;61(2011):212–36.
3. Etchebehere E, Macapinlac HA. The role of 18F-FDG PET/CT in diagnosis and staging of musculoskeletal soft tissue sarcomas. Clin Transl Imaging. 2015;3:111–21.
4. Schulte M, BrechtKrauss D, Heymer B, Guhlmann A, Hartwig E, Sarkar MR, et al. Grading of tumors and tumor-like lesions of bone: evaluation by FDG PET. J Nucl Med. 2000;41:1695–701.
5. Hicks J, Toner GC, Choong PF. Clinical applications of molecular imaging in sarcoma evaluation. Cancer Imaging. 2005;5:66–72.
6. Benz MR, Czernin J, Allen-Auerbach MS, et al. FDGPET/CT imaging predicts histopathologic treatment responses after the initial cycle of neoadjuvant chemotherapy in high grade soft-tissue sarcomas. Clin Cancer Res. 2009;15:2856–63.
7. Folpe AL, Lyles RH, Sprouse JT, Conrad EU, Eary JF. (F-18) fluorodeoxyglucose positron emission tomography as a predictor of pathologic grade and other prognostic variables in bone and soft tissue sarcoma. Clin Cancer Res. 2000;6:1279–87.
8. Bastiaannet E, Groen B, Jager PL, et al. The value of FDGPET in the detection, grading and response to therapy of soft tissue and bone sarcomas; a systematic review and meta analysis. Cancer Treat Rev. 2004;30:83–101.
9. Eary JF, O'Sullivan F, Powitan Y, et al. Sarcoma tumor FDG uptake measured by PET and patient outcome: a retrospective analysis. Eur J Nucl Med. 2001;29:1149–54.
10. Rodriguez-Alfonso B, Mucientes Rasilla J, Mitjavila Casanovasa M, Cardona Arboniésa J, Cubedob JR. 18F-FDG-PET-CT in soft tissue sarcomas: when to image? Rev Esp Med Nucl Imagen Mol. 2014;33:43–9.
11. Arush MW, Israel O, Postovsky S, Militianu D, Meller I, Zaidman I, et al. Positron emission tomography/computed tomography with 18fluoro-deoxyglucose in the detection of local recurrence and distant metastases of pediatric sarcoma. Pediatr Blood Cancer. 2007;49:901–5.
12. Garner HW, Kransdorf MJ, Peterson JJ. Posttherapy imaging of musculoskeletal neoplasms. Radiol Clin North Am. 2011;49:1307–23.
13. Lefkowitz DRA, Landa J, Hwang S, et al. Myxofibrosarcoma: prevalence and diagnostic value of the "tail sign" on magnetic resonance imaging. Skelet Radiol. 2013;42:809–81.
14. Fletcher CDM, Bridge JA, Hogendoorn PCW, et al., editors. WHO classification of tumours of soft tissue and bone. Lyon: International Agency for Research on Cancer; 2013.
15. Ito K, Masuda-Miyata Y, Wada S, Morooka M, Yamasawa K, Hashimoto M, Kubota K. F-18 FDG PET/CT imaging of bulky myxofibrosarcoma in chest wall. Clin Nucl Med. 2011;36(3):212–3. https://doi.org/10.1097/RLU.0b013e318208f2e0.
16. Gronchi A, Ferrari S, Quagliuolo V, Broto JM, Pousa AL, Grignani G, Basso U, Blay JY, Tendero O, Beveridge RD, Ferraresi V, Lugowska I, Merlo DF, Fontana V, Marchesi E, Donati DM, Palassini E, Palmerini E, De Sanctis R, Morosi C, Stacchiotti S, Bagué S, Coindre JM, Dei Tos AP, Picci P, Bruzzi P, Casali PG. Histotype-tailored neoadjuvant chemotherapy versus standard chemotherapy in patients with high-risk soft-tissue sarcomas (ISG-STS 1001): an international, open-label, randomised, controlled, phase 3, multicentre trial. Lancet Oncol. 2017;18(6):812–22.
17. Casali PG, Abecassis N, Aro HT, Bauer S, Biagini R, Bielack S, Bonvalot S, Boukovinas I, Bovee JVMG, Brodowicz T, Broto JM, Buonadonna A, De Álava E, Dei Tos AP, Del Muro XG, Dileo P, Eriksson M, Fedenko A, Ferraresi V, Ferrari A, Ferrari S, Frezza AM, Gasperoni S, Gelderblom H, Gil T, Grignani G, Gronchi A, Haas RL, Hassan B, Hohenberger P, Issels R, Joensuu H, Jones RL, Judson I, Jutte P, Kaal S, Kasper B, Kopeckova K, Krákorová DA, Le Cesne A, Lugowska I, Merimsky O, Montemurro M, Pantaleo MA, Piana R, Picci P, Piperno-Neumann S, Pousa AL, Reichardt P, Robinson MH, Rutkowski P, Safwat AA, Schöffski P, Sleijfer S, Stacchiotti S, Sundby Hall K, Unk M, Van Coevorden F, van der Graaf WTA, Whelan J, Wardelmann E, Zaikova O, Blay JY, ESMO Guidelines Committee and EURACAN. Soft tissue and visceral sarcomas: ESMO-EURACAN clinical practice guidelines for diagnosis, treatment and follow-up. Ann Oncol. 2018;29(Suppl 4):iv51–67.
18. Lunn BW, Littrell LA, Wenger DE, Broski SM. 18F-FDG PET/CT and MRI features of myxoid liposarcomas and intramuscular myxomas. Skelet Radiol. 2018;47(12):1641–50.
19. Jones RL, Constantinidou A, Thway K, Ashley S, Scurr M, Al-Muderis O, Fisher C, Antonescu CR, D'Adamo DR, Keohan ML, Maki RG, Judson IR. Chemotherapy in clear cell sarcoma. Med Oncol. 2011;28(3):859–63.
20. Broto JM, Hindi N, Grignani GE, Martinez Trufero J, Redondo A, Valverde C, Lopez Pousa A, Stacchiotti S, Palmerini E, de Alava E, Moura DS, Perez Vega H, Collini P, Otero I, Ledesma P, Marchesi E, D'Ambrosio L, Lopez Martin JA. IMMUNOSARC: a collaborative Spanish (GEIS) and Italian (ISG) sarcoma groups phase I/II trial of sunitinib plus nivolumab in advanced soft tissue and bone sarcomas: Results of the phase II-soft-tissue sarcoma cohort. Ann Oncol. 2019;30(Suppl 5):684.

21. ESMO/European Sarcoma Network Working Group. Soft tissue and visceral sarcomas: ESMO-EURACAN clinical practice guidelines for diagnosis, treatment and follow-up. Ann Oncol. 2018;29(Suppl 4):iv268–9.
22. Kato A, Nakamoto Y, Ishimori T, Saga T, Togashi K. Prognostic value of quantitative parameters of 18F-FDG PET/CT for patients with angiosarcoma. AJR Am J Roentgenol. 2020;214(3):1–9.
23. Palmerini E, Gambarotti M, Staals EL, Zanella L, Sieberova G, Longhi A, Cesari M, Bonarelli S, Picci P, Ruggieri P, Alberghini M, Ferrari S. Fibrosarcomatous changes and expression of CD34+ and apolipoprotein-D in dermatofibrosarcoma protuberans. Clin Sarcoma Res. 2012;2(1):4. https://doi.org/10.1186/2045-3329-2-4.
24. Maki RG, Awan RA, Dixon RH, Jhanwar S, Antonescu CR. Differential sensitivity to imatinib of 2 patients with metastatic sarcoma arising from dermatofibrosarcoma protuberans. Int J Cancer. 2002;100:623–6.
25. Basu S, Goliwale F. 18F-FDG PET/CT prediction of an aggressive clinical course for dermatofibrosarcoma protuberans. J Nucl Med Technol. 2016;44(2):88–9.
26. Palmerini E, Staals EL, Alberghini M, Zanella L, Ferrari C, Benassi MS, Picci P, Mercuri M, Bacci G, Ferrari S. Synovial sarcoma: retrospective analysis of 250 patients treated at a single institution. Cancer. 2009;115(13):2988–98.
27. Palassini E, Ferrari S, Verderio P, De Paoli A, Martin Broto J, Quagliuolo V, Comandone A, Sangalli C, Palmerini E, Lopez-Pousa A, De Sanctis R, Bottelli S, Libertini M, Picci P, Casali PG, Gronchi. Feasibility of preoperative chemotherapy with or without radiation therapy in localized soft tissue sarcomas of limbs and superficial trunk in the Italian Sarcoma Group/Grupo Español de Investigación en Sarcomas randomized clinical trial: three versus five cycles of full-dose epirubicin plus ifosfamide. J Clin Oncol. 2015;33(31):3628–34.
28. van der Graaf WT, Blay JY, Chawla SP, Kim DW, Bui-Nguyen B, Casali PG, Schöffski P, Aglietta M, Staddon AP, Beppu Y, Le Cesne A, Gelderblom H, Judson IR, Araki N, Ouali M, Marreaud S, Hodge R, Dewji MR, Coens C, Demetri GD, Fletcher CD, Dei Tos AP, Hohenberger P, EORTC Soft Tissue and Bone Sarcoma Group; PALETTE Study Group. Pazopanib for metastatic soft-tissue sarcoma (PALETTE): a randomised, double-blind, placebo-controlled phase 3 trial. Lancet. 2012;379(9829):1879–86.
29. Palmerini E, Paioli A, Ferrari S. Emerging therapeutic targets for synovial sarcoma. Expert Rev Anticancer Ther. 2014l;14(7):791–806.
30. Macpherson RE, Pratap S, Tyrrell H, Khonsari M, Wilson S, Gibbons M, Whitwell D, Giele H, Critchley P, Cogswell L, Trent S, Athanasou N, Bradley KM, Hassan AB. Retrospective audit of 957 consecutive 18F-FDG PET-CT scans compared to CT and MRI in 493 patients with different histological subtypes of bone and soft tissue sarcoma. Clin Sarcoma Res. 2018;8:9.

22 ^{18}F-FDG PET-CT in Treatment Response Evaluation in Cutaneous Malignant Melanoma

Sweni Shah, Salma Audi, and Malavika Nathan

22.1 Introduction

Immunotherapy drugs targeting checkpoint inhibitors on T-cell and tumour cell surfaces have revolutionized the treatment of cutaneous malignant melanoma [1]. These drugs, such as Ipilimumab, Pembrolizumab and Nivolumab, act by inhibiting specific regulatory steps in the immune system, thereby stimulating T-cell proliferation and upregulation of the immune response against cancer cells [2].

The literature has shown that patterns of tumour response to immunotherapy vary from traditional chemotherapy. These novel patterns include [3]:

1. Immediate and complete response with no new lesions.
2. Stable response (sustained response).
3. Initial increase in tumour burden followed by subsequent response, termed as 'pseudo-progression or a flare phenomenon' and due to immune/T-cell infiltration resulting in a temporary increase in size of lesions.
4. Some response (complete or partial) but with the development of new lesions.

Therefore, the Response Evaluation Criteria in Solid Tumors (RECIST) 1.1 categories of response may not always be suitable for immunotherapy. This is particularly true in cases where the tumour has temporarily increased in size or new lesions have developed in the context of response elsewhere. These instances would be categorized as progressive disease by RECIST 1.1, but are actually a novel immunotherapy response.

Therefore, new Immune-related Response Evaluation Criteria In Solid Tumours (iRECIST) have been developed [4], the prefix 'i' specifying 'immune'. The criteria are similar to RECIST1.1 except for definition of progressive disease. Pseudo-progression or flare phenomenon is incorporated into the new criteria and termed immune unconfirmed progressive disease (iUPD) until it is confirmed or refuted on subsequent imaging.

Another caveat when interpreting immunotherapy response is to be aware of immune-related adverse events (irAE), whereby upregulation of the immune response results in autoimmune targeting of non-diseased organs, such as thyroiditis, colitis, adrenalitis and hepatitis. These should be recognized as irAE and not interpreted as sites of tumour infiltration or progressive disease. Metabolically active splenomegaly and lymphadenopathy may also be seen as a feature of immune upregulation.

S. Shah · S. Audi · M. Nathan (✉)
Department of Nuclear Medicine, Royal Free London NHS Foundation Trust, London, UK
e-mail: malavika.nathan@nhs.net

S. Fanti et al. (eds.), *Atlas of Clinical PET-CT in Treatment Response Evaluation in Oncology*,
https://doi.org/10.1007/978-3-030-68858-5_22

22.2 Case 1

Clinical Details A 45-year-old female presented with a cutaneous lesion on the right leg, confirmed to be metastatic malignant melanoma with in-transit metastases up the right leg in 2009. Due to three local recurrences and lumbar metastases, the patient was commenced on Pembrolizumab in 2017.

Images

Case 1A (coronal):

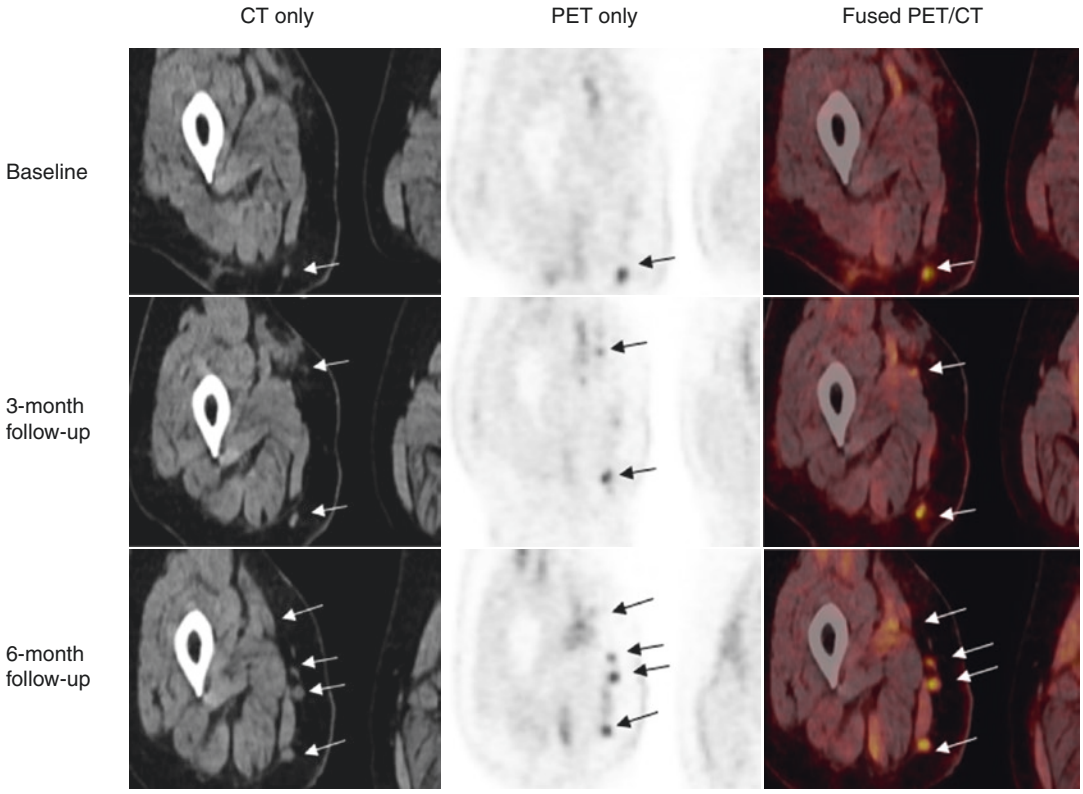

Case 1B (sagittal):

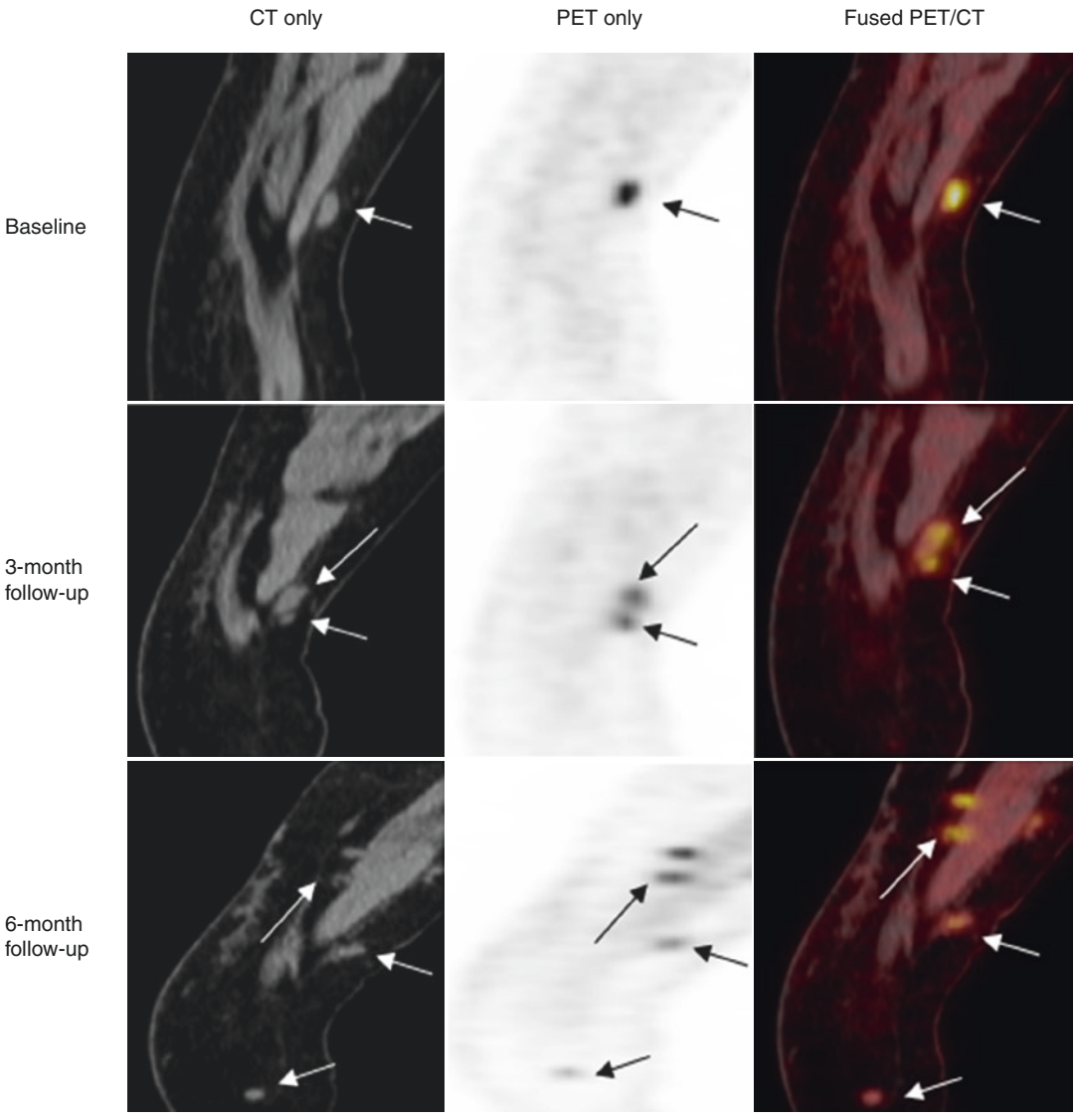

Scan Findings, Case 1 A (Coronal) and 1B (Sagittal)
On the baseline study, only one intensely ^{18}F-FDG avid lymph node was seen in right inferomedial thigh, above the knee (arrow). At 3-month follow-up, at least two nodules were seen in the same region with an increase in size of the initial lesion (arrows). At 6-month follow-up, multiple new nodules were seen in the right thigh, with existing lesions demonstrating an increase in size and intensity.

Interpretation The ^{18}F-FDG PET/CT demonstrates confirmed progressive disease (iCPD) as per the iRECIST criteria.

Comments on Interpretation As the first scan was follow-up post-surgery but before starting immunotherapy it was considered as the new 'baseline'. On the first three-month follow-up, although there are new nodules identified, it is labelled as unconfirmed progressive disease (iUPD) as per the iRECIST criteria. This needs to be confirmed on further follow-up imaging—at least 4 to 8 weeks apart. On subsequent follow-up, these nodules have increased in size, number and intensity, indicating confirmed progressive disease (iCPD).

Teaching Points
- Due to the novel pattern of pseudo-progression, usually seen following initial commencement of immunotherapy, new disease or increase in size or metabolic activity of existing lesions on initial follow-up should be termed unconfirmed progressive disease (iUPD) until it is confirmed or refuted on subsequent imaging 4 to 8 weeks later [4].
- If there is further progression (increase in size, number or intensity of lesions) on follow-up imaging, it is termed confirmed progressive disease (iCPD).

22.3 Case 2

Clinical Details A 56-year-old female with a significant history of sun exposure, presented in 2014 with a two year history of a slowly increasing nodule on the right thigh. This was diagnosed as an 11 mm ulcerated melanoma of the right thigh with two positive sentinel nodes that were excised. Due to disease relapse in 2018 (labial lesion and lung nodules), the patient was commenced on Pembrolizumab. As there was further disease progression on Pembrolizumab. The patient was switched to combination immunotherapy with Ipilimumab and Nivolumab and completed four cycles.

Images

Case 2A (MIP, coronal):

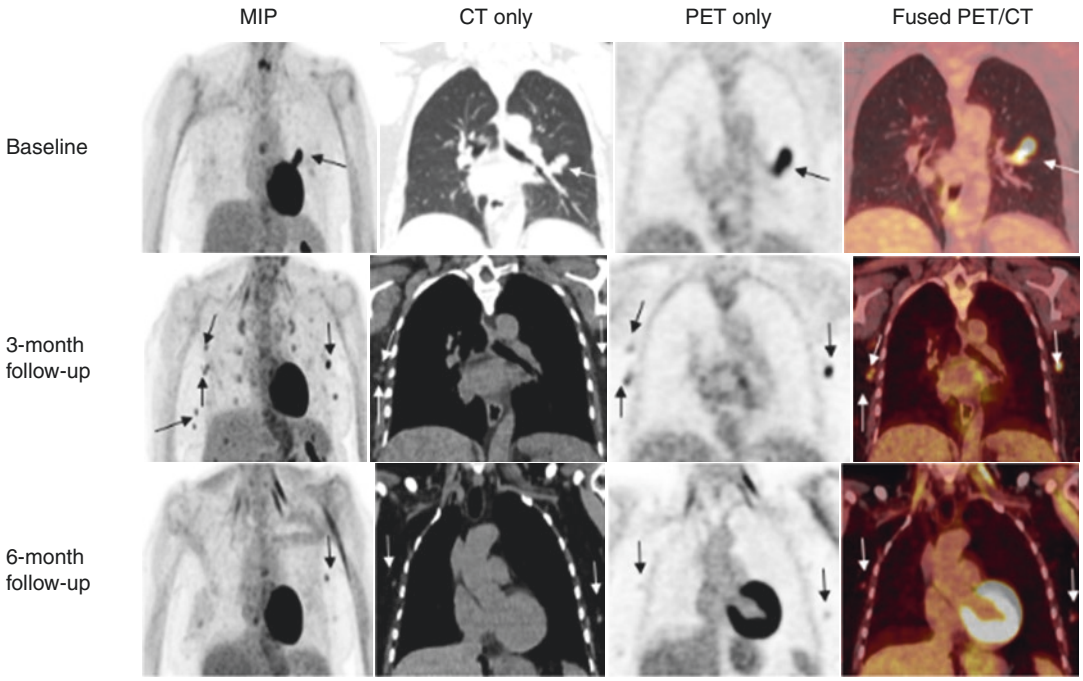

Case 2B (axial):

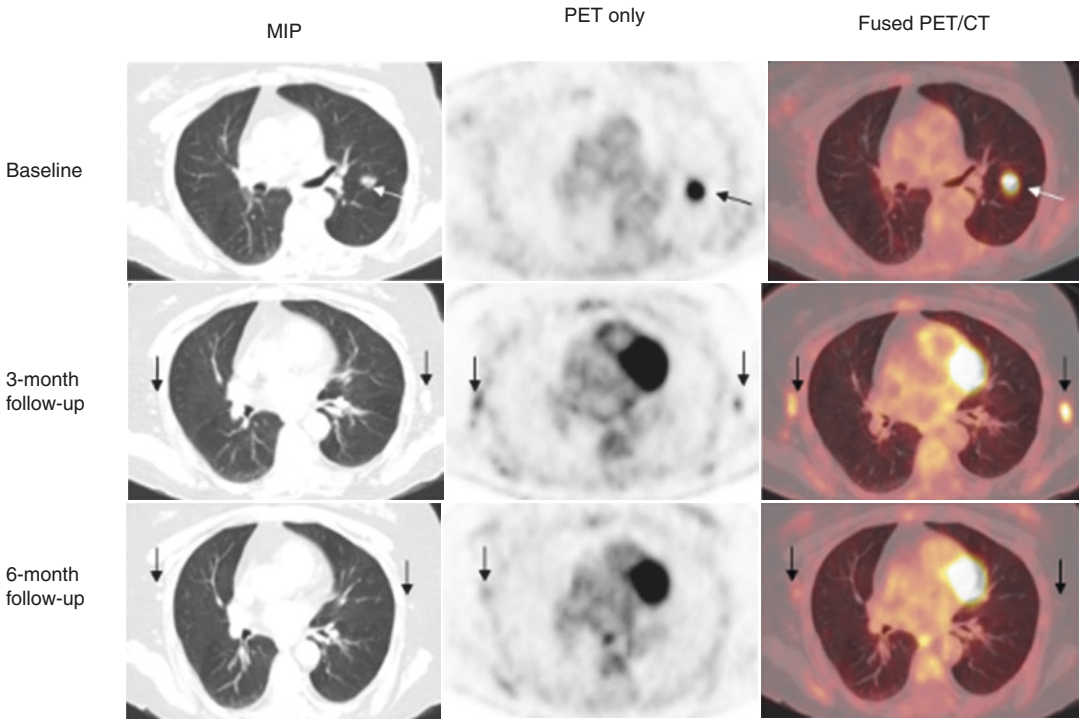

Scan Findings, Case 2 A (MIP, Coronal) and 2B (Axial)

Baseline ^{18}F-FDG PET/CT performed immediately prior to switch to combination immunotherapy with Ipilimumab and Nivolumab depicts two adjacent, intensely ^{18}F-FDG avid nodules in the apical segment of the left lower lobe (arrows) (demonstrated in lung windows on the coronal and axial images). At least four other sub-centimetre lung nodules were seen in both lobes and a hypermetabolic labial lesion was seen (images not shown).

On the 3-month follow-up scan after starting Ipilimumab and Nivolumab, the lung metastases had markedly reduced in size (from 20 mm to 7 mm) and demonstrated no residual metabolic activity. Other sub-centimetre lung nodules seen on the baseline scan had also decreased in size. Intensely ^{18}F-FDG avid (SUVmax 6.5) lymph nodes were seen in bilateral axillae (arrows) and left groin (images not shown) were new compared to previous ^{18}F-FDG PET/CT study. The labial nodule had resolved (images not shown).

On the 6-month follow-up scan, the size, number and intensity of multiple axillary lymph nodes (arrows) and left groin lymph nodes (images not shown) had decreased significantly. The lung metastases had completely resolved.

Interpretation Overall, ^{18}F-FDG PET/CT demonstrates complete response to combination immunotherapy.

Comments on Interpretation On first 3-month follow-up scan, the patient would be diagnosed as iUPD as per iRECIST, due to the development of new ^{18}F-FDG axillary lymph nodes. However, further follow-up images confirm that this is 'pseudo-progression' or flare response and as per iRECIST criteria, response on the interim 3-month scan will change to partial response (iPR); 6-month follow-up imaging confirms complete response.

Teaching Points

- If there is increased or ongoing ^{18}F-FDG uptake in the context of progressive tumour shrinkage or when accompanied by increased activity in the spleen it is considered as 'immune flare'. Symmetric hilar and mediastinal nodal uptake in a pattern similar to sarcoidosis may also occur [5].
- Flare response is unique to immunotherapy, with no similarity among cytotoxic response patterns. It is thought to be due to the immediate recruitment of T-cells with resultant immune system infiltration. The novel pattern may falsely indicate tumour progression if the traditional RECIST 1.1 criteria are used. Therefore, it is also termed as 'pseudo-progression' [6, 7].
- In contrast to the flare response, a subset of patients may demonstrate delayed 'pseudo-progression' due to a prolongation in the time required to build up an immune defence despite having anti-tumour activity. Subsequent confirmatory imaging would depict tumour response [6, 7].
- Following chemotherapy, as per RECIST 1.1, a total increase in tumour burden would immediately result in progressive disease and treatment failure [6]. In immunotherapy, an initial increase in tumour burden would result in unconfirmed progressive disease (iUPD) until confirmation on the follow-up scan. Immunotherapy continues in the interim as long as the patient is clinically stable [7].

22.4 Case 3

Clinical Details A 73-year-old female presented in April 2014 with a lesion behind the right knee, diagnosed as a stage 3B ulcerative malignant melanoma. She underwent wide local excision and nodal clearance due to a positive sentinel node. In 2015, the patient she developed multiple subcutaneous in-transit metastases in the right thigh which were resected, and the patient subsequently commenced on Ipilimumab. Due to further disease progression Ipilimumab, the patient was switched to Pembrolizumab.

Images
Case 3A (coronal):

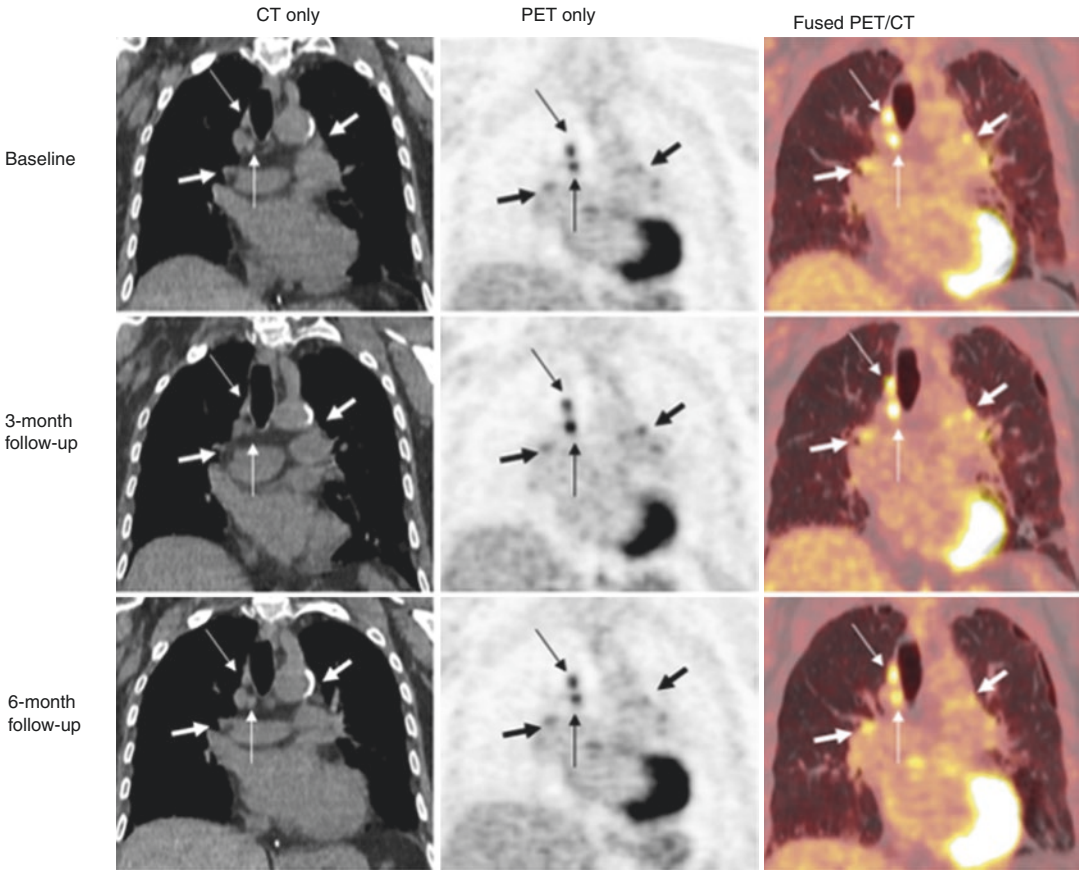

Case 3B (MIP, axial):

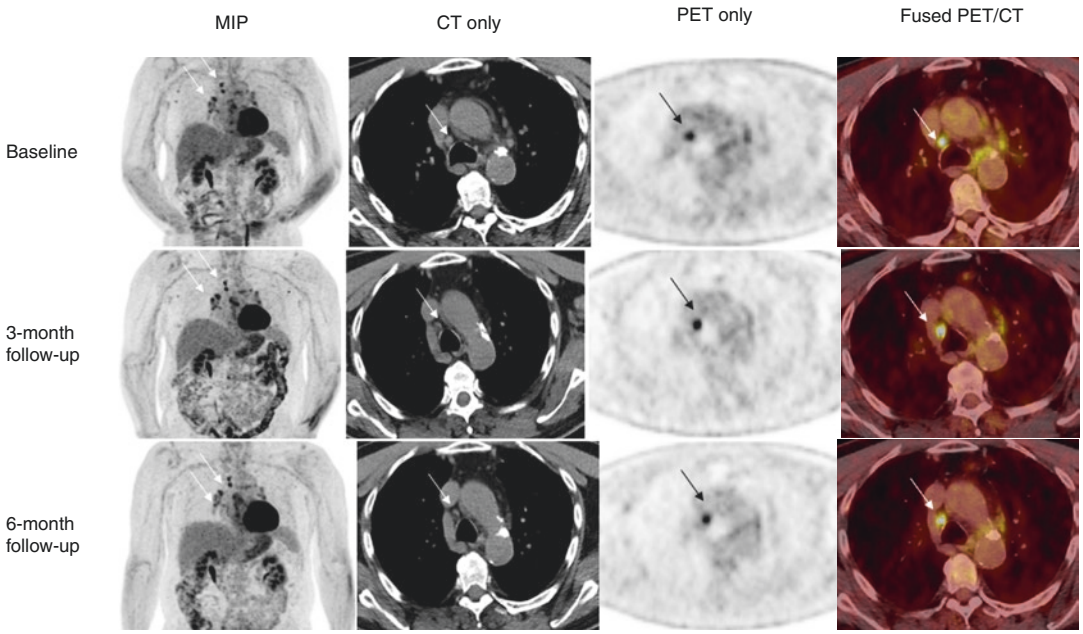

Scan Findings, Case 3A (Coronal) and 3B (MIP, Axial)

On the ^{18}F-FDG PET/CT scan at baseline, prior to the commencement of Pembrolizumab, multiple ^{18}F-FDG avid small volume hilar and mediastinal (paratracheal, pre-tracheal, subcarinal and pre-vascular) lymph nodes were seen (arrows). On the 3- and 6-month follow-up scans, these remained stable in size and intensity of ^{18}F-FDG uptake.

Interpretation ^{18}F-FDG PET/CT demonstrates stable disease on immunotherapy (iSD) as per the iRECIST criteria.

Teaching Points

- As per traditional RECIST 1.1, stable disease (SD) is defined as 'neither sufficient shrinkage to qualify for partial response (PR) nor sufficient increase to qualify for progressive disease (PD)'. In chemotherapy, SD is perceived as a transient phase—a holding period—until further imaging indicates either progression or response [4].
- With immunotherapy, iSD may be durable (i.e. sustained), and this durable state may be associated with improvements in long-term survival [7].
- In some cases a durable SD becomes a gradual modest regression; there is evidence of long-term tumour activity but at thresholds below RECIST 1.1 parameters. In other cases, it is hypothesized that tumour burden does not alter because what is measured is in fact fibrotic tissue with no residual tumour [8].
- For a growing number of immunotherapies, durable SD becomes an important surrogate endpoint for assessing clinical outcomes [9].

22.5 Case 4

Clinical Details A 45-year-old female presented with enlarged lymph nodes in the right axilla that on histopathology demonstrated melanoma of an unknown primary site. Nodal dissection of the right axilla followed by radiotherapy for Stage 3A disease was performed. Multiple relapses occurred over a 5-year period with metastases to the brain, uterus and soft tissues—all of which were resected. On the fifth soft tissue recurrence, the patient was commenced on Pembrolizumab in 2016.

Images

Case 4A (MIP, sagittal upper set, coronal lower set):

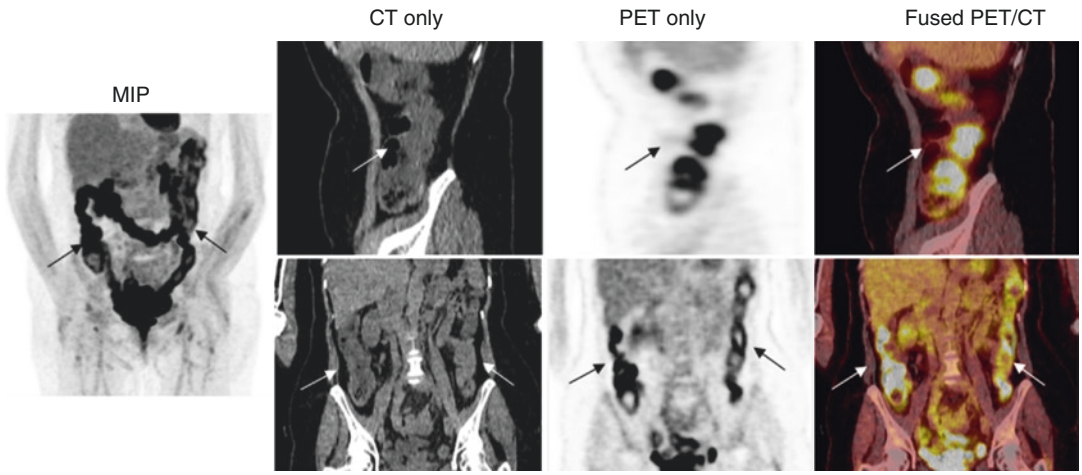

Case 4B (follow-up at 3 months. MIP, coronal upper set, sagittal lower set):

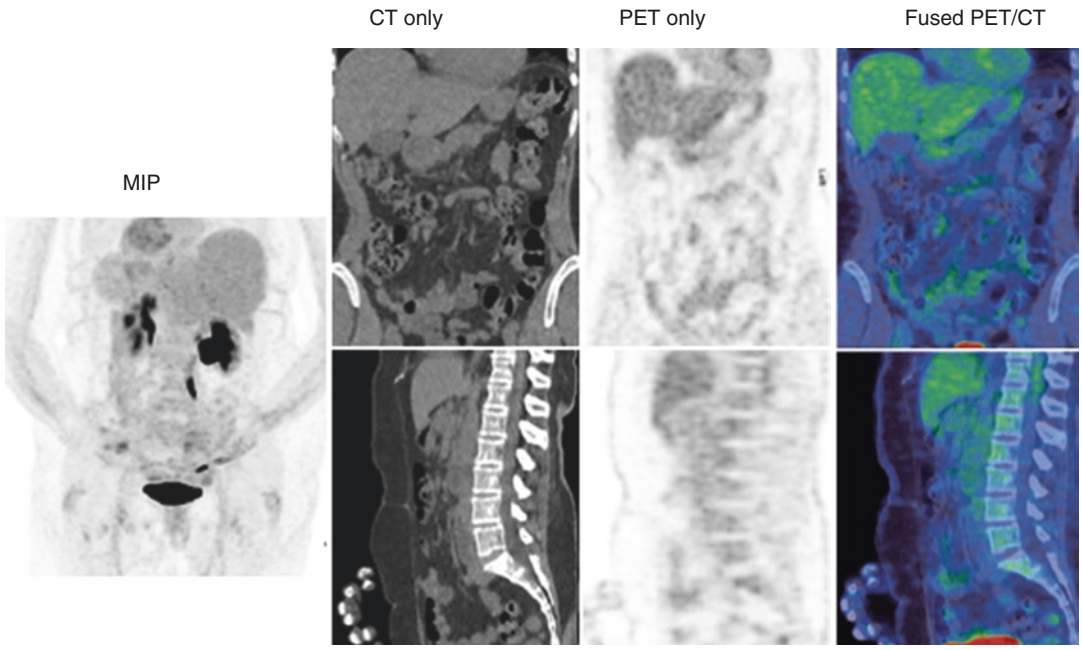

Scan Findings, Case 4A (Colitis) and 4B (Resolved Colitis on 3-month follow-up scan) After two years of complete remission (iCR) (stable sustained response) whilst on Pembrolizumab, the patient demonstrated pan-colonic mucosal thickening and intense ^{18}F-FDG avidity throughout the colon that was new compared to the previous scan. This is demonstrated on the maximum intensity projection (MIP), coronal and sagittal images. The patient did not report any symptoms at the time of the scan. This pattern resolved on follow-up scan at 3 months.

Interpretation ^{18}F-FDG PET/CT demonstrates incidental asymptomatic pancolitis as an adverse event of immunotherapy.

Teaching Points

- Immune-related adverse events (irAE) can occur due to upregulated unfettered autoimmunity.
- Some irAE may initially be asymptomatic and only identified on routine follow-up imaging [10].
- Due to many of these irAEs presenting in asymptomatic patients, reporting radiologists and nuclear medicine physicians need to be aware of these side effects as prompt recognition of drug toxicity is crucial for decision-making regarding further treatment options, including discontinuation of treatment [10].
- Symptomatic patients with colitis can present with diarrhoea or abdominal pain. Imaging features include diffuse colonic inflammation on CT—colonic wall thickening, peri-colonic fat stranding or mesenteric vessel engorgement. Segmental colitis may also occur. ^{18}F-FDG PET/CT may demonstrate pan-colonic intense uptake [11].

22.6 Case 5

Clinical Details A 60-year-old male was diagnosed with melanoma of the toe 15 years prior to recent presentation. The lesion was excised followed by chemotherapy in the patient's native country. More recently, the patient developed inguinal nodal metastases that were excised, but subsequently relapsed again. He was therefore started on combination immunotherapy of Ipilimumab and Nivolumab.

Images

Case 5A (axial):

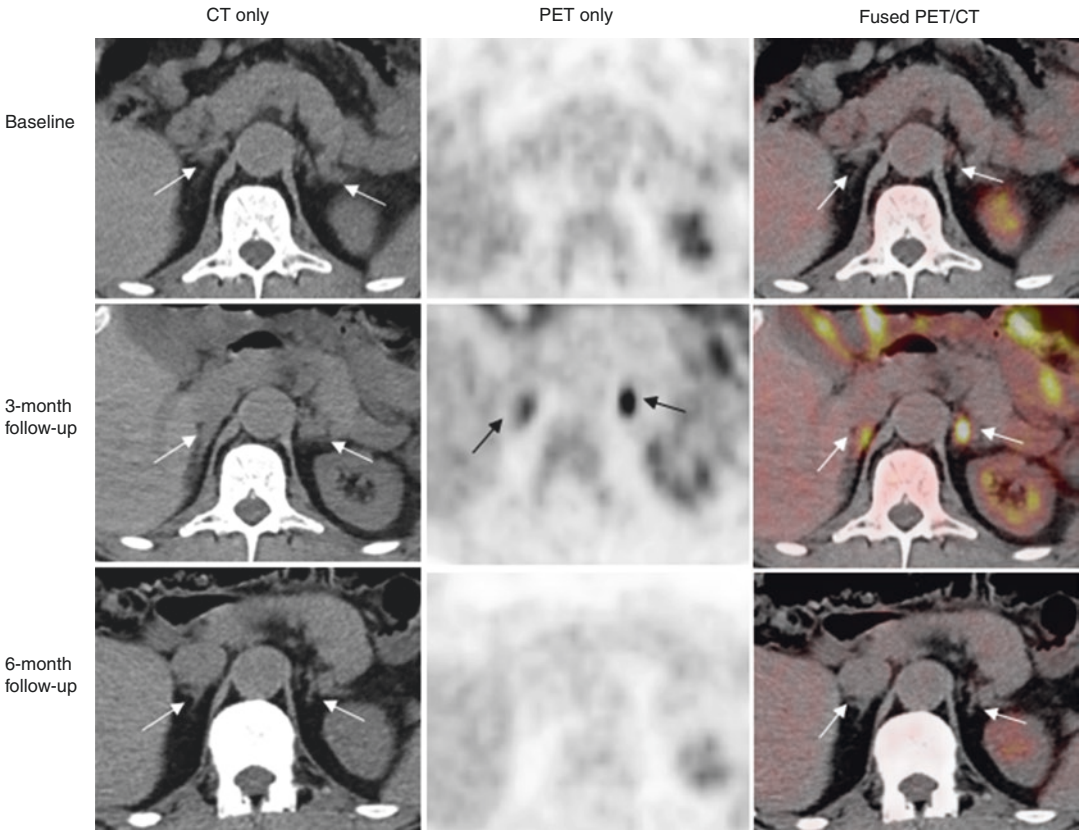

Scan Findings, Case 5A

Baseline imaging demonstrates normal adrenal glands bilaterally. Follow-up imaging at 3 months after commencement of combination immunotherapy demonstrates bilateral adrenal glands enlargement and increased ^{18}F-FDG activity (arrows). There was no focal nodularity. On the 6-month follow-up scan, the adrenal glands had reduced in size and demonstrated physiological activity. The patient was completely asymptomatic.

Interpretation Symmetrical smooth enlargement and increased uptake within both adrenal glands due to transient 'adrenalitis' [12].

Teaching Points

- Ipilimumab is more likely to be associated with severe or life-threatening toxicities compared to other immunotherapies such as Nivolumab or Pembrolizumab [13].
- Adrenalitis is usually asymptomatic; however, it may present with adrenal insufficiency [12].
- The management of these toxicities requires a multi-disciplinary approach. Mild adverse events can be managed conservatively. However, severe or life-threatening toxicities may require immunotherapy discontinuation, high dose corticosteroids or other immune-suppressive agents [13].
- Being aware of the various possible adverse reaction patterns can prevent 'misinterpretation'—for example adrenal hypertrophy and hypermetabolism may misinterpreted as 'new adrenal metastases' [12].

22.7 Case 6

Clinical Details A 53-year-old woman presented with an ulcerated nodule in the left mid back in 2009. Stage 3B melanoma was confirmed following shave excision. In 2016, the patient developed extensive disseminated metastatic disease and was started on combination immunotherapy of Ipilimumab and Nivolumab. The patient developed thyroiditis and pneumonitis whilst on treatment. Immunotherapy was temporarily stopped until the pneumonitis resolved. She was subsequently commenced on Pembrolizumab but demonstrated further disease progression.

Images
Case 6A:

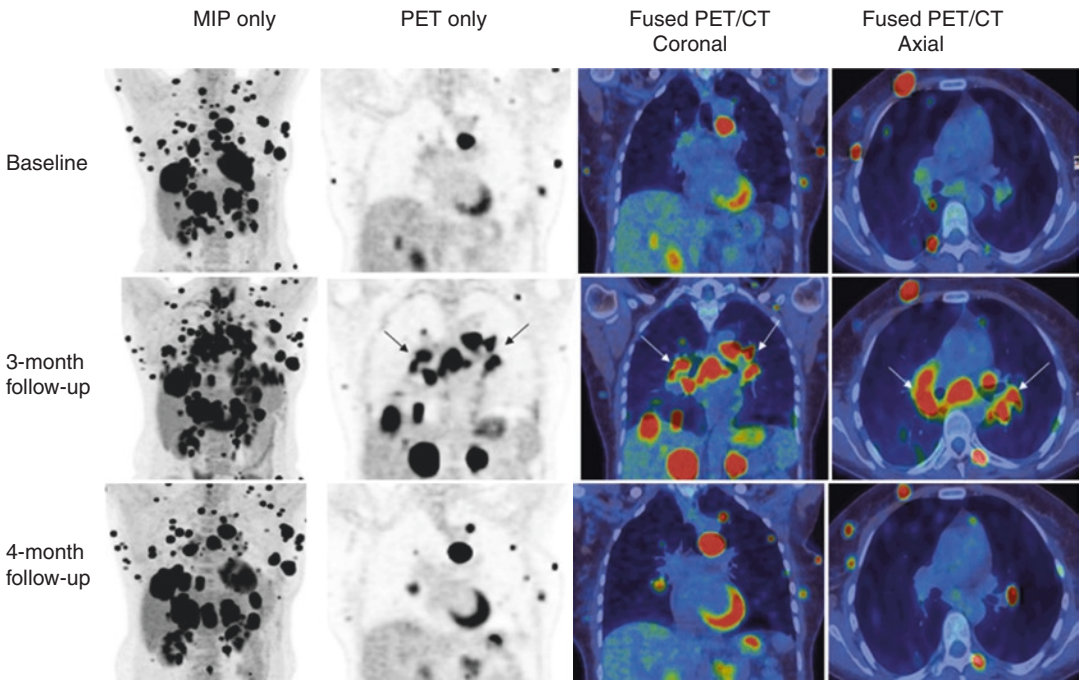

Case 6B:

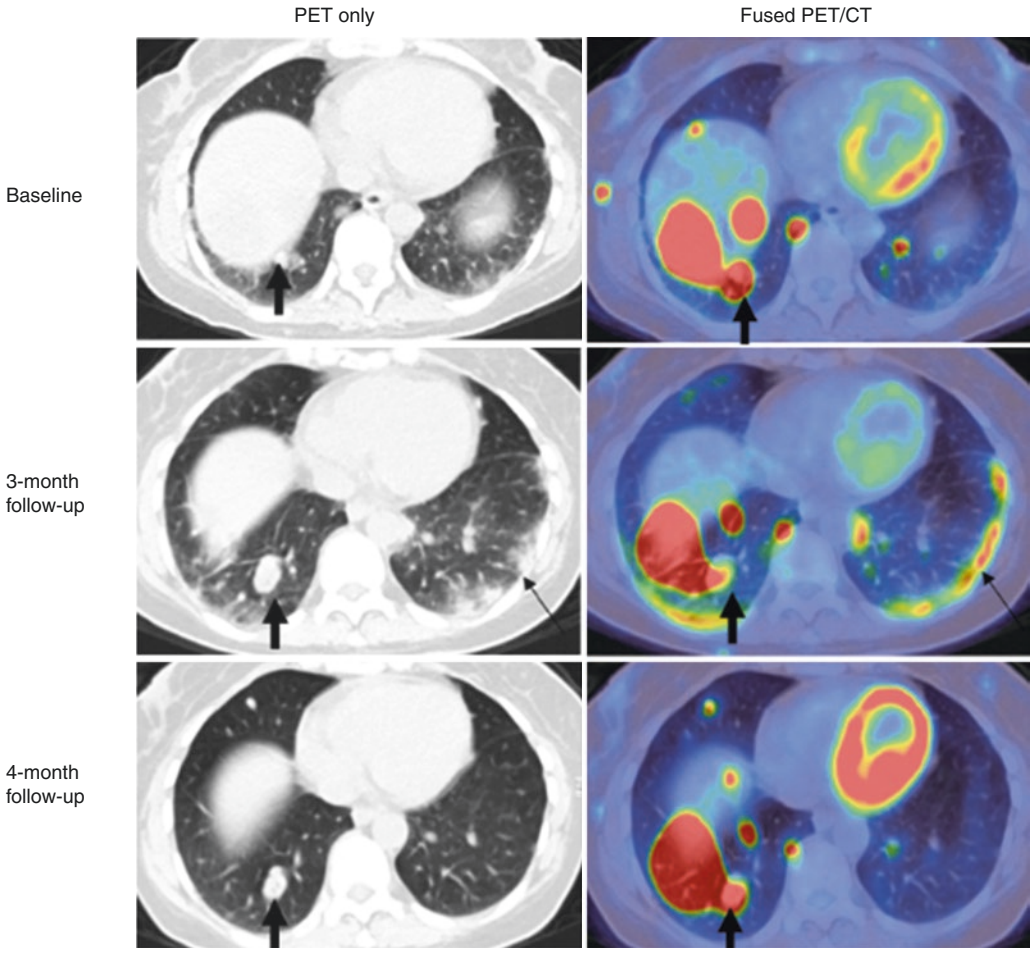
PET only
Fused PET/CT
Baseline
3-month follow-up
4-month follow-up

Scan Findings, Case 6A and 6B

Diffuse metastatic disease is shown throughout the body as seen on serial MIP images. The baseline ^{18}F-FDG PET/CT images demonstrate metastatic uptake in the lungs, liver, adrenal glands, bone and multifocal subcutaneous nodules. At 3-month follow-up, new diffuse mediastinal and hilar uptake (thin arrows) is seen as well as pneumonitis (^{18}F-FDG-avid opacification and nodularity at both lung bases) (thin black arrows), which resolved on subsequent imaging, with only the known metastases persisting (thick black arrows).

Case 6C (axial):

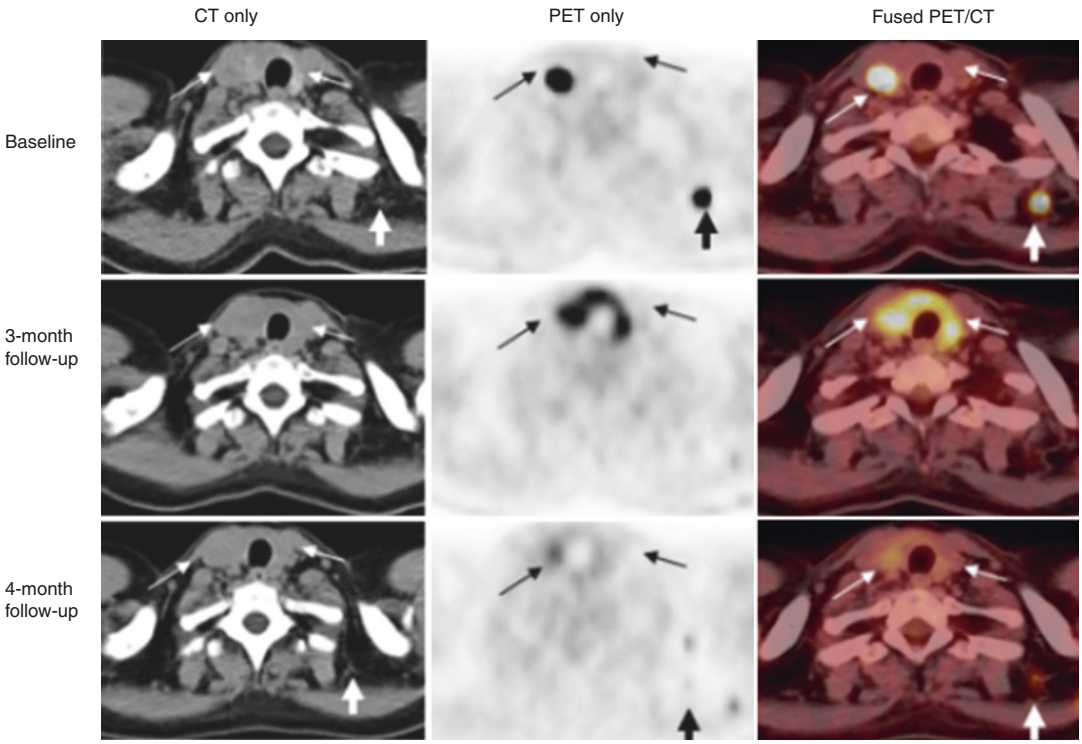

Scan findings 6c (thyroiditis)

Baseline axial images through the thyroid demonstrate a right thyroid nodule with intense avidity. At the 3-month follow-up after starting immunotherapy, increased FDG avidity is seen diffusely throughout the thyroid gland (thin arrows), which resolves on the 4-month follow-up images, highly suggestive of a thyroiditis. Resolution of a left supraclavicular fossa node is seen (thick arrows).

Interpretation ^{18}F-FDG PET/CT demonstrates disseminated metastatic disease with irAE of pneumonitis and thyroiditis following commencement of immunotherapy that subsequently resolved on temporary cessation of immunotherapy and treatment with steroids.

Teaching Points

- Patients with pneumonitis may present with dyspnoea or cough—which may progress to life-threatening respiratory failure. Severe cases may need intubation, treatment with corticosteroids and other immunosuppressants such as Infliximab [10].
- Cryptogenic organizing pneumonia is the most common imaging pattern of pneumonitis caused by Nivolumab. Other imaging features include diffuse ground-glass opacities, reticular opacities, consolidation and/or traction bronchiectasis on CT [14].
- Thyroiditis may initially present as thyrotoxicosis due to the release of thyroid hormone from inflamed thyroid tissue followed eventually by hypothyroidism. On ^{18}F- FDG PET/CT, it can present as diffuse, intense uptake in the thyroid gland [15] and absent uptake on ^{99m}Tc-pertechnetate thyroid imaging.
- Even in the context of widespread metastatic disease, various irAEs can occur which should not be immediately interpreted as progressive disease despite new lesions, new ^{18}F-FDG uptake or new nodal enlargement.

References

1. Robert C, Long GV, Brady B, et al. Nivolumab in previously untreated melanoma without BRAF mutation. N Engl J Med. 2015;372(4):320–30. https://doi.org/10.1056/NEJMoa1412082.
2. Hoos A. Development of immuno-oncology drugs – from CTLA4 to PD1 to the next generations. Nat Rev Drug Discov. 2016;15(4):235–47. https://doi.org/10.1038/nrd.2015.35.
3. Somarouthu B, Lee SI, Urban T, Sadow CA, Harris GJ, Kambadakone A. Immune-related tumour response assessment criteria: a comprehensive review. Br J Radiol. 2018;91(1084):20170457. https://doi.org/10.1259/bjr.20170457.
4. Eisenhauer EA, Therasse P, Bogaerts J, et al. New response evaluation criteria in solid tumours: revised RECIST guideline (version 1.1). Eur J Cancer. 2009;45(2):228–47. https://doi.org/10.1016/j.ejca.2008.10.026.
5. Wong ANM, McArthur GA, Hofman MS, Hicks RJ. The Advantages and challenges of Using FDG PET/CT for response assessment in melanoma in the era of targeted agents and immunotherapy. Eur J Nucl Med Mol Imaging. 2017;44(Suppl 1):67–77. https://doi.org/10.1007/s00259-017-3691-7.
6. Hoos A, Eggermont AMM, Janetzki S, et al. Improved endpoints for cancer immunotherapy trials. JNCI J Natl Cancer Inst. 2010;102(18):1388–97. https://doi.org/10.1093/jnci/djq310.
7. Seymour L, Bogaerts J, Perrone A, et al. iRECIST: guidelines for response criteria for use in trials testing immunotherapeutics. Lancet Oncol. 2017;18(3):e143–52. https://doi.org/10.1016/S1470-2045(17)30074-8.
8. McDermott D, Lebbé C, Hodi FS, et al. Durable benefit and the potential for long-term survival with immunotherapy in advanced melanoma. Cancer Treat Rev. 2014;40(9):1056–64. https://doi.org/10.1016/j.ctrv.2014.06.012.
9. Ratain MJ, Eckhardt SG. Phase II studies of modern drugs directed against new targets: if you are fazed, too, then resist RECIST. J Clin Oncol. 2004;22(22):4442–5. https://doi.org/10.1200/JCO.2004.07.960.
10. Widmann G, Nguyen VA, Plaickner J, Jaschke W. Imaging features of toxicities by immune checkpoint inhibitors in cancer therapy. Curr Radiol Rep. 2017;5(11):59. https://doi.org/10.1007/s40134-017-0256-2.
11. Kim KW, Ramaiya NH, Krajewski KM, et al. Ipilimumab-associated colitis: CT findings. Am J Roentgenol. 2013;200(5):W468–74. https://doi.org/10.2214/AJR.12.9751.
12. Haissaguerre M, Hescot S, Bertherat J, Chabre O. Expert opinions on adrenal complications in immunotherapy. Ann Endocrinol (Paris). 2018;79(5):539–44. https://doi.org/10.1016/J.ANDO.2018.07.002.
13. Haanen JBAG, Carbonnel F, Robert C, et al. Management of toxicities from immunotherapy: ESMO Clinical Practice Guidelines for diagnosis, treatment and follow-up. Ann Oncol. 2017;28(Suppl 4):119–42. https://doi.org/10.1093/annonc/mdx225.
14. Nishino M, Ramaiya NH, Awad MM, et al. PD-1 inhibitor-related pneumonitis in advanced cancer patients: radiographic patterns and clinical course. Clin Cancer Res. 2016;22(24):6051–60. https://doi.org/10.1158/1078-0432.CCR-16-1320.
15. de Filette J, Jansen Y, Schreuer M, et al. Incidence of thyroid-related adverse events in melanoma patients treated with pembrolizumab. J Clin Endocrinol Metab. 2016;101(11):4431–9. https://doi.org/10.1210/jc.2016-2300.

18F-FDG PET-CT in Treatment Response Evaluation: Multiple Myeloma

23

Cristina Nanni

23.1 Introduction

Multiple myeloma (MM) is a plasma cell (PC) disorder characterized by clonal proliferation of malignant PCs in the bone marrow (BM) or in extramedullary tissues. Neoplastic PCs typically synthesize monoclonal proteins (M-protein), which can be either intact immunoglobulins (Ig) or free light chains (FLC). MM accounts for approximately 1% of neoplastic diseases and 13% of hematologic cancers, accounting for 0.9% of all cancer deaths. In Western countries, the annual age-adjusted incidence is five cases per 100,000 persons. Lifetime risk of being diagnosed with MM is about 0.7%. The frequency of MM increases with age and reaches a peak in the sixth to seventh decades of life. The median age of the population affected is about 70 years old, and less than 10% of all patients come to the diagnosis between the second and fourth decades of life. Both genetic and environmental factors are hypothesized to explain racial differences in the incidence of the disease. The main known risk factors are occupational exposure to pesticides, petroleum, and ionizing radiation.

MM may develop de novo or, most commonly, represents the progression of a preceding monoclonal gammopathy of undetermined significance (MGUS). MM onset is clinically asymptomatic in 10–20% of cases and is detected by chance during routine laboratory examinations. In patients with a prior history of MGUS, the progression is characterized by the increase in serum and/or urinary M-protein, and medullary plasmacytosis, with consequent transformation in MM. In the remaining 80–90%, the most common symptoms, for frequency and severity, are skeletal involvement, renal failure, infectious morbidity, myeloid failure, hypercalcemia, neurological complications, hyperviscosity syndrome, and amyloidosis. Regardless of the presence of organ damage, MM is defined as active or symptomatic when at least one of the following conditions (defined as CRAB criteria) are present: hyperCalcemia, Renal failure, Anemia, or Bone lesions.

Recent guidelines identify as myeloma defining events also biomarkers of malignancy (as markers of early evolution to organ damage, i.e., more than 80% of risk within two years), which are defined as high medullary plasmacytosis (≥60%), and/or high serum FLC (sFLC) ratio (involved/uninvolved ≥100), and/or presence of more than one focal lesion identifiable with magnetic resonance (MRI). MM is characterized by the presence of at least one of CRAB criteria or biomarkers of malignancy and requires the start of treatment.

The median survival of patients with MM ranges from few months to more than 10 years

C. Nanni (✉)
Nuclear Medicine Department, AOU S.Orsola-Malpighi, Bologna, Italy
e-mail: cristina.nanni@aosp.bo.it

S. Fanti et al. (eds.), *Atlas of Clinical PET-CT in Treatment Response Evaluation in Oncology*,
https://doi.org/10.1007/978-3-030-68858-5_23

and is influenced by several clinical and laboratory parameters, some of which correlate directly with the tumor burden, others are an expression of the inherent malignancy of the tumor clone and others eventually depend on the patient's response to the therapy. It is generally agreed that a combination of the International Staging System (ISS) and cytogenetic abnormalities allows risk stratification. The ISS identified three subgroups of patients with different prognosis on the basis of two laboratory parameters, albumin and b2-microglobulin. Moreover, cytogenetic-molecular abnormalities split the patients in a high-risk group and standard risk. More recently, the revised ISS (R-ISS) was defined, incorporating high-risk FISH by t(4;14), t(14;16), and del(17p) with ISS and LDH. Other prognostic factors include the number of focal lesions detected at FDG PET/CT or MRI at staging, the age, the performance status, the presence of comorbidities, the presence of extramedullary disease, and the quality of response to therapy.

Due to the prolonged survival related to the introduction, in recent years, of several effective therapeutical lines into the clinical practice, it is becoming more important to have more and more precise prognostic factors and tools able to accurately define complete responders to therapy, beyond the clinical response. FDG PET/CT was proved to provide an important added value in terms of risk stratification for its accurate evaluation of the number of focal lesions at staging, the detection of extramedullary disease, the therapy assessment, and, in recent studies, the detection of minimal residual disease after therapy [1, 2].

23.2 Treatment Response Evaluation

The ability to distinguish between metabolically active and inactive sites of MM renders PET/CT an excellent tool to evaluate and monitor response to treatment. Despite a morphological stability of MM bone lesions, changes in metabolism (reflected in a modification of FDG uptake within lesions) are related to therapy effect and occur in a short time. They can be easily measured both visually and semiquantitatively [3], providing information on therapy efficacy and prognosis (PFS, TTP, OS). This characteristic is clinically relevant especially in patients with nonsecretory multiple myeloma, in whom the clinical assessment of therapy response cannot be achieved through the measurement of the M-component but can be effectively assessed only by changes in SUV max.

The prognostic role of FDG PET/CT for therapy assessment was explored after induction therapy and after transplantation in patients treated with ASCT, and after three cycles and pre-maintenance in patients not transplanted.

In general after treatment or early during therapy reaching a completely negative scan is proved to correlate with high-quality response to therapy.

23.2.1 Early Response

On day 7 after induction or before the first ASCT [4, 5] the persistence of >3 hot focal lesions is an early predictor of significantly shorter PFS and OS [6, 7]. In contrast, complete suppression of FDG avidity in FLs before ASCT is associated with significantly longer progression-free and overall survival. Negativity of PET/CT scans precedes by 12 months the onset of conventionally defined complete response, while resolution of focal lesions at MRI occurs later on (18-month probability of negative images: 92% with PET/CT vs. 29% with MRI).

23.2.2 After Therapy

After ASCT, negative PET/CT scans are associated with prolonged time to progression while a short time to progression can be anticipated in patients with increased metabolic demand persisting after therapy [7, 8]. Absence of FDG uptake after ASCT or improvement of PET response after high-dose therapy increases progression-free survival. At a PET/CT performed before and after allo-SCT, persistence of extramedullary disease after therapy is an inde-

pendent variable predicting for shorter progression-free and overall survival, while patients achieving and/or maintaining PET negativity perform significantly better [9].

23.2.3 PET/CT and MRI

In comparison with contrast-enhanced MRI, FDG PET/CT is related to faster normalization of imaging findings in patients with complete response or very good partial response after therapy [10]. It seems also that PET/CT is superior to whole body MRI (WBMRI) in detecting residual lesions after ASCT (74% vs. 52%, respectively), with a higher specificity and positive predictive value. Results of prospective studies aimed at evaluating the performance of diffusion-weighted imaging (DWI)-WBMRI in assessing response to therapy are still very limited: this is a relevant field of research for the next years.

23.2.4 Minimal Residual Disease

An interesting concept arising regarding the utility of FDG PET/CT in MM is its capacity to detect areas of minimal residual disease (MRD) after therapy that may remain focally active. It was noted, in fact, that among patients in clinical complete response after ASCT, patients with a persistently positive FDG scan had a higher probability of relapse in comparison to patients with a complete suppression of FDG uptake. It is interesting to notice that FDG PET/CT prior to maintenance can be used as a further risk stratificator in patients with negative minimal residual disease at flow cytometry. In fact, those who maintain a positive PET despite no MRD have a significantly worse PFS.

In this context, FDG PET/CT is a powerful tool for evaluating tumor activity and the metabolic response of the tumor clone to a given therapy. Furthermore, among patients in complete response after ASCT, negative PET/CT scans predict better outcomes when compared with persistent FDG avidity, reflecting potentially different levels of MRD [8, 11].

23.2.5 Image Interpretation

Interpretation issues in the evaluation of FDG PET/CT exist and are particularly relevant when therapy assessment is necessary. Doubts may arise especially in case of very recent long bone fractures, vertebral collapses, or recent metallic bone implants aimed at a better skeletal stabilization. Though the presence of metallic prosthesis is not a contraindication to the execution of an FDG PET/CT scan, some artifact may be generated both on PET image series and CT image series. This usually does not compromise significantly the diagnostic potential of the procedure since the diffuse and mild signal eventually detected around the prosthesis can be easily differentiated from a focal FDG accumulation that is expression of a myeloma localization. These artifacts can be minimized thanks to the introduction on new image reconstruction algorithms.

Due to possible interpretation issues and complexity of disease presentation and evolution, there is a need for standardization of PET reading. Mesguich et al. proposed some indications to interpret MM FDG PET/CT in staging, interim evaluation, and after therapy. However, these indications are not yet validated [12].

Recently new criteria (Italian myeloma criteria for PET USe: IMPeTUs) were proposed to standardize FDG PET/CT reading in MM patients. These include the visual interpretation of images based on the standard Deauville 5-point scale, taking into consideration different features of FDG distribution such as the bone marrow nonfocal uptake, focal bone lesions (site, number, and uptake), paramedullary lesions, and extramedullary lesions. These criteria are not validated yet but currently are under perspective and multicenter European validation [13].

Total lesion glycolysis (TLG) and metabolic tumor volume (MTV) are other methods proposed to assess the amount of active disease and its change as a consequence of therapy. TLG and MTV are 3-dimensional regions of interest drawn taking into consideration standard measurement parameters derived for all focal lesions with peak SUV above the background red marrow signal. In a recent study,

these measurements were performed on 192 patients affected by multiple myeloma at baseline and turned out to have significant survival implications, apparently more precise than quantitation of the glycolytic phenotype of active disease [14]. However, there is not a standardized and widely accepted software to harmonize these measurements in the clinical practice and much work is needed in the setting of clinical trials.

23.2.6 Non-FDG Tracers

Despite non-FDG tracers are under evaluation in MM, so far their role is limited to an increase in the detection rate at staging and no data are available for the therapy assessment (Figs. 23.1, 23.2, 23.3 and 23.4).

23.3 Multiple Myeloma Cases

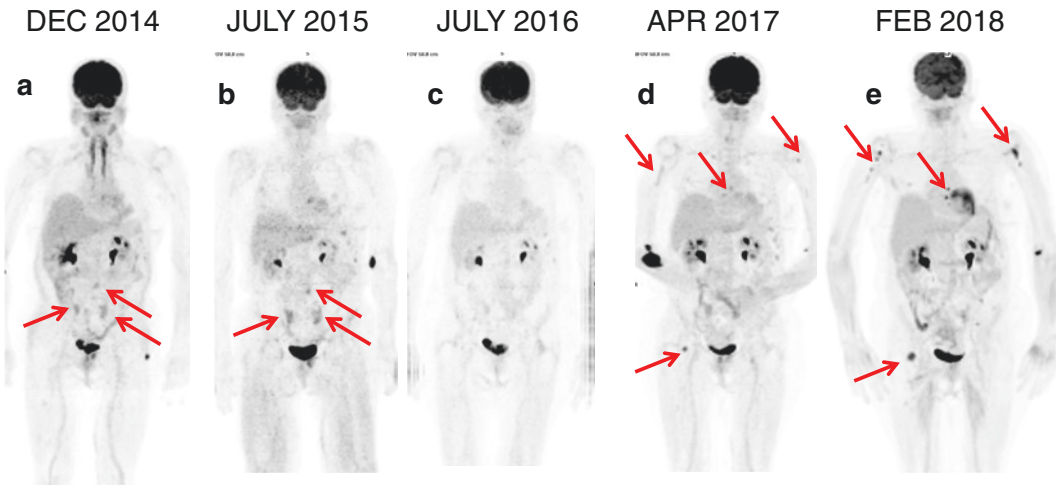

Fig. 23.1 A 74-year-old female with malignant melanoma. (**a**) FDG PET/CT performed at the end of therapy showing the persistence of 3 bone hypermetabolic focal lesions despite a clinical complete response. (**b**) Still positive but stable PET/CT during the maintenance therapy. Focal lesions were radiotreated. (**c**) Negative FDG PET/CT during maintenance and after EBRT showing a complete metabolic response. (**d**, **e**) FDG PET/CT showing a clear and progressive relapse requiring a further treatment. Teaching Point: non-complete normalization of FDG PET/CT despite a clinical complete response is a negative prognostic index predicting for a clinical relapse

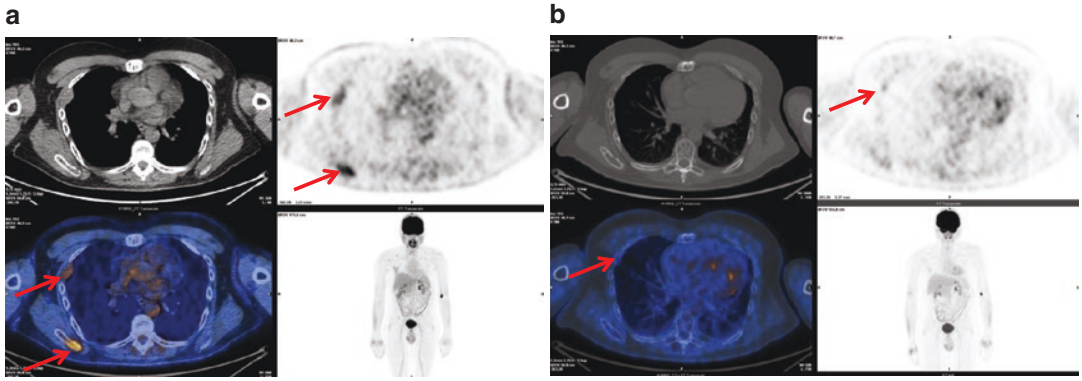

Fig. 23.2 A 63-year-old male with malignant melanoma. (**a**) FDG PET/CT performed at staging showing 2 bone hypermetabolic focal lesions with paramedullary involvement. (**b**) FDG PET/CT performed at the end of therapy still positive (although minimally) in the PM area. PFS of this patient was 11 months, conforming the prognostic value of FDG PET/CT in assessing therapy response. Teaching Point: non-complete normalization of FDG PET/CT in paramedullary sites of disease is a negative prognostic index predicting for a clinical relapse

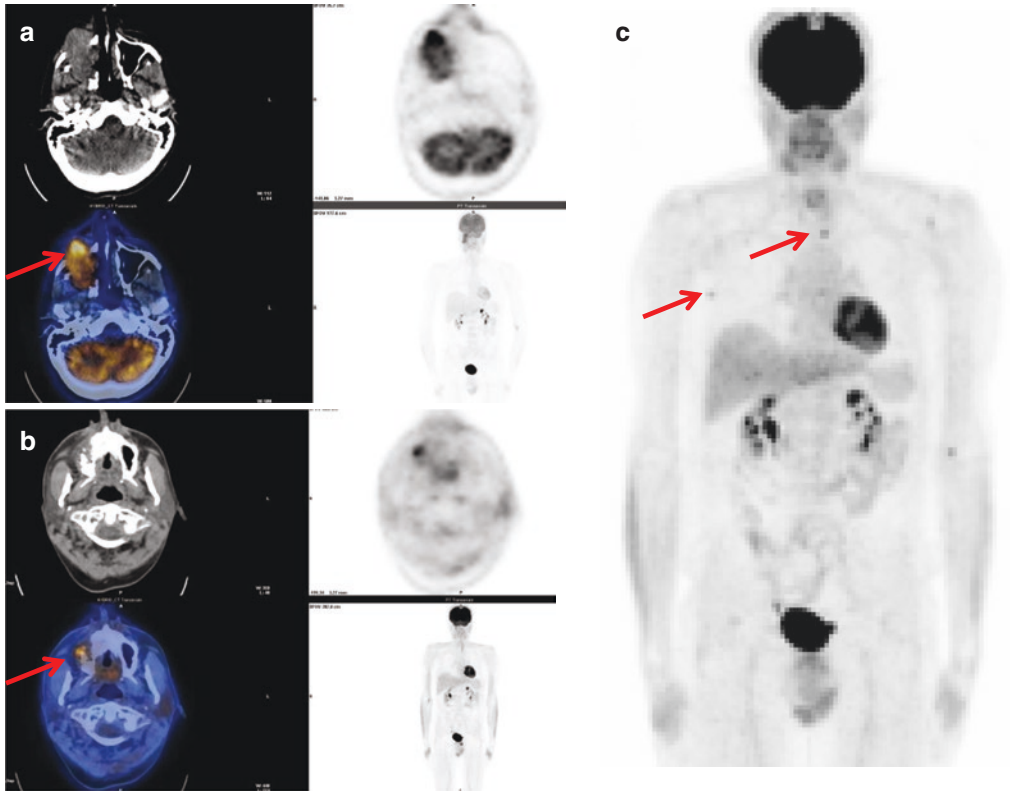

Fig. 23.3 A 71-year-old male. (**a**) FDG PET/CT performed for the evaluation of a plasmacytoma of the right maxillary sinus showing one hot focal lesion with paramedullary involvement. (**b**) FDG PET/CT performed at the end of therapy still positive in the PM area. (**c**) One year after the staging there was a disease relapse at FDG PET/CT showing two hot focal lesions. Teaching Point: non-complete normalization of FDG PET/CT after therapy in paramedullary sites of disease in plasmacytoma is a negative prognostic index predicting for an early relapse

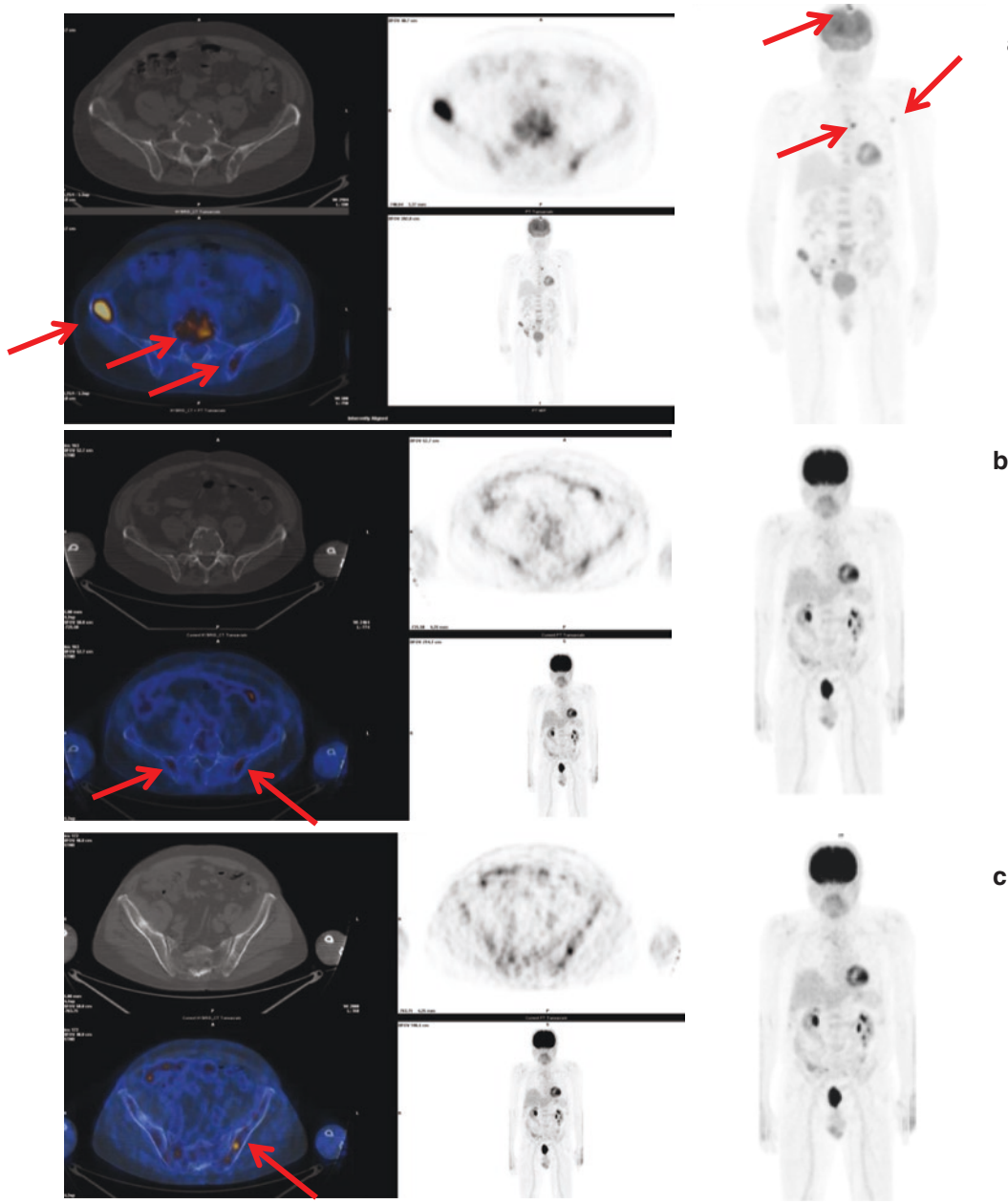

Fig. 23.4 A 69-year-old male. (**a**) FDG PET/CT performed at staging showing 6 bone hypermetabolic focal lesions. (**b**) After induction FDG PET/CT still positive. (**c**) FDG PET/CT performed at the end of therapy showing a clear focal relapse in the bony pelvis. Teaching Point: non-complete normalization of FDG PET/CT after induction is a negative prognostic index predicting for an early relapse

References

1. Moreau P, San Miguel J, Sonneveld P, Mateos MV, Zamagni E, Avet-Loiseau H, Hajek R, Dimopoulos MA, Ludwig H, Einsele H, Zweegman S, Facon T, Cavo M, Terpos E, Goldschmidt H, Attal M, Buske C, ESMO Guidelines Committee. Multiple myeloma: ESMO clinical practice guidelines for diagnosis, treatment and follow-up. Ann Oncol. 2017;28(Suppl 4): 52–61.
2. Cavo M, Terpos E, Nanni C, Moreau P, Lentzsch S, Zweegman S, Hillengass J, Engelhardt M, Usmani SZ, Vesole DH, San-Miguel J, Kumar SK, Richardson PG, Mikhael JR, da Costa FL, Dimopoulos MA, Zingaretti C, Abildgaard N, Goldschmidt H, Orlowski RZ, Chng WJ, Einsele H, Lonial S, Barlogie B, Anderson KC, Rajkumar SV, Durie BGM, Zamagni E. Role of 18F-FDG PET/CT in the diagnosis and management of multiple myeloma and other plasma cell disorders: a consensus statement by the International Myeloma Working Group. Lancet Oncol. 2017;18(4):e206–17.
3. Boellaard R. Standards for PET image acquisition and quantitative data analysis. J Nucl Med. 2009;50:11S–20S.
4. Zamagni E, et al. A prospective comparison of 18F-fluorodeoxyglucose positron emission tomography-computed tomography, magnetic resonance imaging and whole-body planar radiographs in the assessment of bone disease in newly diagnosed multiple myeloma. Haematologica. 2007;92:50–5.
5. Bartel TB, et al. F18-fluorodeoxyglucose positron emission tomography in the context of other imaging techniques and prognostic factors in multiple myeloma. Blood. 2009;114:2068–76.
6. Usmani SZ, et al. Prognostic implications of serial 18-fluoro-deoxyglucose emission tomography in multiple myeloma treated with total therapy 3. Blood. 2013;121:1819–23.
7. Zamagni E, et al. Prognostic relevance of 18-F FDG PET/CT in newly diagnosed multiple myeloma patients treated with up-front autologous transplantation. Blood. 2011;118:5989–95.
8. Moreau P, Attal M, Caillot D, Macro M, Karlin L, Garderet L, Facon T, Benboubker L, Escoffre-Barbe M, Stoppa AM, Laribi K, Hulin C, Perrot A, Marit G, Eveillard JR, Caillon F, Bodet-Milin C, Pegourie B, Dorvaux V, Chaleteix C, Anderson K, Richardson P, Munshi NC, Avet-Loiseau H, Gaultier A, Nguyen JM, Dupas B, Frampas E, Kraeber-Bodere F. Prospective evaluation of magnetic resonance imaging and [18F]fluorodeoxyglucose positron emission tomography-computed tomography at diagnosis and before maintenance therapy in symptomatic patients with multiple myeloma included in the IFM/DFCI 2009 trial: results of the IMAJEM Study. J Clin Oncol. 2017;35(25):2911–8. https://doi.org/10.1200/JCO.2017.72.2975.
9. Patriarca F, et al. The role of positron emission tomography with 18F-fluorodeoxyglucose integrated with computed tomography in the evaluation of patients with multiple myeloma undergoing allogeneic stem cell transplantation. Biol Blood Marrow Transplant. 2015;21(6):1068–73.
10. Spinnato P, et al. Contrast enhanced MRI and (1)(8)F-FDG PET-CT in the assessment of multiple myeloma: a comparison of results in different phases of the disease. Eur J Radiol. 2012;81:4013–8.
11. Kumar S, et al. International Myeloma Working Group consensus criteria for response and minimal residual disease assessment in multiple myeloma. Lancet Oncol. 2016;17:e328–46.
12. Mesguich C, et al. State of the art imaging of multiple myeloma: comparative review of FDG PET/CT imaging in various clinical settings. Eur J Radiol. 2014;83:2203–23.
13. Nanni C, et al. Image interpretation criteria for FDG PET/CT in multiple myeloma: a new proposal from an Italian expert panel IMPeTUs (Italian myeloma criteria for PET USe). Eur J Nucl Med Mol Imaging. 2016;43:414–21.
14. McDonald JE, et al. Assessment of total lesion glycolysis by 18F FDG PET/CT significantly improves prognostic value of GEP and ISS in myeloma. Clin Cancer Res. 2017;23(8):1981–7.

24

^{18}F-FDG PET-CT and ^{18}F-NaF in Treatment Response Evaluation: Bone Metastases and Bone Tumours

Gary J. R. Cook and Sharjeel Usmani

24.1 Introduction

The ability of functional imaging to detect and monitor metastatic disease in the skeleton, with advantages over conventional imaging such as bone scintigraphy or computed tomography (CT), has led to positron emission tomography (PET), particularly with the tracer ^{18}F-fluorodeoxyglucose (^{18}F-FDG), to be adopted into clinical practice [1–4]. This is most commonly in breast cancer, where superiority over conventional methods and prognostic ability have been shown [5–7]. While ^{18}F-FDG is a tumour-specific agent, measuring glucose metabolism in tumour cells, ^{18}F-sodium fluoride (^{18}F-NaF) is a bone-specific tracer with uptake related to local osteoblastic activity and mineralisation and may also be useful in breast, prostate and other cancers [8–12]. The similarity in uptake mechanism of ^{18}F-NaF to conventional bone scintigraphy agents such as ^{99m}Tc-methylene diphosphonate means that it is subject to the flare phenomenon where there can be an initial increase in activity during an osteoblastic healing phase in metastases after successful therapy. Similarly, CT can show an increase in sclerosis as a result of healing following successful treatment. The relationship between tumour activity and osteoblastic activity in skeletal metastases may therefore be complex and a careful assessment with full knowledge of the length and type of therapy is essential to accurately monitor disease response.

G. J. R. Cook (✉)
Cancer Imaging Department, School of Biomedical Engineering and Imaging Sciences, King's College London, London, UK

King's College London and Guy's & St Thomas' PET Centre, St Thomas' Hospital, London, UK
e-mail: gary.cook@kcl.ac.uk

S. Usmani
Department of Nuclear Medicine, Kuwait Cancer Control Center (KCCC), Shuwaikh, Kuwait

S. Fanti et al. (eds.), *Atlas of Clinical PET-CT in Treatment Response Evaluation in Oncology*,
https://doi.org/10.1007/978-3-030-68858-5_24

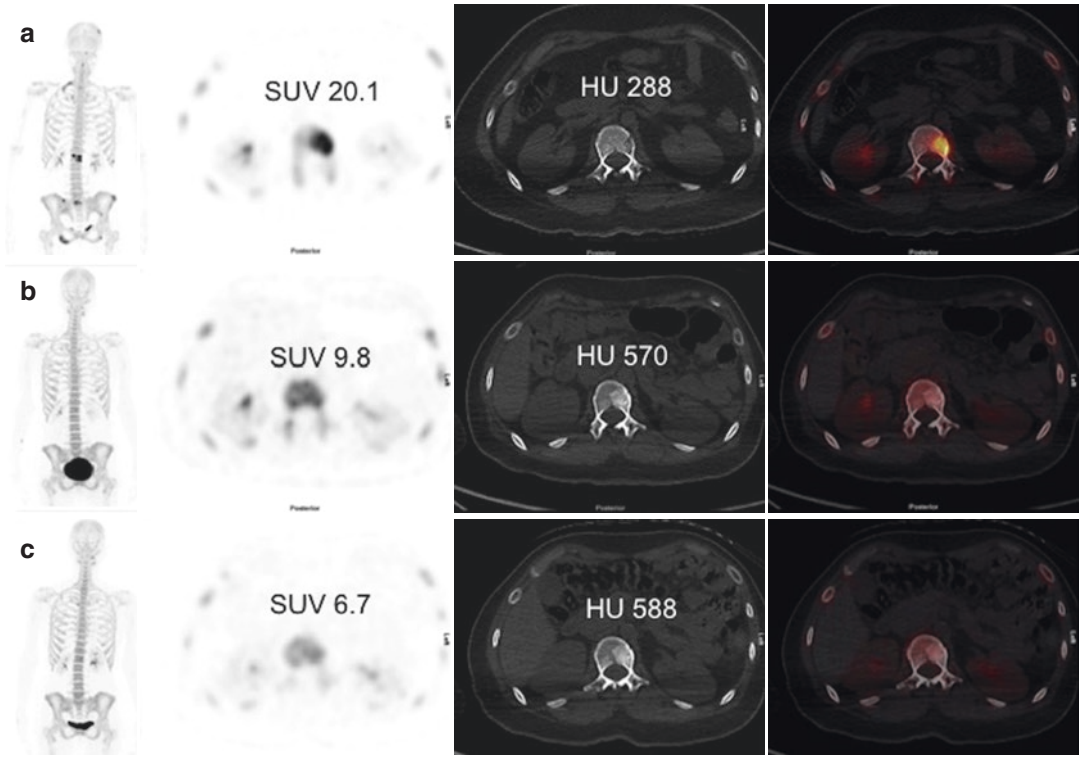

Case 1: A 32-year-old woman with metastatic left breast cancer on endocrine therapy. (**a**) Baseline ^{18}F-NaF PET/CT shows osteoblastic lesions at left parietal bone, right first, seventh, left tenth ribs, L1 vertebral body, sacrum, bilateral iliac and ischial bones. (**b**, **c**) Follow-up scans show resolution of abnormal ^{18}F-NaF activity in keeping with complete response to treatment.

Teaching Point

Note a lytic metastasis shows sclerosis on CT indicating osteoblastic repair as a result of successful treatment with persistent CT sclerosis after ^{18}F-NaF osteoblastic activity has reduced.

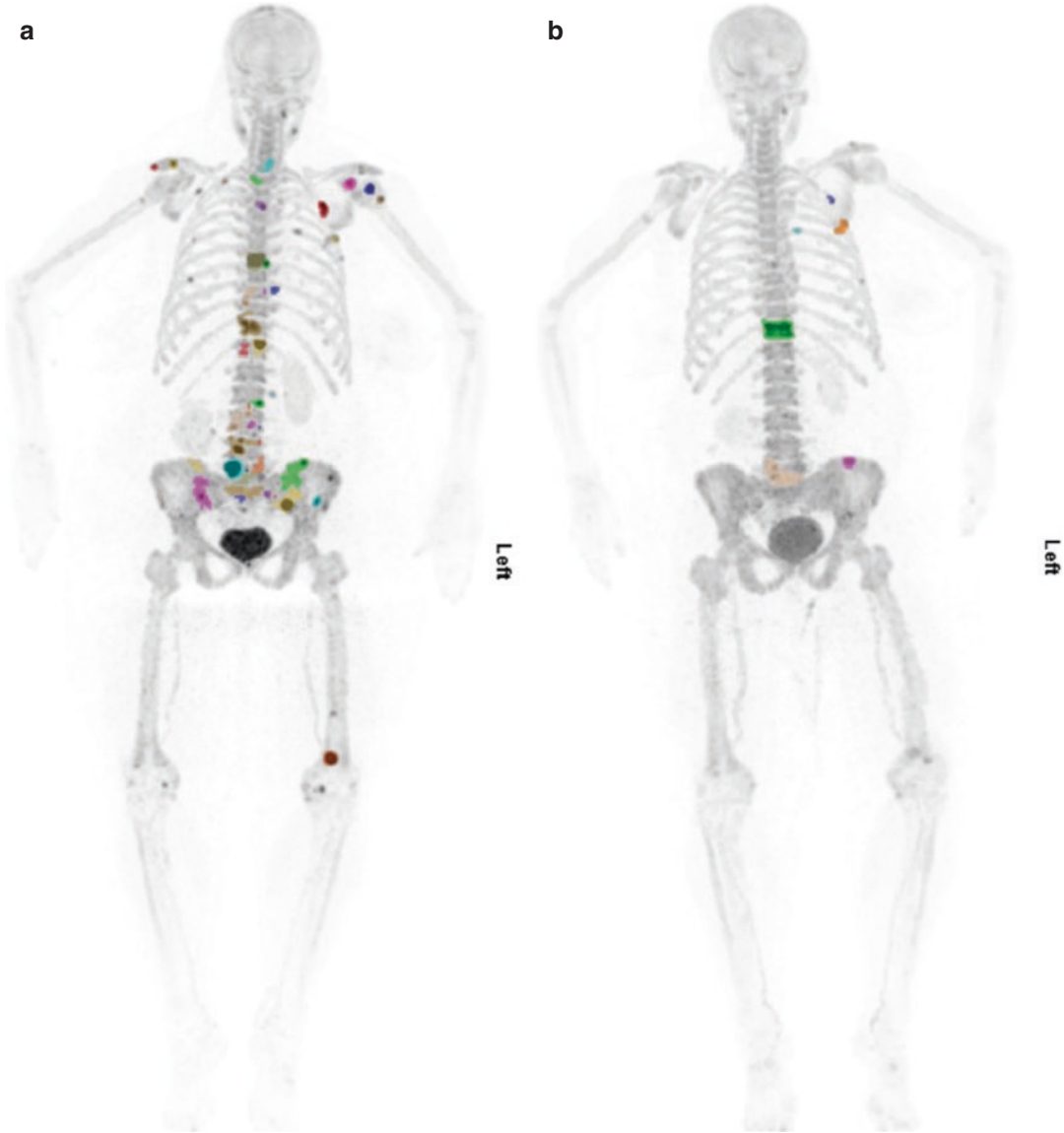

Case 2: A 73-year-old woman with metastatic left breast cancer on letrozole, palbociclib, and faslodex. (**a**) Whole-body ^{18}F-NaF PET/CT image demonstrates multiple osteoblastic metastases. Skeletal tumour burden (TLF_{15} and FTV_{15}) is calculated by semiautomatic VOI delineation in all metastatic lesions with SUVmax threshold of 15. All non-metastatic VOIs (bladder and kidneys) are subtracted from the analysis. Skeletal tumour burden was moderately increased (TLF_{15} = 2607). (**b**) Follow-up scan shows a significant decrease in number and intensity of osteoblastic lesions with skeletal tumour burden reduced by 70% (TLF_{15} = 780).

Teaching Point

It may be helpful to quantify changes in skeletal metastasis activity and volume when monitoring response to therapy.

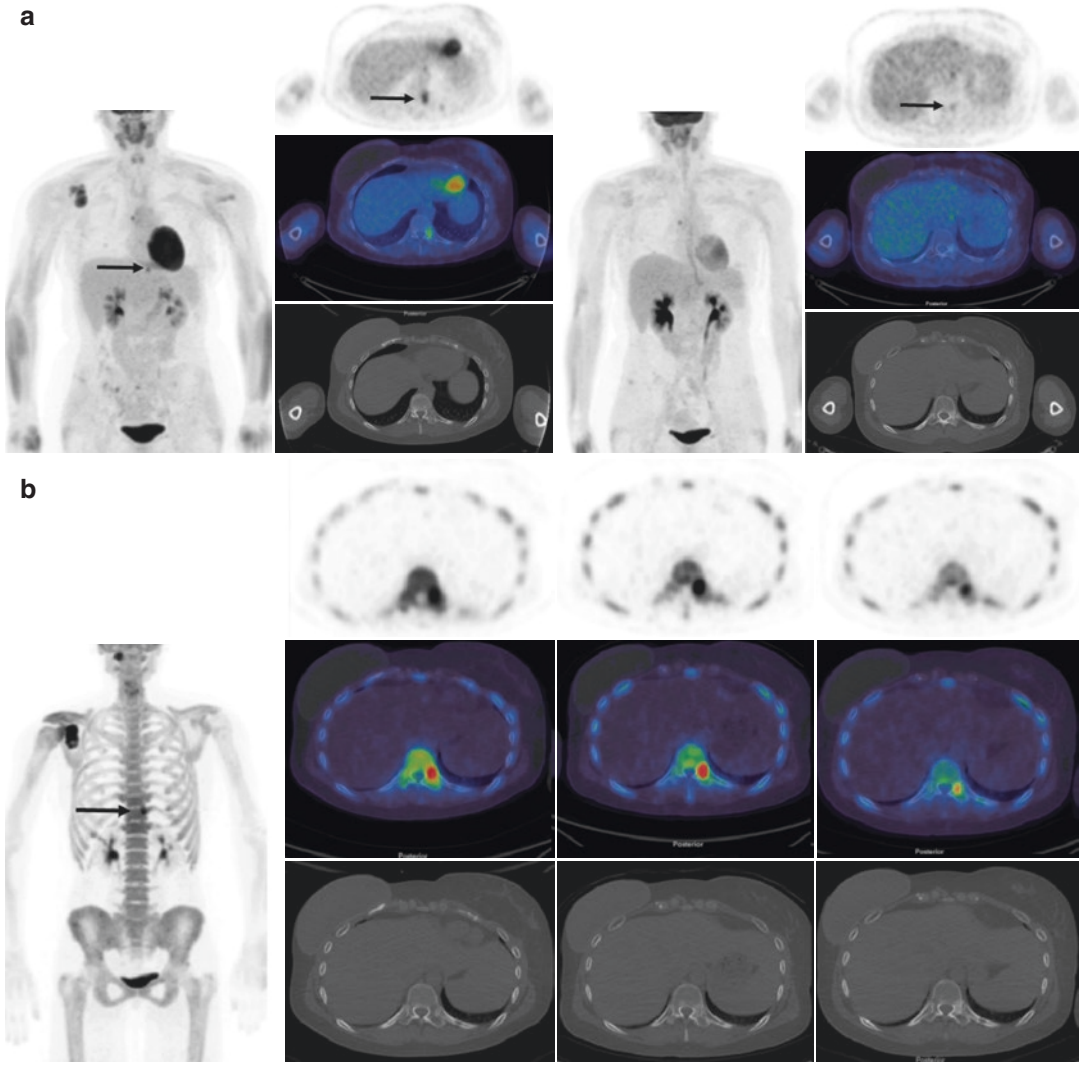

Case 3: A 37-year-old woman with bone predominant metastatic breast cancer before and 8 weeks after commencing endocrine-based systemic therapy. (**a**) Baseline and 8-week ^{18}F-FDG MIP and transaxial scans. (**b**) Baseline MIP and transaxial 0-, 8- and 12-week ^{18}F-NaF scans.

A metabolic response can be seen in a T11 left pedicle (and right scapula) metastasis where the SUVmax decreased from 5.3 to 2.4. The ^{18}F-NaF scans show an initial increase in uptake at 8 weeks followed by a decrease at 12 weeks in keeping with the flare phenomenon (SUVmax 26.5, 40.6, 18.1, respectively).

Teaching Point

The flare phenomenon is relatively common with ^{18}F-NaF PET but not with ^{18}F-FDG [5].

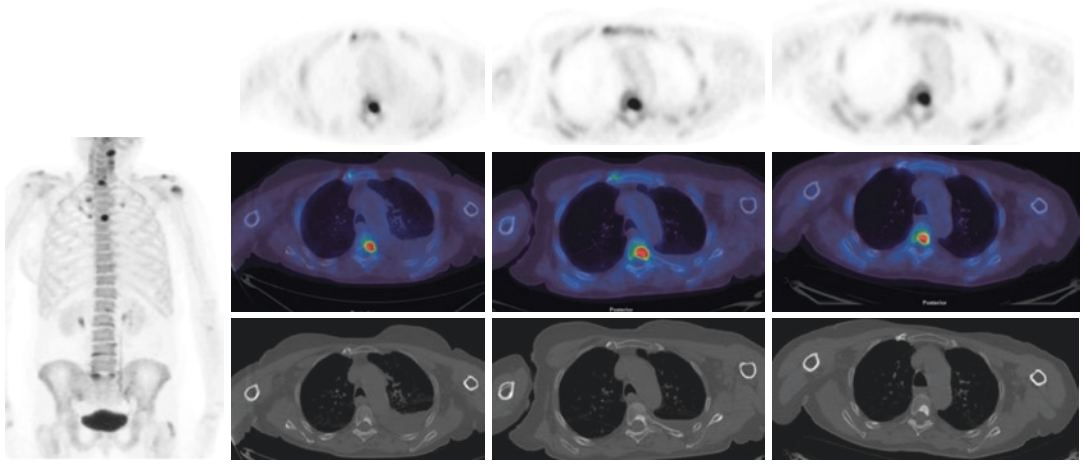

Case 4: A 77-year-old woman with bone predominant metastatic breast cancer treated with endocrine-based systemic therapy. Baseline ^{18}F-NaF MIP and baseline, 8- and 12-week transaxial images at T5.

An initial increase in activity at 8 weeks is followed by a subsequent decrease at 12 weeks in keeping with the flare phenomenon (SUVmax 36.3, 47.3, 34.4, respectively). The woman continued to have a good clinical response to treatment.

Teaching Point

The flare phenomenon is probably maximal at approximately 6–8 weeks and if it is suspected then a subsequent scan after a further interval may help to clarify as a subsequent reduction in activity would be expected [5].

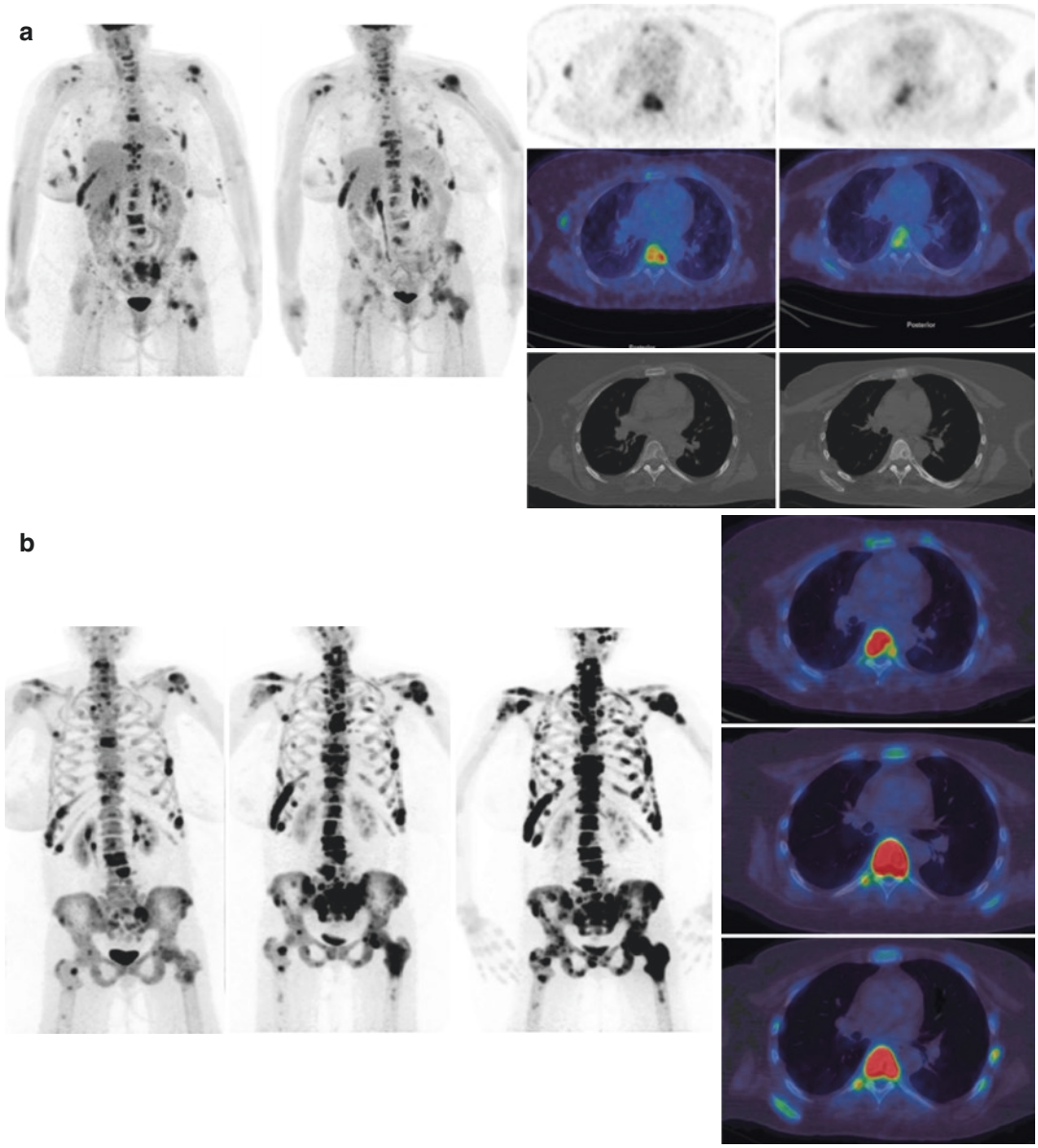

Case 5: A 44-year-old woman with bone predominant metastatic breast cancer treated with endocrine-based systemic therapy. (**a**) ^{18}F-FDG MIP and transaxial images at T6 at baseline and 8 weeks and (**b**) corresponding ^{18}F-NaF MIP and images at baseline, 8 and 12 weeks.

There is a reduction in ^{18}F-FDG uptake in some metastases (e.g. mid-thoracic and mid-lumbar spine, T6 SUVmax reduces from 16.2 to 6.5) with an increase in others (e.g. right ilium, right humerus and scapula) in keeping with a mixed response. There is a clear persistent increase in ^{18}F-NaF activity in most metastases, and this patient continued to show disease progression clinically.

Teaching Point

A mixed response to systemic therapy is not uncommon.

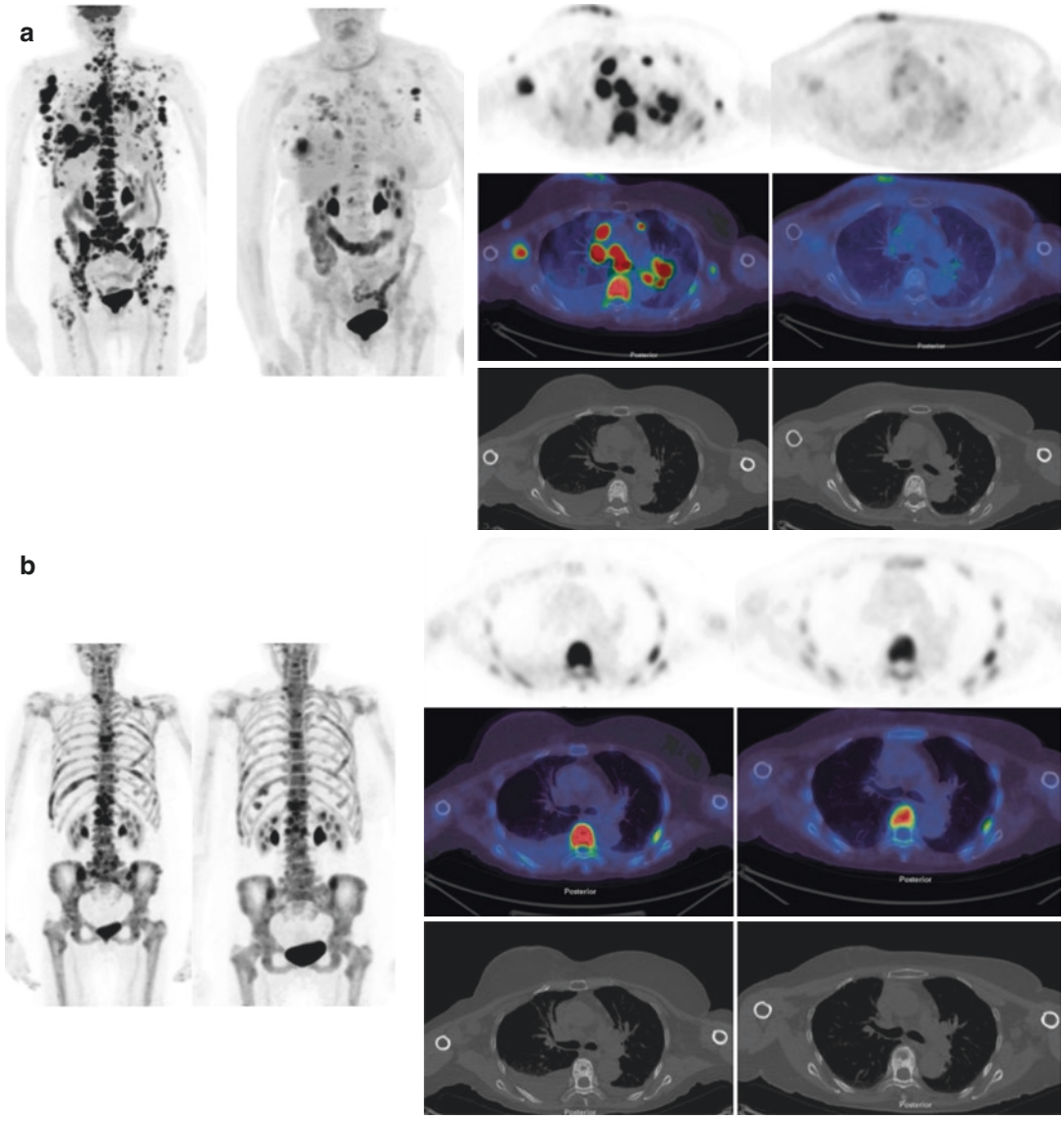

Case 6: A 67-year-old woman with bone predominant metastatic breast cancer (and nodal disease) treated with endocrine-based systemic therapy. (**a**) ^{18}F-FDG MIP and transaxial images at the T6 level and (**b**) corresponding ^{18}F-NaF images.

There is a clear reduction in ^{18}F-FDG uptake in bone and nodal metastases (T6 SUVmax 17.4 and 1.9, respectively) with a corresponding reduction in ^{18}F-NaF activity (T6 SUVmax 33.9 and 23.4, respectively) in keeping with a partial metabolic response.

Teaching Point

A flare phenomenon is not always seen with ^{18}F-NaF PET and often there is corresponding reduction in uptake between ^{18}F-NaF and ^{18}F-FDG after successful treatment at early time points [5].

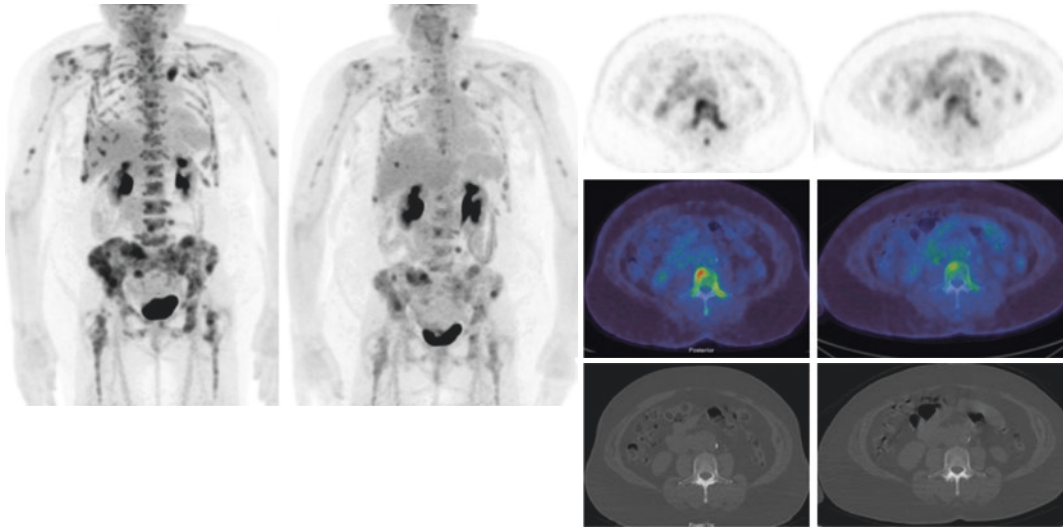

Case 7: A 67-year-old woman with bone predominant metastatic breast cancer treated with endocrine-based systemic therapy. ^{18}F-FDG PET MIP and transaxial L4 images at baseline and 8 weeks.

There is a clear reduction in activity at all sites (L4 SUVmax 11.4 and 5.0, respectively) in keeping with a partial metabolic response.

Teaching Point

Unequivocal reduction in ^{18}F-FDG activity in skeletal metastases indicates a metabolic response to treatment and also infers a better prognosis from patients who do not respond [5–7].

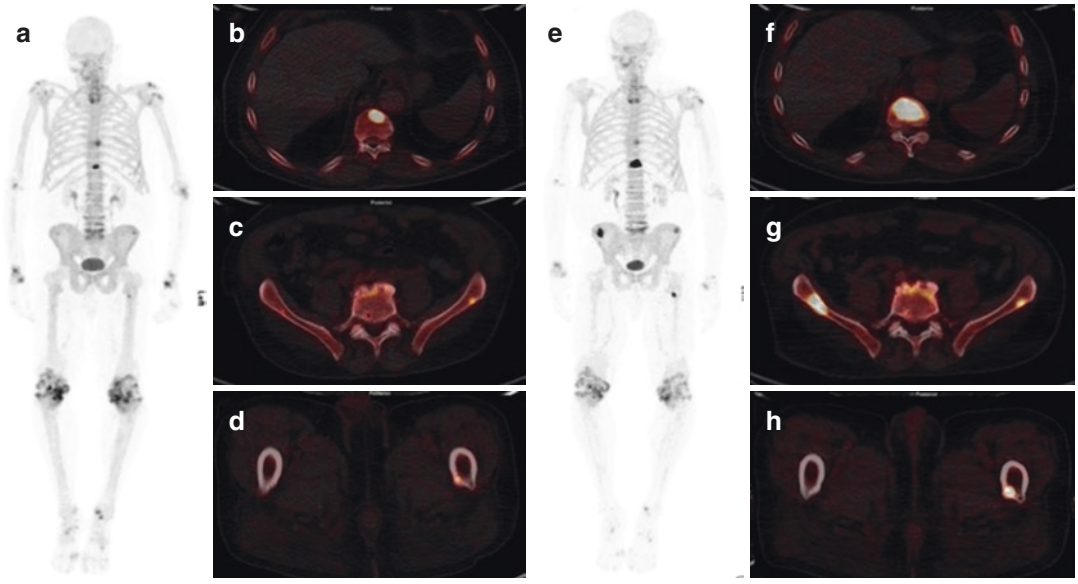

Case 8: A 72-year-old man with metastatic prostate cancer to bone and lymph nodes on hormone therapy. Now presented with rising PSA (**a**–**d**). Initial ^{18}F-NaF PET/CT shows sclerotic lesions with corresponding ^{18}F-NaF uptake at T11, bilateral iliac bones and proximal shaft of left femur (**e**–**h**). Follow-up ^{18}F-NaF-PET/CT after therapy shows increasing pattern of ^{18}F-NaF uptake. Findings are consistent with disease progression as there had been no new treatment or change in treatment to cause a flare.

Teaching Point

A knowledge of the timing and type of therapy is essential when interpreting ^{18}F-NaF PET to help differentiate progressive disease from the flare phenomenon.

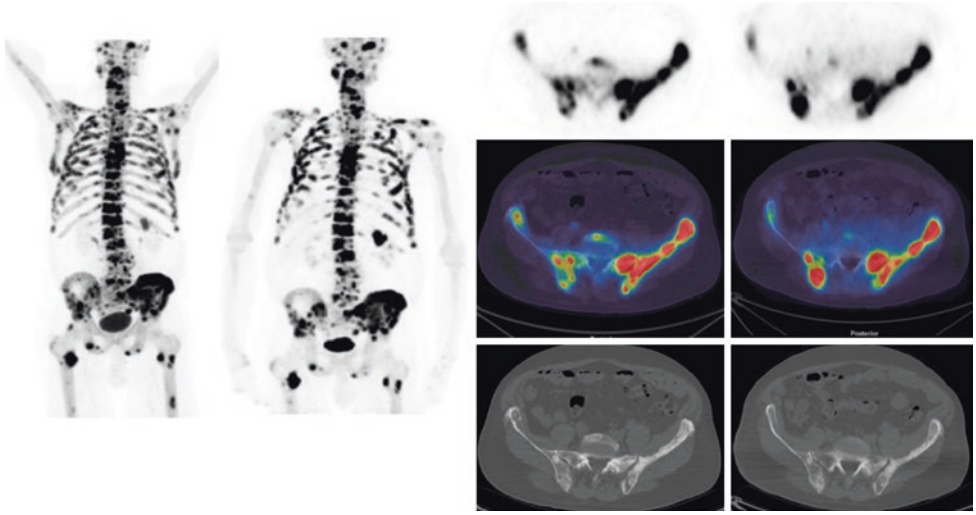

Case 9: A 75-year-old man with bone predominant metastatic prostate cancer treated with docetaxel chemotherapy. ^{18}F-NaF MIP and transaxial pelvis images at baseline and after three cycles of chemotherapy.

The baseline and 8-week images show similar levels of uptake in most sites of disease (L ilium SUVmax 64.5 and 64.2, respectively) in keeping with stable metabolic disease.

Teaching Point

Measuring SUVs may be helpful in assessing treatment response when the qualitative interpretation is difficult.

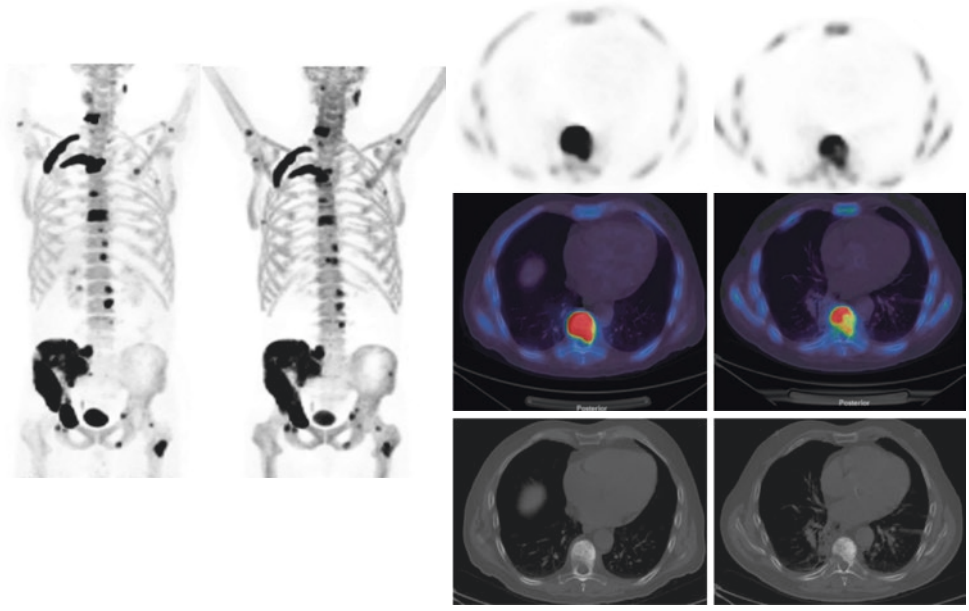

Case 10: A 79-year-old man with bone predominant metastatic prostate cancer treated with docetaxel chemotherapy. [18]F-NaF MIP and transaxial T9 images at baseline and after three cycles of chemotherapy. A reduction in uptake is present in some lesions (T9 SUVmax 68.8 and 34.5, respectively) in keeping with a partial metabolic response. Some lesions show a small increase in activity (e.g. humeri, left ilium) that was assumed to represent the flare phenomenon in some metastases as the patient was significantly improved clinically.

Teaching Point

It may be difficult to differentiate a mixed response to treatment from a combination of treatment response and flare phenomenon and other clinical factors may be required to help interpret the images.

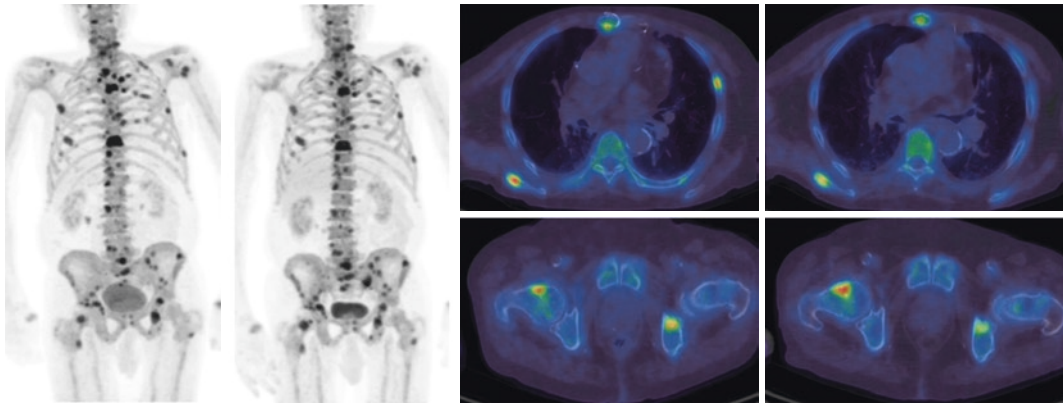

Case 11: A 91-year-old man with bone predominant metastatic prostate cancer treated with docetaxel chemotherapy. ^{18}F-NaF MIP and transaxial thoracic and pelvis images at baseline and after three cycles of chemotherapy.

The baseline and 8-week images show a reduction in activity in most metastases (right scapula SUVmax 20.3 and 14.3, respectively; T9 SUVmax 42.6 and 33.1, respectively) while occasional metastases show an increase (right femoral neck SUVmax 32.6 and 41.0, respectively). This was interpreted as a partial metabolic response with some lesions showing the flare phenomenon as the patient was improving clinically.

Teaching Point

It is not uncommon to see some heterogeneity of response in widespread skeletal metastases with ^{18}F-NaF PET and is more common than with ^{18}F-FDG.

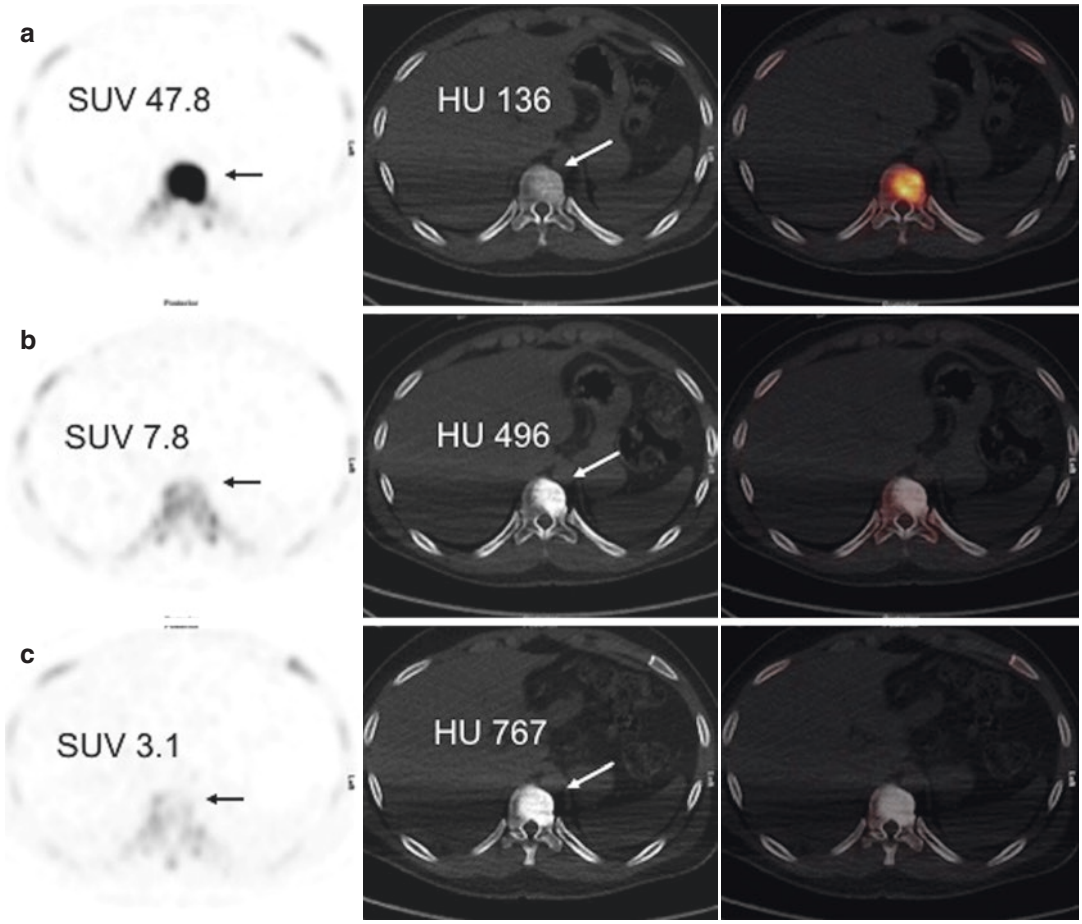

Case 12: A 24-year-old man with metastatic lung cancer to the bone treated with chemotherapy and immunotherapy (Alectinib). (**a**) Baseline transaxial ^{18}F-NaF PET/CT shows a sclerotic lesion (arrow) with corresponding ^{18}F-NaF uptake (arrow) at T8. (**b**, **c**) Follow-up ^{18}F-NaF-PET/CT scans during therapy show a decreasing pattern of ^{18}F-NaF uptake on PET (black arrow), however with increased sclerosis as a repair mechanism shown by an increase in Hounsfield units (HU) on CT (white arrow). Findings indicate a response to therapy.

Teaching Point

Underlying osteoblastic activity on functional ^{18}F-NaF-PET can return to normal despite persistent sclerosis on CT.

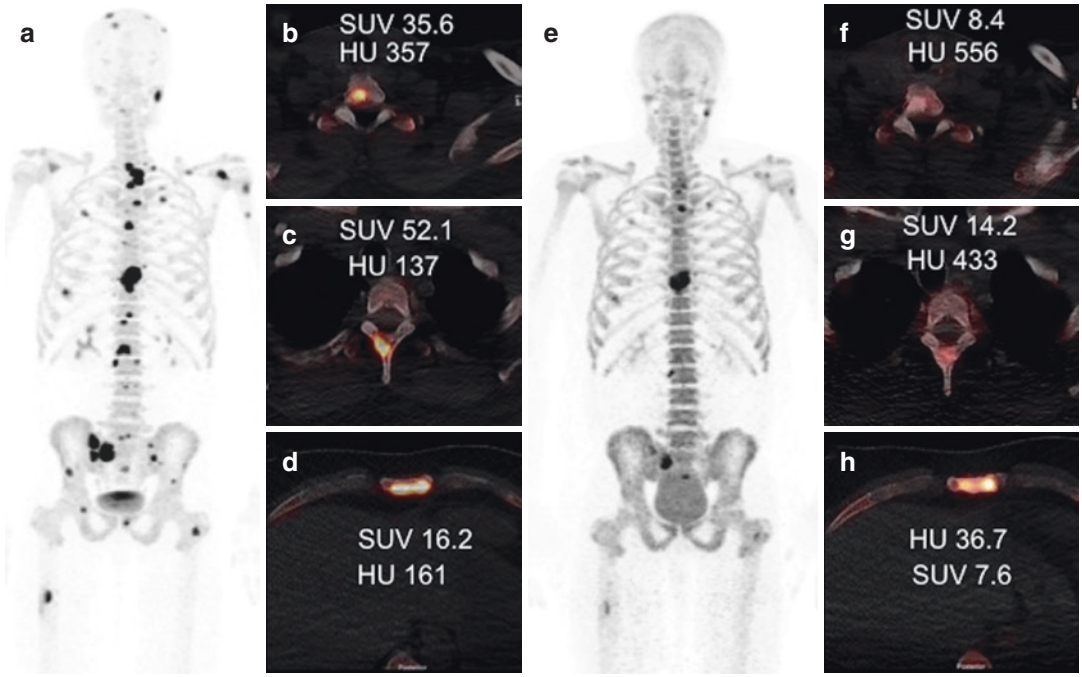

Case 13: A 53-year-old woman with metastatic adenocarcinoma of the left lung. (**a**) Baseline ^{18}F-NaF PET/CT shows multiple osteoblastic lesions involving skull, bilateral scapulae, left humerus, multiple levels in the thoracolumbar spine, sacrum and both iliac bones and femora. (**b**) Post-therapy scan after 8 months of targeted therapy with Erlotinib shows a significant decrease in the number and intensity of osteoblastic lesions with residual osteoblastic activity at T3, sternum and sacrum. Healing sclerosis on CT with increasing HU persists after ^{18}F-NaF osteoblastic activity has reduced. Quantitative analysis shows that skeletal tumour burden is significantly reduced by 92% from TLF_{15} = 8925 to TLF_{15} = 687. Findings are consistent with a response to therapy despite residual lesions and targeted therapy was continued.

Teaching Point

Functional imaging with ^{18}F-NaF PET may be easier to interpret than morphological changes on CT where increasing and persistent sclerosis may indicate a treatment response.

References

1. Cook GJ, Azad GK, Goh V. Imaging bone metastases in breast cancer: staging and response assessment. J Nucl Med. 2016;57(Suppl 1):27S–33S.
2. Mahajan A, Azad GK, Cook GJ. PET imaging of skeletal metastases and its role in personalizing further management. PET Clin. 2016;11:305–18.
3. Azad GK, Cook GJ. Multi-technique imaging of bone metastases: spotlight on PET-CT. Clin Radiol. 2016;71:620–31.
4. Cook GJ, Goh V. Functional and hybrid imaging of bone metastases. J Bone Miner Res. 2018;33:961–72.
5. Azad GK, Taylor BP, Green A, Sandri I, Swampillai A, Harries M, Kristeleit H, Mansi J, Goh V, Cook GJR. Prediction of therapy response in bone-predominant metastatic breast cancer: comparison of [(18)F] fluorodeoxyglucose and [(18)F]-fluoride PET/CT with whole-body MRI with diffusion-weighted imaging. Eur J Nucl Med Mol Imaging. 2019;46:821–30.
6. Tateishi U, Gamez C, Dawood S, Yeung HW, Cristofanilli M, Macapinlac HA. Bone metastases in patients with metastatic breast cancer: morphologic and metabolic monitoring of response to systemic therapy with integrated PET/CT. Radiology. 2008;247:189–96.
7. Specht J, Tam S, Kurland B, Gralow JR, Livingston RB, Linden HM, et al. Serial 2-[18F] fluoro-2-deoxy-d-glucose positron emission tomography (FDG-PET) to monitor treatment of bone-dominant metastatic breast cancer predicts time to progression (TTP). Breast Cancer Res Treat. 2007;105:87–94.
8. Cook GJ, Azad G, Padhani AR. Bone imaging in prostate cancer: the evolving roles of nuclear medicine and radiology. Clin Transl Imaging. 2016;4:439–47.
9. Azad GK, Taylor B, Rubello D, Colletti PM, Goh V, Cook GJ. Molecular and functional imaging of bone metastases in breast and prostate cancers: an overview. Clin Nucl Med. 2016;41:e44–50.
10. Yu EY, Duan F, Muzi M, Deng X, Chin BB, Alumkal JJ, et al. Castration-resistant prostate cancer bone metastasis response measured by 18F-fluoride PET after treatment with dasatinib and correlation with progression-free survival: results from American College of Radiology Imaging Network 6687. J Nucl Med. 2015;56:354–60.
11. Harmon SA, Perk T, Lin C, Eickhoff J, Choyke PL, Dahut WL, et al. Quantitative assessment of early [18F]sodium fluoride positron emission tomography/computed tomography response to treatment in men with metastatic prostate cancer to bone. J Clin Oncol. 2017;35:2829–37.
12. Hillner BE, Siegel BA, Hanna L, Duan F, Quinn B, Shields AF. 18F-fluoride PET used for treatment monitoring of systemic cancer therapy: results from the National Oncologic PET Registry. J Nucl Med. 2015;56:222–88.

25 FDG-PET/CT in Assessment of Treatment Response in Pediatric Lymphoma

Mateos Bogoni, Margaret Masukawa, and Juliano Julio Cerci

25.1 Case 1

Images

Clinical Details Initial staging of Hodgkin's lymphoma in a 1-year-old boy.

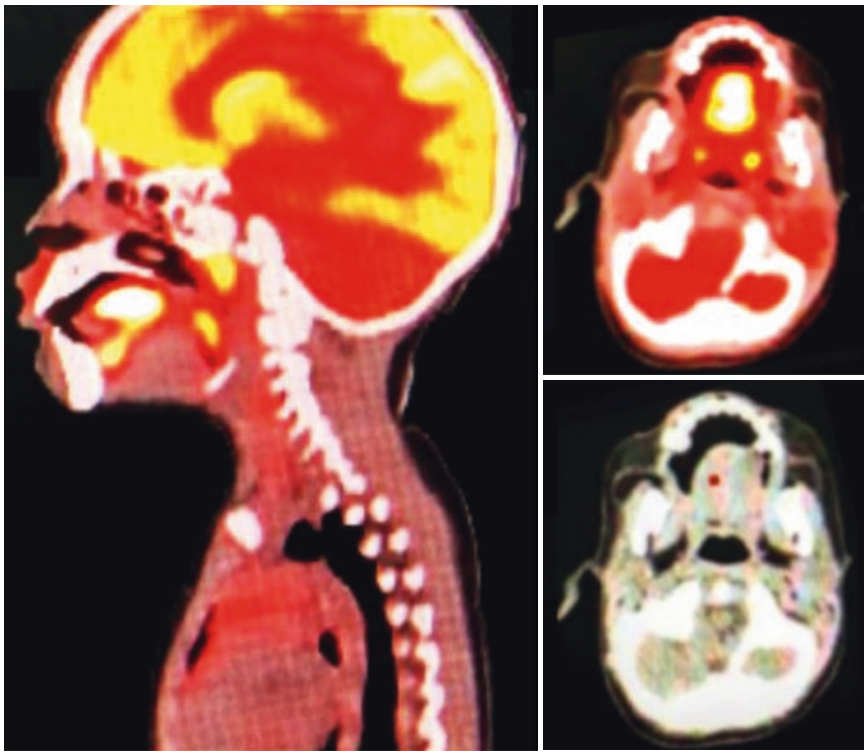

M. Bogoni · M. Masukawa · J. J. Cerci (✉)
PET/CT Center, Quanta – Diagnóstico e Terapia, Curitiba, PR, Brazil

S. Fanti et al. (eds.), *Atlas of Clinical PET-CT in Treatment Response Evaluation in Oncology*,
https://doi.org/10.1007/978-3-030-68858-5_25

Scan Findings

Severe metabolic activity is observed on Waldeyer's ring structures and in the tongue (SUVmax 18.5).

Interpretation It is important to keep in mind that children are not small adults and they do present different physiological FDG uptake (Above Figure). Especially in children, moderate to intense FDG uptake in Waldeyer's ring structures might be physiological due to intense activity in these lymphatic tissues (peaking at 6–8 years of age), and should not be interpreted as disease. The most interesting highlight in this case is the severe uptake in the tongue, which might look suspicious at first, but was considered normal since the patient was a heavy pacifier user. Another pediatric pitfall of which physicians must be aware is FDG uptake related to vaccination. Increased metabolic activity can be seen after vaccine administration not only at the injection sites but also in regional lymph nodes and should not be interpreted as disease. Diffuse and homogeneous FDG uptake might also be seen in the thymus of healthy children [1–3].

Teaching Points

- Recognizing physiological FDG uptake patterns in children is essential to avoid misinterpreting normal studies as positive for disease.
- Common pitfalls in the pediatric population include FDG uptake related to pacifier use, thymus activity, and vaccination (both at the injection site and in regional lymph nodes).

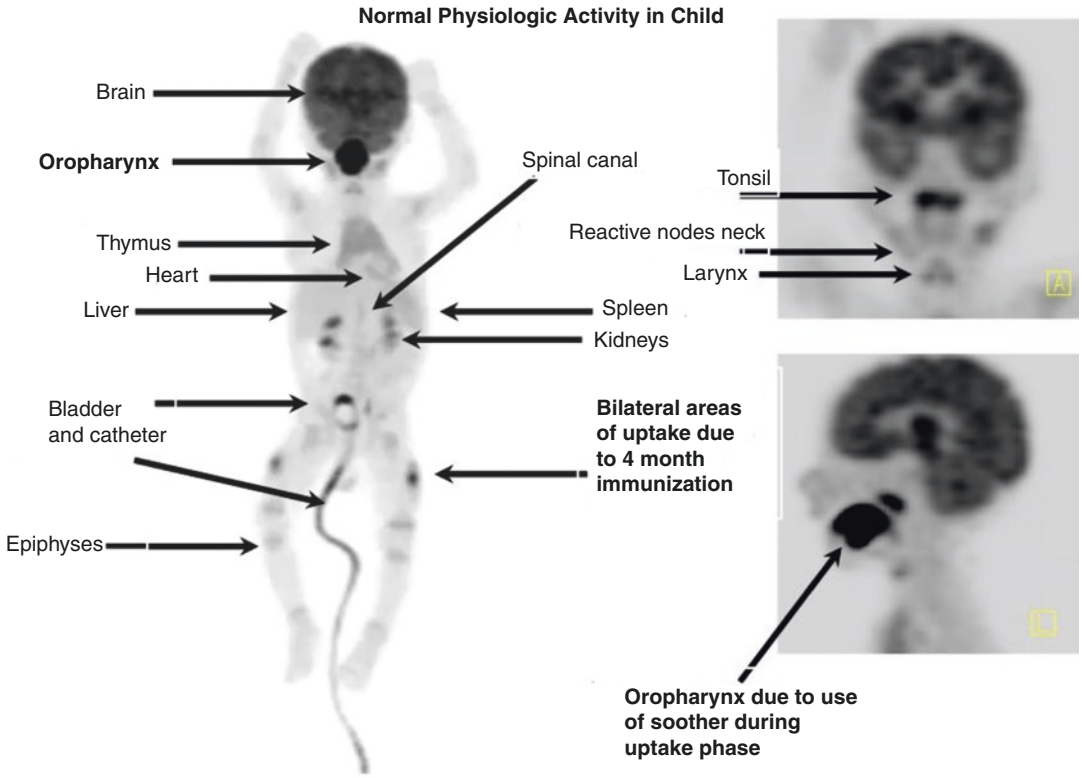

25.2 Case 2

Clinical Details Initial staging of Burkitt's lymphoma in a 12-year-old boy.

Images

Scan Findings: Initial Staging Study

Figure 25.1a–c: MIP images of FDG-PET/CT show high uptake in osseous structures (skull and lower limbs), in a focal site on the liver and in at least two large upper abdominal lesions. Fused FDG-PET/CT images (f, g) reveal the femoral uptake focus to be intramedullar. There are no detectable anatomical changes on CT images (d, e).

Figure 25.2: The liver uptake focus seen on MIP images corresponds to a small nodule in the transition of segments VIII and V of the liver.

Figure 25.3: The high metabolic activity seen on the upper abdomen corresponds to two large pancreatic masses. CT images (d, e) show enlargement of the pancreatic tail secondary to an ill-defined and faintly hypodense lesion. Corresponding fused FDG-PET/CT images (f, g) show intense FDG uptake at the site (SUVmax 5.6).

Figure 25.4: Moderate FDG uptake is observed in the supraclavicular brown fat bilaterally (arrows).

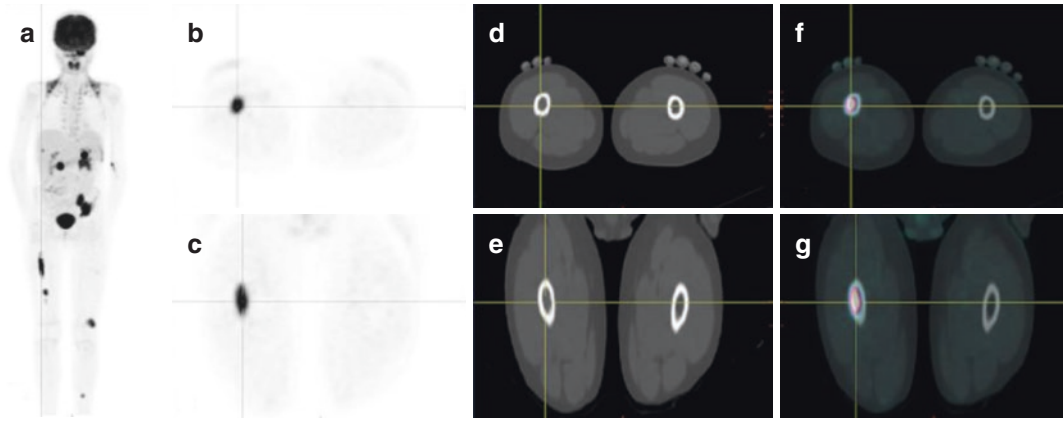

Fig. 25.1 (**a**–**g**) FDG-PET/CT initial staging study

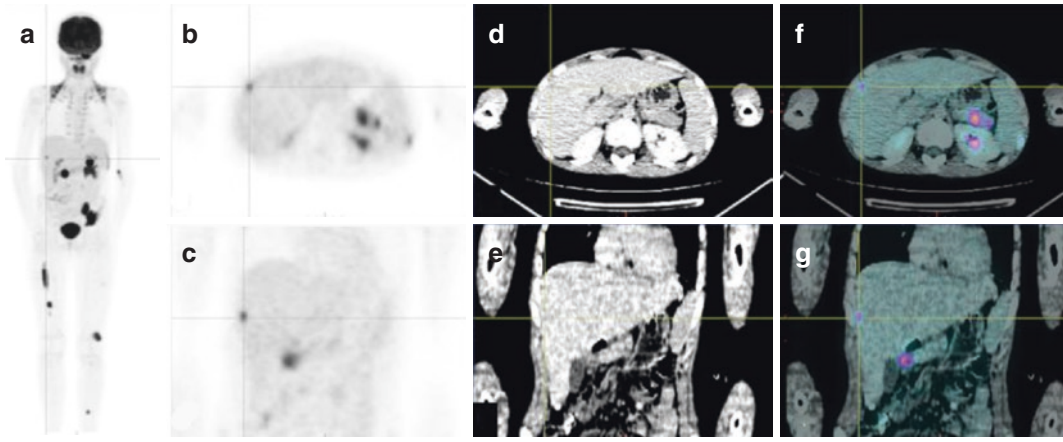

Fig. 25.2 (**a**–**g**) FDG-PET/CT initial staging study

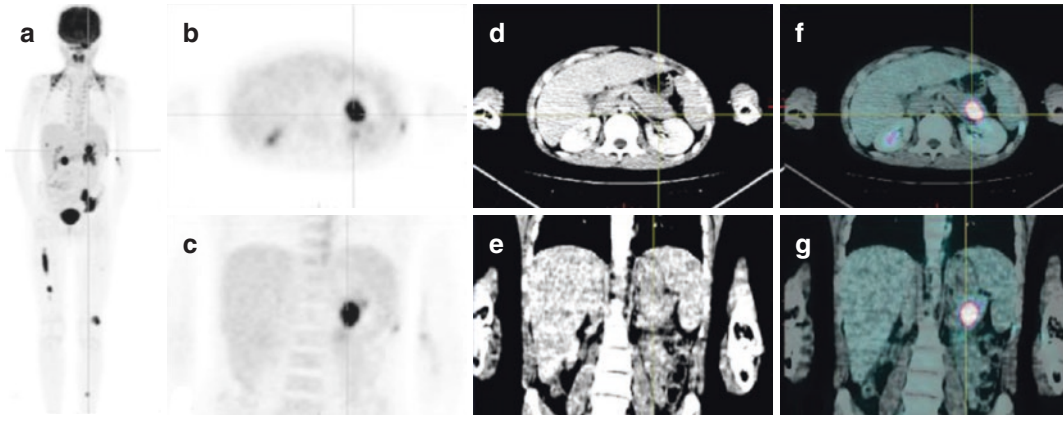

Fig. 25.3 (**a**–**g**) FDG-PET/CT initial staging study

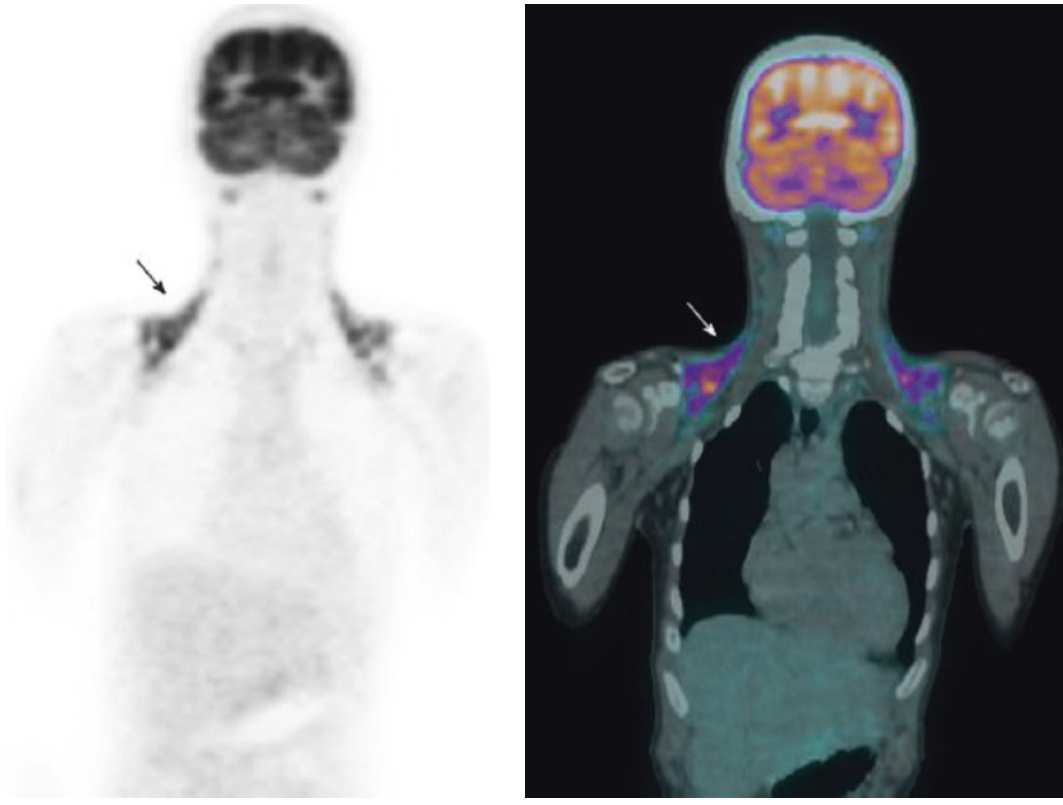

Fig. 25.4 FDG-PET/CT initial staging study

Final treatment study

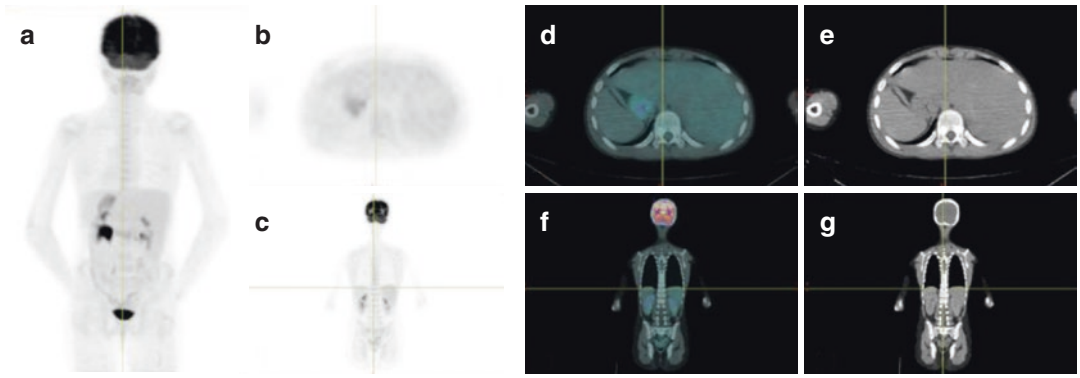

Scan Findings
Follow-up PET/CT evaluation shows no evidence of metabolic activity.

Interpretation Hodgkin's lymphoma (HL) and non-Hodgkin's lymphoma (NHL) account for 10–15% of pediatric malignancies, with HL representing around 40% of cases and NHL around 60%. HL appears rarely widespread at the time of diagnosis, while pediatric NHL is often a rapidly progressing disease and widely spreaded at diagnosis [4]. For HL's management, FDG-PET/CT presents higher sensibility and specificity compared to conventional imaging methods (96.5% vs. 87.5% for sensitivity, 96.7% vs. 85.2% for specificity), thus being well established since the staging phase of the workup [5]. In NHLs' workup, standardization attempts for FDG PET/CT incorporation in different treatment algorithms are challenging. This is mainly due to the fact that NHL comprises several different types of lymphoproliferative entities, among which few explorable common features are found (some not even being FDG avid, such as marginal zone B-cell or small lymphocytic lymphomas). Nevertheless, FDG-PET/CT must also be performed in the management of NHL, whenever feasible, playing a crucial role in staging and response assessments even in the face of such challenges [6].

End treatment assessment is more accurate with FDG-PET/CT, especially for patients with radiologic unknown complete response or partial response in more aggressive lymphomas (HL, DLBCL, and follicular lymphoma). PET/CT and FDG uptake-based criteria eliminate CRu and enhance the prognostic value of PR. In patients with HL (early and advanced stage), a negative predictive value of 95% to 100% and a positive predictive value of more than 90% have been reported [7, 8]. In aggressive NHL, studies have reported a negative predictive value of 80–100% and a positive predictive value of 50–100% [9, 10]. With that in mind, in the presence of a positive FDG-PET/CT scan, if further treatment is being considered, biopsy is advised.

In HL, DLBCL, and follicular lymphoma subtypes, response assessment with PET/CT may be preferred using the Lugano classification 5-point scale (discussed in the next case), whereas CT-based response remains important in lymphomas with low or variable FDG avidity.

An important pitfall highlighted in this case is the metabolic activity seen bilaterally in the supraclavicular region, which represents a classic site of physiologic FDG uptake related to brown adipose tissue and must not be confused with disease. Brown adipose tissue activation can be secondary to low temperature or sympathetic stimulus (e.g., pain or stress), and the metabolic activity observed at this site can mislead the correct interpretation of disease extension. Cautionary measures must be taken in order to ensure that the child is kept adequately warm and as comfortable as possible during the exam [11–14].

Finally, in the end treatment study, there is no FDG uptake (Deauville 5PS: 1), meaning complete response to therapy.

Teaching Points

- Hodgkin's lymphoma (HL) and non-Hodgkin's lymphoma (NHL) account for 10–15% of pediatric malignancies, with HL representing around 40% of cases and NHL around 60%. HL appears rarely widespread at the time of diagnosis, while pediatric NHL is often a rapidly progressing disease and widely spreads at diagnosis.
- FDG PET/CT is better established in HL's staging and response assessments than in NHL's. The great heterogeneity of NHLs hinders the standardization of PET/CT in workup algorithms. Nevertheless, FDG PET/CT must also be performed in the management of NHL, whenever feasible, playing a crucial role in staging and response assessments.
- End treatment assessment is more accurate with FDG-PET/CT, especially for patients with radiologic unknown complete response or partial response in more aggressive lymphomas (HL, DLBCL, and follicular lymphoma). PET/CT and FDG uptake-based criteria eliminate CRu and enhance the prognostic value of PR.
- PET/CT has been increasingly preferred over bone marrow biopsy in both HL and NHL for providing similar or superior results with much less invasiveness.
- Brown adipose tissue FDG uptake presents a common pitfall of which physicians must be aware, since it might be misinterpreted as disease, especially in the neck, supraclavicular and axillary regions. It might be diminished by adequate the scanning room temperature and keeping the patient comfortable.

25.3 Case 3

Clinical Details Initial staging of Hodgkin's lymphoma in a 12-year-old girl.

Images

Scan Findings: Initial Staging Study
a: MIP FDG-PET image shows abnormal uptake in cervical and mediastinal lymph nodes.
b–g: An enlarged anterior mediastinal lymph node is observed, with an SUVmax of 5.6.

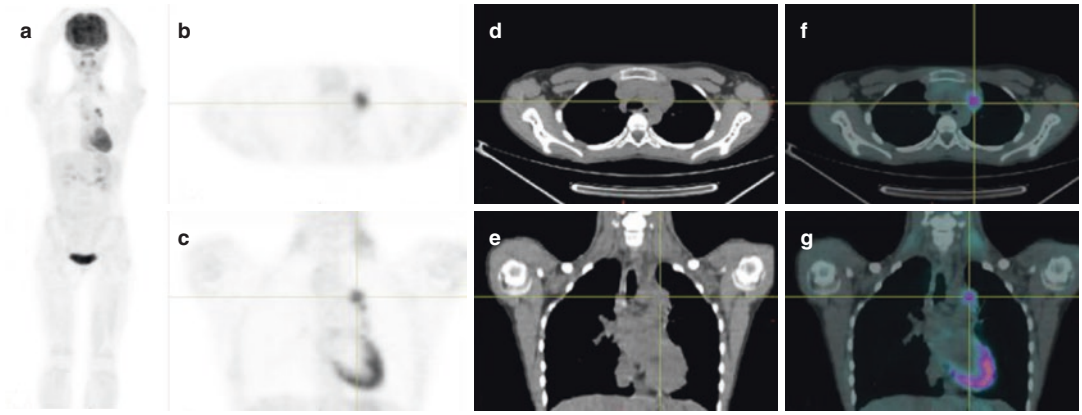

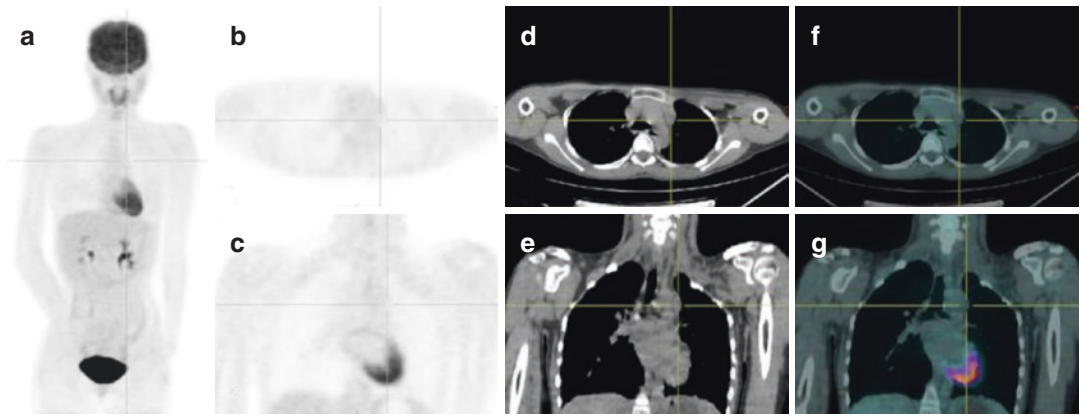

Interim study

Scan Findings: Final study
Interim FDG-PET/CT study shows no evidence of metabolic activity.

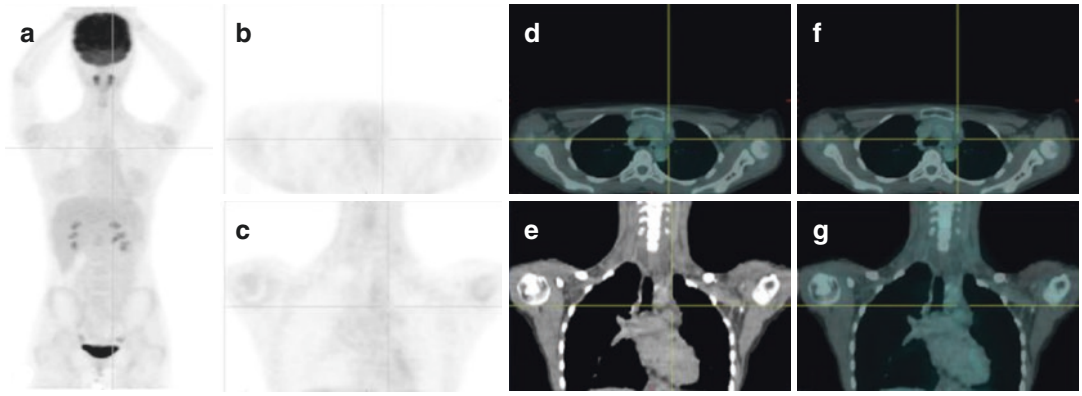

Scan Findings
Sustained complete metabolic response is observed on follow-up PET/CT evaluation.

Interpretation The Lugano Classification was described in 2014 by the International Malignant Lymphoma Working Group for standardization of posttreatment response assessments in lymphoma patients, providing semiquantitative criteria for defining response in PET and conventional imaging techniques [4–6]. Regarding FDG-PET/CT specifically, let us make a brief review on the topic, since it will be useful for the next cases. It is based on the Deauville score, a five-point scoring system (5PS) that is applied to all studies performed after initial staging. Points are designated based on the FDG uptake pattern observed, as follows:

Score	FDG uptake
1	No uptake or no residual uptake
2	Slight uptake, but below blood pool (mediastinum)
3	Uptake above mediastinal, but below or equal to uptake in the liver
4	Uptake slightly to moderately higher than liver
5	Markedly increased uptake or any new lesion
X	Any areas of uptake not likely to be related to lymphoma

After the correct Lugano 5PS category is attributed, its interpretation requires integrated clinical and treatment information.

Score	Interpretation
1 or 2	• Considered to represent complete metabolic response (CMR) at interim and end of treatment
3	• Dependent on the lymphoma subtype and the clinical context • FDG uptake declines during therapy in chemosensitive disease and residual FDG uptake higher than normal liver uptake is frequently seen at interim in patients who achieve CMR at the end of treatment
4 or 5 at interim	• Suggests chemosensitive disease provided uptake has reduced from baseline and is considered to represent partial metabolic response
4 or 5 at the end of treatment	• Represents residual metabolic disease even if the uptake has reduced from baseline

Until very recently, prognostic and outcome evaluations for lymphoma in the pediatric population were based on extrapolated interpretation of studies performed in adult populations. Needless to say, this strategy is far from ideal, given the idiosyncrasies of imaging pediatric patients, with its inherent and frequent pitfalls. A recent multicentric dedicated study [15]

confirmed the value of interim FDG-PET/CT interpreted with the Lugano Classification (both in HL and NHL pediatric patients) as a strong and independent predictor of events (relapse after complete remission, death from any cause, treatment escalation for progressive disease while on treatment and disease progression, or failure to achieve complete remission at end chemotherapy) and overall survival. Our case illustrates the prognostic value given an interim PET/CT's negative Lugano classification, which is associated with fewer events on follow-up and higher overall survival. Since no evidence of metabolic activity is observed on both interim and final PET/CT, the Lugano classification is negative (Deauville 5PS: 1, i.e., complete metabolic response).

Teaching Points

- FDG-PET/CT has great value in assessing therapy response in FDG-avid lymphomas. For this end, the Lugano Classification was developed. In lymphomas with low FDG avidity, conventional CT remains important for posttreatment assessment.
- The Lugano Classification is applied to interim and end treatment CT and MRI studies and establishes a semiquantitative 5-point scoring system (the Deauville score) for determining responses based on FDG-PET/CT, using mediastinal blood pool and hepatic uptake as reference. It is widely accepted and incorporated into both pediatric and adult practice.
- Therapy response assessment through FDG PET/CT holds prognostic value in the pediatric population both for HL and for NHL. Positive interim and end treatment studies are related to more events and reduction in overall survival.

25.4 Case 4

Clinical Details Initial staging of Hodgkin's lymphoma in a 14-year-old girl.

Images

Scan Findings
Figure 25.5a–c: MIP images of initial FDG-PET/CT show intense uptake in the lungs, supradiaphragmatic lymph nodes, and diffusely throughout the skeleton. PET/CT images show large heterogeneous pulmonary masses, with an SUVmax of 10.5 (a–g). Intense FDG uptake is also observed in enlarged thoracic lymph nodes (SUVmax 7.3—Fig. 25.6), with invasion of the 7th thoracic vertebra (SUVmax 7.4—Fig. 25.7).

Scan Findings
Figures 25.8 and 25.9: Interim FDG-PET/CT study reveals partial response to therapy. There was a significant size reduction in the lung masses and enlarged lymph nodes, but persistent metabolic activity was observed (SUVmax 9.6 and 2.6, respectively).

Scan Findings
Final PET/CT study shows minimal FDG uptake in the lungs, associated with radiation pneumonitis seen on CT images (Fig. 25.10). Mild uptake was also noticed in the 11th rib to the left (Fig. 25.11).

Interpretation The 5-year survival rates for HL exceed 98% and are higher than 80% for NHL. Absence of FDG uptake in a residual mass after chemotherapy is predictive of complete remission, while increased FDG uptake may indicate residual disease [4]. Positive PET/CT studies by the Lugano Classification (5PS: 4 or 5) require special caution as to properly interpret what the imaging findings represent in the broader context of the disease. An important observation is that especially in NHL, false positive PET studies due to necrosis or inflammation are relatively common, up to around 40% [16]. In our case (HL), positive classification for the interim study suggests chemosensitive disease, since the FDG uptake has reduced from baseline, and thus is considered to represent partial metabolic response. End treatment evaluation showed no lung uptake and a focal area of uptake in the 11th rib. As the patient did not present lymphoma commitment on that site, it is considered score X not likely related to lymphoma [17].

Teaching Points
- Positive FDG-PET/CT studies by the Lugano Classification (5PS: 4 or 5) require special caution as to properly interpret what the imaging findings represent in the broader context of the disease, especially in NHL cases, due to higher false positive PET studies.
- Positive interim studies might represent disease progression or chemosensitive disease, depending on FDG uptake in comparison to baseline.
- If the end treatment FDG-PET/CT study is positive additional histological evaluation through biopsy must be considered.

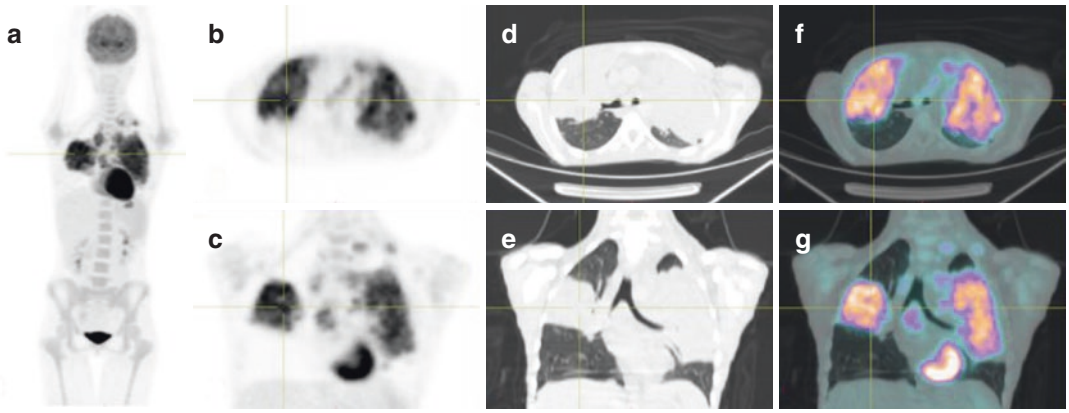

Fig. 25.5 (**a**–**g**) Initial staging study

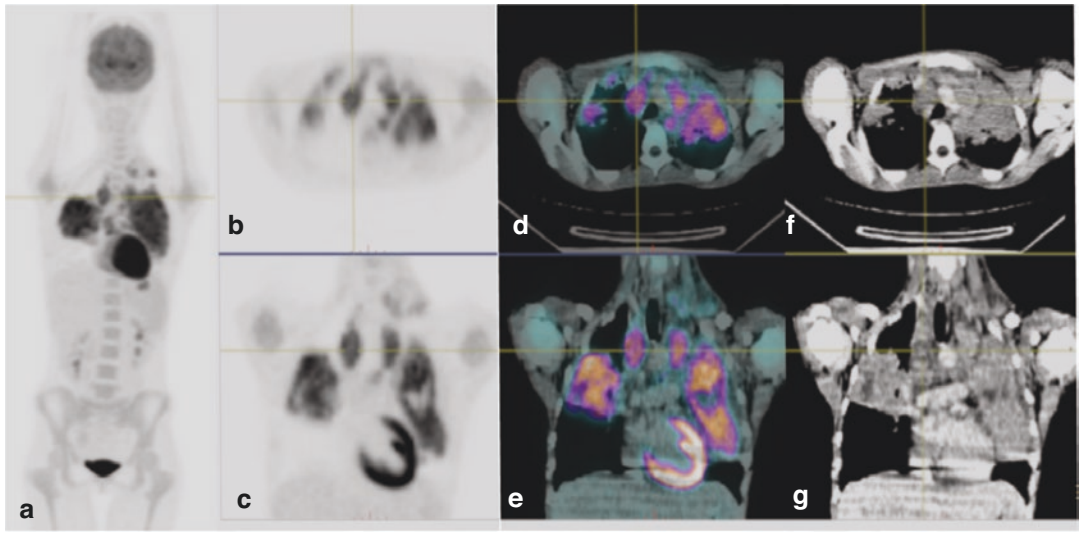

Fig. 25.6 (**a**–**g**) Initial staging study

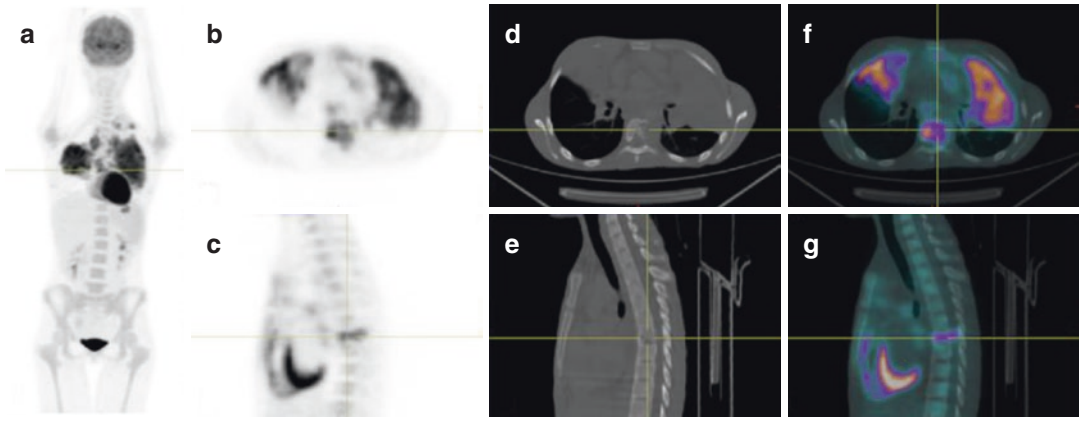

Fig. 25.7 (**a**–**g**) Initial staging study

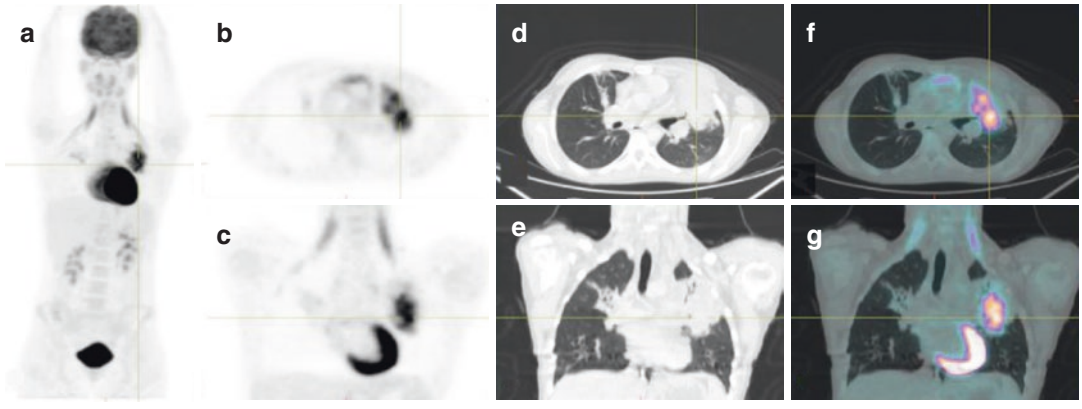

Fig. 25.8 (**a**–**g**) Interim study

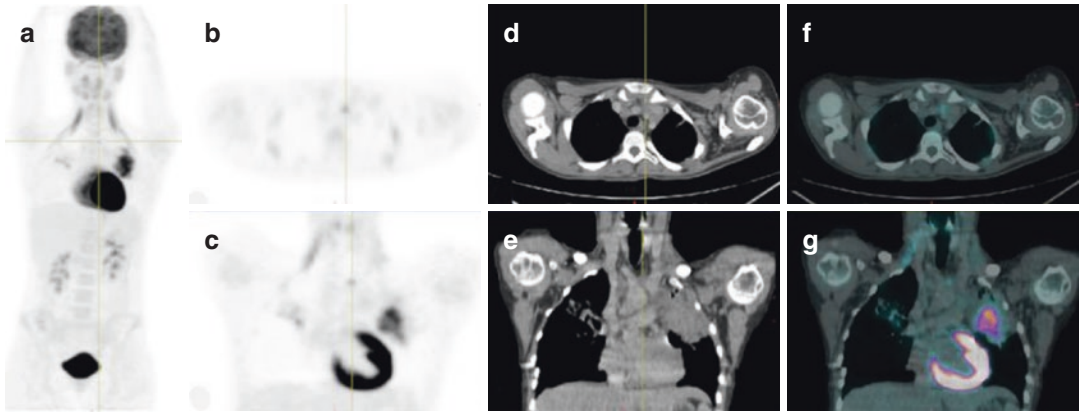

Fig. 25.9 (**a**–**g**) Interim study

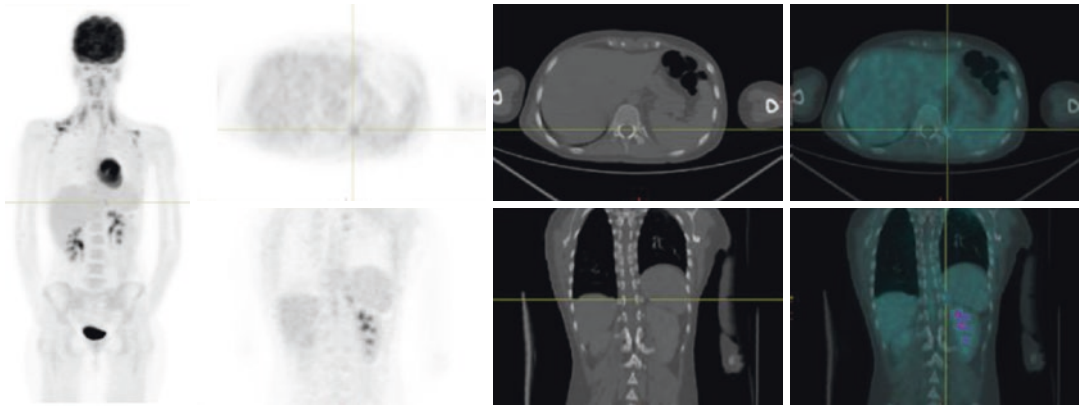

Fig. 25.10 End treatment study

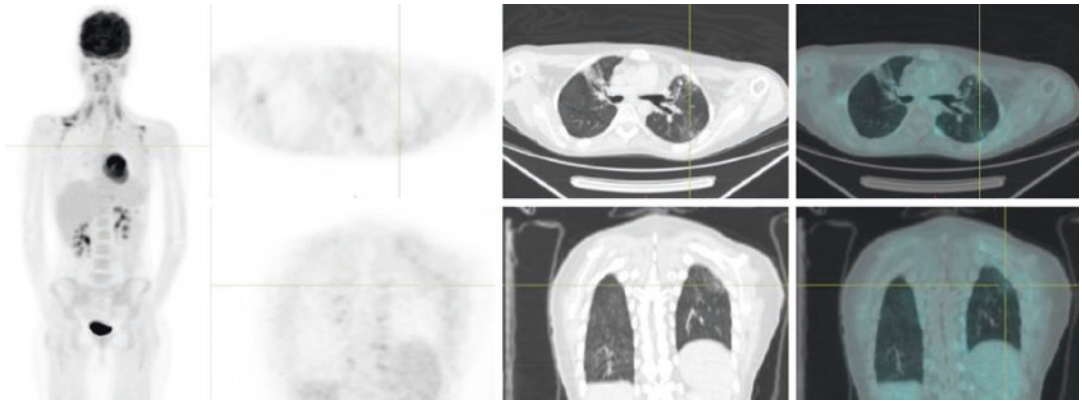

Fig. 25.11 End treatment study

25.5 Case 5

Clinical Details Staging of Hodgkin's lymphoma in a 13-year-old girl presenting with lymphadenopathy.

Images
First study

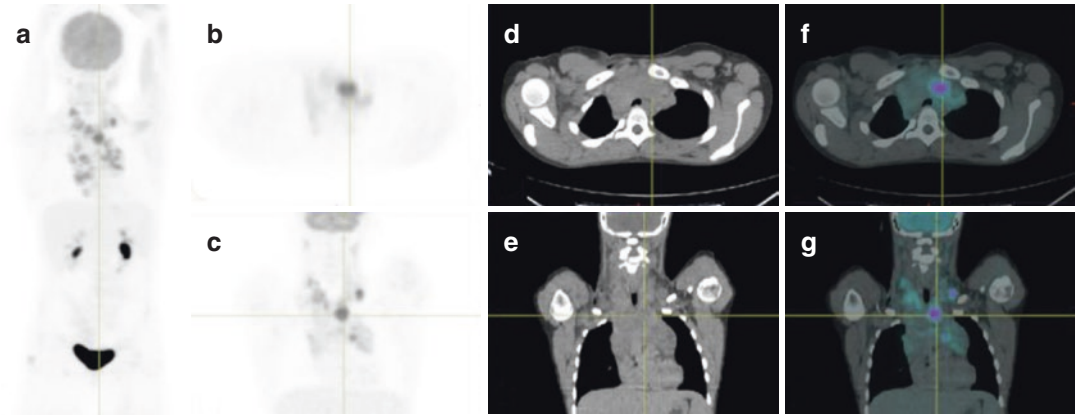

Scan Findings
a: MIP images of FDG-PET/CT show extensive supradiaphragmatic nodal involvement.

b–g: Confluent enlarged anterior mediastinal lymph nodes are observed with severe FDG uptake (SUVmax 10.5).

Interim study

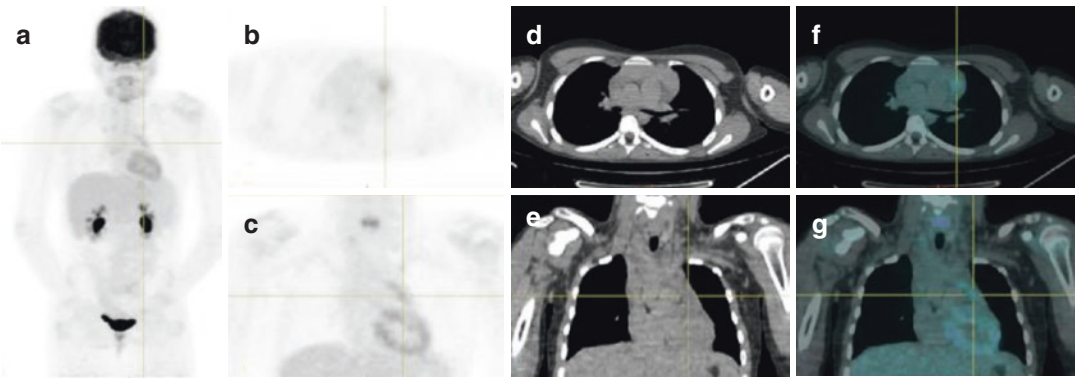

Scan Findings
a–c: Post-chemotherapy MIP FDG-PET/CT images show fewer involved nodes and significantly lower FDG overall uptake. Although important reduction in mediastinal lymph nodes' size is observed on CT (d, e), corresponding fused FDG-PET/CT images reveal faint residual metabolic activity (f, g), with an SUVmax of 2.9 (hepatic SUVmax: 1.8).

Final study

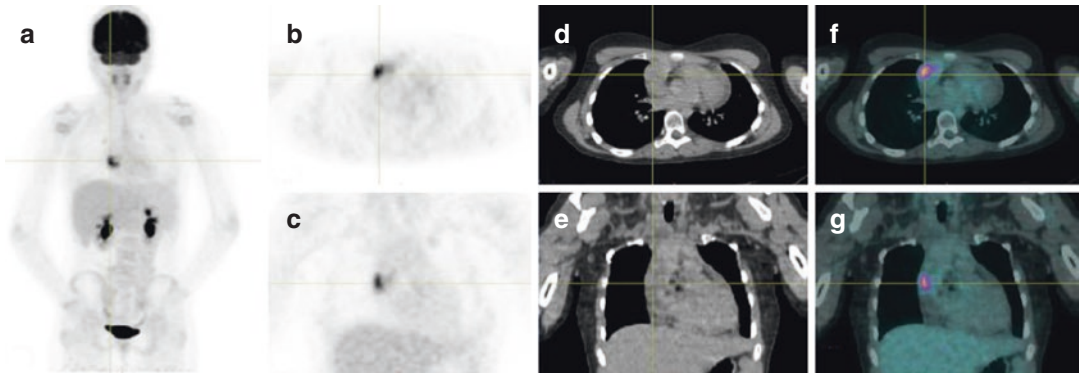

Scan Findings

Follow-up PET/CT study shows a new lesion with high FDG uptake (SUVmax: 10.0) in the anterior mediastinum.

Interpretation Positive FDG-PET/CT results after treatment are associated with higher relapse rates [18]. Patients with residual mass after therapy, including in HL and NHL, with positive FDG-PET/CT results had a 100% relapse rate in contrast to patients who showed no activity of the residual mass with a relapse rate of only 26% [19]. Hence, in the presented case, interim PET/CT's positive Lugano classification has prognostic value, with higher probability of events and lower overall survival. The patient was considered to be in partial metabolic response and started presenting B symptoms again. The final FDG-PET/CT shows increased FDG uptake, thus representing residual metabolic disease (even with reduced uptake from baseline), prompting the need for biopsy to confirm the lymphoma and eventually second-line therapy [14, 20].

Teaching Points

- Therapy response assessment through FDG PET/CT holds prognostic value in the pediatric population both for HL and for NHL. Positive interim and end treatment studies are related to more events and reduction in overall survival.

25.6 Case 6

Clinical Details Initial staging of Hodgkin's lymphoma in a 14-year-old girl.

Images

Initial staging study

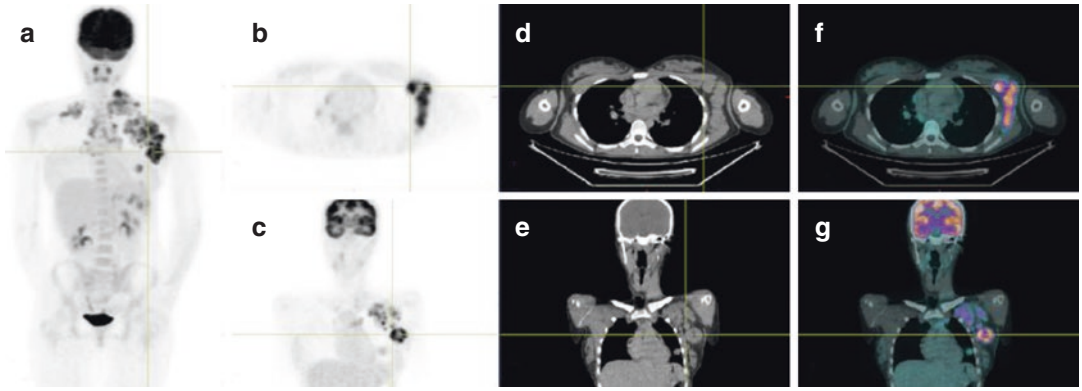

Scan Findings

Extensive supradiaphragmatic disease involving multiple lymph nodes (mediastinal, bilateral supra- and infraclavicular, and left axillary stations). The highest FDG uptake is observed in confluent nodes in the left axillary region (SUVmax 11.0).

Interim study

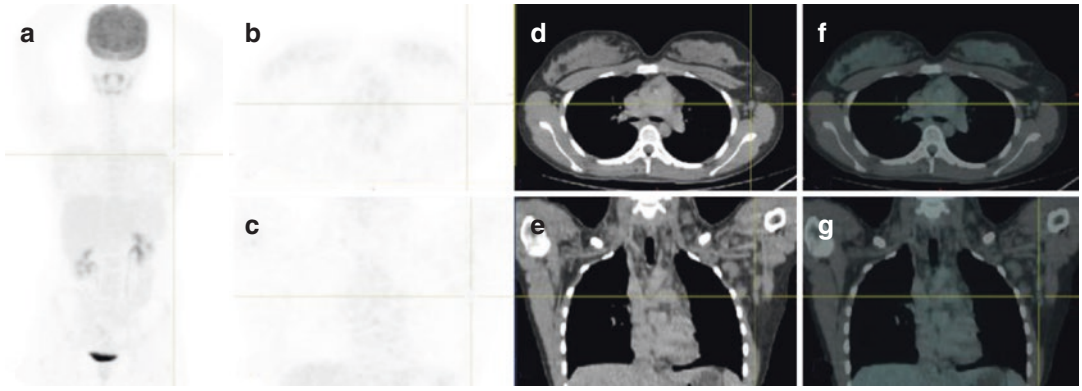

Scan Findings:
Interim FDG-PET/CT study shows no evidence of metabolic activity. CT images (d, e) show significant reduction in axillary lymph nodes' size.

Final study

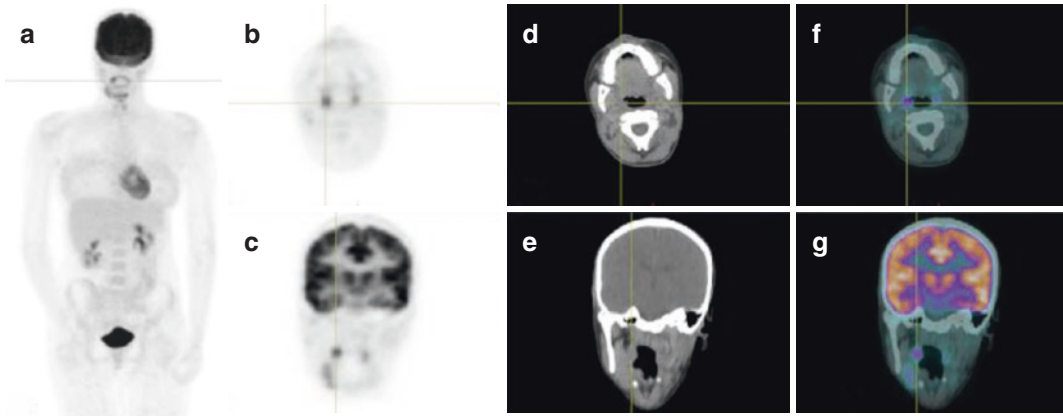

Scan Findings
End treatment FDG-PET/CT study shows asymmetry in the palatine tonsil and submandibular gland.

Interpretation This case highlights the importance of integrating relevant clinical information with imaging findings. Being informed of all previous therapy that the patient might have been exposed to is essential for correct interpretation of FDG-PET/CT images. In this case, the asymmetric metabolic activity observed in the palatine tonsils and submandibular glands is considered secondary to actinic changes, with lower activity on the side of irradiation (the patient was considered in complete metabolic response) [21].

An important topic that has been gaining increasing attention is the necessity of radiotherapy consolidation, since this procedure is associated with higher incidence of new cancers and other disorders (such as cardiovascular disease) in adulthood. Interim FDG-PET/CT has the ability to define certain patient populations that respond greatly to chemotherapy, in which additional radiotherapy can sometimes be deferred [22], while end treatment FDG-PET/CT, especially in Hodgkin lymphoma, plays an important role in the selection of patients to be submitted to radiotherapy, avoiding radiotherapy in patients with a negative FDG-PET/CT scan.

Teaching Points
- Being informed of all previous therapy that the patient might have been exposed to is essential for correct interpretation of FDG-PET/CT images.
- FDG-PET/CT plays an important role in the selection of patients to be submitted to radiotherapy.

25.7 Case 7

Clinical Details Initial staging of lymphoma in a 3-year-old boy.

Images

Initial staging study

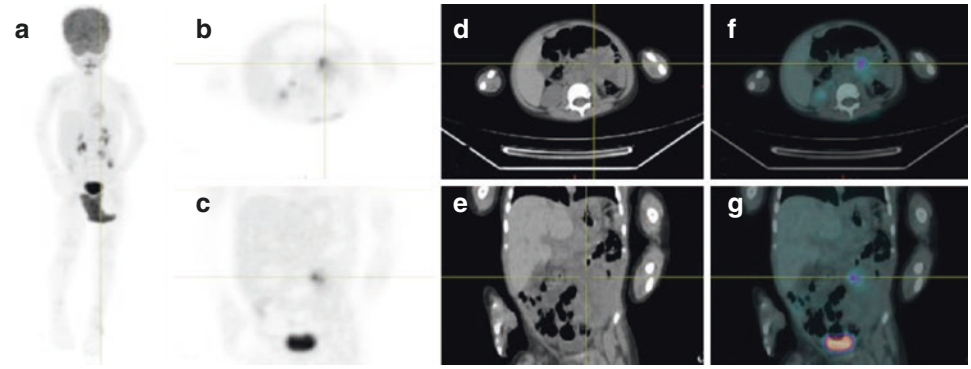

Scan Findings

a–c: MIP FDG-PET/CT images show high metabolic activity on the left side of the abdomen. An ill-defined hypodense mass is observed at the same location on CT (d, e). Corresponding fused FDG PET images (f, g) reveal that a central portion of the mass presents high FDG uptake (SUVmax 5.9).

Interim study

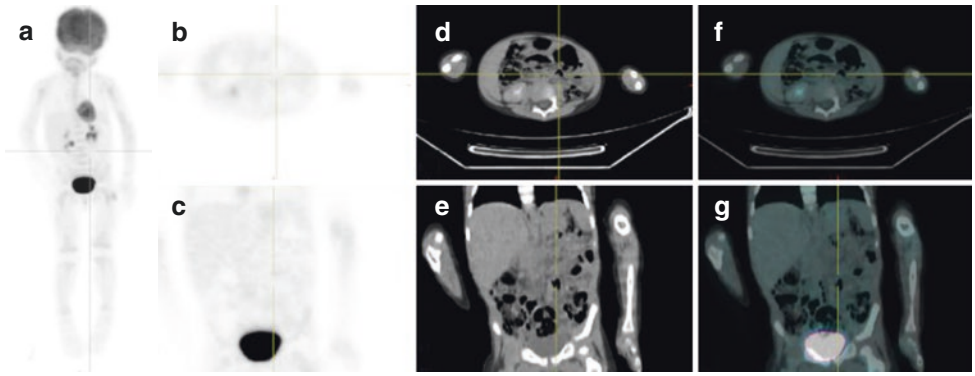

Scan Finding
Follow-up FDG-PET/CT evaluation shows no evidence of metabolic activity.

End treatment study

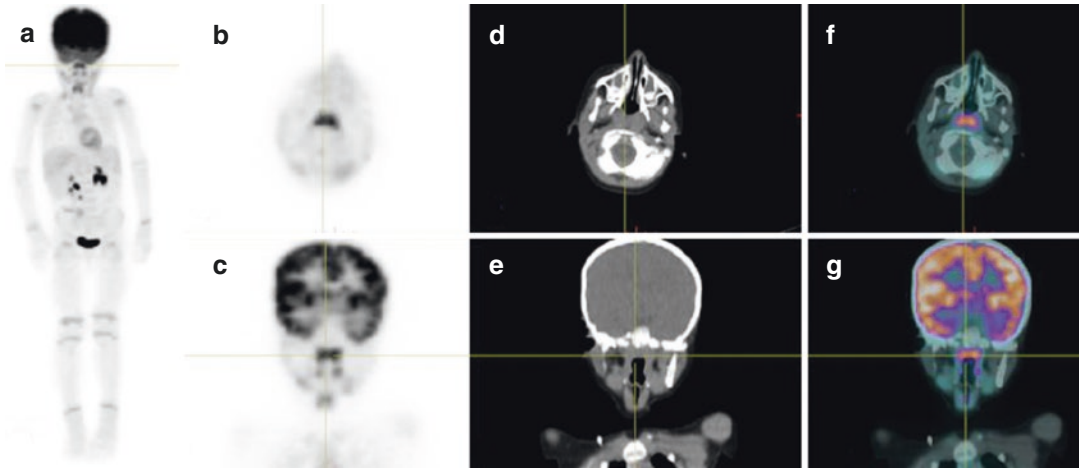

Scan Findings
A new FDG-PET/CT study performed about 1 year later showed high FDG uptake in enlarged pharyngeal tonsils, related to inflammatory/infectious process.

Follow-up study

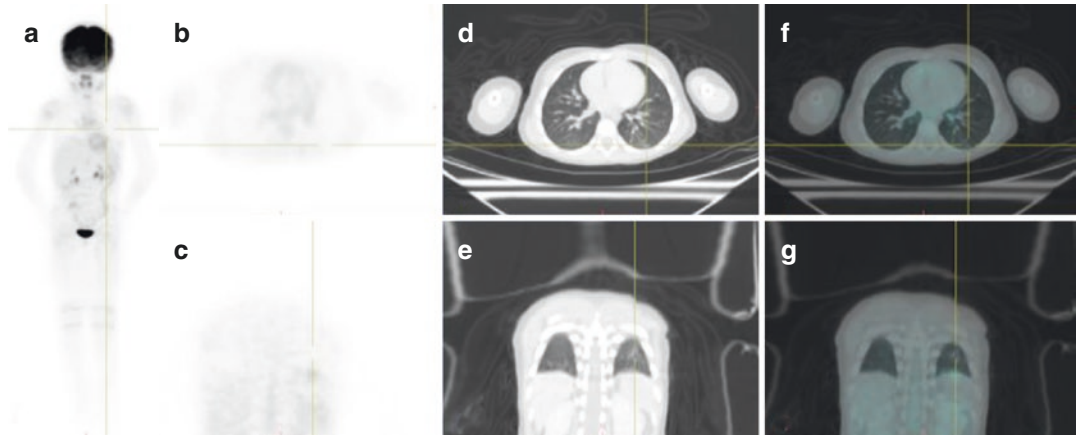

Scan Findings
FDG-PET/CT study only shows discrete metabolic activity in small centrilobular nodules in the left lung (SUVmax 1.6), suggesting inflammatory changes.

Interpretation Interim FDG-PET/CT shows no signs of metabolic activity (Deauville 5PS: 1). Both the final treatment and follow-up studies show new areas of uptake unlikely to be related to lymphoma (pharyngeal tonsils and small centrilobular pulmonary nodules), corresponding to the "X" category of the Lugano classification. This case illustrates another important topic of discussion: follow-up FDG/PET/CT studies or any other imaging method involving radiation must be avoided and performed only in high clinical suspicion. Since the risk of relapse is highest

in the first 2 years after end of treatment, cross-sectional imaging (preferably MRI to avoid radiation exposure) and ultrasound examinations are preferable for evaluating the previously involved lymph node regions in 3–6 monthly intervals. Recent studies reveal that most relapses are found through history and physical examination [23]. After completion of therapy, FDG-PET/CT should only be performed for restaging of a patient with histology-proven relapse or high clinical suspicion of relapse [22].

Teaching Points

- Unnecessary follow-up FDG/PET/CT studies or any other imaging method involving radiation must be avoided, given the relation of excessive radiation exposure in childhood with higher incidence of new cancers and other health conditions in adulthood.
- Most relapses occur in the first 2 years after completion of therapy and are more frequently found through history and physical examination.
- FDG-PET/CT should only be performed for restaging of a patient with histology-proven relapse or high clinical suspicion of relapse.

References

1. Colleran GC, Kwatra N, Oberg L, et al. How we read pediatric PET/CT: indications and strategies for image acquisition, interpretation and reporting. Cancer Imaging. 2017;17(1):28. https://doi.org/10.1186/s40644-017-0130-8.
2. Sheehy N, Drubach L. Pediatr Radiol. 2008;38:246. https://doi.org/10.1007/s00247-007-0686-8.
3. Shammas A, Lim R, Charron M. Pediatric FDG PET/CT: physiologic uptake, normal variants, and benign conditions. Radiographics. 2009;29(5):1467–86. https://doi.org/10.1148/rg.295085247.
4. Huang G. Nuclear medicine in oncology molecular imaging and target therapy: molecular imaging and target therapy. 2019; https://doi.org/10.1007/978-981-13-7458-6.
5. London K, Cross S, Onikul E, Dalla-Pozza L, Howman-Giles R. 18F-FDG PET/CT in paediatric lymphoma: comparison with conventional imaging. Eur J Nucl Med Mol Imaging. 2011;38:274–84.
6. Lisa S, Voss S. PET/CT in pediatric oncology. 2019; https://doi.org/10.1007/978-3-030-03777-2_3.
7. Cerci JJ, Pracchia LF, Linardi CC, et al. 18F-FDG PET after 2 cycles of ABVD predicts event-free survival in early and advanced Hodgkin lymphoma. J Nucl Med. 2010;51:1337–43.
8. Engert A, Haverkamp H, Kobe C, et al. Reduced-intensity chemotherapy and PET-guided radiotherapy in patients with advanced stage Hodgkin's lymphoma (HD15 trial): a randomised, open-label, phase 3 non-inferiority trial. Lancet. 2012;379:1791–9.
9. Cashen AF, Dehdashti F, Luo J, et al. 18F-FDG PET/CT for early response assessment in diffuse large B-cell lymphoma: poor predictive value of international harmonization project interpretation. J Nucl Med. 2011;52:386–92.
10. Pregno P, Chiapella A, Bello M, et al. Interim 18-FDG-PET/CT failed to predict the outcome in diffuse large B-cell lymphoma patients treated at the diagnosis with rituximab-CHOP. Blood. 2012;119:2066–73.
11. Hong TS, Shammas A, Charron M, Zukotynski KA, Drubach LA, Lim R. Brown adipose tissue 18F-FDG uptake in pediatric PET/CT imaging. Pediatr Radiol. 2011;41(6):759–68. https://doi.org/10.1007/s00247-010-1925-y.
12. Lisa S, Voss S. PET/CT in pediatric oncology. 2019; https://doi.org/10.1007/978-3-030-03777-2_3.
13. ESMO E-learning: the Lugano Classification recommendations for Hodgkin's and non-Hodgkin's lymphoma – staging response assessment and follow up. https://oncologypro.esmo.org/content/download/75355/1377102/file/ESMO-E-Learning-The-Lugano-Classification-Recommendations-For-Hodgkins-and-Non-Hodginks-Lymphoma-Staging-Response-Assessment-and-Follow-Up-Zucca-Pavanello.pdf
14. Barrington SF, Mikhaeel NG, Kostakoglu L, Meignan M, Hutchings M, Müeller SP, Schwartz LH, Zucca E, Fisher RI, Trotman J, Hoekstra OS, Hicks RJ, O'Doherty MJ, Hustinx R, Biggi A, Cheson BD. Role of imaging in the staging and response assessment of lymphoma: consensus of the International Conference on Malignant Lymphomas Imaging Working Group. J Clin Oncol. 2014;32(27):3048–58.
15. Nadel H, Etchebehere EC, Cerci JJ, Brink A, Bal CS, Rangarajan V, Pfluger T, Kagna O, Alonso O, Begum F, Mir KB, Magboo VP, Menezes L, Paez D, Pascual TNB. Interim PET/CT predicts response in pediatric lymphoma patients – report of an IAEA multicenter prospective study. 2018; https://doi.org/10.2139/ssrn.3289797. SSRN https://ssrn.com/abstract=3289797
16. Bhojwani D, McCarville MB, Choi JK, et al. The role of FDG-PET/CT in the evaluation of residual disease in paediatric non-Hodgkin lymphoma. Br J Haematol. 2015;168:845–53.
17. Cheson BD, Fisher RI, Barrington SF, Cavalli F, Schwartz LH, Zucca E, Lister TA, Alliance, Australasian Leukaemia and Lymphoma Group;

Eastern Cooperative Oncology Group; European Mantle Cell Lymphoma Consortium; Italian Lymphoma Foundation; European Organisation for Research; Treatment of Cancer/Dutch Hemato-Oncology Group; Grupo Español de Médula Ósea; German High-Grade Lymphoma Study Group; German Hodgkin's Study Group; Japanese Lymphoma Study Group; Lymphoma Study Association; NCIC Clinical Trials Group; Nordic Lymphoma Study Group; Southwest Oncology Group; United Kingdom National Cancer Research Institute. Recommendations for initial evaluation, staging, and response assessment of Hodgkin and non-Hodgkin lymphoma: the Lugano classification. J Clin Oncol. 2014;32(27):3059–68.

18. Buchpiguel CA. Current status of PET/CT in the diagnosis and follow up of lymphomas. Rev Bras Hematol Hemoter. 2011;33(2):140–7. https://doi.org/10.5581/1516-8484.20110035. http://www.scielo.br/scielo.php?script=sci_arttext&pid=S1516–84842011000200013&lng=en&nrm=iso. Accessed 20 Sep 2019. ISSN 1516-8484
19. Jerusalem G, Beguin Y, Fassotte MF, Najjar F, Paulus P, Rigo P, et al. Whole-body positron emission tomography using 18F-fluorodeoxyglucose for post-treatment evaluation in Hodgkin's disease and non-Hodgkin's lymphoma has higher diagnostic and prognostic value than classical computed tomography scan imaging. Blood. 1999;94(2):429–33.
20. Cheson BD, Fisher RI, Barrington SF, Cavalli F, Schwartz LH, Zucca E, Lister TA. Recommendations for initial evaluation, staging, and response assessment of Hodgkin and non-Hodgkin lymphoma: the Lugano classification. J Clin Oncol. 2014;32(27):3059–68.
21. Purandare NC, Puranik AD, Shah S, Agrawal A, Rangarajan V. Post-treatment appearances, pitfalls, and patterns of failure in head and neck cancer on FDG PET/CT imaging. Indian J Nucl Med. 2014;29(3):151–7. https://doi.org/10.4103/0972-3919.136564.
22. Kluge R, Kurch L, Georgi T, Metzger M. Current role of FDG-PET in pediatric Hodgkin's lymphoma. Semin Nucl Med. 2017;47(3):242–57. https://doi.org/10.1053/j.semnuclmed.2017.01.001.
23. Friedmann AM, Wolfson JA, Hudson MM, et al. Relapse after treatment of pediatric Hodgkin lymphoma: outcome and role of surveillance after end of therapy. Pediatr Blood Cancer. 2013;60:1458–63.

26 ^{18}F-FDG PET/CT in Treatment Response Evaluation in Thyroid Cancer

Fahim Ul Hassan and Haseeb Ahmed

26.1 Introduction

^{18}F-FDG PET/CT plays a pivotal role in the management of a number of oncological malignancies. In differentiated thyroid cancer (DTC), it is usually not indicated in initial staging. The whole body scan can have an important role in staging, cancer localisation and treatment planning [1]. However in a group of patients with DTC that have raised thyroglobulins with negative radioiodine scan, FDG PET plays an important role in detection and localisation of metastatic disease [2]. As thyroid cancer cells de-differentiate, their ability to take up radioiodine reduces and glucose metabolic activity increases which explains increased tracer uptake in FDG PET scans [3]. Dong et al. conducted a meta-analysis of 25 studies and concluded that ^{18}F-FDG PET/CT has a sensitivity of 93.5% in detecting recurrence and distant metastases in patients with negative radioiodine scan [4]. ^{18}F-FDG PET is routinely used in patients for response assessment in iodine refractory/negative disease that are on tyrosine kinase (TKI's) and also in patients with thyroid lymphomas [5]. Hurthle cell thyroid carcinoma is relatively aggressive with higher incidence of metastases and worse prognosis in comparison to DTC [6]. They are known to be less avid and show higher FDG uptake [7]. Studies have shown sensitivity and specificity of ^{18}F-FDG PET/CT of 95% and higher mortality rate associated with higher FDG uptake [7]. FDG PET is also useful in detecting recurrence in medullary thyroid carcinoma with evidence of biochemical recurrence, i.e. rising serum calcitonin and carcinoembryonic antigen (CEA) levels [8]. It is also useful in initial staging and response assessment in a rare kind of papillary thyroid cancer (PTC), e.g. columnar variant of PTC [9]. Anaplastic thyroid carcinoma is an aggressive variant and rapidly growing thyroid tumour. Seventy-five percent of the patients present with local invasion and 50% of the cases have distant metastases at the time of diagnosis with the lungs, liver and bones being the most common sites [10]. Despite aggressive treatment the survival is very poor [11]. FDG PET/CT is useful in initial staging and evaluation for surgical suitability and as a follow-up [12]. There are a few relatively new PET tracers being used in the management of various thyroid cancers. ^{124}I PET/CT is useful in detection of residual or recurrent disease in DTC. ^{18}F-DOPA PET demonstrates sensitivity of 81% in medullary thyroid cancer (MTC) [13]. 68-Gallium Dotatate, Dotatoc or Dotanoc can be used in patients with MTC [14], and this can also guide to treat some patients with 177-Lutetium Dotatate therapy.

F. U. Hassan (✉) · H. Ahmed
Department of Nuclear Medicine, Guy's & St. Thomas' NHS Foundation, London, England
e-mail: Fahim-ul.hassan@gstt.nhs.uk; Haseeb.ahmed@gstt.nhs.uk

S. Fanti et al. (eds.), *Atlas of Clinical PET-CT in Treatment Response Evaluation in Oncology*,
https://doi.org/10.1007/978-3-030-68858-5_26

26.2 Case 1: ^{18}F-FDG PET/CT After Thyroid Surgery

Clinical Details A 38 years old female, with a diagnosis of pT4(m)N1b(18/63)M1 papillary thyroid cancer. She underwent total thyroidectomy and bilateral neck dissections. In the context of significant post-operative complications resulting in delay in 131-Iodine treatment, an FDG PET/CT was performed to rule out other sites of metastatic disease.

Images

Scan Findings

Figure 26.1: There are non-FDG-avid bilateral pulmonary nodules with low-grade uptake in the right-sided neck node reported as reactive.

Figure 26.2: Post-therapy radioiodine scan shows intense focal tracer uptake in the thyroid remnant, right Level II cervical lymph node (black arrow), mediastinal lymph node (blue arrow) and extensive pulmonary metastases (black and white arrows on CT and fused images).

Interpretation Non-FDG avid disease is intensely avid on subsequent post-radioiodine scan.

Teaching Points

1. Differentiated thyroid cancers (DTC including PTC and FTC) are usually strongly Iodine avid.
2. DTC usually only shows low-grade FDG uptake. Low-grade tracer uptake in neck nodes on FDG PET/CT scan can raise possibility of metastatic disease rather than simply labelling them as reactive and correlation with further imaging e.g; US neck/FNA should be suggested if clinically appropriate.

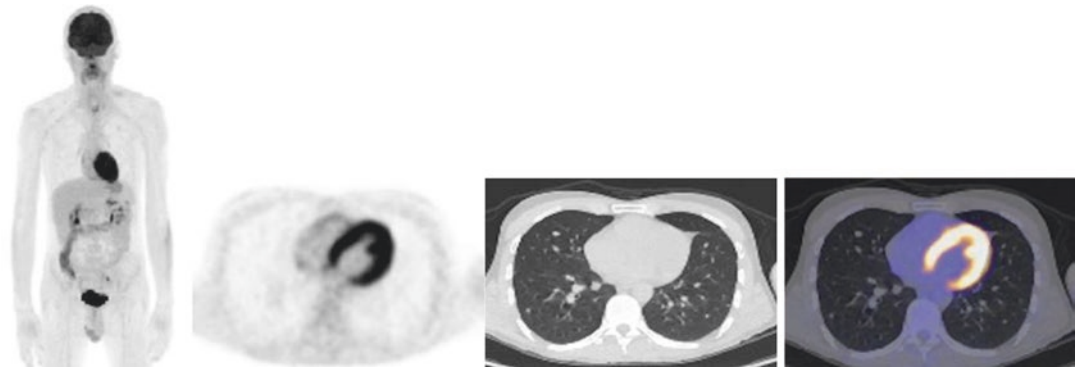

Fig. 26.1 ^{18}F-FDG PET/CT

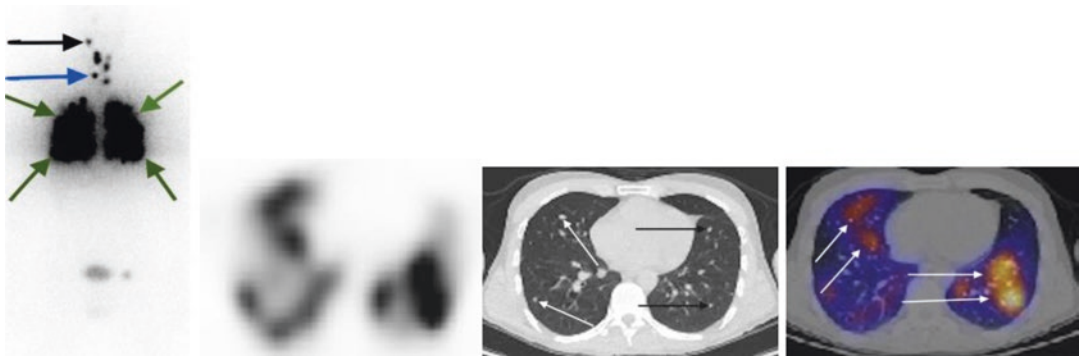

Fig. 26.2 Post treatment radioiodine WB scan supplemented with SPECT/CT of the thorax

26.3 Case 2: Progressive Metastatic Disease After Local Radiotherapy

Clinical Details A 42 years old female with metastatic follicular thyroid cancer (FTC) and non-iodine avid lung and skeletal metastases. Because of severe upper back pain, radiotherapy was given to the lesions in thoracic spine.

Images

Scan Findings

There is FDG-avid disease in the lungs, mediastinum and thoracic spine on the initial scan that has significantly increased in size/number of lesions and as well as metabolic activity.

Figure 26.3 demonstrates metastatic disease involving thoracic spine, most intense at T4 vertebra (green and white arrows) and lungs (blue and yellow arrows).

Figure 26.4: There is metabolic and morphologic progression of metastatic lesions in thoracic spine including T4 vertebra (black and white arrows) that appears to be invading the spinal canal.

Interpretation Disease progression, predominantly related to skeletal metastatic disease with invasion of the spinal canal at T4 vertebra.

Teaching Points

1. Disease progression in thoracic spine after radiotherapy and also in lungs. The patient was started on (TKI).
2. Spinal cord compression cannot be properly assessed on FDG PET study and hence an urgent MRI should be suggested if there is suspicion of impending spinal cord compression.

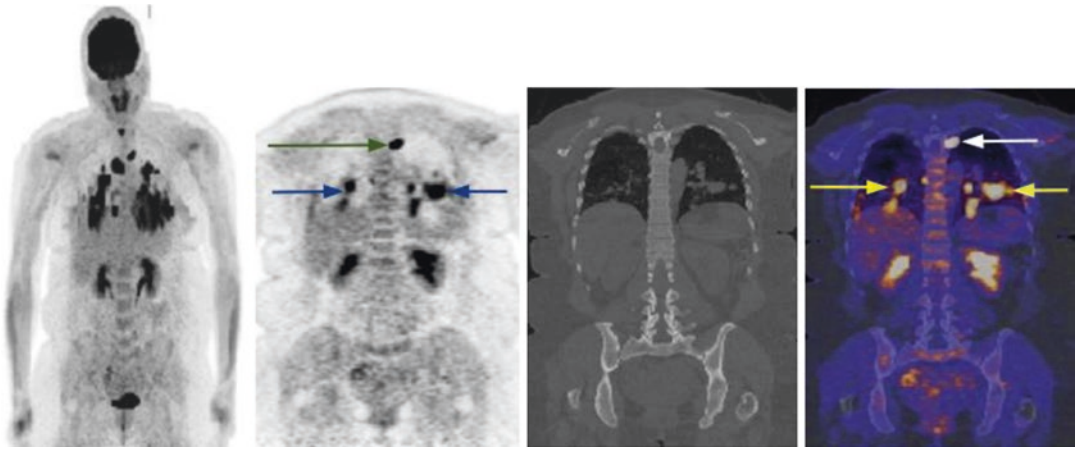

Fig. 26.3 ^{18}F-FDG PET/CT before local radiotherapy

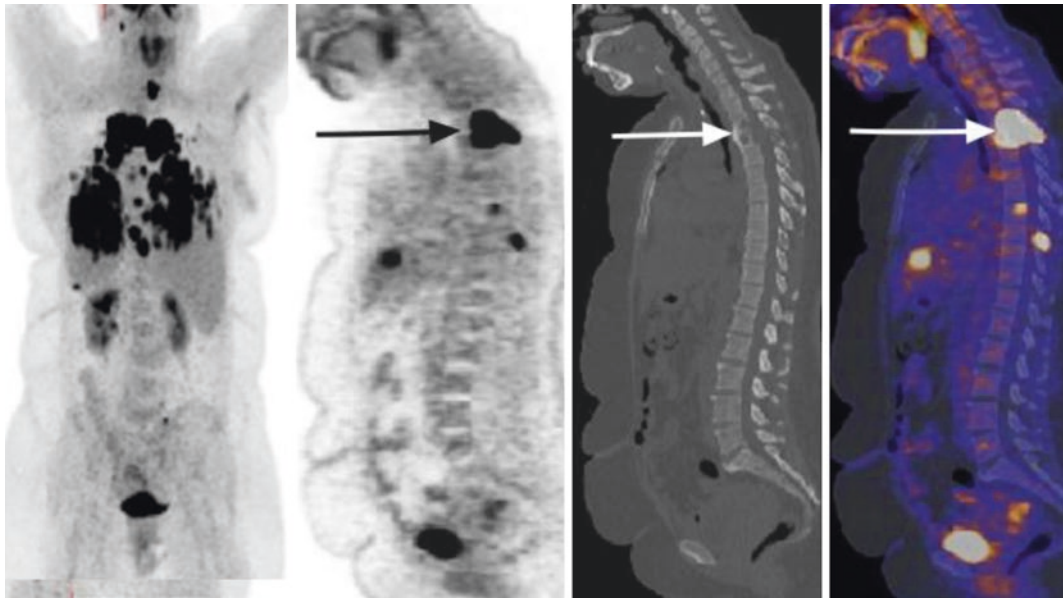

Fig. 26.4 ^{18}F-FDG PET/CT post local radiotherapy

26.4 Case 3: Progressive Disease on Tyrosine Kinase Inhibitor (TKI)

Clinical Details A 52 years old male with a diagnosis of follicular variant of papillary thyroid cancer (pT3N1bM1). Radioiodine treatment did not show any iodine-avid metastatic disease despite increase in thyroglobulin levels. The patient underwent an ^{18}F-FDG PET/CT, which showed metabolically active metastases. The patient was started on Sorafenib but subsequent ^{18}F-FDG PET/CT, 3 months post-initiation of TKI, showed progressive metastatic disease.

Images

Scan Findings
Figure 26.5: There are FDG-avid small volume pulmonary nodules and mediastinal lymph nodes.

Figure 26.6: Overall disease progression including lungs (green, black and white arrows), mediastinal lymph nodes and skeleton. There is increased FDG activity in arms and pelvic muscles that is secondary to strenuous exercise before the scan (blue arrows).

Interpretation There is marked progression of disease in the lungs, mediastinal lymph nodes and skeleton.

Teaching Points
1. Non-avid iodine and FDG-avid disease indicates de-differentiated thyroid cancer. In recent years TKIs can be used to treat these patients.
2. FDG PET/CT is helpful in monitoring metabolic response to TKIs.
3. The patient should not indulge in strenuous exercise before the scan. Exercise can increase the muscular FDG uptake and can make the interpretation of the scan difficult.

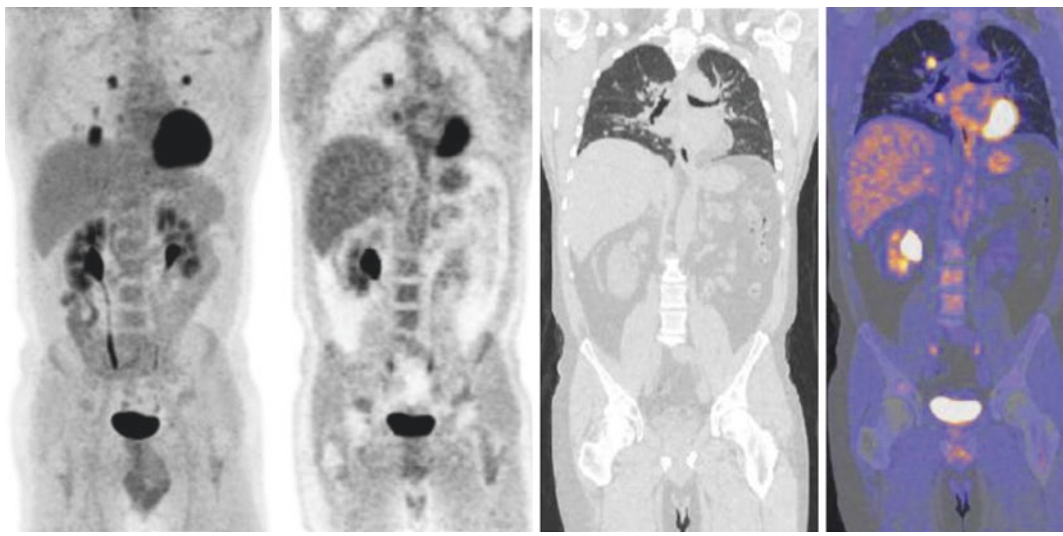

Fig. 26.5 ^{18}F-FDG PET/CT before starting Sorafenib

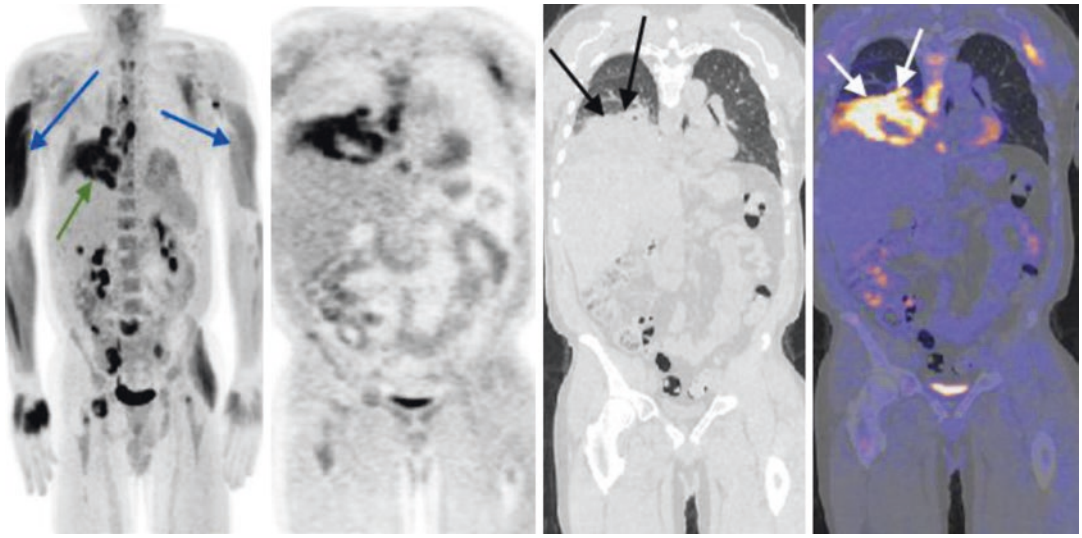

Fig. 26.6 ^{18}F-FDG PET/CT demonstrates progressive metastatic disease

26.5 Case 4: Thyroid Lymphoma

Clinical Details A 75 years old female with history of weight loss underwent FDG PET study. Based on histopathological/PET findings the patient was diagnosed as stage 1E marginal zone lymphoma of the thyroid. She underwent radical radiotherapy of 24 Gy to the thyroid gland.

Images

Scan Findings

Figure 26.7: There is intense diffuse FDG uptake (SUVmax 8) in a bulky enlarged thyroid gland (white arrows).

Figure 26.8: Following radiotherapy there is reduction in size and activity within the thyroid gland (black arrows).

Interpretation The findings suggest possible residual active disease though differential includes inflammatory response. Deauville 4 (FDG uptake > liver background).

Teaching Points

1. Lymphoma involving thyroid gland is rare. Primary thyroid lymphoma is 0.5–5% of all thyroid malignancies and about 2% of extranodal lymphomas.
2. It should be noted that not every uptake in thyroid gland is due to nodular disease/DTC.
3. In lymphomatous process, usually there is intense and diffuse uptake in thyroid.
4. Deauville score is used for response assessment in lymphomas.

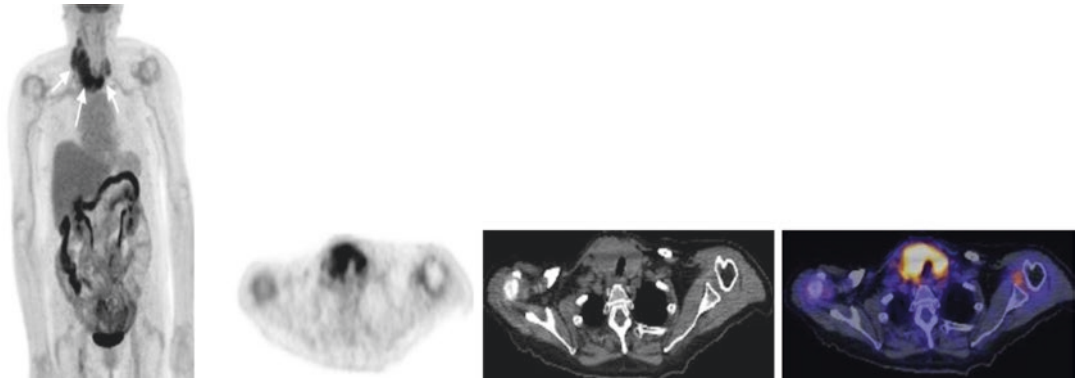

Fig. 26.7 Pre-treatment [18]F-FDG PET/CT

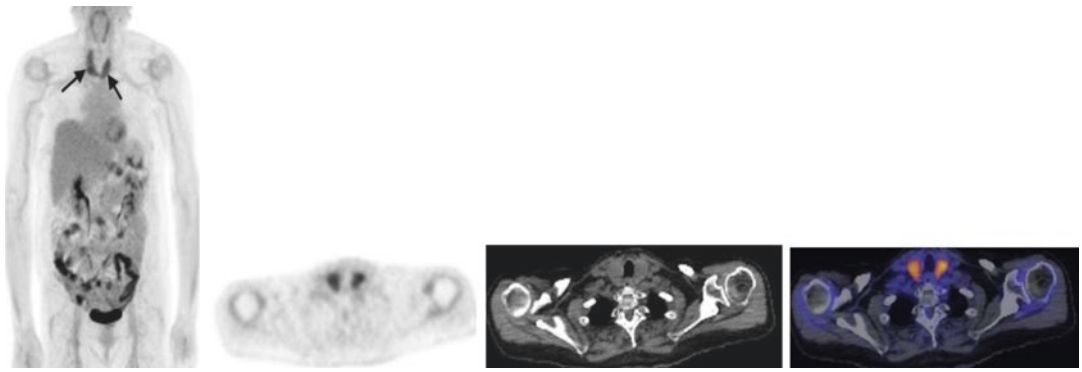

Fig. 26.8 Post-treatment [18]F-FDG PET/CT

26.6 Case 5: Partial Response to Tyrosine Kinase Inhibitors with Increasing Lytic Metastatic Disease

Clinical Details An 82 years old male with known metastatic Hurthle cell carcinoma of thyroid with lung, bone and lymph node metastases. The patient has iodine refractory progressive pulmonary metastases and was commenced on sorafenib.

Images

Scan Findings

Figure 26.9: Metastatic disease in neck, mediastinal nodes and left iliac bone.

Figure 26.10: Following TKI treatment there is reduction in metabolic activity of the metastatic lesions in the mediastinal/hilar nodes from 10.7 to 5 (green arrows) in keeping with partial metabolic response. There are new areas of FDG uptake in the lungs bilaterally (black arrows on axial images) which correspond to consolidation. Metabolic activity in the known left iliac lesion increased (black arrow) and there are random new lytic lesions within the skeleton (black arrow).

Interpretation Partial metabolic response in the known metastatic disease. Taking into account reducing thyroglobulins, increased metabolic activity in known left iliac lesion and new lytic lesions, an alternative diagnosis, e.g. myeloma, should be considered.

Teaching Points

1. Skeletal metastases are usually lytic in thyroid cancers. However, in this case there was response in thoracic nodal disease with reduction in thyroglobulins. Serum protein electrophoresis revealed myeloma.
2. It is important that the reporter hints towards other causes of lytic lesions other than thyroid cancer if discordant findings are found.

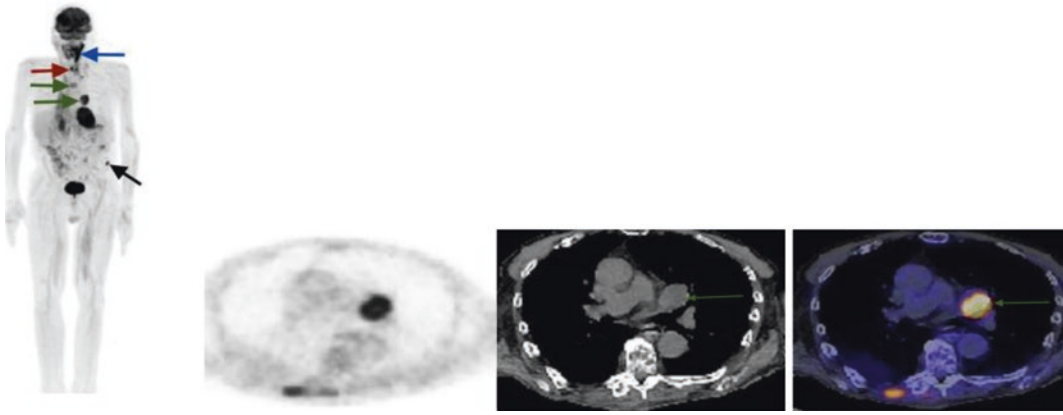

Fig. 26.9 ^{18}F-FDG PET/CT before starting on sorafenib

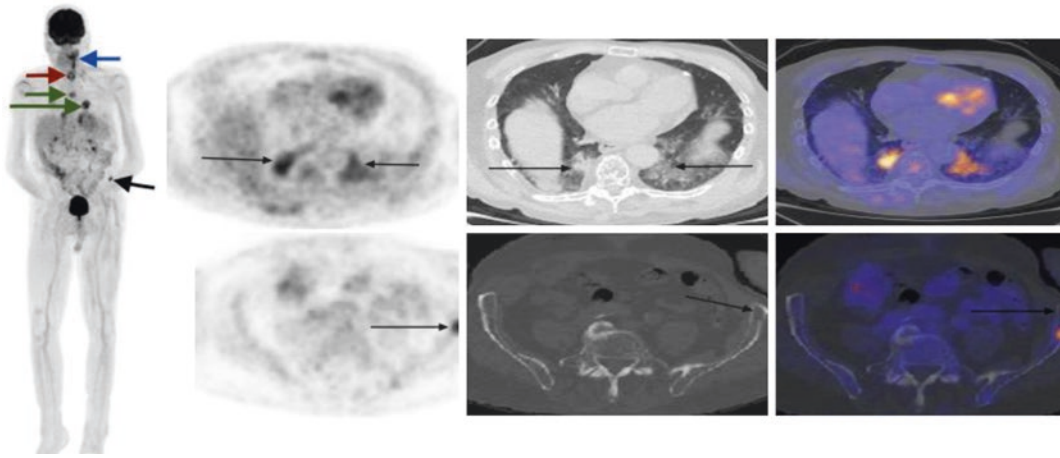

Fig. 26.10 [18]F-FDG PET/CT 6 months after starting on sorafenib

26.7 Case 6: Interesting Finding in a Patient with Anaplastic Carcinoma

Clinical Findings A 60 years old gentleman underwent total thyroidectomy and was diagnosed with pT4N0M0 (anaplastic thyroid carcinoma) followed by chemoradiotherapy. First surveillance scan showed no evidence of metastatic disease. Few months later he complained of gradually worsening upper back pain. Clinical suspicion was of metastatic disease.

Images

Scan Findings

Figure 26.11: There is intense uptake at C5/C6 vertebra (black and white arrows).

Figure 26.12: After a course of antibiotics the previously noted FDG uptake in C5/C6 vertebrae resolved. Linear FDG uptake posteriorly in the pharynx localises to the posterior cricoarytenoid and inferior pharyngeal constrictor muscles which is likely physiological.

Interpretation The focal FDG uptake in C5/C6 was secondary to infection rather than skeletal metastases.

Teaching Points

1. Anaplastic cancers are rare with very high mortality. FDG PET is used for staging and for follow-up following surgery or chemo-radiotherapy

   Although the clinical suspicion was that of metastatic disease, however PET scan appearances were of C5/C6 spondylodiscitis. Not every focal uptake on FDG PET scan is due to metastatic disease. It is important that pattern recognition of FDG uptake along with underlying structural abnormalities is appreciated and correlated with history and biochemical investigations.

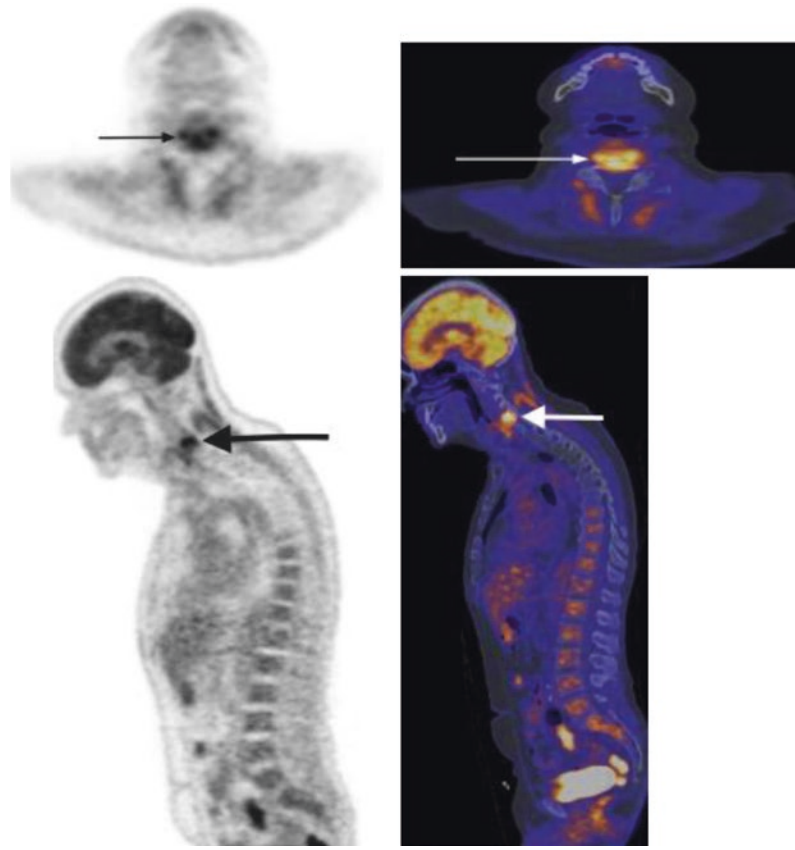

Fig. 26.11 FDG PET for assessment of neck pain

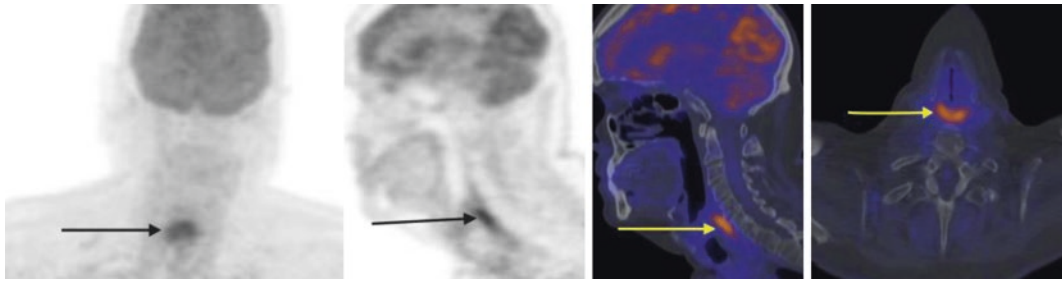

Fig. 26.12 FDG PET following treatment

References

Introduction

1. Grünwald F, Menzel C, Bender H, Palmedo H, Willkomm P, Ruhlmann J, et al. Comparison of 18FDG-PET with 131Iodine and 99mTc-sestamibi scintigraphy in differentiated thyroid cancer. Thyroid. 1997;7(3):327–35.
2. Cooper DS, Doherty GM, Haugen BR, Kloos RT, Lee SL, Mandel SJ, et al. Revised American Thyroid Association management guidelines for patients with thyroid nodules and differentiated thyroid cancer: the American Thyroid Association (ATA) guidelines taskforce on thyroid nodules and differentiated thyroid cancer. Thyroid. 2009;19(11):1167–214.
3. Abraham T, Schöder H. Thyroid cancer—indications and opportunities for positron emission tomography/computed tomography imaging. Semin Nucl Med. 2011;41(2):121–38.
4. Dong M-J, Liu Z-F, Zhao K, Ruan L-X, Wang G-L, Yang S-Y, et al. Value of 18F-FDG-PET/PET-CT in differentiated thyroid carcinoma with radioiodine-negative whole-body scan: a meta-analysis. Nucl Med Commun. 2009;30(8):639–50.
5. Manohar PM, Beesley LJ, Bellile EL, Worden FP, Avram AM. Prognostic value of FDG-PET/CT metabolic parameters in metastatic radioiodine-refractory differentiated thyroid cancer. Clin Nucl Med. 2018;43(9):641–7.
6. Stojadinovic A, Ghossein RA, Hoos A, Urist MJ, Spiro RH, Shah JP, et al. Hürthle cell carcinoma: a critical histopathologic appraisal. J Clin Oncol. 2001;19(10):2616–25.
7. Treglia G, Annunziata S, Muoio B, Salvatori M, Ceriani L, Giovanella L. The role of fluorine-18-fluorodeoxyglucose positron emission tomography in aggressive histological subtypes of thyroid cancer: an overview. Int J Endocrinol. 2013;2013:1–6.
8. Bogsrud TV, Karantanis D, Nathan MA, Mullan BP, Wiseman GA, Kasperbauer JL, et al. The prognostic value of 2-deoxy-2-[18F]Fluoro-d-glucose positron emission tomography in patients with suspected residual or recurrent medullary thyroid carcinoma. Mol Imaging Biol. 2010;12(5):547–53.
9. Vadrucci M, Serio G, Baroli A. ^{18} F-FDG PET/CT-guided clinical management of the rare aggressive "columnar-cell" variant of papillary thyroid cancer. Endocrinol Metab. 2016;31(2):343.
10. Stamatakos M, Paraskeva P, Stefanaki C, Katsaronis P, Lazaris A, Safioleas K, et al. Medullary thyroid carcinoma: the third most common thyroid cancer reviewed. Oncol Lett. 2011;2(1):49–53.
11. Chen J, Tward JD, Shrieve DC, Hitchcock YJ. Surgery and radiotherapy improves survival in patients with anaplastic thyroid carcinoma: analysis of the surveillance, epidemiology, and end results 1983–2002. Am J Clin Oncol. 2008;31(5):460–4.
12. Poisson T, Deandreis D, Leboulleux S, Bidault F, Bonniaud G, Baillot S, et al. 18F-fluorodeoxyglucose positron emission tomography and computed tomography in anaplastic thyroid cancer. Eur J Nucl Med Mol Imaging. 2010;37(12):2277–85.
13. Beheshti M, Pöcher S, Vali R, Waldenberger P, Broinger G, Nader M, et al. The value of 18F-DOPA PET-CT in patients with medullary thyroid carcinoma: comparison with 18F-FDG PET-CT. Eur Radiol. 2009;19(6):1425–34.
14. Treglia G, Castaldi P, Villani MF, Perotti G, de Waure C, Filice A, et al. Comparison of 18F-DOPA, 18F-FDG and 68Ga-somatostatin analogue PET/CT in patients with recurrent medullary thyroid carcinoma. Eur J Nucl Med Mol Imaging. 2012;39(4):569–80.

Case 1

Flavell RR, Naeger DM, Mari Aparici C, Hawkins RA, Pampaloni MH, Behr SC. Malignancies with low fluorodeoxyglucose uptake at PET/CT: pitfalls and prognostic importance: resident and fellow education feature. RadioGraphics. 2016;36(1):293–4.

Case 2

Tam S, Amit M, Boonsripitayanon M, Cabanillas ME, Busaidy NL, Gunn GB, et al. Adjuvant external beam radiotherapy in locally advanced differentiated thyroid cancer. JAMA Otolaryngol Neck Surg. 2017;143(12):1244.

Case 3

Brose MS, Nutting CM, Jarzab B, Elisei R, Siena S, Bastholt L, et al. Sorafenib in radioactive iodine-refractory, locally advanced or metastatic differentiated thyroid cancer: a randomised, double-blind, phase 3 trial. Lancet. 2014;384(9940):319–28.

Surasi DS, Bhambhvani P, Baldwin JA, Almodovar SE, O'Malley JP. 18F-FDG PET and PET/CT patient preparation: a review of the literature. J Nucl Med Technol. 2014;42(1):5–13.

Case 4

Dundar HZ, Sarkut P, Kirdak T, Korun N. Primary thyroid lymphoma. Turk J Surg. 2016;32(1):75–7.

Nakadate M, Yoshida K, Ishii A, Koizumi M, Tochigi N, Suzuki Y, et al. Is 18F-FDG PET/CT useful for distinguishing between primary thyroid lymphoma and chronic thyroiditis? Clin Nucl Med. 2013;38(9):709–14.

Case 5

Cavo M, Terpos E, Nanni C, Moreau P, Lentzsch S, Zweegman S, et al. Role of 18F-FDG PET/CT in the diagnosis and management of multiple myeloma and other plasma cell disorders: a consensus statement by the International Myeloma Working Group. Lancet Oncol. 2017;18(4):e206–17.

Agarwal A, Chirindel A, Shah BA, Subramaniam RM. Evolving role of FDG PET/CT in multiple myeloma imaging and management. Am J Roentgenol. 2013;200(4):884–90.

Case 6

Chen J, Tward JD, Shrieve DC, Hitchcock YJ. Surgery and radiotherapy improves survival in patients with anaplastic thyroid carcinoma: analysis of the surveillance, epidemiology, and end results 1983–2002. Am J Clin Oncol. 2008;31(5):460–4.

Poisson T, Deandreis D, Leboulleux S, Bidault F, Bonniaud G, Baillot S, et al. 18F-fluorodeoxyglucose positron emission tomography and computed tomography in anaplastic thyroid cancer. Eur J Nucl Med Mol Imaging. 2010;37(12):2277–85.

68Ga-DOTA PET-CT in Treatment Response Evaluation: Neuroendocrine Tumours

27

Valentina Ambrosini and Stefano Fanti

27.1 Introduction

Neuroendocrine tumors (NET) are relatively rare disorders that more often present as well-differentiated tumors with a relative good prognosis. However, their prevalence is increasing, mostly as a consequence of more accurate diagnosis, more efficient treatment options, and wider clinical awareness. The well-differentiated tumors (Grade 1, 2 according to the 2010 World Health Organization classification) are generally accurately studied with 68Ga-SA (somatostatin analogs agonists) PET/CT (with either 68Ga-DOTANOC, 68Ga-DOTATOC, 68Ga-DOTATATE) that can demonstrate the presence of somatostatin receptors on tumor cells. However, undifferentiated clones (that can only be visualized on 18F-FDG PET/CT) can become evident during the course of the disease, even when not present at first diagnosis. Therefore, an integrated multidisciplinary approach is highly needed to plan an accurate diagnostic work-up (both at staging and for the assessment of treatment response) that also takes into account the relative long progression-free survival in most cases. According to recent EANM/ENETS guidelines, treatment response should be assessed with morphologic RECIST criteria; however, it is well known that they present several limitations in NET assessment (mostly concerning the relatively small variations in size of generally slow growing disorders and the difficult assessment of the cystic component). Moreover, PET/CT can often detect functional changes indicative of active disease before morphological changes become apparent on CT. Combined functional and morphological imaging may in many cases better reflect the true behavior of the tumor following treatment. The following cases were selected to highlight issues on both image interpretation and choice of the radiopharmaceutical after therapy.

V. Ambrosini (✉) · S. Fanti
Nuclear Medicine, DIMES, S.Orsola-Malpighi Hospital, University of Bologna, Bologna, Italy
e-mail: valentina.ambrosini@unibo.it; Valentina.ambrosini@aosp.bo.it

S. Fanti et al. (eds.), *Atlas of Clinical PET-CT in Treatment Response Evaluation in Oncology*,
https://doi.org/10.1007/978-3-030-68858-5_27

27.2 Clinical Examples

27.2.1 Case 1: 68Ga-DOTANOC PET/CT Biodistribution (Image 27.1)

Clinical Details 68Ga-DOTANOC PET/CT performed in a patient with suspected NET based on biochemical detection of chromogranin A increase.

Interpretation of Image 27.1 68Ga-DOTANOC PET/CT MIP image is negative for neuroendocrine lesions.

Teaching Points—Case 1 (Image 27.1)

- Normal tracer biodistribution includes high uptake at spleen, adrenal glands, pituitary, kidneys, and bladder level.
- When present, accessory spleens may also show increased uptake (the uptake is generally high; however, its intensity also depends on accessory spleens' size).
- The thyroid, the liver, the pancreatic head/uncinate process (variable), and bowel may also show increased uptake.
- The pattern of uptake at pancreatic head/uncinate process level may be diffuse (more frequent) or focal. Careful exclusion of corresponding lesions at morphological diagnostic imaging is crucial to confirm the non-pathologic nature of such finding.
- Increased chromogranin is very non-specific and cannot be considered always indicative of the presence of a neuroendocrine tumor.

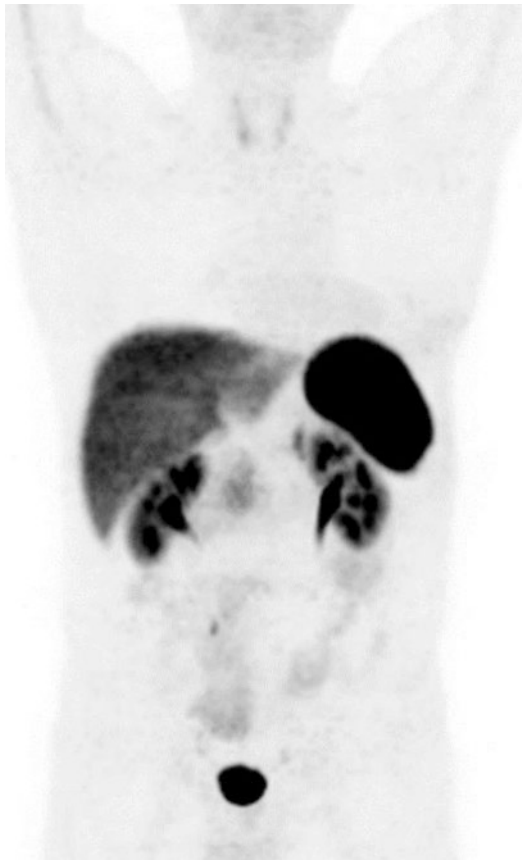

Image 27.1 68Ga-DOTANOC PET/CT MIP image shows no areas of pathological increased uptake

27.2.2 Case 2: Restaging After Radical Surgery (Images 27.2 and 27.3)

Clinical Details Staging (Image 27.2) and restaging (Image 27.3) after radical surgery (splenectomy and left pancreasectomy) and initiation of somatostatin analog therapy of a patient with pancreatic NET G1.

Interpretation of Image 27.2 PET/CT images show intense uptake at the primary pancreatic neoplastic lesion, confirming high somatostatin receptors expression, and therefore a well differentiated NET (high radiopharmaceutical uptake is an indirect measure of better prognosis). Diffuse pancreatic head/uncinate process uptake is to be ascribed to physiologic radiopharmaceutical biodistribution, in the absence of corresponding morphological abnormalities at diagnostic CT.

Interpretation of Image 27.3 PET/CT is negative for NET. The subdiaphragmatic nodule is to be referred to an accessory spleen close to the diaphragm.

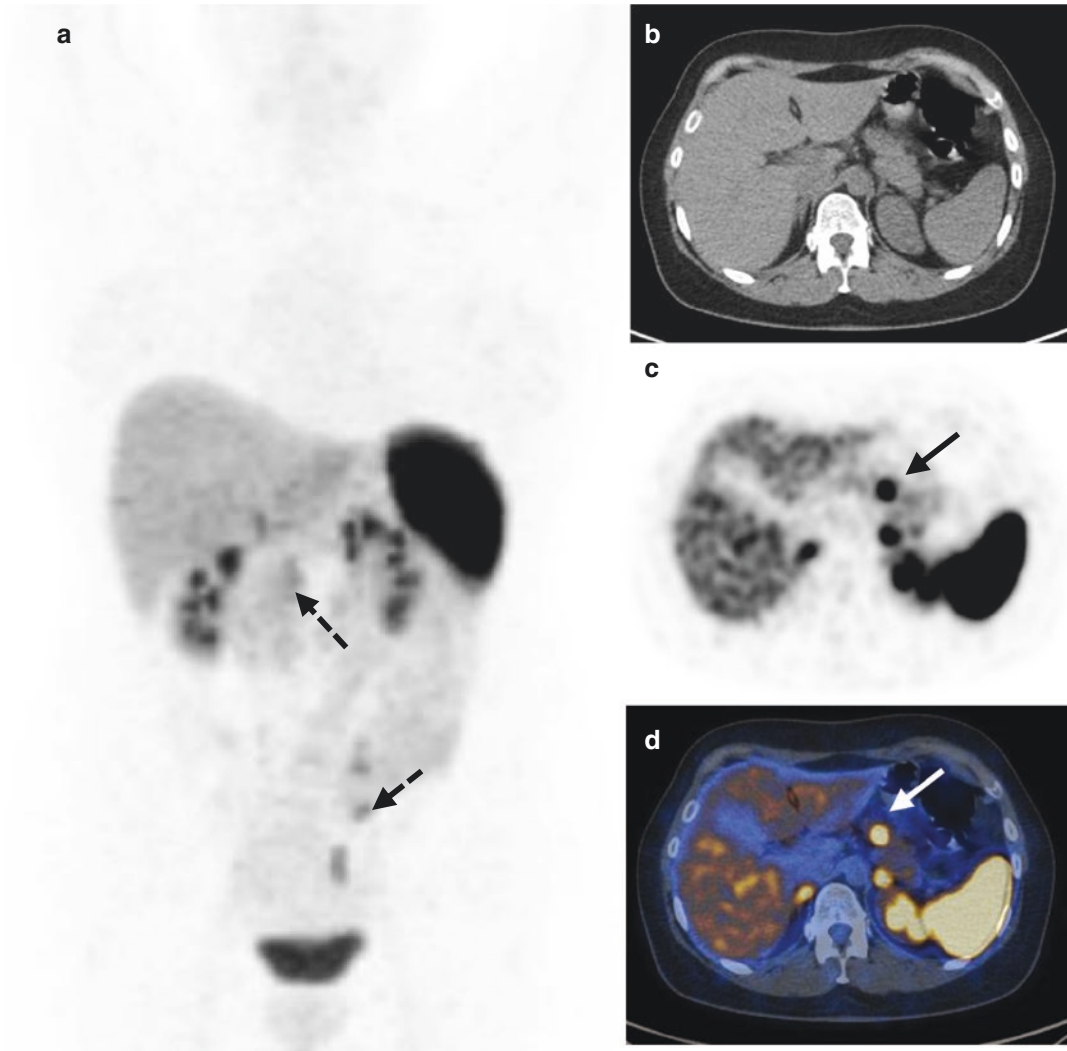

Image 27.2 68Ga-DOTANOC images (**a**: MIP; **b**: non-diagnostic CT; **c**: PET; **d**: fused) show intense (SUVmax = 19.1) focal pancreatic uptake (**d**, white arrow). Dashed black arrows show, respectively, faint and diffuse physiologic pancreatic head/uncinate process uptake and delayed radioactive urine transit in the left ureter

Teaching Points—Case 2 (Images 27.2 and 27.3)

- Accessory spleens are relatively frequent and may represent a potential pitfall in image reading, especially in patients studied for restaging after splenectomy.
- The spleen is the organ presenting the highest 68Ga-SA uptake, due to the high prevalence of lymphocytes (that also express somatostatin receptors).
- Accessory spleens, if present, may also show variable to high 68Ga-SA uptake and should not be erroneously interpreted as disease relapse. Interpretation is easier in cases presenting with accessory spleens in the splenic lodge, while the presence of avid nodules close/adherent to the diaphragm is much more challenging.
- Accessory spleen do not show significant 18F-FDG uptake (e, f) and are easily visualized on 99Tcm-colloid scintigraphy.

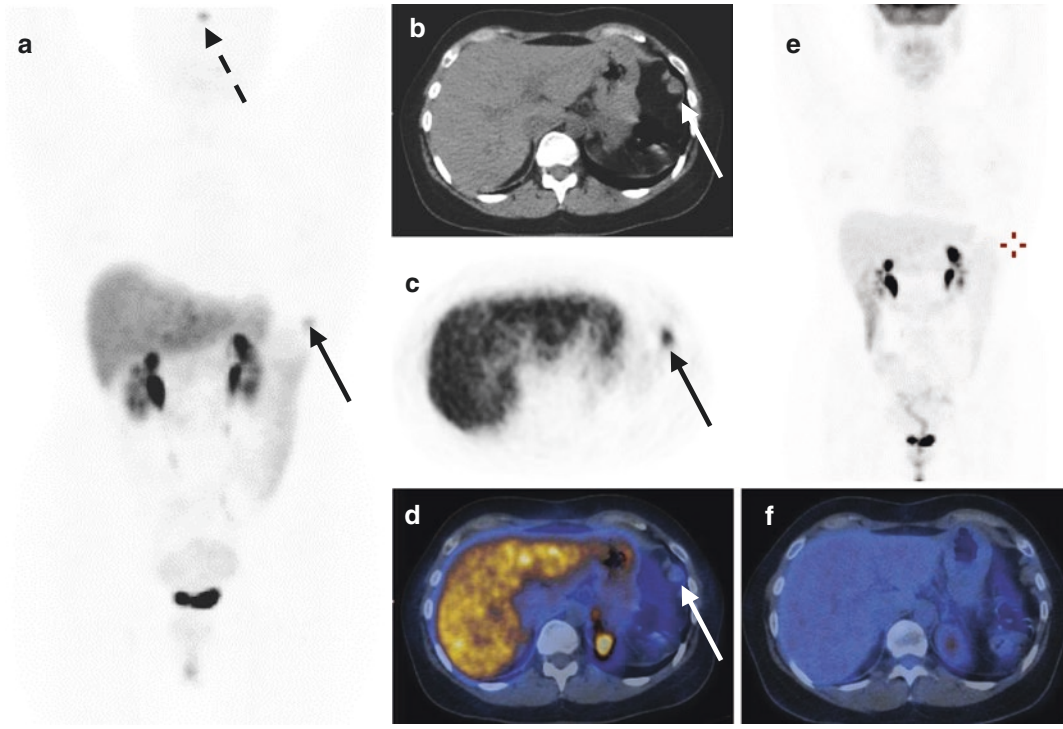

Image 27.3 Restaging of the same patient after surgery and ongoing somatostatin analog therapy. 68Ga-DOTANOC PET/CT images (**a**: MIP; **b**: nondiagnostic CT; **c**: PET; **d**: fused) demonstrate faint uptake at a subdiaphragmatic nodule (arrow, **a**–**d**; SUVmax = 6.7), negative on corresponding 18F-FDG images (**e**: MIP, red pointer; **f**: fused; no uptake is evident on the accessory spleen). Dashed black arrow (**a**) shows normal biodistribution to the hypophysis

27.2.3 Case 3: Restaging After Surgery (Image 27.4)

Clinical Details Staging and restaging after surgery of a pancreatic NET G2.

Interpretation of Image 27.4 there are no areas of pathologic radiopharmaceutical uptake that are suspicious for NET relapse or for the presence of a residual tumor. The focal area of uptake on the surgical margins, associated with the presence of a fluid collection on CT corresponding images, supports the infectious nature (abscess).

Teaching Points—Case 3 (Image 27.4)

- Accurate interpretation of 68Ga-SA PET/CT after surgery requires exclusion of all conditions that could be ascribed to surgery-related inflammation/infection.
- In fact, due to the expression of somatostatin receptors on lymphocytes, inflammatory and infectious findings can be misinterpreted as sites of disease.
- It is mandatory to always evaluate nondiagnostic CT images for accurate PET/CT interpretation.

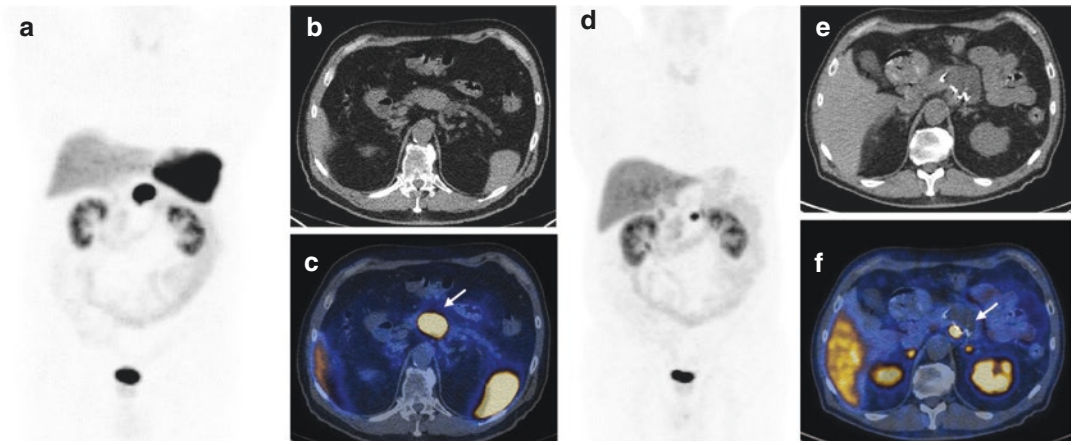

Image 27.4 Presurgical 68Ga-DOTANOC PET/CT images (**a**: MIP; **b**: nondiagnostic CT; **c**: fused) show intense (SUVmax = 42) focal pancreatic uptake at the known NET G2 lesion (**c**: white arrow). After splenopancreasectomy (**d**: MIP; **e**: nondiagnostic CT; **f**: fused), a focal area of intense uptake (SUVmax = 38) is evident at the surgical margins. The corresponding nondiagnostic CT images show a hypodense area suspicious for infection (abscess)

27.2.4 Case 4: Restaging on Somatostatin Analog Therapy (Images 27.5 and 27.6)

Clinical Details A patient with a previously surgically removed ileum NET G2 was studied after surgery (Image 27.5; Panels a–d) and for suspected relapse while undergoing somatostatin analog therapy (Image 27.5; Panels e–k). For the detection of a core cold lesion on 68Ga-DOTANOC PET/CT (Image 27.5), the patient was further studied with 18F-FDG (Image 27.6).

Interpretation Image 27.5 68Ga-DOTANOC PET/CT (a–d) shows a small, though focal, area of increased and pathologic uptake at liver level (SUVmax = 6; c, d: arrow), to be referred to disease relapse.

Subsequent restaging PET/CT (e–l), while on somatostatin analog therapy, shows an increase in the number of liver lesions, compatible with disease progression. In particular, the already documented lesion at the sixth segment shows increased uptake (i, l: SUVmax = 13 vs. c, d: SUVmax = 6). Among new lesions, the biggest one (e, g; white arrow) shows intense tracer avidity at the periphery (SUVmax = 15.7) and a cold core (doughnut-shaped).

Clinical Management After PET/CT Pathological assessment of the biggest doughnut-shaped lesion showed a lower ki67 score at the periphery than at core level (5% vs. 25%), consistent with the co-existence of two distinct cell clones. Therefore, further imaging was prescribed in order to rule out the presence of additional sites of undifferentiated disease.

Interpretation of Image 27.6 disease progression with appearance of an FDG avid single lesion.

Teaching Points—Case 4 (Images 27.5 and 27.6)

- Undifferentiated clones can become evident during the course of the disease (even in cases originally presenting as well-differentiated tumors).
- Management of NET patients requires multidisciplinary discussion in order to establish the most accurate follow-up strategy (also taking into account the expected longer progression-free survival of well-differentiated NET) that may also involve the performance of 18F-FDG additional imaging.
- Since 68Ga-SA PET/CT can only detect somatostatin receptors expressing lesions, in the presence of 68Ga-SA cold areas without CT evidence of corresponding necrosis, an 18F-FDG PET/CT scan should be performed for appropriate disease restaging.

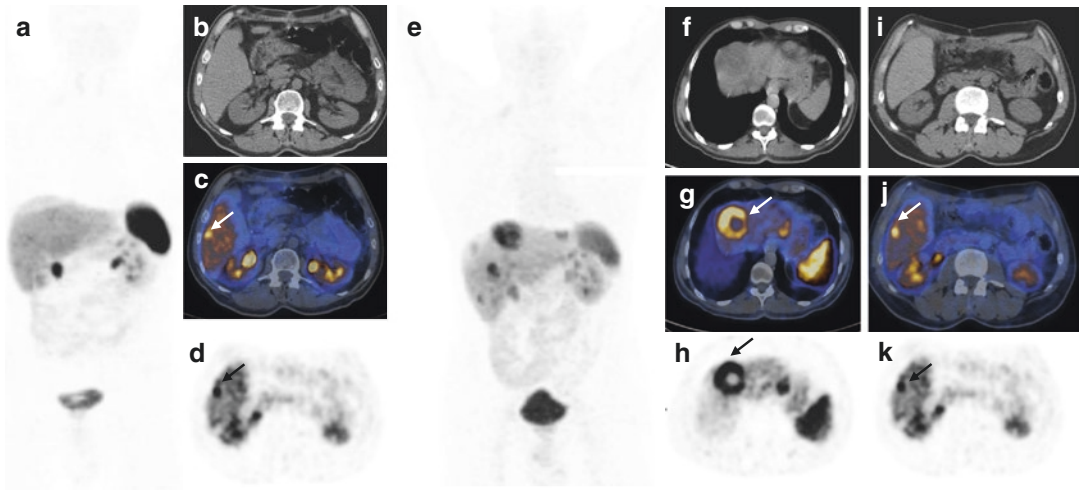

Image 27.5 68Ga-DOTANOC PET/CT was performed after surgery (**a**: MIP; **b**: nondiagnostic CT; **c**: fused; **d**: PET) and for suspected relapse while on-going somatostatin analog therapy (**e**: MIP; **f**, **i**: non-diagnostic CT; **g**, **j**: fused; **h**, **k**: PET)

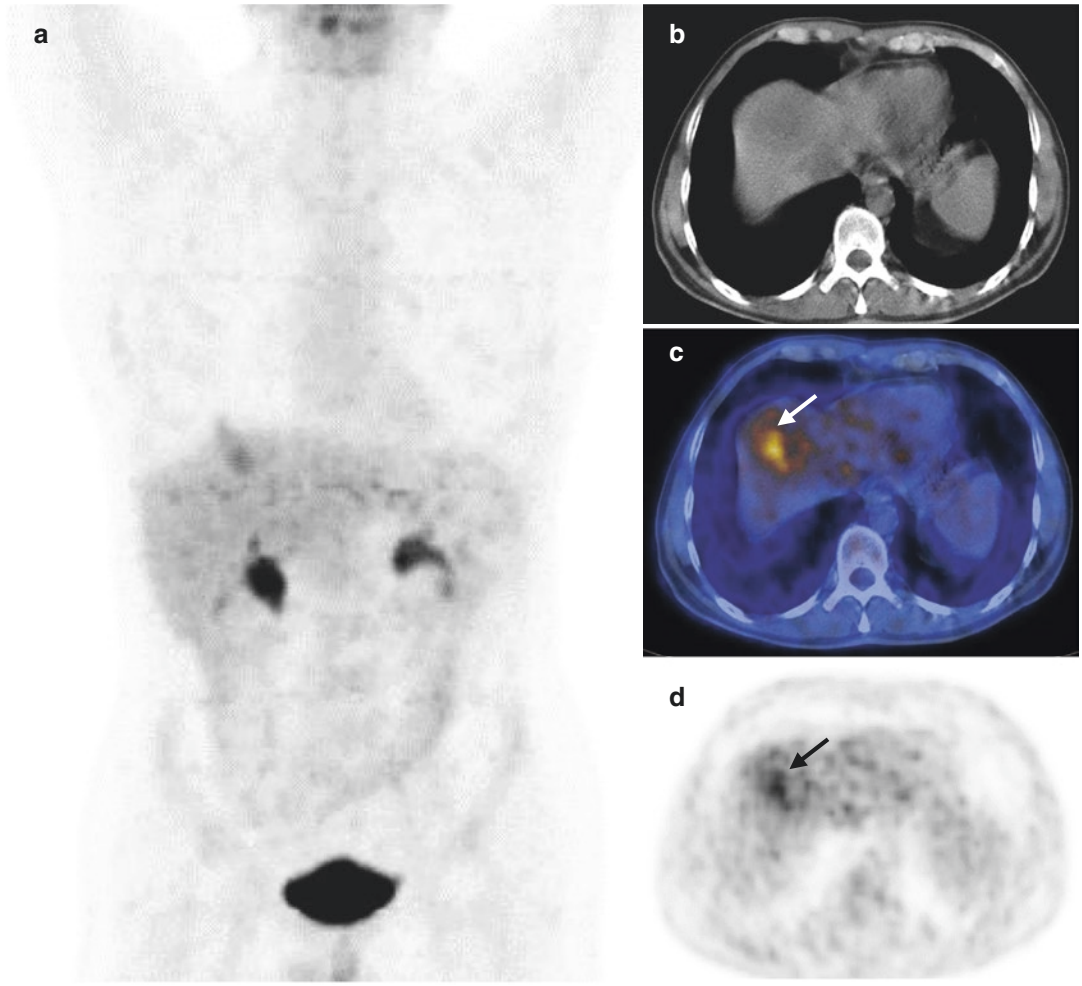

Image 27.6 18F-FDG PET/CT (**a**: MIP; **b**: nondiagnostic CT; **c**: fused; **d**: PET) showed the presence of only one lesion presenting pathological uptake. The FDG avid focus corresponds to the 68Ga-DOTANOC cold core of the previously described doughnut-shaped lesion

27.2.5 Case 5: Restaging After PRRT (Peptide Receptor Radionuclide Therapy) (Images 27.7 and 27.8)

Clinical Details Restaging after PRRT of a patient with advanced unknown primary tumor NET (ki67% = 5%).

Interpretation Images 27.7 and 27.8 68Ga-DOTANOC PET/CT performed before and after PRRT shows a partial response to therapy. Focal and faint uptake in the ureter reflects delayed transit of radioactive urine (dashed arrow).

Teaching Points—Case 5 (Images 27.7 and 27.8)

- 68Ga-SA PET/CT is to be performed before starting PRRT in order to select patients who might benefit from treatment.
- The SUVmax values are an indirect measure of somatostatin receptors expression and therefore an indirect measure of cells differentiation.
- Well-differentiated (Grades 1, 2) tumors are ideal candidates to PRRT as a consequence of high somatostatin receptors expression.
- If different radiopharmaceuticals (DOTANOC, DOTATOC, DOTATATE) were employed before and after therapy, the corresponding SUVmax values are not directly comparable.

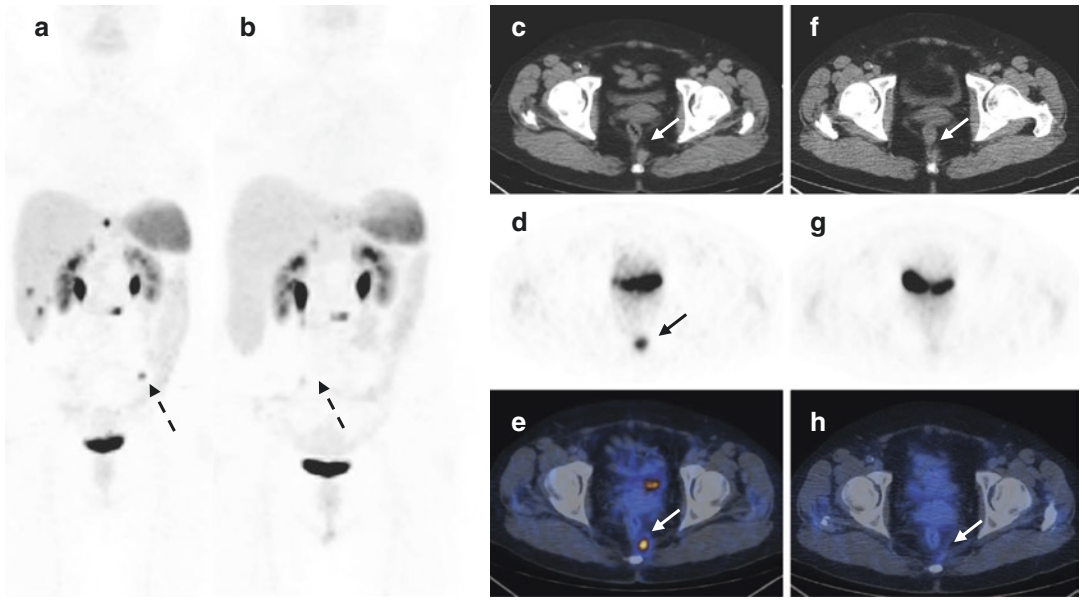

Image 27.7 MIP 68Ga-DOTANOC PET/CT images before (**a**) and after (**b**) PRRT in a patient with advanced CUP NET (ki67% = 5%). Transaxial nondiagnostic CT, PET, and fused images before (**c**–**e**) and after PRRT (**f**–**h**). Images show a complete normalization of a para-rectal node lesion (Panels **c**–**h**; arrows) and of liver lesions

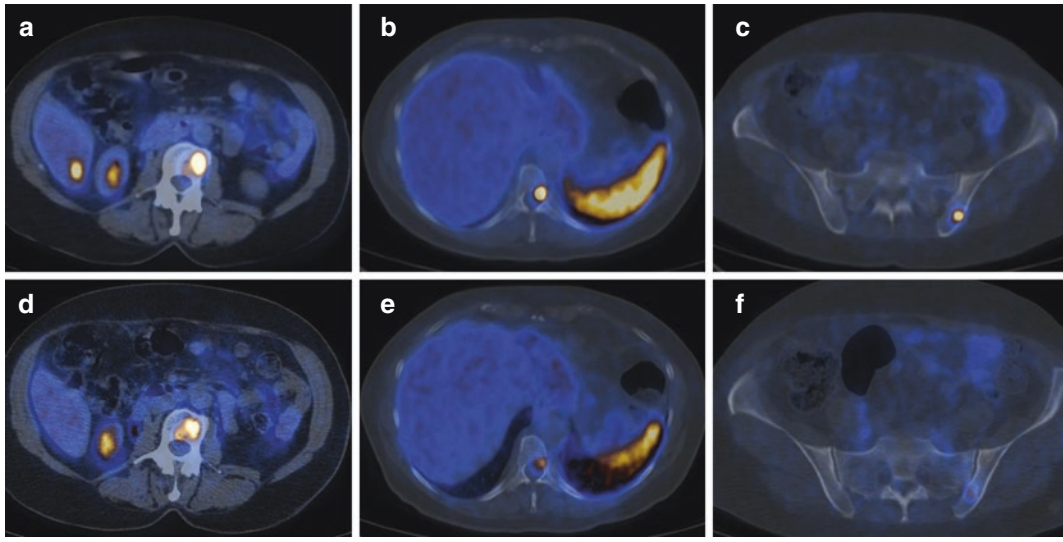

Image 27.8 Transaxial fused images before (**a**–**c**) and after PRRT (**d**–**f**). Images show a complete normalization of liver lesions (Panels **a** and **d**) while bone lesions are still evident in the post-PRRT images, although showing a lower uptake (Panels **a**–**f**)

27.2.6 Case 6: Ileum NET Restaging on Somatostatin Analog Therapy (Image 27.9)

Clinical Details A patient previously surgically treated for an ileum NET G2 (ki67% = 6%) was studied for restaging while on somatostatin analog therapy.

Interpretation of Image 27.9 68Ga-DOTANOC PET/CT shows the presence of a focal and pathologic area of increased tracer uptake at liver level (c: arrow; SUVmax = 7), to be referred to disease progression. Corresponding diagnostic CT images are negative.

Teaching Points—Case 6 (Image 27.9)

- SA PET/CT is very accurate to assess disease progression and can detect the presence of functional changes when morphological abnormalities are not apparent yet.
- Combined functional and morphological imaging may in many cases better reflect the true behavior of the tumor following treatment.

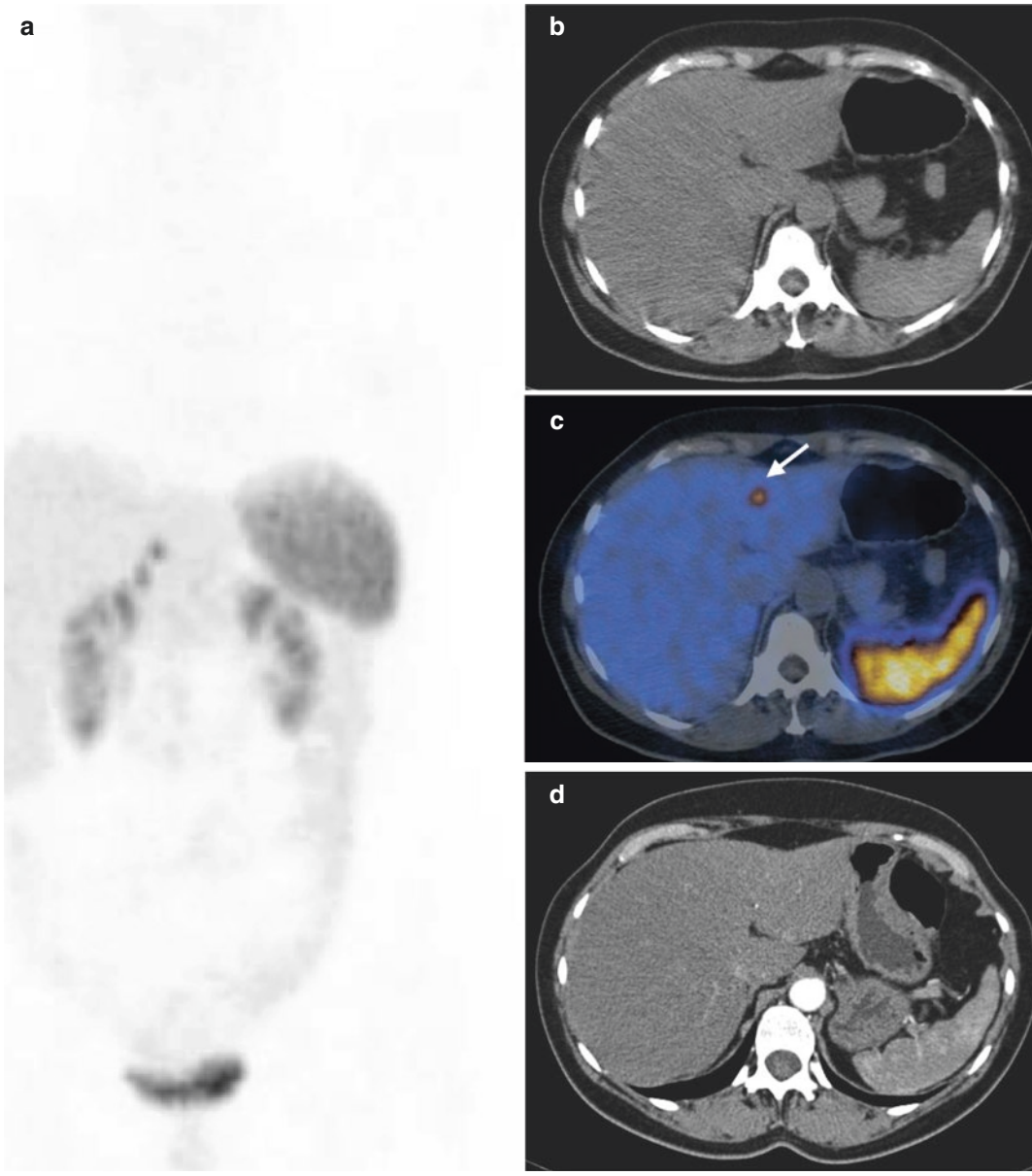

Image 27.9 MIP and transaxial PET images (**a**: MIP; **b**: nondiagnostic CT; **c**: fused) and diagnostic CT (**d**)

27.2.7 Case 7: Nodal Relapse of a Well-Differentiated Ileum NET (Image 27.10) and Further Disease Progression on Somatostatin Analog Therapy (Image 27.11)

Clinical Details—Image 27.10 Restaging of an ileum NET G2 (ki67% = 7%) 2 years after surgical removal of the primary lesion.

Interpretation of Image 27.10 68Ga-DOTANOC PET/CT shows the presence of multiple, focal and pathologic areas of increased tracer uptake at abdominal nodal level (SUVmax = 15; Panels b–d) to be referred to disease progression. Intense radiopharmaceutical uptake indicates well-differentiated tumor lesions. Focal and faint uptake in the right ureter reflects delayed transit of radioactive urine in the ureter (dotted arrow).

Clinical Details—Image 27.11 Restaging of the same patient while on somatostatin analog therapy.

Interpretation of Image 27.11 68Ga-DOTANOC PET/CT shows disease progression at nodal and lung level. Focal and faint uptake in the ureter bilaterally reflects delayed transit of radioactive urine in the ureters (dotted arrow).

Teaching Points—Case 7 (Images 27.10 and 27.11)

- 68Ga-SA PET/CT is accurate to detect somatostatin receptor expressing lesions also at disease progression.
- 68Ga-SA PET/CT is fundamental to select the patients who might benefit from PRRT.
- Lesions showing high 68Ga-SA uptake reflect a high somatostatin receptors expression and therefore are the ideal candidates for PRRT (well-differentiated lesions, Grades 1 and 2).
- Current guidelines recommend PRRT at disease progression; however, the recently published results of the Netter-1 trial will probably lead to further evaluation of the role of PRRT at different disease stages.

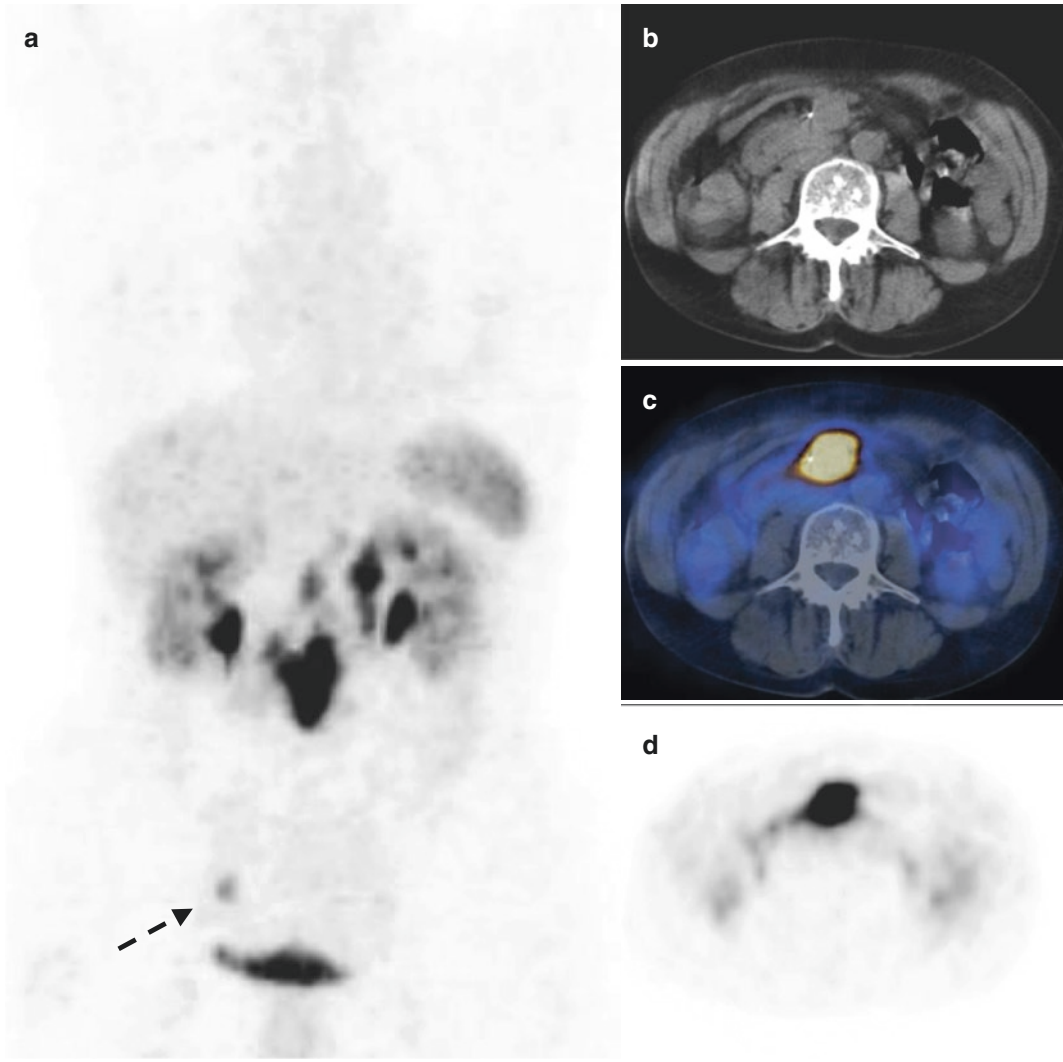

Image 27.10 MIP (**a**) and transaxial PET images (**b**: nondiagnostic CT; **c**: fused images; **d**: PET) show nodal abdominal relapse

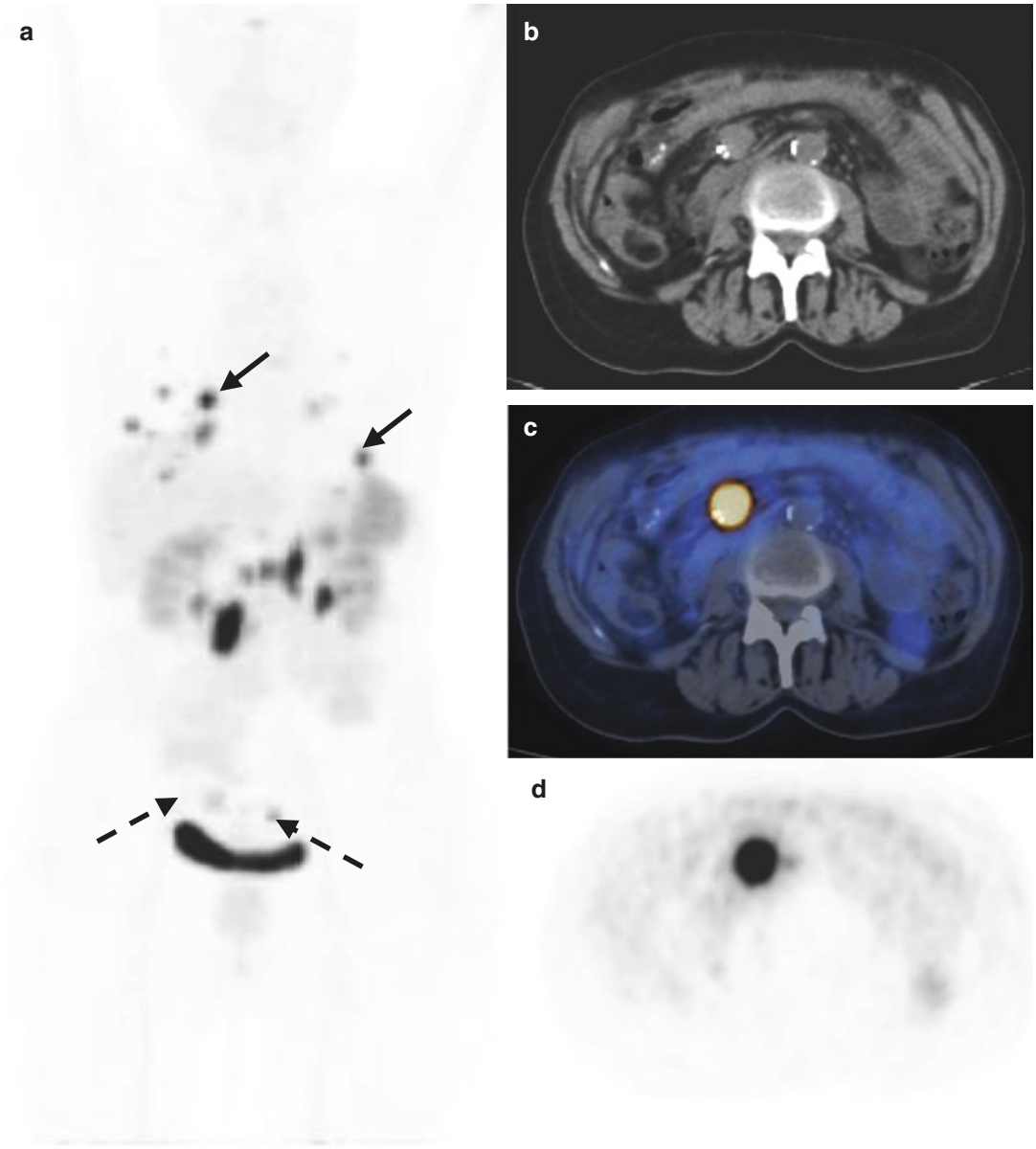

Image 27.11 MIP (**a**) and transaxial PET images (**b**: nondiagnostic CT; **c**: fused images; **d**: PET) show an increase in number of abdominal nodal lesions and occurrence of new multiple lesions at lung level (**a**; black arrows)

27.3 Case 8: Pancreatic NET G1 Studied Before and After PRRT (Partial Response) (Image 27.12)

Clinical Details Patient with pancreatic NET G1 (ki67% = 2%) studied before and after PRRT.

Interpretation of Image 27.12 68Ga-SA PET/CT shows the reduction of the number of somatostatin expressing lesions after PRRT. Post-therapy images show only one single lesion at liver level (white arrow) still presenting significant uptake, although reduced as compared to pre-therapy images (SUVmax post-therapy = 12 vs. SUVmax before therapy = 20). Post-therapy images also show reduced uptake at abdominal nodal level. Partial response to PRRT.

Teaching Points—Case 8 (Image 27.12)

- Although 68Ga-SA PET/CT can be employed to assess changes in radiotracer avidity after PRRT, the internationally standardized method to assess response to therapy is diagnostic CT (by means of the RECIST criteria), although with well-known limitations.
- The definition of more accurate criteria to assess response is mandatory.
- Combined functional and morphological imaging may in many cases better reflect the true behavior of the tumor following treatment.

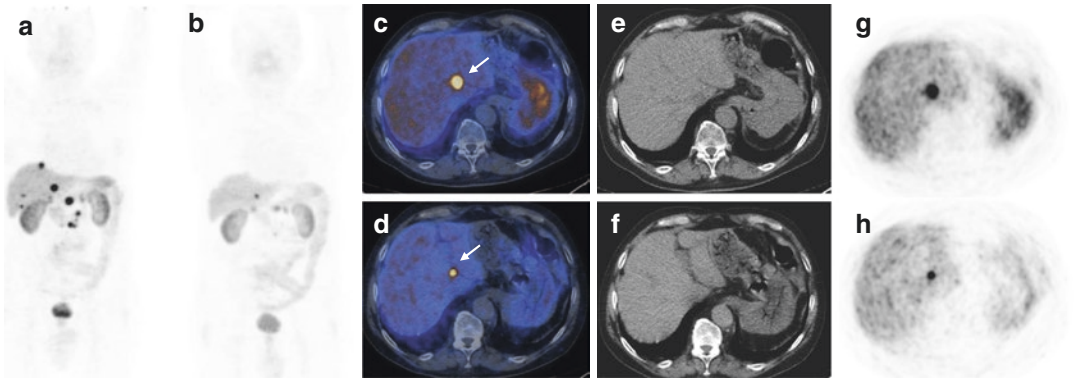

Image 27.12 MIP and transaxial PET images (**a**, **b**: MIP; **c**, **d**: fused; **e**, **f**: nondiagnostic CT; **g**, **h**: PET) acquired before and after PRRT respectively

27.3.1 Case 9: Pancreatic NET G2 Studied Before and After PRRT (Complete Response) (Image 27.13)

Clinical Details Patient with pancreatic (body/tail) NET G2 (ki67% = 4.5%) treated with spleno-pancreasectomy (subtotal) and somatostatin analog therapy. At occurrence of liver progression, the patient was addressed to PRRT.

Interpretation of Image 27.13 Pre-therapy images (a–d) show multiple liver lesions with intense uptake. Post-therapy images show complete response to PRRT. Dashed arrows show the different pattern of uptake at the pancreatic head/uncinated process level (it can change pattern in the same patient over time). Notice that in both set of images the left kidney and the left adrenal are absent due to previous surgical removal for tumor invasion.

Teaching Points—Case 9 (Image 27.13)

- PRRT can achieve complete response in approximately 30% of cases.
- Such estimates are expected to increase when PRRT will be performed earlier in the natural history of the disease (current guidelines indicate PRRT at disease progression or failure of other treatment options).
- PRRT is associated with a low incidence of severe adverse events.

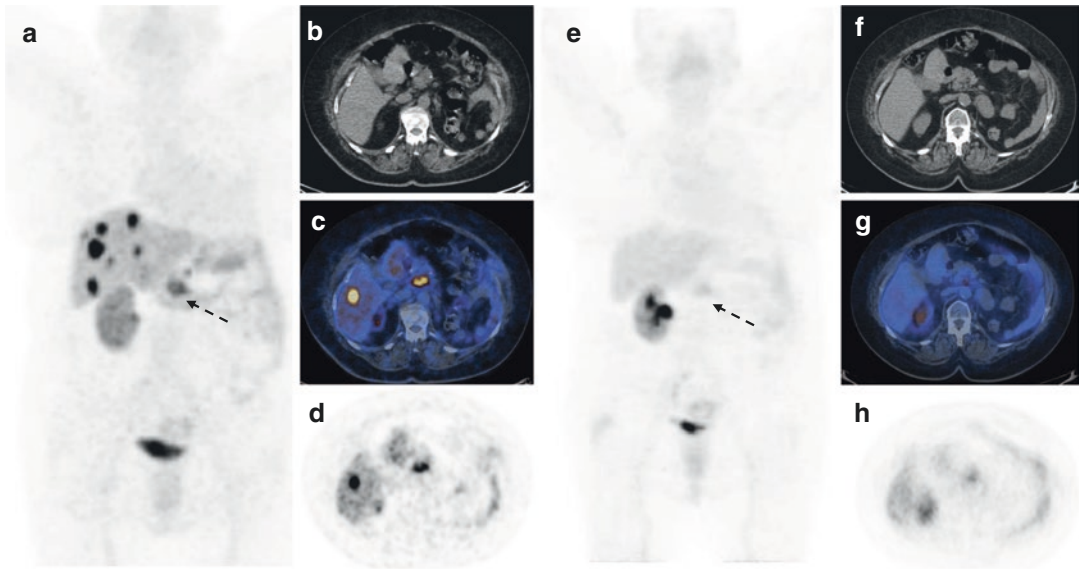

Image 27.13 MIP and nondiagnostic CT, fused and PET transaxial images acquired before (**a**–**d**) and after (**e**–**h**) PRRT respectively

27.4 Case 10: Restaging After Everolimus Therapy (Image 27.14)

Clinical Details A patient with ileum primary NET G2 was surgically radically treated 5 years before. The first relapse occurred at liver level (not shown) and was followed by liver transplantation. After the detection of the second relapse (at nodal, lung, and pancreatic level), Everolimus treatment was initiated.

Interpretation of Image 27.14 Post-therapy images show stable disease at pancreatic (b, d), nodal, and lung level.

Teaching Points—Case 10 (Image 27.14)

- 68Ga-SA PET/CT can be employed to assess response to treatment options other than PRRT.
- The optimal management of the diagnostic work up of a NEN patient requires multidisciplinary discussion in order to evaluate the need of PET re-assessment and the clinical utility (and how frequently) to perform additional imaging (e.g., 18F-FDG).

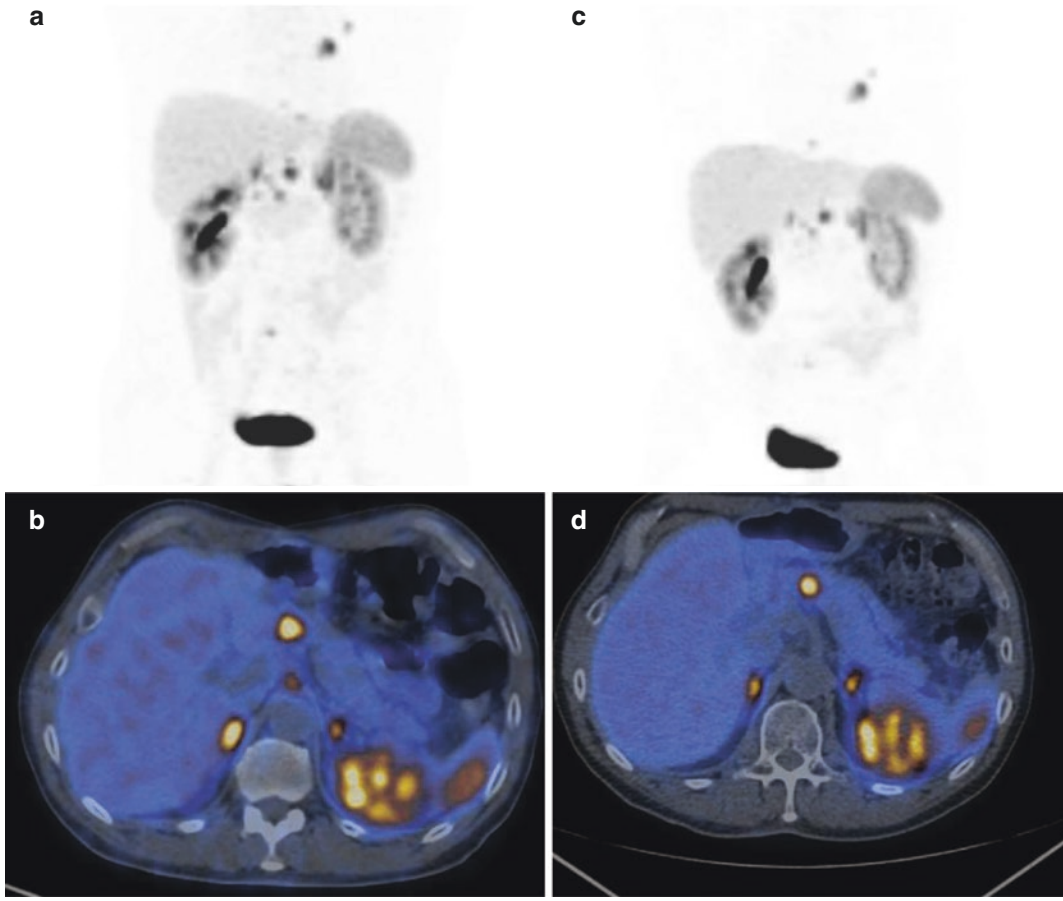

Image 27.14 MIP and transaxial fused 68Ga-DOTANOC PET/CT images acquired before (**a**, **b**) and while on (**c**, **d**) Everolimus treatment respectively

Suggested Reading

Case 1

Bozkurt MF, Virgolini I, Balogova S, Beheshti M, Rubello D, Decristoforo C, Ambrosini V, Kjaer A, Delgado-Bolton R, Kunikowska J, Oyen WJG, Chiti A, Giammarile F, Sundin A, Fanti S. Guideline for PET/CT imaging of neuroendocrine neoplasms with 68Ga-DOTA-conjugated somatostatin receptor targeting peptides and 18F-DOPA. Eur J Nucl Med Mol Imaging. 2017;44(9):1588–601.

Case 2

Bozkurt MF, Virgolini I, Balogova S, Beheshti M, Rubello D, Decristoforo C, Ambrosini V, Kjaer A, Delgado-Bolton R, Kunikowska J, Oyen WJG, Chiti A, Giammarile F, Sundin A, Fanti S. Guideline for PET/CT imaging of neuroendocrine neoplasms with 68Ga-DOTA-conjugated somatostatin receptor targeting peptides and 18F-DOPA. Eur J Nucl Med Mol Imaging. 2017;44(9):1588–601.

Ludtke FE, Mack SC, Schuff-Werner P, Voth E. Splenic function after splenectomy for trauma. Role of autotransplantation and splenosis. Acta Chir Scand. 1989;55(10):533–9.

Rufini V, Inzani F, Stefanelli A, Castaldi P, Perotti G, Cinquino A, Indovina L, Rindi G. The accessory spleen is an important pitfall of 68Ga-DOTANOC PET/CT in the workup for pancreatic neuroendocrine neoplasm. Pancreas. 2017;46(2):157–63.

Case 3

Bozkurt MF, Virgolini I, Balogova S, Beheshti M, Rubello D, Decristoforo C, Ambrosini V, Kjaer A, Delgado-Bolton R, Kunikowska J, Oyen WJG, Chiti A, Giammarile F, Sundin A, Fanti S. Guideline for PET/CT imaging of neuroendocrine neoplasms with 68Ga-DOTA-conjugated somatostatin receptor targeting peptides and 18F-DOPA. Eur J Nucl Med Mol Imaging. 2017;44(9):1588–601.

Case 4

Bozkurt MF, Virgolini I, Balogova S, Beheshti M, Rubello D, Decristoforo C, Ambrosini V, Kjaer A, Delgado-Bolton R, Kunikowska J, Oyen WJG, Chiti A, Giammarile F, Sundin A, Fanti S. Guideline for PET/CT imaging of neuroendocrine neoplasms with 68Ga-DOTA-conjugated somatostatin receptor targeting peptides and 18F-DOPA. Eur J Nucl Med Mol Imaging. 2017;44(9):1588–601.

Sundin A, Arnold R, Baudin E, Cwikla JB, Eriksson B, Fanti S, Fazio N, Giammarile F, Hicks RJ, Kjaer A, Krenning E, Kwekkeboom D, Lombard-Bohas C, O'Connor JM, O'Toole D, Rockall A, Wiedenmann B, Valle JW, Vullierme MP, Antibes Consensus Conference participants. ENETS consensus guidelines for the standards of care in neuroendocrine tumors: radiological, nuclear medicine & hybrid imaging. Neuroendocrinology. 2017;105(3):212–44.

Panagiotidis E, Alshammari A, Michopoulou S, Skoura E, Naik K, Maragkoudakis E, Mohmaduvesh M, Al-Harbi M, Belda M, Caplin ME, Toumpanakis C, Bomanji J. Comparison of the impact of 68Ga-DOTATATE and 18F-FDG PET/CT on clinical management in patients with neuroendocrine tumors. J Nucl Med. 2017;58(1):91–6.

Case 5

Bozkurt MF, Virgolini I, Balogova S, Beheshti M, Rubello D, Decristoforo C, Ambrosini V, Kjaer A, Delgado-Bolton R, Kunikowska J, Oyen WJG, Chiti A, Giammarile F, Sundin A, Fanti S. Guideline for PET/CT imaging of neuroendocrine neoplasms with 68Ga-DOTA-conjugated somatostatin receptor targeting peptides and 18F-DOPA. Eur J Nucl Med Mol Imaging. 2017;44(9):1588–601.

Kim S-J, Pak K, Koo PJ, Kwak JJ, Chang S. The efficacy of (177)Lu-labelled peptide receptor radionuclide therapy in patients with neuroendocrine tumours: a meta-analysis. Eur J Nucl Med Mol Imaging. 2015;42(13):1964–70.

Zaknun JJ, Bodei L, Mueller-Brand J, Pavel ME, Baum RP, Hörsch D, et al. The joint IAEA, EANM, and SNMMI practical guidance on peptide receptor radionuclide therapy (PRRNT) in neuroendocrine tumours. Eur J Nucl Med Mol Imaging. 2013;40(5):800–16.

Fendler WP, Barrio M, Spick C, Allen-Auerbach M, Ambrosini V, Benz M, Bluemel C, Grewal RK, Lapa C, Miederer M, Nicolas G, Schuster T, Czernin J, Herrmann K. 68Ga-DOTATATE PET/CT interobserver agreement for neuroendocrine tumor assessment: results of a prospective study on 50 patients. J Nucl Med. 2017;58(2):307–11.

Case 6

Gabriel M, Decristoforo C, Kendler D, Dobrozemsky G, Heute D, Uprimny C, Kovacs P, Von Guggenberg E, Bale R, Virgolini IJ. 68Ga-DOTA-Tyr3-octreotide PET in neuroendocrine tumors: comparison with somatostatin receptor scintigraphy and CT. J Nucl Med. 2007;48(4):508–18.

Ambrosini V, Nanni C, Zompatori M, Campana D, Tomassetti P, Castellucci P, Allegri V, Rubello D, Montini G, Franchi R, Fanti S. 68Ga-DOTA-NOC PET/CT in comparison with CT for the detec-

tion of bone metastasis in patients with neuroendocrine tumours. Eur J Nucl Med Mol Imaging. 2010;37(4):722–7.
Skoura E, Michopoulou S, Mohmaduvesh M, Panagiotidis E, Al Harbi M, Toumpanakis C, Almukhailed O, Kayani I, Syed R, Navalkissoor S, Ell PJ, Caplin ME, Bomanji J. The impact of 68Ga-DOTATATE PET/CT imaging on management of patients with neuroendocrine tumors: experience from a national referral center in the United Kingdom. J Nucl Med. 2016;57(1):34–40.

Case 7

Bodei L, Mueller-Brand J, Baum RP, Pavel ME, Hörsch D, O'Dorisio MS, O'Dorisio TM, Howe JR, Cremonesi M, Kwekkeboom DJ, Zaknun JJ. The joint IAEA, EANM, and SNMMI practical guidance on peptide receptor radionuclide therapy (PRRNT) in neuroendocrine tumours. Eur J Nucl Med Mol Imaging. 2013;40(5):800–16.
Strosberg J, El-Haddad G, Wolin E, Hendifar A, Yao J, Chasen B, Mittra E, Kunz PL, Kulke MH, Jacene H, Bushnell D, O'Dorisio TM, Baum RP, Kulkarni HR, Caplin M, Lebtahi R, Hobday T, Delpassand E, Van Cutsem E, Benson A, Srirajaskanthan R, Pavel M, Mora J, Berlin J, Grande E, Reed N, Seregni E, Öberg K, Lopera Sierra M, Santoro P, Thevenet T, Erion JL, Ruszniewski P, Kwekkeboom D, Krenning E, NETTER-1 Trial Investigators. Phase 3 trial of 177Lu-dotatate for midgut neuroendocrine tumors. N Engl J Med. 2017;376(2):125–35.

Case 8

Bodei L, Mueller-Brand J, Baum RP, Pavel ME, Hörsch D, O'Dorisio MS, O'Dorisio TM, Howe JR, Cremonesi M, Kwekkeboom DJ, Zaknun JJ. The joint IAEA, EANM, and SNMMI practical guidance on peptide receptor radionuclide therapy (PRRNT) in neuroendocrine tumours. Eur J Nucl Med Mol Imaging. 2013;40(5):800–16.
de Herder WW, Capdevila J, ENETS 2016 Munich Advisory Board Participants. Unmet needs in the field of neuroendocrine neoplasms of the gastrointestinal tract, pancreas, and respiratory system: reports by the ENETS Group. Neuroendocrinology. 2019;108(1):5–6.

Case 9

Kwekkeboom DJ, Teunissen JJ, Bakker WH, Kooij PP, de Herder WW, Feelders RA, et al. Radiolabeled somatostatin analog [177Lu-DOTA0,Tyr3]octreotate in patients with endocrine gastroenteropancreatic tumors. J Clin Oncol Off J Am Soc Clin Oncol. 2005;23(12):2754–62.
Strosberg J, El-Haddad G, Wolin E, Hendifar A, Yao J, Chasen B, Mittra E, Kunz PL, Kulke MH, Jacene H, Bushnell D, O'Dorisio TM, Baum RP, Kulkarni HR, Caplin M, Lebtahi R, Hobday T, Delpassand E, Van Cutsem E, Benson A, Srirajaskanthan R, Pavel M, Mora J, Berlin J, Grande E, Reed N, Seregni E, Öberg K, Lopera Sierra M, Santoro P, Thevenet T, Erion JL, Ruszniewski P, Kwekkeboom D, Krenning E, NETTER-1 Trial Investigators. Phase 3 trial of 177Lu-dotatate for midgut neuroendocrine tumors. N Engl J Med. 2017;376(2):125–35.

Case 10

Bozkurt MF, Virgolini I, Balogova S, Beheshti M, Rubello D, Decristoforo C, Ambrosini V, Kjaer A, Delgado-Bolton R, Kunikowska J, Oyen WJG, Chiti A, Giammarile F, Sundin A, Fanti S. Guideline for PET/CT imaging of neuroendocrine neoplasms with 68Ga-DOTA-conjugated somatostatin receptor targeting peptides and 18F-DOPA. Eur J Nucl Med Mol Imaging. 2017;44(9):1588–601.

28 ^{18}F-FDOPA PET/CT for Treatment Response Assessment

Alessio Imperiale and David Taïeb

28.1 Case 1: Assessment of Response to Chemotherapy in a Patient with Metastatic Ganglioneuroblastoma

Clinical Details Initial staging of a mass located in the left hypochondrium in a 26-year-old woman with a lumbar pain and increased plasma metanephrines levels. (1) Abdomen CT showed a 16-cm heterogeneous mass without signs of local invasion or metastatic spread. (2) ^{123}I-mIBG scintigra phy and ^{18}F-FDG PET/CT showed an intense tumor uptake. (3) ^{18}F-FDOPA PET/CT revealed additional lesions corresponding to small abdominal lymph nodes and bone metastases. (4) The patient underwent complete macroscopic resection of the primary tumor. Pathological examination revealed a ganglioneuroblastoma of adrenal origin. Systemic post-operative chemotherapy was initiated.

A. Imperiale
Biophysics and Nuclear Medicine, University Hospitals of Strasbourg, Strasbourg, France

Molecular Imaging – DRHIM, IPHC, UMR 7178, CNRS/Unistra, Strasbourg, France
e-mail: alessio.imperiale@chru-strasbourg.fr

D. Taïeb (✉)
Department of Nuclear Medicine, La Timone University Hospital, European Center for Research in Medical Imaging, Aix-Marseille University, Marseille, France
e-mail: David.TAIEB@ap-hm.fr

Scan Findings *Baseline ^{18}F-FDOPA PET/CT (Image 28.1a, b):* large left adrenal mass (Image 28.1a, *) characterized by a marked ^{18}F-FDOPA avidity. Additional areas of abnormal radiotracer uptake corresponding to retroperitoneal lymph nodes and bone metastases sometimes with an osteolytic appearance (arrows). *Interim PET/CT (Image 28.1c, d) at the end of first-line chemotherapy (Carboplatin, Etoposide, and Vincristine):* metabolic progression of existing bone metastases, apparition of new bony lesions (black and white arrows), and one isolated retro-diaphragmatic hypermetabolic lymphadenopathy (red arrows). No additional areas of abnormal ^{18}F-FDOPA uptake were found in the remaining parts of the body.

Interim PET/CT (Image 28.1e, f) during second-line chemotherapy (Irinotecan and Temodal): persistent abnormal ^{18}F-FDOPA uptake in bone metastases (white arrows) suggesting partial metabolic response. *Interim PET/CT (Image 28.1g, h) during third-line chemotherapy (Etoposide):* global metabolic regression of existing bone metastases that are only weakly visible on PET scan. Absence of nodal or visceral ^{18}F-FDOPA uptake in the remaining examined body regions.

Interpretation PET scan shows a large mass located in the left hypochondrium with a highly elevated ^{18}F-FDOPA uptake and multiple metastases. In this case, ^{18}F-FDOPA PET was more sensitive than ^{123}I-mIBG scintigraphy for detect-

S. Fanti et al. (eds.), *Atlas of Clinical PET-CT in Treatment Response Evaluation in Oncology*,
https://doi.org/10.1007/978-3-030-68858-5_28

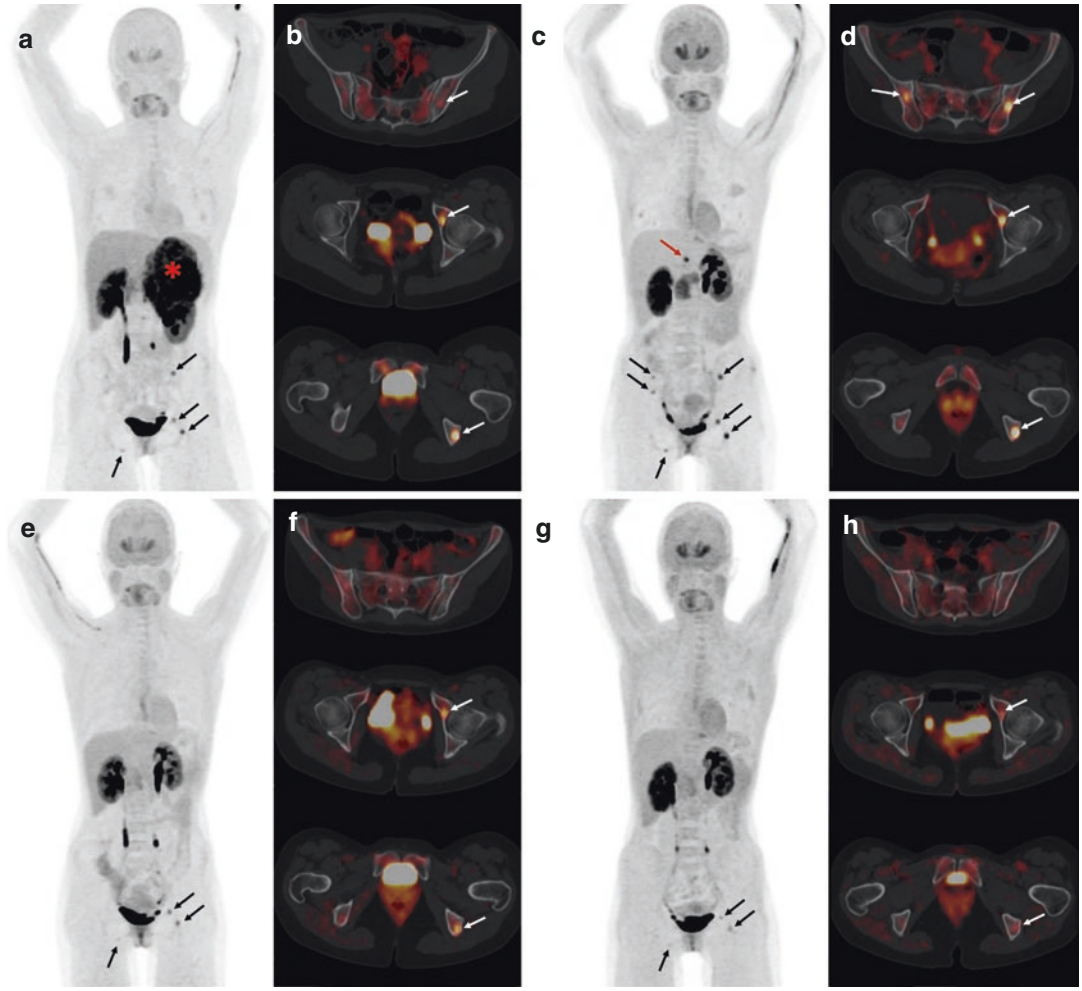

Image 28.1 (**a**–**h**) Treatment response evaluation of a metastatic ganglioneuroblastoma treated by chemotherapy

ing metastatic spread and allows us to assess the efficacy of various systemic treatments. This is important for patients with aggressive tumors where the diagnosis of refractory disease needs to be readily recognized.

Teaching Points

- Neuroblastoma is almost exclusively a pediatric neoplasm: the median age at onset is 2 years, and more than 95% of patients are less than 10 years old at diagnosis [1].
- In similar clinical cases, pheochromocytoma/paraganglioma must be considered as the main differential diagnosis, particularly in adolescent and young adult patients [2, 3].
- Accurate evaluation of disease extension and tumor characterization before starting treatment allow to assess responses during therapies particularly with early identification of non-responders.
- ^{18}F-FDOPA PET has high sensitivity and specificity for staging and restaging neuroblastoma and therefore might be used in complementary to ^{123}I-mIBG scintigraphy.
- ^{18}F-FDOPA PET might serve as a useful imaging tool for the functional assessment of response to treatments of neuroblastoma patients [4, 5].

Acknowledgements Pr. N. Hentzwerle (Pediatric Oncology Department) and Pr. G. Malouf (Hematology and Oncology Department) from the University Hospitals of Strasbourg, France, are kindly acknowledged.

28.2 Case 2: Assessment of Antitumor Effect of Somatostatin Analogs in a Patient with Carcinoid Syndrome

Clinical Details A 79-year-old man with carcinoid syndrome related to metastatic grade-2 (ki67: 3%) neuroendocrine tumor (NET) of unknown origin. (1) Abdomen CT showed 18-mm, retractile, hypervascularized mesenteric adenopathy and multiple bilobar liver metastases. Primary tumor remained unknown. (2) On ^{18}F-FDOPA PET/CT, lymph nodes and liver metastases exhibit a marked avidity. ^{18}F-FDOPA PET/CT also detected the primary ileal tumor. (3) A medical option with somatostatin analogs (SSAs) was chosen as first-line therapy.

Scan Findings *Baseline PET/CT (Image 28.2a, b):* highly elevated ^{18}F-FDOPA uptake by liver metastases (black and white arrows, SUVmax: 51), mesenteric retractile adenopathy (Image 28.2a, *), and ileal primary NET located nearby the ileocecal valve (Image 28.2a, red arrow, SUVmax: 25). No additional areas of abnormal ^{18}F-FDOPA uptake in the remaining parts of the body examined. *Interim PET/CT during long-acting SSAs (Image 28.2c, d):* overall reduction of ^{18}F-FDOPA uptake by liver lesions (black and white arrows, SUVmax: 18), mesenteric node (*), and primary tumor (red arrow, SUVmax: 25). The larger liver metastases also showed a necrotic appearance which corresponded to the central photopenic area (Image 28.2d, upper image).

Interpretation Beyond its ability to detect occult primaries, ^{18}F-FDOPA PET/CT can evaluate the antitumor and antisecretory effects of SSAs. This is due to the high expression of AADC in serotonin-secreting tumors which is at the crossroads between the serotonin and catecholamine secretory pathways. AADC catalyzes the conversion of ^{18}F-FDOPA to ^{18}F-Fdopamine which precludes its internalization into neurosecretory vesicles. ^{18}F-FDOPA PET/CT provides the opportunity to assess the reduction in tumor metabolism at a whole-body scale and therefore could complement biochemical analyses.

Teaching Points

- ^{18}F-FDOPA PET appears to be a sensitive functional imaging tool for the detection of primary NETs, especially tumors with a well-

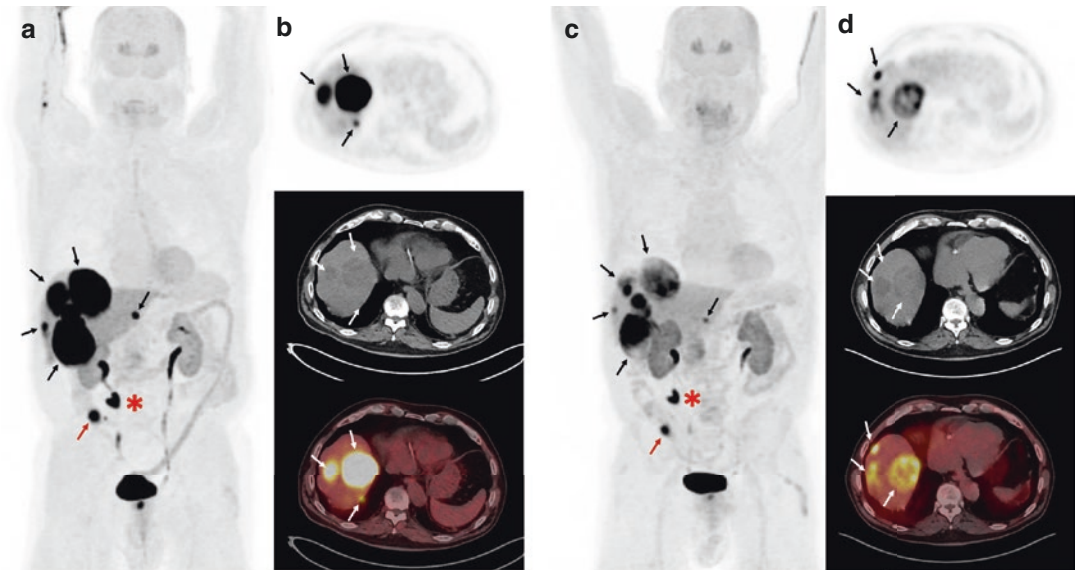

Image 28.2 (**a**–**d**) Treatment response evaluation of a metastatic NET treated by somatostatin analogs

differentiated pattern and serotonin secretion. ^{18}F-FDOPA PET sensitivity is therefore highest in ileal NETs [6].

- ^{18}F-FDOPA PET sensitivity is influenced by the tumor's capacity to take up, decarboxylate, and store amine precursors [7].
- Quantitative assessment of the uptake can be used as a biomarker of efficacy of SSAs.
- In NET patients diagnosed at an advanced stage, SSAs remain the mainstay symptomatic treatment. In addition, several data support an antiproliferative effect of SSAs in patients with well-to-moderately differentiated NETs [8, 9].

Acknowledgements Pr. Ph. Bachellier and Dr. P. Addeo (Hepato-Pancreato-Biliary Surgery and Liver transplantation) from the University Hospitals of Strasbourg, France, are kindly acknowledged.

28.3 Case 3: ^{18}F-FDOPA PET/CT-Guided Radiofrequency Ablation of Liver Metastases

Clinical Details ^{18}F-FDOPA PET/CT-guided radiofrequency (RF) ablation procedure of a single hepatic metastasis in a patient with a previous history of Grade 1 ileal metastatic (liver, nodes) neuroendocrine tumor (NET) and progressive rise of serum biomarkers. No major abnormalities were shown at conventional imaging investigations.

Scan Findings *Baseline PET/CT:* focal and intense ^{18}F-FDOPA uptake in the hepatic Segment VIII (Image 28.3a, d) corresponding to an occult liver metastasis. *During RF procedure (Image 28.3b, e):* RF probe accurately positioned within the metastasis. The total duration of RF ablation was 30 min. No early or late complications were reported. *Post-treatment PET/CT (Image 28.3c, f):* focal photopenic area corresponding to ablated hepatic metastasis (^{18}F-FDOPA PET/CT was performed 30 min after the end of RF ablation). Three months after RF procedure, MRI revealed a parenchymal scar.

Interpretation ^{18}F-FDOPA PET/CT scan revealed a single liver metastasis occult for MRI in a patient with ileal NET, allowing accurate target definition, which is crucial for optimal strategy planification. Efficacy of RF ablation was assessed on ^{18}F-FDOPA PET/CT.

Teaching Points

- ^{18}F-FDOPA PET/CT-guided biopsy may be useful to confirm the neuroendocrine nature of an abnormal foci when conventional imaging is negative [10, 11].
- ^{18}F-FDOPA PET/CT can also be used as a guide for RF ablation of metastases [12].
- ^{18}F-FDOPA can be recommended as a one-step procedure for guiding biopsy and thermoablation and assessing efficacy [13].

Acknowledgements PET/CT-guided radiofrequency ablation procedure was done in collaboration with Pr. A. Gangi and his team, from the Interventional Radiology Unit of the University Hospitals of Strasbourg, France.

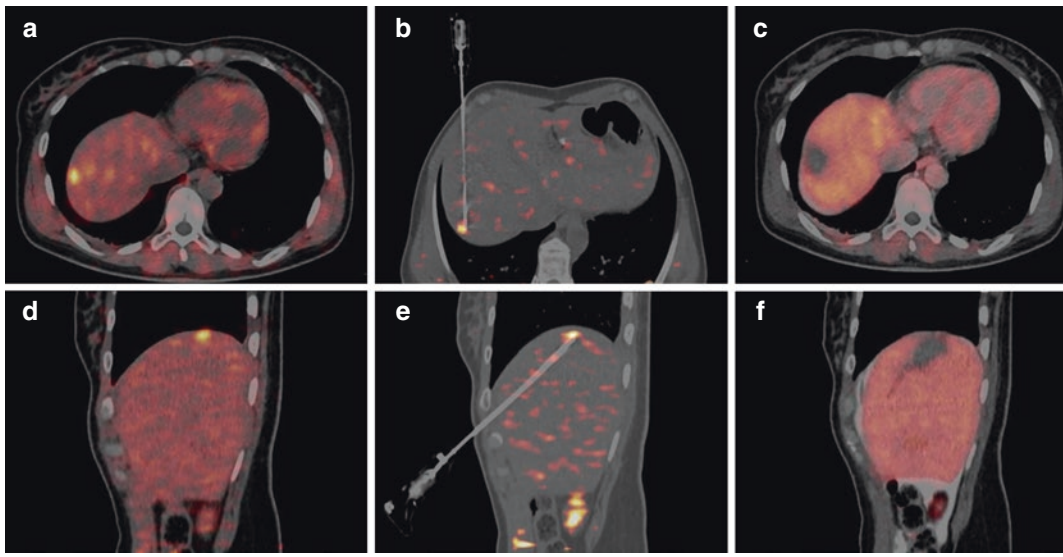

Image 28.3 (**a**–**f**) Treatment response evaluation of a metastatic neuroendocrine tumor treated by radiofrequency ablation

28.4 Case 4: Assessment of Response to Dopamine Agonists Treatment in a Patient with a MEN1-Related Prolactinoma

Clinical Details An asymptomatic 35-year-old woman with type-1 Multiple Endocrine Neoplasia (MEN1) underwent ^{18}F-FDOPA PET/CT for screening of pancreatic NET detected by MRI. A carbidopa-assisted ^{18}F-FDOPA PET/CT protocol was used and showed a single pancreatic tumor and a focal pituitary uptake. Endocrinological work-up found an increased serum prolactin (1920 mUI/L; normal upper range value: 496 mUI/L). All other causes of hyperprolactinemia were excluded. MRI identified a right pituitary microadenoma (10 × 6 mm) leading to the diagnosis of prolactinoma. A medical treatment with dopamine agonists (Cabergoline) was initiated.

Scan Findings *Baseline ^{18}F-FDOPA PET/CT:* focal ^{18}F-FDOPA uptake (arrows) located within the right side of the sella turcica which was consistent with MRI findings (Image 28.4a: MIP image; Image 28.4b: axial attenuation-corrected PET image; Image 28.4c: axial PET/CT fusion image). *Interim PET/CT under dopamine agonists therapy:* 6 months following the initiation of Cabergoline treatment, a complete regression of pituitary ^{18}F-FDOPA pathologic focal uptake was noted (dotted arrows; Image 28.4d: MIP anterior; Image 28.4e: PET axial; Image 28.4f: PET/CT axial). Plasma prolactin levels returned to normal values and MRI showed a reduction in tumor size (8 × 3 mm) on the adenoma.

Interpretation ^{18}F-FDOPA is decarboxylated into ^{18}F-Fdopamine in the dopaminergic tuberoinfundibular hypothalamic neurons and ^{18}F-Fdopamine is released in the hypophyseal portal system where it can bind to D2 dopaminergic receptors (D2DR). Therefore, ^{18}F-FDOPA PET/CT can show D2DR expressing pituitary adenomas and monitor antitumor effect of dopamine agonists. In our case, complete regression of pituitary ^{18}F-FDOPA uptake on interim PET/CT was consistent with normalization of prolactinemia.

Teaching Points

- Prolactin-secreting pituitary adenomas represent about two-thirds of the pituitary adenomas in MEN-1 patients [14].
- Dopamine agonists enable to achieve disease control in about 90% of cases [15]. However, the remaining 10% of cases do not respond to dopamine agonists [16], possibly due to a decrease in D2DR expression or abnormality in the downstream signaling pathway [17].
- In MEN1, a focal pituitary ^{18}F-FDOPA uptake can be suggestive of a D2DR-expressing tumor.
- Similar to the use ^{18}F-FDOPA in the evaluation of presynaptic dopaminergic system in Parkinson' disease, ^{18}F-FDOPA can also be used to assess the D2DR expression on pituitary adenoma [18].
- ^{18}F-FDOPA PET/CT would merit to be specifically evaluated for assessing response to dopamine agonists.

Acknowledgements Pr. B. Goichot (Endocrinology and Internal Medicine Department) from the University Hospitals of Strasbourg, France, is kindly acknowledged.

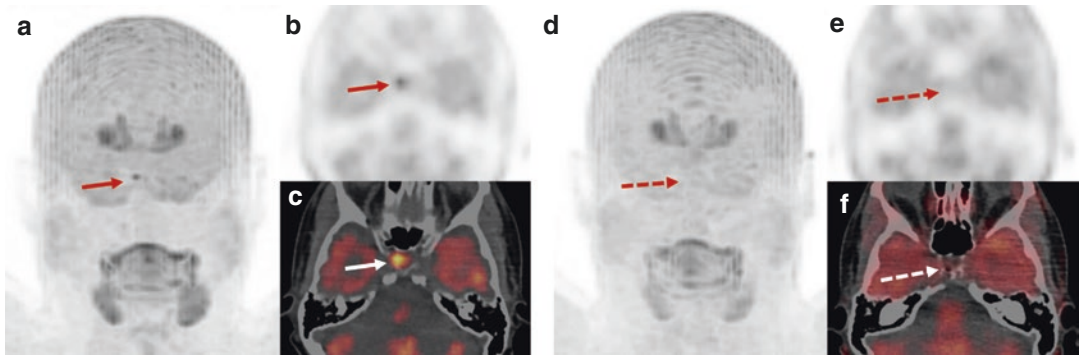

Image 28.4 (**a**–**f**) Treatment response evaluation of a prolactinoma treated by dopamine agonists

28.5 Case 5: Assessment of Response to Peptide Receptor Radionuclide Therapy in a *SDHB*-Related Metastatic Jugular Paraganglioma

Clinical Details An 80-year-old woman with a *SDHB*-related jugular paraganglioma previously treated by subtotal surgery 10-years ago was referred for PRRT. She had worsening dysphagia and weight loss. ^{68}Ga-DOTATOC showed highly elevated uptake values in the primary tumor and multiple vertebral metastases that suggest that the patient was likely to benefit from PRRT. She received four cycles of ^{177}Lu-DOTATATE (7.4 GBq/cycle).

Scan Findings *Baseline ^{18}F-FDOPA PET/CT (Image 28.5a, c, e):* Intense tumor ^{18}F-FDOPA uptake (Image 28.5a: MIP image; Image 28.5b: axial PET/CT fusion image, Image 28.5c: axial MRI). *^{18}F-FDOPA PET/CT PET/CT performed 4 months after the last PRRT cycle:* Decrease of ^{18}F-FDOPA uptake and metabolic tumor burden of the primary tumor which was consistent with decrease of tumor volume on MRI (see Image 28.5f vs. Image 28.5e, asterisk). See a slight decrease in ^{18}F-FDOPA uptake of a bony metastasis (black arrow).

Interpretation The decrease in ^{18}F-FDOPA avidity of PGL lesions can be used as a metabolic response to PRRT.

Teaching Points

- Somatostatin-receptor imaging (preferred PET with ^{68}Ga-DOTA-SSA) is mandatory for selecting candidates to PRRT.
- Molecular imaging can complement anatomical imaging in the assessment of response to PRRT.
- Although ^{68}Ga-DOTA-SSA is currently recommended for staging and restaging of metastatic PPGL, regardless of genotype [19], ^{18}F-FDOPA has a very high sensitivity in metastatic HNPGL, probably due to their very well-differentiated pattern compared to their *SDHx*-related sympathetic counterparts [20].
- The role of ^{18}F-FDOPA by its virtue of phenotyping disease would need to be specifically evaluated in the evaluation of response with head-to-head comparison with ^{68}Ga-DOTA-SSA.

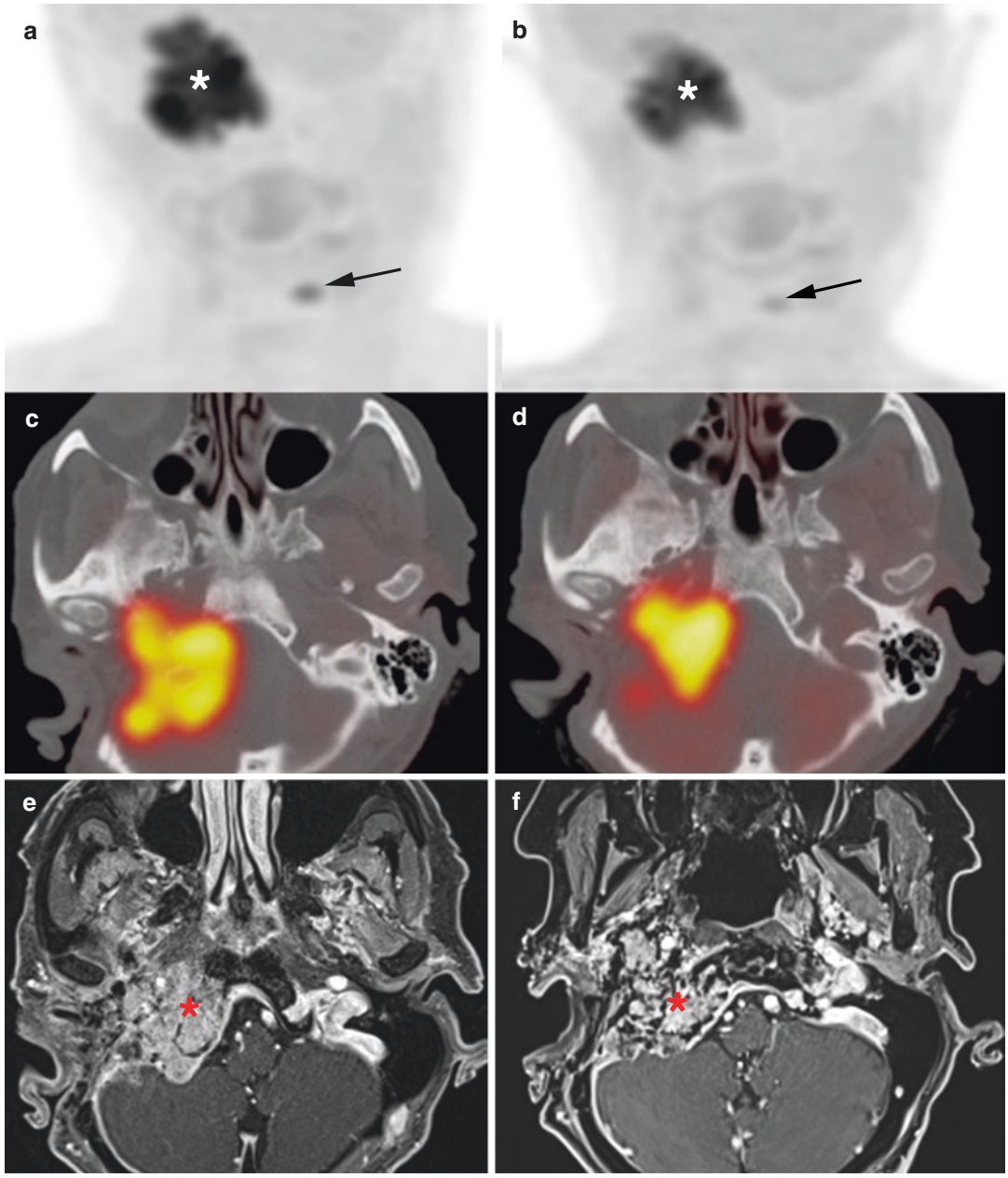

Image 28.5 (**a**–**f**) Treatment response evaluation of a paraganglioma treated by Peptide Receptor Radionuclide Therapy

References

Case 1

1. Evans AE, D'Angio GJ. Age at diagnosis and prognosis in children with neuroblastoma. J Clin Oncol. 2005;23:6443–4.
2. Elsayes KM, Elmohr MM, Javadi S, Menias CO, Remer EM, Morani AC, Shaaban AM. Mimics, pitfalls, and misdiagnoses of adrenal masses on CT and MRI. Abdom Radiol (NY). 2020;45:982.
3. Hanafy AK, Mujtaba B, Roman-Colon AM, Elsayes KM, Harrison D, Ramani NS, Waguespack SG, Morani AC. Imaging features of adrenal gland masses in the pediatric population. Abdom Radiol (NY). 2020;45:964.
4. Lu MY, Liu YL, Chang HH, Jou ST, Yang YL, Lin KH, Lin DT, Lee YL, Lee H, Wu PY, Luo TY, Shen LH, Huang SF, Liao YF, Hsu WM, Tzen KY, National Taiwan University Neuroblastoma Study Group. Characterization of neuroblastic tumors using 18F-FDOPA PET. J Nucl Med. 2013;54:42–9.
5. Liu YL, Lu MY, Chang HH, Lu CC, Lin DT, Jou ST, Yang YL, Lee YL, Huang SF, Jeng YM, Lee H, Miser JS, Lin KH, Liao YF, Hsu WM, Tzen KY. Diagnostic FDG and FDOPA positron emission tomography scans distinguish the genomic type and treatment outcome of neuroblastoma. Oncotarget. 2016;7:18774–86.

Case 2

6. Imperiale A, Rust E, Gabriel S, Detour J, Goichot B, Duclos B, Kurtz JE, Bachellier P, Namer IJ, Taïeb D. [18]F-fluorodihydroxyphenylalanine PET/CT in patients with neuroendocrine tumors of unknown origin: relation to tumor origin and differentiation. J Nucl Med. 2014;55:367–72.
7. Deroose CM, Hindié E, Kebebew E, Goichot B, Pacak K, Taïeb D, Imperiale A. Molecular imaging of gastroenteropancreatic neuroendocrine tumors: current status and future directions. J Nucl Med. 2016;57:1949–56.
8. Enzler T, Fojo T. Long-acting somatostatin analogues in the treatment of unresectable/metastatic neuroendocrine tumors. Semin Oncol. 2017;44:141–56.
9. Rinke A, Müller HH, Schade-Brittinger C, Klose KJ, Barth P, Wied M, Mayer C, Aminossadati B, Pape UF, Bläker M, Harder J, Arnold C, Gress T, Arnold R, PROMID Study Group. Placebo-controlled, double-blind, prospective, randomized study on the effect of octreotide LAR in the control of tumor growth in patients with metastatic neuroendocrine midgut tumors: a report from the PROMID Study Group. J Clin Oncol. 2009;27:4656–63.

Case 3

10. Shyn PB. Interventional positron emission tomography/computed tomography: state-of-the-art. Tech Vasc Interv Radiol. 2013;16:182–90.
11. Cerci JJ, Pereira Neto CC, Krauzer C, et al. The impact of coaxial core biopsy guided by FDG PET/CT in oncological patients. Eur J Nucl Med Mol Imaging. 2013;40:98–103.
12. Imperiale A, Garnon J, Bachellier P, Gangi A, Namer IJ. Simultaneous (18)F-FDOPA PET/CT-guided biopsy and radiofrequency ablation of recurrent neuroendocrine hepatic metastasis: further step toward a theranostic approach. Clin Nucl Med. 2015;40:e334–5.
13. Cazzato RL, Garnon J, Ramamurthy N, Tsoumakidou G, Imperiale A, Namer IJ, Bachellier P, Caudrelier J, Rao P, Koch G, Gangi A. 18F-FDOPA PET/CT-guided radiofrequency ablation of liver metastases from neuroendocrine tumours: technical note on a preliminary experience. Cardiovasc Intervent Radiol. 2016;39:1315–21.

Case 4

14. Molitch ME. Diagnosis and treatment of pituitary adenomas: a review. JAMA. 2017;317:516–24.
15. Faje A, Chunharojrith P, Nency J, et al. Dopamine agonists can reduce cystic prolactinomas. J Clin Endocrinol Metab. 2016;101:3709–15.
16. Gillam MP, Molitch ME, Lombardi G, et al. Advances in the treatment of prolactinomas. Endocr Rev. 2006;27:485–534.
17. Shimazu S, Shimatsu A, Yamada S, et al. Resistance to dopamine agonists in prolactinoma is correlated with reduction of dopamine D2 receptor long isoform mRNA levels. Eur J Endocrinol. 2012;166:383–90.
18. Fine SA, Frohman LA. Loss of central nervous system component of dopaminergic inhibition of prolactin secretion in patients with prolactin-secreting pituitary tumors. J Clin Invest. 1978;61:973–80.

Case 5

19. Reichert T, Fahkry N, Lavieille JP, Amodru V, Sebag F, Romanet P, Loundou A, Castinetti F, Pacak K, Montava M, et al. Exploring the link between tumour metabolism and succinate dehydrogenase deficiency: a (18) F-FDOPA PET/CT study in head and neck paragangliomas. Clin Endocrinol. 2019;91:879.
20. Taieb D, Hicks RJ, Hindie E, Guillet BA, Avram A, Ghedini P, Timmers HJ, Scott AT, Elojeimy S, Rubello D, et al. European Association of Nuclear Medicine Practice Guideline/Society of Nuclear Medicine and Molecular Imaging Procedure Standard 2019 for radionuclide imaging of phaeochromocytoma and paraganglioma. Eur J Nucl Med Mol Imaging. 2019;46:2112–37.

18F-FLT/FET PET-CT in Treatment Response Evaluation

29

Ameya D. Puranik and Yash Jain

29.1 Introduction

In this era of personalized medicine and with the introduction of the concept of precision oncology, molecular imaging with PET/CT is being increasingly implemented in neuro-oncology, as it provides additional biologic information of the tumor. Conventional imaging techniques such as CT and MRI reveal morphologic information but are of limited value for assessment of biology and activity of the tumor. PET can provide additional information on tumor grade, optimal biopsy locations, the degree of intracerebral infiltration, and recurrence. Different molecular processes can be mapped with PET/CT and have been proposed to be useful, like glucose consumption, expression of amino acid transporters, proliferation rate, membrane biosynthesis, and hypoxia. Applications of MR spectroscopy for molecular evaluation are wide ranging, but its utility is limited in comparison to sensitivity of PET. PET can detect biological molecules in the picomolar range whereas MR sensitivity is only in the millimolar range [1].

A. D. Puranik (✉) · Y. Jain
Department of Nuclear Medicine and Molecular Imaging, Tata Memorial Hospital, Homi Bhabha National Institute, Mumbai, India

29.2 Limitations of FDG PET/CT

FDG PET/CT was proposed to be useful for imaging gliomas because of an increased glucose metabolism in high-grade glioma as well as a positive correlation between the glycolysis rate and malignancy [2, 3]. However, the diagnostic accuracy of FDG PET/CT is hampered by the high physiologic glucose metabolism in normal brain parenchyma which significantly limits its sensitivity for detection as well as its specificity for delineation of adjacent glial tissue. This is of particular importance in low-grade gliomas, which anyways show only modest uptake (owing to very low metabolism), similar to that of white matter and decreased uptake when compared with gray matter [4, 5]. Finally FDG is known to accumulate in macrophages and inflammatory tissue, making a distinction between glioma and acute or chronic inflammatory process often difficult.

29.2.1 Amino Acid Tracers

Radiolabeled amino acids were first introduced in 1982 as suitable PET tracers in brain tumors [6]. The use of amino acids is based upon the principle of increased amino acid utilization, which is known to play a key role in cell proliferation, as well as extracellular matrix growth production in glioma [7]. A variety of radiolabeled

S. Fanti et al. (eds.), *Atlas of Clinical PET-CT in Treatment Response Evaluation in Oncology*,
https://doi.org/10.1007/978-3-030-68858-5_29

amino acids, like [11C]methionine ([11C]MET), and aromatic amino acid analogs, like [18F] fluorotyrosine ([18F]TYR), [18F]fluoro-ethyl-tyrosine ([18F]FET), [18F]fluoro-methyltyrosine ([18F]FMT), and [18F]fluorodopa ([18F]DOPA), have been used. FET and MET have been the most widely used amino acid tracers of all, for imaging brain tumors. Amino acid tracers can be used for detection, tumor grading, targeting biopsy, and evaluation of response. Specific advantage of these tracers over FDG is that high-contrast images can be acquired due to high amino acid uptake in both low- and high-grade gliomas and low uptake in normal brain tissue.

29.2.2 FLT and FET PET/CT Imaging

Fluorothymidine (FLT) is a nucleoside thymidine analog. Thymidine is rapidly transported into the cells by means of a nucleoside transporter and is phosphorylated by the enzyme thymidine kinase (TK)-1 to thymidine nucleotides, which are among the molecular building blocks of DNA [8]. TK-1 is highly expressed during DNA synthesis of proliferating cells and leads to intracellular trapping of the radiotracer. Thus retention of [18F]FLT within the cell provides a measure of cellular proliferation. The use of FLT is beneficial because it accumulates at lower levels in most of the brain regions due to a lack of significant neuronal cell division. In gliomas, elevated FLT uptake was associated with increased expression of antigen Ki-67, an index of mitotic activity [9].

[11C]MET and [18F]FET have been the most widely used amino acid tracers in gliomas. Fluoroethyl tyrosine is a tyrosine amino acid analog. FET has shown an increased sensitivity compared to FLT in case of low-grade gliomas and tumors failing to exhibit MR enhancement. This is because FLT cannot cross the intact blood brain barrier (BBB) and hence does not accumulate to a significant extent in low-grade gliomas, which usually show less aggressive and infiltrative behavior. FET however can accumulate in both low- and high-grade gliomas since it is freely mobile across the BBB and its uptake is not dependent on breach of BBB by the tumor [10, 11]. Another advantage of FET over FLT is that it can be used for tumor grading [12]. Recently published data using dynamic analysis of [18F]FET uptake allows a differentiation between low- and high-grade gliomas with high diagnostic power because of different FET kinetic uptake behavior.

29.2.3 Diagnosis and Grading

Management and prognosis of gliomas highly depend on histological grading. The value of conventional MRI is limited in differentiation of low-grade gliomas versus benign nonneoplastic lesions as well as in detection of high-grade gliomas without any obvious MR morphologic signs of malignancy.

FDG was the first PET tracer used; however the sensitivity of FDG PET/CT was found to be limited in primary diagnosis of glioma, because only 3–6% of patients with low-grade gliomas and 21–47% of patients with high-grade gliomas presented with increased tracer uptake. In the past few years amino acid PET tracers have gained importance since they overcome the limitations of FDG by showing much higher tumor to background contrast. Amino acid tracers have shown high sensitivity in differentiation between nonneoplastic lesions and low-grade gliomas (up to 79% positive predictive value). Increased amino acid uptake can be found in 72–76% of low-grade and 95–100% of high-grade gliomas for both [11C]MET and [18F]FET PET/CT [13, 14]. A recently developed dynamic analysis of FET uptake enables the differentiation between low- and high-grade gliomas with high diagnostic power (sensitivity, 94%; specificity, 100%) [15]. Dynamic FET PET/CT typically shows

steadily increasing time-activity curves in WHO Grade II gliomas, as opposed to an early activity peak around 10–20 min after injection, followed by a decrease of FET uptake in WHO Grades III/IV gliomas. This is particularly valuable in the clinical setting of patients with MRI non-contrast-enhancing gliomas suspected of harboring a WHO Grade II glioma.

FET PET has also been demonstrated to reliably detect anaplastic foci and to be able to differentiate between Grades II and III histopathology within one and the same tumor (sensitivity 92%; specificity 82%) when the dynamic analysis was applied; this is of particular importance when planning a biopsy [16].

Multiple histopathological and postmortem series demonstrate the limitations of conventional MRI in defining the extent of glioma [17]. In WHO Grade III/IV gliomas FET PET-based tumor volumes have been shown to extend beyond the contrast-enhancing volume on conventional MRI by 2–3.5 cm for different tracers. In addition, amino acid PET identifies tumor extent within nonspecific regions of T2/FLAIR signal abnormality [18, 19]. Most WHO Grade II gliomas are non-enhancing with infiltrating tumor borders that are difficult to delineate by conventional MRI. Several studies have demonstrated the usefulness of amino acid PET in defining tumor extent. Delineation of tumor borders by amino acid PET is superior to standard MRI in both contrast-enhancing and non-contrast-enhancing Grade II gliomas [20].

29.3 Response Assessment

29.3.1 Radiation Necrosis vs. Recurrence

Assessment of treatment response in gliomas is very challenging. Post-treatment MRIs often show contrast-enhancing lesions that can be associated either with tumor relapse or with treatment-induced changes. Treatment-induced changes can be classified either as "pseudoprogression" (reversible, early radiographic changes) or "radiation necrosis" (subacute radiographic changes, irreversible). In contrast to genuine tumor recurrence, these treatment-induced changes are asymptomatic (especially in case of pseudoprogression), fail to progress, and are associated with prolonged survival. The accuracy of MRI-based predictions of patients disease status remains limited. PET/CT as a supplementary imaging modality has been suggested as a valuable tool for therapy monitoring. FDG was the first tracer used but it proved quite inconsistent and showed limited accuracy for the differentiation of recurrence from treatment-induced changes, with sensitivities between 40% and 90% and specificities between 40% and 80%, respectively, which could lead to an inappropriate treatment in up to one-third of patients.

Amino acid tracers have been proven to be more appropriate. FET PET/CT offers high diagnostic power (sensitivity, 82%; specificity, 100%, positive predictive value, 84%) in this scenario. FET PET with additional dynamic data analysis (sensitivity, 100%; specificity, 93%) was significantly superior to conventional MRI (sensitivity, 94%; specificity, 50%) in discriminating tumor recurrence from post-therapeutic changes [15, 21]. Slightly increasing and homogeneous FET uptake around the tumor cavity points toward benign therapy-related changes, whereas focally increased FET uptake was shown to be an early and reliable indicator of tumor progression. Primarily in WHO Grades III/IV gliomas, current amino acid PET data suggest that a reduction of amino acid uptake and/or a decrease of the metabolically active tumor volume is a sign of treatment response associated with long-term outcome [21]. FET may facilitate the diagnosis of pseudoprogression in glioblastoma patients within the first 12 weeks following completion of chemoradiotherapy [21].

Post-bevacizumab response assessment is even more difficult to monitor by conventional imaging techniques, since treatment-induced reduction of contrast enhancement represents only reduced vascular permeability and provides no significant information on residual or recurrent disease [22]. To date none of the current radiographic modalities, neither conventional or diffusion-weighted imaging-based MRI nor MRS has proven sensitive enough to assess post-bevacizumab treatment effects. Metabolic imaging has been proposed to be an alternative therapy response assessment tool. In a study [18F]FLT PET proved to be superior compared with contrast-enhanced MRI in predicting treatment response of malignant gliomas to bevacizumab plus chemotherapy, in a small group of patients with recurrent malignant gliomas (n = 21) [23]. Furthermore, several other studies suggest that treatment response and outcome in bevacizumab therapy can be assessed by amino acid PET using FET and FDOPA better than by MRI [21].

29.3.2 Post Anti-angiogenic Therapy

In 2010, the RANO group recommended new criteria for response assessment by including FLAIR or T2 signal alterations as criteria for determining tumor response or progression ("non-enhancing tumor progression") [24]. Recent studies indicated that FET and FDOPA PET are useful in detecting pseudoresponse. FET and FDOPA PET have also been used to predict a favorable outcome in responders to bevacizumab [25, 26]. Additionally, the cost effectiveness of FET PET for therapy monitoring of antiangiogenic therapy has been analyzed. The data suggest that the additional use of FET PET in the management of these patients has the potential to avoid overtreatment and corresponding costs, as well as unnecessary patient side effects [27].

29.3.3 Response to Immune Check-Point Inhibitors

The iRANO group noted that to date there is no noninvasive method that can confidently identify pseudoprogression in these patients. Thus, there remains an urgent need for the acquisition of additional information potentially derived from advanced imaging techniques. Recently a small retrospective pilot study addressed this issue and showed for the first time the potential of FET PET to detect pseudoprogression in patients with malignant melanoma brain metastasis treated with ipilimumab or nivolumab [28].

29.4 Conclusion

The present literature in neuroimaging using PET highlights the ability of amino acid PET to quantify biological responses to treatment and allows its application to monitor patients to identify early disease relapse and response to treatment. The more widespread use of amino acid PET for the management of patients with brain tumors has been strongly recommended by the RANO group [29]. However, therapy-monitoring PET data remain limited, necessitating more comprehensive (i.e., biopsy-controlled), prospective studies in larger clinical cohorts. In particular, continued progress is impeded by the lack of stereotactically guided biopsy-controlled studies. Lastly, the diagnostic impact of amino acid PET needs to be compared with a variety of promising advanced MR imaging techniques to develop the most accurate and useful multi-modal biomarkers possible (Figs. 29.1, 29.2, and 29.3).

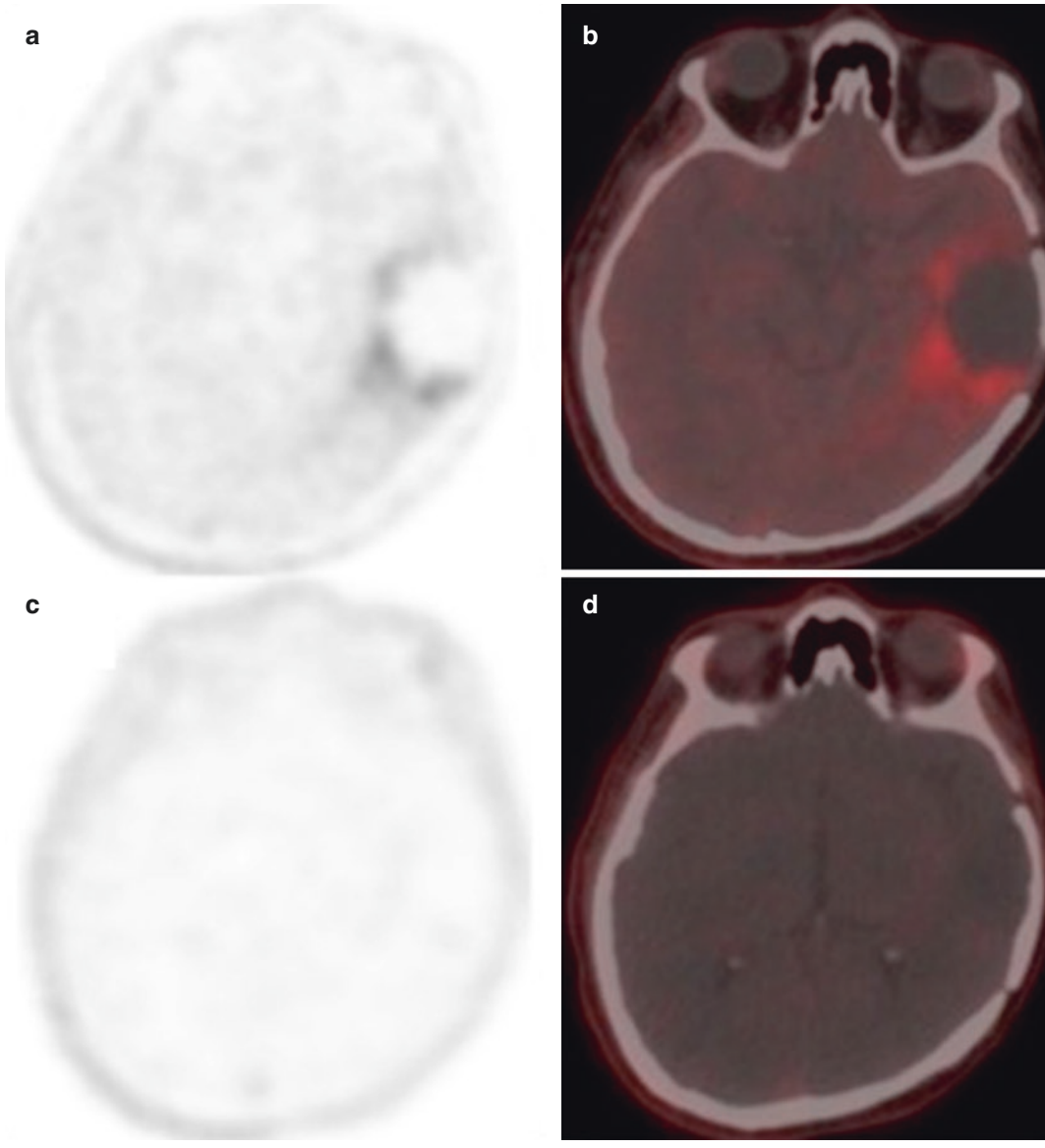

Fig. 29.1 A 37-year-old gentleman, case of GBM, WHO Grade IV, left temporal location, operated in January 2015, received adjuvant radiotherapy and temozolomide (TMZ) followed by concurrent TMZ till December 2015. Patient was on follow-up till 2017, when in June presented with seizures and headache, MRI showed Swiss cheese pattern suggestive of post-treatment changes. FET PET (**a**, **b**) showed increased uptake in the index tumor bed with a tumor-white mater (T-Wm) ratio of 3.5 (normal <2.5) suggestive of recurrent disease. Patient was started on chemotherapy and was asymptomatic a year later, when follow-up FET PET (**c**, **d**) showed no tracer uptake in left temporal region, suggestive of response to treatment. However, MRI showed persistent Swiss cheese pattern

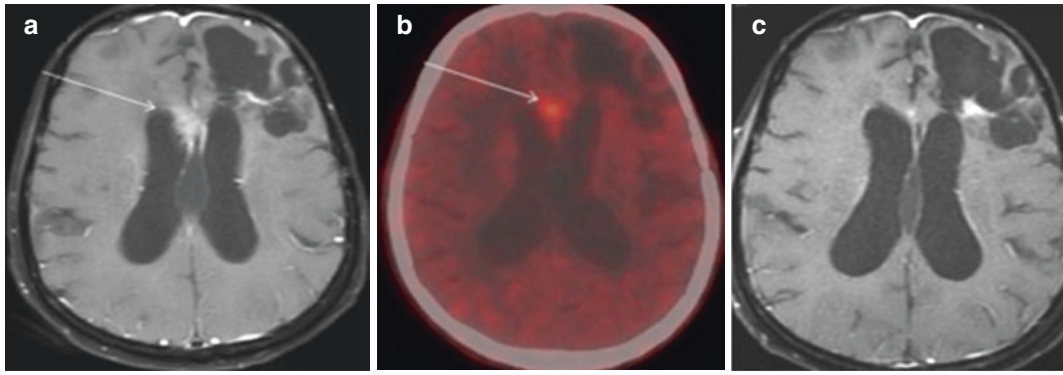

Fig. 29.2 A 67-year-old elderly male, case of WHO Grade III, anaplastic astrocytoma–pericallosal location in midline anteriorly, received radiotherapy followed by concurrent and adjuvant TMZ, was asymptomatic for 1 year, after which, on follow-up MRI (**a**, arrow), ill-defined T1-post-contrast enhancement was seen in anterior genu of corpus callosum (arrow), which was reported as post-treatment changes as it showed hypoperfusion. However, FET PET showed high T-Wm of 4.3 in the same region (**b**, arrow) and was started on chemotherapy. Follow-up MRI (**c**) was done at native place which was shared online, and patient could not travel for FET PET to our institution. Post-contrast T1-weighted image shows reduction in enhancement at the site of recurrence documented on FET PET

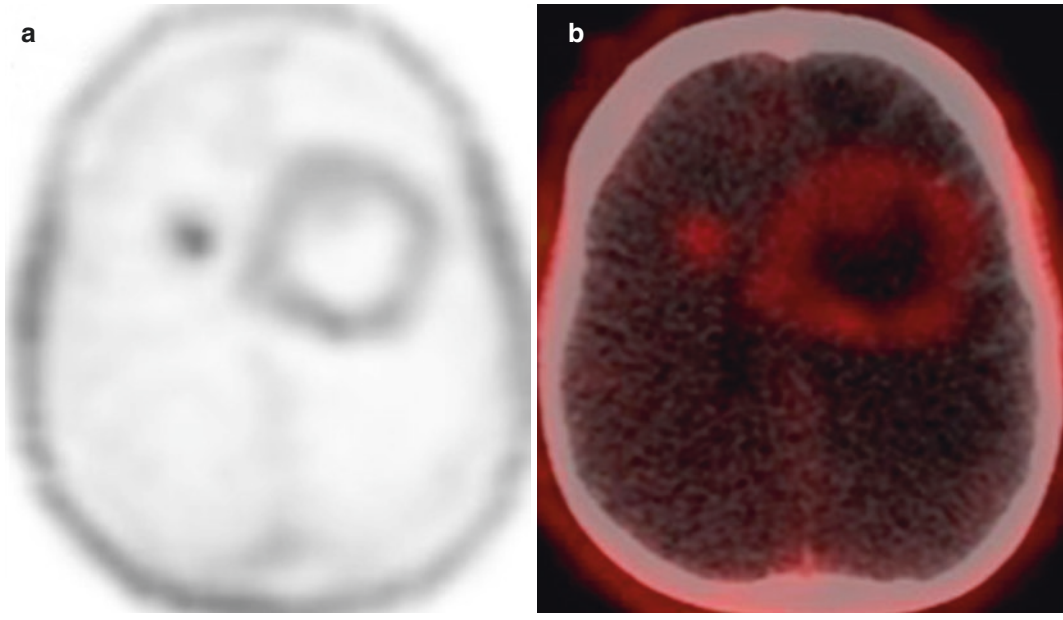

Fig. 29.3 A 27-year-old young male, case of IDH-wild type left frontal GBM, post-radiotherapy and concurrent and adjuvant TMZ, and routine follow-up MRI at 6 months, showed focal enhancing lesion in contralateral frontal region, with post-treatment changes in left frontal region reported on MRI. FET PET (**a**, **b**) showed intense tracer uptake in focal lesion in right frontal (T-Wm ration 2.8) and left frontal ring enhancing lesions (T-Wm of 3.2), both suggestive of tumor recurrence. However, patient was kept on follow-up and FET PET at 3 months (**c**, **d**) showed increase in intensity of tracer uptake and T-Wm ratios (right frontal—3.6, left frontal—3.9) suggestive of disease recurrence. Patient died within 3 months

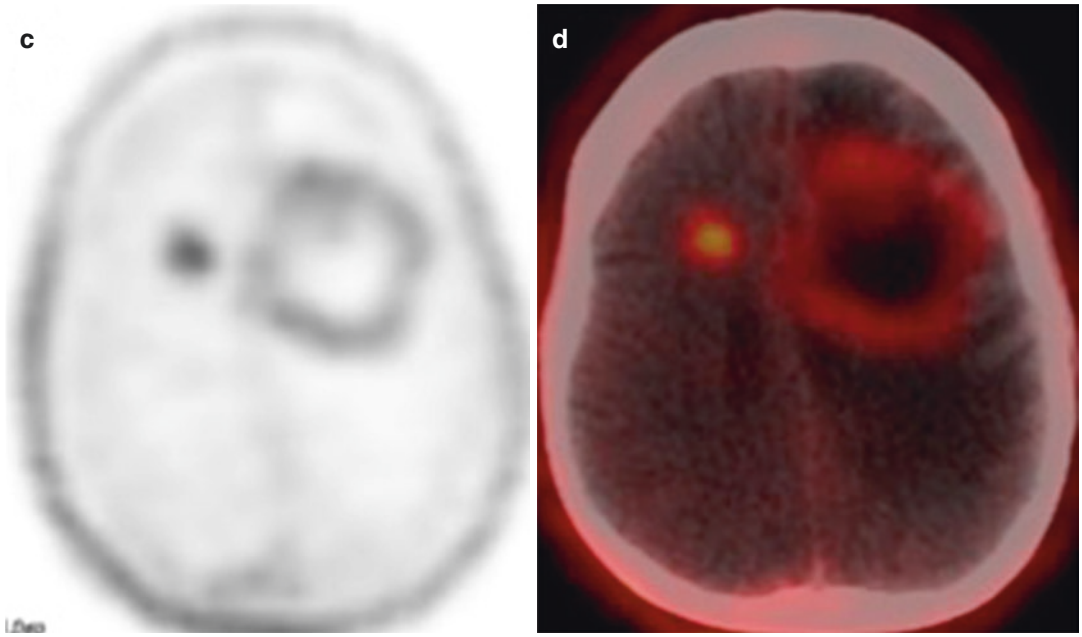

Fig. 29.3 (continued)

References

1. Marmé D, Fusenig N, editors. Tumor angiogenesis: basic mechanisms and cancer therapy. New York, NY: Springer; 2007. p. 726.
2. Di Chiro G, DeLaPaz RL, Brooks RA, et al. Glucose utilization of cerebral gliomas measured by [18F] fluorodeoxyglucose and positron emission tomography. Neurology. 1982;32:1323–9.
3. Alavi JB, Alavi A, Chawluk J, et al. Positron emission tomography in patients with glioma. A predictor of prognosis. Cancer. 1988;62:1074–8.
4. Ricci PE, Karis JP, Heiserman JE, Fram EK, Bice AN, Drayer BP. Differentiating recurrent tumor from radiation necrosis: time for re-evaluation of positron emission tomography? AJNR Am J Neuroradiol. 1998;19:407–13.
5. Weber W, Bartenstein P, Gross MW, et al. Fluorine-18-FDG PET and iodine-123-IMT SPECT in the evaluation of brain tumors. J Nucl Med. 1997;38:802–8.
6. Hubner KF, Purvis JT, Mahaley SM Jr, et al. Brain tumor imaging by positron emission computed tomography using 11C-labeled amino acids. J Comput Assist Tomogr. 1982;6:544–50.
7. Isselbacher KJ. Sugar and amino acid transport by cells in culture–differences between normal and malignant cells. N Engl J Med. 1972;286:929–33.
8. Price SJ, Fryer TD, Cleij MC, et al. Imaging regional variation of cellular proliferation in gliomas using 3!-deoxy-3!-[18F]fluorothymidine positron-emission tomography: an image-guided biopsy study. Clin Radiol. 2009;64:52–63.
9. Arbizu J, Tejada S, Marti-Climent JM, et al. Quantitative volumetric analysis of gliomas with sequential MRI and 11C-methionine PET assessment: patterns of integration in therapy planning. Eur J Nucl Med Mol Imaging. 2012;39(5):771–81.
10. Wienhard K, Herholz K, Coenen HH, et al. Increased amino acid transport into brain tumors measured by PET of L-(2-18F)fluorotyrosine. J Nucl Med. 1991;32:1338–46.
11. Heiss P, Mayer S, Herz M, et al. Investigation of transport mechanism and uptake kinetics of O-(2-[18F] fluoroethyl)-L-tyrosine in vitro and in vivo. J Nucl Med. 1999;40:1367–73.
12. Popperl G, Kreth FW, Mehrkens JH, et al. FET PET for the evaluation of untreated gliomas: correlation of FET uptake and uptake kinetics with tumor grading. Eur J Nucl Med Mol Imaging. 2007;34:1933–42.
13. Ledezma CJ, Chen W, Sai V, et al. 18F-FDOPA PET/MRI fusion in patients with primary/recurrent gliomas: initial experience. Eur J Radiol. 2009;71:242–8.
14. Kunz M, Thon N, Eigenbrod S, et al. Hot spots in 18FET-PET delineate malignant tumor parts within suspected WHO grade II glioma. Neuro-Oncology. 2011;13:307–16.
15. Watanabe M, Tanaka R, Takeda N. Magnetic resonance imaging and histopathology of cerebral gliomas. Neuroradiology. 1992;34(6):463–9.
16. Pope WB, Lai A, Nghiemphu P, Mischel P, Cloughesy TF. MRI in patients with high-grade gliomas treated

with bevacizumab and chemotherapy. Neurology. 2006;66:1258–60.
17. Chen W, Cloughesy T, Kamdar N, et al. Imaging proliferation in brain tumors with 18F-FLT PET: comparison with 18F-FDG. J Nucl Med. 2005;46:945–52.
18. Kato T, Shinoda J, Nakayama N, et al. Metabolic assessment of gliomas using 11C-methionine, [18F] fluorodeoxyglucose, and 11C-choline positron-emission tomography. AJNR Am J Neuroradiol. 2008;29:1176–82.
19. Pauleit D, Stoffels G, Bachofner A, et al. Comparison of (18)F-FET and (18)F-FDG PET in brain tumors. Nucl Med Biol. 2009;36:779–87.
20. Pafundi DH, Laack NN, Youland RS, et al. Biopsy validation of 18F-DOPA PET and biodistribution in gliomas for neurosurgical planning and radiotherapy target delineation: results of a prospective pilot study. Neuro-Oncology. 2013;15:1058–67.
21. Wen PY, Macdonald DR, Reardon DA, Cloughesy TF, Sorensen AG, Galanis E, et al. Updated response assessment criteria for high-grade gliomas: response assessment in neuro-oncology working group. J Clin Oncol. 2010;28:1963–72.
22. Chen W, Delaloye S, Silverman DH, et al. Predicting treatment response of malignant gliomas to bevacizumab and irinotecan by imaging proliferation with [18F] fluorothymidine positron emission tomography: a pilot study. J Clin Oncol. 2007;25:4714–21.
23. Albert NL, Weller M, Suchorska B, Galldiks N, Soffietti R, Kim MM, et al. Response Assessment in Neuro-Oncology working group and European Association for Neuro-Oncology recommendations for the clinical use of PET imaging in gliomas. Neuro-Oncology. 2016;18(9):1199–208.
24. Galldiks N, Rapp M, Stoffels G, Dunkl V, Sabel M, Langen KJ. Earlier diagnosis of progressive disease during bevacizumab treatment using O-(2-18F-fluorethyl)-l-tyrosine positron emission tomography in comparison with magnetic resonance imaging. Mol Imaging. 2013;12:273–6.
25. Galldiks N, Rapp M, Stoffels G, Fink GR, Shah NJ, Coenen HH, et al. Response assessment of bevacizumab in patients with recurrent malignant glioma using [18F]fluoroethyl-l-tyrosine PET in comparison to MRI. Eur J Nucl Med Mol Imaging. 2013;40:22–33.
26. Schwarzenberg J, Czernin J, Cloughesy TF, Ellingson BM, Pope WB, Grogan T, et al. Treatment response evaluation using 18F-FDOPA PET in patients with recurrent malignant glioma on bevacizumab therapy. Clin Cancer Res. 2014;20:3550–9.
27. Heinzel A, Müller D, Langen KJ, Blaum M, Verburg FA, Mottaghy FM, Galldiks N. The use of O-(2-18F-fluoroethyl)-l-tyrosine PET for treatment management of bevacizumab and irinotecan in patients with recurrent high-grade glioma: a cost-effectiveness analysis. J Nucl Med. 2013;54:1217–22.
28. Kebir S, Rauschenbach L, Galldiks N, Schlaak M, Hattingen E, Landsberg J, Bundschuh RA, Langen KJ, Scheffler B, Herrlinger U, Glas M. Dynamic O-(2-[18F]fluoroethyl)-l-tyrosine PET imaging for the detection of checkpoint inhibitor-related pseudoprogression in melanoma brain metastases. Neuro-Oncology. 2016;18(10):1462–4.
29. Langen KJ, Watts C. Neuro-oncology: amino acid PET for brain tumours - ready for the clinic? Nat Rev Neurol. 2016;12:375–6.